Structural Design Methodology for Spray Applied Pipe Liners in Gravity Storm Water Conveyance Conduits



Prepared by:

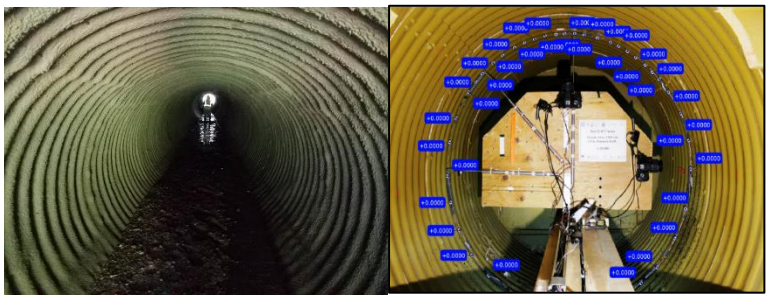
Mohammad Najafi (PI), Xinbao Yu (Co-PI), Zahra Kohankar Kouchesfehani, Amin Darabnoush Tehrani, Seyed Korky, Ramtin Serajiantehrani, Samrat Raut, Ed Kampbell & Lynn Osborn

Prepared for:

The Ohio Department of Transportation, Office of Statewide Planning & Research

Project ID Number: 103453

April 20, 2021



U.S. Department of Transportation
Federal Highway Administration

This Page Left Intentionally Blank.

Technical Report Documentation

1. Report No.	2. Government Accession No.	3. Recipient's Catalog No.
FHWA/OH-2021/10		

4. Title and Subtitle	5. Report Date
Structural Design Methodology for Spray Applied Pipe Liners in Gravity Storm Water Conveyance Conduits	**April 2021** 6. Performing Organization Code

7. Author(s)	8. Performing Organization Report No.
Mohammad Najafi (PI), Xinbao Yu (Co-PI), Zahra Kohankar Kouchesfehani, Amin Darabnoush Tehrani, Seyed Korky, Ramtin Serajiantehrani, Samrat Raut, Ed Kampbell and Lynn Osborn	

9. Performing Organization Name and Address	10. Work Unit No. (TRAIS)
CUIRE/The University of Texas at Arlington **Civil Engineering Laboratory Building (CELB)** **1221 West Mitchell Street, Room #139** **Arlington, TX 76013**	11. Contract or Grant No. **PID: 103453**

12. Sponsoring Agency Name and Address	13. Type of Report and Period Covered
Ohio Department of Transportation **1980 West Broad Street** **Columbus, Ohio 43223**	**Final Report** 14. Sponsoring Agency Code

15. Supplementary Notes

16. Abstract

To reduce high cost of emergency repairs and disruptions to travelling public, and prior to loss of host pipe integrity and soil-structure interaction, departments of transportations (DOTs) can use polymeric or cementitious/geopolymer spray applied pipe linings (SAPLs) to renew deteriorated gravity storm conduits and culverts. The AASHTO – National Transportation Product Evaluation Program (NTPEP) developed a Technical Committee (TC) for SAPL materials to implement this technology. However, no standardized structural design methodology existed, and vendors utilized different design methodologies with some using the cured-in-place pipe (CIPP), and others using various classical analytical structural design equations developed for other purposes. Therefore, the ultimate objective of this project was to develop design equations for structural application of SAPLs for invert-cut (invert deteriorated) circular and arch corrugated metal pipe (CMP) culverts with diameters or spans between 36 and 120 in. To achieve this objective, the project methodology included literature review, survey of U.S. and Canadian transportation agencies, review of CIPP design equations, considerations for use of additional reinforcement and benefits of filling CMP corrugations with cementitious SAPLs, comparison of construction and environmental cost of SAPL with CIPP and sliplining trenchless renewal techniques, inspection and field data collection of past SAPL projects, preparation of performance specifications, soil box testing of bare and renewed CMP samples, and finite element modeling (FEM). As detailed in this report, soil box testing included both intact and invert-cut CMPs of 60-in. diameter/span for circular and arch shapes in both bare (for control test) and renewed (lined) conditions. The CMPs were renewed with polymeric and cementitious SAPLs in three different thicknesses while embedded with poorly graded sand (SP) with shallow cover. A static load with an actuator was continuously applied through a load pad on the soil surface until renewed pipe failed. The results of this project showed that both tested polymeric and geopolymer SAPLs can significantly increase the ultimate loading capacity of invert deteriorated CMPs and be considered as structural solutions.

17. Keywords	18. Distribution Statement
Trenchless Renewal Methods, Spray Applied Pipe Lining (SAPL), Culvert renewal, Structural Design of Culverts	**No restrictions. This document is available to the public through the National Technical Information Service, Springfield, Virginia 22161**

19. Security Classification (of this report)	20. Security Classification (of this page)	21. 582	22. Price
Unclassified	**Unclassified**		

Form DOT F 1700.7 (8-72)	**Reproduction of completed pages authorized**

This Page Left Intentionally Blank.

Authors and Responsibilities

Chapter/Task		Authors/Responsibility
1	Survey	• Seyed Korky • Vasudeva Kaushik Nandyala
2	Literature Review	• Amin Darabnoush Tehrani • Zahra Kohankar Kouchesfehani • Seyed Korky
3	Additional Reinforcement	• Ed Kampbell • Zahra Kohankar Kouchesfehani
4	Evaluation of the Need to Fill the Valleys of Corrugated Pipes	• Ed Kampbell • Amin Darabnoush Tehrani
5	Comparison of Construction and Environmental Cost of SAPL, CIPP and Sliplining	• Ramtin Serajiantehrani
6	Review the Cured in Place (CIPP) Design Equations	• Ed Kampbell
7	SAPL Field Inspection and Data Collection	• Zahra Kohankar Kouchesfehani • Amin Darabnoush Tehrani • Ed Kampbell • Satish Kakkera
8	Development of Structural Design Equations	• Ed Kampbell
9	Performance Construction Specifications	• Lynn Osborn
10	Finite Element Modeling of SAPL Renewed Corrugated Metal Pipes Tested in a Soil Box	• Xinbao Yu • Samrat Raut
11	Laboratory Testing	• Amin Darabnoush Tehrani • Zahra Kohankar Kouchesfehani

This Page Left Intentionally Blank.

Credits and Acknowledgments

Prepared in cooperation with the Ohio Department of Transportation
and the U.S. Department of Transportation, Federal Highway Administration

The contents of this report reflect the views of the authors who are responsible for the facts and the accuracy of the data presented herein. The contents do not necessarily reflect the official views or policies of the Ohio Department of Transportation or the Federal Highway Administration. This report does not constitute a standard, specification, or regulation.

Participating DOTs

This research was conducted under a pool-funded project from National Cooperative Highway Research Program (NCHRP) at the University of Texas at Arlington (UTA), Center for Underground Infrastructure Research and Education (CUIRE). The authors would like to thank Ohio Department of Transportation (Ohio DOT) for leading the project and six other DOTs including DelDOT, FDOT, MnDOT, NCDOT, NYSDOT and PennDOT for funding and contributing to this project. Authors would like to specifically thank Mr. Jeffrey E. Syar, P.E. (Project Leader) and Mr. Thomas K. Birnbrich, P.E. (Ohio DOT), Mr. Brian R. Carmody, P.E. and Mr. Steven Wright, P.E. (NYSDOT), Mr. Matthew Lauffer, P.E. and Mr. Charles Smith P.E. (NCDOT), Mr. Paul Rowekamp and Ms. Aislyn Ryan (MnDOT), Ms. Sheri Little (PennDOT), Mr. Carlton Spirio and Ms. Jennifer Green (FDOT) and Mr. Jonathan Karam and Mr. Nicholas Dean (DelDOT). Authors would like to acknowledge efforts and hard work of ODOT project and contract administrators, Ms. Jill Martindale, Ms. Michelle Lucas, Ms. Cynthia Jones and Ms. Kelly Nye.

Participating Organizations and Individuals

Authors would like to thank Mr. Chip Johnson, Sprayroq, Inc.; and Mr. Mario Tamez, Standard Cement Materials, Inc.; who were instrumental for providing and installing their polymeric and geopolymer SAPL materials, respectively, for the soil box testing. This project could not have been completed without their participation and support. Partner companies and consultants, Rehabilitation Resource Solutions, LEO Consulting LLC., and American Structurepoint, Inc., supported this research project by contributing extra time and efforts. Dr. Firat Sever (formerly with American Structurepoint) contributed to the design equation part of the project. Contech Engineered Solutions LLC (Mr. Darrell Sanders, P.E., Mr. David Horton, and Mr. Hugh Mickel, P.E.) contributed corrugated metal pipes for testing. Mr. Vartan Babakhanian at Forterra Pipe and Precast, provided sandy soil for pipe sample embedment. Principals of: Lane Supply, Madewell Products Corporation, HVJ Associates, MTS Systems Corporation, and Micro-Measurement provided various products and services. Drs. Vinayak "Vinny" Kaushal, Ramtin Serajiantehrani and Reza Malek (former UTA/CUIRE Ph.D. students) provided help during the test setup.

Students

Authors would like to thank CUIRE students who helped with this research project:

- Aaroh Swarup
- Amir Tabesh
- Anushree Nayak
- Ferika Farooghi
- Hiramani Raj Chimauriya
- Charbel Salloum
- Juhil Makwana
- Karthikeyan Loganathan
- Pouria Pourmand
- Sahar Habibzadeh
- Shobhit Srivastava
- Siddharth Raut
- Suhas Patil
- Yasir Sheikh Salman
- Ukendran Gopi
- Kawalpreet Kaur

SI* (MODERN METRIC) CONVERSION FACTORS

APPROXIMATE CONVERSIONS TO SI UNITS

Symbol	When You Know	Multiply By	To Find	Symbol
LENGTH				
in	inches	25.4	millimeters	mm
ft	feet	0.305	meters	m
yd	yards	0.914	meters	m
mi	miles	1.61	kilometers	km
AREA				
in^2	square inches	645.2	square millimeters	mm^2
ft^2	square feet	0.093	square meters	m^2
yd^2	square yards	0.836	square meters	m^2
ac	acres	0.405	hectares	ha
mi^2	square miles	2.59	square kilometers	km^2
VOLUME				
fl oz	fluid ounces	29.57	milliliters	mL
gal	gallons	3.785	liters	L
ft^3	cubic feet	0.028	cubic meters	m^3
yd^3	cubic yards	0.765	cubic meters	m^3
NOTE: Volumes greater than 1000 L shall be shown in m^3.				
MASS				
oz	ounces	28.35	grams	g
lb	pounds	0.454	kilograms	kg
T	short tons (2000 lb)	0.907	megagrams (or "metric ton")	Mg (or "t")
TEMPERATURE (exact)				
°F	Fahrenheit temperature	5(°F-32)/9 or (°F-32)/1.8	Celsius temperature	°C
ILLUMINATION				
fc	foot-candles	10.76	lux	lx
fl	foot-Lamberts	3.426	candela/m^2	cd/m^2
FORCE and PRESSURE or STRESS				
lbf	poundforce	4.45	newtons	N
lbf/in^2 or psi	poundforce per square inch	6.89	kilopascals	kPa

APPROXIMATE CONVERSIONS FROM SI UNITS

Symbol	When You Know	Multiply By	To Find	Symbol
LENGTH				
mm	millimeters	0.039	inches	in
m	meters	3.28	feet	ft
m	meters	1.09	yards	yd
km	kilometers	0.621	miles	mi
AREA				
mm^2	square millimeters	0.0016	square inches	in^2
m^2	square meters	10.764	square feet	ft^2
m^2	square meters	1.195	square yards	yd^2
ha	hectares	2.47	acres	ac
km^2	square kilometers	0.386	square miles	mi^2
VOLUME				
mL	milliliters	0.034	fluid ounces	fl oz
L	liters	0.264	gallons	gal
m^3	cubic meters	35.71	cubic feet	ft^3
m^3	cubic meters	1.307	cubic yards	yd^3
MASS				
g	grams	0.035	ounces	oz
kg	kilograms	2.202	pounds	lb
Mg (or "t")	megagrams (or "metric ton")	1.103	short tons (2000 lb)	T
TEMPERATURE (exact)				
°C	Celsius temperature	1.8°C + 32	Fahrenheit temperature	°F
ILLUMINATION				
lx	lux	0.0929	foot-candles	fc
cd/m^2	candela/m^2	0.2919	foot-Lamberts	fl
FORCE and PRESSURE or STRESS				
N	newtons	0.225	poundforce	lbf
kPa	kilopascals	0.145	poundforce per square inch	lbf/in^2 or psi

* SI is the symbol for the International Symbol of Units. Appropriate rounding should be made to comply with Section 4 of ASTM E380. (Revised September 1993)

(Source: Ohio DOT)

Contents

Chapter Authors v
Problem Statement 1
Research Background 3
Research Approach 11
Task 1: Survey of U.S. Departments of Transportation (DOTs) and Canadian Transportation Agencies 13
Task 2: Literature Review 13
Task 3: Additional Reinforcement 13
Task 4: Evaluation of the Need to Fill the Valleys of Corrugated Pipes 14
Task 5: Comparison of Construction and Environmental Cost of SAPL and other Trenchless Technology Methods 14
Task 6: Review of the Cured in Place (CIPP) Design Equations 15
Task 7: SAPL Field Inspection and Data Collection 15
Task 8: Development of Structural Design Equations 16
Task 9: Performance Construction Specifications 17
Task 10: Finite Element Modeling of SAPL Renewed Corrugated Metal Pipes Tested in a Soil Box 17
Task 11: Laboratory Testing 17
Research Findings and Conclusions 21
Task 1: Survey of U.S. Departments of Transportation (DOTs) and Canadian Transportation Agencies 22
Task 2: Literature Review 23
Task 3: Additional Reinforcement 23
Task 4: Evaluation of the Need to Fill the Valleys of Corrugated Pipes 24
Task 5: Comparison of Construction and Environmental Cost of SAPL and other Trenchless Technology Methods 24
Task 6: Review of the Cured in Place (CIPP) Design Equations 25
Task 7: SAPL Field Inspection and Data Collection 26
Task 8: Development of Structural Design Equations 26
Task 9: Performance Construction Specifications 27
Task 10: Finite Element Modeling of SAPL Renewed Corrugated Metal Pipes Tested in a Soil Box 28
Task 11: Laboratory Testing 29
Recommendations for Implementation 33

Recommendations for Future Work 34
Recommendations for Implementation 35
Chapters and Appendices 36
CHAPTER 1 - SURVEY OF U.S. DOTs AND CANADIAN AGENCIES 38
1.1. Introduction and Background 38
1.2. Part B – Considerations During SAPL Installations 53
1.3. Part C – Considerations After SAPL Installations 54
1.4. Summary 57
Appendix 1- A: Survey Form 58
Appendix 1-B: Survey Respondents Contact Information 71
CHAPTER 2 - LITERATURE REVIEW 76
2.1. Introduction and Background 76
2.1.1. Culverts and Storm Sewers 76
2.1.2. Corrugated Metal Pipe (CMP) 88
2.1.3. Renewal of Deteriorated Culverts using Trenchless Technology 92
2.2. Spray Applied Pipe Linings 100
2.2.1. Polymeric Spray Applied Pipe Liners 100
2.2.2. Cementitious Spray Applied Pipe Liners 109
2.2.3. SAPL Renewed Soil-Pipe System Testing 112
2.3. Structural Analysis of Sewer Linings 120
2.3.1. Structural Classification of Sewer Linings 120
2.4. Standards and Construction Guidelines 121
2.5. Example of Rehabilitation Classification Methods 122
2.6. Summary 123
CHAPTER 3 - ADDITIONAL REINFORCEMENT 126
3.1. Objectives 126
3.2. Background 126
3.3. Introduction 126
3.4. Cementitious Fiber Reinforced SAPL 127
3.5. Structural Strength 128
3.6. Different Types of Reinforcement 129
3.6.1. Micro-Synthetic and Macro-Synthetic Fibers 130
3.6.2. Welded Wire Mesh Reinforcement 133

3.6.3. Non-Metallic Fiber Mesh Reinforcement 134
3.6.4. Basalt Mesh Reinforcement 135
3.6.5. Reinforcement Bars 136
3.7. Summary of Findings 136
3.8. Concluding Remarks 137
CHAPTER 4 - EVALUATION OF THE NEED TO FILL THE VALLEYS OF CORRUGATED PIPES 140
4.1. Introduction 140
4.2. Typical Corrugation Profiles of CMP Structures 142
4.3. Design Goals of Lining CMP Structures 143
4.4. Constructability of Liner Geometry 144
4.5. Increase in Structural Strength 147
4.6. Other Factors 148
4.7. Conclusions 148
CHAPTER 5 - COMPARISON OF CONSTRUCTION AND ENVIRONMENTAL COST OF SAPL, CIPP AND SLIPLINING 152
5.1. Introduction and Background 152
5.1.1. Construction and Environmental Costs Analysis 152
5.1.2. Need Statement 153
5.1.3. Scope of the Work 153
5.2. Cost Data Analysis 153
5.2.1. Dataset Preparation 156
5.2.2. Data Distribution 158
5.3. Results and Comparisons 165
5.3.1. Results 165
5.3.2. Construction Costs Comparison 168
5.3.3. Environmental Costs Analysis 171
5.4. Discussion of Results 177
5.5. Conclusions and Recommendations for Future Work 178
Appendix 5-A Dataset 179
CHAPTER 6 - REVIEW THE CURED IN PLACE (CIPP) DESIGN EQUATIONS 192
6.1. Introduction 192
6.2. WRc SRM Volume III Sewer Renovation 192

6.3. German ATV-DVWK-M 127 E, Part 2 193
6.4. ASCE Pipeline Infrastructure Committee 194
6.5. The ASTM F1216 Design Appendix X1 195
6.5.1. The ASTM Equations for the PD Design Condition 197
6.5.2. The Fully Deteriorated (FD) Pipe Design Condition 199
6.6. Pending ASCE MOP for Design of Flexible Liners 201
6.7. Dealing with the True Design Condition 203
6.8. Summary 208
CHAPTER 7 - SAPL FIELD INSPECTION AND DATA COLLECTION 212
7.1. Objectives 212
7.2 Selection of Culverts 212
7.4. Inspection Tools 214
7.5. Inspection Procedure 214
7.6. SAPL Issues Due to Lack of Standard 215
7.7. SAPL Thickness 219
7.8. Rating Systems 221
7.9. Condition Assessment of SAPLs 229
7.10. Comparative Status of Cementitious and Geopolymer SAPLs. 229
7.11. Numerical Modeling 230
7.12. Limitations, Findings and Recommendations 232
7.13. Summary and Conclusions 234
Appendix 7-A: Inspected SAPL Projects 235
CHAPTER 8 - DEVELOPMENT OF STRUCTURAL DESIGN EQUATIONS 256
8.1. Live and Dead Loads Used for Liner Designs 256
8.2. Design for Liner Thickness Using Polymeric and Cementitious Materials 261
8.2.1. Cementitious Spray Applied Liner Design Procedure 262
8.2.2. Sample Calculations of a Cementitious Liner 265
8.2.3. Development of Proposed Design Equations for Flexible Polymeric Materials 275
8.2.4. Sample Calculations of a Flexible Polymeric Liner 284
8.3. Summary and Recommendations 288
Appendix 8-A: Moment of Inertia Calculation 291
CHAPTER 9 - PERFORMANCE CONSTRUCTION SPECIFICATIONS 294

9.1. POLYMERIC SPRAY APPLIED PIPE LINING 294
9.1.1 - GENERAL 294
9.1.2 - PRODUCTS 298
9.1.3 - EXECUTION 300
9.2 Cementitious Spray Applied Pipe Lining 303
9.2.1 – GENERAL 303
9.2.2 - PRODUCTS 307
9.2.3 - EXECUTION 308
CHAPTER 10 - FINITE ELEMENT MODELING OF SAPL RENEWED CORRUGATED METAL PIPES TESTED IN A SOIL BOX 314
10.1. Finite Element Modeling of Soil Box Tests of CMPs 314
10.1.1. Model Setup 314
10.1.2. Boundary Condition and Loading 315
10.1.3. Material Model 315
10.1.4. Soil-CMP and Liner-CMP Interaction 317
10.1.5. Elements 317
10.1.6. Mesh Size Analyses 319
10.1.7. Modeling Steps 321
10.2. Simulation Results of the Control Test 322
10.2.1. Intact CMP Loaded with a 10x20 in.^{2} Load Pad 322
10.2.2. Intact CMP (20x40 in2 load pad) 326
10.2.3. Invert-Cut CMP 329
10.3. Results from Circular polymeric SAPL Lined CMPs 332
10.3.1. 0.25-in. thick polymeric SAPL 333
10.3.2. 0.5-in. thick polymeric SAPL 337
10.3.3. 1-in. thick polymeric SAPL 338
10.4. Parametric Analysis on Lined Invert-Removed Circular CMP pipe 339
10.4.1. 0.75-in thick polymeric SAPL 340
10.4.2. 1.5-in. thick polymeric SAPL 340
10.4.3. 2-in. thick polymeric SAPL 342
10.4.4. 0.25-in thick (over the Crest) polymeric SAPL (Filled Corrugation) 343
10.5. Polymeric SAPL Performance Comparison 346

10.6. Results for Arch Control Test 347
10.6.1. Invert-Cut Arch CMP 348
10.6.2. Intact Arch CMP 349
10.7. Results from invert removed arch CMPs lined with polymeric SAPL 350
10.7.1. 0.25-in. thick Arch polymeric SAPL 351
10.7.2. 0.5-in. thick polymeric SAPL 354
10.7.3. 1-in. thick polymeric SAPL 355
10.7.4. 0.75 -in. thick polymeric SAPL 359
10.7.5. 1.5 -in. thick polymeric SAPL 360
10.7.6. 2 -in. thick polymeric SAPL 361
10.7.7. 0.25 in. thick (over the Corrugation) filled polymeric SAPL 362
10.7.8. Comparison of Liner Performance 364
10.8. Summary and Conclusions 365
10.8.1. Circular CMPs lined with polymeric SAPL 366
10.8.2. Arch CMP lined with polymeric SAPL 366
10.8.3. Limitations 367
Appendix 10–A: Invert-cut Circular CMP 368
Appendix 10-B: Invert-cut circular CMP with polymeric SAPL 372
Appendix 10–C: Invert-cut Arch CMP 379
Appendix 10–D: Parametric Study of Invert-cut Circular 380
CMPs Repaired with polymeric SAPL 380
Invert-cut circular 60 in. CMPs with 3 ft. Cover and 0.25, 0.5, and 1 in. thick polymeric Liner 380
Invert-cut circular 60 in. CMPs with 1 ft. cover and 0.25, 0.5, and 1 in. thick polymeric circular liner 382
Appendix 10E: Invert-cut Arch CMP with polymeric Liners 383
Invert-cut Circular 48 in. CMPs with 3 ft. Cover and 0.25, 0.5, and 1 in. Thick polymeric Liner 389
Invert-cut Circular 48 in. CMPs with 2 ft. Cover and 0.25, 0.5, and 1 in. thick polymeric Liner 391
Invert-cut Circular 48 in. CMPs with 1 ft. Cover and 0.25, 0.5, and 1 in. Thick Liner 392

Invert-cut Circular 36 in. CMPs with 3 ft. Cover and 0.25, 0.5, and 1 in. Thick polymeric Liner....394
Invert-cut Circular 36 in. CMPs with 2 ft. Cover and 0.25, 0.5, and 1 in. Thick polymeric Liner....395
Invert-cut Circular 36 in. CMPs with 1 ft. Cover and 0.25, 0.5, and 1 in. Thick polymeric Liner....397
Material Model....398
Soil and CMP interaction....399
Results and discussion....399
CHAPTER 11 - LABORATORY TESTING....406
11.1 OVERVIEW....406
11.2 EXPERIMENTAL TEST DESIGN AND SETUP PREPARATION....408
11.3 BURIAL CONFIGURATION....410
11.4 COMPACTION METHODOLOGY AND MEASUREMENT....415
11.4.1 Laboratory Compaction of Granular Soils....416
11.4.2 Field Compaction of Granular Soils....416
11.4.3 Soil-box Compaction....417
11.4.4 Measurement of Field Compaction....417
11.4.5 Nuclear Density Gauge....417
11.4.6 Time Domain Reflectometry (TDR)....418
11.5 PIPE SAMPLES....419
11.6 PIPE INSTALLATION AND EMBEDMENT....422
11.7 LOAD PADS....423
11.7.1 Test Operation and Load Rate....424
11.8 INSTRUMENTATION....424
11.8.1 Strain Gauges....425
11.8.2 Earth Pressure Cells....427
11.8.3 LVDT and CDS....428
11.8.4 DIC Measurement and Pipe Monitoring....429
11.8.5 SAPL Thickness Measurement....431
11.9 POLYMERIC SAPL....432
11.9.1 CMP Surface Preparation and Polymeric SAPL Installation....432

11.9.2 Polymeric SAPL Installation 433
11.9.3 Polymeric SAPL Sampling for Material Property Testing 434
11.10 CEMENTITIOUS SAPL 435
11.10.1 CMP Surface Preparation 435
11.10.2 SAPL Installation 436
11.10.3 SAPL Mechanical Properties Testing Samples 438
11.10.4 SAPL Visual Inspection and Internal Instrumentation 440
11.10.5 CMP Arch samples Renewed with Cementitious SAPL 440
11.10.6 Circular CMPs Renewed with Cementitious SAPL 441
11.10.7 SAPL Thickness Measurement 441
11.11 TESTING RESULTS AND DISCUSSIONS 442
11.11.1 CMP Control Test 442
11.11.2 Polymeric SAPL 460
11.11.3 Cementitious SAPL 492
11.12 Conclusions 549
APPENDIX A Design Spreadsheet ..... **Error! Bookmark not defined.**
GENERAL REFERENCES 563

Figures

Figure 1. Structural condition of the culvert 2
Figure 2. Research methodology. 12
Figure 3. Macro-fibers used in concrete linings: (a) polypropylene fibers, (b) fiberglass, (c) polyolefin fibers, and (d) steel fibers. 13
Figure 4. Micro-fibers used in concrete linings: (a) acrylic fiber, (b) alkali resistant (AR) glass fiber, (c) PVA fiber, and (d) alkali resistant glass scrim..... 14
Figure 5. Two common SAPL installation methods: (a) following and (b) filling the corrugation pattern..... 14
Figure 6. (a) and (b) Field data collections of SAPL installations..... 16
Figure 7. Design Equation Development Methodology..... 16
Figure 8. Finite element modeling of the soil box testing. 17
Figure 9. The CMPs' burial configuration (control test set): (a) plan view, (b) profile view of the aligned CMPs in the soil box, and(c) cross sectional view of both circular and CMP arch samples. 19
Figure 1-1. Survey respondents from U.S. 39
Figure 1-2. Survey respondents from Canadian Transportation Agencies. 40
Figure 1-3. Decision making priorities for using SAPL in RCP culverts, ... 41
Figure 1-4. Decision making priorities for using SAPL in CMP culverts, ... 42
Figure 1-5. Reasons for selecting structural SAPL for RCP culverts, ... 43
Figure 1-6. Reasons for selecting structural SAPL for CMP culverts 44
Figure 1-7. Factors influencing circular CMP, ... 46
Figure 1-8. Factors influencing pipe arch CMP, ... 47
Figure 1-9. Factors influencing circular RCP..... 48
Figure 1-10. Factors influencing pipe arch RCP. 49
Figure 1-11. Percentage of existing culverts, (15 Respondents)..... 50
Figure 1-12. Permitted reinforcement material, (10 Respondents). 51
Figure 1-13. Required adhesion in cementitious materials, (15 Respondents). 51
Figure 1-14. Required adhesion in polymeric materials, (14 Respondents). 52
Figure 1-15. Minimum thickness requirement in cementitious material, (11 Respondents). 52
Figure 1-16: Minimum thickness requirement in polymeric material, (9 Respondents). 52
Figure 1-17. Prohibited weather conditions, (9 Respondents). 53
Figure 1-18. Expected design life, (17 Respondents)..... 55
Figure 2-1. American society of civil engineers' report card for America's infrastructure (2017). 76
Figure 2-2. Corrugated metal pipe culverts (CMPs): (a) multi-cell CMPs (Source: Contech), and (b) invert deteriorated CMP (Source: Metal Culverts Inc.). 77
Figure 2-3. Commonly used culvert shapes: (a) closed conduit culvert shapes, and (b) open-bottom culvert shapes (FHWA 2012). 78
Figure 2-4. Culvert materials (ODOT 2018). 79
Figure 2-5. Typical "inlet control" flow section for a partly full culvert (FHWA 2012). 80

Figure 2-6. Typical “outlet control” flow in both full flow (submerged) and partly full flow (unsubmerged) conditions (FHWA 2012)..... 81
Figure 2-7. Deflection of a circular flexible pipe (Najafi 2008)..... 82
Figure 2-8. Failure modes of flexible conduits: (a) wall crushing, (b) seam separation, (c) elastic local buckling, (d) inelastic (snap-through) buckling, and(e) plastic yielding (excessive deflection) (Leonards and Stetkar 1978). 83
Figure 2-9. Active pressure distribution around circular conduit..... 86
Figure 2-10. Bresse Model for calculating the critical buckling pressure of a thin unconstraint circular ring under external hydrostatic pressure. 87
Figure 2-11. Rigid pipes under vertical loading: (a) rigid pipe stress zones (Hydraulics Manual M 23-03.06 2019), and (b) finite element modeling of a rigid reinforced concrete pipe (RCP) (Darabnoush Tehrani 2016). 88
Figure 2-12. Types of corrugated metal pipes (CMPs): (a) helical, (b) annular and (c) spiral rib CMPs..... 89
Figure 2-13. Common Defects of Culverts: (a) invert corrosion, (b) invert abrasion, (c) joint separation, (d) crack, (e) joint infiltration, (f) spalling in concrete culverts, (g) wall damages in plastic culverts, (h) piping beneath a culvert and (i) outlet scour (Piratla et al. 2017). 91
Figure 2-14.Trenchless renewal solutions. 93
Figure 2-15. Segmental sliplining method (Source: Hobas Pipe USA). 94
Figure 2-16. CIPP method installation process (Source: Insituform Technologies)..... 95
Figure 2-17. Pipe bursting method (Source: google images). 96
Figure 2-18. Three main variations of ThP process (Najafi and Gokhale 2005)..... 97
Figure 2-19. Corrugated metal pipe culverts (CMPs) before and after SAPL rehabilitation: (a) cementitious SAPL installation using spin casting machine (Source: CentriPipe) and (b) polymeric SAPL installation with hand spray (Source: Sprayroq). 98
Figure 2-20. A sample of SAPL renewed twin culvert, North Carolina. 99
Figure 2-21. Significant increase in renewed CRP structural capacity (Entezarmahdi, 2015).....102
Figure 2-22. Performance comparison of polyurea, polyurea hybrid, polyurethane and epoxy coatings applied on steel substrate (Adapted from Cain 2016). 104
Figure 2-23. CMP renewal using SprayWall® polyurethane SAPL, Norristown, PA: (a) before renewal, and (b) CMP renewal during SAPL application, 2007 (Sprayroq Inc.). 106
Figure 2-24. Comparison of spray-on lining methods using material property testing: (a) long-term flexural testing, (b) long-term creep tensile testing and (c) hydrostatic test setup (Motlagh et al. 2013). 107
Figure 2-25. Dead-load testing of reinforced concrete pipes (RCPs) renewed with polymeric SAPLs: (a) tested concrete rings covered by polyurea coating, (b) spraying polyurea coating system on concrete ring, and (c) D-load testing frame (Szafran and Matusiak 2017). 108
Figure 2-26. The structural behavior and performance of a fast-setting polyurea–urethane (PUU) SAPL as a structural lining material for rehabilitating water pipes (Ha et al. 2016). 109
Figure 2-27. Axial forces, T (left) and bending moments, M (right) at the CMP crown (Davidson et al. 2008).....112

Figure 2-28. Soil box laboratory testing of corrugated metal pipes: (a) single axle loading configuration, and (b) schematic tandem axle loading configuration (Garcia and Moore 2015). 114
Figure 2-29. Comparison of longitudinal strain at peak of corrugation 116
Figure 2-30. Comparison of longitudinal strain at valley of corrugation 116
Figure 2-31. Culvert loading positions in the field (Masada et al. 2017). 117
Figure 2-32. Field testing of a shallow cover severely deteriorated arch CMP (Sargand et al. 2018). 118
Figure 2-33. Cross section of culvert position and load applied 119
Figure 3-1. Bridging behavior of fiber reinforcements to limit the cracks, ... 128
Figure 3-2. FEM analysis of an RCP under TBT setup: inner sides of crown (0^0) and invert (180^0) are in tension and need to be reinforced (Darabnoush Tehrani 2016). 129
Figure 3-3. Macro fibers used in concrete lining; (a) polypropylene fibers, (b) fiberglass, (c) polyolefin fibers and (d) steel fibers. 130
Figure 3-4. (a) Acrylic fiber, (b) alkali resistant (ar) glass fiber, (c) PVA fiber, and (d) alkali resistant glass scrim (Source: http://www.buddyrhodes.com). 131
Figure 3-5. Types of Mesh. (a) Hexagonal Iron Mesh, (b) Woven PP, (c) Woven Nylon 66, (d) Expanded Metal Mesh. 135
Figure 3-6. (a) Basalt Mesh Grid with 10 mm by 10 mm Opening, (b) Basalt Mesh Placed into Wet Concrete Prior to Final Layer's Placement. 136
Figure 4-1. The Upper section of the concrete lining was made by spinning the pipe, ... 141
Figure 4-2. CMP profiles in North America, (Source: PCPIPE, Website: http://www.pcpipe.com). 142
Figure 4-3. 2⅔×½-in. CMP profile lined with an SAPL. 144
Figure 4-4. 3×1-in. CMP profile lined with SAPL. 145
Figure 4-5. Linings in a 6×2-in. corrugation profile CMP: (a) not filling the corrugations and (b) filling the corrugations. 147
Figure 4-6. Cementitious SAPL thickness versus cracking moment. 148
Figure 5-1. Location of the data points throughout the US map. 154
Figure 5-2. Frequency of data in each state DOT. 158
Figure 5-3. (a) Frequency of letting year (descending order), and (b) frequency of letting year based on the individual state contribution. 160
Figure 5-4. (a) Frequency of trenchless methods (descending order), and (b) frequency of trenchless method in each year. 161
Figure 5-5. Frequency of pipe diameters. 162
Figure 5-6. Frequency of pipe lengths. 163
Figure 5-7. Frequency of renewal thicknesses (descending order). 164
Figure 5-8. Frequency of unit cost in 2019 dollars. 165
Figure 5-9. Scatter boxplot of unit cost and pipe diameter. 166
Figure 5-10. Scatter Boxplot of unit cost and location. 167
Figure 5-11. Mean unit cost in 2019 dollars based on the location. 168
Figure 5-12. Mean construction costs comparison of SAPL, CIPP, and Sliplining in 2019 dollars. 170
Figure 5-13. Environmental costs comparison of SAPL, CIPP, and Sliplining in 2019 dollars (Serajiantehrani, 2020). 172

Figure 5-14. Environmental and construction costs composite comparison of SAPL, CIPP, and Sliplining in 2019 dollars. 173
Figure 5-15. Environmental and construction costs proportioning comparison of SAPL, CIPP and sliplining for diameter of 30 in. to 54 in. 174
Figure 5-16. Environmental and construction costs proportioning comparison of SAPL, CIPP and sliplining for diameter of 60 in. to 84 in. 175
Figure 5-17. Environmental and construction costs proportioning comparison of SAPL, CIPP, and sliplining for diameter of 90 in. to 108 in. 176
Figure 6-1. Partially and fully deteriorated pipe terminologies according to the ASTM F1216 (2016). 197
Figure 6-2. Restrained (non-linear) theory, Glock (1977). 198
Figure 6-3. Buckling Mode, Thépot (2000). 202
Figure 6-4. Buckling strength reduction for fractured sewer with close fitting liner (Source: Moore, 2008). 207
Figure 6-5. Bending limit state (Moore, 2008). 208
Figure 7-1. Geographical distribution of selected SAPL culverts. 212
Figure 7-2. Issues found with SAPLs. 216
Figure 7-3. SAPL measured thicknesses versus 2 in. design thickness, ... 220
Figure 7-4. SAPL average installed thicknesses versus 1.5 in. design thickness 221
Figure 7-5. Conditions assessment of SAPLs, (a) SAPL original condition given as percent of liner condition, (b) SAPLs structural condition given as percent of liner structural condition. 229
Figure 7-6. Correlation of Age, H/R, Thickness and AOR of SAPLs, (a) A, H/R and AOR (b) A, T and (AOR), (C) H/R, T and AOR. 231
Figure 8-1 Diagram for coefficient Ct (Figure 9-13 in ASCE MOP 60). 259
Figure 8-2 Dead loads acting on pipe. 261
Figure 8-3 Typical corrugation profile showing tangent angle. 265
Figure 8-4 Cross-section on 1.0-inch-thick liner in soil box testing. 265
Figure 8-5 Key Dimensions of 47"x71" Pipe-arch 272
Figure 8-6 Pipe arch shape showing bottom arc angle 281
Figure 10-1. FE model of the soil-pipe-liner system. 315
Figure 10-2. Soil model in FE with 2.4 in. mesh size. 318
Figure 10-3. CMP model in FE. 318
Figure 10-4. 1 in. liner model in FE. 319
Figure 10-5. Load displacement plot for the soil (Chimauriya, 2019). 320
Figure 10-6. Mesh size distribution in the soil. 320
Figure 10-7. Load displacement plot for the pipe at the crown. 321
Figure 10-8. Von Mises Stress in the pipe. 321
Figure 10-9. Plastic strain due to the soil failure in the loaded area at 5-inch settlement. 323
Figure 10-10. Progression of plastic strain under the load pad in soil ((a) at 1 in. settlement, (b) at 4 in. settlement (c) at 5 in. settlement 323
Figure 10-11. Plastic strain and deflection pattern in CMP (a) Experimental Result (b), (c) and (d)FEM Result (scaled up by 5 times). 324
Figure 10-12. Load displacement curve for soil at 5 in. displacement of soil of intact CMP. 325

Figure 10-13. Load displacement curve for the crown at 5 in. displacement of the soil of intact CMP. 325
Figure 10-14 Earth pressure distribution just above the crown of the pipe of the intact pipe. 326
Figure 10-15. Plastic strain and the deformation of the pipe loaded under the 20x40 in2 load pad. 327
Figure 10-16. Effect of load pad size on the load-displacement at the crown. 328
Figure 10-17. Effect of load pad size on the load- soil settlement under the load. .. 328
Figure 10-18. Earth pressure comparison for the bigger and smaller load pad conditions. 329
Figure 10-19. (a) Reduction in the invert gap from FEM (b) Experimental recording of the reduction in invert gap by Digital Image Processing (Darabnoush Tehrani, et al., 2020) (c) Vertical diameter change from FEM after invert removal. 330
Figure 10-20. Complete closure of the invert after loading (a), (c) from FEM (b) closure of invert seen in the Experiment (d) plastic strain at the spring line area. .. 331
Figure 10-21. (a) 1st plastic strain in the CMP (b) 1st crack in the model for 0.25 in. thick polymeric SAPL 333
Figure 10-22. (a) Plastic strain at the ultimate load in the FE model (b) Crack in the model at the end of the test for 0.25 in. thick polymeric SAPL 334
Figure 10-23. (a) Deformation of CMP at the time of the 1st plastic strain, and (b) Deformation of CMP at the ultimate load condition for 0.25 in. thick polymeric SAPL 334
Figure 10-24. Stress distribution in the pipe at the ultimate load conditions for 0.25 in. thick polymeric SAPL 334
Figure 10-25. Comparison of the liner displacement at crown for 0.25 in. thick polymeric SAPL between experiment and FEM results. 335
Figure 10-26. Comparison of the earth pressure at crown plotted against the liner displacement for 0.25 in thick polymeric SAPL 336
Figure 10-27. Comparison of the earth pressure at crown plotted against the applied load for 0.25 in. thick polymeric SAPL..... 337
Figure 10-28. Crack in the CMP (Left) Plastic strain in the crown from FE model (Right) of the CMP at the ultimate load conditions for 0.5 in. thick polymeric SAPL. 337
Figure 10-29. Plastic strain in the inside and outside the liner for 1 in. thick polymeric SAPL..... 338
Figure 10-30. (a) Development of plastic strain in the inside polymeric liner for 0.75 in. thickness, and (b) Deformation pattern of the polymeric liner..... 340
Figure 10-31. (a) Ultimate von Mises stress distribution around the liner, and (b) Deformation pattern for 1.5- in. thick polymeric SAPL 341
Figure 10-32. (a) Development of plastic strain (b) Deformation pattern for 2- in. thick polymeric SAPL..... 343
Figure 10-33. (a) Development of plastic strain (b) Deformation pattern for 0.25-in thick polymeric SAPL with filled corrugation. 343
Figure 10-34. Load displacement plot for the liner displacement at crown and settlement of soil from FE analysis for 0.25-in. thick (filled over the crest) polymeric SAPL..... 344

Figure 10-35. Load displacement plot from FE analysis for 0.25-in. thick (over the crest) polymeric SAPL. 345
Figure 10-36. Comparison of the load-displacement plot at the crown obtained from all the FE results. 346
Figure 10-37. (a) Bending of the arch CMP along the crown after complete loading (b) Vertical diameter change from FEM after complete loading. 348
Figure 10-38. Deformation of the invert cut arch CMP from the FE model. 349
Figure 10-39. (a) Vertical diameter change from FEM after complete loading, and (b) ultimate Mises stress in around the arch CMP. 350
Figure 10-40. Load displacement plot for intact arch CMP. 350
Figure 10-41. (a) Deformation of arch CMP at 1st plastic strain in the 0.25-in. thick arch liner, and (b) 1st plastic strain in 0.25-in. thick polymeric SAPL. 351
Figure 10-42. Deformation of the CMP at ultimate load condition for 0.25-in thick polymeric SAPL. 351
Figure 10-43. Stress Distribution (a) Soil (b) in the SAPL at the ultimate load conditions for 0.25 in. thick arch polymeric SAPL. 352
Figure 10-44. Comparison of the liner displacement at crown and soil settlement for 0.25 in. thick arch polymeric SAPL between Experiment and FEM results. 352
Figure 10-45. Comparison of the earth pressure at crown plotted against the soil displacement for 0.25 in thick arch polymeric SAPL 353
Figure 10-46. Comparison of the earth pressure at crown plotted against the applied load for 0.25 in. thick arch polymeric SAPL 354
Figure 10-47. First plastic strain from FE model for 0.5 in. thick arch polymeric SAPL. 354
Figure 10-48.1st plastic strain in the liner for 1 in. thick arch polymeric SAPL 355
Figure 10-49. Development of the plastic strain in 1-in. thick arch polymeric SAPL along with the crown. 356
Figure 10-50 1 in. thick polymeric SAPL liner showing the restriction of the vertical movement at two ends 357
Figure 10-51 Load displacement curve comparison between FEM and Experiment for 1-in. thick SAPL with the boundary conditions at the end 358
Figure 10-52 Load displacement curve comparison between FEM and Experiment for 0.5-in. thick polymeric SAPL with the boundary conditions at the end 358
Figure 10-53 Load displacement curve comparison between FEM and Experiment for 0.5-in. thick polymeric SAPL with the boundary conditions at the end 359
Figure 10-54. (a) Development of plastic strain in the inside liner for 0.75 in. thick arch liner (b) Deformation pattern of 0.75-in. thick arch polymeric SAPL. 360
Figure 10-55. (a) Development of plastic strain in the inside liner for 1.5 in. thick arch SAPL, and (b) Deformation pattern for 1.5- in. thick arch polymeric liner. 361
Figure 10-56. (a) Development of mises stress, and (b) Deformation pattern for 2- in. thick arch polymeric SAPL. 362
Figure 10-57. Load displacement curve for 0.25-in. thick polymeric SAPL (filled corrugations). 363
Figure 10-58. Comparison of the performance of 0.25-in. thick filled corrugated polymeric SAPL for arch with liner thickness following the corrugation. 363

Figure 10-59. Comparison of the load-displacement plot at the crown obtained from all the FE results for arch CMP lined with polymeric SAPL. 364
Figure D10-1. Load displacement plot for 60 in. invert-cut circular CMP with 3ft. cover and 0.25, 0.5, and 1 in. thick polymeric circular liner. 380
Figure D10-2. Earth pressure at 4 in. above the crown vs. crown displacement for 60 in. invert-cut circular CMP with 3ft. cover and 0.25, 0.5, and 1 in. polymeric circular thick liner. 381
Figure D10-3. Load displacement plot for 60 in. invert-cut circular CMP with 1 ft. cover and 0.25, 0.5, and 1 in. thick polymeric circular liner. 382
Figure D10-4. Earth pressure 4 in. above the crown vs. crown displacement for 60 in. invert-cut circular CMP with 1 ft. cover and 0.25, 0.5, and 1 in. polymeric circular thick liner. 383
Figure E10-5. Load displacement plot for 48 in. invert-cut circular CMPs with 3 ft. cover and 0.25, 0.5, and 1 in. thick polymeric liner. 390
Figure E10-6. Earth pressure at 4 in. above the crown vs. crown displacement for 48 in. invert-cut circular CMPs with 3 ft. cover and 0.25, 0.5, and 1 in. thick polymeric liner. 390
Figure E10-7. Load displacement plot for Invert-cut Circular 48 in. CMPs with 2 ft. cover and 0.25, 0.5, and 1 in. thick polymeric liner. 391
Figure E10-8. Earth pressure at 4 in. above the crown vs. crown displacement for Invert-cut Circular 48 in. CMPs with 2 ft. cover and 0.25, 0.5, and 1 in. thick polymeric liner. 392
Figure E10-9. Load displacement plot for Invert-cut circular 48 in. CMPs with 1 ft. cover and 0.25, 0.5, and 1 in. thick polymeric liner. 392
Figure E10-10. Earth pressure at 4 in. above the crown vs. crown displacement for Invert-cut circular 48 in. CMPs with 1 ft. cover and 0.25, 0.5, and 1 in. thick polymeric liner. 393
Figure E10-11. Load displacement plot for invert-cut circular 36 in. CMPs with 3 ft. cover and 0.25, 0.5, and 1 in. thick polymeric liner. 394
Figure E10-12. Earth pressure at 4 in. above the crown vs. crown displacement for Invert-cut circular 36 in. CMPs with 3 ft. cover and 0.25, 0.5, and 1 in. thick polymeric liner. 395
Figure E10-13. Load displacement plot for invert-cut circular 36 in. CMPs with 2 ft. cover and 0.25, 0.5, and 1 in. thick polymeric liner. 396
Figure E10-14 Earth pressure at 4 in. above the crown vs. crown displacement for invert-cut circular 36 in. CMPs with 2 ft. cover and 0.25, 0.5, and 1 in. thick polymeric liner. 396
Figure E10-15. Load displacement plot for invert-cut circular 36 in. CMPs with 1 ft. cover and 0.25, 0.5, and 1 in. thick polymeric liner. 397
Figure E10-16. Earth pressure 4 in. above the crown vs. crown displacement for invert-cut circular 36 in. CMPs with 1 ft. cover and 0.25, 0.5, and 1 in. thick polymeric liner. 397
Figure 11-1. CUIRE laboratory at the University of Texas at Arlington. 406
Figure 11-2. Soil box details. 406
Figure 11-3. Soil box configuration for three CMP samples divided by wooden partition walls. 405

Figure 11-4. Initial schematic design of the wooden partition wall. 409
Figure 11-5. Soil box ventilation..... 409
Figure 11-6. Foundation compaction: (a) schematic illustration of soil compaction, (b) soil compaction using a 4,496 lbs vibratory plate compactor. 410
Figure 11-7. Embedment soil characteristics: a) soil sieve analysis, and b) standard Proctor test. 411
Figure 11-8. The CMPs' burial configuration (control test set): (a) plan view, (b) profile view of the aligned CMPs in the soil box, and(c) cross sectional view of both circular and CMP arch samples. 412
Figure 11-9. The CMPs' burial configuration (SAPL renewed testing): (a) plan view, (b) profile view of the aligned CMPs in the soil-box, and (c) cross sectional view of the circular CMP. 413
Figure 11-10. The CMP arch samples' burial configuration (SAPL renewed testing): (a) plan view, (b) profile view of the aligned CMP arch samples in the soil-box, and (c) cross sectional view of the CMP arch. 414
Figure 11-11. Nuclear density measurement. 415
Figure 11-12. Compaction Curve for a Granular Soil (Drnevich, Evans, & Prochaska, July 2007). 416
Figure 11-13. Modes of operation of nuclear density gauge (MULTIQUIP, 2018). 417
Figure 11-14. Measurement of soil moisture content using TDR method (Siddiqui & Drnevich, 1995). 418
Figure 11-15. Intact and invert-cut CMP samples. 421
Figure 11-16. Detachable invert section for control test. 421
Figure 11-17. Detachable invert mechanism (in four stages) for SAPL renewed CMP samples before and during the SAPL installation. 422
Figure 11-18. Pipe installation and preparation before backfilling. 423
Figure 11-19. Steel load pads. 423
Figure 11-20. Strain gauges configuration and details: (a) schematic profile view at the crown of the bare circular CMP, (b) schematic profile view at the crown of Polymeric SAPL renewed circular CMP, schematic profile view of the cementitious SAPL renewed pipe samples (d) physical protection of outer surface strain gauges, and (r) installed strain gauges on the inner surface of the SAPL renewed circular CMP. . 426
Figure 11-21. Strain gauges connected to a data acquisition system (DAQ). 427
Figure 11-22. Earth pressure cell. (a) Geokon 4800 series, (b) 4 in. distance from the CMP at the springline, and (c) connection to a data acquisition system (DAQ). 427
Figure 11-23. LVDTs and cable displacement sensors. 428
Figure 11-24. LVDT and CDS DAQ, and alternating current (AC) to direct current (DC) convertor (from left to right). 428
Figure 11-25. Pipe monitoring: (a) cameras used for capturing changes, and (b) DIC targets for pipe profiling. 429
Figure 11-26. Instrumentation: LVDTs, CDSs, DIC targets and cameras inside the pipe sample. 430
Figure 11-27. Instrumentation: (top) LVDTs, CDSs, DIC targets and cameras inside the pipe sample, (bottom) data acquisition systems. 430

Figure 11-28. SAPL thickness measurement: (a) thickness gauge and calibration sample, (b) longitudinal measured locations, (c) circular CMP circumferential measured locations, and (d) CMP arch circumferential measured locations. 431
Figure 11-29. CMP surface preparation for SAPL installation: (a) dirt and dust on the CMP, and (b) CMP after power wash without any dirt and dust. 432
Figure 11-30. SAPL installation of invert-cut circular CMPs: (a) before SAPL installation (stage 2), (b) after SAPL installation (stage 3), and (c) end strips detachment (stage 4 of). 433
Figure 11-31. CMP arch preparation for SAPL installation: (a) CMP arch before gap sealing, (b) the invert-cut gap sealing with Styrofoam and plastic sheets, (c) Sprayroq's vendor working inside the CMP arch samples, (d) the prepared pipe prior to the SAPL installation, and (e) the SAPL renewed CMP arch samples. 433
Figure 11-32. Hand spray SAPL installation. 434
Figure 11-33. SAPL sampling for circular CMPs test setup: (a) sample plates prior to the cut into required shape for flexural and tensile test, and (b) the sampling site with Sprayroq installation truck. 435
Figure 11-34. Plate sampling from the SAPL batch to provide material test samples for CMP arch test setup. 435
Figure 11-35. End-strip detachment: (a) end-strip preparation, (b) end-strip before SAPL installation, end-strip detachment after SAPL installation. 436
Figure 11-36. Cementitious SAPL installation on: (a) CMP arch and (b) circular CMPs. 437
Figure 11-37. Thickness measurement using a depth gauge at the time of SAPL installation. 438
Figure 11-38. Mechanical properties testing samples: (a) compressive testing cylinders molds, (b) mold preparation, and (c) sample storage at a curing room. 440
Figure 11-39. SAPL thickness measurement: (a) measurements in circumferential direction on circular and, (b) pipe arch SAPL samples, (c) measurements in longitudinal direction on circular and, (d) pipe arch SAPL samples. 441
Figure 11-40. CMP movement due to the invert detachment (without any end strips) before loading. 442
Figure 11-41. 60 in. invert-cut circular bare CMP, pipe profiling using DIC technique. 443
Figure 11-42. Control test - applied load through the steel load pad versus soil settlement. 444
Figure 11-43. Control test - pressure on the soil surface under the load pad versus soil settlement. 444
Figure 11-44. Control test - pressure on top of the CMP samples vs soil settlement. 445
Figure 11-45. Results of DIC measurement for 60 in. intact circular CMP: (a) before loading, and (b) after loading at the end of the test. 446
Figure 11-46. Circular CMP movement due to the invert detachment: (a) the movement mechanism, and (b) The gap closure at the cut location due to vertical loading. 447
Figure 11-47. 60 in. Invert-cut circular CMP soil box testing: (a) before loading, and (b) after loading. 448

Figure 11-48. Results of DIC measurement at the end of the test (60 in. invert-cut circular CMP). 448
Figure 11-49. CMP arch movement due to the invert detachment: (a) the movement mechanism, and (b) the uplift of the invert-cut CMP arch after loading and soil compaction under the haunch area after exhuming the CMP. 449
Figure 11-50. 47×71 in. invert-cut CMP arch soil box testing: (a) before loading, and (b) the local buckling failure of the pipe sample after loading. 450
Figure 11-51. Results of DIC measurement at the end of the test (47×71 in. invert-cut CMP arch). 451
Figure 11-52. Load versus displacement of CMPs at different locations for the control test: (a) intact 60 in. circular CMP under a 10×20 in. steel load pad, (b) invert-cut 60 in. circular CMP under a 20×40 in. steel load pad, and (c) invert-cut 47×71 in. CMP arch under a 20×40 in. steel load pad. 452
Figure 11-53. Results of earth pressure cells for the CMP control test: (a) intact circular CMP, (b) invert-cut circular CMP, and (c) invert-cut CMP arch. 454
Figure 11-54. Results of strain gauges for the CMP control test: (a) intact circular CMP, (b) invert-cut circular CMP, and (c) invert-cut CMP arch. 457
Figure 11-55. Internal forces on intact, invert-cut circular and invert-cut CMP arch samples: (a) bending moment, and (b) thrust forces for the invert-cut arch, invert-cut circular and circular intact CMPs. 458
Figure 11-56. Pipe profiling using DIC results before loading and after loading at the ultimate load carrying capacity of the samples: (a) intact CMP, (b) invert-cut circular CMP, and (c) invert-cut CMP arch. 459
Figure 11-57. Polymeric SAPL material property test results: (a) flexural test (ASTM D790), and (b) tensile test (ASTM D638). 461
Figure 11-58. Thickness measurement results of polymeric SAPL renewed circular CMPs: (a) 0.25 in. thick SAPL, (b) 0.5 in. thick SAPL, (c) 1 in. thick SAPL, and (d) measured locations in circumferential and longitudinal direction. 463
Figure 11-59. Load vs. displacement results for CMP samples and soil: (a) bare invert cut CMP, (b) 0.25 in. SAPL renewed CMP, (c) 0.5 in. SAPL renewed CMP and (d) 1 in. SAPL renewed CMP. 466
Figure 11-60. Formation of the first structural crack. It shows (a) 0.25 in. SAPL renewed circular CMP at 39 kips, (b) 0.5 in. SAPL renewed circular CMP at 42.78 kips, and (c) 1 in. SAPL renewed circular CMP at 66.26 kips. 467
Figure 11-61. Load improvement by SAPL application: (a) ultimate load comparison of renewed SAPL circular CMPs with bare CMP, and (b) load comparison of renewed SAPL CMPs with bare CMP at 2 in. pipe deflection. 468
Figure 11-62. Earth pressure cells' results: (a) bare circular CMP, (b) 0.25 in. SAPL renewed circular CMP (c) 0.5 in. SAPL renewed circular CMP and (d) 1 in. SAPL renewed circular CMP. 470
Figure 11-63. Strain gauge results for SAPL renewed circular CMP: (a) at the crown and (b) around the SAPL at the time of first structural crack. 471
Figure 11-64. DIC results of SAPL renewed circular CMP: (a) and (b) bare CMP, (c) and (d) 0.25 in. SAPL renewed CMP, (e) and (f) 0.5 in. SAPL renewed CMP, (g) and (h) 1 in. SAPL renewed CMP. 473

Figure 11-65. Pipe profiling using DIC technique at the time of failure: (a) 0.25 in. SAPL, (b) 0.5 in. SAPL, and (c) 1.0 in. SAPL renewed circular CMP. 474
Figure 11-66. Thickness measurement results of polymeric SAPL renewed CMPAs: (a) quarter, (b) half, (c) one inch SAPL renewed CMP arch samples, and (d) measured locations in circumferential direction. 477
Figure 11-67. Invert-cut CMP arch end-strip detachment to remove the host pipe's ring stiffness: (a) over-sprayed SAPL and cutting process on the end-strip location, and (b) unbolted end-strip. 478
Figure 11-68. Bare and SAL renewed CMP arch samples Load-Displacement graphs: (a) invert-cut bare CMP arch, (b) 0.25 in. SAPL renewed CMP arch, (c) 0.5 in. SAPL renewed CMP arch, and (d) 1 in. SAPL renewed CMP arch. 481
Figure 11-69. Formation of the first structural crack: (a) 0.25 in. SAPL renewed CMP arch at 29.32 kips, (b) 0.5 in. SAPL renewed CMP arch at 26.27 kips, and (c) 1 in. SAPL renewed CMP arch at 41.08 kips. 482
Figure 11-70. Fully Invert deteriorated CMP arch samples ultimate load carrying capacity improvement through SAPL application. 482
Figure 11-71. Pressure vs. crown displacement graphs: (a) invert-cut bare CMP arch, (b) 0.25 in. SAPL renewed CMP arch, (c) 0.5 in. SAPL renewed CMP arch, and (d) 1 in. SAPL renewed CMP arch. 484
Figure 11-72. CMP arch behavior due to the vertical load, where the red boxes show the soil support under the pipe on the west haunch area and the blue boxes illustrates the pipe upward movement. 485
Figure 11-73. Strain gauge results: (a) invert-cut bare CMP arch, (b) 0.25 in. SAPL renewed CMP arch, (c) 0.5 in. SAPL renewed CMP arch, and (d) 1 in. SAPL renewed CMP arch. 487
Figure 11-74. Pipe profiling using DIC results: (a) and (b) bare CMP arch, (c) and (d) 0.25 in. SAPL renewed CMP arch, (e) and (f) 0.5 in. SAPL renewed CMP arch, and (g) and (h) 1 in. SAPL renewed CMP arch. 489
Figure 11-75. Pipe profiling using DIC technique at the time of failure: (a) 0.25 in. SAPL, (b) 0.5 in. SAPL, and (c) 1.0 in. SAPL renewed CMP arch samples. 490
Figure 11-76. CMP arch behavior due to the vertical load, where the red boxes show the soil support under the pipe on the west haunch area and the blue boxes illustrates the pipe upward movement. 493
Figure 11-77. Invert-cut CMP arch renewed with 3 in. cementitious SAPL: (a) before loading, (b) after loading, (c) after unloading, and (d) delamination in the West springline 494
Figure 11-78. Invert-cut CMP arch renewed with 3-in. thick cementitious SAPL subjected to static live load: (top) load-time and (bottom) load-soil displacement graphs. 495
Figure 11-79. Earth pressure cell results for the 3-in. thick SAPL renewed invert-cut CMP arch with respect to: (top) time, and (bottom) crown displacement. 496
Figure 11-80. Mechanical sensors result for 3-in. thick SAPL renewed invert-cut CMP arch. 497
Figure 11-81. Strain gauges reading for the 3-in. thick SAPL renewed invert-cut CMP arch. 497

Figure 11-82. Pipe profiling using DIC for the 3-in. thick SAPL renewed invert-cut CMP arch. 498
Figure 11-83. Load vs. displacement of the soil surface, crown, springline, and shoulder of the 3-in. thick SAPL renewed invert-cut CMP arch due to the applied static load. 499
Figure 11-84. Load vs. pressure for the 3-in. thick SAPL renewed invert-cut CMP arch. 499
Figure 11-85. Thickness measurement for the 3-in. thick cementitious SAPL renewed CMP arch. 500
Figure 11-86. Invert-cut CMP arch renewed with 2 in. cementitious SAPL: (a) before loading, and (b) after loading. 501
Figure 11-87. Invert-cut CMP arch renewed with 2-in. thick cementitious SAPL subjected to static live load: (top) load-time and (bottom) load-soil displacement graphs. 502
Figure 11-88. Earth pressure cell results for the 2-in. thick SAPL renewed invert-cut CMP arch with respect to: (top) time, and (bottom) crown displacement. 503
Figure 11-89. Mechanical sensors result for 2-in. thick SAPL renewed invert-cut CMP arch. 504
Figure 11-90. Strain gauges reading for 2-in. thick SAPL renewed invert-cut CMP arch. 504
Figure 11-91. Pipe profiling using DIC for the 2-in. thick SAPL renewed invert-cut CMP arch. 505
Figure 11-92. Load vs. displacement of the soil surface, crown, springline, and shoulder of the 2-in. thick SAPL renewed invert-cut CMP arch due to the applied static load. 506
Figure 11-93. Load vs. pressure for the 2-in. thick SAPL renewed invert-cut CMP arch. 506
Figure 11-94. Thickness measurement for the 2-in. thick cementitious SAPL renewed CMP arch. 507
Figure 11-95. Invert-cut CMP arch renewed with 1 in. cementitious SAPL: (a) before loading, where the East haunch had a shrinkage crack and (b) after loading, where the shrinkage crack is closed. 508
Figure 11-96. Invert-cut CMP arch renewed with 1-in. thick cementitious SAPL subjected to static live load: (top) load-time, and (bottom) load-soil displacement graphs. 509
Figure 11-97. Earth pressure cell results for the 1-in. thick SAPL renewed invert-cut CMP arch with respect to: (top) time, and (bottom) crown displacement. 510
Figure 11-98. Mechanical sensors result for 1-in. thick SAPL renewed invert-cut CMP arch. 511
Figure 11-99. Strain gauges reading for 1-in. thick SAPL renewed invert-cut CMP arch. 511
Figure 11-100. Pipe profiling using DIC for the 1-in. thick SAPL renewed invert-cut CMP arch. 512
Figure 11-101. Load vs. displacement of the soil surface, crown, springline, and shoulder of the 1-in. thick SAPL renewed invert-cut CMP arch due to the applied static load. 513

Figure 11-102. Load vs. pressure for the 1-in. thick SAPL renewed invert-cut CMP arch. 513
Figure 11-103. Thickness measurement for the 1-in. thick cementitious SAPL renewed CMP arch. 514
Figure 11-104. Load vs. soil settlement comparison graph. 515
Figure 11-105. Load vs. crown displacement comparison graph. 516
Figure 11-106. Load vs. springline displacement comparison graph. 516
Figure 11-107. Load vs. pressure comparison graph. 517
Figure 11-108. Compression and tension zones of a circular pipe subjected to a vertical load. 518
Figure 11-109. Invert-cut circular CMP renewed with 3 in. cementitious SAPL: (a) before loading, and (b) after loading. 519
Figure 11-110. Invert-cut circular CMP renewed with 3-in. thick cementitious SAPL subjected to static live load: (top) load-time, and (bottom) load-soil displacement graphs. 520
Figure 11-111. Earth pressure cell results for the 3-in. thick SAPL renewed invert-cut circular CMP with respect to: (top) time, and (bottom) crown displacement. 521
Figure 11-112. Mechanical sensors result for 3-in. thick SAPL renewed invert-cut circular CMP. 522
Figure 11-113. Strain gauge result for 3-in. thick SAPL renewed invert-cut circular CMP. 522
Figure 11-114. Pipe profiling using DIC for the 3-in. thick SAPL renewed invert-cut circular CMP. 523
Figure 11-115. Load vs. displacement of the soil surface, crown, springline, and shoulder of the 3-in. thick SAPL renewed invert-cut circular CMP due to the applied static load 524
Figure 11-116. Load vs. pressure for the 3-in. thick SAPL renewed invert-cut circular CMP. 524
Figure 11-117. Thickness measurement for the 3-in. thick cementitious SAPL renewed circular CMP. 525
Figure 11-118. Invert-cut circular CMP renewed with 2 in. cementitious SAPL: (a) before loading, and (b) after loading. 526
Figure 11-119. Invert-cut circular CMP renewed with 2-in. thick cementitious SAPL subjected to static live load: (top) load-time, and (bottom) load-soil displacement graphs. 527
Figure 11-120. Earth pressure cell results for the 2-in. thick SAPL renewed invert-cut circular CMP with respect to: (top) time, and (bottom) crown displacement. 528
Figure 11-121. Mechanical sensors result for 2-in. thick SAPL renewed invert-cut circular CMP. 529
Figure 11-122. Strain gauges result for 2-in. thick SAPL renewed invert-cut circular CMP. 529
Figure 11-123. Pipe profiling using DIC for the 2-in. thick SAPL renewed invert-cut circular CMP. 530
Figure 11-124. Load vs. displacement of the soil surface, crown, springline, and shoulder of the 2-in. thick SAPL renewed invert-cut circular CMP due to the applied static load 531

Figure 11-125. Load vs. pressure for the 2-in. thick SAPL renewed invert-cut circular CMP. 531
Figure 11-126. Thickness measurement for the 2-in. thick cementitious SAPL renewed circular CMP. 532
Figure 11-127. Invert-cut circular CMP renewed with 1 in. cementitious SAPL: (a) before loading, and (b) after loading. 533
Figure 11-128. Invert-cut circular CMP renewed with 1-in. thick cementitious SAPL subjected to static live load: (top) load-time, and (bottom) load-soil displacement graphs. 534
Figure 11-129. Earth pressure cell results for the 1-in. thick SAPL renewed invert-cut circular CMP with respect to: (top) time, and (bottom) crown displacement. 535
Figure 11-130. Mechanical sensors result for 1-in. thick SAPL renewed invert-cut circular CMP. 536
Figure 11-131. Strain gauges result for 1-in. thick SAPL renewed invert-cut circular CMP. 537
Figure 11-132. Pipe profiling using DIC for the 1-in. thick SAPL renewed invert-cut circular CMP. 538
Figure 11-133. Load vs. displacement of the soil surface, crown, springline, and shoulder of the 1-in. thick SAPL renewed invert-cut circular CMP due to the applied static load. 539
Figure 11-134. Load vs. pressure for the 1-in. thick SAPL renewed invert-cut circular CMP. 539
Figure 11-135. Thickness measurement for the 1-in. thick cementitious SAPL renewed circular CMP. 540
Figure 11-136. Load vs. crown displacement comparison graph. 542
Figure 11-137. Load vs. springline displacement comparison graph. 542
Figure 11-138. Load vs. soil surface settlement comparison graph. 543
Figure 11-139. Load vs. pressure comparison graph. 543
Figure 11-140. Cube samples taken from SAPL batch sprayed on circular CMPs. 545
Figure 11-141. Box plot for the 3 × 6-cylinder samples taken from SAPL batch sprayed on circular CMPs: (top) spray cast, (bottom) hand cast. 546
Figure 11-142. Box plot for the 4 × 8-cylinder samples taken from SAPL batch sprayed on circular CMPs: (top) spray cast, (bottom) hand cast. 547
Figure 11-143. Box plot for the 6 × 12-cylinder samples taken from SAPL batch sprayed on circular CMPs. 548
Figure 11-144. Bar chart results for: (a) 7 days, and (b) 28 days samples. 548

Tables

Table 1. Accomplished tasks for the SAPL research project. 5
Table 2. A summary of key literature search. 6
Table 1-1. Decision making priorities for using SAPL in RCP culverts with “1” highest priority, (17 Respondents)..... 40
Table 1-2. Decision making priorities for using SAPL in CMP culverts with “1” highest priority, (20 Respondents)..... 41
Table 1-3. Reasons for selecting a structural SAPL for RCP culverts with “1” highest priority, (17 Respondents)..... 43
Table 1-4. Reasons for selecting structural SAPL for CMP culverts with “1” highest priority, (13 Respondents)..... 43
Table 1-5. Reasons for a culvert to be identified as fully deteriorated with “1” highest priority. 44
Table 1-6. SAPL materials ranking (15 Respondents) with “1” highest priority. 50
Table 2-1. Common CMP corrugation profile in North America (PCPIPE 2016). 89
Table 2-2. Main characteristics of Sliplining methods (Najafi 2016). 93
Table 2-3 Main characteristics of Sliplining methods (Najafi 2016). 94
Table 2-4 Main characteristics of CIPP method (Najafi 2016). 95
Table 2-5 Main characteristics of in-line replacement method (Najafi 2016). 95
Table 3-1. Fiber reinforced concrete classification (According to ASTM C1116/C1116M 2015).....129
Table 3-2 Volume fraction of fibers (Ramakrishnan et al. 1998) 130
Table 3-3 Fibers classifications (FRCA 2015).....131
Table 4-1 CMP profiles and their respective size ranges.....142
Table 4-2 Coefficient of roughness of CMP structures (Source: AISI,1999).....143
Table 4-3. Pipe barrel hydraulics example.....144
Table 5-1 Scope of work. 153
Table 5-2. Dataset included features. 154
Table 5-3. Dataset parameters classification and value. 155
Table 5-4 Type of dataset parameters. 155
Table 5-5. Sample of the raw dataset. 156
Table 5-6 Sample of the final dataset. 157
Table 5-7. Trenchless SAPL, CIPP, and Sliplining mean unit cost in 7 locations.....169
Table 7-1 List of selected SAPL culverts for field inspection.....213
Table 7-2 SAPL and existing culvert defects. 215
Table 7-3 SAPL field inspection findings. 217
Table 7-4 SAPLs’ issues found for each culvert. 219
Table 7-5. Rating modifier values (Masada et al. 2007).....222
Table 7-6 Rating scale to evaluate general conditions of SAPLs. 223
Table 7-7 SAPLs overall average rating score (OAR) and adjusted overall structural rating score (AOR). 227
Table 7-8 Comparative Status of Cementitious and Geopolymer SAPLs, (According to OAR). 230
Table 7-9 Summary of findings and recommendations. 232
Table 7-10 Inspection plan. 233

Table 8-1 Recommended Safe Values of Cohesion 259
Table 8-2 Soil Box Pipe Deformation (in inches) (+ means outward and – means inward movement). 267
Table 8-3 Soil Box Hoop Strain Measurements, (+ means tension and – mean compression) 268
Table 8-4 Soil Box Hoop Stress Measurements (psi), (+ means tension and – mean compression) 269
Table 8-5 Soil Box Hoop Strain Measurements, ... 269
Table 8-6 Soil Box Hoop Stress Measurements (psi) 270
Table 8-A 1. Moment of inertia (3.0 in. cementitious SAPL – corrugation filled). 284
Table 8-A 2. Moment of inertia (2.0 in. cementitious SAPL – corrugation filled). 284
Table 8-A 3. Moment of inertia (1.0-in. cementitious SAPL – corrugation filled). 285
Table 8-A 4. Typical Moment of Inertia values for a corrugated profile to be considered for different SAPL Thicknesses 285
Table 10-1. Soil properties. 316
Table 10-2. Properties of steel. 316
Table 10-3. Properties of polymeric liner material used in FEM models. 317
Table 10-4. Run time for different mesh sizes. 319
Table 10-5. Comparison of the results from FEM and experiment 326
Table 10-6. Comparison of the results for the intact CMP for smaller and bigger load conditions. 328
Table 10-7. Comparison of the change in dimension of the pipe after the removal of the invert. 330
Table 10-8. Comparison of the load-displacement between FE model and the experimental results for 0.25-in. thick polymeric SAPL. 336
Table 10-9. Comparison of the load and displacement at the crack and ultimate load conditions for 0.5-in. thick polymeric SAPL 338
Table 10-10. Comparison of the load and displacement at crack and ultimate load conditions for 1-in. thick polymeric liner. 339
Table 10-11. Predicted crack and ultimate load and displacement 340
Table 10-12. Predicted crack and ultimate load for 1.5 in. thick polymeric SAPL 341
Table 10-13. Predicted crack and ultimate load for 2-in. thick polymeric SAPL 343
Table 10-14. Prediction of crack and ultimate load for 0.25-in. thick filled corrugated polymeric SAPL CMP. 344
Table 10-15. Comparison of the result for filling the corrugations and following the corrugations. 346
Table 10-16 Comparison of the reduction in diameter and the ultimate load obtained from FEM. 347
Table 10-17. Comparison of load and displacement for invert cut arch CMP 349
Table 10-18. Comparison of the load and displacement between the FE model and the experimental results for 0.25 in. thick arch polymeric SAPL. 353
Table 10-19. Comparison for the load-displacement plots from the FE model and test for 0.5 in. thick arch polymeric SAPL 355
Table 10-20. Comparison of the test and FE model results for 1 in. thick arch polymeric SAPL 356

Table 10-21. Crack and Ultimate load prediction for 0.75-in. thick arch polymeric SAPL. 360
Table 10-22. Crack and Ultimate load prediction for 1.5-in. thick arch polymeric SAPL. 361
Table 10-23. Crack and ultimate load prediction for 2-in. thick arch polymeric SAPL. 362
Table 10-24. Comparison of the reduction in the diameter and the ultimate load obtained from FEM for arch CMP lined with polymeric SAPL 365
Table D10-1: Comparison of applied load, displacement, and earth pressure at the first crack point and ultimate point for 60 in. invert-cut circular CMP with 3ft. cover 381
Table D10-2. Comparison of applied load, displacement, and earth pressure at the first crack point and ultimate point for 60 in. invert-cut circular CMP with 1 ft. cover and 0.25, 0.5, and 1 in. thick polymeric circular liner. 382
Table E10-3. Comparison of the applied load, displacement, and earth pressure at the first crack and ultimate load for 48 in. invert-cut circular CMP with 3 ft. cover and 0.25, 0.5, and 1 in. thick polymeric liner. 389
Table E10-4. Comparison of applied load, displacement, and earth pressure at the first crack and ultimate load for Invert-cut Circular 48 in. CMPs with 2 ft. cover and 0.25, 0.5, and 1 in. thick polymeric liner. 391
Table E10-5. Comparison of applied load, displacement, and earth pressure at the first crack and ultimate load for Invert-cut Circular 48 in. CMPs with 1 ft. cover and 0.25, 0.5, and 1 in. thick polymeric liner. 393
Table E-10-6. Comparison of applied load, displacement, and earth pressure at the first crack and ultimate load for invert-cut circular 36 in. CMPs with 3 ft. cover and 0.25, 0.5, and 1 in. thick polymeric liner. 394
Table E-10-7. Comparison of applied load, displacement, and earth pressure at the first crack point and ultimate load for invert-cut circular 36 in. CMPs with 2 ft. cover and 0.25, 0.5, and 1 in. thick polymeric liner. 395
Table E10-8. Comparison of applied load, displacement, and earth pressure at the first crack and ultimate load for invert-cut circular 36 in. CMPs with 1 ft. cover and 0.25, 0.5, and 1 in. thick polymeric liner. 398
Table 11-1. Soil box test setups at CUIRE laboratory at UTA 407
Table 11-2. Summary of materials and test options for the soil used in soil box test. 419
Table 11-3. CMP samples' geometric details (NCSPA 2008). 420
Table 11-4. Instrumentation used in the soil box testing. 424
Table 11-5. Compressive testing samples for CMP arches renewed 439
Table 11-6. Compressive testing samples for circular CMPs renewed with cementitious SAPL. 439
Table 11-7. Control test of bare CMPs - the ultimate load and pressure and the maximum displacement at the time of failure. 455
Table 11-8. The circular CMPs' load bearing capacity, crown deflection and the soil displacement at initial crack and failure. 467
Table 11-9. Soil pressure results around the circular CMPs at the time of failure. 469

Table 11-10. The circular CMPs' load bearing capacity, crown deflection and the soil displacement at initial crack and failure. 485
Table 11-11. Soil pressure results around the CMP arch samples..... 486
Table 11-12. CMP arch samples test results. 514
Table 11-13. Circular CMP test results. 541

Problem Statement

Culverts and drainage structures are an integral part of roadway assets that deteriorate overtime and require maintenance and renewal. Failure of these conduits is costly for DOTs both directly due to emergency cost of replacement of the failed conduit and indirectly due to social costs of traffic interruptions and inconvenience to commuters. Further challenges are the variety in host conduit material types, level of deterioration, shapes, embedment materials, types of roads, depth of cover from road surface, size (diameter), length, condition of substrate, accessibility, wide geospatial distribution, water table, and environmental exposures that makes every single culvert unique. There are several trenchless technology methods available to renew and replace these deteriorated culverts with different degrees of installation experiences, costs, advantages, limitations and applicability. These methods, as described in this report, include Cured-in-Place Pipe (CIPP), Sliplining (SL), Modified Sliplining (MSL), Pipe Bursting (PB), and Spray Applied Pipe Lining (SAPL). Among these methods, SAPLs provide more flexibility of installation, specifically for tight to reach areas, higher speed of mobilization and installation, and less social costs. While CIPP and sliplining have a long history of use and can be utilized for structural applications, dependent on the project conditions, they may decrease hydraulic capacity and may not be applicable due to limited access, size, shape and other features of host culvert, while SAPLs can be used in those conditions. In addition, SAPLs can improve or maintain hydraulic capacity of culverts and inhibit further deterioration and corrosion. However, currently there is not much history of SAPL use for structural application and there are no SAPL standard specifications and design guidelines.

The key factor in current design guidelines is whether an existing pipe is structurally sound enough to continue to carry the earth, live and hydrostatic loads imposed on it. It is well known that existing flexible pipes gain structural strength through the soil-structural interaction, thus making them a composite system. There are many documented instances of existing corrugated metal pipes with significant invert loss that continue to hold their shape due to the load carrying capacity of the surrounding soil. Figure 1 illustrates the structural condition of a CMP culvert in partially and fully deteriorated conditions.

The main objectives of this research were to address structural application of SAPLs and to develop design equations and performance specifications for both cementitious and resin-based materials for circular and non-circular (arch) shapes up to 120 in. diameter. The developed design equations considered loading conditions as detailed in the AASHTO's Load and Resistance Factor Design (LRFD) Bridge Design Specifications.

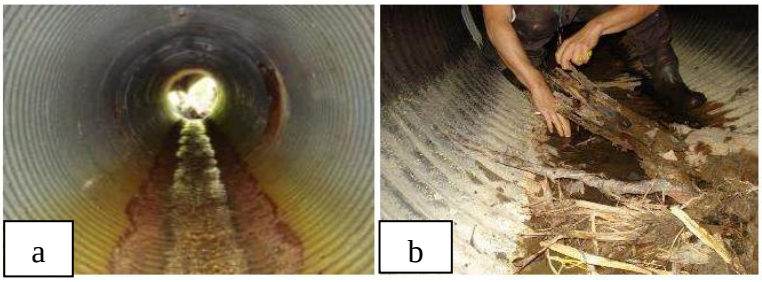
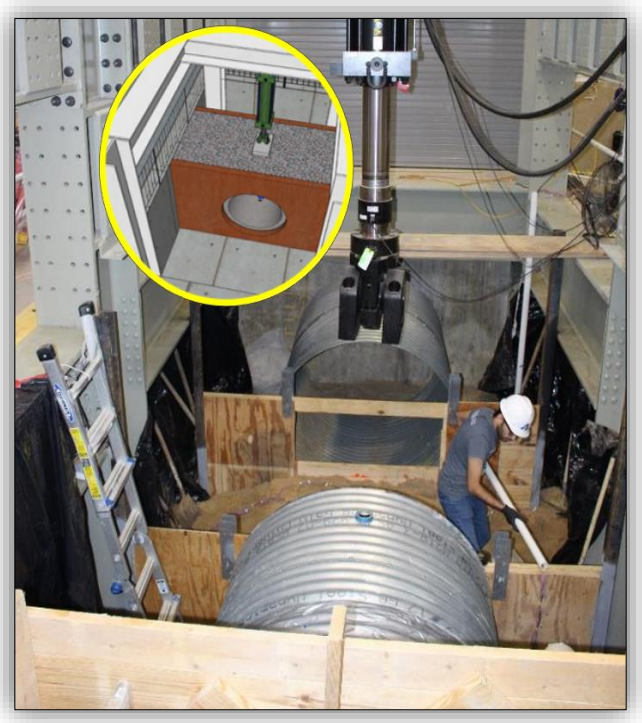


Figure 1. Structural condition of the culvert:
(a) partially deteriorated and (b) fully deteriorated.

Research Background



To reduce emergency projects and impacts to the traveling public, departments of transportation (DOTs) can use SAPLs to renew deteriorated gravity storm water conveyance conduits and culverts provided they are discovered prior to loss of soil-structure interaction. The American Association of State Highway Transportation Officials (AASHTO) National Transportation Product Evaluation Program (NTPEP) developed a Technical Committee for Spray-Applied Pipe Liners to implement this new technology. The SAPL Task Committee (TC) consists of DOTs, manufactures of resin-based material, and manufactures of cementitious-based materials. An early request from the DOT members was to ensure that the spray-applied lining functioned as a structural liner. However, it was quickly realized that no standardized structural design methodology existed for this technology. Manufacturers utilize different design methodologies with some using the CIPP ASTM F1216 methodology and others using various classical analytical structural design equations developed for other purposes. A gap in knowledge was identified and preliminary discussions for research among the SAPL TC members were formed.



The research needs statement was posted through Ohio DOT's Research Program and the National Cooperative Highway Research Program (NCHRP), and CUIRE was selected. The primary objective of this three-year research was to develop design equations for structural renewal of gravity storm water conveyance culverts using spray-applied pipe linings for both cementitious and resin-based materials and for large diameter ($\geq 36\ in.$) circular and non-circular shapes. These design equations developed with this project used loading as detailed in the AASHTO's Load and Resistance Factor Design (LRFD) Bridge Design Specifications. Practical limitations on the use of these design equations were included.

Data collected via the SAPL NTPEP program was incorporated into the pooled funded research project in addition to field and laboratory testing via the research

project. The development of practical spray applied structural culvert pipe linings is of enormous benefit to the DOTs. Such linings could be a key strategy in extending service life and managing the future burden expected from the aging network of culverts and storm sewers. Compared to other culvert rehabilitation systems, SAPLs promise greater cost effectiveness and less community disruptions. Table 1 presents accomplished tasks. Table 2 presents a summary of key literature search findings.

Table 1. Accomplished tasks for the SAPL research project.

Structural Design Methodology for Spray Applied Pipe Liners in Gravity Storm Water Conveyance Conduits	
Task No.	**Description**
1	*Survey of US DOTs and Canadian Agencies*
2	*Literature Search/Participation Material Vendors*
3	*Additional Reinforcement*
4	*Evaluation if Corrugations Needed to be Completely Filled by the Spray Applied Liner as Part of the Structural Design*
5	*Comparison of Construction and Environmental costs for SAPL, Sliplining and CIPP*
6	*Review the Cured in Place (CIPP) Design Equations*
7	*Field Data Collection and Assistance from DOT Partners*
8	*Develop a Recommended Structural Design Equations*
9	*Develop Performance Construction Specification*
10	*Computational Modeling*
11	*Soil Box Testing*
12	*QA/QC*

Table 2. A summary of key literature search findings.

Author	Ellison, D. (2003)
Title	Investigation of pipe cleaning methods. AWWA Research Foundation and American Water Works Association, Denver, CO.
Key Points	• Spray applied pipe liners in gravity storm sewers and culverts can be considered "structural" with implementation of proper design equations (does not exist). • It has been recognized for decades that cementitious and polymeric linings provide structural benefits. • Both field experience and laboratory experiments have shown that these linings are certainly capable of spanning over pits, holes, and gaps in the host pipe material, thereby preventing leaks. • Simply by decreasing leakage and soil erosion around culvert, the longevity of culverts can be increased. • The risk of pipe breaks can be reduced.
Author	**Motlagh G. S., Jain. A, Najafi M., (2013)**
Title	Comparison of Spray-on Linings for Water Pipeline Renewal Application
Objective	• To compare different SAPL materials (cement mortar, epoxy, polyurethane, and polyurea linings) using the vendors material property testing results. • To provide an overview of the advantages and limitations of different SAPL materials. • To provide the physical properties of different SAPL materials available in the market.
Methodology	• Short-term material property testing. • Long-term tensile creep testing plans of polymer spray-on linings.
Results	• Rapid reaction and curing time characteristics of polymers may provide an effective solution to other pipeline renewal technologies.
Critique	• No structural testing.
Author	**Entezarmahdi A. (2015)**
Title	Testing, Analysis and Classification of No-dig Manhole Rehabilitation Materials
Objective	To study the impact of several SAPL materials including cement mortar, epoxy, polyurethane, cured-in-place composites, and a multi-layer structure material on increasing the structural capabilities of deteriorated manholes.
Methodology	**Conducted Experimental Testing Using:** - ASTM C39: compression test of cylinder concrete specimens. - ASTM C293: flexural testing of concrete beam specimens using 3 points loading. - ASTM C497: 17 three-edge bearing test of reinforced concrete pipes (4 ft long, 24 in. Dimeter, 3 in. thickness) using different SAPL materials. • SAPL Thickness: (125, 150, 250, 500, and 1000 mills).

	• Material: epoxy, polyurethane, multi structural liners with modified polyurea and foam, cementitious, resin impregnated cured-in-place lining (CIPP)
Results	The results showed that tested SAPL materials can significantly improve structural performance of deteriorated pipes and manholes.
Authors	**Garcia D. B. and Moore I. D. (2015)**
Title	Performance of deteriorated corrugated steel culverts rehabilitated with sprayed-on cementitious liners subjected to surface loads.
Objective	To examine the performance of deteriorated steel culverts rehabilitated with spray-on liners when subjected to surface loads.
Methodology	**Conducted Large Scale Soil Box Testing:** • Compared two 4 ft diameter deteriorated CMPs (different levels of deterioration). - Bare condition (without liner). - Renewed with 2 different cementitious SAPL thicknesses (2 in. and 3 in.). • Bare CMPs were tested under designated service load (4 ft of soil cover). • The pipelines were then renewed with cementitious SAPL. • Renewed CMPs were examined again under the designated service load (single axle load frame - 4 ft of soil cover). • Then tested employing a tandem axle load frame (4 ft and 6 ft of soil cover). • Evaluated ultimate strength of the two deteriorated CMPs, renewed with cementitious SAPL. • Evaluated the applied SAPL thicknesses.
Results	• The flexible CMPs responded like semi-rigid structures after rehabilitation. • No signs of failure were observed prior to the rehabilitation. • Corroded CMPs had still sufficient amount of structural capacity. • Renewed pipe showed smaller curvature change when subjected to the same load configuration (stiffer response). • The higher the cover, the lower the strain in the pipe.
Critique	• Basically, every test was a new test, which is hard to compare their results. • The CMPs were able to sustain the load, therefore it is still unknown that the SAPL is fully structural or not. • Ultimate capacity of the renewed culverts is unknown. • There is too much variation in pipe thickness which directly affects the results.
Authors	**Yu, X., Riahi, E., Entezarmahdi, A., Najafi, M., and Sever, V. F. (2016)**
Title	Experimental and Numerical Analyses of Strength of Epoxy-Coated Concrete under Different Load Configurations.
Objective	To evaluate the strength of ultra-high epoxy-coated concrete specimens under different load configurations.

Methodology	• **Experimental testing:** - *ASTM D4541* Pull-off Testing to measure the adhesion strength between the epoxy coating and concrete specimens. - *ASTM C39* Uniaxial compression for 17 cylindrical concrete specimens (with and without epoxy coating) - *ASTM C293* Three-point bending for 5 beam concrete specimens (with and without epoxy coating) - *ASTM C497* Three-edge bearing for 17 concrete pipe specimens (with and without epoxy coating) • **Finite-element modeling (FEM)**
Results	• The epoxy lining can **improve the flexural strength** of a concrete beam by **80%**. • The epoxy lining can **improve the compressive strength** of a concrete cylinder by **10%**. • The epoxy lining can **increase the pipe's structural capacity**.
Critique	• Design methodology not covered.
Author	**Mai, V. T., Hoult, N. A., and Moore, I. D. (2013)**
Title	Effect of Deterioration on the Performance of Corrugated Steel Culverts.
Objective	To compare the performance of a largely intact steel culvert in well-compacted backfill condition with a corroded culvert in loose backfill condition.
Methodology	**Soil-Pipe Testing** • Extensive corroded and lightly corroded CMPs • Compared the behaviors of CMPs (6 ft diameter, 10 ft long) during backfilling. • Compared the behaviors of CMPs under the standard American and Canadian design trucks at two burial depths (2 ft and 3 ft) • Loaded under single axle and tandem load configuration
Results	• Higher deflection occurred at lower cover with single axle loading configuration. • Despite the pipes were loaded several times under different conditions, which caused irrecoverable deformations, they were able to take the full-service load of 38.22 kips in tandem configuration.
Critique	• Design methodology not covered.
Author	**Masada T. (2017)**
Title	Structural Benefit of Concrete Paving of Steel Culvert Inverts
Objective	To compare the structural performance of CMPs in intact, partially deteriorated invert, and paved invert conditions
Methodology	**Field and Laboratory Testing** • Intact CMP • Partially deteriorated invert

	• An invert paved CMP using mesh reinforced cementitious material
Results	• The intact CMP, under an incremental loading, buckled at one of the shoulders at a load of 923 kips. • The partially invert deteriorated culvert had 26.6% load carrying capacity reduction compared to intact CMP. • The remaining invert sections partially maintained the resistance to ring compression and played an important role in the CMP's stability and load carrying capacity. • The invert paved pipe sample failed at 13.3% lower load carrying capacity of the intact CMP at the load of 800-kips.
Critique	The structural behavior and loading carrying capacity of fully deteriorated invert condition is unknown.
Author	**Sargand, S. M., Khoury, I., Hussein, H. H., and Masada, T. (2018)**
Title	Load Capacity of Corrugated Steel Pipe with Extreme Corrosion under Shallow Cover
Objective	To investigate the load capacity of an extreme corroded CMP sample
Methodology	**Field testing of a shallow cover and severely deteriorated arch CMP** • Asphalt concrete pavement was applied on the half of a CMP sample's invert. • Static loading was applied on top of the crown of the paved and unpaved sections of a CMP sample, respectively. • Invert paving was done in the half of the culvert toward its outlet end. • Fully cured concrete pavement. • Each half was tested under an external load of up to 60-kip placed over the crown.
Results	• Despite the highly deteriorated conditions and the shallow cover (1 ft), the culvert structure supported a load considerably larger than 18 kips. • The invert-paved section of the culvert responded to the load with smaller strains, deflections, and thrusts and moments. • The stresses at the interface of the steel culvert and the poured concrete treatment were not very large.
Critique	• Design methodology not covered.
Author	**Szafran J. and Matusiak A. (2017)**
Title	Structural Behavior and Compressive Strength of Concrete Rings Strengthened with a Polyurea Coating System.
Objective	To evaluate and determine structural behavior and increased compressive strength of RCPs lined with polyurea SAPL.
Methodology	**D-Load Testing** • Static compressive testing on RCP with and without internal and external polyurea SAPL application.
Results	• Using polyurea SAPL on both internal and external surfaces of RCP increased the peak load of failure by about 21.9%. • Polyurea SAPL increases the compressive strength of RCP.

Critique	• The authors used external coating and internal spraying, which are not usable for trenchless renewal of existing culverts.
Author	**Ward, D.C. (2018)**
Title	NCHRP Synthesis 519 The Renewal of Stormwater Systems Using Trenchless Technologies.
Objective	To summarize six trenchless technologies (cured-in-place pipe (CIPP), sliplining (SL), modified sliplining (MSL), In-line replacement (ILR), spray-in-place pipe (SIPP) and close-fit pipe (CFP) used for renewal stormwater systems. The use of manhole renewal and invert paving are also discussed.
Methodology	• Literature review, survey of DOTs and interviews on methods used, decision criteria to select a renewal method, and limiting factors on applicability of specific trenchless renewal methods.
Results	• Survey results indicated that SL and CIPP the most commonly used methods for stormwater system renewal. The need to maintain the existing hydraulic capacity was identified as the primary reason not using trenchless renewal. Survey results indicated that while 88% of DOT respondents have experience with trenchless renewal, 60% have experience one or two methods. Only 8% of DOT respondents have experience with all six primary methods.
Recommendations	• The author recommended additional research and synthesis of structural testing and analysis of SIPP (such as current research) and CIPP liners. Additional information needed on less commonly used ILR methods, detailed cost data and standardized trenchless renewal and replacement selection guidelines.

Research Approach

The primary objective of this research project was to develop design equations and performance specifications for structural renewal of gravity storm water conveyance culverts using spray-applied pipe linings for both cementitious and resin-based materials and for circular and non-circular (arch) shapes. The developed design equations utilized loading as detailed in the *AASHTO's Load and Resistance Factor Design (LRFD)—Bridge Design Specifications* and will be applicable for round and arch shapes up to 120 in. diameter or span. As shown in Figure 2, and illustrated in below sections, to achieve the objectives of this research project, 12 tasks were defined to provide essential components for different aspects of the design equations and performance specifications.

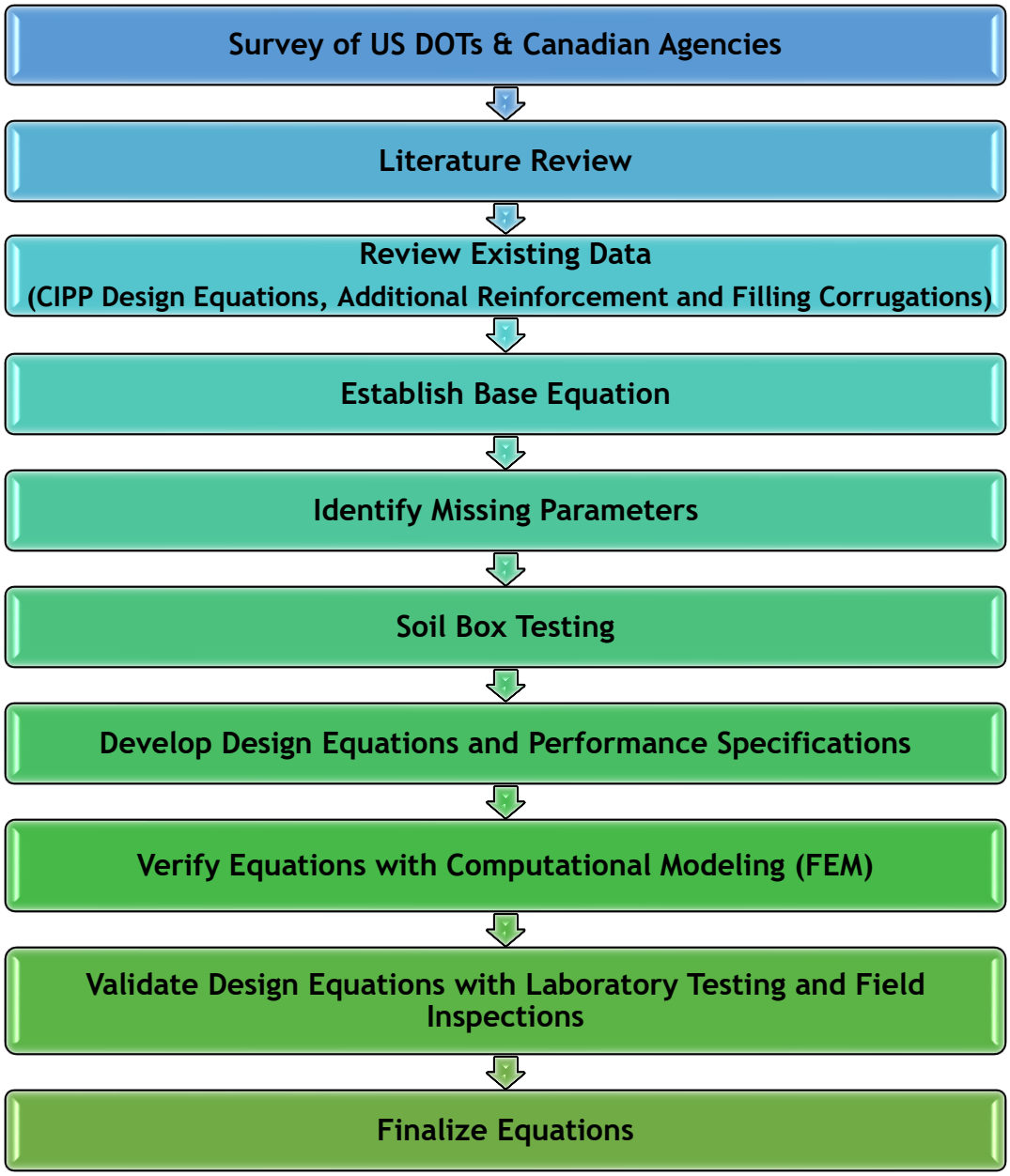


Figure 2. Research methodology.

Task 1: Survey of U.S. Departments of Transportation (DOTs) and Canadian Transportation Agencies

A survey of U.S. Departments of Transportation (DOTs) and Canadian Transportation Agencies was conducted to identify advantages and limitations of SAPLs. The survey sought DOT experiences in three stages of planning and design (pre-installation), during the installation, and after installation was completed. This survey was beneficial to identify the gap in the knowledge and identified the following:

1. Which DOTs used or planned to use SAPLs.
2. Design procedure.
3. Existing SAPL specifications.
4. Applicability of SAPLs for culvert renewal.
5. Environmental and host culvert requirements for SAPL application.

Task 2: Literature Review

A literature review was conducted to utilize findings of previous researchers and to identify gaps in the knowledge that previous researchers had confronted. The literature review provided significant understanding of the subject matter through assessment of the past research projects to develop research needs for this project.

Task 3: Additional Reinforcement

To evaluate structural application, first the SAPL material should be assessed to see if it is capable to structurally resist all the applied loads. Then, if needed, applicability of using reinforcements can be considered to further increase the mechanical properties of SAPL material. **Error! Reference source not found.**Figures 3 and 4 **Error! Reference source not found.**illustrate different types of macro-fiber and micro-fiber reinforcements that potentially can be used.

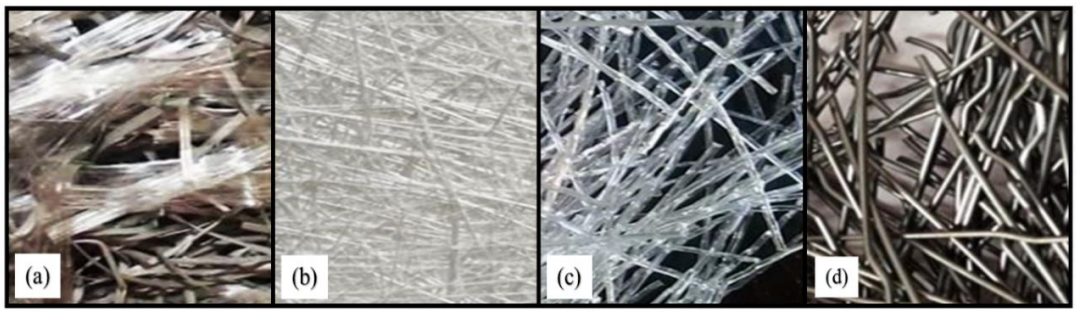


Figure 3. Macro-fibers used in concrete linings: (a) polypropylene fibers, (b) fiberglass, (c) polyolefin fibers, and (d) steel fibers.

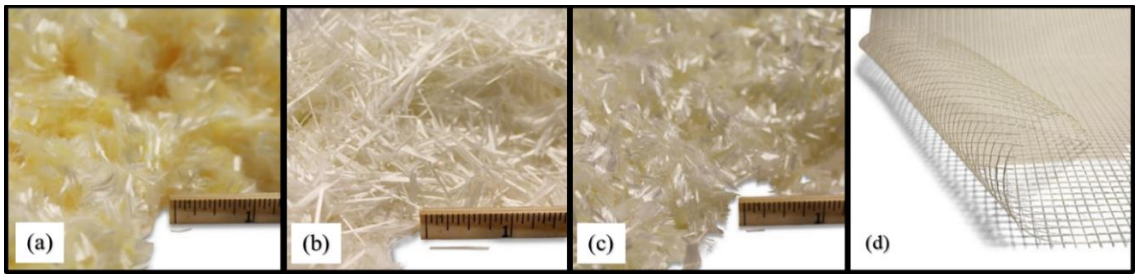


Figure 4. Micro-fibers used in concrete linings: (a) acrylic fiber, (b) alkali resistant (AR) glass fiber, (c) PVA fiber, and (d) alkali resistant glass scrim.

Task 4: Evaluation of the Need to Fill the Valleys of Corrugated Pipes

In absence of previous standard guidelines for application of SAPLs on CMPs, the objective of this task was to investigate two different installation approaches (filling corrugations or not filling corrugations) to come up with a preferred installation method. This task was accomplished by consideration of hydraulic and structural effects of each installation methods. Figure 5 illustrates two common SAPL installation methods on inner surface of corrugated metal pipes.



(a) (b)

Figure 5. Two common SAPL installation methods:
(a) following and (b) filling the corrugation pattern.

Task 5: Comparison of Construction and Environmental Cost of SAPL with Cured-in-Place Pipe (CIPP) and Sliplining (SL)

The life cycle cost of a project includes direct and indirect cost of construction, social and environmental costs as well as planning, design, operation and maintenance costs. The construction and environmental cost analysis performed in this task evaluated construction as well environmental cost of SAPL, CIPP and sliplining installations. This comparison can be useful during planning and design phase of a culvert renewal to select a method with lowest construction and environmental costs.

Task 6: Review of the Cured in Place Pipe (CIPP) Design Equations

To evaluate all the parameters needed for development of new design equations, it was crucial to investigate applicability of current design methodologies to SAPLs, mainly CIPP (ASTM F1216 design Appendix X1). Additionally, this task included consideration of WRc Sewerage Rehabilitation Manual, the German Static Calculation for the Rehabilitation of Drains and Sewers Using Lining and Assembly Procedures (ATV-DVWK-M 127 E, Part 2), and the ASTEE 3R2014 Structural Design for Non-Circular Linings under Groundwater Pressure, as well as pending ASCE Manual of Practice for the Design of Flexible Liners (currently in press).

Task 7: SAPL Field Inspection and Data Collection

In addition to property of material, performance of any trenchless renewal method and specifically SAPLs, is dependent on the quality of installation. Appropriately designed and properly installed liner systems will generally perform well throughout their design life. Proactive maintenance strategies can be scheduled based on the structural condition and performance assessments of the existing structures through the field inspection and collected data. To identify the most common issues with SAPL installations, a comprehensive field inspection program was prepared and conducted. The objective of this task was to collect data through in-situ inspections of past SAPL projects. This information was used to prepare performance specifications (Task 9) and to identify and categorize installation issues. The data collected through this task will improve design and installation of future SAPL projects. Figure 6 (a and b) illustrates some samples of SAPL installation issues.



(a)



(b)

Figure 6. (a) and (b). Some samples of SAPL installation issues.

Task 8: Development of Structural Design Equations

This task produced design equations for both polymeric and cementitious types of SAPLs using data and information from other tasks of this project, mainly finite element modeling (FEM) and soil box testing (Tasks 10 and 11). The equations are addressed both circular and arch geometries. As per Task 6, first existing design methods were evaluated and analyzed for their applicability to SAPLs. Design loading as per AASHTO's Load and Resistance Factor Design (LRFD) Bridge Design Specifications was used. Then limitations with existing design equations were considered and design thickness results were compared with the data obtained from numerical and experimental studies in Tasks 10 and 11. Once the applicable equation was identified, it was further calibrated using regression curves to conform with test results. Figure 7 illustrates the design equation development methodology.

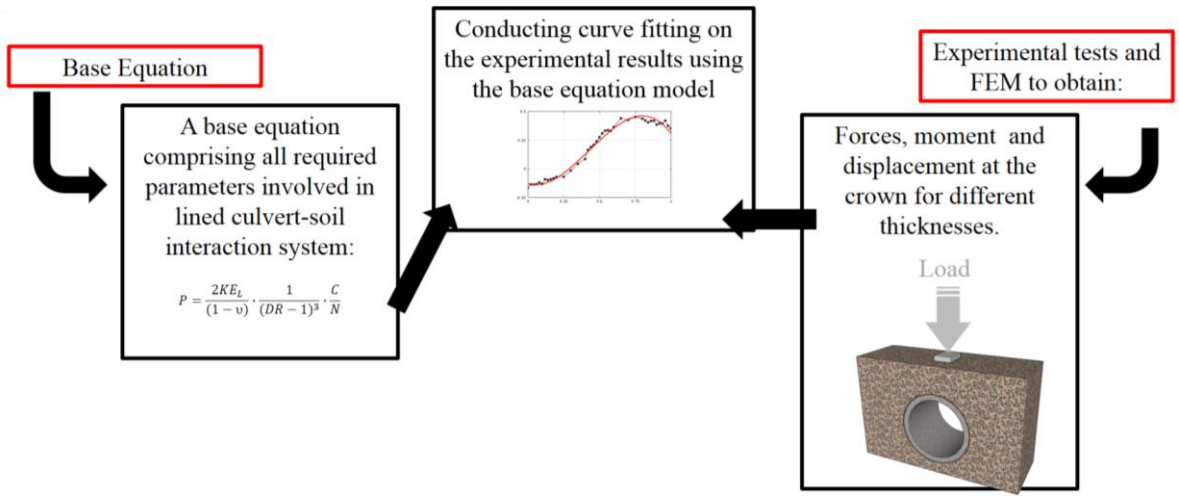


Figure 7. Design equation development methodology.

Task 9: Performance Construction Specifications

In the absence of standard installation guidelines, this task investigated, and prepared performance construction specifications based on the outcomes of the previous tasks to ensure structural integrity of the SAPL is not jeopardized due to faulty installation.

Task 10: Finite Element Modeling of SAPL Renewed Corrugated Metal Pipes Tested in a Soil Box

This task included preparation of finite element modelling (FEM) and simulation of the soil box test results for other similar conditions. Once the FEM models were validated with the results of the soil box, different conditions and situations were simulated, which were not considered in the soil box testing. ABAQUS was used to perform FEM simulations and analyses. The simulations included three CMP pipes without linings, three invert-removed circular CMP lined with a SAPL, and three invert-removed arch CMP lined with a SAPL. The three CMP pipes without linings are one bare intact circular CMP, one bare invert-cut circular CMP, and one bare invert-cut arch CMP. These three bare CMP pipes were used as the control tests to provide baseline results of the CMP pipes before lining. The FEM results simulated other conditions that were not considered during soil box testing Figure 8. *Finite element modeling of the soil box testing.*
 illustrates the FEM modeling of soil box testing.

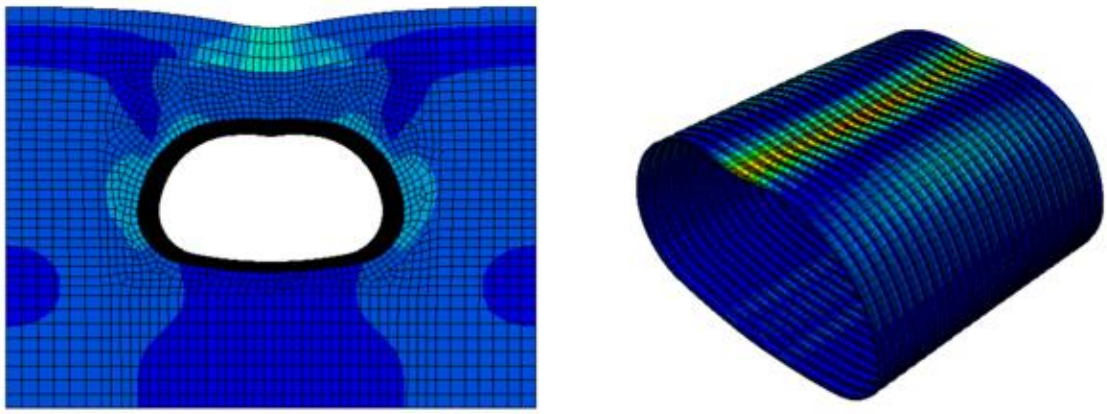


Figure 8. Finite element modeling of the soil box testing.

Task 11: Laboratory Testing

The laboratory testing of this study was designed to include both structural and material evaluations. The tests were conducted at the Center for Underground Infrastructure Research and Education (CUIRE) laboratory facility located at the University of Texas at Arlington (UTA). The soil box is equipped with a 330-kips MTS actuator installed on a steel reaction frame designed for this type of experimental project. The material testing program included results of tensile and flexural resistance

evaluations of polymer as well as compressive and flexural strength of cementitious SAPLs. As stated previously, the experimental structural testing program consisted of five sets of full-scale laboratory tests including (1) control test, (2) circular CMPs renewed with polymeric SAPL, (3) CMP arch pipes renewed with polymeric SAPL, (4) circular CMPs renewed with cementitious SAPL, and (5) CMP arch pipes renewed with cementitious SAPL. The control test consisted of one intact circular CMP, one invert-cut circular CMP, and one invert cut CMP arch. The SAPL liner thickness for the polymeric circular and arch pipe samples were 0.25, 0.5, and 1-in. The circular and CMP arch cementitious SAPL test series consisted of three separate invert-cut CMP samples each, renewed with 1, 2, and 3-in. thick cementitious SAPL. To acquire the structural capacity of the SAPLs, the invert section of the CMPs were cut and detached after backfilling. Therefore, no ring compression was existed in the CMP sample and the load was resisted by the SAPL only. The soil-pipe structure was subjected to statistical vertical load, applied at the soil surface, simulating a truck load. The outcomes of the soil box testing can reveal the true renewed pipe-soil structural capacity and failure modes, which were crucial for design equation development. Figure 9 illustrates CUIRE soil box testing setups.

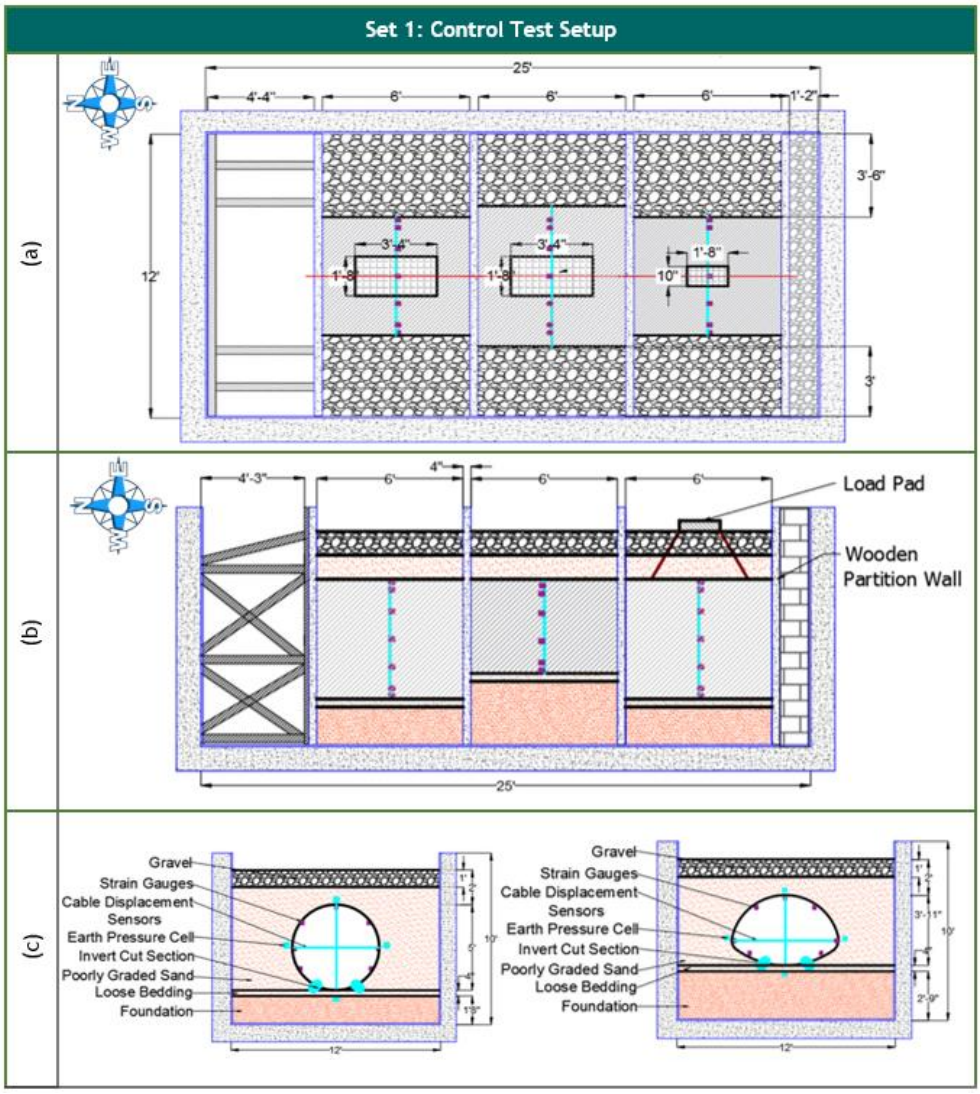


Figure 9. The CMPs' burial configuration (control test set): (a) plan view, (b) profile view of the aligned CMPs in the soil box, and(c) cross sectional view of both circular and CMP arch samples.

This Page Left Intentionally Blank.

Research Findings and Conclusions

Task 1: Survey of U.S. Departments of Transportation (DOTs) and Canadian Transportation Agencies

A survey of U.S. Departments of Transportation (DOTs) and Canadian Transportation Agencies was conducted to identify advantages and limitations of SAPLs. The survey sought DOT experiences in three stages of *(1) planning and design (pre-installation), (2) during the installation, and (3) after installation was completed*. This survey was beneficial to identify the gap in the knowledge and identified which DOTs used or planned to use SAPLs, design procedure, existing SAPL specifications, applicability of SAPLs for culvert renewal, and environmental and host culvert requirements for SAPL application.

Issues before and during SAPL installations included:

- The most common deficiency in the CMP material is invert deterioration (invert loss).
- The common most deficiency in the RCP material is longitudinal cracking.
- The SAPL protects the interior surface from corrosion and it can be helpful against abrasion.
- It can be interpreted that cementitious SAPL, alone, does not have structural integrity.
- Cementitious SAPL's structural capacity is dependent on the bonding with the host culvert.
- Weather conditions must be considered before design of cementitious SAPL and/or selection of the cementitious SAPL materials.
- Weather conditions have a significant impact on the cementitious SAPL during and after installation.
  Issues after cementitious SAPL installations included:

    - **Ordinary Portland Cement Mortar:**
        - Longitudinal and circumferential cracking,
        - Hairline cracking with rust bleeding through cracks,
        - Cracking at joints,
        - Spalling,
        - Delamination,
        - Rough application,
        - Rust-through,
        - Slumping from ceiling,
        - Buildup of material due to poor installation,
        - Lack of uniform application,
        - Groundwater infiltration before cure time, and
        - Cracking and infiltration of groundwater through the centrifugally cast concrete pipe (CCCP) was observed approximately one year after installation.

- **Geo-polymer:**
  - Leaking ground water,
  - Cracking at joints,
  - Spalling,
  - Delamination,
  - Rough application,
  - Rust-through,
  - Slumping from ceiling, and
  - Buildup of material due to poor installation.

Task 2: Literature Review

- Spray applied pipe lining (SAPL) in literature are also called spray-in-place pipe (SIPP) and spray-on lining (SOL) and underground coatings and lining (UCL).
- SAPLs have the potential to renew deteriorated culvert pipes and can be used as structural applications to renew the existing culverts.
- The host culvert conditions have minor impact on the structural capacity of the SAPL.
- There are no comprehensive studies that produced design equations and performance specifications for SAPL projects.

Task 3: Additional Reinforcement

- Crack control and post-cracking behavior are the most important advantages of inclusion of additional fiber reinforcements to the cementitious SAPL.
- Use of fiber reinforcements may substantially increase the cementitious SAPL matrix tensile strength.
- A medium volume fraction of fibers (1%-3%) can enhance post crack load-carrying capacity, tensile stress, flexural stress, shrinkage cracking resistance, durability modulus of rupture, energy absorption, fracture toughness and impact resistance of the fiber reinforced cementitious SAPL mortar.
- The magnitude of enhancements needs to be verified through the experimental tests.
- A high aspect ratio (fiber length divided by fiber dimeter) produces a higher strength composite.
- Various literatures show inconsistent effect of fibers on the compressive strength of the FRC.
- Presence of fiber reinforcement can enhance the bond strength between the old substrate (host culvert) and the repair material (SAPL).
- Micro-Synthetic Fibers and Basalt Mesh Grid can fit with the SAPL application.
- As the SAPLs are thin shelled structures, the macro-synthetic fibers, as they are big in length and diameter, do not fit well with this application which mostly ranges from 1 to 3 in.
- Steel WWM is not a viable option for SAPLs.

Task 4: Evaluation of the Need to Fill the Valleys of Corrugated Pipes

- While the engineer could design a theoretical wall thickness that followed the corrugation profile of a particular CMP; it would be impractical to install such in the field. Further, the likelihood that the finished cross-section of the lining would resemble that design would be low. The site installation inspections conducted this past summer clearly showed how difficult it was to get the required thickness of the liner. During the installation process the crests of the corrugations provide the reference points needed to assure the owner of the pipe that the specified thickness is being installed. This is true of both cementitious and flexible polymeric material. Further, beyond the structural performance issues, it has been shown that pipe barrel hydraulics also favors a smooth interior surface profile. From an operational standpoint, this can be true even when the culverts are in inlet control.
- Operational considerations favor a smooth surface profile for the lining. Maintaining flows through a culvert rewards a surface profile that lowers its tendency to catch and hold onto debris swept up by the storm water flows. Minimizing the impacts of large rocks and boulders passing through the culvert minimizes the potential for losing parts of the lining.
- The guidance provided by ARMCO's engineering team in the 1980s and defined in the ASTM standard A979, Concrete Pavements and Linings Installed in Corrugated Steel Structures in the Field, which still exists today specifying the production of a smooth interior surface profile liner, is the best long-term design solution for this new generation of SAPL's. While their focus was to produce a pipe that could compete competitively with smooth bore concrete pipes; lining existing corrugated metal pipes with a liner that produces a new smooth bore path not only produces a more hydraulically efficient pipe, but also a more structurally sound pipe.

Task 5: Comparison of Construction and Environmental Cost of SAPL and other Trenchless Technology Methods

- This study used bid tabs for evaluation of construction costs, however for an accurate estimate of costs, more detailed project information regarding construction equipment, depth of culvert and accessibility, weather conditions, level of host culvert deterioration and required cleaning, etc., are required.
- The data points for diameter of 84 in. and above were significantly less than that of 30 in. to 84 in. By adding more data for SAPL projects, the accuracy of the entire analysis can be improved. Analysis of liner thickness for each trenchless renewal requires more data. This study can be expanded to other locations and states.
- It can be concluded that SAPL, CIPP, and sliplining have the lowest to highest construction costs in culvert with diameter range of 30 in. to 108 in., respectively.

- Due to data availability, only one material from each trenchless method was considered for the analysis and comparisons. There is a need to obtain the project data for all other types of materials for each trenchless method to have a better comparison among different renewal methods.
- SAPL concept for large diameter gravity culverts is a more recent technique rather than CIPP and sliplining, so fewer projects are conducted with this method until now. With more use of SAPL method, more data becomes available to improve accuracy of the cost comparison analysis.
- Environmental and construction costs play essential roles in the decision-making to select the most appropriate trenchless method for culvert renewals. It is recommended to investigate influence of other factors, such as, social costs.

Task 6: Review of the Cured in Place (CIPP) Design Equations

- While the non-mandatory design appendix of ASTM F1216 is the design procedure currently specified by North American engineers, it has been found by academicians and specialist engineers as being unrealistic for designing flexible liners like CIPP for a variety of reasons. While it can be said that it is overly conservative in many aspects, it also has the potential to understate long-term performance in other aspects.
- While engineers have thought for years that specifying the FD design condition for CIPP liners is conservative, they inadvertently ended up over designing this class of liners. With excessive thickness comes issues with the installation process as liners go into larger and larger diameter pipes (e.g., full curing throughout the full thickness of the liner). Excessive CIPP thickness may add issues with proper fit and finish issues (e.g., fitting tightly to current shape, wrinkles and fins, etc.). In the case of flexible host pipes like CMP, the dominant structure for resisting the load coming onto the CIPP was the host pipe and/or the surround soil. This meant that knowledge of the current performance properties of the soil surround are critical to the performance of the rehabilitated soil-structure interaction system, which was often given as some arbitrary minimum values in the project specifications.
- The only true design methodology existing for non-circular shaped pipe geometries is developed by Olivier Thépot which was subsequently presented in the ASTEE 3R2014 Structural Design for Non-Circular Linings Under Groundwater Pressure.
- Except in some rare cases, the loads that will be transferred onto a CIPP liner will come from the deflections that are induced in the host pipe structure from additional soil dead loads, any surface live loads, and any external groundwater loads. Any design procedure used for CIPP must recognize the differences in how rigid pipe structures versus flexible pipe structures will transfer these loads to consider the stresses and strains created in the CIPP liner itself. In reality, CIPP can be a reinforcing material as opposed to a standalone structure. If at some point in the future the host pipe will truly be gone, it will be the soil structure that dominates the survival of this hydraulic structure. Therefore, the

surrounding soil will be important to the engineer who is preparing the plans and specifications for the design of the liner.

Task 7: SAPL Field Inspection and Data Collection

- Spray applied pipe linings (SAPLs) structurally renew existing pipes and provide a protective interior coating, thus inhibiting further deterioration of the interior of culverts and drainage pipes. Currently no standard design methodology and performance construction specification exist for SAPLs. Vendors have their own design approaches and installation procedures which highly impact the performance of the applied SAPL. SAPL field data collection presented in this chapter identified and addressed the existing issues with the applied liner on the interior surface of the culverts which highlights the needs for comprehensive performance construction specifications to satisfy the liner design requirements. The common cementitious/geopolymer SAPL issues (due to lack of any standard) identified in this chapter includes circumferential crack, fracture, infiltration weeper, efflorescence, rust staining and non-uniform thickness. The condition of inspected SAPLs summarized and evaluated using an established numerical scale rating system from 0 (Failed) to 9 (Excellent). This chapter depicted that besides the design, liner installation process is a main key to reach a uniform thickness of SAPL and to achieve its structural application. It was observed that the corrugated aluminum pipes experienced less effect of corrosion on the surface of SAPL compared with the corrugated steel pipes. It implies that corrugated aluminum performs better in locations with high levels of corrosive environments. Due to different crack patterns in cementitious and geopolymers, it is recommended to select the type of SAPL materials in accordance with the deteriorated culvert's condition, geographical and weather conditions (freeze/thaw), cover depth and skew angle of culvert with the road for each location. Finally, authors used the available ASTM and AASHTO standards for other purposes and provided recommendations (Table 7-9) for proper SAPL installation to address the issues as well as having a robust quality control and inspection plans for stages of pre-installation, installation and post-installation.

Task 8: Development of Structural Design Equations

- The objective of this task was to develop a set of structural design equations for polymeric and cementitious SAPLs for renewing CMP culverts up to 120 in. diameter. After deterioration of CMP, SAPL would perform as a standalone pipe in the embedment soil.
- The current design method presently in use for polymeric materials consists of following the design appendix X1 of the ASTM Standard F1216. The fully deteriorated design case (standalone pipe) follows an old design used for the installation of fiberglass pipe by the AWWA Committee C950 in 1987. It calculated the allowable buckling strength of the liner. It did not address the liner providing any resistance to bending as some may have thought. The

resistance to bending would come in equation 8-24, which is the Spangler or modified Iowa equation. As the AWWA committee evolved and the fiberglass pipe design was put into a Manual of Practice (M45), it has undergone numerous improvements over the years and has become the state of the art for these type of pipe installations.

- For the polymeric materials it was found that Article 12.12 of the AASHTO Design Manual already contained much of the latest iteration of the AWWA M45 design method for plastic materials. However, as it has been drafted from the standpoint of an open cut excavation installation, it needed to be streamlined and defined in terms required to address a pipe being installed using a trenchless method into the site-specific conditions of an existing pipe; and what loads were probable to come onto the new pipe (liner) after its installation. This mission was accomplished by showing the relevant current M45 design equations in this document along with definitions of the variables with changes given that would be appropriate to the lining process over a new direct bury process. More study is needed to determine the bedding coefficient needed for a mature soil-structure interaction system.
- For the cementitious materials there was no design method given in the AASHTO Design Manual that could be easily taken and adapted by the research team. Darabnoush Tehrani (2020) found that a modified Iowa equation for deflection of buried pipes gave a suitable enough solution to be used for circular pipe shapes. Limiting the predicted deflection to 1.0 percent or less he stated provided a safe estimate against cracking of the cementitious liner. Again, this equation (the modified Iowa equation) will not accommodate pipe-arch shapes. Therefore, a mechanical analysis of a thin-walled ring structure was formulated to analyze the critical top curved beam element to the load coming onto the pipe structure. This analysis zooms in on the critical crown location identifying the impact of thrust and bending stresses generated by the dead and live loading conditions acting thereon based upon the distributional effects of the live loading at the surface and the depth of cover. The 60-inch circular pipe example using the equation presented herein appeared to agree well with the experimental testing contained within this project as stated earlier. The predicted stress level in the liner corresponding well with the strain measurements in the soil box testing.
- Filling the valley of the corrugations and then applying the calculated thickness of the SAPL increases the moment of inertia of the cross-section which in turn reduces the magnitude of the bending moment induced in the liner by the live loading. In the example calculation presented the thrust (compression) in the liner became the dominant stress at the interior wall surface of the liner.

Task 9: Performance Construction Specifications

- Performance specifications were developed to allow for contractor innovation and utilization of the most current products and techniques.
- The specifications were the result of input from the UTA team and consultants and several rounds of reviews and comments by the DOTs.

- The polymer and cementitious specifications are structured from the same outline with many portions of the individual specifications identical, with obvious differences where required because of product and installation differences.

Task 10: Finite Element Modeling of SAPL Renewed Corrugated Metal Pipes Tested in a Soil Box

- **Circular CMPs**
  - Prediction of different parameters by the FE model showed reasonable accuracy for all cases except for the control test on the invert-cut CMP.
  - Intact pipe FEM results for load-displacement, earth pressure at the crown, strains, and bending moments compared well with the test results with a discrepancy of less than 5%.
  - When the load pad size was increased from 10x20 $in.^2$ to 20x40 $in.^2$, the load-carrying capacity of the intact CMP soil-box system increased by about 90%, and the bearing failure of the soil was not observed before the pipe failures.
  - For invert cut pipe, the FE model over predicted the load by about 145% before the invert edges meet. The FEM over-prediction is caused by the soil model's limitation to replicate the collapse behavior of the soil during the invert removal process.
  - FE analyses of the invert-removed CMPs with liners predict load - displacement, earth pressure curves, ultimate load with less than 10% discrepancy with the measured values.
  - Also, the prediction of the first crack, which was represented by the appearance of the first plastic strain in FE model matches the test results with less than 10% discrepancy.
  - The lost load capacity of intact CMP due to the complete removal of invert from the CMP could be restored with the application of only 0.25-in. thick liner. With the liner thickness of 0.5-in. thick the load capacity of the invert cut CMP increased by 10% compared to its intact capacity.
  - The parametric analysis for the rehabilitated invert removed circular CMP showed that thickness and the capacity of the liner have a linear relationship.
  - The FE analysis for the filled corrugation with 0.25-in thick over the crest provided the load capacity in between the load capacity for 0.5-in. thick and 0.75-in. thick liner that was applied by following the corrugation.
  - Also, through parametric analysis, FE model clearly shows the increase in the rigidity of the circular CMP pipe with the increase in the thickness in the liner as we can see the reduction in the deformation of the liner at first plastic strain condition and ultimate load condition.

- **Arch CMP**
  - The FE analysis shows that the load-carrying capacity of the intact arch CMP is 20% less than the equivalent intact circular CMP.

- Like the invert removed circular CMP, the invert removed arch FE model also could not predict the collapse behavior of soil during the invert removal process. Although the FEM could not predict the collapse behavior, the ultimate load and displacement results were predicted within the discrepancies of 20%. Also, the load-displacement curve comparison between the test and FE simulation showed a similar response.
- For the lined invert cut arch CMPs, the FE model predicted the ultimate load and the displacement with discrepancies of less than 20% for all the tests. During the test, there were circumferential cracks present in the liner before loading, which could have resulted in less load carrying capacity of the system. The FE model did not account for the attachment of the liner to the boundary wall due to over-spraying.
- The response of the liner in the test was stiffer than the response of the liner from the FE model before the occurrence of the major crack.
- From parametric and calibration of FE models, it was found that the plastic strain on the CMP would appear when the system is near the ultimate load conditions.
- Like the lined invert cut circular CMPs the FE model also predicted that the 0.25-in. thick SAPL would be enough to re-establish the lost capacity of the CMP through invert removal. While 0.5-in. thick SAPL and 0.75-in. thick SAPL, when compared to intact arch CMP capacity, would increase the capacity by 9% and 18%, respectively. The 1-in. thick SAPL and 2-in. thick SAPL would increase the load capacity by nearly.
- The load-carrying capacity of the rehabilitated invert-cut circular CMPs is greater than the load-carrying capacity of rehabilitated invert-cut arch CMPs for the same thickness of the liner.

- **Limitations**
  - The FE model was implicit and thus could not predict the load drop after the ultimate load.
  - The Drucker Prager model is not suitable for modeling the soil collapse behavior observed in the test of the invert-removed circular CMP pipe.
  - Since the brittle polymeric material of the liner was modeled using the simple elastic-plastic model instead of crack models, a drop in load at first crack was not observed in the FE model.
  - FEM models for the CMP pipes and liners were based on the nominal geometry specified in the design. Actual geometry discrepancies were not evaluated in the FEM models.

Task 11: Laboratory Testing

A total of 15 large diameter pipes, including 3 bare CMPs (control samples) and 12 SAPL renewed CMPs, were buried under 2 ft of soil cover comprising layers of poorly graded sand (SP) and TxDOT 247 grade 1 type D aggregates. A static load with a displacement-control regime was continuously applied with a load rate of 0.03 in./min through a rigid 20 × 40 in. steel load pad on the soil surface over crown of the pipe.

The results and discussions were presented in this report and the conclusions are summarized as follows:

- The mechanical property test results showed that the polymeric SAPL had the flexural modulus of 850,000 psi, the averaged maximum tensile stress of 8,600 psi, and the elastic modulus of 329,000 psi.
- The mechanical property test results showed that the cementitious SAPL had an average compressive strength of 2,700 psi after 24 hours of curing. After 7 days the strength of the samples was increased up to 4,400 psi. The compressive strength increased further for 56.6% at the end of 28 days where the compressive strength reached average value of 6,900 psi.
- For polymeric SAPL, the results of thickness measurement showed that the utilization of hand spray installation of the polymeric SAPL resulted in a thicker liner at the springline for renewed CMPs than the designated thickness. However, the SAPL was installed closer to the required thickness at crown and both shoulders.
- For cementitious SAPL, the liner's thickness was variable along the circumference of the pipes, which emphasizes on the superiority of centrifugal casting machine over the hand sprayed method to provide uniform thickness in large thicknesses. However, the applied thickness was generally either higher or about the design thickness on the crown and both shoulder locations.
- The invert-cut bare CMP in the absence of the ring stiffness was not able to resist the applied load beyond its frictional resistance limit. The CMP continuously squeezed until both sides of the invert-cut sections contacted the main body of the CMP and retrieved the ring stiffness. The invert-cut bare CMP structurally failed at the load of 39.9 kips.
- All polymeric SAPL renewed circular CMPs cracked at about 3% of pipe deflection, where at this deflection the application of 0.25 in., 0.5 in., and 1 in. polymeric SAPLs increased the load carrying capacity for 471.7%, 482.8%, and 802.7% respectively.
- Application of the polymeric SAPL increased the stiffness of the invert-cut circular CMP. The SAPL renewed CMPs with the thicknesses of 0.25 in., 0.5 in., and 1 in. increased the ultimate load bearing capacity of the fully invert deteriorated CMPs for 16.2%, 31.4%, and 80.8%, respectively.
- Application of the polymeric SAPL increased the stiffness of invert-cut pipe arch CMPs. The SAPL renewed CMPAs with the thicknesses of 0.25 in., 0.5 in., and 1 in. increased the ultimate load carrying capacity of the invert deteriorated pipe arch CMPs for 23.1%, 32.1%, and 98.9%, respectively.
- The cementitious SAPL with the thicknesses of 1 in., 2 in., and 3 in. increased the ultimate load bearing capacity of the invert-cut circular CMPs for 79.7, 113.9, 174.7% respectively. These values for the pipe arch CMPs were 72.3, 104.4, and 151.4% respectively.
- It was observed that both polymeric and cementitious SAPLs were able to increase the structural capacity of the fully invert deteriorated CMPs and retrieve the ring compression resistance of the renewed pipes. In addition to that, since the polymeric SAPL did not crack at the invert-cut location, even at

the ultimate loading stage, it can be concluded that the polymeric liner was structurally capable to perform as a new pipe inside the host pipe (i.e., pipe-in-pipe) and could solely resist the applied ring compression.

This Page Left Intentionally Blank.

Recommendations for Implementation

Recommendations for Future Work

- The experimental study included the shallow cover condition in the absence of hydrostatic pressure. In addition, the ovality of the host pipe was not considered in the problem statement. Furthermore, the length of the CMPs could be an important factor affecting the ring compression resistance. It is recommended in the future studies these parameters to be investigated either through experimental or numerical studies. These parameters can further optimize the proposed design equations.
- Investigate centrifugally-cast SAPL using spin-caster robots to install the SAPL at higher pressure with more uniformly installed thickness. The thickness variation along the circumference of the pipe can distribute the applied stress incommensurate, which results in asymmetrical crack formation and affect the structural load carrying capacity of the liner. It is highly recommended to further investigate the benefit of using robotically centrifugally-cast SAPL and compare it with the results of this study.
- Investigate the SAPL's load carrying capacity installed on previously failed host pipe, which can assure that all the resistance from the renewed pipe comes from the liner solely.
- Develop advanced soil and liner FEM simulations to improve post-failure behaviors of the lined CMPs.
- Perform simulations of traffic loads representing true load configurations on the lined CMPs to study the effect of load configuration.
- Investigate the effect of pipe shape imperfections in the FEM simulations. All FEM simulations were based on CMP pipes with nominal geometry and shape provide in design drawings. Actual pipe shape and liner thickness variation should be evaluated and modeled in FEM simulations.
- More testing is recommended to further confirm the validity of the equations for the cementitious liners proposed herein over a much larger number of installations. It is also recommended that this testing be conducted on existing installations to reflect the actual support provided by the surrounding soil (constrained soil modulus).
- Due to the unique circumstances encountered in the field, the quality of application under field conditions varies from that of liner preparation in the laboratory, and the final liner may have different structural properties. Therefore, a comprehensive testing program is needed to evaluate the performance of actual in-service SAPLs from the field. Material property tests as well as full-scale tests on the lined pipe can be conducted. It is recommended to take coupons from aging polymeric and cementitious SAPL installations, after 5 and 10 years of installation, to conduct physical testing to assess performance of field aged SAPLs and how these materials lose their structural properties over time. Recommended material testing methods includes:
    - ASTM D2412 – Liner extraction, and parallel plate loading tests on the lined pipe composites loaded until failure of the host pipe.
    - ASTM D638 – Tensile test

- ASTM D790 – Flexural test
- X-ray CT tests – This test may reveal internal structure as air voids are common.

Additional recommendations for future work can be summarized as following:

- Develop design equations for culvert diameters larger than 120 in.
- For cementitious SAPLs, investigate structural enhancement of filling corrugations vs. following the corrugations.
- For flexible liners, investigate bedding coefficient.
- For cementitious liners, monitor existing SAPL installations to verify field performance compared with the ones installed using developed equations in this research, especially for pipe arches.
- Investigate existence of external hydrostatic head in the soil, especially in the embankment fill condition, should be undertaken.
- Investigate impact of cracks in cementitious SAPL.
- Investigate seismic loads over SAPL conduit.
- Investigate load bearing capacity of longitudinal steep slope for deep SAPL conduit.
- Analyze SAPL conduit buoyancy and/or uplift load.
- Investigate impacts of voids around the host culvert.
- Investigate impact of infiltration through cementitious SAPLs.

Recommendations for Implementation

It is recommended that results of this project be implemented and monitored under active traffic with lining a deteriorated CMP culvert divided in two or more sections and each section lined with different polymeric and cementitious/geopolymer SAPL. The contractors should use developed design equations and performance specifications presented in Chapters 8 and 9 of this report. During this implementation project, any strategies to overcome potential risks and obstacles will be identified. The quality of installation should be compared with recently installed SAPLs. Soil movement around the culvert should be monitored at least for one year using horizontal inclinometers. Surface settlement, infiltration, and condition of invert should be monitored and documented. Such parameters as water pH, abrasion, embedment material around host culvert, host culvert movements, voids around host pipe, depth cover and traffic loads, use of reinforcement and infiltration on SAPL must be studied. Additional numerical methods using FEM can expand results of field evaluation to other scenarios.

Chapters and Appendices

Chapter 1
Survey

CHAPTER 1 - SURVEY OF US DOT's AND CANADIAN AGENCIES

1.1. Introduction and Background

Spray Applied Pipe Linings (SAPLs) inside a host culvert are used to renew deteriorated gravity storm water conveyance conduits (storm drains and culverts). A structurally SAPL is an application that provides a protective interior surface to against abrasive material and can structurally support severely damaged culvert and drainage conduits. The primary materials used for SAPLs generally fall into two broad categories of cementitious materials and polymers such as epoxies, polyurethanes and polyureas. SAPLs can be a key strategy in extending service life and managing the future burden expected from the aging network of culverts and drainage structures. Compared to other trenchless culvert renewal methods, SAPLs can accommodate limited access and has less community disruptions. This survey includes corrugated metal pipe (CMP) and reinforced concrete pipe (RCP) culverts in circular and arch shapes.

To supplement the literature review, a survey of U.S. Departments of Transportation (DOTs) and Canadian Transportation Agencies was conducted. Appendix 1-A includes a copy of the survey. Appendix 1-B presents contact information of respondents.

The primary objectives of this survey were to determine:

6. Which DOTs used or plan to use SAPLs.
7. Existing SAPL specifications.
8. Applicability of SAPLs for culvert renewal.
9. Environmental and host culvert requirements for SAPL application.
10. The quality of SAPL installations.

Respondents were asked to share their experiences for considerations Part **A, before**, Part **B, during** and Part **C, after** installation of SAPLs.

Figure 1-1 and Figure 1-2 illustrate the geographical locations of survey respondents. Overall, 32 (62%) state DOTs and one Canadian agency responded to the survey.

Appendix 1-A includes abbreviations.

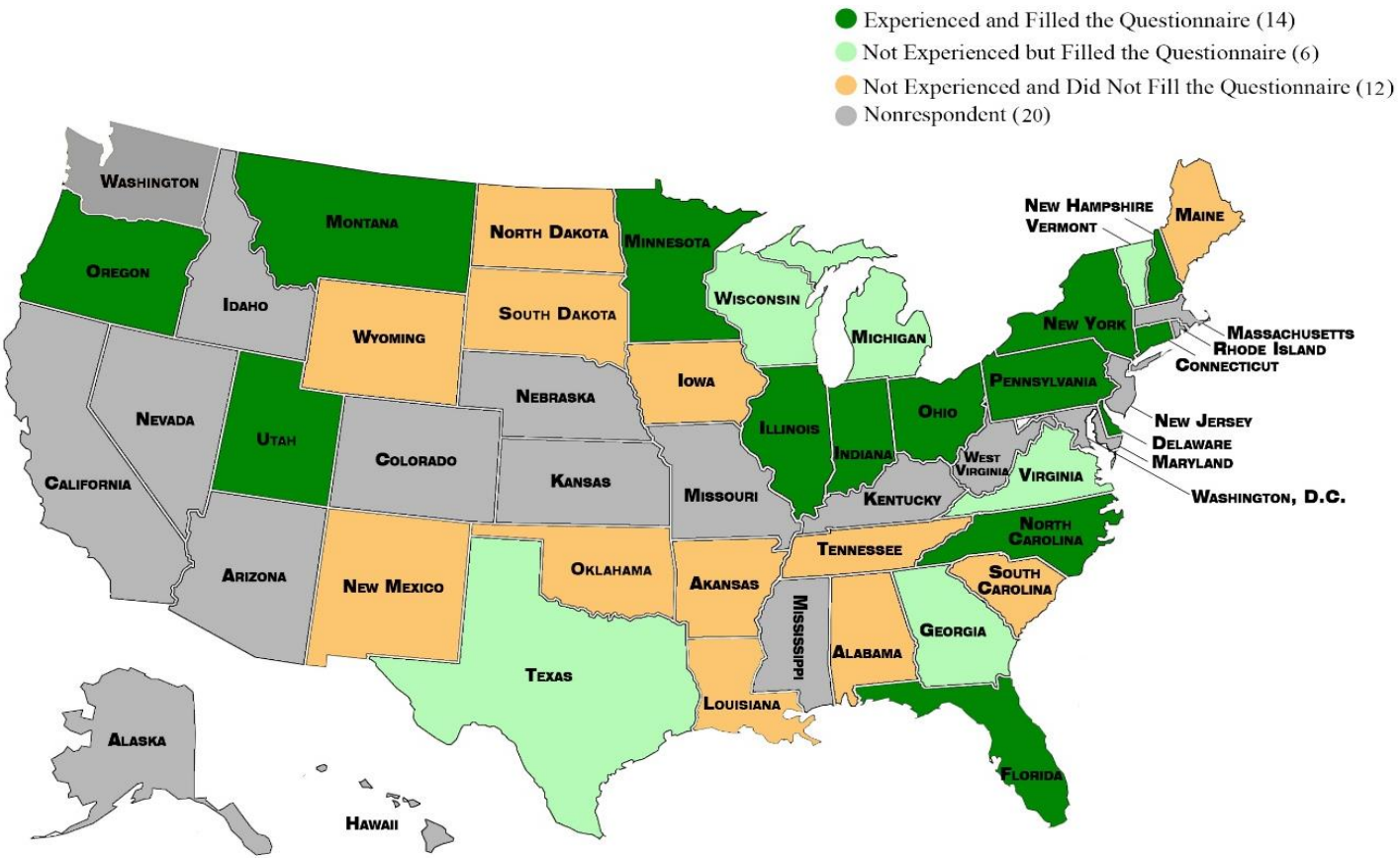


Figure 1-1. Survey respondents from U.S.



Figure 1-2. Survey respondents from Canadian Transportation Agencies.

Part A – Considerations Before SAPL Installation

Question A.1 – Decision Making Priorities When Using a SAPL

Table 1-1. and Table 1-2 present the priorities set by respondents based on their experiences for RCP and CMP culverts, respectively. Figure 1-3 and Figure 1-4 illustrate same information. Overall, for both RCP and CMP, durability, hydraulic capacity, impact to travelling public, project economics, minimum thickness, contractor experience, project schedule are major considerations. Some respondents stated other priorities, which included fish passage, host culvert condition, feasibility, and benefit/cost ratio for both RCP and CMP renewals.

Table 1-1. Decision making priorities for using SAPL in RCP culverts with "1" highest priority, (17 Respondents).

Decision Making Priorities	Rank
Hydraulic Capacity Due to Liner	1
Durability	2
Impact to Travelling Public	3

Project Economics	4
Minimum Thickness	5
Contractor Experience	6
Project Schedule	7
Others: Fish Passage, Host Pipe Condition, Feasibility, and Benefit/Cost Ratio	8

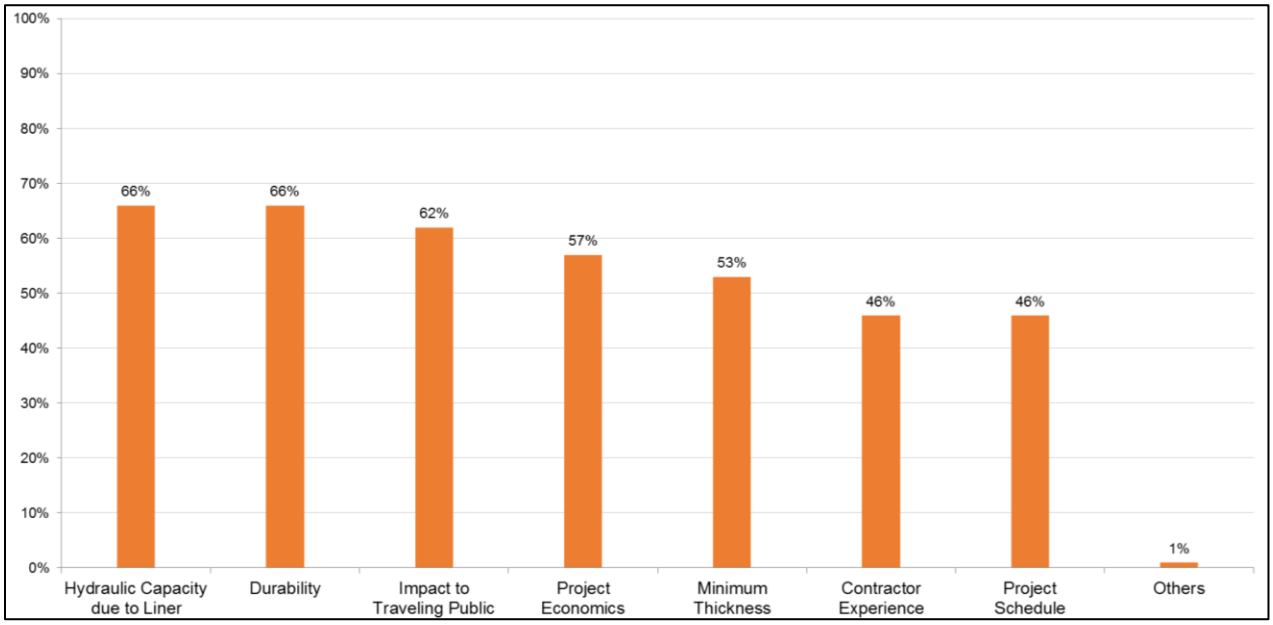


Figure 1-3. Decision making priorities for using SAPL in RCP culverts, (17 Respondents).

Table 1-2. Decision making priorities for using SAPL in CMP culverts with "1" highest priority, (20 Respondents).

Decision Making Priorities	Rank
Durability	1
Hydraulic Capacity Due to Liner	2
Impact to Travelling Public	3
Project Economics	4
Minimum Thickness	5
Contractor Experience	6
Project Schedule	7
Others: Fish Passage, Host Pipe Condition, Feasibility, and Benefit/Cost Ratio	8

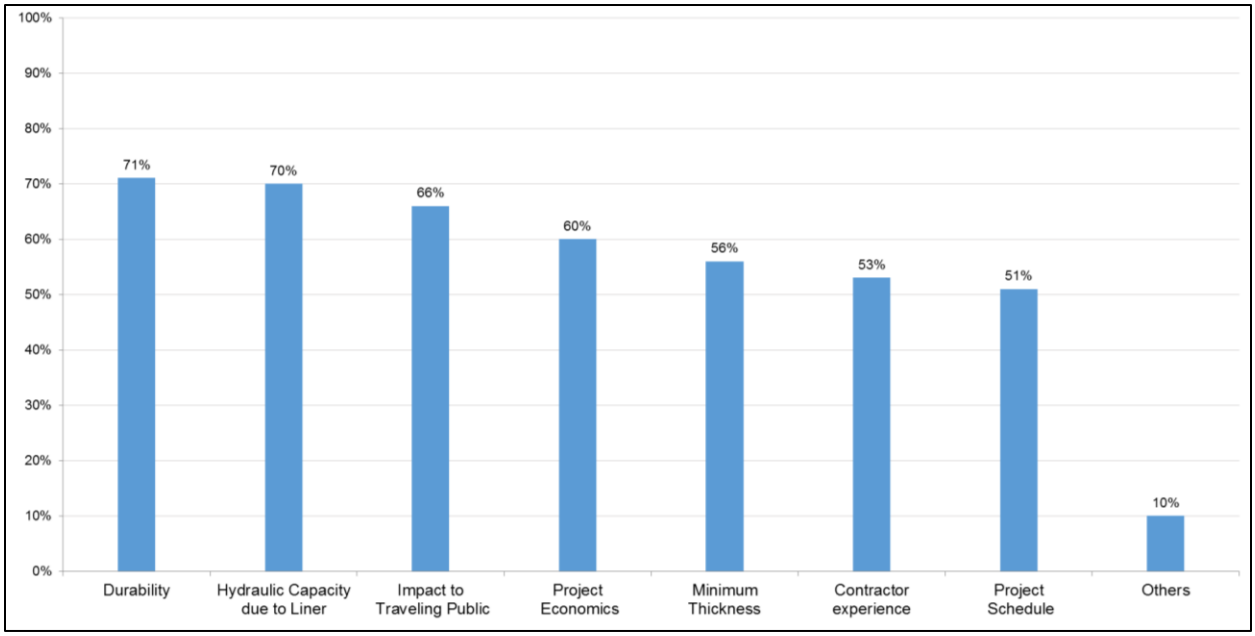


Figure 1-4. Decision making priorities for using SAPL in CMP culverts, (20 Respondents).

Question A.2 – The Main Reasons for Selecting a Structural SAPL

Table *1-3* and Table 1-4 present priorities selected by respondents for structural application of SAPL for RCP and CMP culverts, respectively. Figure 1-5 and Figure 1-6 illustrate the same information.

For RCP, respondents considered *longitudinal* and *circumferential cracking* as the most common problems for selecting a structural SAPL. *Invert loss or erosion*, *joint separation*, *delamination* and *spalling* are other important categories. Other factors stated include *environmental footprint* and *large diameter* culverts.

The most common CMP culvert problem to apply a structural SAPL is invert loss. Respondents ranked *invert loss* as the first issue for selecting SAPL and *access to culvert* as the second ranked parameter. Survey results show that 74% of the respondents ranked *deflection/ovality/flattening/racking* as the third reason. Respondents ranked *conservative design to avoid future failures* as the fourth reason. Additionally, respondents ranked other priorities which inluded *corrosion* and *environmental footprint*.

Table 1-3. Reasons for selecting a structural SAPL for RCP culverts with “1” highest priority, (17 Respondents).

RCP Culvert	Rank
Conservative Design to Avoid Future Failures	1
Longitudinal Cracking	2
Circumferential Cracking	3
Invert Loss/Erosion	4
Joint Separation	5
Delamination	6
Spalling	7
Access to Culvert	8
Others: Corrosion and Environmental Footprint	9

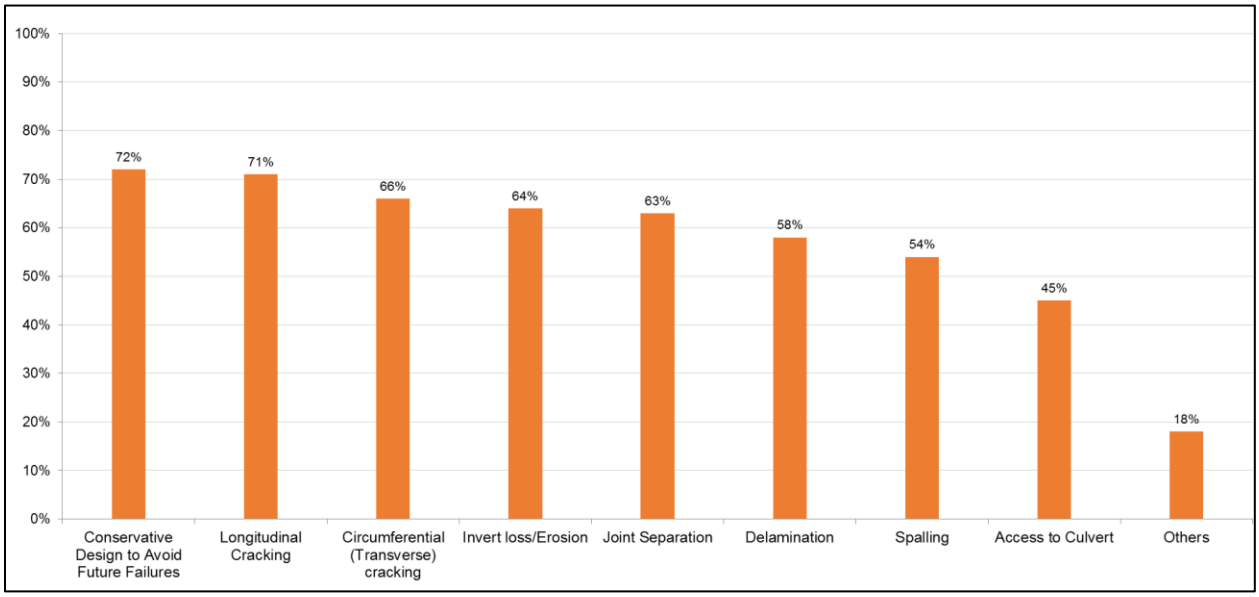


Figure 1-5. Reasons for selecting structural SAPL for RCP culverts, (17 Respondents).

Table 1-4. Reasons for selecting structural SAPL for CMP culverts with “1” highest priority, (13 Respondents).

CMP Culvert	Rank
Invert Loss	1
Access to Culvert	2
Deflection/Ovality/Flattening/Racking	3
Conservative Design to Avoid Future Failures	4
Abrasive Conditions	5
Others: Corrosion and Environmental Footprint	6

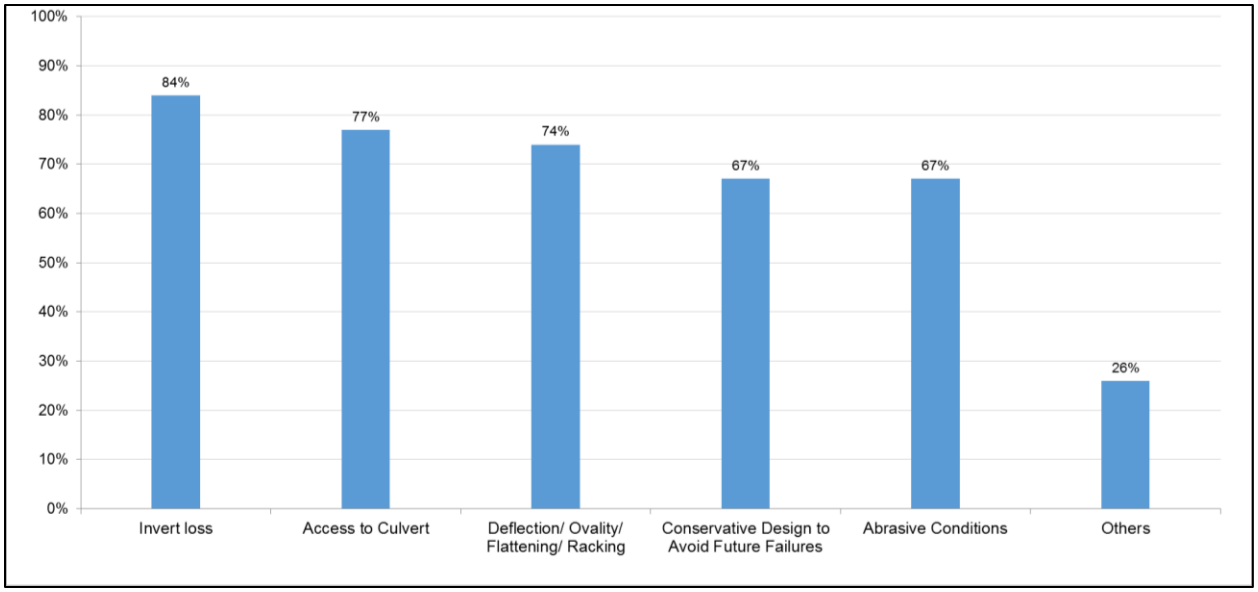


Figure 1-6. Reasons for selecting structural SAPL for CMP culverts (13 Respondents).

Question A.3 – Conditions for Considering a Culvert as a "Fully Deteriorated" Culvert (1 is the highest rank)

This question includes circular and arch RCPs and CMPs. Table 1-5 presents how respondents ranked conditions for a fully deteriorated culvert.

Table 1-5. Reasons for a culvert to be identified as fully deteriorated with "1" highest priority.

RCP				CMP	
Circular		Arch		Circular and Arch	
Issues	Rank	Issues	Rank	Issues	Rank
Longitudinal Cracking and Joint Separation	1	Longitudinal Cracking and Joint Separation	1	Corrosion at Invert	1
Erosion, Pop-outs and Delamination	2	Circumferential Cracking, Pop-outs and Delamination	2	Deflection/Ovality and Seam Defects/Cracks	2
Circumferential Cracking and Spalling	3	Erosion and Spalling	3	Abrasion	3
Corrosion	4	Corrosion, Abrasion and Honeycombs	4	-	-
Abrasion and Honeycombs	5	Scaling and Efflorescence	5	-	-
Scaling	6	-	-	-	-
Efflorescence	7	-	-	-	-

Question A.4 – Limitations of SAPL Due to Culvert and Site Conditions (19 Respondents)

Respondents considered the following general culvert conditions for both RCP and CMP:

- Size
- Shape
- Level of deterioration
- Hydraulic capacity
- Partially collapsed
- Host pipe condition related to its viability as a "form"
- Mostly shape (deflection) and alignment (joints)
- Past performance

Site Conditions for both RCP and CMP

- High ADT
- Utilities
- Detours
- Site access
- Manholes on each end (limited access)
- Environmental issues
- High groundwater and infiltration
- High bed load that could crack SAPL
- Flowing water and Aquatic Organism Passage (AOP)
- Deep cover and culvert no longer aligned as originally installed

Specific Conditions - RCP

- Joint separation or movement that is likely to continue.
- Large offset of joints.
- Collapsed pipe with longitudinal cracking.
- Cracks due to joint seperation.

Specific Conditions - CMP

- Significant deviation from original shape.
- Severe deflection/ovality.
- Completely rusted out on the bottom.

Questions A.5 and A.6 – Factors for Decision Making for SAPL Use

Figure 1-7, Figure *1-8*, Figure *1-9* and Figure *1-10* illustrate a comparison of using SAPL between cementitious and polymeric materials for circular CMP, arch CMP, circular RCP and arch RCP respectively.

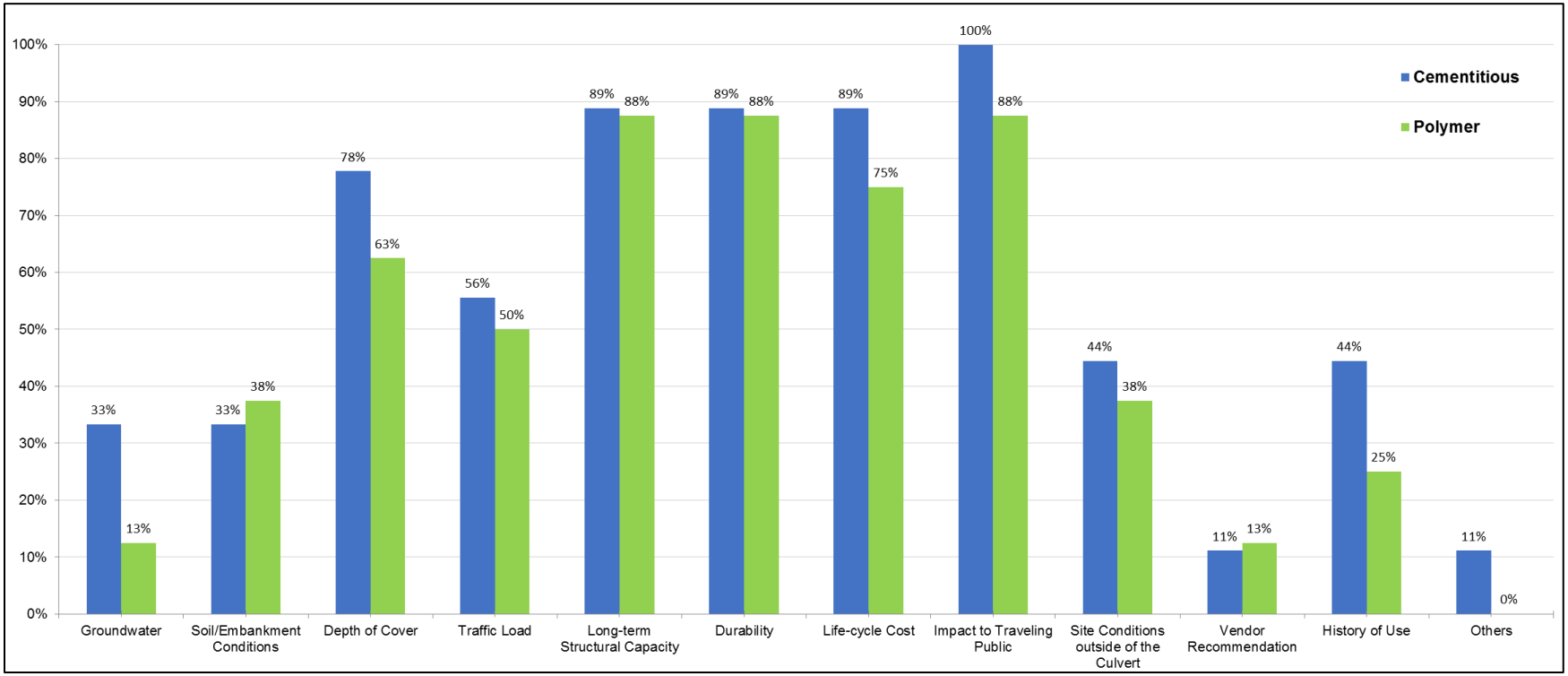


Figure 1-7. Factors influencing circular CMP,
(No. of Respondents: Cementitious = 8; Polymer = 8).

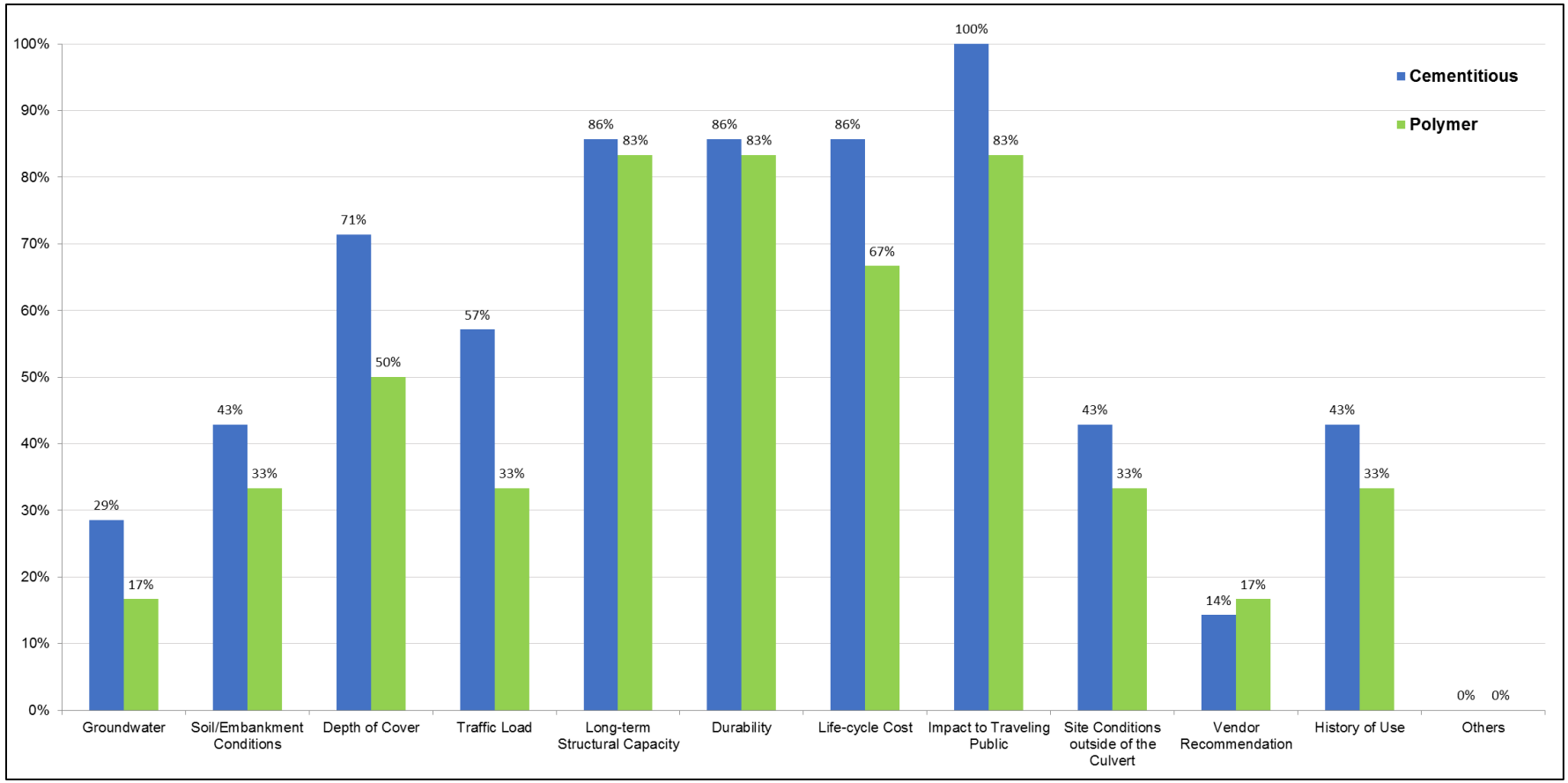


Figure 1-8. Factors influencing pipe arch CMP,

(No. of Respondents: Cementitious = 7; Polymer = 6).

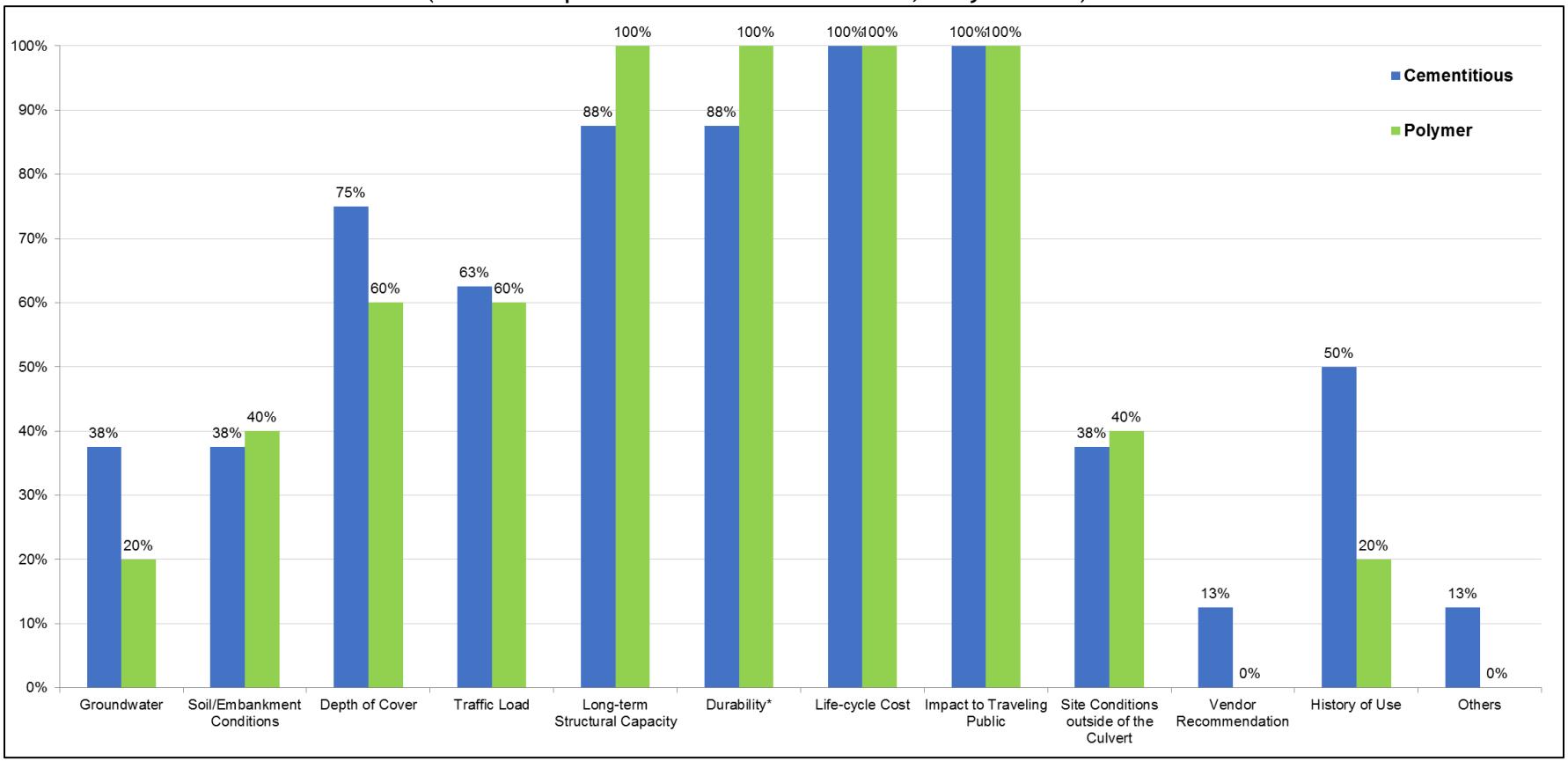


Figure 1-9. Factors influencing circular RCP.
(No. of Respondents: Cementitious = 7; Polymer = 5).

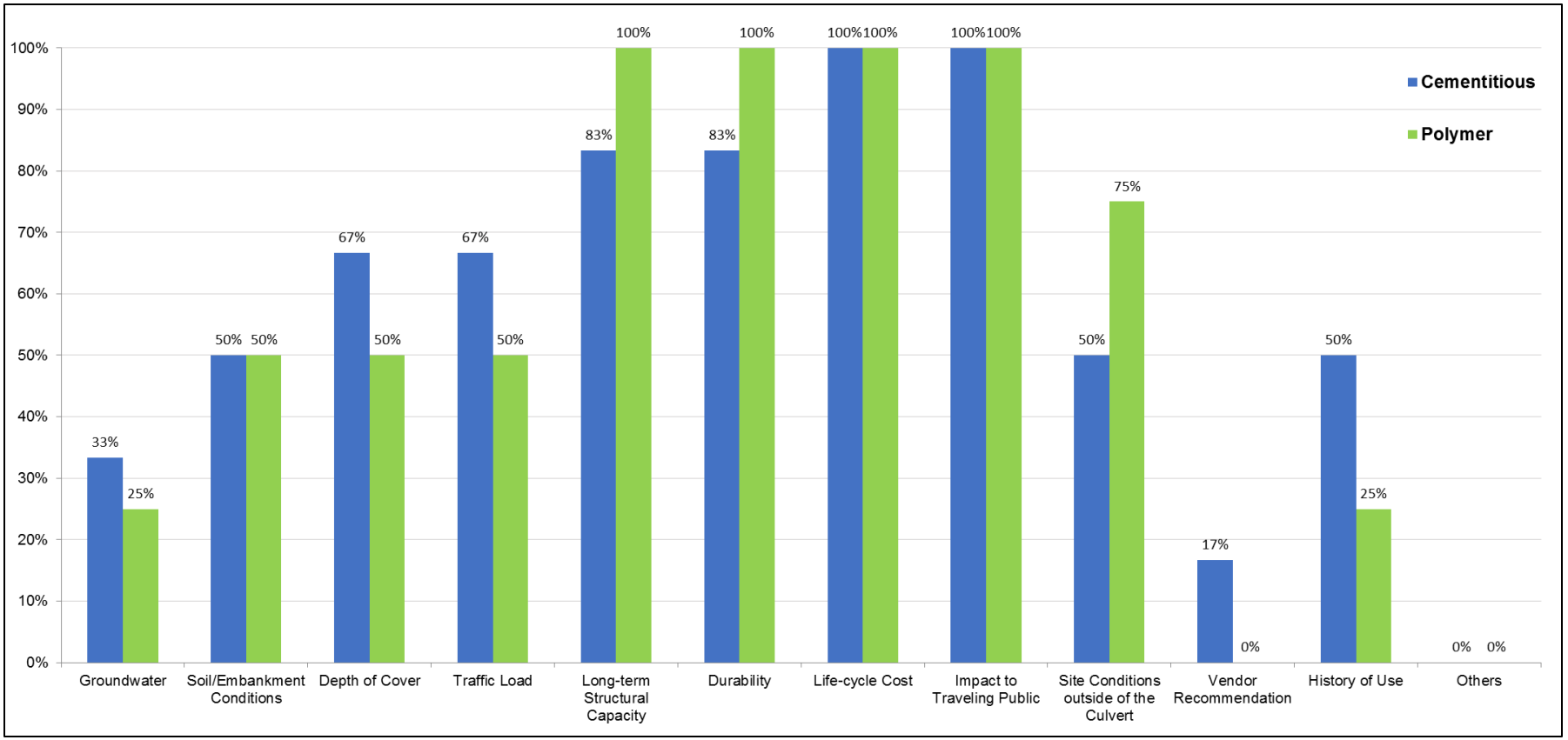


Figure 1-10. Factors influencing pipe arch RCP.
(No. of Respondents: Cementitious = 6; Polymer = 4).

Question A.7 – Percentage of Existing Culverts Based on Shape

Figure 1-11 illustrates that 86% of the existing culverts are circular and 14% are pipe arch shape.

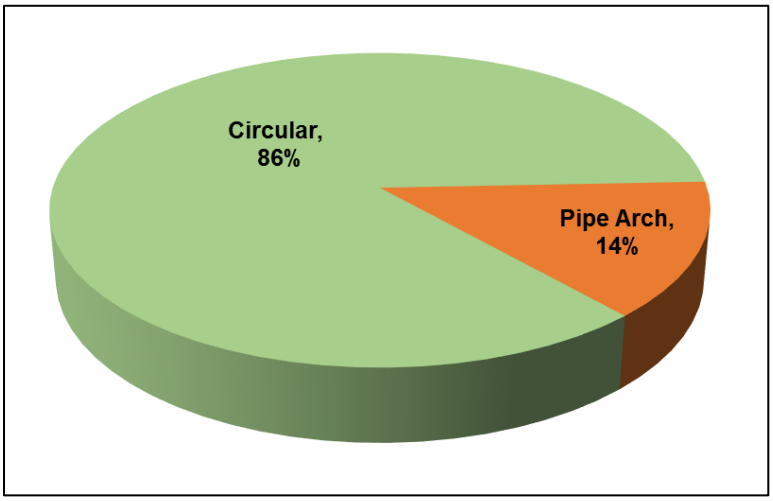


Figure 1-11. Percentage of existing culverts, (15 Respondents).

Question A.8 – Priority of Material Selection

Table 6 presents which SAPL material is more likely to be used.

Table 1-6. SAPL materials ranking (15 Respondents) with "1" highest priority.

Material	Rank
Cementitious	1
Geo-polymer	2
Polyurethane	3
Polyurea	4
Epoxy	4

Question A.9 – Prohibited Reinforcement Materials (14 Respondents)

Approximately 70% of the respondents answered *none* to this question; however, three of the DOTs had limitations on using cementitious SAPL materials (see Question A.10 below).

Question A.10 – SAPL Permitted Reinforcement Materials

Figure 1-12 illustrate permitted SAPL reinforcement material.

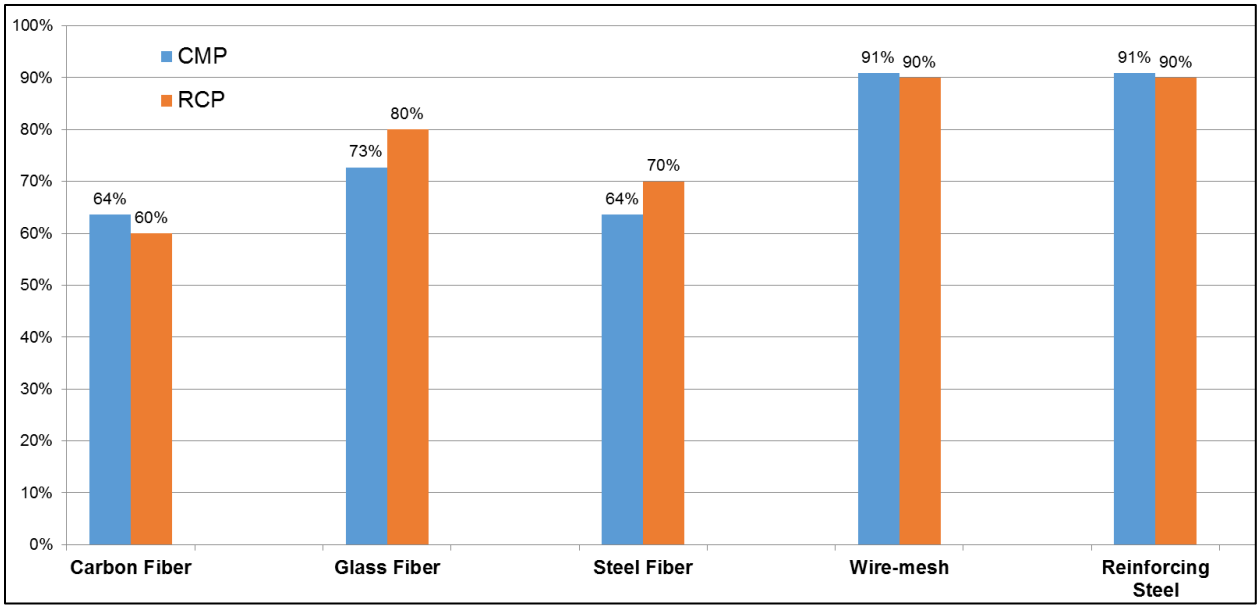


Figure 1-12. Permitted reinforcement material, (10 Respondents).

Question A.11 – Necessity of Considering Adhesion of SAPL with the Host Culvert for Structural Application

Figure 1-13 and Figure 1-14 illustrate what percentage of the respondents believe that adhesion of cementitious and polymer SAPLs to the host culvert is required in the design phase.

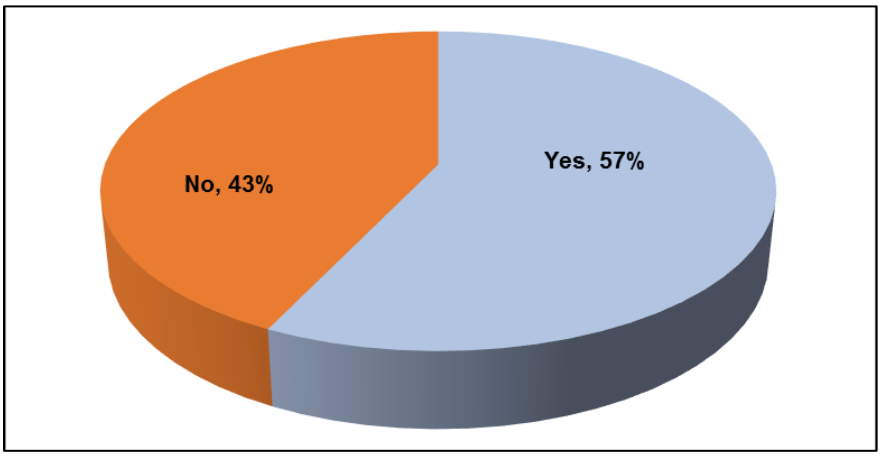


Figure 1-13. Required adhesion in cementitious materials, (15 Respondents).

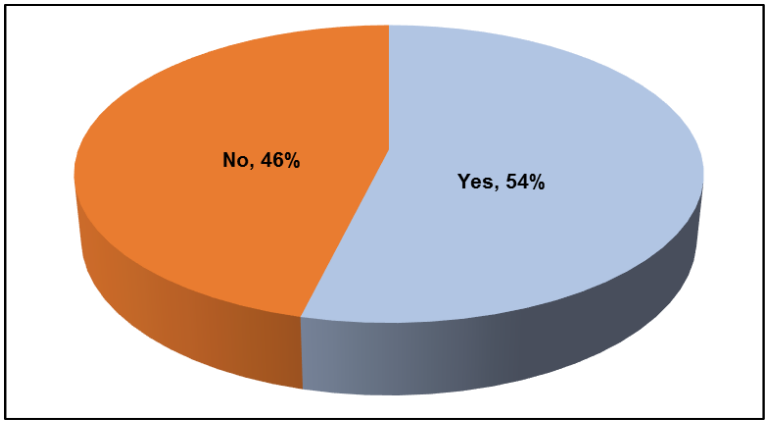


Figure 1-14. Required adhesion in polymeric materials, (14 Respondents).

Question A.12 – Minimum Thickness Requirements for SAPL

Figure 1-15 and Figure 1-16 illustrate what percentage of the respondents required a minimum thickness for cementitious and polymer SAPLs.

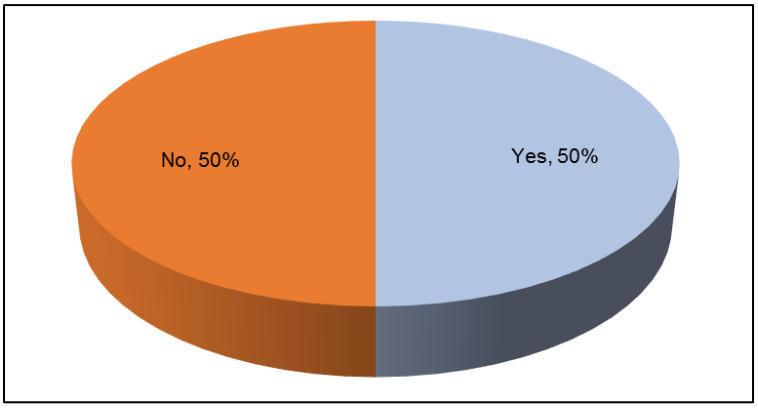


Figure 1-15. Minimum thickness requirement in cementitious material, (11 Respondents).

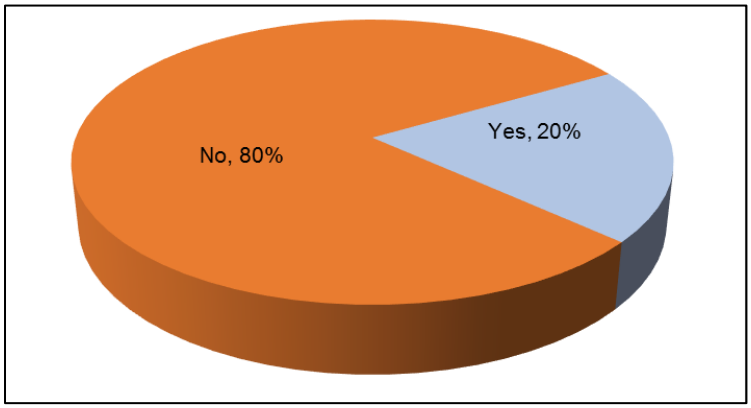


Figure 1-16: Minimum thickness requirement in polymeric material, (9 Respondents).

1.2. Part B – Considerations During SAPL Installations

Question B.1 – Type of Weather Conditions Prohibiting Installation of SAPL

According to respondents, during installation, when SAPL projects encounters cold weather, wetness and freeze/thaw conditions, cementitious material is prohibited and polymeric SAPLs are more resistant. In hot weather and humid conditions, cementitious SAPLs are considered to have a better performance and polymeric SAPLs are prohibited (Figure 1-17).

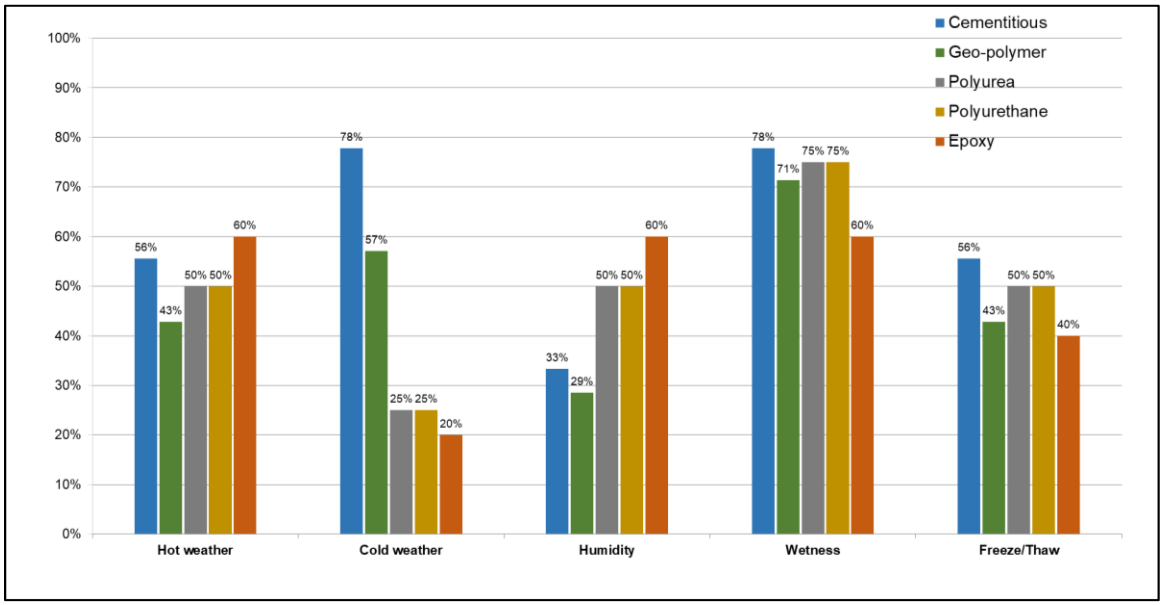


Figure 1-17. Prohibited weather conditions, (9 Respondents).

Question B.2 – Jurisdiction Having a Protocol for QA/QC of SAPL Installation, Testing and Inspection

Respondents provided the following comments for this question:

- "No. Looking for official direction on this - something in addition to what salesperson suggests."
- "For past installations, no to all. However, testing requirements are included in new contract special provision."
- "No QA/QC. Standards are under development. Until that time will be determined on a project by project basis and manufacturer-provided final material properties."
- "Not specifically. Standard construction specs must be met (installation, material, etc). Sites are reviewed regularly as part of our inspection program."

Question B.3 – Jurisdiction Having Additional Safety Protocols in Addition to OSHA Confined Space Entry (21 Respondents)

According to respondents, there are no additional safety protocols for SAPL projects; however, respondents used OSHA standard safety protocols.

1.3. Part C – Considerations After SAPL Installations

Question C.1 – Tools and Techniques to Measure the Thickness of SAPL (16 Respondents)

- Nails and cores (one respondent)
- Yardstick for thickness measurement (one respondent)
- Based on particular SAPL product (one respondent)

One respondent stated:

"The Contractor shall provide means necessary using depth gauges or other approved methods to check the thickness of the proposed lines in at least three locations around the inner surface of the pipe every twenty linear feet of pipe. Depth gauges may be left in place within the liner. These measurements must be written down in a log-book, which will be submitted to the department."

Twelve respondents stated that they did not use any tools.

Question C.2 – Type of Problems After SAPL Application (7 Respondents)
Cementitious:

- Longitudinal and circumferential cracking
- Hairline cracking with rust bleeding through cracks
- Cracking at joints
- Spalling
- Delamination
- Rough application
- Rust-through
- Slumping from ceiling
- Buildup of material due to poor installation
- Lack of uniform application
- Groundwater infiltration before cure time.
- Cracking and infiltration of groundwater through the centrifugally cast concrete pipe (CCCP) was observed approximately one year after installation

Geo-polymer:

- Leaking ground water
- Cracking at joints
- Spalling
- Delamination
- Rough application

- Rust-through
- Slumping from ceiling
- Buildup of material due to poor installation

Question C.3 – Expected SAPL Design Life

Figure 1-18 illustrates that the most probable design life is between 50 to 75 years.

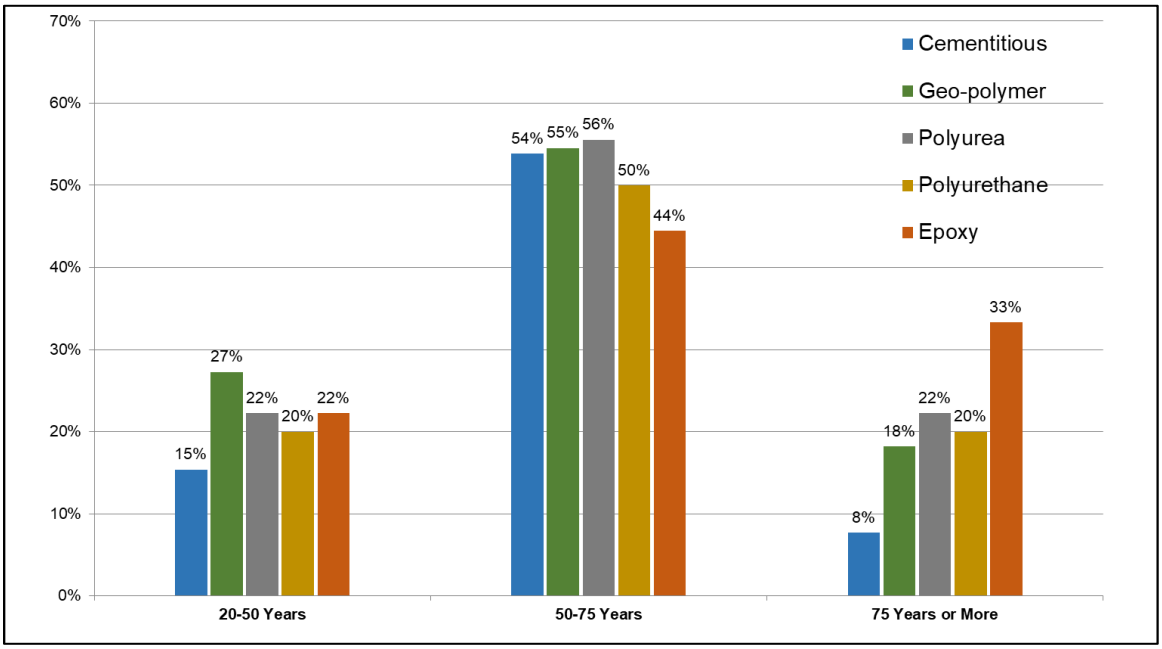


Figure 1-18. Expected design life, (17 Respondents).

Question C.4 – Additional Information Regarding the Experiences and Concerns with SAPLs (9 Respondents)

Respondents stated the following:

- "Structural capacity of liner is not defined by AASHTO design specification. Therefore, it cannot be load-rated in accordance with the MBE." (One Respondent)
- "Concerns with suppliers meeting spec/number of suppliers able to meet spec." (One Respondent)
- "Specifications being too stringent." (One Respondent)
- "Size limits." (One respondent)
- "Durability." (One Respondent)
- "I've been on site when SAPL is being used. I have seen the material not stick as it is supposed to ("*pipe not clean enough*" was the excuse given, also "*sprayed to heavy in this area*"). Generally, the soughing off occurred in the upper third of the pipe. The mixing of the product was sited another time as the issue with

lack of adhesion. In returning to these sites, it was noted that the structural integrity of the pipe was not enhanced, and the pipe had to be replaced, wasting the money and effort spent on lining." (One Respondent)

- "Structural capacity is the most important factor. We need a way to estimate minimum required liner thickness and to check structural designs submitted by Contractors." (One Respondent)
- "Concrete spray liner quality seems to be extremely dependent on installation quality. A few poor installations have been seen, that are starting to deteriorate after less than a year. Field offices continue to use concrete liners, but they are met with suspicion by the central office." (One Respondent)
- "Manufacturers have not yet provided data we need for structural design. No agreed structure design method. Vendors are not familiar with AASHTO design methods or structural design in general." (One Respondent)
- "A geo-polymer liner was specified for a large diameter pipe with a high fill depth. It was caught in construction and found to not meet the unique structural requirements of the site. The pipe was eventually replaced conventionally (open-cut)." (One Respondent)
- "At this time, the following minimum design conditions shall be considered if a culvert or storm sewer is lined by methods other than sliplining such as CIPP, cast or SAPLs (One Respondent):

  - Pipes 48-inch equivalent diameter and less can be verified by empirical analysis for structural capacity, stamped by a professional engineer registered in the state and submitted to the project for review 14 days prior to delivery of the material. The analysis should assume a fully deteriorated pipe. For CIPP systems the structural analysis for pipes under 48-inches shall be performed using Appendix XI from ASTM F1216-16 Standard Practice for Rehabilitation of Existing Pipelines and Conduits by the Inversion and Curing of a Resin-Impregnated Tube. For other non-traditional methods of culvert rehabilitation, such as cast or spray-on liners, a manufactured-recommended empirical analysis for structural capacity can be utilized.

  - Pipes larger than 48-inch equivalent diameter cannot be lined with spray, cast or similar liner systems. CIPP installations larger than 48-inch equivalent diameter require a site-specific numerical (finite-element) structural analysis that incorporates soil boring data from the site and any additional anticipated loadings from dead, live, or adjacent foundation sources, stamped by a professional engineer registered in the state and submitted to the project for review 30 days prior to the delivery of the material. It is recommended that a geotechnical subsurface investigation be performed during the design process and an initial liner analysis be performed by the design engineer to determine the feasibility of lining pipes greater than 48 inches in diameter using CIPP methods. The geotechnical subsurface investigation should provide the necessary level of detail to allow the accurate computational analyses of pipe lining design. The actual geology and site conditions will determine how many, and what spacing of, borings are required.

- Our environmental services section is also concerned with CIPP and SAPL liners. Liability during construction and from eventually disposal is a concern. Consideration is being given to submittal requirements that will allow the inventorying and classification of these liner materials."

1.4. Summary

DOTs preferred SAPLs due to less impact to traveling public compared with the other trenchless renewal methods; however, most of the respondents expressed concerns about SAPL structural capabilities. 60 % of the respondents have used cementitious materials. They preferred cementitious material to polymeric material due to their experiences.

CMP culverts with deteriorated inverts and RCP culverts with longitudinal cracking and joint separation are the most common reasons for considering a culvert as fully deteriorated. Results of survey show that the respondents expect to have an independent SAPL design methodology. Most of the respondents stated that they do not currently have SAPL construction guidelines and specifications.

Additionally, respondents stated that, during the installation, they prohibit cementitious SAPL if the project encounters cold weather, wetness and freeze/thaw conditions. They stated that in hot weather and humid conditions, cementitious SAPLs have better performance. They prohibited polymeric SAPLs in hot weather and humid conditions.

After installation, some respondents experienced longitudinal and circumferential cracking, hairline cracking with rust bleeding through cracks, cracking at joints, spalling, delamination, rough application (corrugation issues), rust-through, slumping from crown, buildup of material due to poor installation, lack of uniform application, groundwater infiltration before cure time, and leaking groundwater as previously stated in this report.

Appendix 1- A: Survey Form



Please save your document as you complete the survey

Introduction:

Spray Applied Pipe Lining (SAPL) inside a host culvert is used to renew deteriorated gravity storm water conveyance conduits (storm drains and culverts). This project will develop a structural design methodology for SAPL in gravity storm culverts for large diameter (up to 10 ft) Concrete Pipe (CP) and Corrugated Metal Pipe (CMP). The objective of this project is to develop design methodologies and equations for structural application of SAPL for Circular Pipe and Pipe Arch shapes with span larger than 36 inches. The funding commitment was achieved by DelDOT, FDOT, MnDOT, NCDOT, NYSDOT, ODOT, and PennDOT led by Ohio DOT.

This project is conducted by the Center for Underground Infrastructure Research and Education (CUIRE) (www.cuire.org) which is a research, education and outreach organization and is a part of the University of Texas at Arlington's (UTA's) Department of Civil Engineering.

Please submit your completed survey by Thursday, May 31th, 2018, to Ms. Cynthia Jones at the Ohio Department of Transportation (Ohio DOT), Phone: 614-466-1975, Email: cynthia.jones@dot.ohio.gov.

If you have any questions or concerns regarding this survey, please contact Mr. Jeffrey Syar, P.E., Administrator, Ohio DOT Office of Hydraulic Engineering, Phone: 614-275-1373, Email: Jeffrey.Syar@dot.ohio.gov; or Dr. Mo Najafi, P.E., Phone: 817-272-9177, Email: najafi@uta.edu, the Principal Investigator for this project.

Your assistance in completing this survey will be kept confidential. We will acknowledge your help in completing this survey in our final report, but we will not refer to your individual responses. Upon completion of this project, expected in December 2019, we will send you a copy of the final report.

We thank you in advance. **Please submit by May 31th**
Email: cynthia.jones@dot.ohio.gov

Contact Information

Respondent's Agency:	
Respondent's Name:	
Title:	
Phone Number:	
Email Address:	

Are you in charge of culvert renewal in your agency?

☐ Yes, *if yes, approximately how many culverts have been renewed by SAPL?*

☐ No, *please forward this to the appropriate subject matter expert within your agency.*

**All terms with "*" are defined in the Glossary section at the end of this survey*

Please save your document as you complete the survey

Part A. SAPL* BEFORE Installation

A.1. What are your decision making priorities when using a SAPL* (1 is high priority through 8 to less priority)?

Rank	Concrete Pipe Culvert	Rank	Corrugated Metal Culvert
--	Contractor experience	--	Contractor experience
--	Project Economics	--	Project Economics
--	Project Schedule	--	Project Schedule
--	Durability*	--	Durability*
--	Hydraulic Capacity due to Liner	--	Hydraulic Capacity due to Liner
--	Minimum Thickness	--	Minimum Thickness
--	Impact to Traveling Public	--	Impact to Traveling Public
--	Others *(please specify)*	--	Others *(please specify)*

Comments:	

A.2. Rank the main reasons for selecting fully structural SAPL* with "1" as the highest priority.

Rank	Concrete Pipe Culvert
--	Conservative Design to Avoid Future Failures
--	Longitudinal Cracking*
--	Circumferential (Transverse) cracking*
--	Invert loss/Erosion*
--	Joint Separation*
--	Delamination*
--	Spalling*
--	Access to Culvert
--	Other *(please specify)*

Rank	Corrugated Metal Culvert
--	Conservative Design to Avoid Future Failures
--	Deflection*/Ovality*/Flattening*/Racking*
--	Invert loss*
--	Abrasive Conditions*
--	Access to Culvert
--	Other *(please specify)*

Comments:	

**All terms with "*" are defined in the Glossary section at the end of this survey*

A.3. In what conditions do you consider the culvert "fully deteriorated*"? (Check as many as required)

Concrete Pipe Culvert			
Circular		Pipe Arch*	
☐	Longitudinal Cracking*	☐	Longitudinal Cracking*
☐	Circumferential (Transverse) Cracking*	☐	Circumferential (Transverse) Cracking*
☐	Corrosion*	☐	Corrosion*
☐	Joint Separation*	☐	Joint Separation*
☐	Erosion*	☐	Erosion*
☐	Pop-outs*	☐	Pop-outs*
☐	Abrasion*	☐	Abrasion*
☐	Honeycombs*	☐	Honeycombs*
☐	Scaling*	☐	Scaling*
☐	Delamination*	☐	Delamination*
☐	Spalling*	☐	Spalling*
☐	Efflorescence*	☐	Efflorescence*

Corrugated Metal Culvert			
Circular*		Pipe Arch*	
☐	Deflection*/Ovality*	☐	Deflection*/Ovality*
☐	Corrosion at Invert*	☐	Corrosion at Invert*
☐	Abrasion*	☐	Abrasion*
☐	Seam Defects/Cracks*	☐	Seam Defects/Cracks*

Comments:	

A.4. What existing Culvert Conditions and Site Conditions limit application of SAPL*?

	Concrete Pipe Culvert	Corrugated Metal Culvert
Culvert Conditions		
Site Conditions		

Comments:	

Please save your document as you complete the survey

A.5. What factors influence your decision to select a specific SAPL* material for Corrugated Metal Culvert? (Check as many as possible)

	Corrugated Metal Culvert			
	Circular		Pipe Arch	
	Cementitious	Polymer	Cementitious	Polymer
Groundwater	☐	☐	☐	☐
Soil/Embankment Conditions	☐	☐	☐	☐
Depth of Cover	☐	☐	☐	☐
Traffic Load	☐	☐	☐	☐
Long-term Structural Capacity	☐	☐	☐	☐
Durability*	☐	☐	☐	☐
Life-cycle Cost	☐	☐	☐	☐
Impact to Traveling Public	☐	☐	☐	☐
Site Conditions outside of the Culvert	☐	☐	☐	☐
Vendor Recommendation	☐	☐	☐	☐
History of Use	☐	☐	☐	☐
Others *(please specify)*		☐	☐	☐	☐

Comments:	

A.6. What factors influence your decision to select a specific SAPL* material for Concrete Pipe Culvert? (Check as many as possible)

	Concrete Pipe Culvert			
	Circular		Pipe Arch	
	Cementitious	Polymer	Cementitious	Polymer
Groundwater	☐	☐	☐	☐
Soil/Embankment Conditions	☐	☐	☐	☐
Depth of Cover	☐	☐	☐	☐
Traffic Load	☐	☐	☐	☐
Long-term Structural Capacity	☐	☐	☐	☐
Durability*	☐	☐	☐	☐

**All terms with "*" are defined in the Glossary section at the end of this survey*

Please save your document as you complete the survey

Life-cycle Cost				
Impact to Traveling Public				
Site Conditions Outside of the Culvert				
Vendor Recommendation				
Establish History of Use				
Others *(please specify)*				

Comments:	

A.7. Approximately what percentage of your existing culverts are Circular and Arch Pipe?

Shape of Culvert	Approximate Percentage (%)
Circular 	
Arch Pipe 	

Comments:	

A.8. Which material is more likely to be used for SAPL*? (Rank from one to five with one to be most likely)

1	--
2	--
3	--
4	--
5	--

Comments:	

**All terms with "*" are defined in the Glossary section at the end of this survey*

Please save your document as you complete the survey

A.9. Which SAPL* material is prohibited in your jurisdiction, if any? (Please Explain Below)

A.10. Which reinforcement material is permitted? (Check all that applies)

Culvert Type	Carbon Fiber*	Glass Fiber*	Steel Fiber*	Wire-mesh* (Worker Entry)	Reinforcing Steel (Worker Entry)	Other *(please specify)*
Corrugated Metal						
Concrete Pipe Culvert						

Comments:	

A.11. Do you consider adhesion of SAPL* with the host culvert necessary for structural application?

1	Cementitious*	--
2	Polymer*	--
3	Other *(please specify)*	

Comments:	

A.12. Do you have a minimum thickness requirement for SAPL*? (In SI Unit per mm)
If Yes, please answer the following options
If No, please go to the next question

Type of SAPL	Minimum Thickness
Cementitious*	--
Polymer*	--

Comments:	

**All terms with "*" are defined in the Glossary section at the end of this survey*

Please save your document as you complete the survey

Part B. SAPL* DURING Installation

B.1. What type of weather conditions prohibit installation of SAPL*? (Check as many as possible)

	Hot weather	Cold weather	Humidity	Wetness	Freeze/thaw	Others *(please specify)*
Cementitious*						
Geo-polymer*						
Polyurea*						
Polyurethane*						
Epoxy*						

Comments:	

B.2. Does your jurisdiction have a protocol for QA/QC of SAPL* installation, testing and inspection?

	Installation, Testing, Inspection, and Others	If yes, please provide a copy of link or email us the protocol (See note below).
Cementitious*	--	
Geo-polymer*	--	
Polyurea*	--	
Polyurethane*	--	
Epoxy*	--	

Note: Please attach a copy of your QA/QC protocol if no link is available.

Comments:	

B.3. Does your jurisdiction have additional safety protocols in addition to OSHA confined space entry? If yes, please provide a copy or link.

**All terms with "*" are defined in the Glossary section at the end of this survey*

Please save your document as you complete the survey

Part C. SAPL* AFTER Installation

C.1. Do you use any tools or techniques to measure the thickness of SAPL*?

○	Yes (random)
○	Yes (continuously)
○	No
If yes, *(please specify what type of equipment)*	

Comments:	

C.2. What type of problems do you face **AFTER** SAPL* application? If possible, specify the cause, location, and orientation (longitudinal, circumferential, etc.) of the defect such as cracks.

Material	Explanation
Cementitious*	
Geo-polymer*	
Polyurea*	
Polyurethane*	
Epoxy*	

Comments:	

C.3. What is your expected design life for the SAPL*?

Material	Years
Cementitious*	
Geo-polymer*	
Polyurea*	
Polyurethane*	
Epoxy*	

Comments:	

**All terms with "*" are defined in the Glossary section at the end of this survey*

Please save your document as you complete the survey

C.4. Additional information regarding your experiences and concerns with SAPL*:

Please make sure you save the file before submitting

If you have projects using SAPL that you would like to share with us, please email to Jeffrey.Syar@dot.ohio.gov or najafi@uta.edu. We would like to know successful and unsuccessful experiences.

Once again, we greatly appreciate your help in advance for completing this survey. We understand your time and efforts are valuable, however, your input and feedback will provide a comprehensive research that will help the transportation industry.

Please feel free to call or email us if you would like to provide your comments over the phone or email or would like to join this important pooled study (Jeffrey Syar, 614-275-1373, Jeffrey.Syar@dot.ohio.gov ; and Mo Najafi, 817-272-9177, najafi@uta.edu).

Please submit your survey **BY THURSDAY, MAY 31th**

Thank you again.

Please save your file and submit as an attachment to Ms. Cynthia Jones at Ohio Department of Transportation (Ohio DOT), Phone: 614-466-1975, Email: cynthia.jones@dot.ohio.gov

**All terms with "*" are defined in the Glossary section at the end of this survey*

Please save your document as you complete the survey

GLOSSARY

Abrasion	Abrasion is the gradual wearing away of the culvert wall due to the impingement of bed load and suspended material.
Carbon Fiber	A material consisting of thin, strong crystalline filaments of carbon, used as a strengthening material, especially in resins and ceramics.
Cementitious	Having the properties of a cement
Corrosion	It is a deterioration or dissolution of a material by a chemical or electrochemical reaction with its environment.
Corrugated Pipe	Pipe with ridges (corrugations) going around it to make it stiffer and stronger. The corrugations are usually in the form of a sine wave and are usually made of galvanized steel or aluminum.
Cracking	A fissure in an installed precast concrete culvert. - Circumferential (Transverse) cracking - Longitudinal cracking
Deflection	Change in diameter due to stress, temperature, time and other factors.
Delamination	Splitting apart of material into layers.
Durability	Ability to withstand wear, pressure, or damage.
Efflorescence	Efflorescence is a combination of calcium carbonate leached out of the cement paste and other recrystallized carbonate and chloride compounds. It is a white crystalline or powdery deposit on the surface of the concrete surface and is caused by water seeping through the culvert wall. The water dissolves salts inside the concrete surface, while moving through it, and then evaporates leaving the salts on the surface.
Erosion (Culvert)	Wearing or grinding away of culvert material by water laden with sand, gravel or stones; generally referred to as abrasion.
Fully Deteriorated	A culvert which has insufficient strength to support all soil and live loads.
Flattening	A critical decrease of vertical diameter due to loading that makes the circular shape similar to rectangular shape.
Geo-polymer	Geo-polymers are chains or networks of mineral molecules linked with co-valent bonds.
Glass Fiber	A strong plastic, textile, or other material containing embedded glass filaments for reinforcement.

**All terms with "*" are defined in the Glossary section at the end of this survey*

Honeycomb	Improper vibration of concrete leads to exposure of aggregate. This exposure of aggregate is called as honeycomb.
Host Culvert	An **e**xisting, old, or deteriorated culvert.
Invert-deteriorated	Progressive worsening of part of a culvert below the spring line that represents the lowest point in the internal cross section.
Joints	The means of connecting sectional lengths of culvert system into a continuous line using various types of joining materials.
Joint Failure	Failures which occur in the joints due to uneven bedding, poorly compacted backfilling operations, or unexpected settlements.
Joint Separation	Separation in joint that occurs due to failure in the type of joining material used.
Ovality	The difference between the maximum and mean diameter, divided by the mean diameter, or the difference between the mean and the minimum, divided by the mean. Expressed in percentage.
Partially Deteriorated	A culvert which may have displaced joints, cracks or corrosion, but is structurally able to support all soil and surface loads.
Polymer	A compound of high molecular weight derived either by the addition of many smaller molecules, as polyethylene, or by the condensation of many smaller molecules with the elimination of water, alcohol, or the like, as nylon.
Polyurea	The polymerization of isocyanates with polyamines result in the urea linkage. Generally, polyureas appear to have better elongation properties than polyurethanes; on the other hand polyurethanes provide more stiffness.
Polyurethane	Polyurethane is formed by reaction (or addition) of an isocyanate (-N=C=O) group with a hydroxyl (-OH) group or a polyol. This reaction is triggered by catalysts. Other typical components of the polyurethanes include cross linkers, surfactants, blowing agents, pigments, and fillers.
Popouts	Popouts are conical fragments that break out of the surface of the concrete leaving small holes
Racking	The movement of structural elements out of level or plumb by forces such as stress, material shrinkage or expansion.
Renewal	All aspect of upgrading with a new design life for the performance of existing culvert system. Includes rehabilitation, renovation, and replacement.
Repair	Reconstruction of short culvert lengths, but not the reconstruction of the whole culvert. Therefore a new design life is not provided. In contrast, in culvert renewal, a new design life is provided to existing culvert system.
Replacement	All aspects of upgrading with a new design life for the performance of the existing culvert. Includes rehabilitation and renovation.

Please save your document as you complete the survey

Scaling	Build-up of material on the inside portion of the culvert.
Seam Defects/Cracks	Defects and cracks at the joint of CMP.
Spalling	Breaking of part of culvert into small pieces.
Spring-line	(1) An imaginary horizontal line across the pipe that passes between the points where the pipe has its greatest cross-sectional width. (2) Midpoint of a pipe cross section (equal vertical distance between the crown and the invert of the pipe).
Steel Fiber	A material consisting of thin, strong crystalline filaments of steel, used as a strengthening material, especially in resins and ceramics.
Wire-mesh	A series of horizontal and vertical reinforcement welded together at a specific center-center distance

List of Acronyms

DelDOT	Delaware Department of Transportation
CMP	Corrugated Metal Pipe
CP	Concrete Pipe
CUIRE	Center for Underground Infrastructure Research and Education
FDOT	Florida Department of Transportation
MnDOT	Minnesota Department of Transportation
NCDOT	North Carolina Department of Transportation
NYSDOT	New York State Department of Transportation
ODOT	Ohio Department of Transportation
QA/QC	Quality Assurance / Quality Control
PennDOT	Pennsylvania Department of Transportation
SAPL	Spray Applied Pipe Lining

**All terms with "*" are defined in the Glossary section at the end of this survey*

Appendix 1-B:
Survey Respondents Contact Information

Acknowledgements

This survey was performed by the Center for Underground Infrastructure Research and Education (CUIRE) at The University of Texas at Arlington (UTA). Mr. Jeffrey Syar, P.E. Administrator, Ohio DOT Office of Hydraulic Engineering is the project leader and Dr. Mohammad Najafi (CUIRE at UTA) is the principal investigator. We are grateful to Ohio DOT, New York State DOT, North Carolina DOT, Minnesota DOT, Penn DOT, Delaware DOT and Florida DOT for funding this project and participating in this survey. We would like to thank the following members of U.S. DOTs and Canadian Agencies for providing feedback. We understand that their time was valuable, and we could not have accomplished this work without their input.

Jonathan Karam, Delaware DOT
Andrea Hendrickson, Minnesota DOT
Thomas K. Birnbrich P.E., Ohio DOT
Charles Smith, North Carolina DOT
Chad C. Ingram, P.E., Texas DOT
Kevin Riechers, Illinois DOT
Therese R. Kline, PE, Michigan DOT
Carlton D. Spirio, Jr., Florida DOT
Jerry Chaney, Utah DOT
Lee Tsiantis, South Carolina DOT
Mark Bailey, Indiana DOT
David Hedstrom, Montana DOT
Brian Carmody, New York State DOT
Robert Trevis, P.E., Oregon DOT
Nexa M. Castro, Pennsylvania DOT
Sven Scribner, Vermont DOT
Jason F. Moore, Georgia DOT
John Schuler, Virginia DOT
Michael Hogan, Connecticut DOT
Edward G. Lilla, P.E., Wisconsin DOT
Ted Kniazewycz, P.E., Tennessee DOT
Mitra Hashemieh, Louisiana DOT
Caroline Watt, Alberta Transportation
Christopher Carucci, New Hampshire DOT

Contact Information of Survey Questionnaire Respondents

Respondent's Agency:	**Delaware DOT**
Respondent's Name:	**Jonathan Karam**
Title:	Project Engineer
Phone Number:	302-760-2312
Email Address:	Jonathan.karam@state.de.us

Respondent's Agency:	**Indiana DOT**
Respondent's Name:	**Mark Bailey**
Title:	Office of Hydraulics Manager
Phone Number:	(317) 233-2096
Email Address:	mbailey1@indot.in.gov

Respondent's Agency:	**Minnesota DOT**
Respondent's Name:	**Andrea Hendrickson**
Title:	State Hydraulic Engineer
Phone Number:	(651) 366-4466
Email Address:	andrea.hendrickson@state.mn.us

Respondent's Agency:	**Montana DOT**
Respondent's Name:	**David Hedstrom**
Title:	State Hydraulic Engineer
Phone Number:	406-444-7961
Email Address:	dhedstrom@mt.gov

Respondent's Agency:	**New Hampshire DOT**
Respondent's Name:	**Christopher Carucci, PE**
Title:	Civil Engineer, Bureau of Highway Design, Specialty Section (Hydraulics)
Phone Number:	603-271-3252
Email Address:	christopher.a.carucci@dot.nh.gov

Respondent's Agency:	**New York State DOT**
Respondent's Name:	**Brian Carmody**
Title:	Professional Engineer
Phone Number:	518-457-4571
Email Address:	Brian.Carmody@dot.ny.gov

Respondent's Agency:	**Ohio DOT**
Respondent's Name:	**Thomas K. Birnbrich P.E.**
Title:	Bridge Hydraulic Engineer
Phone Number:	614-752-2974
Email Address:	tom.birnbrich@dot.ohio.gov

Respondent's Agency:	**Oregon DOT**
Respondent's Name:	**Robert Trevis, P.E.**
Title:	Culvert Engineering Program Lead
Phone Number:	503-986-3860
Email Address:	robert.e.trevis@odot.state.or.us

Respondent's Agency:	**North Carolina DOT**
Respondent's Name:	**Charles Smith**
Title:	Engineer, Hydraulics Unit
Phone Number:	919-707-6716
Email Address:	crsmith1@ncdot.gov

Respondent's Agency:	**Pennsylvania DOT**
Respondent's Name:	**Nexa M. Castro**
Title:	Senior Civil Engineer Supervisor
Phone Number:	717-705-6184
Email Address:	necastro@pa.gov

Respondent's Agency:	**Texas DOT**
Respondent's Name:	**Chad C. Ingram, P.E.**
Title:	Director of Construction, Paris District
Phone Number:	903-737-9207
Email Address:	chad.ingram@txdot.gov

Respondent's Agency:	**Vermont DOT**
Respondent's Name:	**Sven Scribner**
Title:	Bridge Maintenance Engineer
Phone Number:	(802) 522-8090
Email Address:	sven.scribner@vermont.gov

Contact Information of Survey Questionnaire Respondents

Respondent's Agency:	**Illinois DOT**
Respondent's Name:	**Kevin Riechers**
Title:	Policies and Standards Group Engineer
Phone Number:	(217) 782-9109
Email Address:	kevin.riechers@illinois.gov

Respondent's Agency:	**Georgia DOT**
Respondent's Name:	**Jason F. Moore**
Title:	District Seven Maintenance Manager (Metro Counties)
Phone Number:	770-216-3841
Email Address:	jason.moore@dot.ga.gov

Respondent's Agency:	**Michigan DOT**
Respondent's Name:	**Therese R. Kline, PE**
Title:	Flexible Pipe Specialist
Phone Number:	517-241-0082
Email Address:	klinet@michigan.gov

Respondent's Agency:	**Virginia DOT**
Respondent's Name:	**John Schuler**
Title:	Material Program Manager
Phone Number:	804-328-3140
Email Address:	john.schuler@vdot.virginia.gov

Respondent's Agency:	**Florida DOT**
Respondent's Name:	**Carlton D. Spirio, Jr.**
Title:	State Drainage Engineer
Phone Number:	(850) 414-4351
Email Address:	carlton.spirio@dot.state.fl.us

Respondent's Agency:	**Connecticut DOT**
Respondent's Name:	**Michael Hogan**
Title:	Transportation Supervising Engineer
Phone Number:	860-594-3241
Email Address:	michael.hogan@ct.gov

Respondent's Agency:	**Utah DOT**
Respondent's Name:	**Jerry Chaney**
Title:	Senior Hydraulics Engineer
Phone Number:	801 633-6218
Email Address:	jchaney@utah.gov

Respondent's Agency:	**Wisconsin DOT**
Respondent's Name:	**Edward G.Lilla, PE**
Title:	Statewide Drainage Engineer
Phone Number:	608-266-2312
Email Address:	edward.lilla@dot.wi.gov

Respondent's Agency:	**South Carolina DOT**
Respondent's Name:	**Lee Tsiantis**
Title:	Maintenance Contracts Manager
Phone Number:	803-737-1290
Email Address:	tsiantisls@scdot.org

Respondent's Agency:	**Tennessee DOT**
Respondent's Name:	**Ted Kniazewycz, P.E.**
Title:	Director - Structures Division
Phone Number:	615-741-3351
Email Address:	ted.kniazewycz@tn.gov

Respondent's Agency:	**Alberta Transportation**
Respondent's Name:	**Caroline Watt**
Title:	Bridge Planning Specialist
Phone Number:	7804151013
Email Address:	caroline.watt@gov.ab.ca

Respondent's Agency:	**Louisiana DOT**
Respondent's Name:	**Mitra Hashemieh**
Title:	Hydraulic Design Engineer Administrator
Phone Number:	(225)379-1482
Email Address:	mitra.hashemieh@la.gov

This Page Left Intentionally Blank.

Chapter 2
Literature Review

CHAPTER 2 - LITERATURE REVIEW

2.1. Introduction and Background

Drainage infrastructure systems including culverts, storm sewers, outfall and related drainage elements represent an integral portion of Department of Transportations' assets that routinely require inspection, maintenance, repair, and renewal. According to ASCE Infrastructure Report Card (2017), illustrated in Figure 2-1, America's cumulative infrastructure grade is D+, which means the condition and performance is in a poor quality and needs investments and improvements. Failure of these systems is costly for DOTs both directly due to the replacement of the failed system and indirectly due to the time and money and even in some cases lives lost for commuters. Further challenges are the variety in material types, shapes, backfill materials, types of roads, wide geospatial distribution and environmental exposures that makes every single culvert unique (Najafi et al, 2008). Therefore, drainage infrastructure systems need special attention in terms of proactive/preventive asset management strategy.

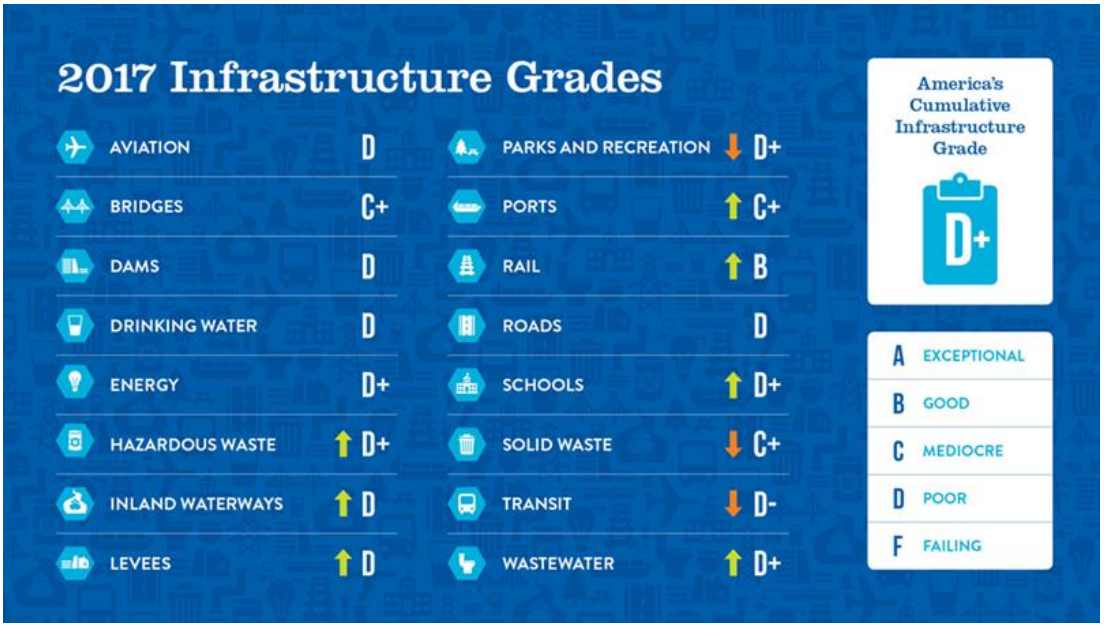


Figure 2-1. American society of civil engineers' report card for America's infrastructure (2017).

2.1.1. Culverts and Storm Sewers

Culverts and storm sewers are important components of highway infrastructures. Corrugated metal pipes (CMPs) and reinforced concrete pipes (RCPs) are commonly used as culverts in the United States (Darabnoush Tehrani et al. 2019). Assessment and Rehabilitation of Existing Culverts by the National Cooperative Highway Research Program (NCHRP), Synthesis 303, defines storm sewers as any "structure used to convey

storm runoff where storm sewers and storm drains are connected, that sometimes called a pipe or culvert". Culvert is a structure that conveys water or forms a passageway through an embankment (Najafi and Gokhale 2005).

According to the federal highway administration (FHWA), the United States has approximately 4.12 million miles (6.63 million kilometers) of roadways, making it the largest in the world with millions of culverts hidden underneath. The Culvert Management Manual by the Ohio Department of Transportation (ODOT) defines culverts as "any structure that conveys water or forms a passageway through an embankment and is designed to support a super-imposed earth load or other fill material plus live loads (even though they may support traffic loads directly) with a span, diameter, or multi-cell (with a total span) less than 10 ft (3.1 m) when crossing the centerline of the roadway," as shown in Figure 2-2 (ODOT 2018).

Culverts are designed to withstand soil overburden, pavement and traffic loadings. Among different types of culverts, Corrugated Metal Pipes (CMPs) are the most common in the United States, however, they are exposed to abrasion and corrosion damage (Arnoult 1986). Many culverts in the United States have reached their service life and need to be repaired, renewed, or replaced (Wyant 2002).

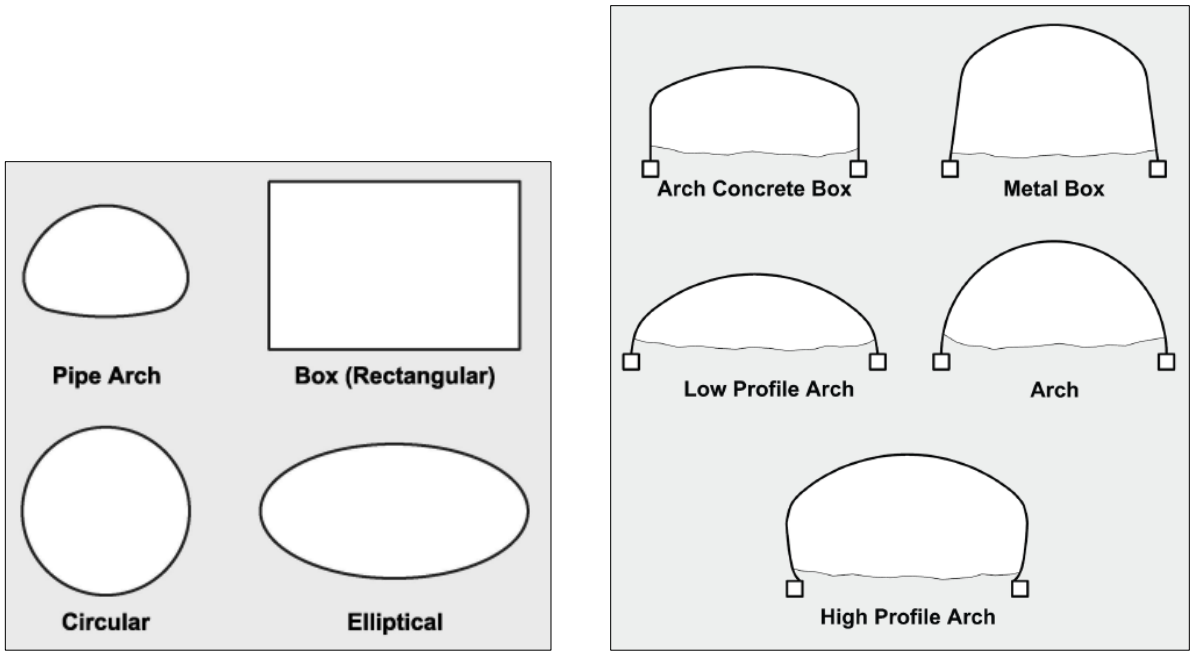


(a) (b)

Figure 2-2. Corrugated metal pipe culverts (CMPs): (a) multi-cell CMPs (Source: Contech) and (b) invert deteriorated CMP (Source: Metal Culverts, Inc.).

2.1.1.1. Culvert Shapes

Culverts are available in variety of shapes for both, closed conduits, and open-bottom conduits. The most common shapes for closed conduits are circular, box (rectangular), elliptical, and pipe-arch, as illustrated in Figure 2-3 (a). Open-bottom culverts are mostly found in an arch configuration, as illustrated in Figure 2-3 (b). These typical culvert shapes have the same material on the entire perimeter (FHWA 2012).



(a) (b)

Figure 2-3. Commonly used culvert shapes: (a) closed conduit culvert shapes, and (b) open-bottom culvert shapes (FHWA 2012).

2.1.1.2. Culvert Materials

According to the Culvert Management Manual by Ohio Department of Transportation (ODOT 2018), the most commonly used culvert materials are plain or reinforced concrete, corrugated metal (aluminum or steel), verified clay, cast or ductile iron, aluminum alloy, brick, field tile (clay), corrugated plastic, steel casing, stone, timber, polyvinyl chloride (PVC) and high-density polyethylene (HDPE), as illustrated in Figure 2-4. The selection of a culvert material may depend upon structural strength, hydraulic roughness, durability (corrosion and abrasion resistance) and constructability (FHWA 2012).





Figure 2-4. Culvert materials (ODOT 2018).

2.1.1.3. Culvert Hydraulics and Flow Conditions

Culverts may flow partly full (free surface flow or open channel flow), or full over the entire length (full flow or pressure flow), which rarely happens. Water surface profile calculations determine the flow level in the culvert barrel (FHWA 2012). Froude number, F_r (dimensionless), determines the appropriate flow regime, as presented in Equation 2-1.

$$F_r = \frac{V}{\sqrt{gy}} \qquad \text{Eq.2-1}$$

Where,

v the average velocity of flow, ft/s,
g the gravitational acceleration, ft/s^2, and
y a representative depth, ft, (typically the equivalent depth in circular sections or the hydraulic depth for other shapes).

In circular sections, the equivalent depth is the square root of one-half of the cross-sectional flow area $(A/2)^{0.5}$ and for other shapes the hydraulic depth is cross-sectional flow area divided by the width of the free water surface (A/T). By evaluating the Froude number, three flow regimes are defined as subcritical, critical, and supercritical. The flow is considered subcritical and is characterized as tranquil if the Froude number, F_r is less than 1, and is called critical if Froude number, F_r is equal to 1. The flow is called supercritical and is characterized as rapid if the Froude number, F_r is greater than 1. For a culvert in a partly full flow condition, as illustrated in Figure 2-5, the subcritical flow exists in the upstream channel, the critical depth occurs at the inlet location and the supercritical flow in the culvert barrel (FHWA 2012).

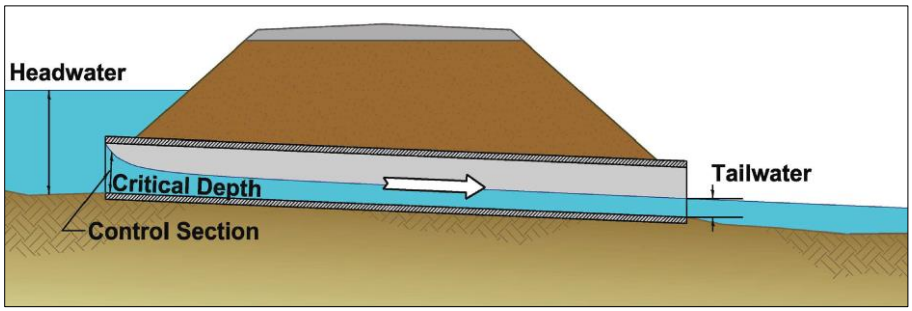


Figure 2-5. Typical "inlet control" flow section for a partly full culvert (FHWA 2012).

2.1.1.4. Types of Flow Control

A culvert capacity is affected by its shape, geometry, skew angle of inlet, and most importantly the inlet edge configuration. Two types of flow control in a culvert are called inlet control and outlet control.

2.1.1.4.1. Inlet Control

The culvert is called "inlet control" flow condition if its barrel can convey more flow than the inlet will accept. The critical depth for an inlet control culvert occurs at entrance, as illustrated in Figure 2-5. In the inlet control condition, the culvert capacity is not impacted by downstream hydraulic characteristics.

2.1.1.4.2. Outlet Control

The culvert is called "outlet control" flow condition if its barrel capacity is not enough to convey as much flow as the inlet will receive. In an outlet control flow condition, the culvert capacity is determined by its geometry, hydraulic characteristics, and the elevation of water surface at the outlet. In an "outlet control" flow condition, the control section is located at the culvert downstream, as illustrated in Figure 2-6.

Full flow culverts (pressure flow) or subcritical flow culverts are considered as outlet control conditions (FHWA 2012; Wisconsin DOT 1997).

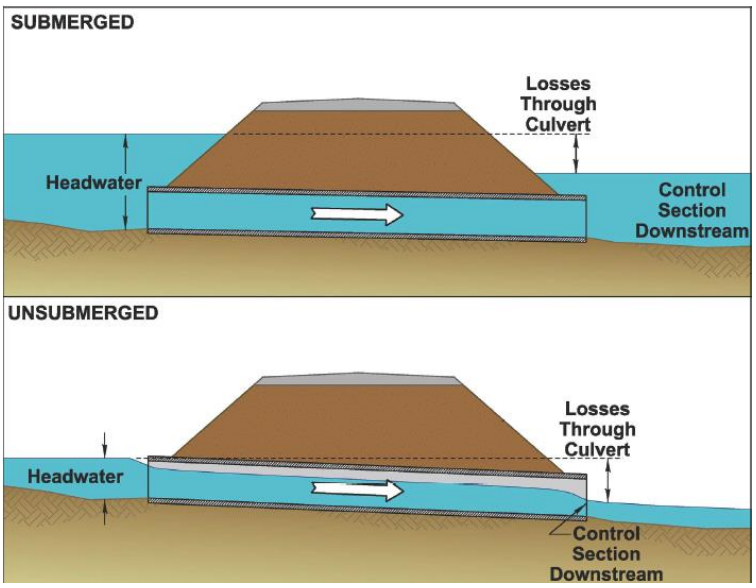


Figure 2-6. Typical "outlet control" flow in both full flow (submerged) and partly full flow (unsubmerged) conditions (FHWA 2012).

2.1.1.5. Culvert Structural Behavior

Buried conduits obtain their structural capacity to withstand the imposed loads from two sources (Spangler 1960):

(a) The inherent strength of the pipe to bear the external pressures.
(b) The lateral pressure of the soil at the pipe sides.

Pipe culverts structurally can be classified as flexible and rigid, based on material type and how they perform when installed (Hydraulics Manual M 23-03.06 2019). A proper backfill is required for both flexible and rigid pipes to allow the load transfer from the pipe to the soil. Flexible pipes under loading deflect against the backfill, and the load is transferred to and carried by the backfill. In case of rigid pipes under loading, the load is transferred through the pipe wall into the bedding material (Omara 1997).

2.1.1.5.1. Flexible Pipe

Flexible pipes are made of materials such as corrugated metal or thermoplastic. Flexible pipes can be flexed or distorted significantly without cracking (Hydraulics Manual M 23-03.06 2019). A flexible culvert is a composite structure of culvert barrel and the surrounding soil (Najafi 2008). Proper soil support is an important element to the flexible culvert structural performance. Soil support degradation and embankment settlement can occur due to soil erosion and scour through the culvert voids, poor backfill material, inadequate compaction, lack of headwall or cutoff walls in granular soil types and insufficient surface drainage design (FHWA 2012). Flexible pipes under

loading attempt to deflect. In case of a circular flexible pipe under loading, the vertical diameter decreases, and the horizontal diameter increases, as shown in Figure 2-7. Soil pressure resists the increase in horizontal diameter of a flexible pipe due to loading. The thrust force can be calculated, based on the diameter of the pipe and the load placed on the top of the pipe.

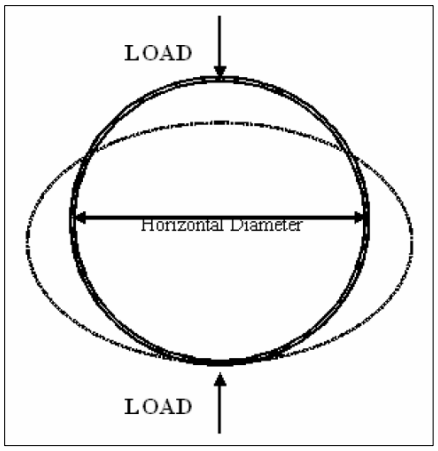
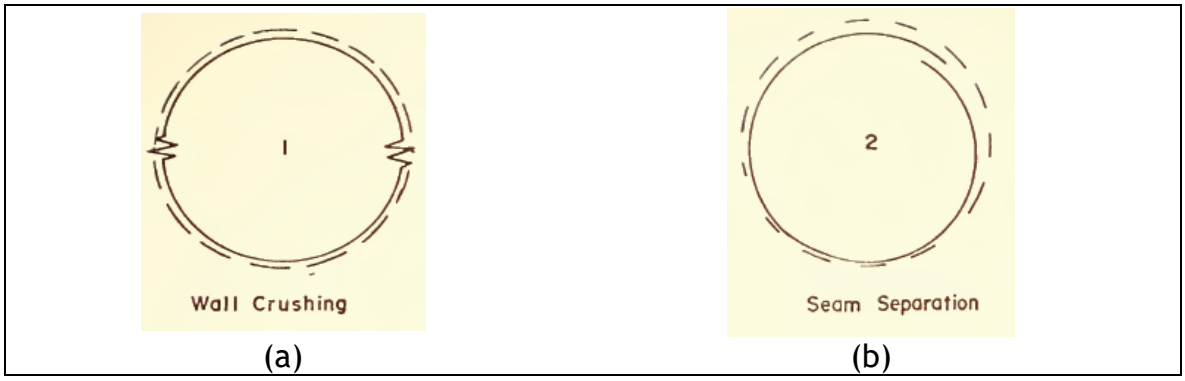


Figure 2-7. Deflection of a circular flexible pipe (Najafi 2008).

2.1.1.5.1.1. Flexible Pipe Modes of Failure

Flexible conduits, as illustrated in Figure 2-8 are designed to withstand five primary modes of failure including:

1) Wall crushing (compressive stress due to circumferential thrust exceeds the yield stress),
2) Separation of seams (thrust exceed the seam strength),
3) Initial buckling (elastic state of stress),
4) Inelastic buckling, and
5) Excessive deflection or flattening (plastic yielding under combined compressive and bending stresses) (Leonards and Stetkar 1978).



(a) (b)

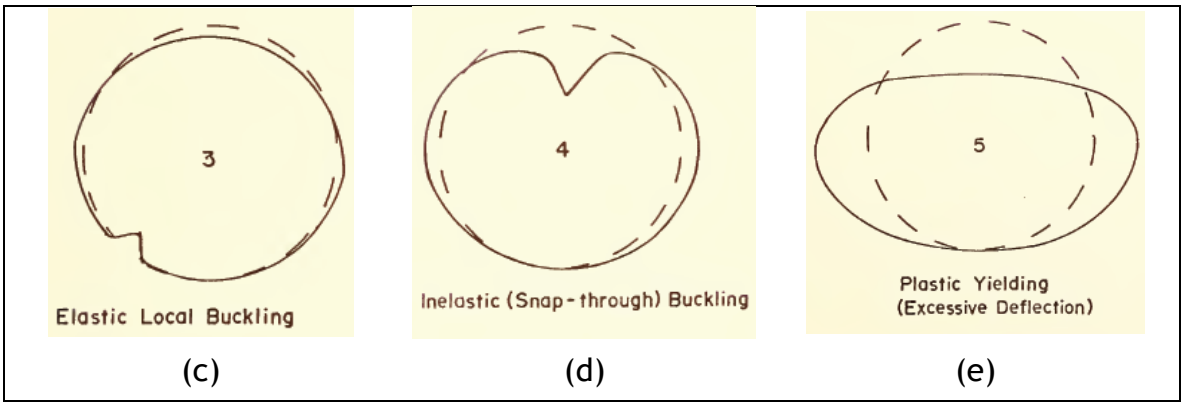


Figure 2-8. Failure modes of flexible conduits: (a) wall crushing, (b) seam separation, (c) elastic local buckling, (d) inelastic (snap-through) buckling, and(e) plastic yielding (excessive deflection) (Leonards and Stetkar 1978).

For the first two modes of failures, the magnitude of circumferential thrust can be less impacted by the soil properties or pipe stiffness. For initial buckling, inelastic buckling and excessive modes of failures, the pipe bending stress is impacted by soil properties and pipe stiffness.

Elastic Buckling

Elastic buckling of flexible conduits can occur in a high mode with many waves around the pipe circumference, or in a low mode with a small number of waves around the entire circumference. Elastic local buckling can occur with a crimp or crease in a small portion of the pipe circumference. A flexible conduit due to the residual stresses and geometric imperfection can exhibit different types of elastic buckling which cannot be easily distinguished by visual inspection (Leonards and Stetkar 1978).

Inelastic Buckling

Inelastic buckling of a flexible conduit wall occurs in a low mode after passing the plastic yielding point. Snap-through buckling of a flexible conduit can manifest itself as a sudden inversion or curvature reversal in the pipe wall that can results in instability. Local buckling of a flexible conduit wall may not immediately results in instability (Leonards and Stetkar 1978).

2.1.1.5.1.2. Buckling Theories of Cylindrical Shells or Rings

Shell elements are used to model structures in which one dimension, the thickness, is significantly smaller than the other dimensions. The thickness of a cylindrical shell element is very small compared with the radii of curvature. The following have presented different theories regarding buckling of cylindrical shells or rings:

- **Timoshenko and Gere 1961** (Elastic Buckling in High Modes)

Buckling of buried flexible conduits was modeled by a circular ring subjected to a uniform hydrostatic external pressure and the critical external normal pressure, p, was derived by Timoshenko and Gere (1961) and given as Eq. 2-2 .

$$P_c = \frac{EI(n^2-1)}{R^3} \qquad \text{Eq. 2-2}$$

Where,

E Young's modulus, psi,

I moment of inertia of ring wall, in.^{4}/in.

R radius, in.

n buckling mode $=\frac{\pi R}{l}$, where l = half wavelength of the buckled shape.

The Eq. 2-2 is resulted from the equilibrium of a deformed ring element in which only circumferential stresses were considered by Timoshenko and Gere. In this equation nonlinear deflection terms were neglected (Leonards and Stetkar 1978).

- **Klöppel and Glock 1970** (Elastic Local Buckling)

For flexible steel pipes, vertical deflection to a magnitude of 20% of the pipe diameter results in conduit instability (Spangler 1941). Spangler stated that using a safety factor of 4, limits the permissible vertical deflection to 5 percent of the pipe diameter that is a criterion in culvert design.

The instability of initially deflected buried flexible conduits was developed by Kloppel and Glock (1970). Two interaction zones at the crown (upper portion of the conduit wall) and springline (lower portion of the conduit wall) of the flexible buried conduits are introduced by them. At the upper portion interaction zone, the pipe wall is subjected to active earth pressure and deflects away from the surrounding soil. At the lower portion interaction zone, the pipe wall is subjected to the passive pressure and deflects or presses into the surrounding soil. An instability is most probable to occur at the crown or upper portion interaction zone due to a reduction in the soil support (Klöppel and Glock 1970; Leonards and Stetkar 1978). Kloppel and Glock (1987) modeled the upper portion interaction zone of a buried flexible conduit wall by a hinged arch with circumferential radial elastic soil support $\left[\frac{E_S}{R(1+\nu_S)}\right]$ as well as tangential (K_T) and rotational (K_R) elastic soil support at hinges that are restrained by the lower section of conduit (Leonards and Stetkar 1978). The developed model by Kloppel and Glock considered:

i. Elliptical flexible conduits as well as circular flexible conduits,
ii. Friction at the conduit-soil interface,
iii. Non-uniform radial pressures having a maximum value at the crown (hence, buckling was always initiated at the crown),
iv. Modulus of soil restraint either constant or stress-level dependent,
v. Symmetric displacements prior to buckling,

vi. The influence of a plastic hinge at the crown.

The horizontal active pressure at the springline was given by Eq. 2-3.

$$P_{springline} = P_S \lambda \qquad \text{Eq. 2-3}$$

Where,
P_S the vertical crown pressure (overburden pressure + live load pressure), psi, and
λ coefficient of active earth pressure (commonly λ=0.5).

The active radial pressure distribution around the conduit circumference, as illustrated in Figure 2-9 (a), was expressed by Eq. 2-4.

$$P = P_S \cos\left[\frac{\pi}{2}.\frac{\psi}{\psi_B}\right] \qquad \text{Eq. 2-4}$$

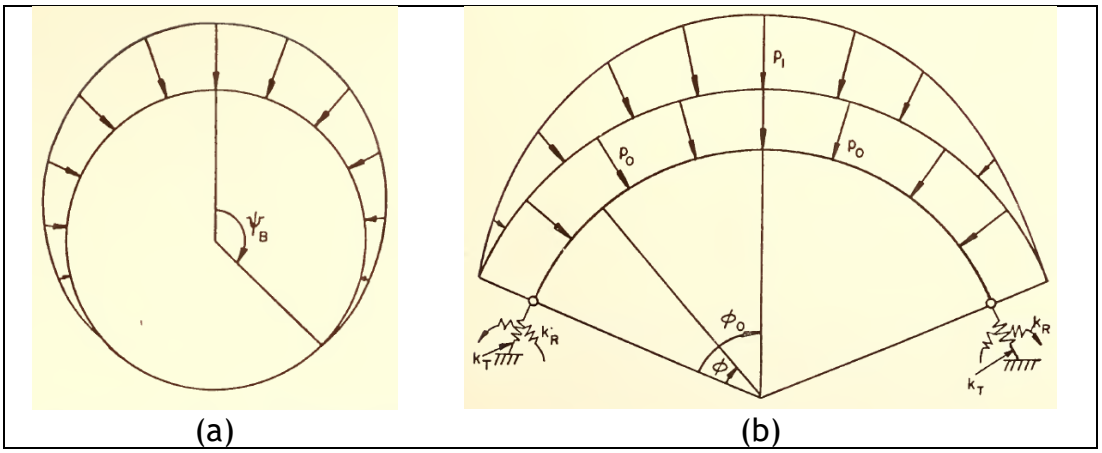
$$\psi_B = \frac{\pi^2}{4\cos^{-1}\lambda} \qquad \text{Eq. 2-5}$$

Assuming the common value of λ = 0.5, the ψ_B will be equal to $\frac{3\pi}{4}$ radians.

To solve the instability issue, an arch section of the conduit (defined by 2 $\emptyset_o$), as illustrated in Figure 2-9 (b), was analyzed by Kloppel and Glock. The provided restraint by the bottom portion of the conduit was introduced by rotational (K_R) and tangential (K_T) elastic moduli at the arch supports. The boundary pressure distribution around the conduit circumference on the arch section was divided into a uniform pressure of P_O, and a nonuniform pressure of P_1, as described in Eq. 2-6.

$$P = P_O + P_1 \sin\left[\frac{\pi}{2}.\frac{\phi}{\phi_O}\right] \qquad \textit{Eq. 2-6}$$

Where,
$P_O = P_S \cos\frac{\pi\emptyset_O}{2\psi_B}$, and
$P_S = P_O + P_1$ = vertical overburden plus live load pressures at crown, psi.



(a) (b)

Figure 2-9. Active pressure distribution around circular conduit (Klöppel and Glock 1970; Leonards and Stetkar 1978).

- **Cheney (1963)**

Cheney (1963) studied the hydrostatic buckling pressure of a thin ring encased in rigid cavity using the small-deflection linear theory. He analyzed the stability of a circular ring under plane stress conditions, subject to circumferential support by elastic springs, under a uniform external pressure distribution on the ring wall. Cheny's model is presented by Eq. 2-7.

$$P_{cr} = \frac{(K_{cr}^2)EI}{R^3} \qquad \text{Eq. 2-7}$$

where,
P_{cr} critical buckling pressure (psi),
i radius of gyration, in.,
R radius of the ring, in.,
E Young's modulus, psi,
I Modulus of Elasticity, in.^{4}/in.
$K_{cr} = 1.57(R/i)^{2/5}$.

For relatively thin infinitely long pipes (e.g., DR > 30), the critical pressure can be expressed as Eq. 2-8.

$$P_{cr} = \frac{2.55E}{1-\nu^2}\left(\frac{t}{D}\right)^{11/5} \qquad \text{Eq. 2-8}$$

Where,
P_{cr} critical buckling pressure, psi,
t thickness of the ring, in.,
D diameter of the ring, in.,
E Young's modulus, psi,
I Modulus of Elasticity, in.^{4}/in.

ν Poisson's ratio.

- **Bresse (1866)**

Bresse (1866), using the small deflection theory, studied the stability of a thin unconstraint circular ring under external hydrostatic pressure, as it is given by Eq. 2-9. Bresse's model is illustrated in Figure 2-10.

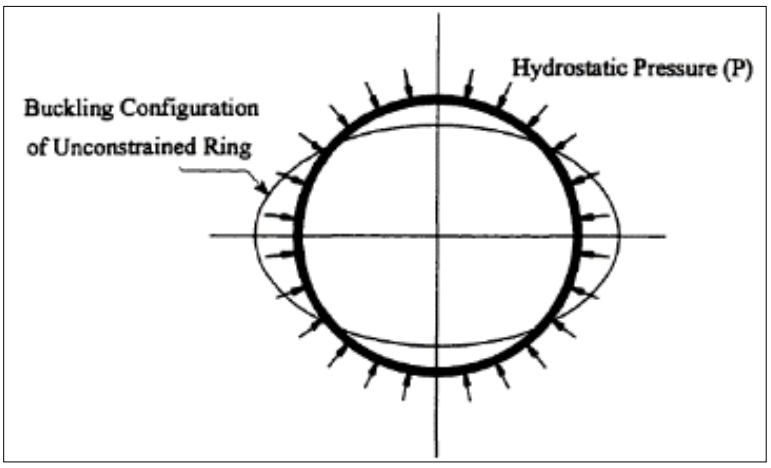


Figure 2-10. Bresse Model for calculating the critical buckling pressure of a thin unconstraint circular ring under external hydrostatic pressure.

$$P_{cr} = \frac{3EI}{R^3} \qquad \text{Eq. 2-9}$$

Where,
P_{cr} critical buckling pressure, psi,
E Young's modulus, psi,
I Modulus of Elasticity, in.^{4}/in.

- **G.H. Bryan (1888)**

G. H. Bryan (1888), using the minimum potential energy criterion of stability, studied the critical buckling pressure for an infinitely long free-standing pipe under hydrostatic external pressure, as it is given by Eq. 2-10. In this equation the term of $\frac{E}{(1-\nu^2)}$ accounts for the plain strain condition of the infinitely long pipe.

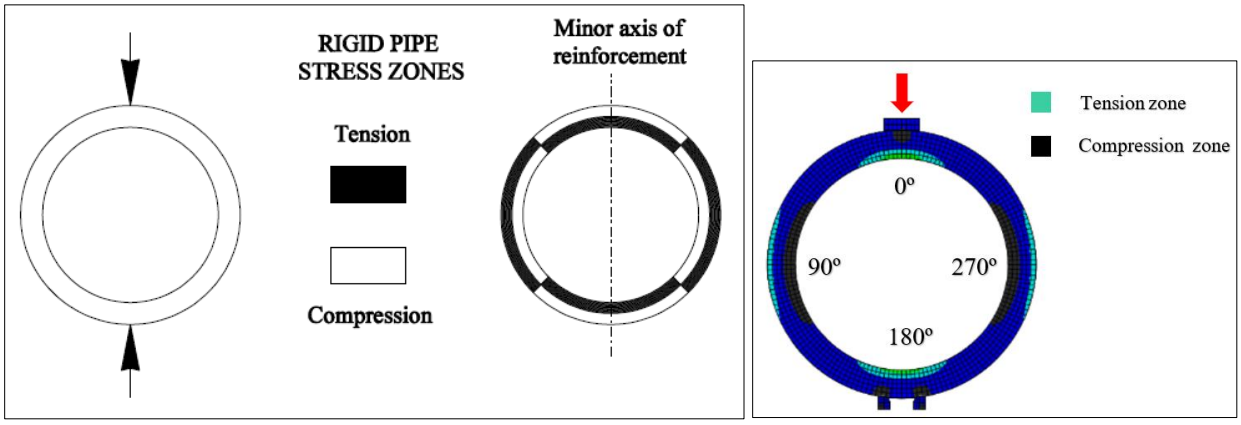
$$P_{cr} = \frac{2E}{(1-\nu^2)}\left(\frac{t}{D}\right)^3 \qquad \text{Eq. 2-10}$$

Where,
P_{cr} critical buckling pressure, psi,
t thickness of the ring, in.,
D diameter of the ring, in.,

E Young's modulus, psi,
I Modulus of Elasticity, in.^{4}/in.
ν Poisson's ratio.

2.1.1.5.2. Rigid Pipe

Rigid pipes are stiff and do not deflect appreciably. Rigid pipes are unable to deflect more than 2% without significant structural distress such as cracking (Omara 1997). Rigid pipes are made of materials such as concrete that provides the primary resistance to bending. The load carrying capacity of a rigid pipe is provided by the structural strength of the pipe itself, with some additional support from the surrounding bedding and backfill. A rigid pipe under vertical loads, that is prone to tension and compression in different zones, is illustrated in Figure 2-11. Steel reinforcement can be added to the tension zones to enhance the tensile strength of a concrete pipe. A rigid pipe is stiffer than the surrounding soil and it carries a substantial portion of the applied load. Shear stress in the haunch area can be critical for heavily loaded rigid pipe on hard foundations, especially if the haunch support is inadequate (Hydraulics Manual M 23-03.06 2019). The performance of rigid pipes is dependent on foundation and bedding stability (*AASHTO LRFD Bridge Design Specifications* 2020).



(a) (b)

Figure 2-11. Rigid pipes under vertical loading: (a) rigid pipe stress zones (Hydraulics Manual M 23-03.06 2019), and (b) finite element modeling of a rigid reinforced concrete pipe (RCP) (Darabnoush Tehrani 2016).

2.1.2. Corrugated Metal Pipe (CMP)

Corrugated metal pipe (CMP) and concrete culverts have been in service in the U.S. storm/sanitary system for more than 70 years. Availability of CMP in variety of shapes and sizes, and modification capability to increase their durability has made this material preferable in many sites. CMP is ideal for shipping due to its light weight and is easy to assemble and install. However, CMPs are sensitive to high or low soil pH or water pH which may result in CMP corrosion. Due to presence of sand and/or rock in a high velocity stream, abrasion may cause loss of CMP metal (Najafi 2008).

2.1.2.1. CMP Types and Corrugation Profiles

There are generally three types of CMP: helical, spiral rib, and annular (Darabnoush Tehrani et al. 2019). Helical CMP is a corrugated tube, fabricated with a tube-shaped shell in a spiral arrangement, as illustrated in Figure 2-12 (a). Spiral rib CMP is similar to helical CMP, where the pipe is manufactured from a continuous metallic strip passed through a roll forming line that forms the external ribs, edges and joined by lock seaming, as illustrated in Figure 2-12 (b) (NCSPA 2017). The annular CMP is usually fabricated from bent hot-dip galvanized steel[1] sheets along their edges using bolts or rivets, as illustrated in Figure 2-12 (c). CMP, due to its corrugation profile, has higher hoop and bending strengths compared with a same thickness plane steel pipe. Several CMP profiles have been used across the North America since its introduction in 1896, which are the 1½×¼ in., 2⅔×½ in., 3×1 in., and 5×1 in. The CMP industry later added the 6×2 in. metal sheets for erecting pipe arch structures of sizes 61 in. by 55 in., and larger. From these available sizes, the most common encountered corrugation profiles are the 2⅔×½ in., 3×1 in., and 6×2 in. Common CMP corrugation profiles in the North America are presented in Table 2-1. The 2⅔×½ in. and 3×1 in. corrugation profile may have a riveted construction (annular corrugations) or lock seam construction (helically wound corrugations), while the 6×2-in. corrugation profile is made up by bolting standard panels together.

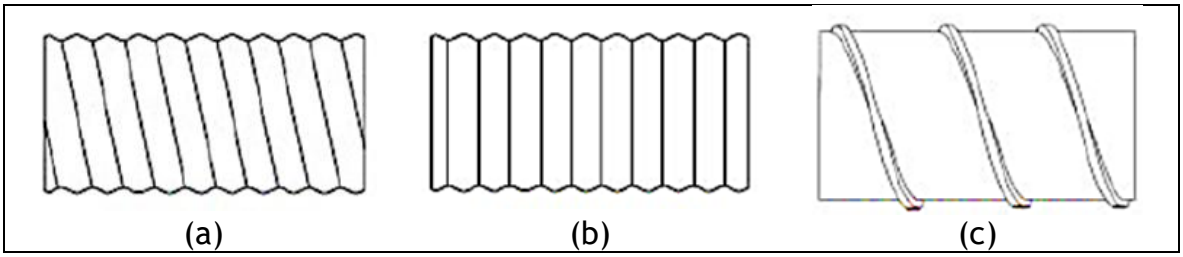
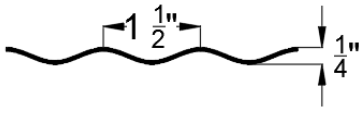
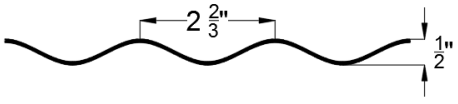
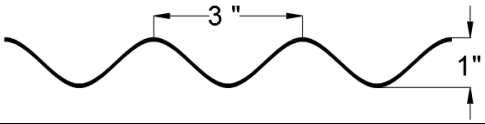
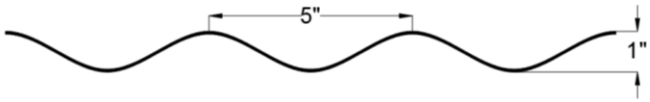
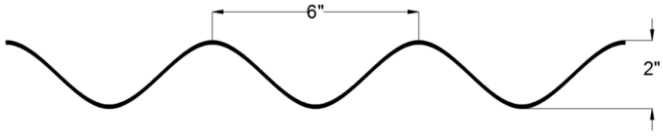


Figure 2-12. Types of corrugated metal pipes (CMPs): (a) helical, (b) annular and (c) spiral rib CMPs.

Table 2-1. Common CMP corrugation profile in North America (PCPIPE 2016).

CMP Type	Corrugation Profile	Thickness (in.)
Helical and Annular		0.052” and 0.064”
		0.064” - 0.168”

[1] The process of dipping fabricated steel into a kettle or vat containing molten zinc.

CMP Type	Corrugation Profile	Thickness (in.)
		0.064”- 0.168”
		0.064”- 0.168”
Annular		0.1” - 0.168”

2.1.2.2. Durability and Structural Performance of CMPs

Many culverts in the United States that were installed four to five decades ago, now have reached their design life and need to be repaired, renewed, or replaced (Najafi 2008). In the pipeline industry, problems with corroded metallic and fiber reinforced concrete pipes are of the major concerns. The pipeline deterioration has a direct impact on economics and public services.

The durability of a CMP is mainly impacted by duration of water contact, pH, dissolved salts, alkalinity, hardness, and abrasiveness. Due to the abrasion, the CMP corrosion rate (for both inner and outer surfaces) increases. The occurrence of waterside (inner surface) corrosion is faster compared to the soil side (outer surface) corrosion. Hence, the CMP waterside corrosion is considered as the controlling factor (Bednar n.d.).

Culvert deterioration can be classified as serviceability-related and strength-related issues, as follows (Najafi 2008):

Serviceability-related deterioration:

- Scour and erosion of streambed and embankments,
- Inadequate flow capacity,
- Corrosion and abrasion of metal culverts,
- Abrasion and deterioration of concrete and masonry culverts,
- Sedimentation and blockage by debris,
- Separation and/or drop-off of sections of modular culverts, and
- Inadequate length.

Strength-related deterioration:

- Cracking of rigid culverts,

- Undermining and loss of structural support,
- Loss of the invert of culverts due to corrosion or abrasion,
- Over-deflection and shape deformation of flexible culverts, and
- Stress cracking of plastic culverts.

Common defects in culverts can include crack, corrosion, loss of pipe wall thickness, joint infiltration, joint exfiltration, invert deterioration, joint misalignment, shape distortion, debris, loss of wall thickness, and bedding voids, as illustrated in Figure 2-13 (Piratla et al. 2017).

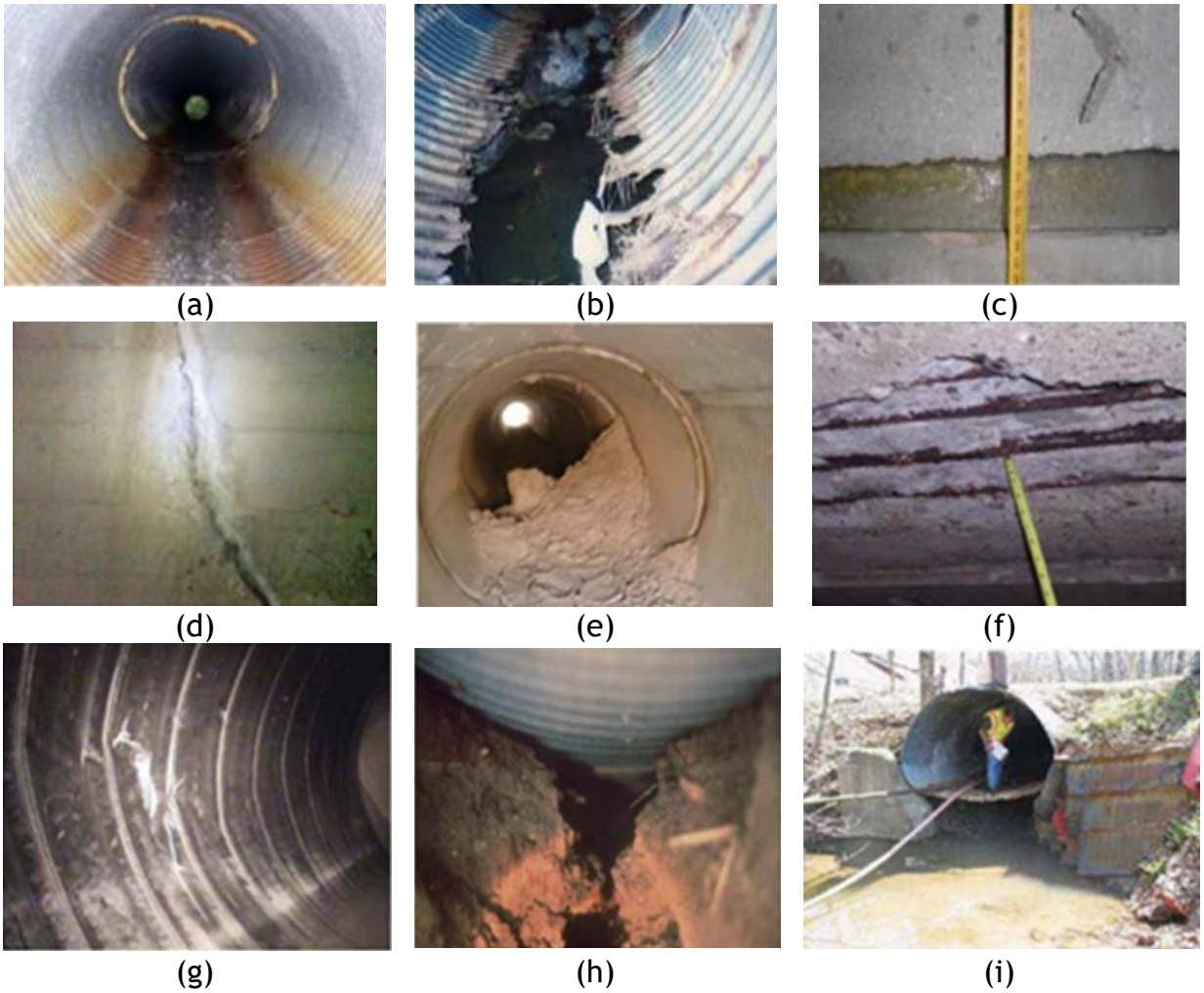


Figure 2-13. Common Defects of Culverts: (a) invert corrosion, (b) invert abrasion, (c) joint separation, (d) crack, (e) joint infiltration, (f) spalling in concrete culverts, (g) wall damages in plastic culverts, (h) piping beneath a culvert and (i) outlet scour (Piratla et al. 2017).

The structural performance of a CMP is impacted by the improper backfill material, the level of backfill soil compact and the presence of groundwater or hydrostatic pressure (Sehn and Duncan 1994). Culvert failures are sudden and may cause

flooding potholes or total failure of the roadway. Four examples of culvert failures follow:

2.1.3. Renewal of Deteriorated Culverts using Trenchless Technology

Trenchless renewal and replacement methods can be used to line, rehabilitate, upgrade, or renovate existing pipelines (Najafi 2010). Although, one of the solutions is open-cut replacement of the deteriorated pipe and reconstruction, it is disruptive to traffic. To reduce social cost to commuting public, trenchless technology can offer innovative and nondestructive approaches, which make pipe renewal easier (Kohankar Kouchesfehani et al. 2017). A pipe renewal technique takes the advantage of employing the remaining usable pipe and extending its design life by the application of lining methods (Najafi 2010). If a pipe exceeds the preventative maintenance stage but still maintains its structural integrity, then using trenchless renewal methods is the proper corrective action. If a pipe deteriorates to a point where its structural integrity or soil support is lost, then trenchless pipe replacement can be an appropriate corrective action (Wyant 2002).

The most important step in designing a trenchless renewal technique is selection of the most appropriate, cost-effective and reliable method. Decision making process for the selection of a pipeline renewal solution should consider many factors such as existing pipeline conditions, constructability and site limitations, strengths and limitations of potential renewal methods, pipe geometry, costs and availability of contractor and technology providers (Najafi 2016). The design of a pipeline renewal system involves 1) identification of pipe conditions, problem recognition and classification, 2) prioritization of problem considering strategies and long-term plans, 3) selection of an appropriate pipeline renewal method and 4) designing renewal methods based on project specific conditions (Kouchesfehani et al. 2018; Najafi and Gokhale 2005).

Trenchless renewal methods include several techniques. Sliplining (SL), cured-in-place pipe (CIPP), close-fit pipe (CFP), spiral wound lining, fold-and-form PVC lining, and spray applied pipe lining (SAPL) are some of the trenchless rehabilitation techniques, as shown in Figure 2-14 (Syar et al. 2019). SIPP and SAPL are conceptually the same, however, SIPP applies to potable water pipelines constructed of metallic or asbestos cement piping in the diameter ranges of 4 in. to 36 in., (F3182-16 2016). SAPL is a pipeline renewal solution to support severely damaged large diameter (larger than 36 in. span) gravity storm pipes such as culverts and drainage structures to protect these pipes from further deterioration (Najafi 2016). These trenchless renewal methods have many social and environmental benefits over traditional open-cut or cut-and-cover methods. These methods should be used when the project surface and subsurface conditions allow utilizing the trenchless technology. Compared with other trenchless methods, SAPL methodology has the benefit of fast installation, is cost effective, environmentally friendly, corrosion and erosion resistant without hydraulic capacity loss and minimum laydown area (Darabnoush Tehrani et al. 2019; Kohankar Kouchesfehani et al. 2019).

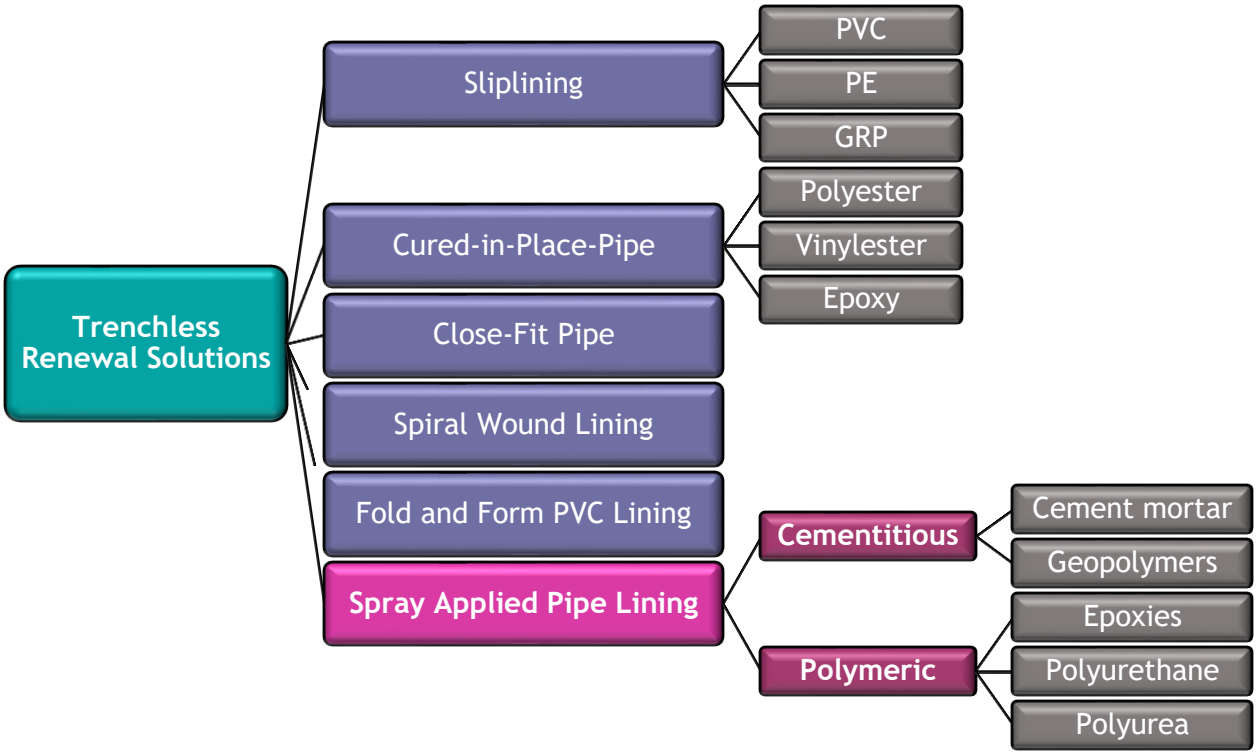


Figure 2-14.Trenchless renewal solutions.

2.1.3.1. Sliplining

Sliplining trenchless renewal technique is mainly used for structural applications when the old pipe does not have joint settlements or misalignments. In this method, a new pipeline of smaller diameter is inserted into the old pipe and usually the annulus space between the old pipe and new pipe is grouted. This installation method has the merit of simplicity and is relatively inexpensive. However, there can be a significant loss of hydraulic capacity. This method is applicable for diameters greater than 24 in. Figure 2-15 illustrates a segmental sliplining method (Najafi and Gokhale 2005). Table 2-2 presents the main characteristics of the sliplining method.

Table 2-2. Main characteristics of Sliplining methods (Najafi 2016).

Method	Diameter Range (in.)	Maximum Installation (ft)	Liner Material	Applications
Segmental	4-158	1,000	HDPE, PVC, and GRP	Gravity Pipelines
Continuous	4-63	1,000	HDPE and PVC	Pressure Pipelines



Figure 2-15. Segmental sliplining method (Source: Hobas Pipe USA).

2.1.3.2. Modified Sliplining

Modified sliplining is usable for large diameter (worker entry) gravity pipes including culverts (Najafi, 2016). The scope of using this method is for both structurally application and non-structurally application. It is applicable for different shapes and is used in sewer lines. “Modified sliplining liners (panels) usually have tongue-and-groove joints that are sealed with either rubber sealing rings or polyurethane or epoxy filler” (Najafi, 2016). There will be reduction in cross-sectional area of the pipe, which must be compared with any improvements due to a better coefficient of roughness of the lined pipe. As a conclusion of using this method, it is useful when the culvert needs structural rehabilitation. Table 2-3 shows the main characteristics of the modified sliplining method.

Table 2-3 Main characteristics of Modified Sliplining methods (Najafi 2016).

Method	Diameter Range (in.)	Maximum Installation (ft)	Liner Material	Applications
Panel Lining	>48	varies	GRP	Gravity Pipelines
Spiral Wound	36 -100	1,000	PE and PVC	Gravity Pipelines

2.1.3.3. Cured-in-Place Pipe Lining (CIPP)

The cured-in-place pipe lining (CIPP) process involves the insertion of a resin-impregnated fabric tube into an old pipe by use of water inversion or winching. The resin impregnation is referred to “wet out.” Usually, the fabric is a polyester material, fiberglass reinforced or similar. Usually, hot water or steam is used for the curing process. The pliable nature of the resin-saturated fabric prior to curing allows installation around curves, filling of cracks, bridging of gaps, and maneuvering through pipe defects. CIPP can be applied for structural or non-structural purposes. Figure 2-16 illustrates CIPP installation process (Najafi and Gokhale 2005). Table 2-4 presents the main characteristics of the CIPP method.

Table 2-4 Main characteristics of CIPP method (Najafi 2016).

Method	Diameter Range (in.)	Maximum Installation (ft)	Liner Material	Applications
Inverted-In-Place	3-120	3,000	Thermoset Resin/ Fabric Composite	Gravity and Pressure Pipelines
Winched-In-Place	4-54	1,000	Thermoset Resin/ Fabric Composite	Gravity and Pressure Pipelines



Figure 2-16. CIPP method installation process (Source: Insituform Technologies).

2.1.3.4. In-Line Replacement

"When capacity of deteriorated pipelines is found to be inadequate, the In-Line Replacement (ILR) should be considered. There are two categories representing ILR, Pipe Bursting and Pipe Removal. Pipe bursting, as the name implies, uses a pulling head or a vibrating hammer to break the existing host pipe and force broken particles in the earth while a new pipe is pulled and/or pushed in its place simultaneously. Pipe removal on the other hand, can be performed by use of horizontal directional drilling, horizontal auger boring or microtunneling equipment. In this method, the existing pipe is broken into small pieces and taken out of borehole by means of slurry or auger" (Najafi 2016). Table 2-5 shows the main characteristics of ILR method. Figure 2-22 illustrates the pipe bursting process.

Table 2-5 Main characteristics of in-line replacement method (Najafi 2016).

Method	Diameter Range (in.)	Maximum Installation (ft)	Liner Material	Applications
Pipe Bursting	4-140	750	PE, Clay, PVC, GRP and DI	Gravity and Pressure Pipelines
Pipe Removal	Up to 36	300	PE, PVC, GRP and DI	Gravity and Pressure Pipelines

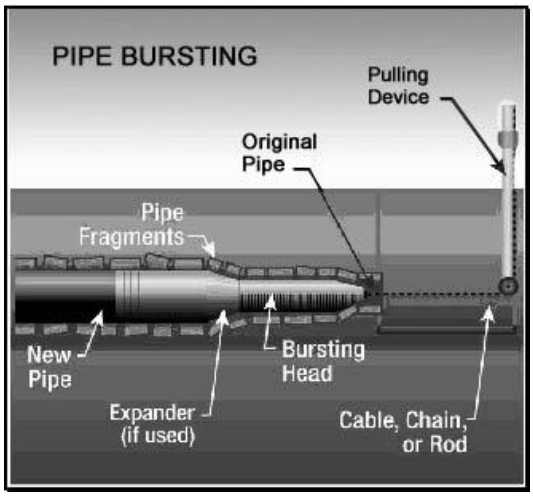


Figure 2-17. Pipe bursting method (Source: google images).

2.1.3.5. Close-fit Pipe Lining

Not commonly used for culvert renewal, close-fit pipe trenchless renewal temporarily reduces the cross-sectional area of the new pipe before it is installed, then expands it to its original size and shape after placement to provide a close fit with the existing pipe. This method can be used for both structural and non-structural purposes. Lining pipe can be reduced on-site or in the manufacturing plant and reformed by heat and/or pressure or naturally. There are three versions of this approach: Fold and Formed (F&F), Drawdown (DD) and Rolldown (RD) (Najafi and Gokhale 2005).

2.1.3.6. Spiral Wound Lining (SWP)

Spiral wound trenchless renewal method is used for gravity sewers only. In this process, a new pipe is installed inside the existing pipe from a continuous strip of PVC 20 to 30 cm width. The strip has tongue-and-groove castings on its edges. It is fed to a special winding machine placed in a manhole, which creates a continuous helically wound liner that proceeds through the host pipe. The continuous spiral joint, which runs the length of the pipe, is watertight. Upon completion of the lining process, grouting of the annulus space between the lining and the host pipe wall is usually required, although there is a technique in which the lining is close-fit to the existing wall, thereby removing the need for grouting (Najafi and Gokhale 2005).

This process can be used for circular and non-circular pipe. Further, as the new pipe is formed directly against the wall of the host pipe, this method can be used to renew an existing pipe with a minimal loss of diameter as compared to conventional sliplining processes that rely on prefabricated pipes of fixed diameters. Hydraulic capacity of pipes lined in this manner may minimally increase because of reduction in flow area (Najafi and Gokhale 2005).

2.1.3.7. Thermoformed Pipe (ThP)

Not commonly used for culvert renewal, thermoformed pipe trenchless renewal technique can be used for sewers systems, potable water and gas supply lines, and industrial applications. ThP can be used for structural (including renewal of severely distressed pipeline) or nonstructural purposes and for pipelines from 4 in. to greater than 30 in. diameter and for lengths up to 1,500 ft. This technology can negotiate bends in the existing pipeline and generally provides a small footprint, minimal community disruption, and very brief service disruption. There are three methods of ThP as illustrated Figure 2-18 (Najafi and Gokhale 2005).

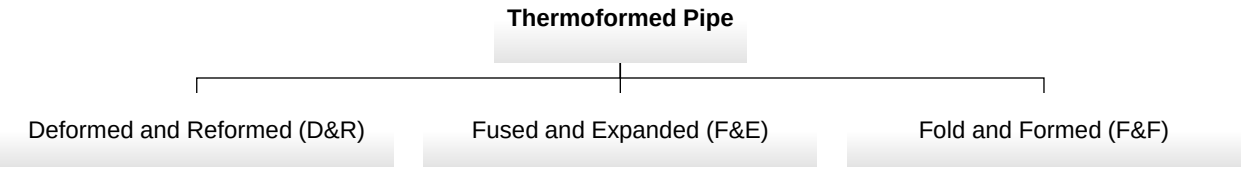


Figure 2-18. Three main variations of ThP process (Najafi and Gokhale 2005).

2.1.3.8. Fold & Formed (F&F)

In the first method of ThP, called fold and formed (F&F), PVC pipes are flattened in the factory during production, then wound onto large reels, and folded during insertion. F&F methods can be used for gravity and/or pressure pipelines, including sanitary sewer, storm sewer and culvert, and potable water pipes and can be designed to provide full, independent structural integrity. Following the delivery to the renewal site, the new PVC pipe is heated with steam until it becomes flexible. Once in place, the new pipe is forced against the inside surface of the existing pipe using steam and air pressure to form a new PVC pipeline tightly inside the old pipe. Maximum diameter varies across vendors with sizes available up to 24 in. (Najafi and Gokhale 2005).

2.1.3.9. Deformed and Reformed (D&R)

The second ThP method is deformed and reformed (D&R), where high-density polyethylene (HDPE) pipe is deformed into a U shape in the factory and wound into large coils. This method is used for gravity and/or pressure pipelines and for structural purposes. The new HDPE pipe is pulled at ambient temperature from manhole-to-manhole with a winch cable through the existing pipe. After the new pipe is inserted into position, it is heated with steam to revert it to its round memory and pressurized to push it out against the host pipe. Maximum diameter is 24 in. with sizes above 18 in. butt-fused and deformed in the field immediately prior to installation (Najafi and Gokhale 2005).

2.1.3.10. Fused and Expanded (F&E)

With the third method, called fused and expanded (F&E), PVC pipes are fused in the field prior to insertion. F&E pipes can be used for high-pressure pipelines exceeding 150 psi, including potable water pipes. Following delivery to the renewal site, the new PVC pipe is butt-fused and inserted through access pits as would be typical of sliplining. Once in place, the new pipe is heated with a hot liquid and highly pressurized to thermoform the new pipe tightly against the inside surface of the existing pipe. The maximum available diameter continues to expand with sizes exceeding 30 in. having been installed (Najafi and Gokhale 2005).

2.1.3.11. Spray Applied Pipe Lining (SAPL)

Spray applied pipe lining (SAPL) is a trenchless renewal methodology and an application that inhibits further deterioration and can structurally support severely damaged pipes, culverts and drainage structures. SAPL can potentially be used for structural renewal and load carrying capacity enhancement of culverts by applying a monolithic layer, ranging approximately 1.0 in. to 3.0 in., to the culvert inner surface (Darabnoush Tehrani 2016; Syar et al. 2020). SAPL can be installed either manually with hand spray or with a rotatory spin casting machine using a sled, as illustrated in Figure 2-19. The primary materials used for SAPLs can be categorized into (1) cementitious such as geopolymers and (2) polymeric materials such as polyurethanes (Johnson and Hammon 2017). SAPLs can be a key strategy in extending service life and managing the future burden expected from the aging network of culverts, as shown in Figure 2-20. SAPL is environmentally friendly, compatible with complex geometry, durable, corrosion and erosion resistant and fast for installation without hydraulic capacity loss of the culvert (Syar et al. 2019).



(a) (b)

Figure 2-19. Corrugated metal pipe culverts (CMPs) before and after SAPL rehabilitation: (a) cementitious SAPL installation using spin casting machine (Source: CentriPipe) and (b) polymeric SAPL installation with hand spray (Source: Sprayroq).

To reduce emergency projects and impacts to the travelling public, departments of transportation (DOTs) can use spray applied pipe linings (SAPLs) to renew deteriorated gravity storm water conveyance conduits and culverts provided they

discovered prior to loss of soil-structure interaction. However, currently no standardized structural design methodology exists for this technology. Most lining vendors utilize cured-in-place pipe (CIPP), ASTM F1216 design methodology. Others use various classical analytical structural design equations, such as beam element or shell element. The development of a practical spray-applied culvert/pipe lining methodology could be of enormous benefit to the DOTs. Such linings could be a key strategy in extending service life and managing the future burden expected from the aging network of culverts and storm sewers.



Figure 2-20. A sample of SAPL renewed twin culvert, North Carolina.

The key factor in a design guideline for SAPL is whether the existing pipe is structurally sound enough to support the earth, live, and hydrostatic loads imposed on it. It is well known that existing flexible pipes gain structural strength through the soil-structural interaction, thus making them a composite system (Syar et al. 2019). There are many documented instances of existing corrugated metal pipes with significant invert loss that continue to hold their shape due to the load carrying capacity of the surrounding soil. If the existing pipe is structurally sound enough to continue to maintain shape and carry the earth and live loads imposed on it then several internal lining techniques might be applicable, including sliplining (SL), cured-in-place pipe (CIPP), spray applied pipe lining (SAPL), and close-fit pipe (CFP) (Najafi 2016).

ASTM F1216-16 divides deterioration of existing pipe conditions into two classes: “partially deteriorated” and “fully deteriorated” (F1216-16 2016). The assignment of a partially or a fully deteriorated design procedure depends upon condition of existing pipe or its expected structural contribution over the liner design period. The main objective of a structural renewal is to inhibit further deterioration and be able to structurally renew the severely damaged culverts and drainage structures (Najafi 2016).

2.2. Spray Applied Pipe Linings

Spray applied pipe lining (SAPL) application dates to 1930s, which is the pioneer technique for pipe renewal (Najafi 2010). SAPL applies layers of liner on the interior surface of the host pipe to provide corrosion protection and structural capacity enhancement. SAPL substances can be cementitious such as cement mortar and geopolymers, or polymeric material including epoxy, polyurethane, and polyurea. Uncertainty about the structural capacity of same SAPL materials have categorized their application in the past as a non-structural renewal method (Ellison et al. 2010; Najafi et al. 2019).

Sever et al. (2013) discussed manhole rehabilitation knowledge gaps based on a SEPA/Water Environment Research Foundation (WERF) sponsored project. The objective of this paper was to focus on the materials and methods used for pipeline rehabilitation from structural, hydraulic, and economic perspectives. Authors defined three different opinion of structural behavior of SAPL, which were 1) SAPL increases the stiffness of manhole, 2) SAPL supports all the loads applied although the host manhole has structural resistance during the application, and 3) SAPL carries the load independently. They defined three classes of structural conditions of manhole rehabilitation including structural (class A), semi-structural (class B) and non-structural (class C). They defined a decision support tool (DST) for manhole rehabilitation. Not only DST is related to the structural capacity of the SAPL, but some other factors, such as, manhole condition, site condition (soil, groundwater, traffic and other loads), cost of the rehabilitation system, and overall objective of the rehabilitation project must be considered. In conclusion, following seven items need to be considered to pass gaps in the knowledge of manhole rehabilitation:

- Classify manhole rehabilitation materials per their structural capabilities.
- Determine to what extent structural rehabilitation is necessary for the utilities.
- Pros and cons of testing manufactured samples versus those obtained from field (in service).
- Develop a comprehensive decision support tool specifically designed for manhole rehabilitation.
- Prepare a manhole rehabilitation manual that will complement the existing ASCE Manual (ASCE MOP 92 – Manhole Inspection and Rehabilitation).
- Develop an ASTM Standard for cured-in-place manhole rehabilitation and other methods.
- Determine the number of manholes in the USA and provide a better estimate of their age and condition, thereby overall value.

2.2.1. Polymeric Spray Applied Pipe Liners

Accelerated corrosion problems in today's infrastructure have led to development and use of coatings and linings to enhance infrastructure life

expectancies. Due to inherent safety, performance, and quick return to service attributes, solvent-free 100% solids polymers have advantages for successful structural renewal and corrosion protection of infrastructures. Polymers can be formulated for structural or nonstructural pipeline renewal/rehabilitation applications (ASCE Manual of Trenchless Renewal of Culverts and Storm Sewers, 2010). There are two major categories of protective polymeric coating technologies: epoxies and polyurethane-type systems, which include polyurethanes, polyureas and hybrids of these two chemistries (Cain 2016). Protective coating SAPL is a problem for DOT's because these pipes are not designed to be pressurized from the inside to keep the lining pressed against the host pipe. Culverts usually have water pressure coming through the soil-tight joints that easily fail the protective coating type of SAPL products. Polymeric SAPL needs to always be structural to withstand the water pressure.

2.2.1.1. Epoxy

Epoxy coatings are used as corrosion protection for factory-applied metals and as primers (sometimes zinc-rich) in multi-coat systems. Epoxies can provide a good adhesion to metals and are highly moisture resistant. High-build or 100%-solids are the most common used epoxies. However, epoxies do not exhibit a good performance and become brittle at low temperatures. Epoxies are not very flexible and can crack in applications with any substrate movement. Hence, polyurethane and its derivative coatings, due to their higher flexibility compared with epoxies, are widely used as metal corrosion protection with a high level of adhesion and moisture resistant (Cain 2016).

Riahi et al. (2014) used Finite Element Model (FEM) for simulating the epoxy lining of manhole rehabilitation. The objective of this paper was to explore the use of FEM to predict the integral structural performance of SAPL on concrete manholes. Methodology started first by laboratory testing on the concrete and then materials. Compression strength of concrete for bare specimen was 5,083 psi and increased to 5,633 for specimen with SAPL; however, flexural strength of concrete for bare specimen was 916 psi and increased to 1,657 for specimen with SAPL. FEM were performed on three cases: flexural beam test, pipe crushing test, and manhole structure under uniform soil and hydrostatic pressure. In the FEM model, the loading condition was simplified to parallel plate loading condition. Both bare concrete pipe and lined concrete pipe were simulated. For the lined pipe, a 0.25-in. layer of epoxy was applied to the inside of the concrete pipe. Overall, three cases, flexural strength test of beams, pipe crushing, and uniform pressure were modeled in FE. The deflection for case I is 0.0019 in. for bare concrete with increasing to 0.0051 in. in the peak load. The deflection for case II is 0.021 in. for bare concrete. In case III, there was no contribution of concrete to the structural capacity. For 10.2-psi peripheral pressure, the lining has a radial deformation of 0.006 in. Authors concluded that the adhesion of lining could affect the structural capacity of host manhole when linings are subjected to tension stress normal to the contact surface.

Entezarmahdi (2015) conducted structural evaluation on 17 reinforced concrete pips (CRPs), renewed with epoxy lining and tested through three-edge bearing test. The

pipe samples had 24 in. inside diameter and were selected from class II category of the ASTM C76 (2015). Different types of liners including epoxy, Polyurethane, Multi structural liners with modified pleurae and foam, cementitious, and resin impregnated cured-in-place lining (CIPP) were applied on different layers and thicknesses. The author summarized the results in one graph as the significant increase in renewed CRP structural capacity by using different liners, showed in Figure 2-21.

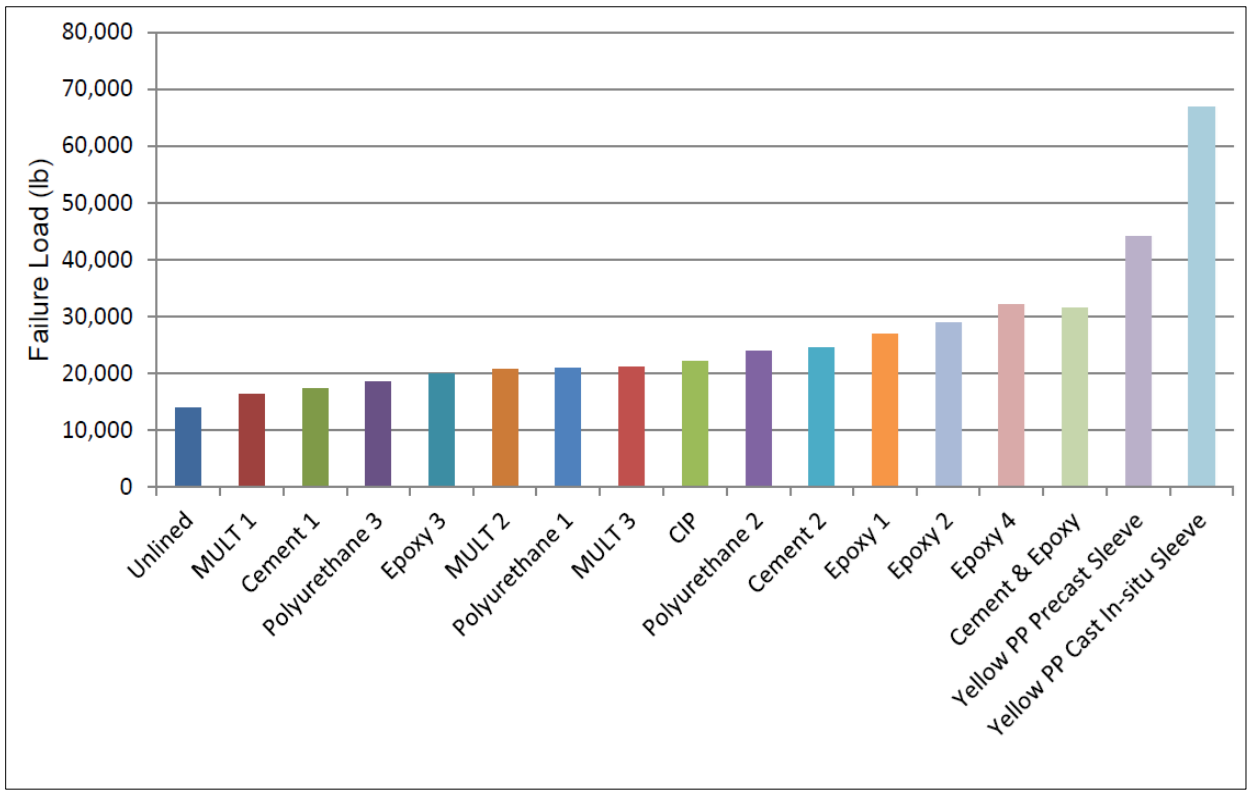


Figure 2-21. Significant increase in renewed CRP structural capacity (Entezarmahdi, 2015).

2.2.1.2. Polyurethane

Polymeric SAPL was developed in 1970s. Initially, it was based on 100% solid elastomeric polyurethane. In the mid-1990s 100% solids rigid polyurethane coating were developed, which was able to form a three-dimensional cross-linked structure, resulted in a superior resistance to chemicals, water penetration, and high temperatures (Matthews and Simicevevic, 2012). Polymeric SAPLs can be applied through a spin caster machine or hand sprayed. Polyurea, provides high degree of chemical resistance and is able to cure rapidly (about 5 to 15 seconds). Many Departments of Transportation (DOTs) have already approved polymeric coatings for rehabilitation of culverts in the United States, such as Ohio DOT, Virginia DOT, Florida DOT, etc. (Ellison et al. 2010).

Polyurethane coatings can range from very flexible (elastomeric) to very rigid. Polyurethane coatings can exhibit a good combination of flexibility/elongation and

harness compared with epoxy coatings. Polyurethane coatings have excellent adhesions to different substrates. Polyurethane coatings cure rapidly, even at lower temperatures, but most require a catalyst. Compared to epoxies, and polyureas, most 100%-solids polyurethane coatings are sensitive to moisture and susceptible to blistering. Solvent-based polyurethane coatings are typically applied as a thin layer of less than 5 mil using airless sprayers. Compared to solvent-based polyurethanes, 100% solid polyurethanes can be applied at a thicker layer of greater than 20 mils. Installation of 100% solid polyurethanes need the use of a plural component spray technique that can mix the resin and catalyst components together prior to spraying (Cain 2016).

2.2.1.3. Polyurea

Polyurea coatings are 100% solids, zero-Violate Organic Compound (zero-VOC) formulations. Polyurea coating cures rapidly in around 30 seconds without use of a catalyst or heat at low temperatures. Polyurea coatings are not sensitive to moisture due to the existence of the urea linkage. Polyurea coatings are water resistant, and no blistering occurs when they are applied on substrates in the presence of liquid water. Polyurea coatings exhibit excellent mechanical properties (stiffness, tear and abrasion resistance, thermal shock and impact resistance) (Cain 2016).

Polyureas can be applied at very high thickness, compared with polyurethane, and enhance the structural integrity of the substrate. Installation of polyurea coatings need the application of high-pressure, plural component sprayers, and a trained applicator. Polyurea elastomers are unsuitable for applications requiring less than 5 mil thickness coatings. Polyureas are used a replacement for epoxies in applications that mechanical properties such as elongation and impact resistance are important. A performance comparison using the mechanical properties of polyurea, polyurea hybrid, polyurethane and epoxy coatings applied on steel substrate is illustrated in Figure 2-22.

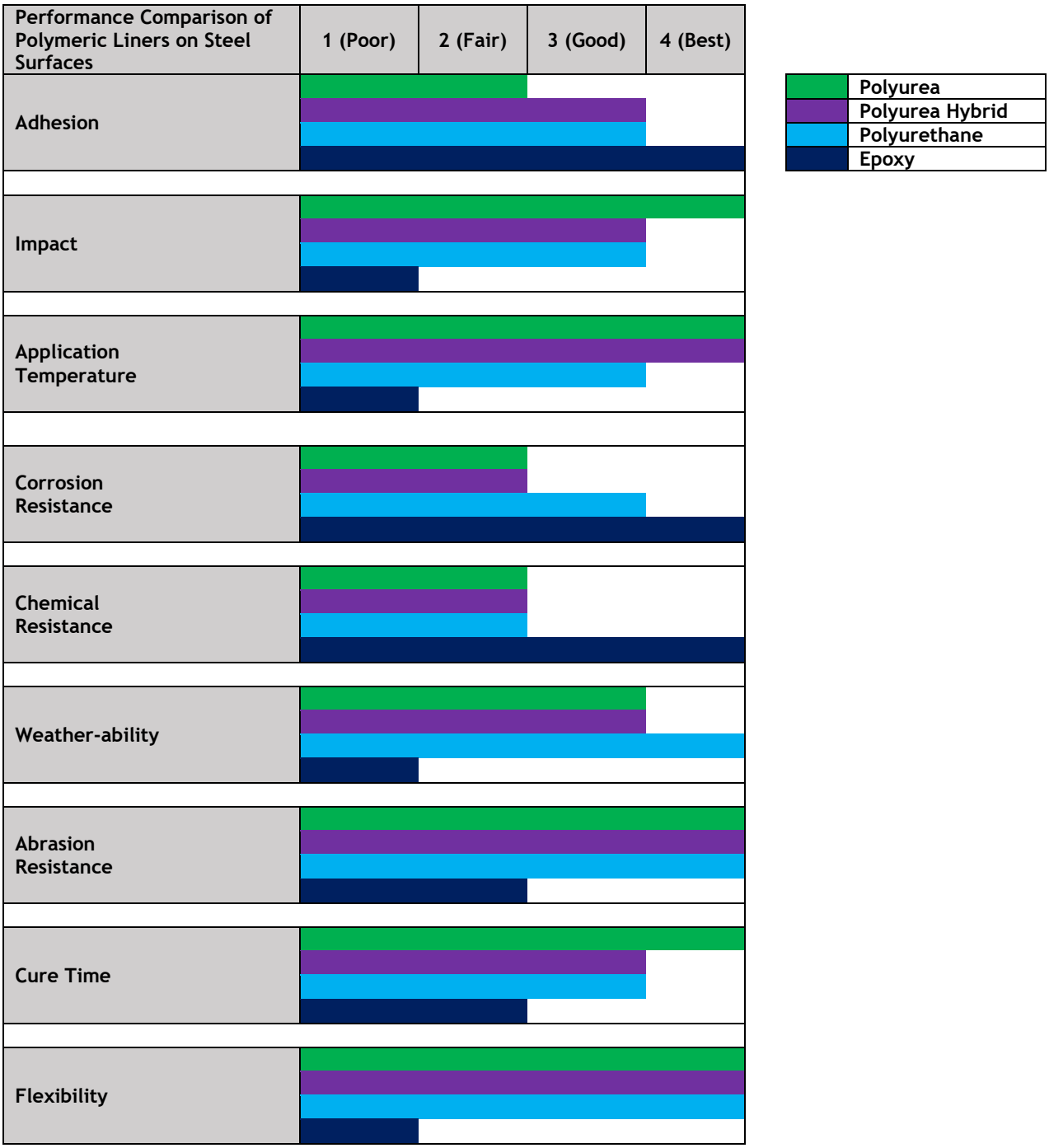


Figure 2-22. Performance comparison of polyurea, polyurea hybrid, polyurethane and epoxy coatings applied on steel substrate (Adapted from Cain 2016).

Walker and Guan (Walker and Guan 1997) conducted a set of material property tests in accordance with ASTM standards and reviewed the performance of five primary materials of sprayed liners used in North America. Their tests included 100% solids rigid polyurethane, 100% solids epoxy, solvent amine-based epoxy, 100% solids elastomeric polyurethane and cement mortar lining for the internal renewal of potable water steel pipelines. Their study stated the 100% solids polyurethane had a better performance to

be used in potable water steel pipelines. (Ha et al. 2016) conducted a series of laboratory testing to investigate the applicability of the fast-setting polyurea-urethane (PUU) lining as a structural lining material, applied inside of small diameter (5.91 in.) water pipes. Their study included pull off bond test, hole or gap spanning test, angular displacement test, transverse shear test and fatigue cyclic tests. It was concluded the fast-setting PUU lining can be used as a structural lining material for water pipelines. Szafran and Matusiak (Szafran and Matusiak 2017) studied the structural behavior of reinforced concrete rings renewed from inside and outside surfaces with polyurea SAPL through the three-edge bearing test (Al-Lami 2020). They concluded the used polyurea SAPL membrane for standard application in two layers on both surfaces increased the compressive capacity of concrete rings by 21.9%. Authors stated further research is needed to explore the performance of polyurea SAPL in the existence of soil-pipe interaction system.

Primeaux II (Primeaux 1989) introduced the concept of 100% solids spray elastomer polyurea coatings that differentiated polyurea coatings (products based on isocyanates/amines) from polyurethane coatings (products based on isocyanates/ polyols). Since then, 100% solids polyurea spray elastomers have been promoted as a new coating technology with polyurea advantage (Broekaen 2002). The author concluded that spray polyurea elastomers is capable and versatile for different variety of applications due to its several advantages as: fast reactivity and cure, relative water insensitivity, two-component, 100% solids (1:1 volume ratio) , excellent physical properties, high thermal stability (up to 350 ºF), wide formulation flexibility, easily pigmented, and ease of application (spray or pour techniques).

In 2000, the industry formed the Polyurea Development Association (https://www.pda-online.org/) to promote market awareness, and the understanding and acceptance of polyurea technology through the development of educational programs, product standards, safety, environmental, and usage recommendations. Guan (2003) studied the chemistry, history, and the developments of 100% elastomeric polyurethane, 100% elastomeric polyurea, and 100% solids rigid (structural) polyurethane. He discussed a newly developed ceramic-modified 100% solids rigid polyurethane coatings that meet the challenge of highly abrasive or high-flow applications and offer ultimate durability and impact resistance. Another improvement of 100% solids polyurethane/polyurea involves incorporating a non-leachable antimicrobial additive, that enables these coatings to provide long-term corrosion protection. The development of a 100% solids rigid aliphatic polyurethane coating is another improvement, which has a better adhesion on non-primed steel or galvanized surfaces, faster initial film development, and superior corrosion and chemical resistance. The author concluded the developed ceramic-modified 100% solids rigid polyurethane coatings meet the challenge of highly abrasive or high-flow applications and offer ultimate durability and impact resistance.

Guan (Guan et al. 2004) studied an advanced 100% solids rigid (or structural) polyurethane coating used for rehabilitating of welded joints, (steel) oil/gas and water/wastewater pipelines. Traditionally, most pipe rehabilitation field applications

have been based on 100% solids elastomeric polyurethane; however, since the mid-1990s, the movement in North America has been toward the development and use of 100% solids rigid polyurethane coatings. The 100% solids rigid polyurethane forms a 3-dimensional cross-linked structure resulting in a coating with superior resistance to chemicals, water penetration, and extreme temperatures. The sprayable resin has a 1:1 mixing ratio with balanced viscosities between two reactive components, which enables easier metering of the components in the field. The author concluded the 100% solids rigid polyurethane field-applied coating technology outperforms the 100% solids elastomeric polyurethanes.

Performance of pipeline lining systems depends on several factors. Guan (Guan et al. 2004) listed twelve most essential performance properties of a coating system for pipeline rehabilitation: adhesion to pipe substrate, abrasion, impact and penetration resistance (hardness), chemical and corrosion resistance, dielectric strength and resistance to cathodic disbondment, flexibility, stability at low or elevated temperatures and service conditions, water absorption or water vapor permeability.

For example, SprayWall® is a self-priming polyurethane lining from Sprayroq Protecting Lining System Company for pipeline rehabilitation that reinstates structural integrity, provides infiltration control and chemical resistance. It may be applied up to 0.25" thick in a single application or lift. It begins to gel in about 8 seconds, with a tack-free condition after 2 minutes. Within 60 minutes, the initial cure is complete, and the structure is capable of accepting flow, while complete curing continues over the next 72 hours. A galvanized corrugated steel pipe culvert, 60 in. diameter and 1,800 ft in length, was renewed with SprayWall® polyurethane, using the SAPL technique in Norristown, PA, 2007, as illustrated in Figure 2-23 (a) and (b).



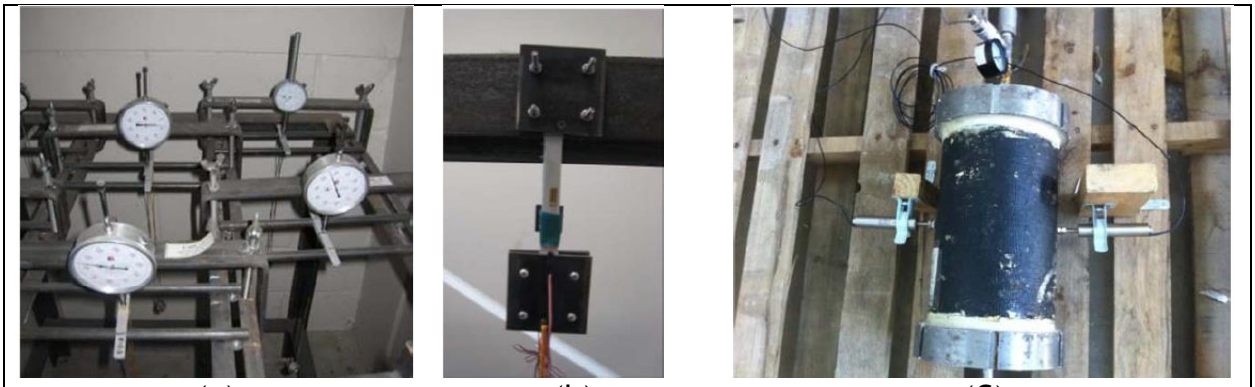
(a) (b)

Figure 2-23. CMP renewal using SprayWall® polyurethane SAPL, Norristown, PA: (a) before renewal, and (b) CMP renewal during SAPL application, 2007 (Sprayroq Inc.).

Entezarmahdi (Entezarmahdi 2015) conducted laboratory testing according to the ASTM standards C39, C76 and C497 to examine the structural capabilities of

renewed RCP samples with different SAPL materials including epoxy, multi structural liners with modified pleurae and foam, polyurethane, and cement mortar. It was concluded that all the tested lining materials enhanced the structural capacity of the pipe samples.

Motlagh et al. (2013) studied and compared spray-on linings applications used in renewal of water pipeline. The objectives of their study were to provide a comparison of spray-on lining methods, including cement mortar, epoxy, polyurethane, and polyurea linings, and to provide an overview of their advantages and limitations. Their methodology involved short-term material property testing (according to different ASTM standards) and long-term tensile creep testing plans of polymer spray-on linings, which were commercially available. Experimental procedure followed for carrying out the long-term tensile creep testing (10,000 hours) was being conducted at the Center for Underground Infrastructure Research and Education (CUIRE) Laboratory, as illustrated in Figure 2-24. The authors discussed the advantages and limitations of spray-on lining methods including cement mortar linings, epoxy linings, polyurea linings and polyurethane linings. Their paper concluded rapid reaction and curing time characteristics of polymers may provide an effective solution to other pipeline renewal technologies (Motlagh et al. 2013).



(a) (b) (C)

Figure 2-24. Comparison of spray-on lining methods using material property testing: (a) long-term flexural testing, (b) long-term creep tensile testing and (c) hydrostatic test setup (Motlagh et al. 2013).

Szafran and Matusiak (2017) studied the structural behavior and compressive strength of reinforced concrete pipes (RCPs) renewed with polyurea SAPL through D-Load testing, which ignored the impact of soil-pipe-structure interactions. The objective of their study was to evaluate and determine structural behavior and increased compressive strength of RCPs lined with polyurea SAPL. Their methodology was involved static compressive testing on RCP with and without internal and external polyurea SAPL application. Results of these tests indicated that using polyurea SAPL on both internal and external surfaces of RCP increased the peak load of failure by about 21.9%. These results concluded that polyurea SAPL increases the compressive strength of RCP. The authors used external coating and internal spraying, as illustrated in Figure

2-25, which are not usable for the application of renewal of existing culverts (Szafran and Matusiak 2017).

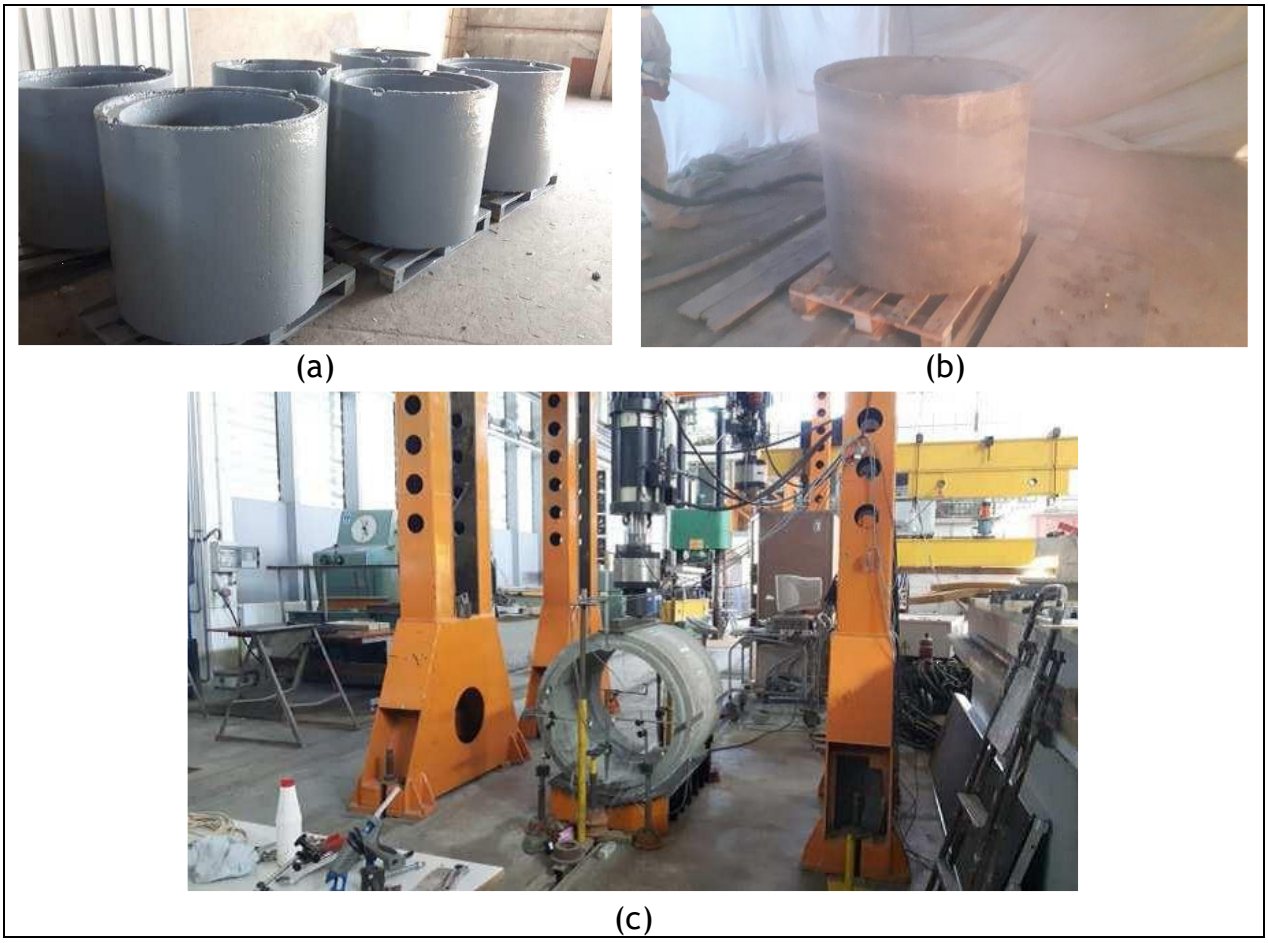


Figure 2-25. Dead-load testing of reinforced concrete pipes (RCPs) renewed with polymeric SAPLs: (a) tested concrete rings covered by polyurea coating, (b) spraying polyurea coating system on concrete ring, and (c) D-load testing frame (Szafran and Matusiak 2017).

Allouche (2017) studied maximizing the service life of culverts by rehabilitation while minimizing direct costs and traffic disruptions. The objectives of rehabilitation were to address stability, bedding deficiencies and hydraulic capacity of culverts. A series of decision-making procedures for rehabilitation of concrete, metal and thermoplastic culverts were prepared. Spray-on coating of metal pipes (SAPL) was part of this study which explained SAPLs were used with different thicknesses. For instance, a 60-in. pipe with a length of 1,800 ft was sprayed with polyurethane at a thickness of 0.3-in. (300 mils). Authors concluded that the main advantage of polymer SAPL is to protect against corrosion, although it increases structural capacity of the host culvert.

Ha et al. (2016) studied the structural behavior and performance of a fast-setting polyurea–urethane (PUU) SAPL as a structural lining material for rehabilitating water pipes, as showed in Figure 2-26. The objectives of their study were to investigate the

bonding between a fast-setting PUU SAPL and steel specimens, the spanning capability of the lining on the water pipes, the bending and shear behavior of PUU lining, and the fatigue behavior of a renewed water pipe with PUU. Their methodology involved a series of experimental tests to assess the bond strength, hole and gap spanning capabilities, angular displacement ability, transverse shear resistance, and fatigue cyclic loading resistance. From these tests, the hole spanning capability of water pipe with 0.2 in. hole was observed to be 1,595 psi. Peel off failure of PUU occurred at an angular displacement capacity of 6.74° and no failure of PUU was observed at a transverse shear capacity of 25% of the diameter. The fatigue resistance of PUU in the range of 10^5 cyclic loadings was achieved. As the result, the authors found that the fast-setting PUU lining can be used in renewal of water pipes. Their paper ignored the impact of soil-pipe-structure interactions (Ha et al. 2016).

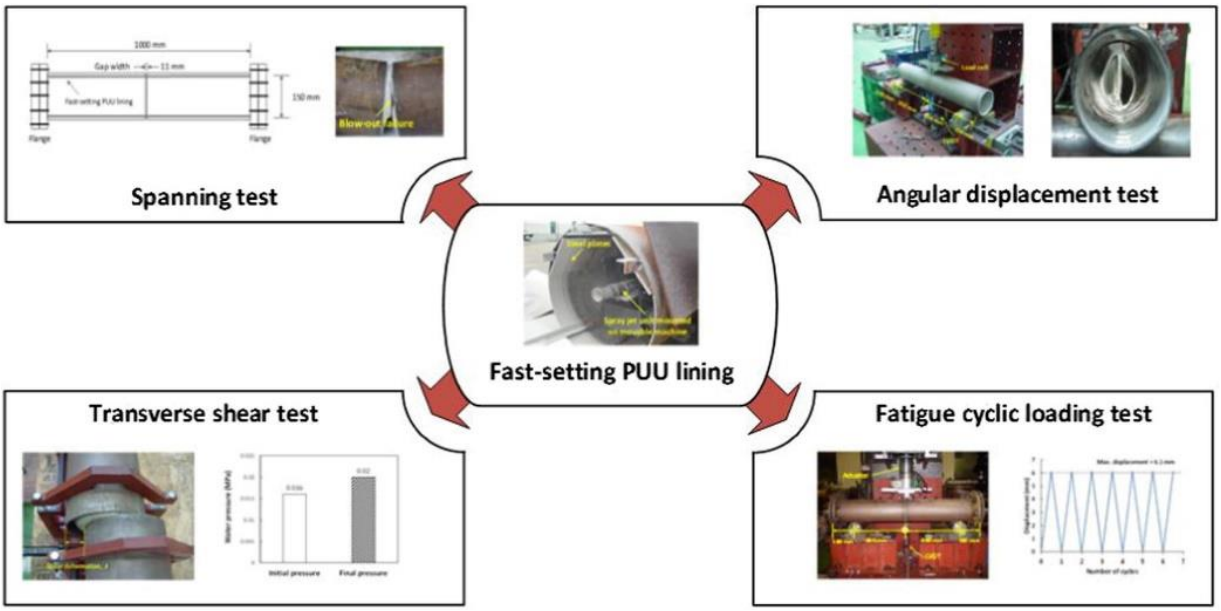


Figure 2-26. The structural behavior and performance of a fast-setting polyurea-urethane (PUU) SAPL as a structural lining material for rehabilitating water pipes (Ha et al. 2016).

2.2.2. Cementitious Spray Applied Pipe Liners

Cementitious SAPL is the oldest method to line culverts. Cement mortar SAPL, has been in existence since the 1900s and is one of the most common lining methods used today. The first successful trial of cementitious SAPL took place in early 1930s (AWWA-C602, 2000). Cementitious SAPL can be classified as ordinary Portland cement mortar and geopolymer.

Kampbell (2016) studied on lining large diameter pipes with cementitious materials. The objective of this paper was to discuss the performance considerations of design and development of a new generation of cementitious material to be used for SAPL. Kampbell presented the characteristics of these materials by describing

thixotropy, permeability, modulus of rapture, thin-shell toughness, and freeze-thaw performance. Author concluded that due to soil structure behavior under hydrostatic and live loads, SAPL needs a comprehensive evaluation of site conditions.

2.2.2.1. Fiber Reinforced Concrete

Fiber reinforced mortar is a composite material of fibers as reinforcing and cement mortar as the binding matrix (Luk 2001). Addition of fibers to cement mortar adds resistance to it by bridging the cracks and limiting the crack propagation which will delay the perfusion of shrinkage cracks (El Debs and Naaman 1995). The cohesive and adhesive characteristics of binding matrix help to transfer stress from matrix to fibers through the interface(Luk 2001). Additional fibers improve the durability of composite reinforced cement mortar like abrasion resistance and freeze thaw resistance by its impermeability and cracking control capability (Izaguirre et al. 2011; Luk 2001; Spadea et al. 2015). Moreover, presence of fiber reinforcement can enhance the bond strength between the old substrate (host pipe) and the repair material (SAPL) (Dawood and Ramli 2011; Iucolano et al. 2013; Luo et al. 2013; Zanotti et al. 2014).

2.2.2.2. Ordinary Portland Cement

Conventional cement mortar has brittle behavior and is easy to crack due to the shrinkage of the materials, concentration of stress and low tensile stress (Banthia et al. 2014). Under an applied load, the existing micro-cracks in concrete propagate and results in formation of macro-cracks. The macro-cracks allow moisture and chloride penetration into the cement mortar. By increasing the load, the condition of macro-cracks can be critical which causes a reduction in the load-bearing capacity of the structure, and a failure is expected (Kohankar Kouchesfehani et al. 2019). Therefore, cracks act as a detrimental agent resulting in steel corrosion, freeze-thaw damage, scaling, discoloration and early saturation (Banthia et al. 2014). To enhance the mechanical properties of conventional mortar, adding fibers of different materials in different sizes such as steel, carbon, polypropylene, polyester, nylon, glass and cellulose can limit the formation, growth of cracks and chemical intrusion (Banthia et al. 1994, 2014; Chiaia et al. 2009; Hsie et al. 2008).

The U.S. Army Corps of Engineers released the results of their field study on the performance of concrete-lined corrugated metal pipe (CLCMP) for use as an alternative to reinforced concrete pipe in November of 1986. Approximately 12,000 linear feet of concrete-lined pipe were inspected during their 15-month long study. Essentially, all were relatively new installations (less than two years old) with the concrete lining installed at the manufacturing plant. The pipe manufacturer was ARMCO. The objective of this evaluation was to verify the manufacturer's claims, that this product offered the hydraulic efficiency of concrete pipe and the structural efficiency of corrugated metal pipe. All these pipes had the valleys of the corrugations filled and a specified minimum lining of 0.375-in. over the crests of the corrugations; but the actual minimum thickness was found to usually be 0.750 in. The result of this study led to development of the ASTM A979 - Concrete Pavements and Linings Installed in corrugated steel structures in

the field standard. It was recommended in this standard to fill the corrugation valleys with concrete lining (ASTM A979, 2003). The result of the Army Corps study showed that the concrete liner increased the load bearing capacity of the pipes.

2.2.2.3. Geopolymer

Geopolymer Spray Applied Pipe Lining (SAPL) material compared with the ordinary Portland cement mortar or reinforced cementitious material provides less shrinkage cracks, high chemical resistance, low creep, and less CO_2 emissions, as well as better physical properties. Geopolymer SAPL is achieved by a mixture of aluminosilicate materials such as fly ash, metakaolin, silica fume, slag, rice-husk ash, or red mud with highly alkaline solutions such as hydroxides or silicates (Darabnoush Tehrani 2020).

Matthews et al. (2014) presented a report to the U.S. Environmental Protection Agencies (EPA) entitled "Performance Evaluation of an Innovative Fiber Reinforced Geo-polymer Spray Applied Mortar for Large Diameter Wastewater Main Rehabilitation in Houston, Texas." The objective of this report was to describe the performance of a fiber reinforced geo-polymer spray applied mortar as a structural lining in a 60 in. circular reinforced concrete pipe (RCP) under 25 ft soil cover. "A lining thickness of approximately 3.3 in. was sprayed in the pipe, which is more than the design minimum value of 1.9 in. The design methodology used was for resisting against first, hydrostatic pressure (Eq. 2-11) and soil loads (Eq. 2-12).

$$t_{pd}^{2.5} = N\frac{P_w l_r^{1.5}\left(1-\mu^2\right)^{0.75}}{0.807E} \qquad \text{Eq. 2-11}$$

Where,

t_{pd} minimum thickness required, partially deteriorated pipe, in.
P_w external hydrostatic pressure due to groundwater = 0.433(H_w+D/12), psi,
H_w height of ground water above pipe, ft,
D inside diameter of the host pipe, in.,
l effective length caused by surface traffic wheels, in.
r inside radius of the host pipe = D/2, in.
μ Poisson's ratio of concrete (0.15),
N safety factor (2.0 default),
E initial long-term modulus of elasticity = 2,000, ksi.

$$t_{fd}^{2.5} = N\frac{W_t l_r^{1.5}\left(1-\mu^2\right)^{0.75}}{0.807E} \qquad \text{Eq. 2-12}$$

Where,

t_{fd} minimum thickness required, fully deteriorated pipe, in.
W_t total loads = P_w + W'_s, psi,
W'_s soil and live loads = W_c/12/D, psi,
W_c loads on pipe = $C_d \times w_s \times (B_d/12)^2$, lb/ft,

C_d load coefficients,
ku' soil coefficients,
H depth of cover from ground surface to top of pipe, ft,
B_d width of trench (inches) = D + 24, in.
w_s unit weight of soil, lb/ft^3.

Selvakumar et al. (2014) used above study to evaluate technologies that have the potential to reduce costs and increase the effectiveness of the operation, maintenance, and renewal of aging water distribution and wastewater collection systems. The main objectives of this study were: (a) to use an innovative large-diameter structural rehabilitation technology on a severely deteriorated pipe located beneath a large open storm water channel, and (b) to assess the new technology by an independent third party. The authors once again concluded that the geo-polymer could be used as a structural alternative instead of traditional repair and replacement methods.

2.2.3. SAPL Renewed Soil-Pipe System Testing

2.2.3.1. Cementitious SAPL

Davidson et al. (2008) studied polyvinyl alcohol (PVA) fiber reinforced concrete. The objective of their paper was to analyze the use of PVA fiber reinforced concrete on corrugated metal pipes (CMPs) to rehabilitate using SAPL. Five topics are included in this study: (1) background review, (2) designing, optimizing, and testing the material formulation, (3) outlining design methodology, (4) demonstrating the application approach and strength, and (5) documenting the technology and results of the project. Finite element analysis was used to evaluate the soil-structure interaction of cementitious liners for CMPs, which was validated by coupon testing and D-load testing of full-scale composite host pipe with liner. Finite Element Modelling (FEM) indicated that the optimum thickness would be 1-in. Figure 2-27 illustrates the results of FEM. An analytical approach was derived for designing the required liner thickness. Authors concluded that PVA offers intriguing and unique characteristics that would minimize the required liner thickness, while providing tension, strength, rigidity and ductility.

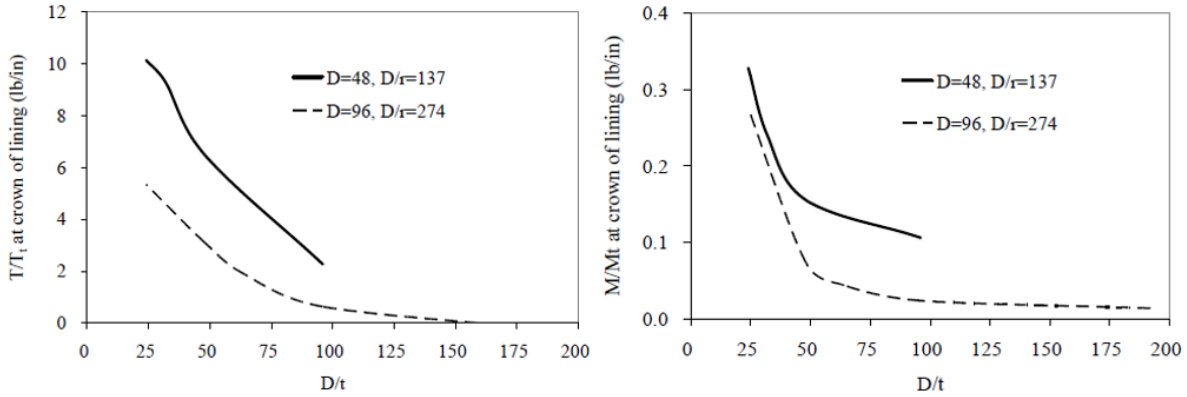


Figure 2-27. Axial forces, T (left) and bending moments, M (right) at the CMP crown (Davidson et al. 2008).

Moore and García (2013) compared two deteriorated CMPs with and without cementitious SAPLs. The objectives of this report were: (1) to monitor the vertical and horizontal diameter changes, as well as deflection of the culverts under different loading conditions before and after the lining, (2) to observe and monitor the cracks occurred on liners before failure, and (3) to assess the interaction between the pipe and liner for flexural loadings. Two deteriorated CMPs of 48-in., 23-ft length were embedded with poorly graded sandy gravel (GP-SP). Both culverts were instrumented with strain gauges and string potentiometers (sensors). Simulated single and tandem axle truck loads were applied over these lined CMPs gradually. Geo-polymer material with 2- and 3-in. thicknesses were used as SAPLs and included 48-in. and 83-in. soil covers. Results showed that deteriorated CMPs with SAPLs survived H-20 and HL-93 loads. The loading continued until lined CMPs failed. First crack was at a loading of 146 kips, and then with increasing loads, larger cracks started at 169-180 kips.

Mai et al. (2013) conducted experimental study on two deteriorated 71-in. CMPs (Mai et al. 2013). The pipe samples had different level of deterioration. They were corroded and perforated along both side of the invert. Both CMPs had bitumen asbestos protective coating, which was removed prior to the testing. The pipe samples were embedded with well-graded sandy gravel soil with 95% of the maximum dry unit weight achieved in a standard Proctor test (Standard Proctor Dry Density or SPDD). The CMPs were backfilled and tested with two different cover of 2 and 3 ft using single axle and tandem load configuration. The result showed that higher deflection occurs at lower cover with single axle loading configuration. In addition, despite the pipes were loaded several times under different conditions, which caused irrecoverable deformations, they were able to take the full-service load 38.22 kips in tandem configuration.

Moore and Garcia (2015) analyzed ultimate strength of cementitious SAPLs. Authors conducted laboratory testing to evaluate the performance of deteriorated helical corrugated metal pipes renewed with cementitious spray applied liners under different burial depths and truck axles, as illustrated in Figure 2-28 (García and Moore 2015). The objectives were: (1) to observe the failure of the CMPs with cementitious SAPL and to determine whether their strength was controlled by cracking of SAPL along crowns and inverts, and (2) to obtain measurements to permit quantitative evaluation of SAPL design methodologies. The CMP diameters were 47 in. and were corroded at the invert location with some perforations at haunch area. The pipe samples were buried at the 47.2 in. and 82.6 in. (4 ft and 8 ft) cover depths using poorly graded sandy gravel (GP-SP) backfill material. The compaction rate of backfill under the haunch area was 84.8% of the SPDD and from haunch to top cover was 92% of SPDD. The testing was conducted for axial and tandem configuration using hydraulic jack to simulate the Canadian design truck before and after pipe sample rehabilitation. For bare CMP (i.e., without liner), the loads were applied in two cycles for full-service load of 45.6-kips. The first cycle applied in one increment and immediately removed to settle the system and to eliminate the effect of irrecoverable ground deformations. Then, the second cycle was applied in 20% increments to represent the incremental response of the system under repeated surface loads, like the pipeline in service. The pipes responses were higher at the first cycle (before consolidation). The tandem axle showed lower

diameter change than single axle. At the end, no sign of structural failure observed at any stage of testing (García and Moore 2015).

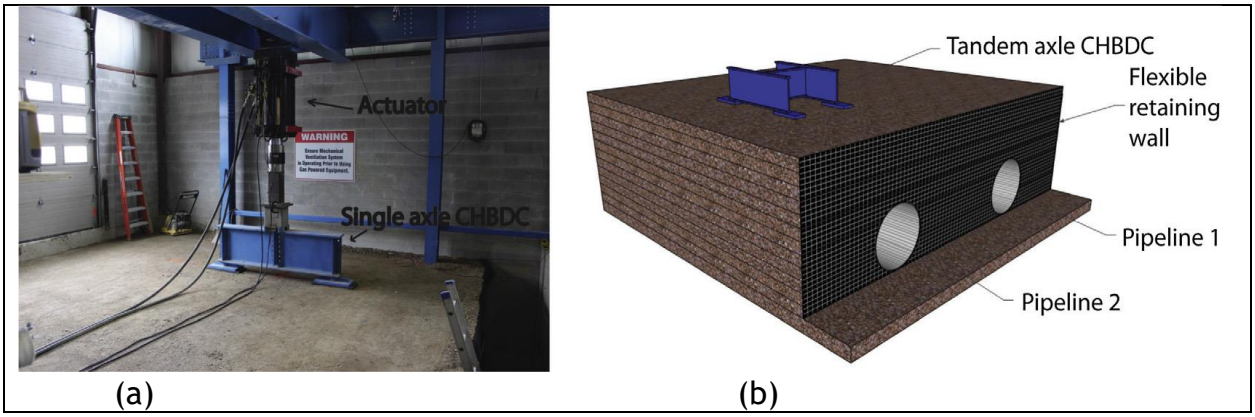


Figure 2-28. Soil box laboratory testing of corrugated metal pipes: (a) single axle loading configuration, and (b) schematic tandem axle loading configuration (Garcia and Moore 2015).

Moore and Garcia (2015) studied the ultimate strength of two deteriorated metal culverts renewed with cementitious SAPL. The specimen size and burial configuration is same as their previous study. However, the load was applied until the failure of the system was achieved. The load-control loading regime was applied and consequently, the post failure behavior of the system was not obtained. The results showed that the liner increased the ultimate bearing capacity of the deteriorated culverts. The sample 1 with 2 in. of SAPL failed at 200 kips and the sample 2 with 3 in. of SAPL failed at 260 kips in tandem axle configuration. It was noted that the thickness of the SAPL was not the same everywhere, and its variation at some location was almost two times greater than the designed thickness.

Royer and Allouche (2016) conducted laboratory testing of RCP and CMP with and without SAPL. The tests were performed on 24-in., 36-in. and 48-in. pipe diameters. For considering the ovality in the CMP host culverts, 24-in. diameter pipes were preloaded to obtain 12% deformation. Compressive strength tests were conducted as per ASTM C39, tensile tests as per ASTM C307 and flexural strength tests as per C78. D-Load values were scaled assuming Type IV bedding factor (Bf) of 1.5. Authors recommended a minimum thickness of 1-in. for pipes smaller than 54-in. and a minimum of 1.5-in. for larger pipes to compensate for local variations in the installed thickness and material properties.

2.2.3.1.1. Invert Paving

Hurd (1984) studied 624 CMP culverts, in which 127 pipes were bituminous coated and 302 pipes were bituminous coated with cementitious paved inverts. The selected culvert sites were located throughout the state of Ohio. The required data pertinent to culvert durability were collected at each site, which included pipe size, pH of water, presence of abrasive material, etc. Regression analysis was performed using field data

collected. Results showed pH of water and abrasiveness of flow have a significant impact on the deterioration rate of CMPs. Innumerable predictive metal-loss equations were developed using the age, water pH, and abrasion for various combinations of CMPs. Bituminous coating with paved inverts increased the durability of CMPs for an average of 12 and more years.

Lougheed (2008) used 0.039 in./min for testing a buried deep corrugated large-span arch culvert in an incremental regime where the displacement is applied at a predefined increment and held for a known period of time before exerting the next increment (Lougheed 2008). ASTM D2412 suggests 0.5 in./min for testing flexible pipes, such as CMPs, under the parallel-plate testing configuration (ASTM-D2412 2018). However, Schluter and Shade (1999) studied the effect of load rate on the parallel-plate testing and suggested 0.05 in./min instead of 0.5 in./min and stated that the 0.5 in./min does not ASTM D2414 deflection rate does not relate to the real world behavior of pipes (Darabnoush Tehrani et al. 2020c; Schluter and Shade 1999). Similar study has been done by Sargand and Hazen (1998) for plastic pipes and a rate between 0.01 to 0.06 in./min is suggested. In addition to the suggested load rates for flexible pipes, ASTM D1633 suggests 0.05 in./min loading rate for testing compressive strength of soil-cement cylinders (ASTM D1633 2013). Therefore, a reasonable load rate value should be within the range of the numbers in agreement with soil and pipe testing values.

Sargand et al. (2015) studied a CMP arch culvert based on the level of corrosion in Muskingum County, Ohio. This case study included replacement of invert with concrete, which had soil cover of approximately 4-in. with asphalt pavement. The deflection of culvert was analyzed, before and after rehabilitation. Concrete placement had a variation in thickness from 2- to 5-in. over the invert. Loading on crown was applied in increments of 18 kips, 40 kips and 60 kips. Results show that under service load, there is no difference between paved and original CMP. Figure 2-29 and Figure 2-30 show longitudinal strain at the peak and valley of CMP before and after paving.

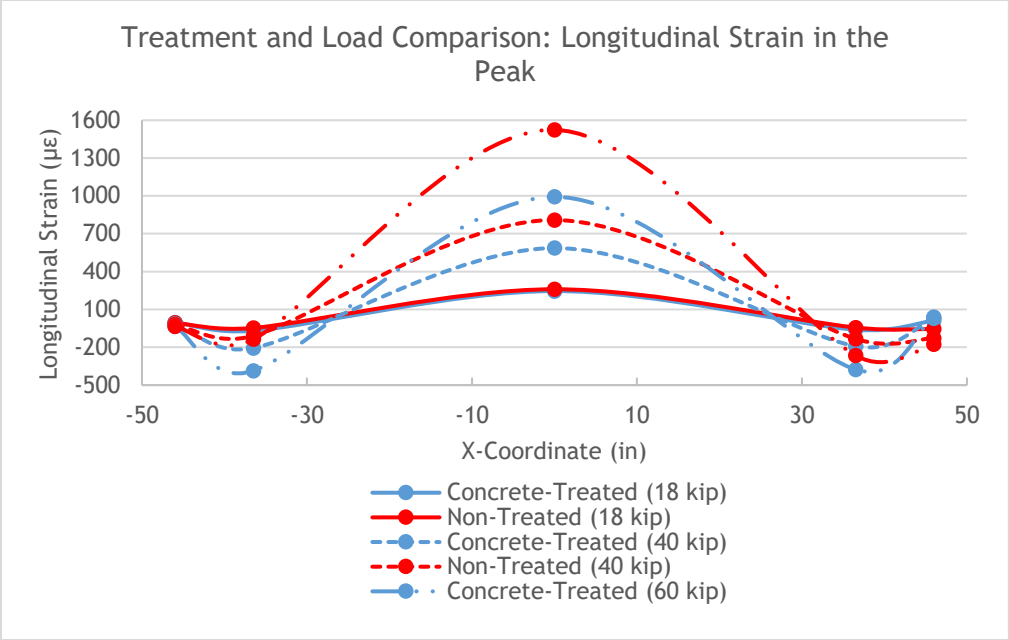


Figure 2-29. Comparison of longitudinal strain at peak of corrugation before and after paving (Sargand et al. 2015).

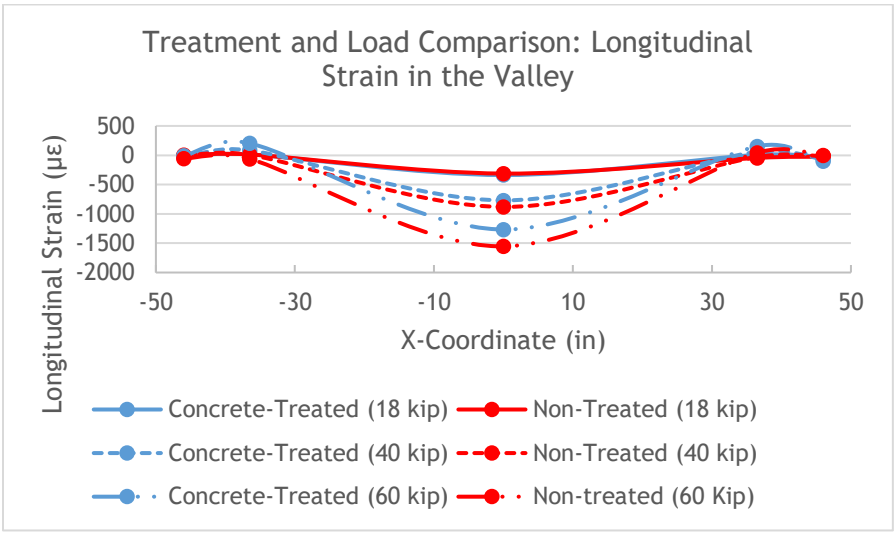


Figure 2-30. Comparison of longitudinal strain at valley of corrugation before and after paving (Sargand et al. 2015).

Masada (2017) carried out field and laboratory testing on an intact, a deteriorated invert, and an invert paved 60-in. CMP. The field test was conducted using H20 truck placed on the top of the culvert (Masada 2017a; b). The laboratory testing was carried out using a hydraulic jack at the outdoor load frame facility, which provided a controlled-testing condition including load rate and loading method. The first laboratory test was conducted on an intact helical CMP using 68 in. by 108 in. load pad over the crown of the buried pipe sample. The load was applied incrementally until the pipe sample wall at one of the shoulders buckled at 923-kips. The second test was carried out on another CMP, backfilled in the same procedure similar to the first test.

The invert of the installed CMP was cut partially to simulate perforations in the invert of a deteriorated culvert in field. The result showed the partially invert deteriorated culvert had 26.6% capacity reduction under relatively large distributed load (with a load pad size of 68×108 in.) applied over the pipe's crown. During the test, a separation of pipe sample's helical interlocking seems separation was observed at 81% of the ultimate load carrying capacity of 667-kips. The third set of tests was carried out similar to the second test, except the whole invert was paved with mesh reinforced cementitious material. The pipe sample failed at 13.3% lower load carrying capacity of the intact CMP at the load of 800-kips. However, it should be considered that none of the tested pipe samples had a fully deteriorated invert. The remaining invert sections partially maintained the resistance to ring compression and played an important role in the CMP's stability and load carrying capacity. While, there are still many culverts in service with fully invert section gone and their structural behavior and load carrying capacity are yet unknown.

Masada et al. (2017) studied structural contribution of paving the invert of culvert. The objective of this study was to present structurally contribution of paving invert of culvert. Two field studies as well as Ohio University's outdoor loading tests facilities were performed to obtain actual data. Study continued by engineering analysis and computer simulations. Selecting the suitable culvert in the field was based on cover depth over crown between 1 to 2 ft, span 5 to 10 ft, no or little sediment, shallow flow depth if it is normal, moderate to severe deterioration (perforations) concentrated on the invert or interface area in the haunch, and good site accessibility. Culvert was tested under an H-20 gravel loaded truck before and after paving in different loading position. Figure 2-31 illustrates the position of wheel loading over the culvert after paving the invert.

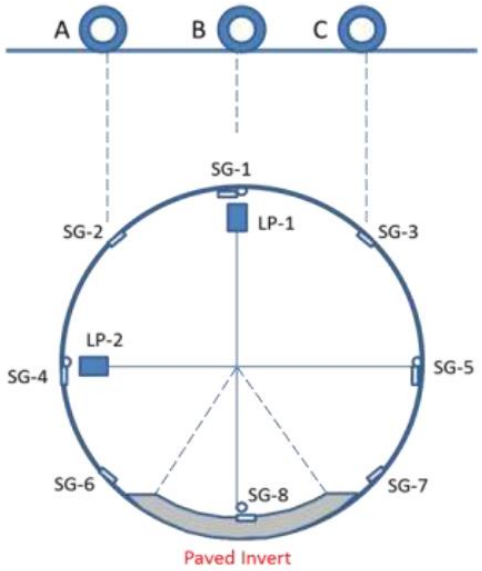


Figure 2-31. Culvert loading positions in the field (Masada et al. 2017).

Authors continued testing in an outdoor site with a 60-in. diameter CMP, 16-ft length and 2-2/3 in. (pitch) corrugation by ½ in. (depth). This CMP had a thickness of 0.109 in. (gage 12) and the pipe wall moment of inertia was 3.425 x 10-3 in.^{4}/ft. This

CMP was tested three times, including baseline performance, removal of 1/3 of the bottom and after paving CMP. Authors presented the following results in the testing task of this study:

- More settlement of the soil cover and more deflection when the CMP invert is severely deteriorated.
- After removing the invert, the load capacity of CMP dropped to 73% (considering a 60 in. CMP).
- The structural behavior of a paved CMP culverts can be considered similar to the original CMP
- Welding #4 rebars to the CMP is recommended to get 100% of structural capacity due to providing better bonding.

Sargand et al. (2018) conducted field testing of a shallow cover severely deteriorated arch CMP at Coopermill Road in Muskingum County, Ohio, illustrated in Figure 2-32. Asphalt concrete pavement was applied on the half of the pipe sample's invert as a repair method and the other half was left unpaved. Static loading was applied at the top of the paved and unpaved pipe sample sections respectively. The test results showed that the unpaved section was subjected to higher transverse strain at the crown compared to the paved section, while transverse strain difference at the springline was inconsequential. Moreover, despite the advanced level of deterioration, both sections of the culvert carried significant load capacity. For untreated section the plastic limit of the steel was exceeded at the crown with the load of 60-kip. It should be noted that, due to different levels of water exfiltration, soil strength around different locations of the pipe sample may not have been the same and level of CMP's deterioration might not have been the same along the culvert (Sargand et al. 2018).



Figure 2-32. Field testing of a shallow cover severely deteriorated arch CMP (Sargand et al. 2018).

The synopsis of similar studies, presented above, discusses laboratory testing conditions. However, there are generally two methods of soil-pipe testing; placing the pipe sample in the field and backfilling to a required cover height and passing or placing a truck with a specified weight and wheel size on the top of the pipe sample (Chaallal et al. 2014; Darabnoush Tehrani et al. 2020c; Rakitin and Xu 2014). In this method, the load is applied continuously and fast. Basically, to prevent damage to the truck and instrumentations, these tests are not designed to monitor soil-pipe structure failure. The other method is to carry out the tests in the laboratory condition using a hydraulic actuator that provides more control on the applied loading rate and condition (García and Moore 2015; Khatri et al. 2015; Kunecki and Kubica 2004). However, in many similar studies, particularly when it is in displacement control, the load rate is not reported.

Tetreault et al. (2018) analyzed a shallow depth horizontal 5.3-ft span and 4.3-ft rise ellipse CMP culvert (1.6 m span and 1.35 m rise). Their objectives were to examine the corroded ellipse culvert behavior before and after paved invert rehabilitation under service load and to check the ultimate load bearing capacity. Experimental methodology included first putting an intentionally corroded elliptical culvert under one and half feet (0.45 m) of soil cover with service load of a tandem axle wheel pad. Second, the invert of the culvert was paved with concrete and tested under load. Figure 2-33 illustrates the schematic of CMP culvert position for the soil box testing.

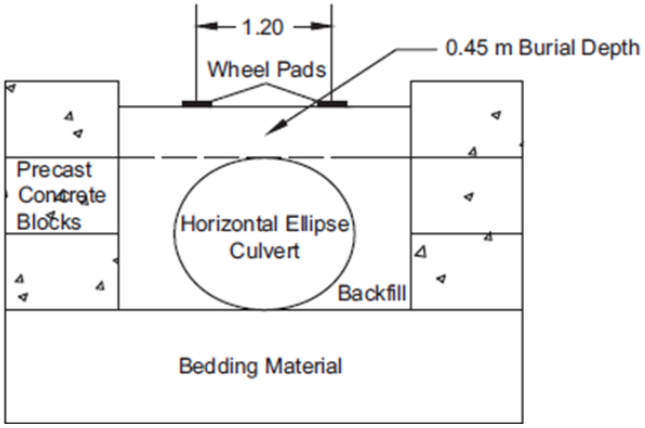


Figure 2-33. Cross section of culvert position and load applied (Tetreault et al. 2018).

In this study, thickness of a CMP culvert was reduced in different locations by 10 to 20%. A poorly graded sandy gravel (AASHTO soil classification GP-SP) was selected for embedment and bedding with 95% of standard Proctor. However, in other part of this paper, authors mentioned that loose material was used for bedding. The selected rehabilitation methodology was paving the invert with 4-in. (100 mm) thickness of concrete layer in 5.3 ft (1.6 m) of the inside sector of the horizontal ellipse with a 4 x 4 galvanized mesh. A 23- by 10-in. (600- by 25-mm) steel load pad was used for service load and a 37- by 14-in. (950- by 370-mm) wooden load pad was used for ultimate load. The deflection and average strains of intact culvert versus deteriorated culvert under service load, same results for deteriorated versus rehabilitated culvert, and finally, strains of paved invert. The conclusions were:

- The loading zone area is more critical,
- The corrosion at the invert of the horizontal ellipse did not have a significant impact on the performance of the culvert under service loads,
- The paved invert rehabilitation technique seemed to improve the structural performance of the horizontal ellipse under service loads,
- The bending capacity increased from 180 Kips (800 kN) to 214 Kips (950 kN), and
- Both intact and rehabilitated horizontal ellipse culverts experienced similar failure mechanisms. The intact culvert failed under 298 Kips (1,325 kN) and rehabilitated culvert failed under 360 Kips (1,600 kN).

2.3. Structural Analysis of Sewer Linings

Trenchless renewal applications are being widely used to restore hydraulic integrity of sewer pipes and to provide them with a new design life. Spray applied pipe linings (SAPL) and cured-in-place pipe linings (CIPP) can benefit from their compatibility with different geometries and taking the shape of host pipe. The imposed deformations of the host pipe and the existing hydrostatic pressure impacts a liner installed inside the old pipe. The originated stresses in the liners due to the deformations of buried structure (that are generally small) are almost negligible. Conversely, the existing groundwater pressure can cause lining failure or material breakdown. Hence, a liner must be designed to resist the external hydrostatic pressure that is the only loading case with a high probability of occurrence. If the host pipe material is damaged or degraded after the liner installation or if the sewer is in an unstable condition, the surrounding static soil load transfers partially from the host pipe to the liner that causes deformation. But, in most cases, the existing pipe-soil structure continues to carry soil load and traffic loads (Thepot 2000).

2.3.1. Structural Classification of Sewer Linings

Falter (1996) classified sewer linings into two categories of Type 1 and Type 2:

- Type 1: Liner is bonded to the existing pipe. The liner and existing pipe both behave as a rigid structure.
- Type 2: Liner is not bonded to the existing pipe and behaves as a flexible pipe. Liner receives support from the existing pipe and soil.

According to the Falter (1996) classification, the discussed and tested polymeric material in this research is under Type 2 category which the liner was not bonded to the host pipe. Many of polymeric materials are brittle and fail in fracture and hence the limiting tensile strain is the suitable failure criteria. Therefore, an appropriate polymeric material used for sewer pipe lining fails in tension not compression. Any failure of polymeric sewer lining materials will happen due to either elastic buckling itself or a sharp increase in displacement, stress and strain that may result in instability and the occurrence of buckling failure and material failure simultaneously (Boot and Gumbel 1997).

2.4. Standards and Construction Guidelines

ASTM F-1216-16 divides existing pipe conditions into two classes: “partially deteriorated” condition and “fully deteriorated” condition. The assignment of a partially or a fully deteriorated design procedure depends upon the existing condition of the existing pipe or its expected structural contribution over the liner design period. Studies (ASCE, 2007) have shown that the term “fully deteriorated” is fundamentally flawed because the existing pipe structure, even in its fully deteriorated state, is holding the soil load and live loads and is not fully collapsed. However, most design methodologies used in practice today follow ASTM F1216.

In 2010, American Society of Civil Engineers (ASCE) published a manual of practice (MOP) for trenchless renewal of culverts and storm sewers (ASCE, 2010). After an introduction, such topics as safety consideration, cleaning and inspection, evaluation and condition assessment, a detailed description of all renewal methods are included. SAPLs are separated into coatings and linings. Coatings are considered as barriers for corrosion protection. Linings are used as corrosion protection, as well as structural enhancement. Both coatings and linings can mitigate further degradation of culverts, but only linings can structurally enhance or structurally repair culverts and storm sewers. The most common materials used for renewal of these structures are cementitious, polymers and sheet linings, which include polyvinyl chloride (PVC) and polyethylene (PE) liners.

NCHRP (2002) has a synthesis of highway practice over the assessment and rehabilitation of existing culverts entitled SYNTHESIS 303. “This synthesis study was initiated to determine the state of the practice of pipe assessment, the selection of appropriate repair or rehabilitation methods, and the management aspects of a pipe/culvert program.” The methodology of this research was based on a survey that was collected data from local, state and federal transportation agencies. Results of survey show that there are no comprehensive methods/manuals for repair; therefore, personal experiences were used for repair. As a conclusion of this study and survey results, most of the respondents wanted to rehabilitate the existing culvert rather than replacing it. Respondents requested the need for SAPLs.

Wagener and Leagjeld (2014) studied over culvert rehabilitation methods and practices. The main objective of this research was to develop the best practices guidelines for rehabilitation and replacement methods for deteriorating culverts. The methodology of this research includes the collection of survey data from Minnesota State and other states of U.S. Rehabilitation methods discussed in this report were the most common culvert rehabilitation and repair methods identified during survey program. The culvert repair process includes these steps: (1) Identify the Problem, (2) Determine the Causes of Deterioration, (3) Evaluate the Hydraulic Condition, (4) Evaluate the Structural Condition, (5) Evaluate Repair, Rehabilitation, and Replacement Options, (6) Implement the Design, and (7) Maintain the Repairs. Culverts with diameters greater than 36” can receive paved inverts since personnel entry is

possible. SAPL can be applied to culverts at early stages of deterioration to increase the service life.

2.5. Example of Rehabilitation Classification Methods

According to another manual published by ASCE (2016), the proper selection of lining materials, their physical properties, and application methodology provide a way to find suitable solutions for a range of pipe and pipe conditions. This includes consideration for host pipe valves and appurtenances, bends, and service connections. Other factors include pipe material and conditions, operating pressures, number of service connections, installation length, renewal objectives, structural capabilities of the host pipe, and soil and live loadings. If a lining is proposed, determination of the liner thickness is an important design parameter, and the physical properties of the liner material have great bearing on it. Depending on how much deterioration is present in the pipe to be renewed, project designers may choose to utilize liners among the categories described in AWWA Structural Classifications of Pressure Pipe Linings (AWWA 2019) as summarized and quoted in the following:

"***Class I linings:***

These linings are nonstructural systems used primarily to protect the inner surface of the host pipe from corrosion, such as the traditional cement mortar lining (CML) and nonstructural polymers such as epoxy.

Class II and III linings:

These linings are called semi-structural because they interact with the host pipe. According to AWWA M28 (AWWA 2014), Class II and III liners are not expected to survive burst failure of the host pipe, because their long-term (50 year) internal burst strength is less than the maximum allowable operating pressure (MAOP) of the host pipe. These liners are capable of bridging certain holes and gaps. Class II liners have minimal ring stiffness and depend entirely on adhesion to the pipe wall to prevent collapse if the pipe is depressurized. Class III liners are self-supporting with no dependency on the pipe wall adhesion. Use of Class II and III liners is recommended when the host pipe has discernible internal corrosion leading to pinholes and leakage, leakage from faulty joints, and localized external corrosion. Examples of Class II and III liners are close-fit semi-structural linings that can span holes and gaps in the host pipe but have minimal thickness and may require bond to the host pipe to prevent collapse during depressurization.

Class IV linings:

These linings are fully structural essentially a pipe within a pipe and they possess a 50-year internal burst strength, when tested independently from the host pipe, equal to or greater than MAOP of the host pipe. They also can survive any dynamic loading or short-term effects associated with sudden failure of the host pipe due to internal

pressure loads. Class IV linings are sometimes considered to be equivalent to replacement pipe, although such linings may not be designed to meet the same requirements for external buckling or have the same longitudinal/bending strength as the original pipe. It should be noted that some renewal technologies can offer Class II, III, and IV linings, depending on the type of application, their material characteristics, design thickness, and installation method."

2.6. Summary

The literature review concludes that SAPLs have potentials for renewing deteriorated culvert pipes and can be used as structural applications to renew/replace the existing culverts. Many structural and construction issues as well as applicability to specific host culvert conditions must be investigated. The objective of current research is to highlight these considerations for proper renewal of existing large diameter (more than 36 in.) circular and arch culverts to develop proper design methodologies/equations for structural application of SAPLs for large diameter deteriorated CMP culverts up to 120 in. diameter or span.

This Page Left Intentionally Blank.

Chapter 3

Additional Reinforcement

CHAPTER 3 - ADDITIONAL REINFORCEMENT

3.1. Objectives

The research team was tasked to determine the benefits of adding reinforcement to SAPL applications. The objectives of this task are to decide when, how, and how much additional reinforcement would be required if the load-response mode is found to be dominated by bending that exceeds the capabilities of the proposed SAPLs modulus of rupture (or flexural strength). Several options of reinforcement including non-metallic fabric, welded wire fabric, traditional reinforcing steel, micro-fibers, and macro-fibers were considered. The specific objectives are:

1. When to add additional reinforcement?
2. How to add additional reinforcement?
3. How much additional reinforcement needed?
4. What are the benefits of non-metallic tensile reinforcement like a basalt mesh?

3.2. Background

SAPLs for buried pipe structures are thin-shell structures having thicknesses typically ranging from 1 in. to 3 in. Additional reinforcement to these thin-shelled systems must fit within the typical thicknesses. The magnitude of bending that the SAPL will experience as part of the existing soil-structure interaction system will determine the selection of the reinforcement system(s) and at what level. The following sections discuss reinforcement alternatives commercially available along with their potential performance enhancement capabilities and constructability.

3.3. Introduction

SAPLs can be used to protect and renew storm sewer conveyance conduits and have many benefits of trenchless technologies (Najafi 2016). The principal objective of a SAPL is to apply a monolithic layer that inhibits further deterioration and/or provides structural replacement. Type of deterioration is dependent upon existing structure under consideration. According to Najafi (2016), the main objective of a structural renewal is to inhibit further deterioration and can structurally renew severely damaged culverts and drainage structures.

In the SAPL technology, the existing host pipe is as a form to a thin layer of SAPL. These thin-shell structures have thicknesses typically ranging from 1 in. to 3 in. The primary materials used for SAPL, generally fall into two broad categories of cementitious such as geopolymers and polymeric materials, such as epoxies, polyurethanes, etc. The environment of the drainage structures such as gravity storm conduits expose the ordinary Portland cement (OPC) and concrete to deteriorate. Moreover, other problems with ordinary cement mortar are lime leaching and

nonstructural nature of its mixture, which is the major issue with rehabilitated deteriorated pipelines (Luk 2001). Additional reinforcement can provide higher tensile strength compared with conventional cement mortar and help with corrosive environment (Matthews, et al. 2015). Thus, this report discusses additional reinforcement in case of cementitious SAPLs.

3.4. Cementitious Fiber Reinforced SAPL

Conventional cement mortar has brittle behavior and is easy to crack due to the shrinkage of the materials and low tensile strength (Banthia, et al. 2014). Under an applied load, the distributed micro-cracks in concrete propagate and result in macro-cracks. The macro-cracks allow moisture and chloride penetration into the cement mortar. By increasing the load, the condition of the macro-cracks will be critical as the load-bearing capacity will be decreased, and a failure is expected. Thus, crack routs act as a detrimental path resulting in corrugated metal pipe and reinforcement corrosion in concrete, freeze-thaw damage, scaling, discoloration and early saturation (Banthia, et al. 2014). To enhance the mechanical properties of conventional cement mortar such as flexural strength, splitting tensile strength and ductility behavior, several previous studies have presented the type and optimum percentage of reinforcement (Hsie, et al. 2008 and Banthia, et al. 1994). Adding fibers of different materials such as steel, carbon, polypropylene, polyester, nylon, glass and cellulose with different sizes can limit the formation, growth of described cracks and chemical intrusion (Banthia, et al. 2014 and Chiaia, et al. 2009).

Fiber reinforced cement mortar is a composite material of fibers as reinforcing and cement mortar as the binding matrix (Luk 2001). Addition of fibers to cement mortar, adds resistance to it by bridging the cracks and limiting the crack propagation which will delay the perfusion of shrinkage cracks (El Debs and Naaman 1995), as illustrated in Figure 1. The cohesive and adhesive characteristics of binding matrix help to transfer stress from matrix to fibers through the interface (Luk 2001). Additional fibers improve the durability of composite reinforced cement mortar like abrasion resistance and freeze thaw resistance by its impermeability and cracking control capability (Luk 2001; Spadea, et al. 2015 and Izaguirre, et al. 2011). Moreover, presence of fiber reinforcement can enhance the bond strength between the old substrate (host culvert) and the repair material (SAPL) (Zanotti, et al. 2014; Luo, et. al 2013; Dawood, et al. 2011 and Lucolano, et al. 2013).

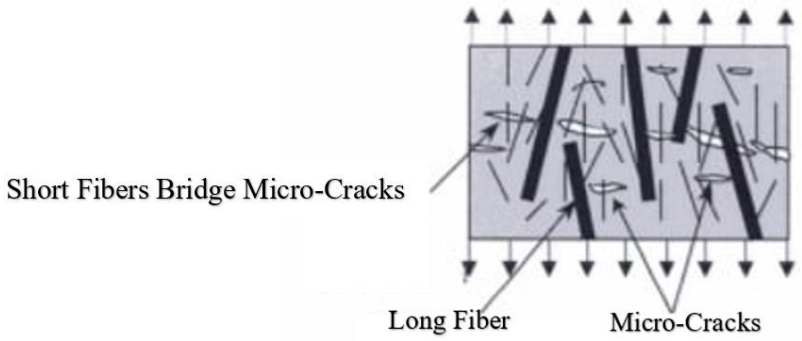


Figure 3-1. Bridging behavior of fiber reinforcements to limit the cracks, (Source: https://theconstructor.org/concrete/hybrid-fiber-reinforced-concrete/17204/).

3.5. Structural Strength

Fiber reinforcement in SAPL rehabilitation technology is used to enhance the structural performance of conventional cementitious mortars. Like concrete, SAPL is an inhomogeneous composite material that is strong in compression but weak in tension and needs to be reinforced at the zones subjecting to tensile stress to keep it from pulling apart. Darabnoush Tehrani (2016) analyzed the reinforced concrete pipe (RCP) behavior under vertical loading according to the ASTM-C76 (Standard Specification for Reinforced Concrete Culvert, Storm Drain, and Sewer Pipe) and studied the effect of various reinforcement location along the pipe thickness. Figure 3-2 shows tension zones of a 48-in. RCP configuration under the three-edge bearing test (TBT) using finite element analysis. As Figure 3-2 shows, the green regions of the pipe are subjected to tension and yellow regions are subjected to compression. However, due to the higher moment exerted at the crown, the crack initiates at the inner side of this crown and propagates along the pipe thickness.

Likewise, the cementitious SAPL in a renewed CMP is prone to crack at crown. The host culvert, in presence of sufficient bond with the SAPL (composite structure), acts as a reinforcement at the outer surface of SAPL, although it cannot provide any resistance to the inner surface of the cementitious SAPL as well as cracking at crown and invert. Therefore, inclusion of fiber reinforcements in cementitious SAPL mortar strengthens the SAPL against the crack initiation at the interior surface of the crown and invert.

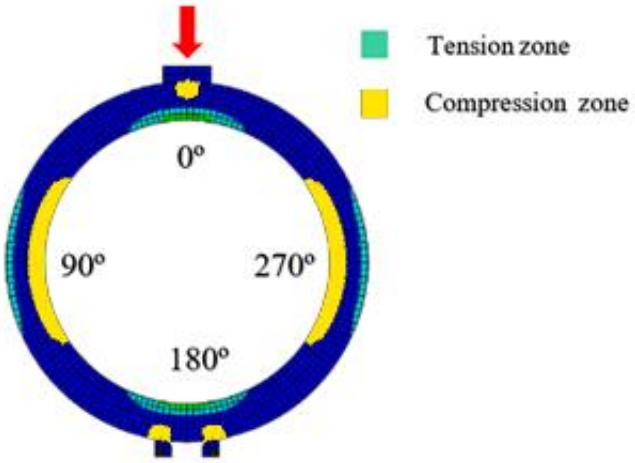


Figure 3-2. FEM analysis of an RCP under TBT setup: inner sides of crown (0º) and invert (180º) are in tension and need to be reinforced (Darabnoush Tehrani 2016).

3.6. Different Types of Reinforcement

Fiber reinforcements used in cementitious SAPL are from different materials, qualities, geometries, shapes, and sizes. According to the ASTM C1116/C1116M (2015), Fiber Reinforced Concrete (FRC) is classified as: Steel Fiber-Reinforced Concrete (SFRC), Glass Fiber-Reinforced Concrete (GFRC), Synthetic Fiber-Reinforced Concrete (SNFRC) and Natural Fiber Reinforced Concrete (NFRC) which are presented in Table 3-1.

Table 3-1. Fiber reinforced concrete classification (According to ASTM C1116/C1116M 2015)

Type	Reinforcement Material		
Type I	Steel Fiber-Reinforced Concrete (SFRC) (ASTM A820)	Stainless Steel Fibers Alloy Steel Fibers Carbon Steel Fibers	Carbon fibers with Petroleum and Coal Pitch
Type II	Glass Fiber-Reinforced Concrete (GFRC) (ASTM C1666)	Alkali-Resistant (AR) Glass Fibers	
Type III	Synthetic Fiber-Reinforced Concrete (SNFRC) (ASTM C1116)	Polyolefin Fibers	Polypropylene Polyethylene Other Polymer Blends
Type IV	Natural Fiber-Reinforced Concrete (NFRC) (ASTM D7357)	Cellulose Fibers	

Additional reinforcement to the thin-shelled SAPL systems must fit within the typical thicknesses ranging from 1 in. to 3 in. The magnitude of bending that the SAPL will experience as part of the existing soil-structure interaction will determine the selection of the reinforcement system(s). Fiber reinforcement can increase the flexural

strength by 25%-55% compared to conventional Portland cement (Roesler and Gaedicke 2004).

The fiber properties, bonding mechanism and its volume fractions (Table 3.2) affect the strength of the reinforced cement (Luk 2001). However, a larger volume fraction of fibers provides a higher strength composite cement mortar. Due to the mixing and workability problems, the maximum volume fraction of fibers should not exceed 3% of cement mortar (Luk 2001 and Naaman 2003).

Table 3-2 Volume fraction of fibers (Ramakrishnan et al. 1998)

Fiber Addition	Percentage (%) of Total Volume of Concrete
High	3% - 12%
Intermediate	1% - 3%
Low	0.1% - 1%

3.6.1. Micro-Synthetic and Macro-Synthetic Fibers

According to the Fiber Reinforced Concrete Association (FRCA 2015), the synthetic fibers are classified in Micro-Synthetic and Macro-Synthetic fibers (Table 4). This class of fibers has emerged over the last 15 years as a suitable alternative to steel fibers when dosed properly. Typical materials include polypropylene and other polymer blends with the same physical characteristics (e.g., length, shape) as steel fibers. These fibers can be dosed from 3 to 20 lb/cy (1.8 to 12 kg/m^3). Macro-synthetic fibers can perform a greater structural role in cementitious linings compared with micro-synthetic fibers. The manufacturer's recommended liner application method will dictate if macro-fibers are an option for a particular liner system. Macro-synthetic fibers cannot be used in the centrifugal casting in place process due to issues with passing through the spin-casting head. To validate the macro-synthetic fiber's performance characteristics, it must be tested in the SAPL mixture to which it will be added. Figures 3 and 4 show a few types of fiber reinforcements.



(a) (b) (c) (d)

Figure 3-3. Macro fibers used in concrete lining; (a) polypropylene fibers, (b) fiberglass, (c) polyolefin fibers and (d) steel fibers.
(Source: Rehabilitation Resource Solutions)



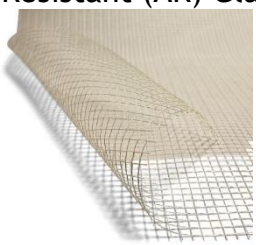
(a) Acrylic Fiber



(b) Alkali Resistant (AR) Glass Fiber



(c) PVA Fiber



(d) Alkali Resistant Glass Scrim

Figure 3-4. (a) Acrylic fiber, (b) alkali resistant (ar) glass fiber, (c) PVA fiber, and (d) alkali resistant glass scrim (Source: http://www.buddyrhodes.com).

According to the Fiber Reinforced Concrete Association (FRCA 2015), micro-synthetic fibers are generally used for the protection and mitigation of plastic shrinkage cracking in concrete. Most fiber types are manufactured from polypropylene, polyethylene, polyester, nylon and other synthetic materials, such as aramid and acrylics. These fiber types are generally dosed at low volumes ranging from 0.03 to 0.2% by volume of concrete, 0.5 to 3.0 lb/cy (0.3 to 0.9 kg/m^3). Microfibers provide the possibility of thin-shell structures without any conventional steel reinforcement (Pigeon et. al., 1996). Micro-synthetic fiber reinforcement is currently being used in at least some, if not all the commercially available cementitious SAPL systems. However, adding micro-synthetic fibers as reinforcement in the SAPL and shotcrete application may cause workability issues with the centrifugal casting process in some cases. Table 3.3 present fibers classifications.

Table 3-3 Fibers classifications (FRCA 2015).

Fiber Type	Specification	Dose
Steel Fibers	• Used for providing concrete with enhanced toughness and post-crack load carrying capacity. • Typically, loose or bundled. • Made from **carbon** or **stainless steel**. • Shaped into varying geometries such as crimped, hooked-end or wit other mechanical deformations for anchorage in the concrete. • Fiber types are classified within ACI 544 as Types I through V • Maximum lengths ranging from 1.5” to 3” (30 to 80 mm). **Carbon Fibers:**	10 to 100 lb/cy (6 to 67 kg/m^3).

Fiber Type		Specification	Dose
		• Very light. • Specific gravity of about 1.9. • Inert to most of the chemicals. • Have potential for special applications that require high tensile and flexural strength. • Elastic modulus as high as steel. • Two to three times stronger than steel.	
Glass Fibers		**Alkali-resistant**	
Macro-Synthetic Fibers	**Polypropylene** **Basalt Macro-Fibers** Other polymer blends with the same physical characteristics (e.g., length, shape) as steel fibers	• Diameter equal to or greater than 0.012 in. (0.3 mm). • Lengths varying from 0.5 to 2.5 in. (12.7 to 63.5 mm). • To perform a greater structural role in cementitious lining concrete mortars. • The Basalt Minibars™ will satisfy the relevant residual strength requirements based on ASTM C1609 tests as specified in ACI 318-08 when used as shear reinforcement in concrete slabs and beams. • Suitable alternative to steel fibers when dosed properly. • Can be used as **structural reinforcement** in concrete or shotcrete. • Can be used as a replacement for long-term crack control steel meshes. • Can be used when an increase in residual (post-cracking) flexural strength is required (ASTM C1609) • Can be used when the application of the lining is either by pumping and troweling or the shotcrete process. • The manufacturer's recommended liner method will dictate if macro-fibers are an option for a particular liner system.	3 to 20 lb/cy (1.8 to 12 kg/m^3).
Micro-Synthetic Fibers	**Polypropylene** **Polyethylene** **Polyester** **Nylon** **Carbon** **Aramid** **Acrylics**	• Diameter less than 0.012 in. (0.3 mm). • Length less than 0.5 in. (12.7 mm or smaller). • **Noticeable improvements to some of the hardened materials' modulus of rupture.** • To be used for the protection and mitigation of plastic shrinkage cracking in concrete. • To minimize early age cracking; or cracking that can occur during the first 24 hours of curing. • To facilitate moisture retention during the curing process (depending on the manufacturer). • To enhance adherence of the mortar mixture to itself during the casting in place process (depending on the manufacturer). • To improve workability due to the smaller size of fibers. • Micro polypropylene (PP) improves the fire protection. • **Micro-Fiber Reinforcements** are currently **being used in** at least some, if not all the commercially available cementitious **SAPL systems.** • They are **not being used as a structural reinforcement** in the current commercially offered cementitious SAPL systems.	• Low volumes ranging from 0.03 to 0.2% by volume of concrete. • 0.5 to 3.0 lb/cy (0.3 to 0.9 kg/m^3).

Fiber Type	Specification	Dose
Poly-Vinyl Alcohol (PVA) Fibers	• Synthetic-made fibers. • Can alter the flexural and compressive performance of concrete when used at higher volumes.	N/A
Natural Fibers	• Manufactured from processed wood pulp products. • To be used in similar manner as micro-synthetic fibers for the control and mitigation of plastic shrinkage cracking. • To be used to reinforce cement-based products in non-commercial applications worldwide. • Has been predominantly used in architectural applications and modified cement-based panel structures.	N/A
Cellulose Fibers		N/A
Steel & Micro/Macro Blends	• They are combination or blending of steel and/or macro-synthetic fibers with various types of micro-synthetic fibers. • These blends help control plastic shrinkage cracking (i.e., micro-synthetics). • They provide concrete with enhanced toughness and post-crack load carrying capacity achieved only with the use of steel and macro-synthetic fibers	N/A

The amount of synthetic macro-fibers used is typically between 6.6 and 13.2 lb per cubic yard of concrete. Actual field performance is influenced not only by the dosing rate, but also the following three characteristics; tensile strength, aspect ratio (calculated as the length/diameter), and anchorage (hooked, crimp, emboss, fibrillation, etc.). And it should be noted that one characteristic does not outweigh another; all three items must work together for optimal performance to be achieved.

As fiber reinforced concrete materials are a composite material, all proposed fiber packages must be tested in the concrete mixture to which it will be added to validate its performance characteristics for use in thin shell linings. Testing done by the University of Akron (Adhikari, 2013) using the ReforceTech BFRP Minibars™ (basalt macro-fibers) demonstrated increases in the modulus of rupture of the concrete up to 2,465 psi using a percentage volume fraction of 4.0%. The testing also demonstrated that these Minibars™ will satisfy the relevant residual strength requirements based on ASTM C1609 tests as specified in ACI 318-08 when used as shear reinforcement in concrete slabs and beams.

Other than the above explained fiber reinforcements, there are also some types of mesh reinforcement applicable for the SAPL rehabilitation technology which are described here briefly.

3.6.2. Welded Wire Mesh Reinforcement

Welded Wire Mesh (WWM) is the standard reinforcement used by most DOT's for minimizing old-age cracking in slabs not subject to "structural" loading (ACI318.2-14). WWM is cross wires laid on top of long wires, welded together at each intersection and creating very even square openings. Welded mesh is more rigid (less flexible) than woven wire mesh. An internet review of specifications currently being used by various

DOTs showed a required minimum cover between 0.75 in. and 1.00 in. Table 5.10.1-1 in the latest edition of the AASHTO LRFD Bridge Design Specifications requires a minimum cover between 1.0 in. and 4.0 in. depending on the application. At a minimum 1.0 in. of cover in a 2.0 in. thick liner the steel would be essentially at the neutral axis of the cross-section. Thus, this would mean that the use of steel WWM for liners 3.0 in. in thickness and smaller would be at odds with this minimum cover requirement. Therefore, steel WWM is not a viable option for SAPL's used in the rehabilitation of culverts.

3.6.3. Non-Metallic Fiber Mesh Reinforcement

Non-Metallic Fiber Mesh (NMFM) significantly increase the flexural strength of this class of cementitious liners without having to resort to metallic reinforcement. Polymeric fiber reinforcement meshes such as woven nylon 66 meshes and Woven polypropylene (PP) meshes are some types of non-metallic fiber mesh reinforcements. Rahman et al (2013) presented a comparison in properties between polymeric fiber reinforcement meshes and conventional ferrous reinforcement meshes under flexural load for a thin (1.0 in. thick) concrete beam. The conducted study took hexagonal and expanded metal meshes, nylon 66 and polypropylene woven mesh placed in a single layer within the 1.0 in. thick cast concrete. The meshes were placed at 0.25 in. from the tensile face of the concrete slabs that would ultimately be cut into 3.0 in. wide beams set to span 11.0 in. in a three-point bending test. The results of their testing found that the expanded metal mesh beams had a modulus of rupture between 2,155 psi and 2,464 psi, the Polypropylene (PP) woven mesh beams had a modulus of rupture between 2,155 psi and 2,218 psi, and the Nylon 66 woven mesh beams produced a modulus of rupture between 2,587 psi and 2,772 psi. Thus, NMFM would be a viable reinforcement alternative for SAPLs used in the lining of culverts. Figure 5 shows some types of these fiber mesh reinforcements.

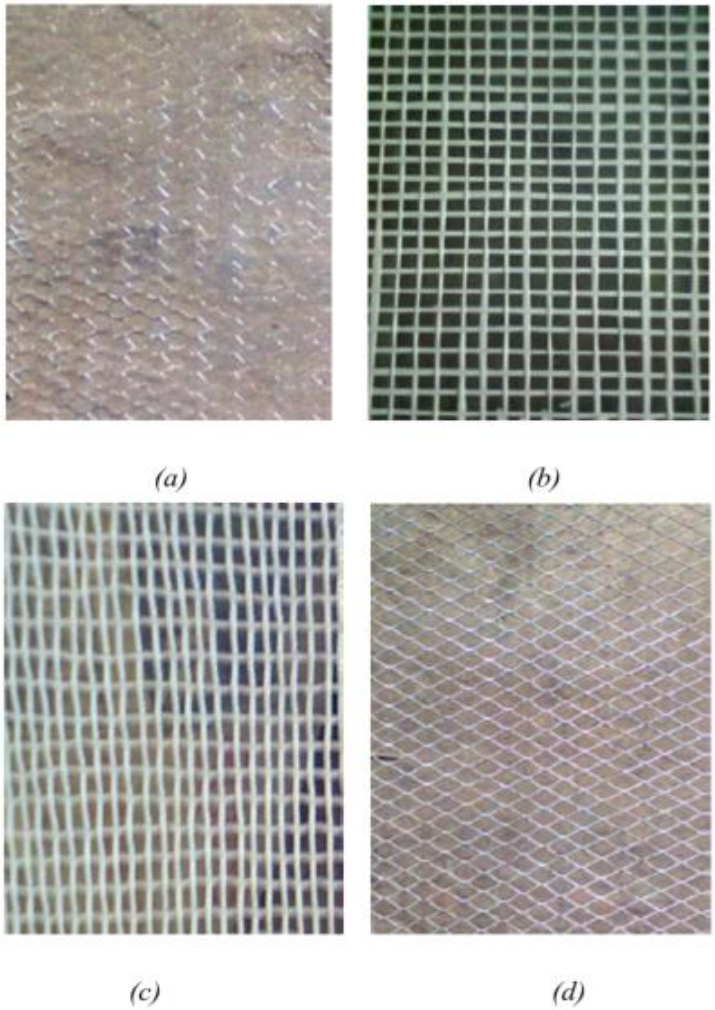


Figure 3-5. Types of Mesh. (a) Hexagonal Iron Mesh, (b) Woven PP, (c) Woven Nylon 66, (d) Expanded Metal Mesh.

3.6.4. Basalt Mesh Reinforcement

Basalt fiber (BF) is a kind of inorganic fiber made by the extrusion of melted basalt rock and is available in the commercial market. The BF has better tensile strength than the E-glass fiber, greater failure strain than the carbon fiber as well as good resistance to chemical attack, impact load and fire with less poisonous fumes. So, BF has a potential to be a suitable replacement for glass, steel, and carbon fibers in many construction applications (Kizilkanat et al. 2015). Basalt even can be in the forms of textile reinforced mortar (TRM) technology (Larrinaga et al. 2014) or mesh reinforcement. Basalt reinforcement mesh geo-grid is available in different sizes (5x5 mm, 10x10 mm, 25x25 mm and 50x50 mm) with epoxy coatings for concrete. They can be stronger than steel wire of comparable size, lighter and easier to handle and install (no nasty cuts). Basalt reinforcement mesh geo-grid will not rust or corrode or cause cracking of concrete. Basalt does not conduct electricity or induce electric fields.

Figure 6 below shows (a) basalt mesh grid with 10 mm by 10 mm opening, and (b) a basalt mesh placed into wet concrete prior to final layer's placement and set to achieve a minimum cover depth of 0.375 in. from the interior face of the liner.



(a) (b)

Figure 3-6. (a) Basalt Mesh Grid with 10 mm by 10 mm Opening, (b) Basalt Mesh Placed into Wet Concrete Prior to Final Layer's Placement.

The advantage of using a basalt mesh grid over a polymeric mesh grid for reinforcement of the SAPL is that it is not affected by hot or cold temperatures as the polymeric meshes used in the cited study. Additionally, because of their volcanic origins they are bonded quite well by the cementitious component (i.e., Portland cement) of the SAPL.

3.6.5. Reinforcement Bars

The remaining category of reinforcement to be considered would be the standard tensile reinforcing bars; made from either ferrous or non-ferrous materials. However, given the thinness of these liners and the strengths that can be achieved using either macro-fibers or non-metallic woven meshes suggests that the expense of employing this type of reinforcement renders it to be not cost-effective. Further, the better distribution of the tensile reinforcement throughout the liner's cross-section and the issues of placing the liner around bars tied on 3.0 in. to 6.0 in. centers (ACI 318.2, 2014) render this alternative as also very low in terms of constructability given their application method.

3.7. Summary of Findings

Thin-shell structures require reinforcement that fits within the typical thickness of 1-3 in. when additional flexural strength is required. Further, they require reinforcement which fits the application of the sprayed in place material. Most, if not all the manufacturers making a fine aggregate concrete liner for SAPL applications are currently using one or more micro-fibers in their mix design to aid in the material's structural performance and to minimize short-term shrinkage cracking. None are currently employing macro-fibers in their mix designs to improve flexural and shear strength or to minimize long-term shrinkage cracking.

Steel fibers should be avoided in components that would be exposed to chloride penetration. Given the strength enhancements available from using synthetic macro-fibers, it is recommended that steel macro-fibers not be used in spray applied cementitious liners (Ghadban, et al. 2017 and Luk 2001). Further, the minimum fiber dosage(s), 1%-3%, that satisfies the required physical properties should be chosen as this will ensure cost-effectiveness and the fluidity (high slump) needed to pump the FRC to the application head.

The Departments of Transportation (DOTs) have two alternatives for increasing the flexural strength of the cementitious liners for specific design requirements. Based on the working environment of culverts and storm sewers these are: 1) the addition of basalt macro-fibers to the mix design or 2) the placement of a NMFM prior to the last layer of the liner being installed. Regarding the latter, it is suggested that the NMFM be installed as close to the surface of the face of the liner as is practical (within 0.375 to 0.500 in.). It should be noted that the thickness of the liner may be increased to reduce the bending stress level on the liner if the pipe barrel hydraulics of the subject culvert will allow the needed increase.

3.8. Concluding Remarks

The following are conclusions based on the literature review presented in this chapter:

- Crack control and post-cracking behavior are the most important advantages of inclusion of additional fiber reinforcements to the cementitious SAPL.
- Use of fiber reinforcements may substantially increase the cementitious SAPL matrix tensile strength.
- A medium volume fraction of fibers (1%-3%) may enhance post crack load-carrying capacity, tensile stress, flexural stress, shrinkage cracking resistance, durability modulus of rupture, energy absorption, fracture toughness and impact resistance of the fiber reinforced cementitious SAPL mortar (Ostertag and Blunt 2008; Luck 2001). The magnitude of enhancements needs to be verified through the experimental tests.
- A high aspect ratio (fiber length divided by fiber dimeter) produces a higher strength composite (Luk 2001).
- Various literatures show inconsistent effect of fibers on the compressive strength of the FRC (Noushini, et al. 2013; High C, et al. 2015; Benaimeche, et al. 2018; Banthia, et al. 2014; Błaszczyński, et al. 2015; Spadea, et al. 2015; Rodin III, et al. 2018; Yoo and Banthia 2016; Ayub, et al. 2014; Tassew and Lubell 2014; Kizilkanat, et al. 2015).
- The presence of fiber reinforcement can enhance the bond strength between the old substrate (host culvert) and the repair material (SAPL) (Zanotti, et al. 2014; Luo, et. al 2013; Dawood, et al. 2011 and Iucolano, et al. 2013).
- Micro-Synthetic Fibers and Basalt Mesh Grid can fit with the SAPL application.

- As the SAPLs are thin shelled structures macro-synthetic fibers do not fit well with this application which mostly ranges from 1 to 3 in. Steel fiber are not applicable either due to their size as well.
- Steel WWM is not a viable option for thin-shelled SAPLs.

Chapter 4

Evaluation of the Need to Fill Valleys of Corrugated Pipes

CHAPTER 4 - EVALUATION OF THE NEED TO FILL THE VALLEYS OF CORRUGATED PIPES

4.1. Introduction

This objective of this task is to address the differences in opinion in the cementitious Spray Applied Pipe Liner industry as to whether the valleys of corrugated metal pipes should be filled prior to application of the design thickness or merely follow the corrugation profile of the pipe being lined. Currently, when cementitious (and polymeric) liners are applied in manhole structures the consensus is that the specified liner's thickness will be measured from the peaks of the irregular surface. This also applies to brick pipe structures, stone pipe structures, and badly eroded (what had been smooth) concrete structures. But, given the uniform shape of the corrugations, some cementitious SAPL suppliers propose that the wall thickness can follow the profile of the corrugations in the pipe. This task will consider the need for filling the valleys of the corrugations with cementitious SAPL material considering the criterion of structural strength, constructability of the liner, and pipe barrel hydraulics performance. Flexible materials are dependent on the soil surround and the stiffness it can provide against deflection. The moment of inertia for a flexible polymeric material, even if one were to fill the corrugations, provides relatively little resistance to the deflection versus the soil's contribution.

The Army Corps of Engineers released the results of their field study on the performance of concrete-lined corrugated metal pipe (CLCMP) for use as an alternative to reinforced concrete pipe in November of 1986. A total of almost 12,000 linear feet of concrete-lined pipe were inspected during their 15-month long study. Essentially, all were relatively new installations (less than two years old) with the concrete lining installed at the manufacturing plant. The only exception to this was a 26-year-old installation that had the concrete lining installed in the field. The pipe manufacturer was ARMCO. The objective of this evaluation was to verify the manufacturer's claims, that this product offered the hydraulic efficiency of concrete pipe and the structural efficiency of corrugated metal pipe. All these pipes had the valleys of the corrugations filled and a specified minimum lining of 0.375-inches over the crests of the corrugations; but the actual minimum thickness was found to usually be 0.750 inches. Figure 4-1 illustrates the upper and lower sections of the concrete lining.

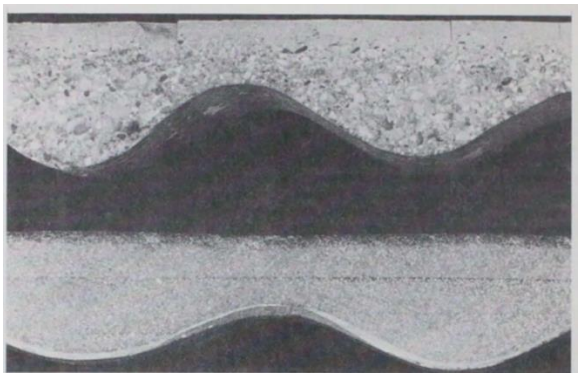


Figure 4-1. The Upper section of the concrete lining was made by spinning the pipe, the lower section was made with the pipe stationary, (Source: Construction Products Division of Armco, Inc.).

The report noted that the CLCMPs appeared to be behaving as a flexible rather than a rigid conduit. It was also noted that rigid conduits such as RCPs cannot deflect more than about 0.1 percent of their diameter without damage (i.e., 0.01-inch crack). Therefore, they must be designed to carry the load of the soil above the pipe including negative arching loads from the soil adjacent to that directly above the pipe. Flexible conduits can deflect 5.0 percent or more under load without damage. During the pipe inspections in their study, the Corps found deflections of the installed pipe ranged from -1 to +6 percent of the nominal diameter; but generally being less than 3.0 percent. They noted that no popping or spalling resulted from these deflections. The characteristic, randomly spaced, circumferential and longitudinal cracks were observed in uninstalled pipe at both the plant and the job sites, indicating that they resulted from plastic shrinkage of the concrete during curing and/or handling. They also noted that the cracks remained tightly closed in the installed pipe except when the deflection exceeded approximately 5.0 percent of the nominal diameter.

The results of the above evaluation led to the production of two ASTM standards for CLCMP:

1. ASTM A849 - *Post-Applied Coatings, Pavings, and Linings for Corrugated Steel Sewer and Drainage Pipe*
2. ASTM A979 - *Concrete Pavements and Linings Installed in Corrugated Steel Structures in the Field*

In the latter standard's paragraph 5.3.1 it reads:

"*The lining for all straight pipes shall be placed, in one or more passes, by a machine that progresses uniformly through the pipe and applies concrete against the pipe surface fully filling the corrugation and providing a uniform thickness over the corrugation crests…*"

This reflected the fact that writers of the standard expected that conventional cement mortar lining equipment would be employed in the installation of the liner in the field.

As the above linings were meant for new CMP installations, the minimum finished thickness specified in these two ASTM standards was "0.125-inches above the crests of the corrugations or structural plate bolts or nuts as applicable".

4.2. Typical Corrugation Profiles of CMP Structures

Several CMP profiles have been used across North America since its introduction in 1896. They are the 1½×¼ in., 2×½ in., 2⅔×½ in., 3×1 in, and 5×1 in. The CMP industry has added the 6×2 in metal plates for erecting pipe arch structures of sizes 61 in. by 55 in., and larger. Of these sizes, the most commonly encountered corrugation profiles today are the 2⅔×½ in., 3×1 in., and 6×2 in. Table 4-1 presents CMP profiles and their respective size ranges. Figure 4-2 illustrates CMP Profiles in the North America.

The 2⅔×½ in. and 3×1-in. corrugation profiles may have a riveted construction (annular corrugations) or lock seam construction (helically wound corrugations), while the 6×2-in. corrugation profile is made up by bolting standard panels together. Values of the coefficient of roughness (n) for standard corrugated steel pipe published in AISI (1999) for use in the Manning's Formula are presented in the Table 4-1.

Table 4-1 CMP profiles and their respective size ranges.

Corrugation Profile	Circular Pipe Size Range	Pipe Arch Size range
2⅔× ½ in.	12" – 96"	18"×11" to 85"×54"
3 × 1 in.	36" – 120"	43"×27" to 142"×91"
6 × 2 in.	60" – 312"	61"×55" to 247"×158"

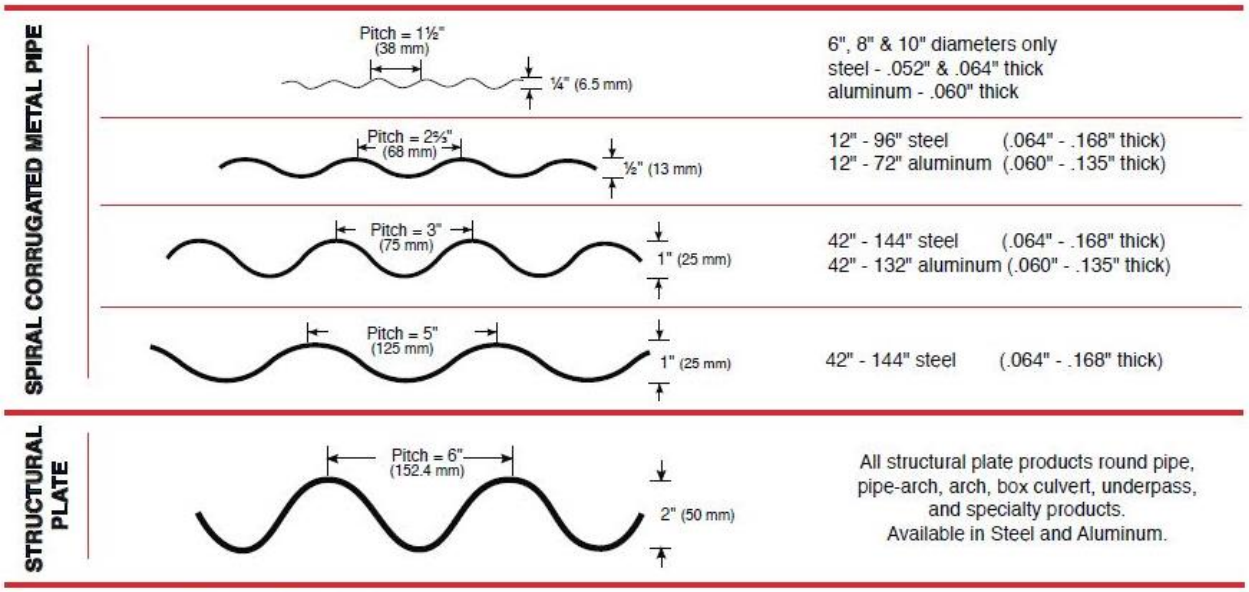


Figure 4-2. CMP profiles in North America, (Source: PCPIPE, Website: http://www.pcpipe.com).

Table 4-2 Coefficient of roughness of CMP structures (Source: AISI,1999).

Corrugations	**Annular 2⅔×½ in.**	**Helical 2⅔x ½ in.**								
	All Sizes	36"	48"	60" and Larger						
Unpaved	0.024	0.019	0.020	0.021						
25% Paved	0.021	0.017	0.020	0.019						
Fully Paved	0.012	0.012	0.012	0.012						
Corrugations	**Annular 3×1 in.**	**Helical 3×1 in.**								
	All Sizes		48"	54"	60"	66"	72"	78" and Larger		
Un-Paved	0.027		0.023	0.023	0.024	0.025	0.026	0.027		
25% Paved	0.023		0.020	0.020	0.021	0.022	0.022	0.023		
Fully Paved	0.012		0.012	0.012	0.012	0.012	0.012	0.012		
Corrugations - 6×2 in.					60"		72"		120"	180"
Un-Paved					0.033		0.032		0.030	0.028
25% Paved					0.028		0.027		0.026	0.024
Fully Paved					0.012		0.012		0.012	0.012

4.3. Design Goals of Lining CMP Structures

While the purpose of the SAPL study is to produce a set of design equations for arriving at a minimum wall thickness to renew the structural performance of existing culverts and conduits, an engineer cannot forget to address the other design performance parameter, which is the hydraulic performance of the structure. Given that the existing pipe size was originally selected upon the ability to convey a certain level of storm, the decision becomes, whether to produce a relatively smooth interior wall surface profile of the lined pipe or to emulate the corrugated surface profile of the host pipe (if that is possible). Table 4-3 presents a 66-in. diameter circular CMP with 3×1-in. corrugation profile that is 200 feet in length, which is found to be in outlet control. The proposed lining thickness is 1.5 in. Assuming the Manning “n” value for the smooth liner (corrugations filled) will be 0.017 (conservative) and the Manning n for the corrugated liner will match that of the host pipe, which is 0.025, the estimated hydraulic capacity after lining was calculated. The estimated change in capacity for the relatively smooth lined culvert was found to be +41%; while the corrugated finished liner was found to produce a net loss of 4% for the subject culvert. Thus, one can see that if preservation of the existing culvert's hydraulic capacity is indeed a design consideration for the DOT then filling of the corrugations and then applying the 1.5-in. liner thickness is the recommended alternative when that particular structure is in outlet control. More study is recommended to confirm the range of Manning's "n" value for spray applied linings.

Table 4-3. Pipe barrel hydraulics example.

Host Pipe		Lining Thickness, in.	Corrugations	Manning n	% Change
Diameter, in.	Length, feet				
66	200	---	---	0.025	0
66	200	1.50	Not Filled	0.025	−4
66	200	1.50	Filled	0.017	+41

4.4. Constructability of Liner Geometry

Task 3 of this project discussed the incorporation of additional reinforcement into the SAPL considering the methodologies of applying the SAPL to the host pipe structure. This section addresses the constructability of SAPL application methodologies in the context of the need to fill the valleys of the corrugations prior to applying the liner for the 2⅔×½ in., the 3×1-in., and the 6×2-in. profiles.

Given that the cementitious liners typically start at pipes around 36 in. in diameter, the minimum finished thickness of these liners is going to be between 0.50 and 1.0-in. (depending on the conservatism of the design engineer or pipe owner). For a pipe having a 2⅔×½ in. profile, rational thinking would conclude that it is not practical to follow such a shallow corrugation profile for any thickness of liner as filling the corrugations first would be unavoidable for all three application methodologies: centrifugally casting in place, pumping, and troweling on, and shotcreting.

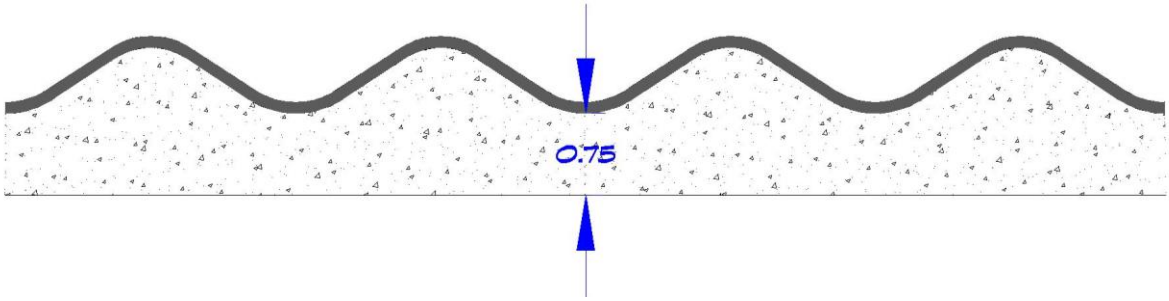


Figure 4-3 shows a ¾ in. thick liner in this profile to graphically illustrate this to the reader.

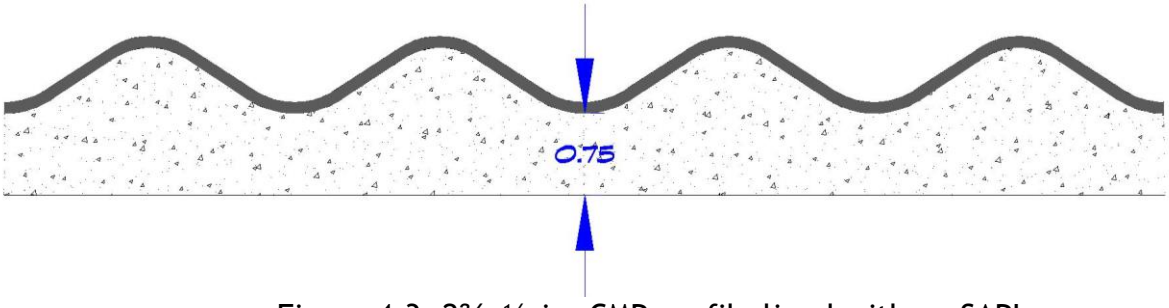


Figure 4-3. 2⅔×½-in. CMP profile lined with an SAPL.

The 3×1-in. corrugation profile shown in the Figure 4-4 illustrates the issues with trying to follow the corrugations when trying to install a 1.00-in. thick liner (top left) and a 1.50-in. thick liner (top right). Passing a spin-casting unit through the pipe at a uniform speed and using the crests and/or the valleys for thickness control points would almost certainly create a shortfall in the thickness on the sloping areas of the CMP wall surface of approximately 29% or more. This is because the tangent angle for the 3x1 and 6x2 profiles is 45°. This means if you are measuring a 1.0 thickness in the valleys and on the crests, the tangential distance (or thickness) for the sloping portions of the corrugations is at best going to be 0.707 times this value. There is not an easy way of controlling this shortfall other than increasing the thickness on the crests (i.e., increase the 1.00-in. thickness to 1.40-in. to assure the 1.0-in. required). Again, it is clear from the bottom part of the Figure 4-4 that filling the corrugations first and subsequently using the crests of the corrugations to confirm thickness applied is the only practical way of ensuring the required thickness per the design calculations is applied with the least amount of material.

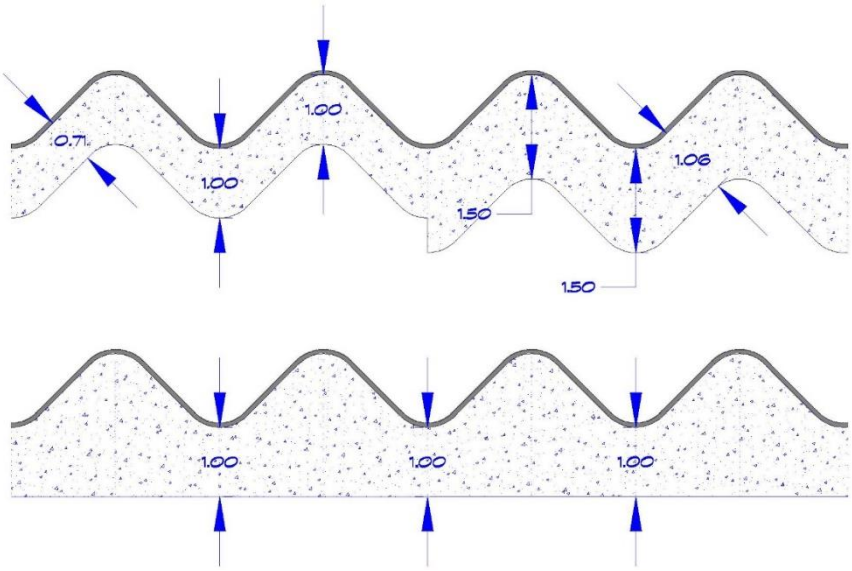
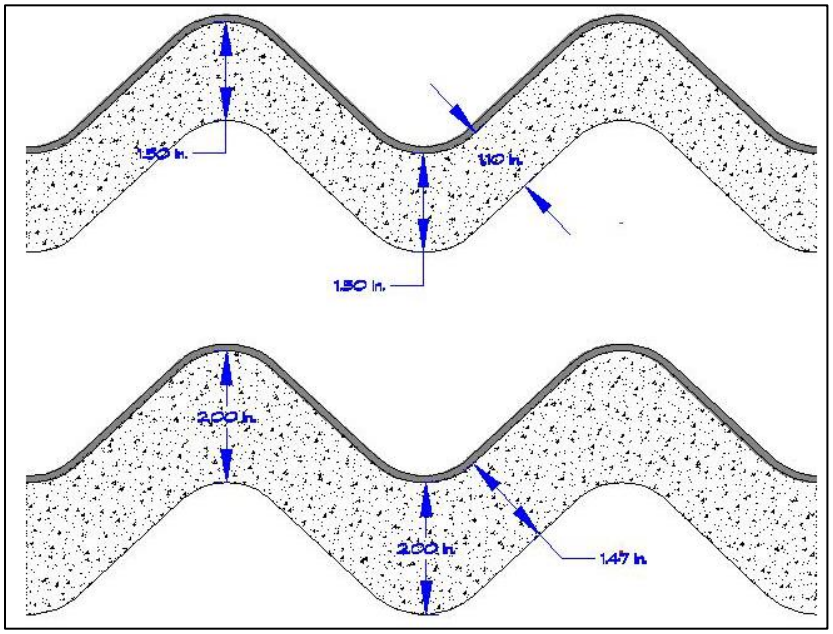


Figure 4-4. 3×1-in. CMP profile lined with SAPL.

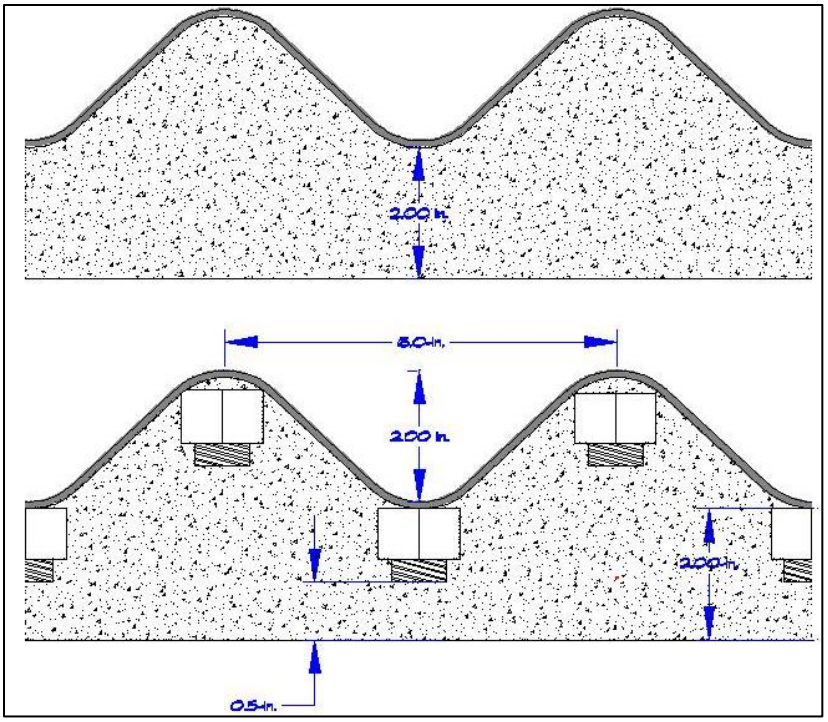
Considering a 6×2-in. corrugation profile, a 1.5-in. and 2.0-in. thick SAPL should be applied (Figure 4-5 a and b). Given the deepness of this profile and the span between the crests, the possibility of saving a significant amount of material following the profile on these CMPs demands a serious consideration of this alternative. However, a graphical analysis of the lining process shows that using a spin-caster pulled at a constant rate of speed through such a pipe would result in a shortfall of approximately 29% on the sloped surfaces of the pipe's wall section. Again, this can also be arrived at analytically using the tangent angle of the sloped wall surface of the 6×2-in. corrugated metal profile which is 45°. At this angle, the measurement of the thickness measured perpendicular to the sloped wall would be 0.707 times the thickness measured on the crest or valley of the corrugation (i.e., 0.707 x 1.5 = 1.06 inches). To compensate this, an increase of thickness to the crest of the corrugations is needed (i.e., increasing the thickness of

1.50-in. to approximately 2.00-in.). For the pump-trowel and shotcrete methodologies, more controls need to be used on the sloped surfaces, but this puts too many expectations on the installer (nozzleman) and the quality assurance inspection process itself to assure that the specified thickness can be "uniformly" applied.

The hydraulics requirement of the 6x2 corrugation profile lined pipe is more significant than the smaller sizes. The earlier example on this subject shows the differences in the pre- and post-coefficients of roughness for the "follow the corrugation profile" versus filling the corrugation profile and then lined, produces a significant difference in the hydraulic capacity of the culvert when in outlet control. For the example's 66-in. diameter 3×1-in. corrugation profile the pre-lining coefficient of roughness was 0.025. If the same 66-in. diameter CMP had a 6×2-in. profile, the pre-lining coefficient of roughness is approximately 0.033, making the pipe barrel hydraulics performance difference even more significant.



(a)



(b)

Figure 4-5. Linings in a 6×2-in. corrugation profile CMP: (a) not filling the corrugations and (b) filling the corrugations.

4.5. Increase in Structural Strength

Filling in the corrugations can also lead to a noticeable increase in the ring stiffness and strength of the liner and thus can be advantageous to the structure's performance as the size of the structure increases. As an example, let us consider a 72-inch diameter pipe with a 6×2-in. corrugation profile filled with a 2.0-in. thick liner (measured above the crest of the corrugations). Ring stiffness is a function of the modulus of the material, the area moment of inertia, and the diameter of the ring; RS = EI/D^3. Stating the area moment of inertia of the CMP cross-section as I, a cementitious liner that follows the corrugation profile has an area moment of inertia of 11.9I; and a cementitious liner that fills the corrugation valleys and then forms a 2.0-inch-thick liner over the crests of the corrugations has an area moment of inertia of 20.9I. The neutral axis of these various configurations produces effective diameters of 74, 72, and 71.24 inches, respectively. Using a modulus of elasticity of 30,000,000 psi for the steel and 5,260,000 psi for the cementitious liner demonstrates that the ring stiffness of the liner following the corrugations is 2.3 times that of the unlined CMP (when new); and when the corrugation profile is filled and then the 2.0-inch-thick liner is applied the ring stiffness is 4.0 times that of the unlined CMP. The flexible polymeric liner used in the study at 2.0 inches thick would have a ring stiffness of 0.32 and 0.57 times that of the unlined CMP, respectively. This difference in ring stiffness demonstrates that the new liner becomes the dominant structure independent of any contribution by the existing

structure. This dominant performance is verified by the lack of any significant strain increases seen in the 156-inch diameter CMP under SR 16 in Clay County Florida in testing by Resensys.

Figure 4-6 illustrates a graphical representation of the increase in cracking moment with increases in the cementitious liner thickness for filling versus following the corrugations. In these plots the contribution from a composite action of the CMP with the new liner is considered. The relative separation between the followed and the filled cracking moments and the increase in separation between them are notable in the curves. Therefore, the filled corrugations provide a stronger, more robust design.

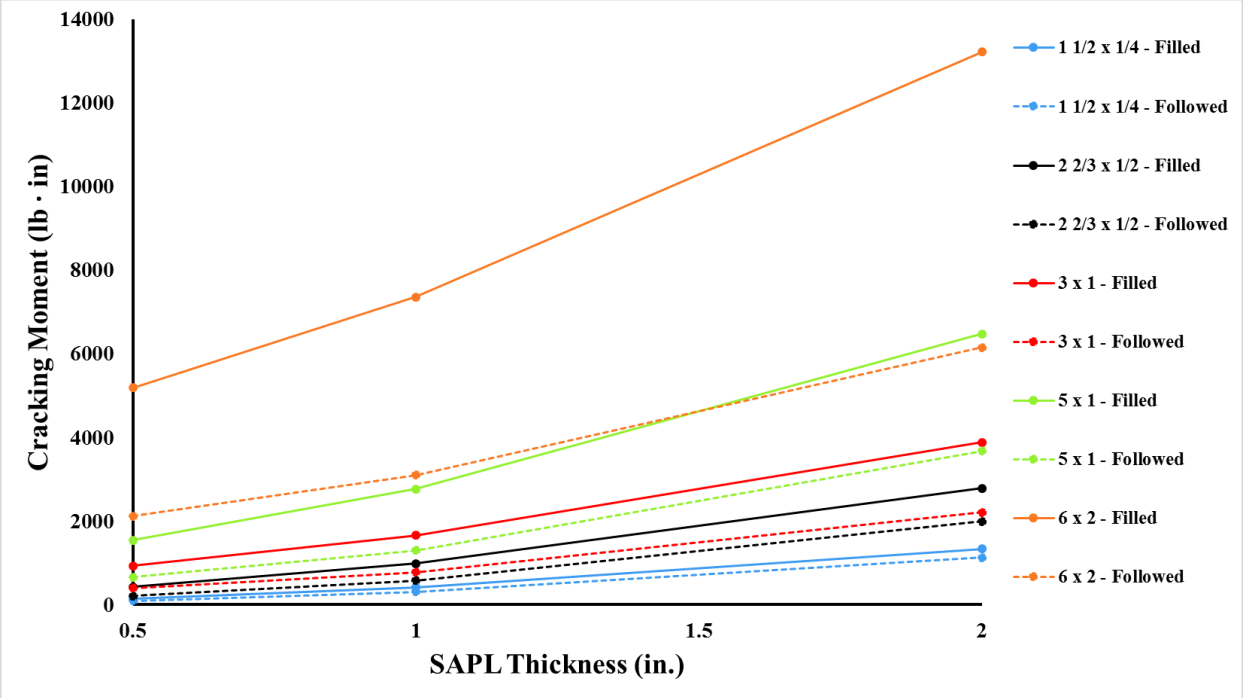


Figure 4-6. Cementitious SAPL thickness versus cracking moment.

4.6. Other Factors

In addition to the practicality of applying the liner to the pipe wall as designed and the pipe barrel hydraulics, there is also the consideration of the operational issues of a corrugated profile versus a smooth surface profile. A smooth surface profile will produce:

- A lowered tendency to catch debris (i.e., tree limbs) as it is moved through the pipe barrel.
- Protection against impact damage from large rocks and boulders as they pass through the culvert.

- Better corrosion coverage over any protruding CMP assembly hardware. To achieve a minimum cover thickness in the valley area basically demands filling the valley area (as illustrated in Figure 4-5).

4.7. Conclusions

In summary, while the engineer could design a theoretical wall thickness that followed the corrugation profile of a particular CMP; it would be impractical to install such in the field. Further, the likelihood that the finished cross-section of the lining would resemble that design would be low. The site installation inspections showed how difficult it was to get the required thickness of the liner. During the installation process the crests of the corrugations provide the reference points needed to assure the owner of the pipe that the specified thickness is being installed. This is true of both cementitious and flexible polymeric material. Further, beyond the structural performance issues, it has been shown that pipe barrel hydraulics also favors a smooth interior surface profile. From an operational standpoint, this can be true even when the culverts are in inlet control.

Operational considerations favor a smooth surface profile for the lining. Maintaining flows through a culvert rewards a surface profile that lowers its tendency to catch and hold onto debris swept up by the storm water flows. Minimizing the impacts of large rocks and boulders passing through the culvert minimizes the potential for losing parts of the lining.

Thus, the guidance provided by ARMCO's engineering team in the 1980s and defined in the ASTM standard A979, *Concrete Pavements and Linings Installed in Corrugated Steel Structures in the Field*, which still exists today specifying the production of a smooth interior surface profile liner, is the best long-term design solution for this new generation of SAPL's. While their focus was to produce a pipe that could compete competitively with smooth bore concrete pipes; lining existing corrugated metal pipes with a liner that produces a new smooth bore path not only produces a more hydraulically efficient pipe, but also a more structurally sound pipe.

This Page Left Intentionally Blank.

Chapter 5

Comparison of Construction and Environmental Cost of SAPL, CIPP and Sliplining

CHAPTER 5 - COMPARISON OF CONSTRUCTION AND ENVIRONMENTAL COST OF SAPL, CIPP AND SLIPLINING

Glossary

Air Quality Monitoring	The systematic, long-term assessment of pollutant levels by measuring the quantity and types of certain pollutants in the surrounding, outdoor air.
Analysis of Variance	A statistical method in which the variation in a set of observations divided into distinct components.
Granular Activated Carbon	A highly porous adsorbent material, produced by heating organic matter, such as coal, wood and coconut shell, in the absence of air, which is then crushed into granules.
Total Organic Carbon	The amount of carbon found in an organic compound and used as a non-specific indicator of water quality.
Vinyl Ester Resin	A resin produced by the esterification of an epoxy resin with an unsaturated monocarboxylic acid.

5.1. Introduction and Background

5.1.1. Construction and Environmental Costs Analysis

The construction cost of a trenchless renewal project includes planning and engineering costs, direct and indirect costs, and operation and maintenance costs, which are associated with the entire life of the project (Najafi and Gokhale, 2005). The environmental cost analysis is used to identify and evaluate the environmental impacts associated with the energy and resources to create materials or services throughout the product's entire lifespan (Theis and Tomkin, 2013). The cost of the maintenance of traffic (MOT) is not considered in this analysis. It is a significant cost to consider because

in some instances the MOT can cost more than actual construction cost. This is particularly true on roadways with high ADT that may require multiple phases to accommodate construction such as interstates. However, this cost could be considered equal across the three rehabilitation methods shown in this section. It needs to be mentioned that this may be a significant cost when comparing these rehab methods to open-cut. This is the primary reason why trenchless methods are sought after by DOT's.

In this study, State DOT bid tabs (lowest contractor's costs) were used to represent the construction cost as well as the environmental cost analysis by Serajiantehrani (2020). For environmental costs an analysis of materials and equipment for trenchless SAPL, CIPP, and sliplining renewal for large diameter culverts were used.

5.1.2. Need Statement

In response to the growing usage of SAPL, CIPP, and sliplining installations, an analysis was performed to compare the total construction and environmental costs of these technologies. A social and environmental comparison of SAPL, CIPP, and sliplining can be an effective tool for planning design phases of a trenchless culvert renewal project (CUIRE, 2018). Table 5-1 presents scope of work.

5.1.3. Scope of the Work

Table 5-1 Scope of work.

TRM	Included	Not Included
SAPL, CIPP, and Sliplining	• Location: 7 DOTs • Diameter: 30-108 in. • Time: Year 2010-2019 • SAPL material: Cementitious • CIPP material: Polyester • Sliplining material: HDPE • Host Pipe: Corrugated Metal Pipe (CMP)	• Soil condition • Depth of culvert • Watertable • SAPL polymeric material • CIPP different resins • Sliplining different materials • Host Pipe: Concrete Pipe

5.2. Cost Data Analysis

The cost data was collected from 7 U.S. Department of Transportations (DOTs) including Delaware, Florida, Minnesota, New York, North Carolina, Ohio, and Pennsylvania. Figure 5-1 presents the location of the data points in the U.S. map. The data for more than 400 projects of large diameter culverts using trenchless SAPL, CIPP, and sliplining renewal were used. The data was prepared and stored into Microsoft Excel 2016 and then Python 3.7 was used for further processing, data preparation, and data analysis. Subsequently, different data visualization techniques such as histogram, scatter plot, and pie chart were used to visualize the dataset.

Overall, 417 bid items (data points) of trenchless SAPL, CIPP, and sliplining renewal methods in large diameter[1] culverts from 2010 to 2019 of 7 DOTs were gathered and analyzed. All culverts were round using corrugated metal pipe (CMP). Based on the data availability, several parameters from each bid item were collected as below:

- Location of the culvert,
- Type of the trenchless renewal method,
- Letting year of the renewal,
- Diameter of the culvert (30-108 in.),
- Length of the culvert,
- Thickness of the trenchless renewal method, and
- Unit cost of the trenchless renewal method.

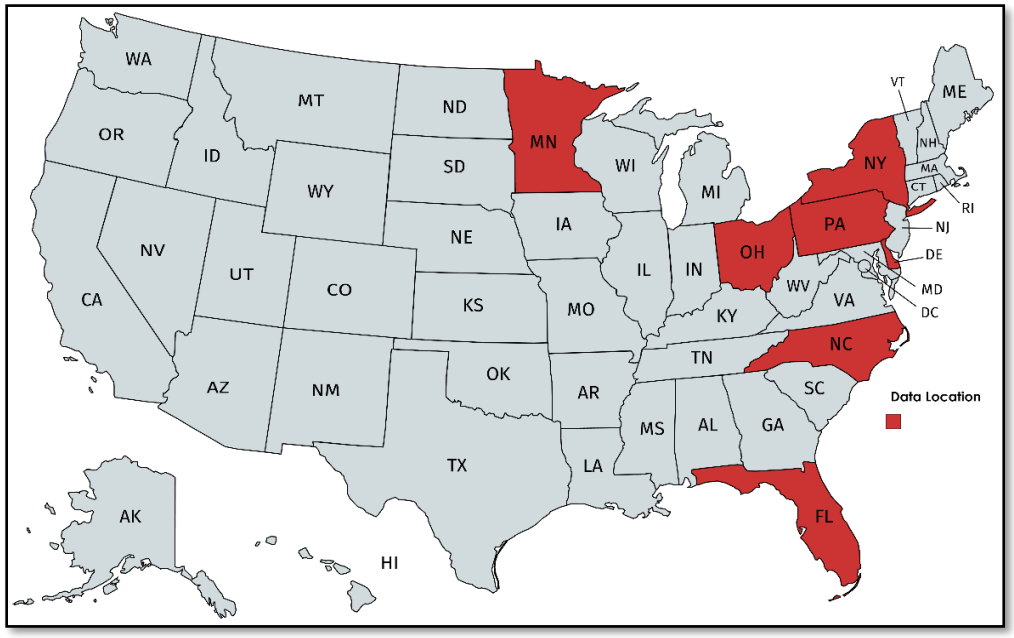


Figure 5-1. Location of the data points throughout the US map.

Table 5-2 shows a summary of the included and excluded features in the dataset to analyze the construction costs.

Table 5-2. Dataset included features.

Feature	Included	Excluded
Culvert Shape	Round	Arch, Ellipse, Box

[1] Large diameter for this report is considered to be 36 in. to 120 in.

Culvert Material	CMP	Concrete
SAPL Material	Cementitious	Polymeric
CIPP Material	Polyester	Fiberglass Reinforced
Sliplining Material	HDPE	PVC and FRP

There are different types of parameters in the dataset including:

- Nominal categorical parameter, which is the one that has two or more categories, but there is no intrinsic ordering to the categories.
- Interval continuous parameter, which can be measured along a continuum that has fixed values between two points but does not have a meaningful zero-point.
- Ratio Continuous parameter, which are interval variables, but with the added condition that zero.

Table 5-3 illustrates the types of parameters in the dataset. Table 5-4 illustrates the raw data sample.

Table 5-3. Dataset parameters classification and value.

Parameter	Location	Time	Renewal Method	Renewal Thickness	Diameter	Length	Unit Cost
Unit/Type	State	Year	Trenchless	t (in.)	D (in.)	L (ft)	2019 Dollars ($)
Value/Classification	Delaware Florida Minnesota New York North Carolina Ohio Pennsylvania	2010 2011 2012 2013 2014 2015 2016 2017 2018 2019	SAPL CIPP Sliplining	0.5 1 1.5 1.75 2 2.25	30 36 42 48 54 60 66 72 78 84 90 96 102 108	5–46,950	105–1,275

Table 5-4 Type of dataset parameters.

Parameter	Type	Parameter	Type
Location	Nominal Categorical	Diameter	Ratio Continuous
Renewal Method		Length	
Time	Interval Continuous	Unit Cost	
Renewal Thickness			

5.2.1. Dataset Preparation

Data preparation included discovery, cleansing, transforming, and storing the final dataset. After scrubbing 412 data, 401 data points are remained in the dataset to proceed for analysis. Samples of raw and final datasets are presented in Tables 5-5 and 5-6.

Table 5-5. Sample of the raw dataset.

Project General Information					Independent Variables of Large Diameter Renewal Culverts (larger than 30 inches)								
No	Project ID/ Letting ID	Owner (Agency)	Contractor	Location (County)	Letting Year	Trenchless Method	Host Pipe Diameter (in.)	Host Pipe Length (ft)	Host Pipe Shape (ft)	Host Pipe Material	Rehab Thickness (in.)	Trenchless Method Cost ($/LF)	Data Source (website, link, etc.)
1	6.1E+09	PennDOT	xcon Chemicals , I	Schuylkill	2017	SAPL	74*132	66.5	Arch	Metal	2	$ 1,141.28	PennDOT Excel File
2	6.1E+09	PennDOT	AP/M Permaform	Washington	2015	SAPL	54	60	Round	Metal	1	$ 1,053.33	PennDOT Excel File
3	6.1E+09	PennDOT	AP/M Permaform	Washington	2015	SAPL	48	55	Round	Metal	1	$ 957.58	PennDOT Excel File
4	6.1E+09	PennDOT	AP/M Permaform	Washington	2015	SAPL	68	50	Round	Metal	1	$ 877.78	PennDOT Excel File
5	6.1E+09	PennDOT	AP/M Permaform	Delaware	2015	SAPL	48	30	Round	Metal	1	$ 1,266.67	PennDOT Excel File
6	82470, SI	PennDOT	SprayRoq	Lancaster	2012	SAPL	72	325	Round	Metal	0.5	$ 955.00	PennDOT Excel File
22	82162	PennDOT	ıaCure inversion li	Warren	2012	CIPP	48	216	Round	Metal	N/A	$ 300.00	PennDOT Excel File
23	62082	PennDOT	ıaCure inversion li	McKean	2009	CIPP	60	75	Round	Metal	N/A	$ 200.00	PennDOT Excel File
24	N/A	NCDOT	N/A	N/A	2016	SAPL	30	188	Round	Metal	1.5	$ 307.00	NCDOT Bid Avg, Centrally Let
25	N/A	NCDOT	N/A	N/A	2014	SAPL	30	208	Round	Metal	1.5	$ 650.00	NCDOT Bid Avg, Centrally Let
26	N/A	NCDOT	N/A	N/A	2014	SAPL	42	68	Round	Metal	1.5	$ 750.00	NCDOT Bid Avg, Centrally Let
50	N/A	NCDOT	N/A	N/A	2011	Slip Line	60	358	Round	Metal	N/A	$ 450.00	NCDOT Bid Avg, Centrally Let
51	N/A	NCDOT	N/A	N/A	2011	Slip Line	66	185	Round	Metal	N/A	$ 590.00	NCDOT Bid Avg, Centrally Let
52	N/A	NCDOT	N/A	N/A	2011	Slip Line	72	345	Round	Metal	N/A	$ 498.00	NCDOT Bid Avg, Centrally Let
53	98201	ODOT	Eclipse Co LLC	N/A	2018	CIPP	36	246	Round	Metal	N/A	$ 139.50	ODOT Official Bid Tabulation
157	D261944	NYSDOT	N/A	N/A	2012	CIPP	30	666	Round	Metal	N/A	$ 352.00	NYSDOT Official Bid Tabulation
158	D261954	NYSDOT	N/A	N/A	2012	CIPP	30	1,291	Round	Metal	N/A	$ 253.77	NYSDOT Official Bid Tabulation
159	D261998	NYSDOT	N/A	N/A	2012	CIPP	30	60	Round	Metal	N/A	$ 280.00	NYSDOT Official Bid Tabulation
160	D262078	NYSDOT	N/A	N/A	2012	CIPP	30	100	Round	Metal	N/A	$ 280.00	NYSDOT Official Bid Tabulation
161	D262091	NYSDOT	N/A	N/A	2013	CIPP	30	820	Round	Metal	N/A	$ 400.00	NYSDOT Official Bid Tabulation

Table 5-6 Sample of the final dataset.

No.	Location	Letting Year	Trenchless Method	Pipe Diameter (in.)	Pipe Length (ft)	Renewal Thickness (in.)	Unit Cost Converted to 2019 ($/ft)
1	PA	2015	SAPL	54	60	1	741.49
2	PA	2015	SAPL	48	55	1	674.08
3	PA	2015	SAPL	68	50	1	950.64
4	PA	2015	SAPL	48	30	1	891.67
5	PA	2018	SAPL	48	440	1.75	888.83
6	PA	2018	SAPL	60	450	2.25	1,027.09
7	PA	2016	CIPP	36	62		444.88
8	PA	2016	CIPP	30	125		220.67
9	PA	2016	CIPP	36	70		394.04
17	NC	2016	SAPL	30	188	1.5	328.49
18	NC	2014	SAPL	30	208	1.5	387.99
19	NC	2014	SAPL	42	68	1.5	831.41
20	NC	2014	SAPL	54	64	1.5	942.26
28	NC	2015	CIPP	60	269		850.16
29	NC	2017	CIPP	30	580		167.51
30	NC	2019	CIPP	30	264		140
31	NC	2019	Sliplining	32	211		250
33	NC	2019	Sliplining	54	578		260
34	NC	2011	Sliplining	30	452		492.96
35	NC	2010	Sliplining	36	135		359.2

5.2.2. Data Distribution

The construction cost analysis was performed, and the distribution of each parameter was executed using the histogram plot. The following sections are provided to illustrate the histogram analysis of each parameter.

5.2.2.1. Location

The dataset was gathered from 7 states in the U.S. The number of data points in each state was different from another. There were 201 projects in the dataset which were in New York state. Also, Delaware State with only 4 data had the least projects in the dataset. The histogram of the location distribution for 7 states is presented in Figure 5-2.

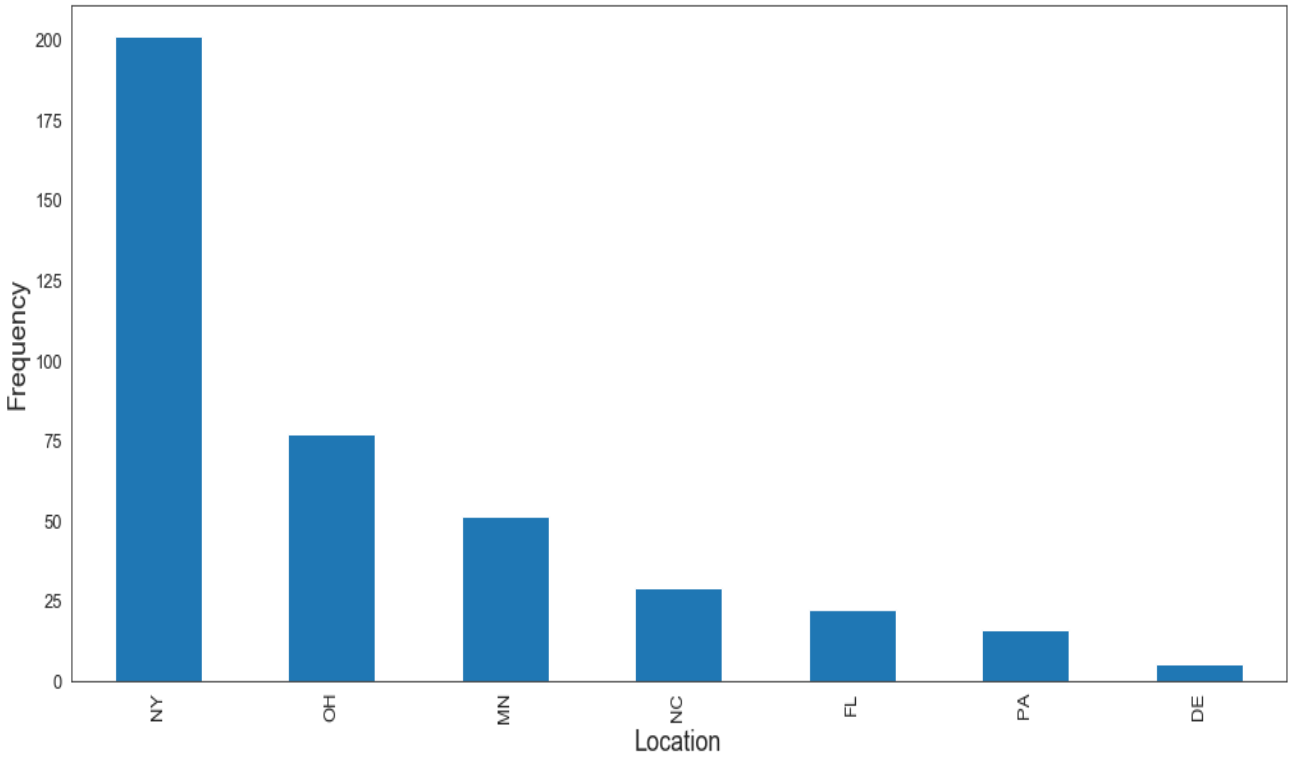
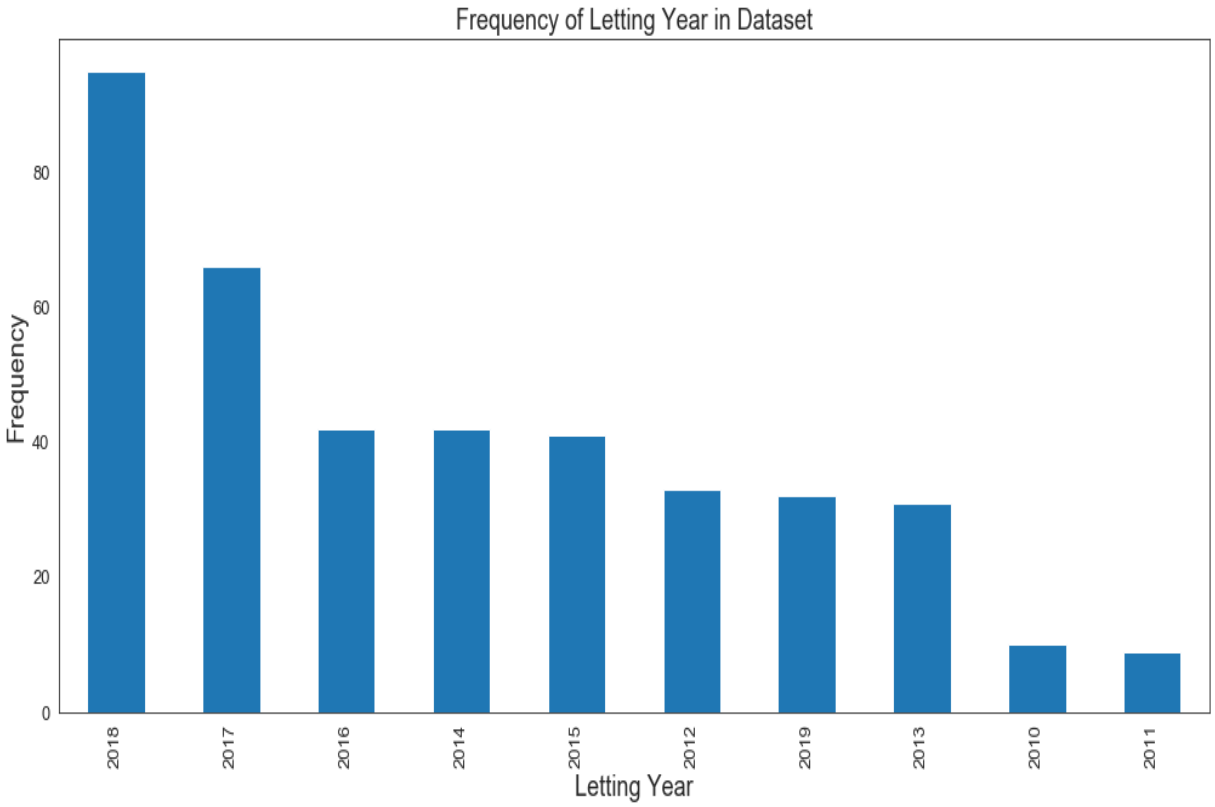


Figure 5-2. Frequency of data in each state DOT.

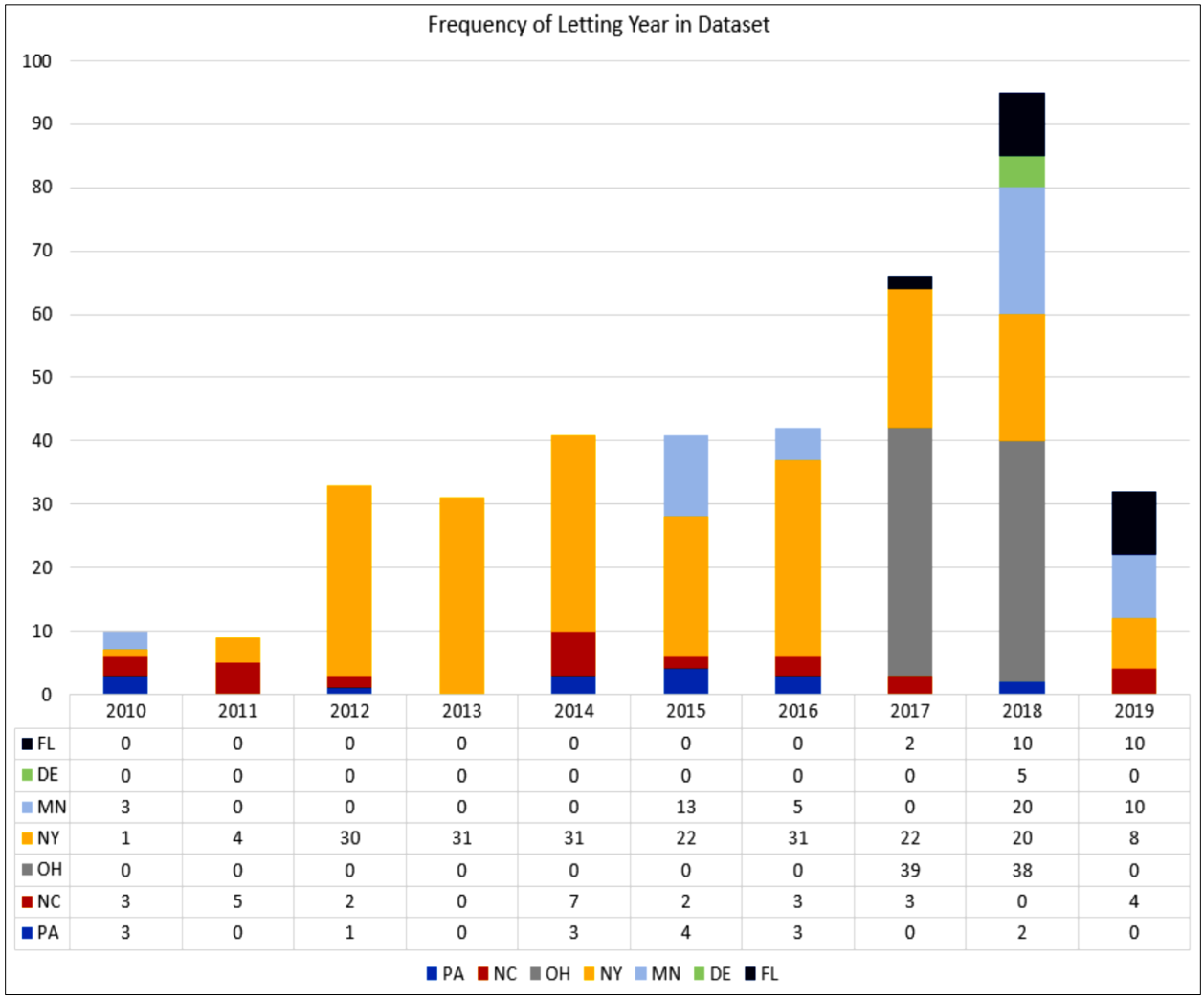
5.2.2.2. Letting Year

The letting year of the dataset was from 2010 to 2019. Most of the collected projects were coming from 2018 with 95 data points and 2011 consisted of the least collected data points with only 9 projects. It can be seen from the trend that using the trenchless technology renewals are increased over the time.

However, since there were many on-going projects in 2019, the number of data for 2019 was less than that of 2018. The histogram of the letting year distribution of the dataset is presented in Figure 5-3 a. Also, the breakdown of contribution of each individual state contribution to the total in each year is shown in Figure 5-3 b.



(a)



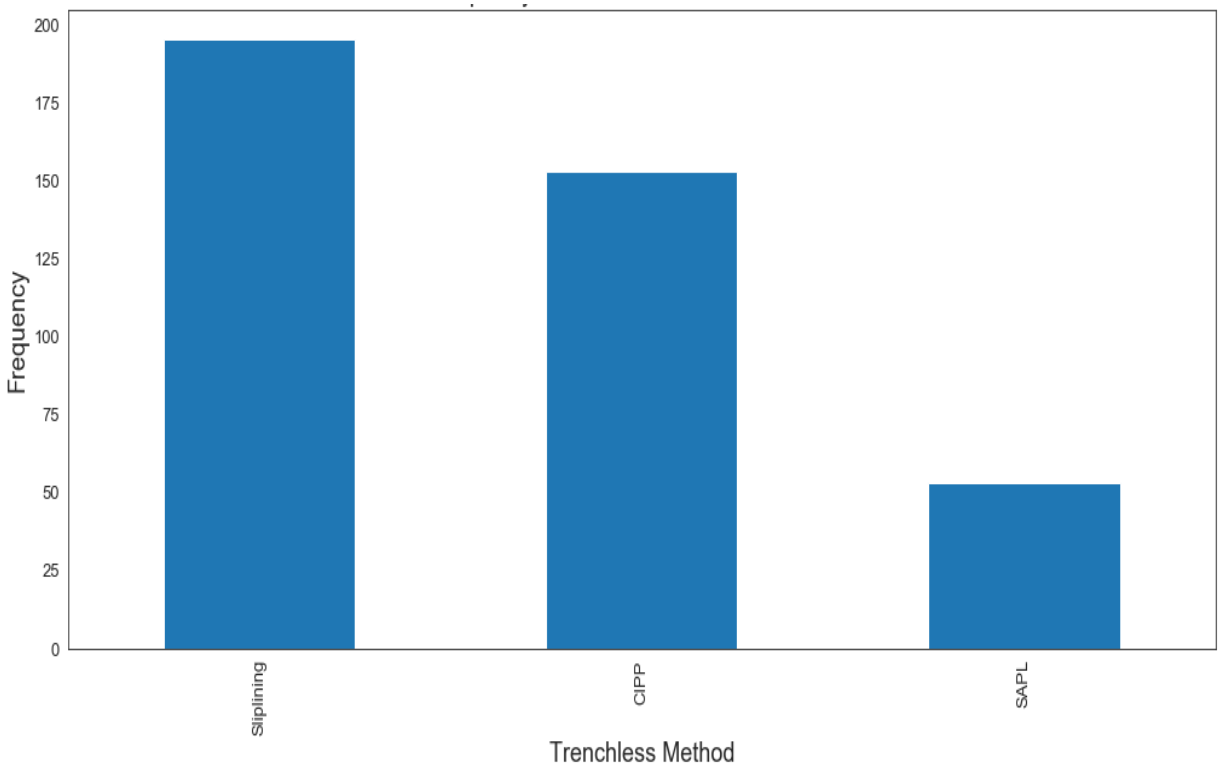
	2010	2011	2012	2013	2014	2015	2016	2017	2018	2019
FL	0	0	0	0	0	0	0	2	10	10
DE	0	0	0	0	0	0	0	0	5	0
MN	3	0	0	0	0	13	5	0	20	10
NY	1	4	30	31	31	22	31	22	20	8
OH	0	0	0	0	0	0	0	39	38	0
NC	3	5	2	0	7	2	3	3	0	4
PA	3	0	1	0	3	4	3	0	2	0

(b)

Figure 5-3. (a) Frequency of letting year (descending order), and (b) frequency of letting year based on the individual state contribution.

5.2.2.3. Trenchless Method

As stated earlier, the trenchless methods studied in this chapter were SAPL, CIPP, and sliplining. Sliplining is the most widely used trenchless renewal technology with 195 data points in the dataset. SAPL is the newest method in the trenchless renewal technology field. As a result, fewer projects can be found for this technology. Only 53 of the collected projects were SAPL projects among 401 projects. The histogram of the trenchless method distribution is plotted in Figure 5-4.



(a)

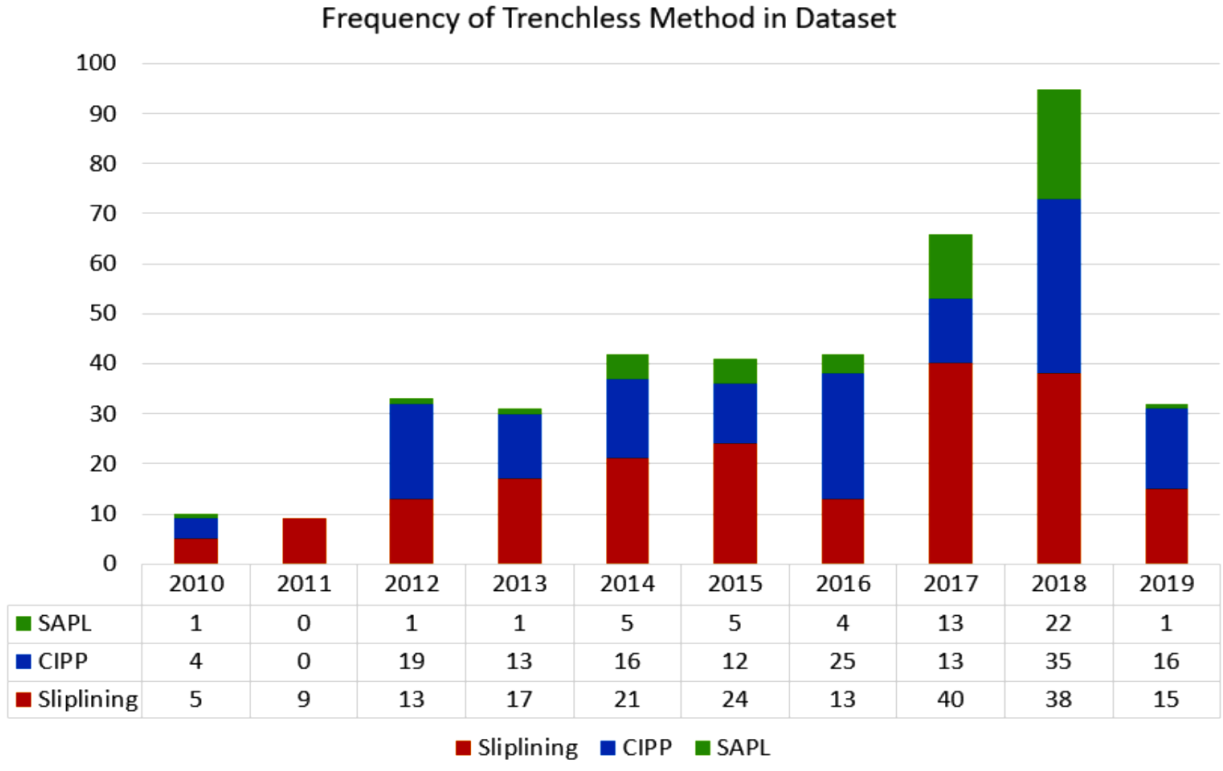


Figure 5-4. (a) Frequency of trenchless methods (descending order), and (b) frequency of trenchless method in each year.

5.2.2.4. Pipe Diameter

Most data points were pipe diameters 36 in., 48 in., and 60 in. and the least collected projects were including pipes with 90 in., 102 in., and 108 in. diameter. The histogram of the pipe diameter distribution is illustrated in Figure 5-5.

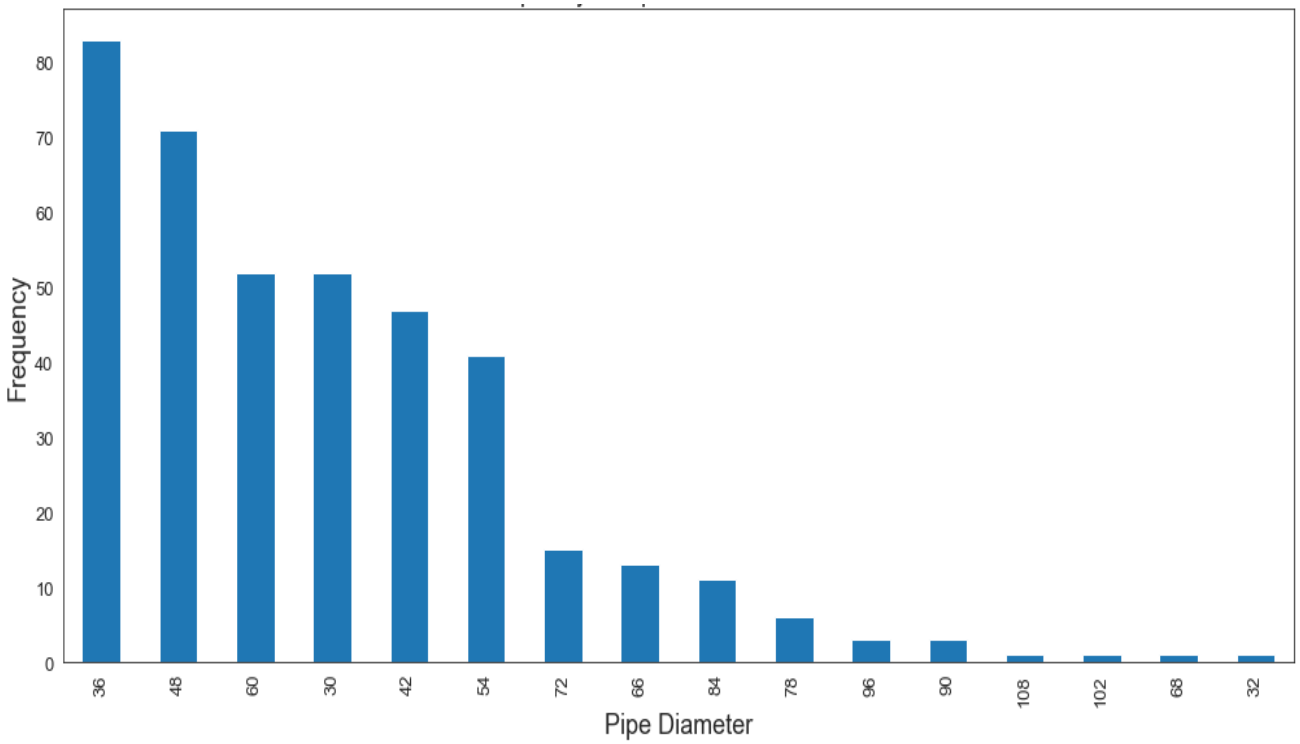


Figure 5-5. Frequency of pipe diameters.

5.2.2.5. Pipe Length

Pipe length was another independent variable, which was included in the dataset with a range of 5 ft to almost 5,000 ft. The histogram of the pipe length distribution is depicted in Figure 5-6.

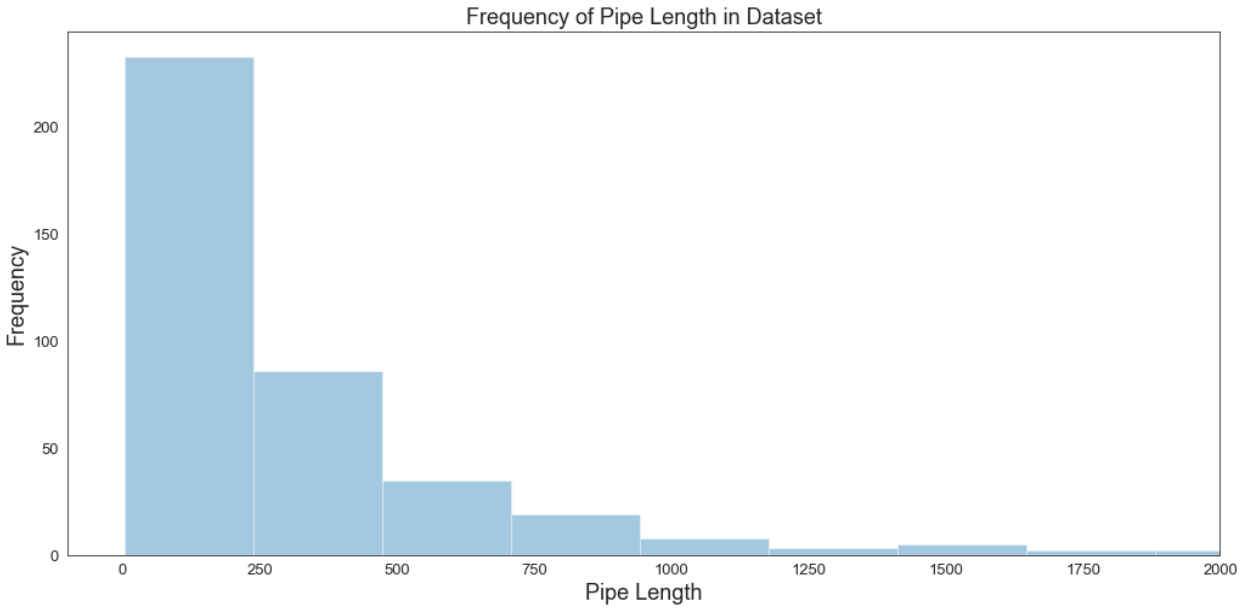


Figure 5-6. Frequency of pipe lengths.

5.2.2.6. Renewal Thickness

The renewal thickness parameter, which represents the thickness of the SAPL, CIPP, and sliplining renewal method was varied in the dataset from 0.5-in. to 2.25-in. Most of the collected projects were 1.5-in. and 2-in. The histogram of the renewal thickness distribution is presented in Figure 5-7.

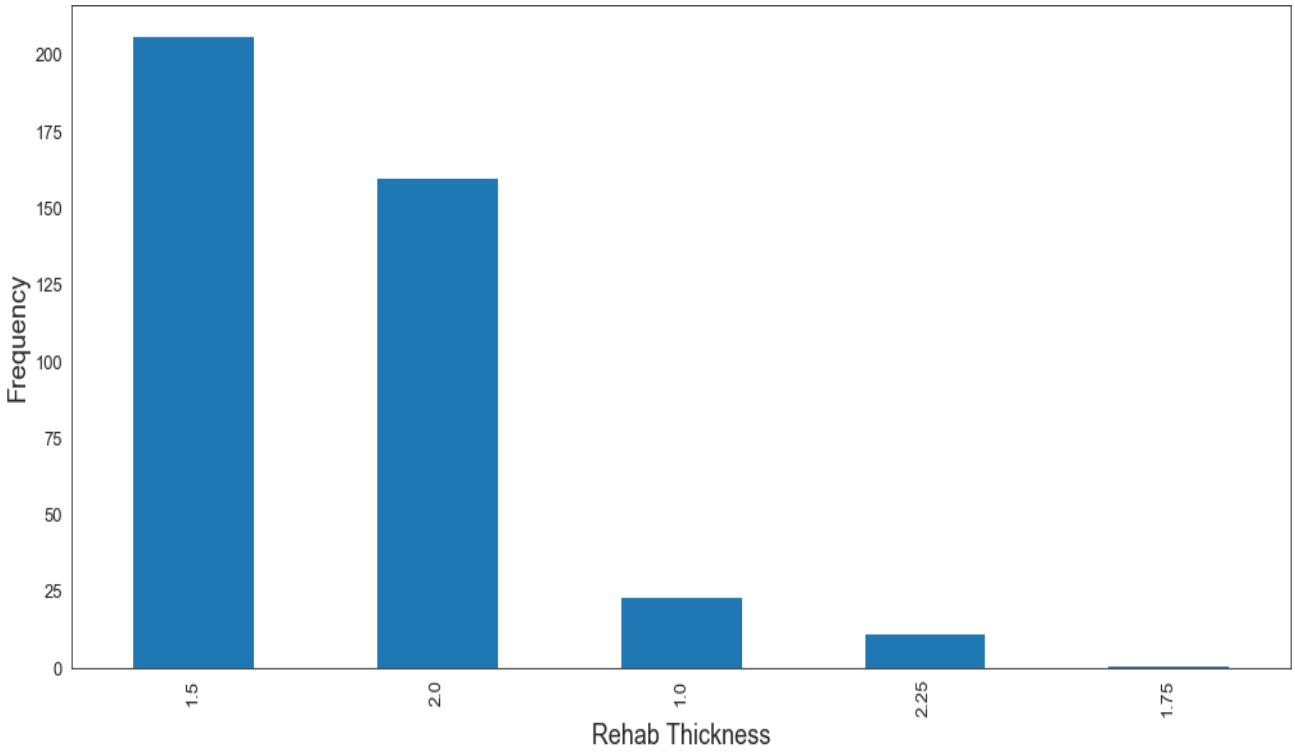


Figure 5-7. Frequency of renewal thicknesses (descending order).

5.2.2.7. Unit Cost

Unit cost as a dependent variable in the dataset was the dollar value per linear feet of each trenchless culvert renewal method. As it is mentioned earlier in the data preparation section, since the cost of projects was associated with their letting year, which was varied from 2010 to 2019, all costs were adjusted to the equal dollar value in 2019. Figure 5-8 presents the distribution of the unit costs of all projects in the dataset.

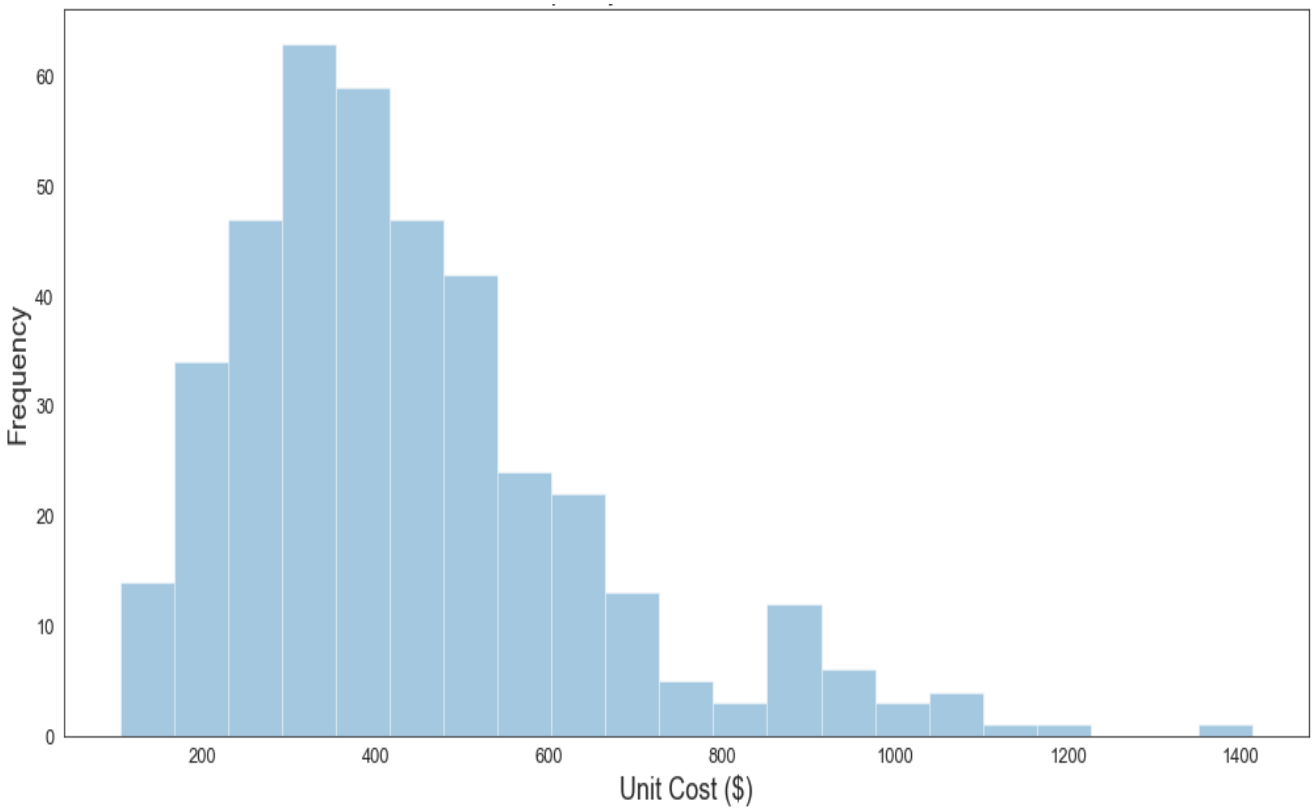


Figure 5-8. Frequency of unit cost in 2019 dollars.

5.3. Results and Comparisons

In this section, the results, which show the distribution of each independent and dependent variable (unit cost), as well as the comparison of the mean construction costs of SAPL, CIPP and sliplining are discussed.

5.3.1. Results

Scatter boxplot in Python was employed to visualize the data parameters over each other and to identify the thresholds. Figure 5-9 shows the distribution of the unit cost and pipe diameter. This figure shows the thresholds of the median, lower quartile, upper quartile, lower extreme, and upper extreme of the unit cost for each pipe diameter. In addition, it shows that by increasing the pipe diameter, the unit cost of the project regardless of other factors are increased.

Congestion of data points for each diameter shows a range which majority of the projects having the approximate same unit cost. There are considerable variations in the unit cost for the various pipe diameters. The medians vary from about 300 $/LF to

1,100 $/LF. It is noted that there is some variation in the scale of the unit cost for each pipe diameter.

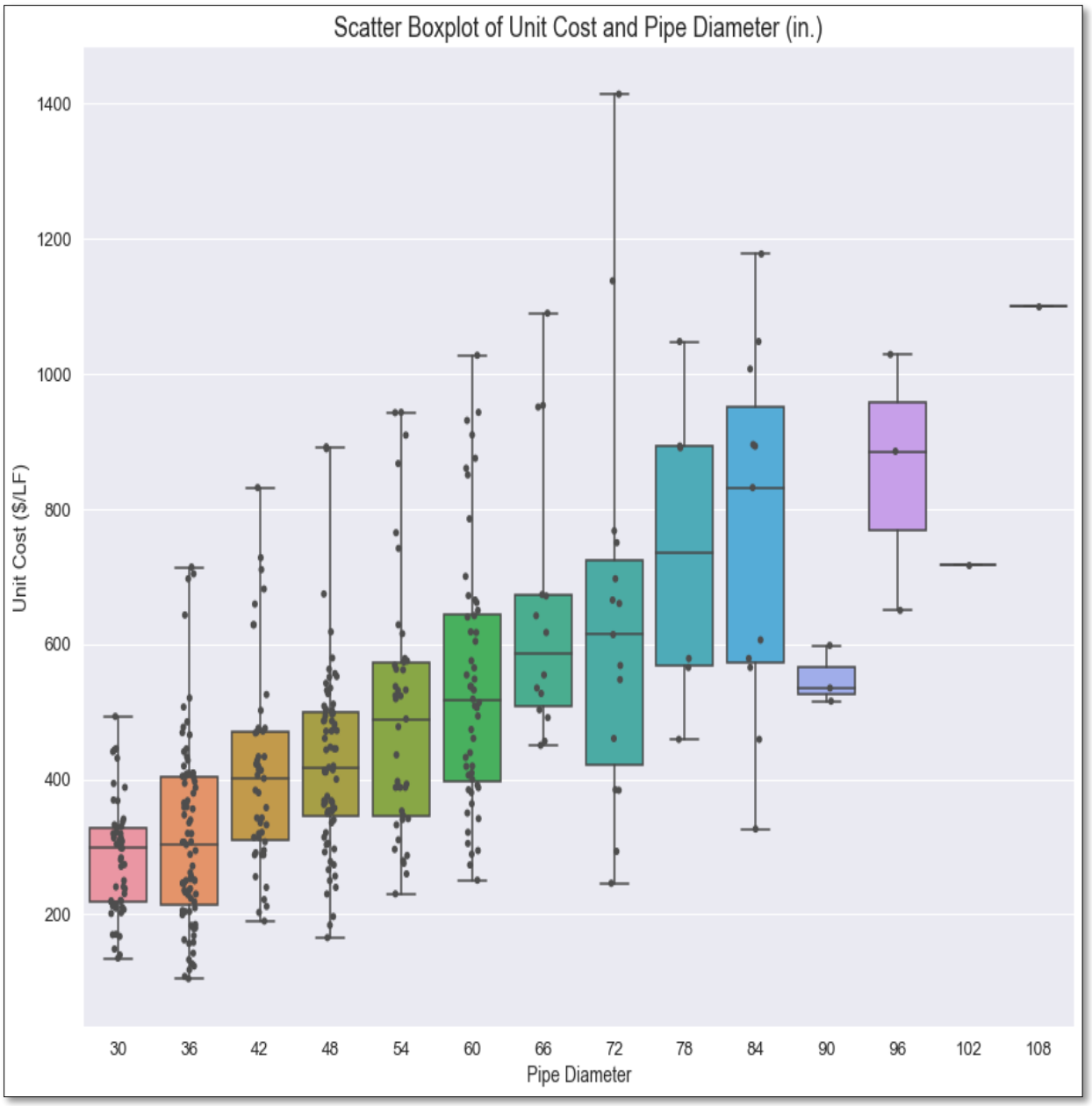


Figure 5-9. Scatter boxplot of unit cost and pipe diameter.

Figure 5-10 shows distribution of the unit cost with the location. This figure shows that Florida State has the lowest and North Carolina State has the highest unit cost medians regardless of the trenchless methods used. In addition, Pennsylvania, North Carolina, Ohio, New York, and Delaware states have almost the same unit cost. The medians for different locations vary from about 250 $/LF to 510 $/LF. Lastly, there

is some variation in the scale of the unit cost for each location, however, this variation for North Carolina and Minnesota states is much more than other locations.

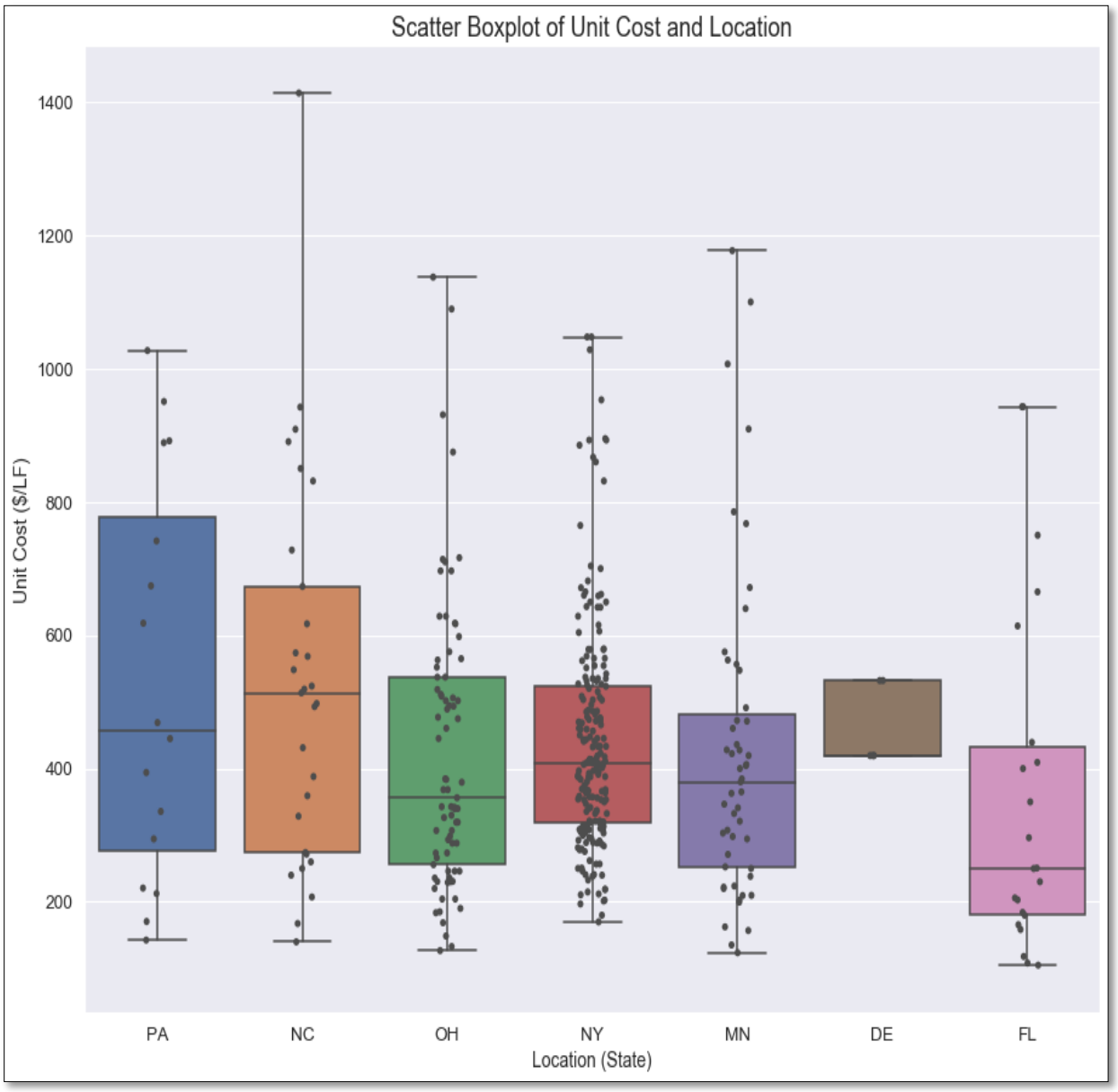


Figure 5-10. Scatter Boxplot of unit cost and location.

Figure 5-11 highlights the distribution of the unit cost with the trenchless method. Comparing the medians of the trenchless technology options together, it can be found that the SAPL has the highest unit cost and the CIPP has the lowest. Also, the unit cost data points in SAPL are not congested while the CIPP has the high congested data points. This shows that the unit cost for the SAPL can be varied based on the other parameters while the unit cost for the CIPP can be less related to the other parameters.

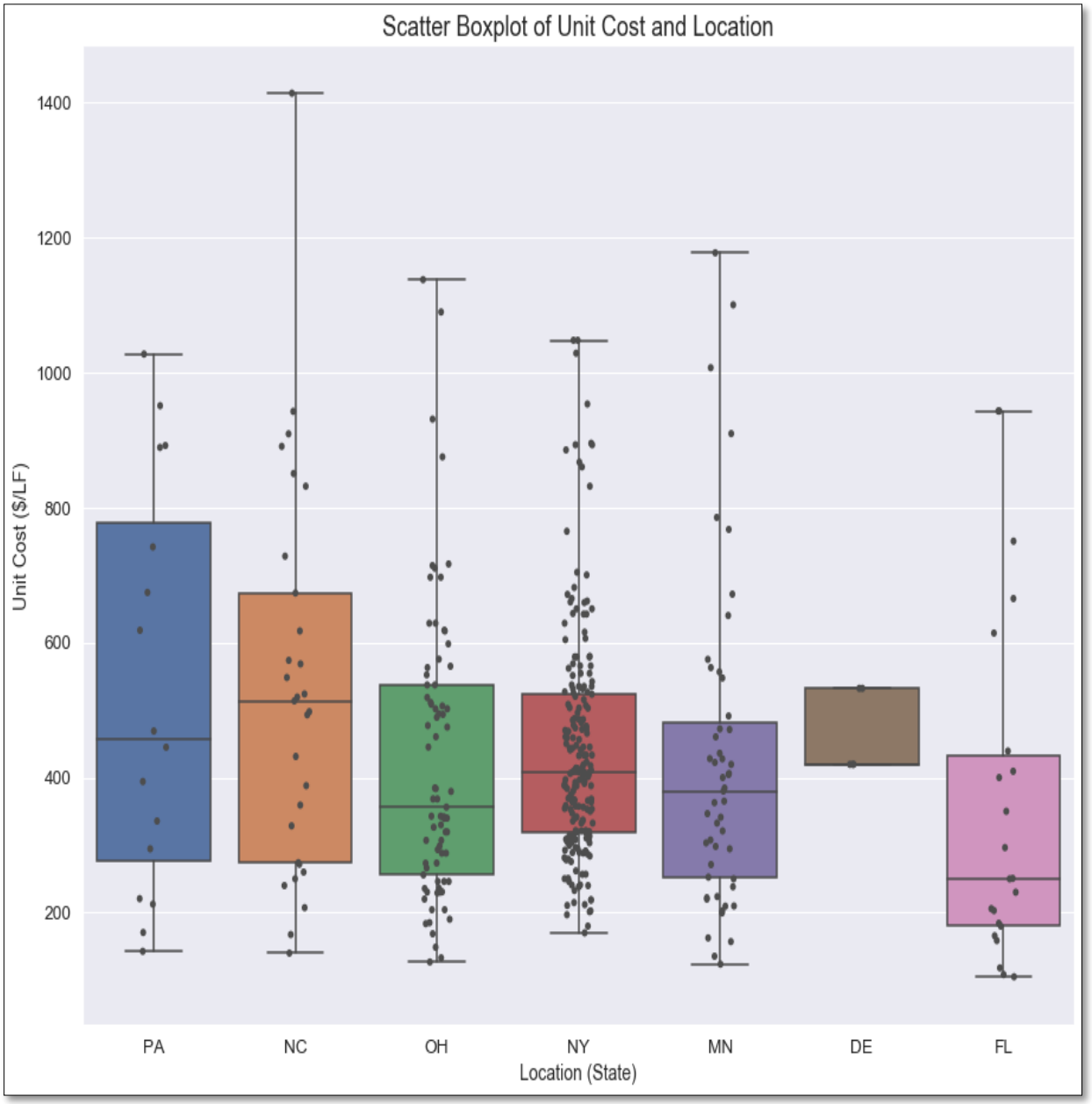


Figure 5-11. Mean unit cost in 2019 dollars based on the location.

5.3.2. Construction Costs Comparison

The results for the mean unit cost of each trenchless technology method including SAPL, CIPP, and sliplining in 7 DOTs concluded the ranking for the locations with the least expensive mean unit cost to the most expensive one (see Table 5-7).

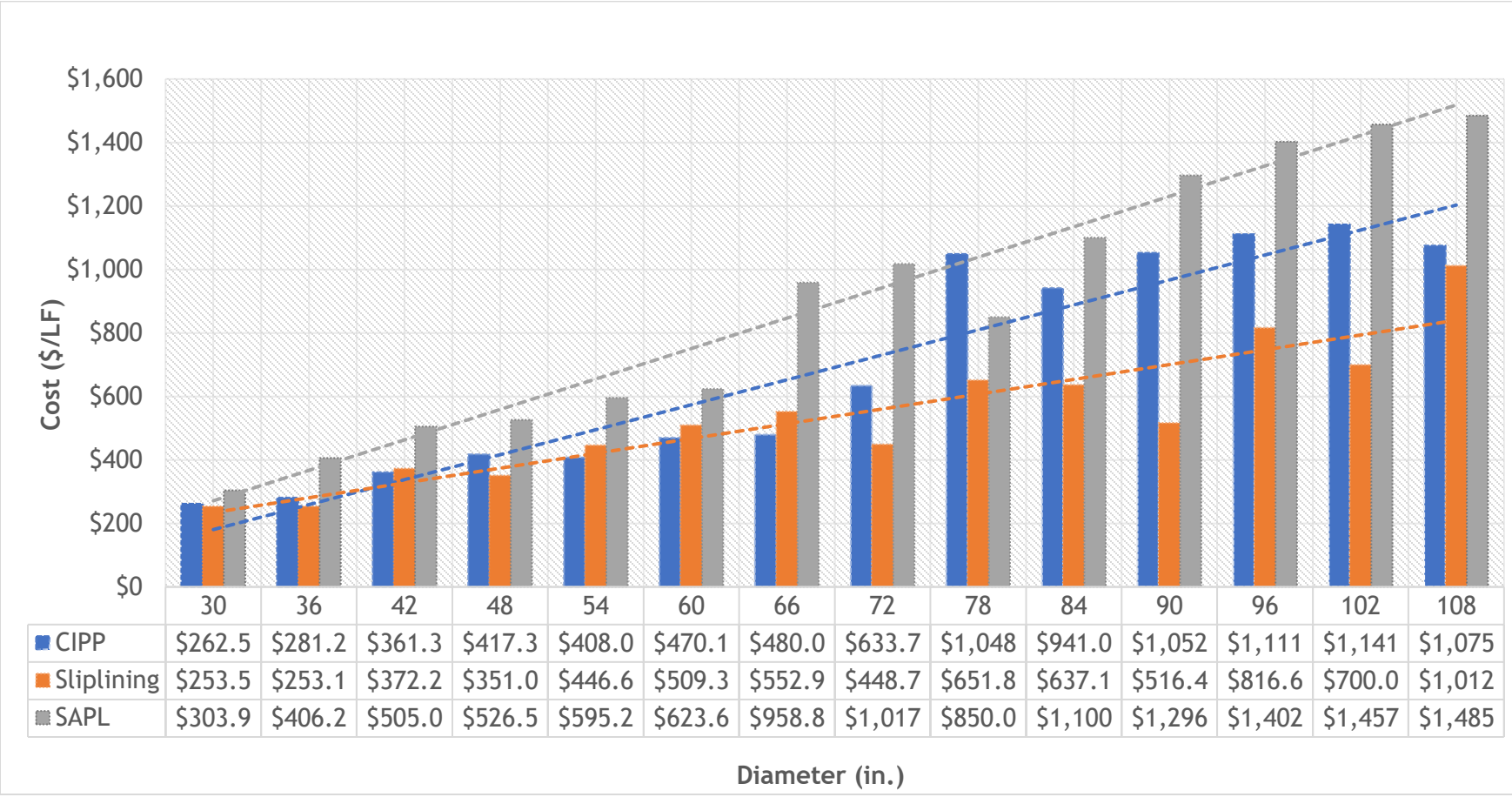
A comprehensive comparison of unit cost for all three renewal options was done for 7 DOT States in the U.S., which can be found in Figure 5-12. It can be observed that from 30 in. to 42 in. the mean unit cost of CIPP is the lowest and SAPL is the highest

construction costs. However, from 48 in. and above the sliplining has the lowest construction cost while SAPL still has the highest construction cost in compare with CIPP and sliplining.

Table 5-7. Trenchless SAPL, CIPP, and Sliplining mean unit cost in 7 locations.

TRM	SAPL	CIPP	Sliplining
Lowest to Highest Mean Unit Cost	Location (Mean Unit Cost)		
	Florida ($350.00)	Ohio ($224.04)	Minnesota ($301.94)
	New York ($422.95)	Florida ($272.50)	Ohio ($398.09)
	Delaware ($454.00)	Pennsylvania ($297.85)	North Carolina ($448.13)
	Ohio ($517.76)	North Carolina ($319.99)	New York ($452.26)
	Minnesota ($593.49)	New York ($346.04)	Florida ($563.33)
	North Carolina ($668.38)	Minnesota ($432.69)	Pennsylvania (N/A*)
	Pennsylvania ($813.45)	Delaware (N/A*)	Delaware (N/A*)

*N/A: The data was not available.



	30	36	42	48	54	60	66	72	78	84	90	96	102	108
CIPP	$262.5	$281.2	$361.3	$417.3	$408.0	$470.1	$480.0	$633.7	$1,048	$941.0	$1,052	$1,111	$1,141	$1,075
Sliplining	$253.5	$253.1	$372.2	$351.0	$446.6	$509.3	$552.9	$448.7	$651.8	$637.1	$516.4	$816.6	$700.0	$1,012
SAPL	$303.9	$406.2	$505.0	$526.5	$595.2	$623.6	$958.8	$1,017	$850.0	$1,100	$1,296	$1,402	$1,457	$1,485

Figure 5-12. Mean construction costs comparison of Cementitious SAPL, CIPP, and Sliplining in 2019 dollars.

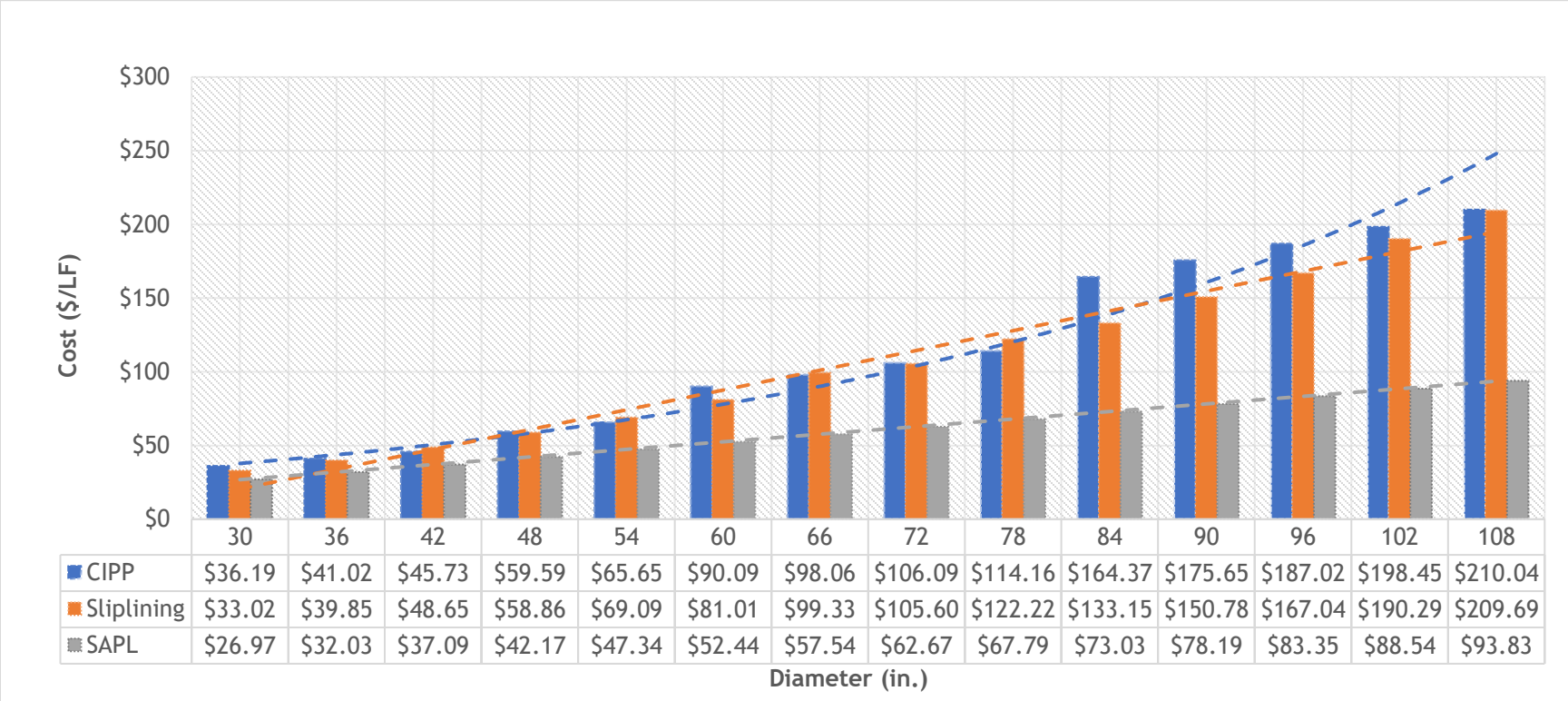
5.3.3. Environmental Costs Analysis

Environmental impact assessment, also known as life-cycle assessment (LCA), is a systematic tool used to identify and evaluate the environmental impacts associated with the energy and resources to create materials or services throughout the product's entire lifespan (Theis and Tomkin, 2013).

Serajiantehrani (2020) conducted a research on analysis of environmental impact for cementitious SAPL, CIPP with polyester resin, and sliplining with HDPE pipe. SimaPro software was used to perform environmental analysis. The output of the SimaPro software for each diameter of each trenchless renewal was the emission amount of 10 environmental impact categories using the Tool for Reduction and Assessment of Chemicals and Other Environmental Impacts (TRACI). TRACI is an environmental impact assessment tool created by the U.S. Environmental Protection Agency (EPA) which calculates impact assessments based on ten impact categories (USEPA, 2016):

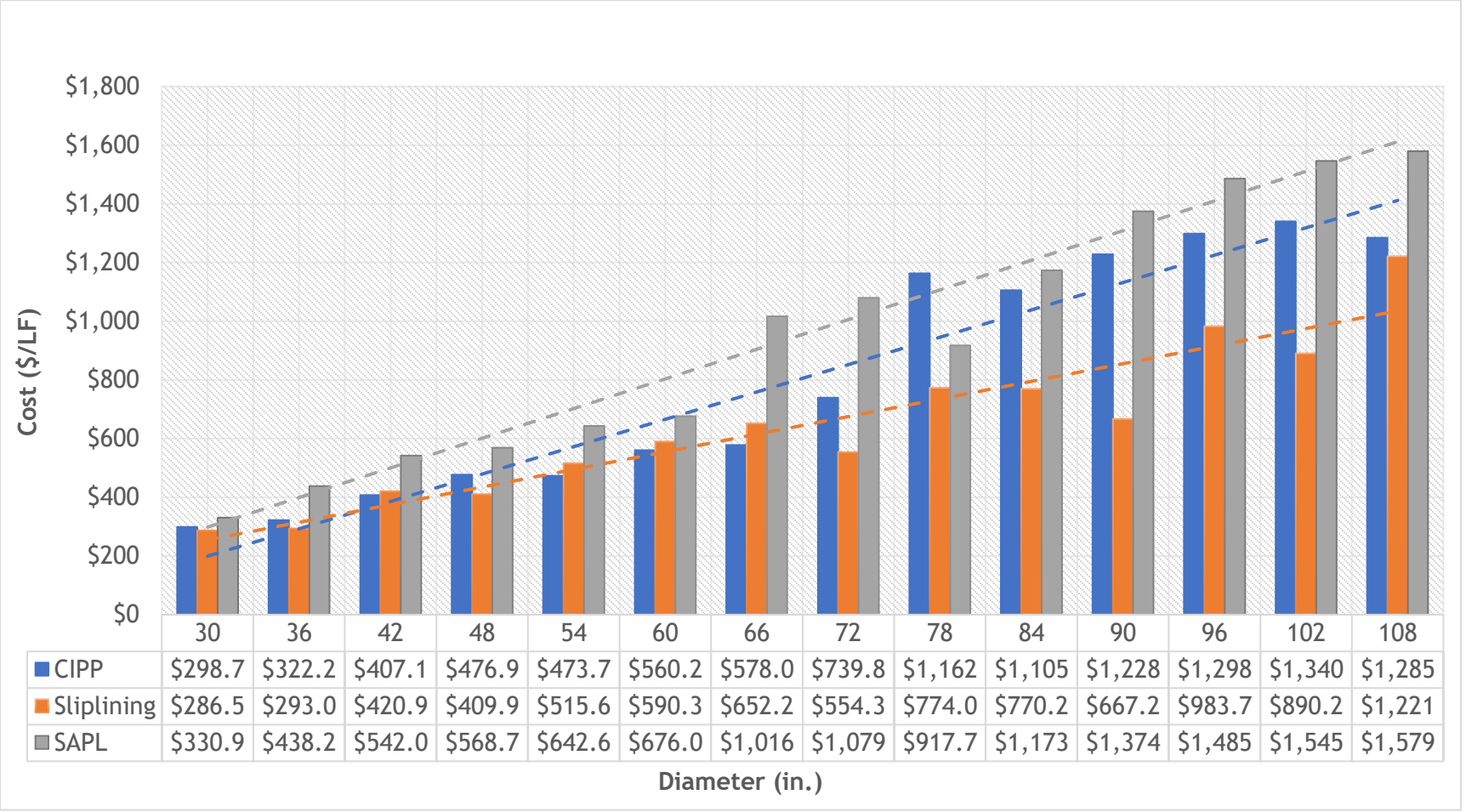
1. Ozone depletion (measured in kg CFC-11 (Freon-11) equivalents)
2. Global warming (measured in kg CO_2 equivalents)
3. Smog (measured in kg O_3 equivalents)
4. Acidification (measured in kg SO_2 equivalents)
5. Eutrophication (measured in kg N equivalents)
6. Carcinogenic (measured in comparative toxic units (CTU) for morbidity (h))
7. Non-carcinogenic (measured in CTUh)
8. Respiratory effects (measured in kg particulate matter (PM) 2.5 equivalents)
9. Ecotoxicity (measured in CTU for aquatic Ecotoxicity (CTUe))
10. Fossil Fuel Depletion (measured in MJ)

The environmental impacts in unit cost per length can be found in Figure 5-13. In addition, the composite graph of construction and environmental of cementitious SAPL, CIPP, and sliplining can be found in Figure 5-14. Lastly, the proportion of the environmental costs to the sum of the environmental and construction costs are depicted in Figure 5-15 to Figure 5-17. Figure 5-18 shows the portion of environmental costs to the total costs is increasing by increasing the diameter for trenchless CIPP and sliplining renewal methods. However, the portion of environmental costs to the total cost is decreasing for SAPL method by increasing the diameter. These figures indicate that SAPL for certain diameters is the most expensive option. However, access and lack of right-of-way are real concerns that are part of the decision process. The cost of access and lack of right-of-way is not something that can readily be added into this analysis but should be noted that time to allocate the right-of-way and the associated cost of the purchase is significant.



	30	36	42	48	54	60	66	72	78	84	90	96	102	108
CIPP	$36.19	$41.02	$45.73	$59.59	$65.65	$90.09	$98.06	$106.09	$114.16	$164.37	$175.65	$187.02	$198.45	$210.04
Sliplining	$33.02	$39.85	$48.65	$58.86	$69.09	$81.01	$99.33	$105.60	$122.22	$133.15	$150.78	$167.04	$190.29	$209.69
SAPL	$26.97	$32.03	$37.09	$42.17	$47.34	$52.44	$57.54	$62.67	$67.79	$73.03	$78.19	$83.35	$88.54	$93.83

Figure 5-13. Environmental costs comparison of Cementitious SAPL, CIPP, and Sliplining in 2019 dollars (Serajiantehrani, 2020).



	30	36	42	48	54	60	66	72	78	84	90	96	102	108
CIPP	$298.7	$322.2	$407.1	$476.9	$473.7	$560.2	$578.0	$739.8	$1,162	$1,105	$1,228	$1,298	$1,340	$1,285
Sliplining	$286.5	$293.0	$420.9	$409.9	$515.6	$590.3	$652.2	$554.3	$774.0	$770.2	$667.2	$983.7	$890.2	$1,221
SAPL	$330.9	$438.2	$542.0	$568.7	$642.6	$676.0	$1,016	$1,079	$917.7	$1,173	$1,374	$1,485	$1,545	$1,579

Figure 5-14. Environmental and construction costs composite comparison of Cementitious SAPL, CIPP, and Sliplining in 2019 dollars.

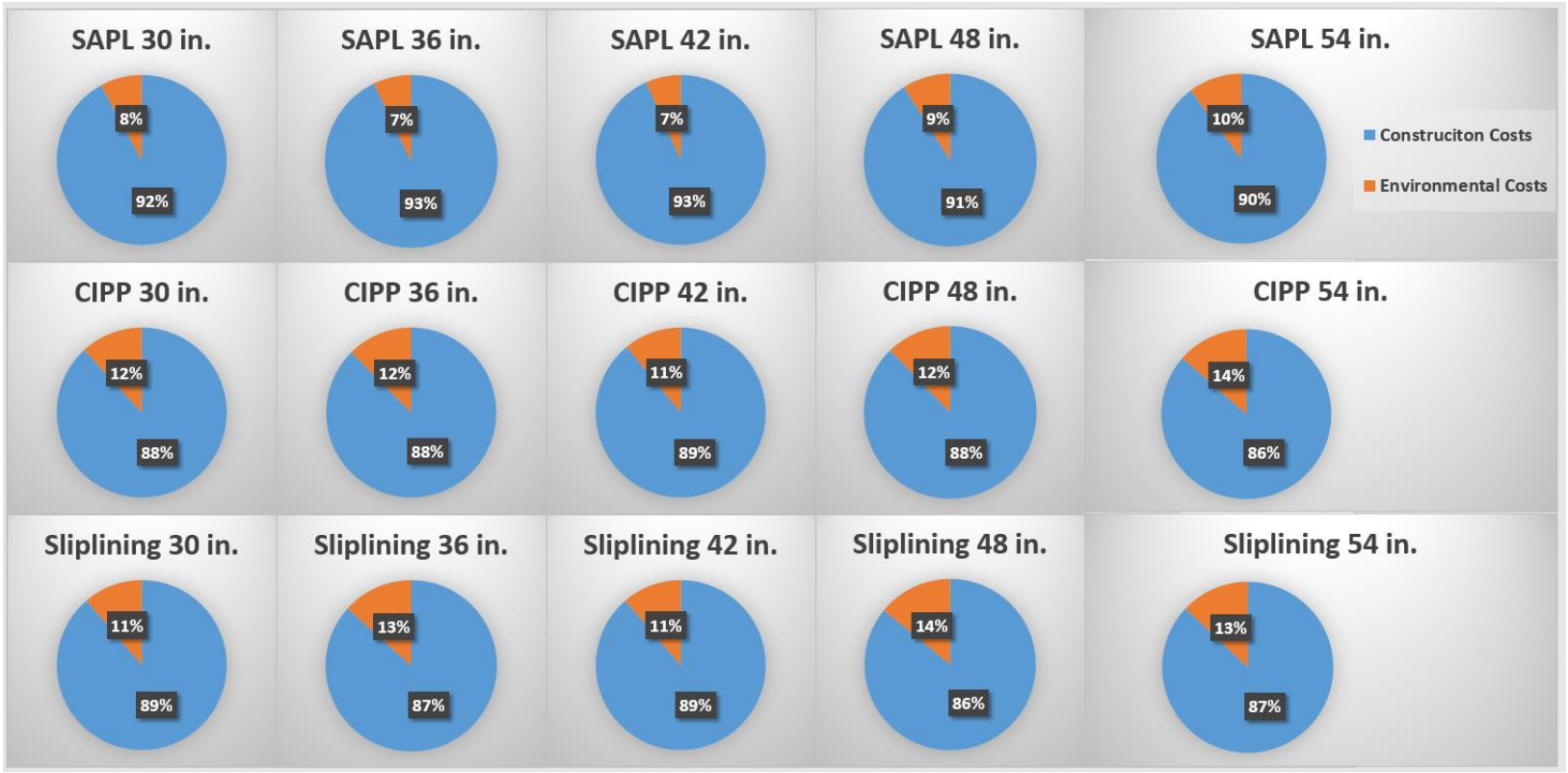


Figure 5-15. Environmental and construction costs proportioning comparison of Cementitious SAPL, CIPP and sliplining for diameter of 30 in. to 54 in.

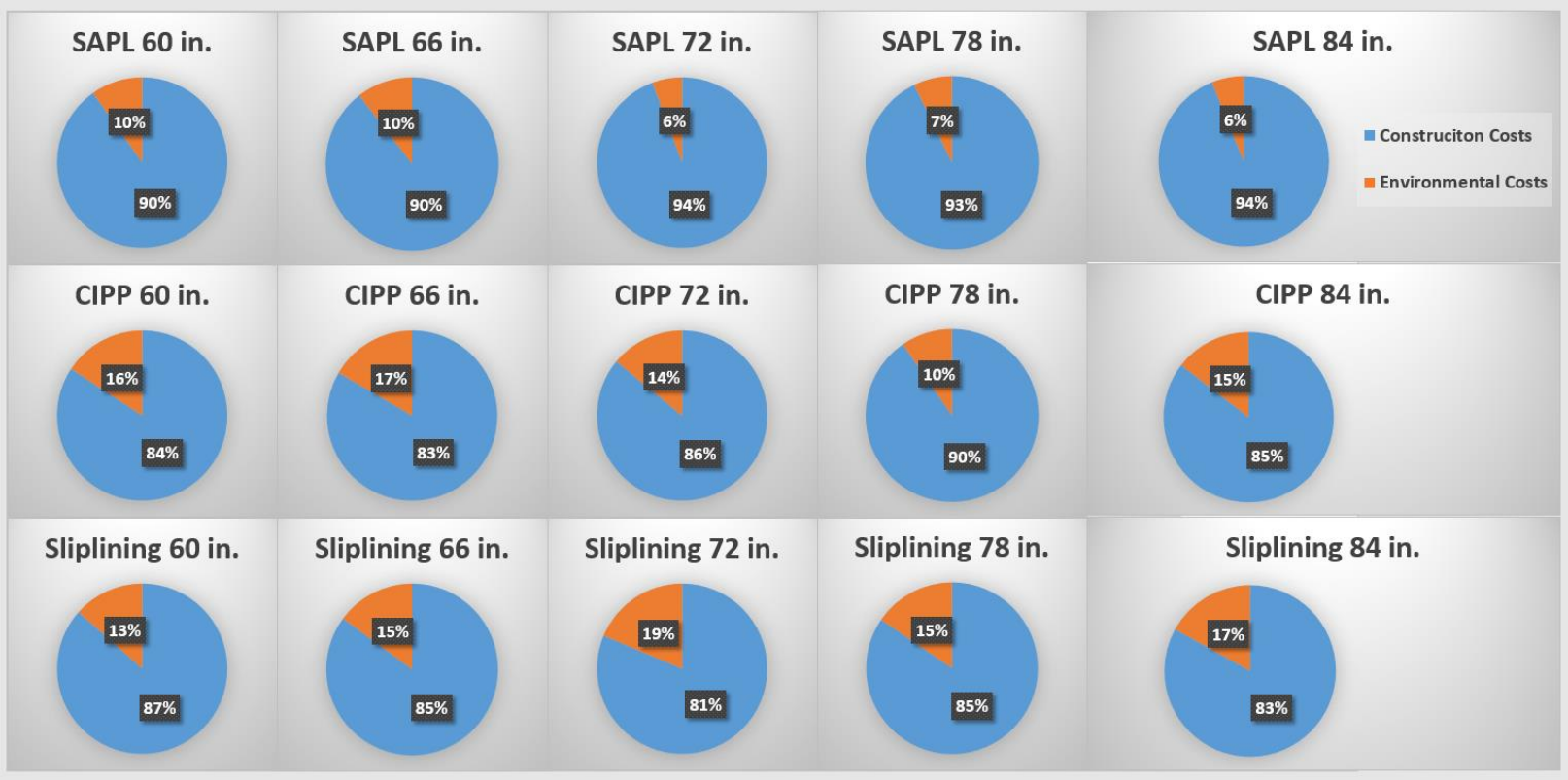


Figure 5-16. Environmental and construction costs proportioning comparison of Cementitious SAPL, CIPP and sliplining for diameter of 60 in. to 84 in.

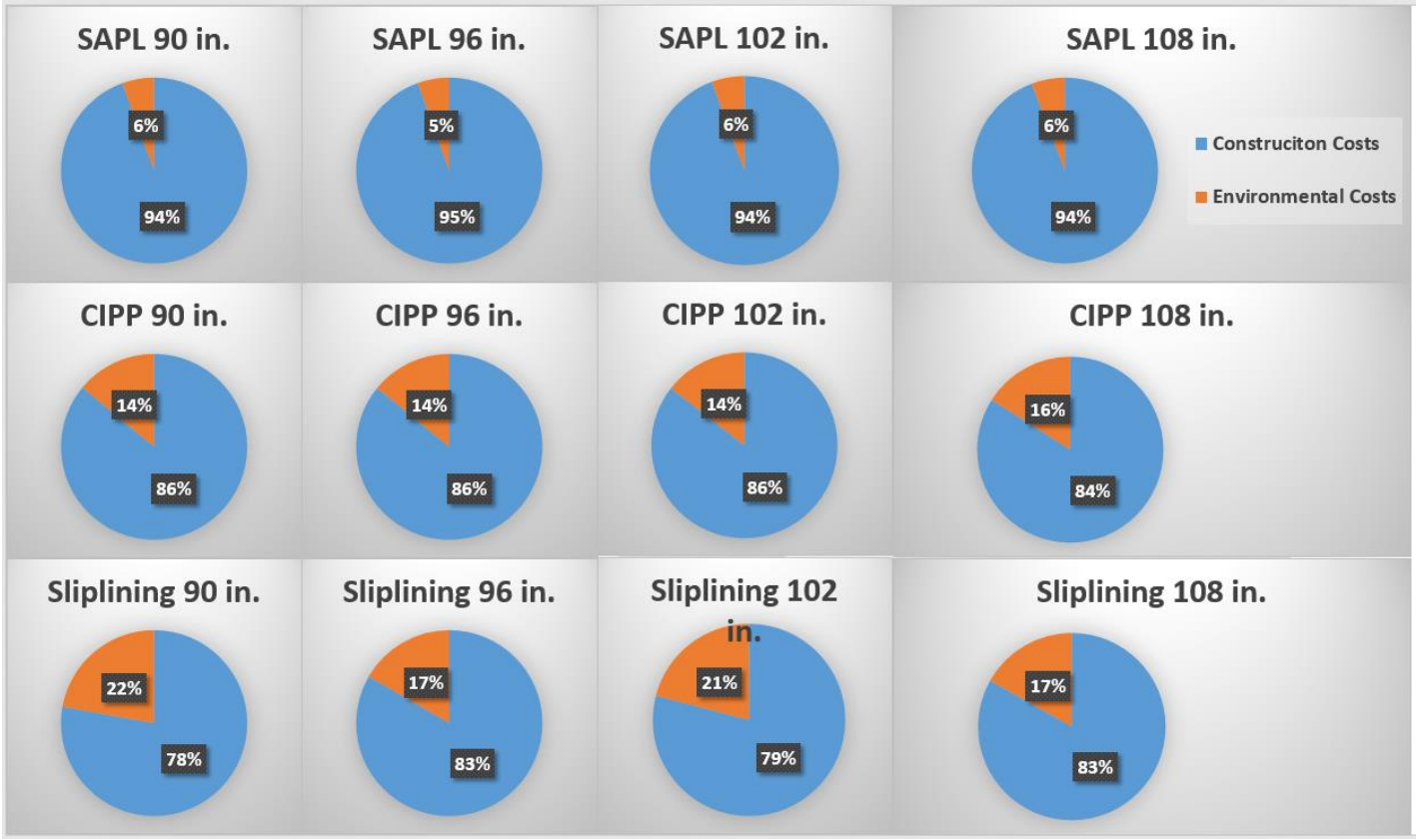


Figure 5-17. Environmental and construction costs proportioning comparison of Cementitious SAPL, CIPP, and sliplining for diameter of 90 in. to 108 in.

5.4. Discussion of Results

This section presents a discussion of results for SAPL, CIPP and sliplining with in large diameter culverts as follows:

Compared with CIPP and sliplining, SAPL has least overall environmental costs. After 60-in. diameter, the difference between CIPP environmental costs and SAPL will increase by more than 50%.

For 78 in. to 108 in. diameters, the environmental costs of CIPP and sliplining are almost the same. For the same range, the environmental costs of both CIPP and sliplining are twice than SAPL application.

The difference between mean construction costs of sliplining and SAPL for 72 in. diameter is 120 times more than that of 30 in. diameter. This shows a significant increase in difference of construction costs for SAPL and sliplining by increasing the diameter from 30 to 72 in.

The difference between mean construction costs of CIPP and SAPL in 72 in. diameter is 500% more than that of 30 in. diameter. This shows a significant increase in difference of construction costs of CIPP and SAPL by increasing the diameter of the culverts.

According to Figure 5-18, the ratio of environmental costs to total costs of CIPP is roughly constant for 30- to 108-in. diameter range. However, for sliplining, the same category is increasing and for SAPL is decreasing.

Table 5-7 illustrates that SAPL is least expensive in Florida and most expensive in Pennsylvania. The ratio of mean construction unit cost of Pennsylvania to Florida is more than 200%. For CIPP, Minnesota experienced higher cost by a factor of 1.9 with reference to Ohio. For sliplining, Minnesota is less expensive than Florida. This difference between mean unit cost is approximately 85%.

The CIPP has least mean unit cost in Florida compared with sliplining, which most expensive. In Minnesota, sliplining is least expensive and SAPL is the most expensive renewal method. In Pennsylvania, SAPL is 170% more expensive than CIPP, while this difference in Florida is 55%.

In New York, SAPL and sliplining are about the same price, while CIPP is least expensive one. In Ohio, compared with CIPP, SAPL has higher mean unit cost by a factor of 1.3.

5.5. Conclusions and Recommendations for Future Work

The data points for diameter of 84 in. and above were significantly less than that of 30 in to 84 in. By adding more data for SAPL projects, the accuracy of the entire analysis can be improved. Analysis of liner thickness for each trenchless renewal requires more data. This study can be expanded to other locations and states. This study used bid tabs for evaluation of construction costs, however for an accurate estimate of costs, more detailed project information regarding construction equipment, depth of culvert and accessibility, weather conditions, level of host culvert deterioration and required cleaning, etc., are required.

It can be concluded that SAPL, CIPP, and sliplining have the highest to lowest construction costs in culvert with diameter range of 30 in. to 108 in., respectively.

In this chapter, due to data availability, only one material from each trenchless method was considered for the analysis and comparisons. There is a need to obtain the project data for all other types of materials for each trenchless method to have a better comparison among different renewal methods.

SAPL concept for large diameter gravity culverts is a more recent technique rather than CIPP and sliplining, so fewer projects are conducted with this method until now. With more use of SAPL method, more data becomes available to improve accuracy of the cost comparison analysis.

Environmental and construction costs play essential roles in the decision-making to select the most appropriate trenchless method for culvert renewals. In addition, it is recommended to investigate influence of other factors, such as, social costs.

Appendix 5-A
Dataset

Dataset

No	Latitude	Longitude	Location	Letting Year	Trenchless Method	Pipe Diameter	Pipe Length	Rehab Thickness	Unit_Cost_19
1	41.2033	-77.1945	PA	2015	SAPL	54	60	1	741.49
2	41.2033	-77.1945	PA	2015	SAPL	48	55	1	674.08
3	41.2033	-77.1945	PA	2015	SAPL	66	50	1	950.64
4	41.2033	-77.1945	PA	2015	SAPL	48	30	1	891.67
5	41.2033	-77.1945	PA	2018	SAPL	48	440	1.75	888.83
6	41.2033	-77.1945	PA	2018	SAPL	60	450	2.25	1027.09
7	41.2033	-77.1945	PA	2016	CIPP	36	62		444.88
8	41.2033	-77.1945	PA	2016	CIPP	30	125		220.67
9	41.2033	-77.1945	PA	2016	CIPP	36	70		394.04
10	41.2033	-77.1945	PA	2014	CIPP	36	145		468.9
11	41.2033	-77.1945	PA	2014	CIPP	48	110		618.1
12	41.2033	-77.1945	PA	2014	CIPP	30	320		212.47
13	41.2033	-77.1945	PA	2010	CIPP	36	445		142.68
14	41.2033	-77.1945	PA	2010	CIPP	30	116		170.57
15	41.2033	-77.1945	PA	2012	CIPP	48	216		335.61
16	41.2033	-77.1945	PA	2010	CIPP	60	75		294.43
17	35.7596	-80.7935	NC	2016	SAPL	30	188	1.5	328.49
18	35.7596	-80.7935	NC	2014	SAPL	30	208	1.5	387.99
19	35.7596	-80.7935	NC	2014	SAPL	42	68	1.5	831.41
20	35.7596	-80.7935	NC	2014	SAPL	54	64	1.5	942.26
21	35.7596	-80.7935	NC	2017	SAPL	78	405	1.5	890.38
22	35.7596	-80.7935	NC	2016	SAPL	48	160	1.5	497.55
23	35.7596	-80.7935	NC	2014	SAPL	72	253	1.5	1413.39
24	35.7596	-80.7935	NC	2017	SAPL	54	56	1.5	523.75
25	35.7596	-80.7935	NC	2014	CIPP	30	143		207.3
26	35.7596	-80.7935	NC	2016	CIPP	30	105		431.21
27	35.7596	-80.7935	NC	2014	CIPP	36	131		271.59
28	35.7596	-80.7935	NC	2015	CIPP	60	269		850.16
29	35.7596	-80.7935	NC	2017	CIPP	30	580		167.51
30	35.7596	-80.7935	NC	2019	CIPP	30	264		140
31	35.7596	-80.7935	NC	2019	Sliplining	30	211		250
32	35.7596	-80.7935	NC	2019	Sliplining	42	195		240
33	35.7596	-80.7935	NC	2019	Sliplining	54	578		260
34	35.7596	-80.7935	NC	2011	Sliplining	30	452		492.96
35	35.7596	-80.7935	NC	2010	Sliplining	36	135		359.2
36	35.7596	-80.7935	NC	2010	Sliplining	54	64		573.54

37	35.7596	-80.7935	NC	2010	Sliplining	66	110		617.11
38	35.7596	-80.7935	NC	2011	Sliplining	30	150		273.87
39	35.7596	-80.7935	NC	2015	Sliplining	42	19		727.78
40	35.7596	-80.7935	NC	2012	Sliplining	54	408		519.08
41	35.7596	-80.7935	NC	2014	Sliplining	54	244		909
42	35.7596	-80.7935	NC	2012	Sliplining	60	168		548.16
43	35.7596	-80.7935	NC	2011	Sliplining	60	358		513.5
44	35.7596	-80.7935	NC	2011	Sliplining	66	185		673.25
45	35.7596	-80.7935	NC	2011	Sliplining	72	345		568.27
46	40.4173	-82.9071	OH	2018	CIPP	36	246		183.66
47	40.4173	-82.9071	OH	2018	CIPP	36	262		230.22
48	40.4173	-82.9071	OH	2018	CIPP	42	286		255.8
49	40.4173	-82.9071	OH	2017	CIPP	36	265		246.16
50	40.4173	-82.9071	OH	2017	CIPP	36	210		235.69
51	40.4173	-82.9071	OH	2017	CIPP	42	218		288.06
52	40.4173	-82.9071	OH	2017	CIPP	30	173		219.98
53	40.4173	-82.9071	OH	2017	CIPP	36	265		246.16
54	40.4173	-82.9071	OH	2017	CIPP	36	210		235.69
55	40.4173	-82.9071	OH	2017	CIPP	42	218		288.06
56	40.4173	-82.9071	OH	2018	CIPP	36	264		133.01
57	40.4173	-82.9071	OH	2018	SAPL	36	496	1.5	306.96
58	40.4173	-82.9071	OH	2018	SAPL	42	298	1.5	342.77
59	40.4173	-82.9071	OH	2018	SAPL	48	476	1.5	368.35
60	40.4173	-82.9071	OH	2018	SAPL	54	1064	2	562.76
61	40.4173	-82.9071	OH	2017	SAPL	36	154	1	696.59
62	40.4173	-82.9071	OH	2017	SAPL	42	145	1	628.5
63	40.4173	-82.9071	OH	2018	SAPL	60	125	2	537.18
64	40.4173	-82.9071	OH	2017	SAPL	48	94	1.5	552.03
65	40.4173	-82.9071	OH	2017	SAPL	54	158	1.5	489.18
66	40.4173	-82.9071	OH	2017	SAPL	72	154	2	696.59
67	40.4173	-82.9071	OH	2017	SAPL	42	145	1.5	628.5
68	40.4173	-82.9071	OH	2017	SAPL	66	88	2	1089.4
69	40.4173	-82.9071	OH	2017	SAPL	60	489	2	505.94
70	40.4173	-82.9071	OH	2017	SAPL	48	332	2	501.75
71	40.4173	-82.9071	OH	2017	SAPL	60	279	2	518.51
72	40.4173	-82.9071	OH	2018	SAPL	36	496	1.5	306.96
73	40.4173	-82.9071	OH	2018	SAPL	42	298	1.5	342.77
74	40.4173	-82.9071	OH	2018	SAPL	48	476	1.5	368.35

75	40.4173	-82.9071	OH	2018	SAPL	60	1064	2	460.44
76	40.4173	-82.9071	OH	2018	SAPL	30	61	1.5	230.73
77	40.4173	-82.9071	OH	2018	SAPL	72	51	2	1137.29
78	40.4173	-82.9071	OH	2018	Sliplining	36	16		229.2
79	40.4173	-82.9071	OH	2018	Sliplining	36	42		713.86
80	40.4173	-82.9071	OH	2018	Sliplining	36	38		185.08
81	40.4173	-82.9071	OH	2018	Sliplining	42	36		190.18
82	40.4173	-82.9071	OH	2018	Sliplining	48	35		339.91
83	40.4173	-82.9071	OH	2018	Sliplining	48	52		266.14
84	40.4173	-82.9071	OH	2018	Sliplining	60	44		493.5
85	40.4173	-82.9071	OH	2018	Sliplining	60	386		617.06
86	40.4173	-82.9071	OH	2017	Sliplining	30	18		319.49
87	40.4173	-82.9071	OH	2017	Sliplining	36	40		204.26
88	40.4173	-82.9071	OH	2018	Sliplining	36	5		339.7
89	40.4173	-82.9071	OH	2017	Sliplining	30	18		319.49
90	40.4173	-82.9071	OH	2017	Sliplining	48	14		494.42
91	40.4173	-82.9071	OH	2017	Sliplining	54	32		230.45
92	40.4173	-82.9071	OH	2017	Sliplining	36	40		204.26
93	40.4173	-82.9071	OH	2017	Sliplining	60	105		618.03
94	40.4173	-82.9071	OH	2017	Sliplining	72	68		293.3
95	40.4173	-82.9071	OH	2017	Sliplining	72	84		246.16
96	40.4173	-82.9071	OH	2017	Sliplining	30	203		298.54
97	40.4173	-82.9071	OH	2017	Sliplining	36	110		356.15
98	40.4173	-82.9071	OH	2018	Sliplining	36	16		126.88
99	40.4173	-82.9071	OH	2018	Sliplining	60	94		874.84
100	40.4173	-82.9071	OH	2018	Sliplining	60	256		273.19
101	40.4173	-82.9071	OH	2018	Sliplining	48	154		445.09
102	40.4173	-82.9071	OH	2018	Sliplining	90	120		597.94
103	40.4173	-82.9071	OH	2018	Sliplining	60	53		508.53
104	40.4173	-82.9071	OH	2018	Sliplining	60	96		341.75
105	40.4173	-82.9071	OH	2018	Sliplining	72	85		383.7
106	40.4173	-82.9071	OH	2018	Sliplining	84	81		326.4
107	40.4173	-82.9071	OH	2018	Sliplining	42	82		710.1
108	40.4173	-82.9071	OH	2018	Sliplining	48	163		474.76
109	40.4173	-82.9071	OH	2018	Sliplining	60	317		564.81
110	40.4173	-82.9071	OH	2018	Sliplining	60	125		537.18
111	40.4173	-82.9071	OH	2018	Sliplining	102	452		716.24
112	40.4173	-82.9071	OH	2017	Sliplining	30	64		148.75

113	40.4173	-82.9071	OH	2017	Sliplining	36	76		168.65
114	40.4173	-82.9071	OH	2017	Sliplining	72	68		384.43
115	40.4173	-82.9071	OH	2017	Sliplining	30	204		329.96
116	40.4173	-82.9071	OH	2017	Sliplining	48	226		511.18
117	40.4173	-82.9071	OH	2017	Sliplining	48	226		273.4
118	40.4173	-82.9071	OH	2017	Sliplining	36	8		379.44
119	40.4173	-82.9071	OH	2017	Sliplining	60	77		575.26
120	40.4173	-82.9071	OH	2017	Sliplining	60	97		930.75
121	40.4173	-82.9071	OH	2017	Sliplining	36	128		477.02
122	40.4173	-82.9071	OH	2017	Sliplining	42	120		501.84
123	40.73061	-73.9352	NY	2012	CIPP	30	606		201.37
124	40.73061	-73.9352	NY	2012	CIPP	30	666		393.78
125	40.73061	-73.9352	NY	2012	CIPP	30	1291		283.89
126	40.73061	-73.9352	NY	2012	CIPP	30	60		313.24
127	40.73061	-73.9352	NY	2012	CIPP	30	100		313.24
128	40.73061	-73.9352	NY	2013	CIPP	30	820		440.89
129	40.73061	-73.9352	NY	2013	CIPP	30	190		304.21
130	40.73061	-73.9352	NY	2013	CIPP	30	248		281.26
131	40.73061	-73.9352	NY	2013	CIPP	30	132		369.24
132	40.73061	-73.9352	NY	2013	CIPP	30	50		308.62
133	40.73061	-73.9352	NY	2013	CIPP	30	100		445.16
134	40.73061	-73.9352	NY	2014	CIPP	30	140		443.42
135	40.73061	-73.9352	NY	2014	CIPP	30	325		308.26
136	40.73061	-73.9352	NY	2014	CIPP	30	270		210.62
137	40.73061	-73.9352	NY	2014	CIPP	30	100		310.39
138	40.73061	-73.9352	NY	2015	CIPP	30	880		202.52
139	40.73061	-73.9352	NY	2015	CIPP	30	2025		218.77
140	40.73061	-73.9352	NY	2015	CIPP	30	50		368.22
141	40.73061	-73.9352	NY	2016	CIPP	30	424		309.23
142	40.73061	-73.9352	NY	2016	CIPP	30	610		240.75
143	40.73061	-73.9352	NY	2016	CIPP	30	100		299.6
144	40.73061	-73.9352	NY	2016	CIPP	30	50		337.05
145	40.73061	-73.9352	NY	2017	CIPP	30	500		240.93
146	40.73061	-73.9352	NY	2018	CIPP	30	1094		214.87
147	40.73061	-73.9352	NY	2018	CIPP	30	100		332.54
148	40.73061	-73.9352	NY	2012	CIPP	36	912		246.11
149	40.73061	-73.9352	NY	2012	CIPP	36	270		307.64
150	40.73061	-73.9352	NY	2012	CIPP	36	122		520.2

151	40.73061	-73.9352	NY	2012	CIPP	36	1587		368.31
152	40.73061	-73.9352	NY	2012	CIPP	36	60		408.33
153	40.73061	-73.9352	NY	2012	CIPP	36	100		408.33
154	40.73061	-73.9352	NY	2013	CIPP	36	840		440.89
155	40.73061	-73.9352	NY	2013	CIPP	36	122		347.2
156	40.73061	-73.9352	NY	2015	CIPP	36	500		250.17
157	40.73061	-73.9352	NY	2013	CIPP	36	64		484.98
158	40.73061	-73.9352	NY	2013	CIPP	36	50		402.31
159	40.73061	-73.9352	NY	2013	CIPP	36	100		506.8
160	40.73061	-73.9352	NY	2014	CIPP	36	880		465.59
161	40.73061	-73.9352	NY	2014	CIPP	36	606		319.98
162	40.73061	-73.9352	NY	2014	CIPP	36	1120		232.79
163	40.73061	-73.9352	NY	2014	CIPP	36	100		404.62
164	40.73061	-73.9352	NY	2015	CIPP	36	810		218.77
165	40.73061	-73.9352	NY	2015	CIPP	36	3997		238.26
166	40.73061	-73.9352	NY	2015	CIPP	36	50		433.2
167	40.73061	-73.9352	NY	2016	CIPP	36	704		408.74
168	40.73061	-73.9352	NY	2016	CIPP	36	300		256.8
169	40.73061	-73.9352	NY	2016	CIPP	36	130		288.9
170	40.73061	-73.9352	NY	2016	CIPP	36	184		363.8
171	40.73061	-73.9352	NY	2016	CIPP	36	100		358.45
172	40.73061	-73.9352	NY	2016	CIPP	36	50		406.6
173	40.73061	-73.9352	NY	2017	CIPP	36	1500		261.88
174	40.73061	-73.9352	NY	2018	CIPP	36	426		250.68
175	40.73061	-73.9352	NY	2018	CIPP	42	100		414.4
176	40.73061	-73.9352	NY	2017	CIPP	42	850		314.25
177	40.73061	-73.9352	NY	2016	CIPP	42	50		433.35
178	40.73061	-73.9352	NY	2016	CIPP	42	100		433.35
179	40.73061	-73.9352	NY	2016	CIPP	42	188		659.12
180	40.73061	-73.9352	NY	2015	CIPP	42	50		525.26
181	40.73061	-73.9352	NY	2015	CIPP	42	363		314.07
182	40.73061	-73.9352	NY	2014	CIPP	42	100		471.13
183	40.73061	-73.9352	NY	2014	CIPP	42	575		288.22
184	40.73061	-73.9352	NY	2013	CIPP	42	50		468.44
185	40.73061	-73.9352	NY	2012	CIPP	42	100		475.45
186	40.73061	-73.9352	NY	2012	CIPP	42	60		475.45
187	40.73061	-73.9352	NY	2012	CIPP	42	433		422.94
188	40.73061	-73.9352	NY	2012	CIPP	42	1158		335.61

189	40.73061	-73.9352	NY	2012	CIPP	48	2008		413.92
190	40.73061	-73.9352	NY	2012	CIPP	48	60		503.42
191	40.73061	-73.9352	NY	2012	CIPP	48	100		531.38
192	40.73061	-73.9352	NY	2013	CIPP	48	50		551.11
193	40.73061	-73.9352	NY	2014	CIPP	48	100		526.56
194	40.73061	-73.9352	NY	2015	CIPP	48	356		357.39
195	40.73061	-73.9352	NY	2015	CIPP	48	50		579.41
196	40.73061	-73.9352	NY	2016	CIPP	48	200		353.1
197	40.73061	-73.9352	NY	2016	CIPP	48	180		535
198	40.73061	-73.9352	NY	2016	CIPP	48	100		502.9
199	40.73061	-73.9352	NY	2016	CIPP	48	50		508.25
200	40.73061	-73.9352	NY	2017	CIPP	48	450		366.63
201	40.73061	-73.9352	NY	2017	CIPP	48	188		471.38
202	40.73061	-73.9352	NY	2018	CIPP	48	100		486.02
203	40.73061	-73.9352	NY	2018	CIPP	48	180		486.21
204	40.73061	-73.9352	NY	2012	SAPL	36	890	1.5	335.61
205	40.73061	-73.9352	NY	2013	SAPL	36	46950	1.5	319.64
206	40.73061	-73.9352	NY	2015	SAPL	36	724	1.5	703.95
207	40.73061	-73.9352	NY	2014	SAPL	36	790	1.5	642.95
208	40.73061	-73.9352	NY	2016	SAPL	36	30768	1.5	396.6
209	40.73061	-73.9352	NY	2017	SAPL	36	15510	1.5	387.58
210	40.73061	-73.9352	NY	2018	SAPL	36	800	1.5	409.28
211	40.73061	-73.9352	NY	2019	Sliplining	30	266		170
212	40.73061	-73.9352	NY	2019	Sliplining	36	438		180
213	40.73061	-73.9352	NY	2010	Sliplining	48	50		353.31
214	40.73061	-73.9352	NY	2011	Sliplining	48	30		410.8
215	40.73061	-73.9352	NY	2011	Sliplining	48	50		410.8
216	40.73061	-73.9352	NY	2011	Sliplining	48	117		542.03
217	40.73061	-73.9352	NY	2012	Sliplining	48	124		374.76
218	40.73061	-73.9352	NY	2012	Sliplining	48	356		196.89
219	40.73061	-73.9352	NY	2013	Sliplining	48	520		413.33
220	40.73061	-73.9352	NY	2014	Sliplining	48	30		443.42
221	40.73061	-73.9352	NY	2015	Sliplining	48	295		303.24
222	40.73061	-73.9352	NY	2017	Sliplining	48	350		445.19
223	40.73061	-73.9352	NY	2018	Sliplining	48	251		417.47
224	40.73061	-73.9352	NY	2019	Sliplining	48	85		240
225	40.73061	-73.9352	NY	2011	Sliplining	60	400		473.56
226	40.73061	-73.9352	NY	2016	Sliplining	60	678		363.8

227	40.73061	-73.9352	NY	2019	Sliplining	60	96		700
228	40.73061	-73.9352	NY	2019	Sliplining	60	95		350
229	40.73061	-73.9352	NY	2012	Sliplining	84	165		894.96
230	40.73061	-73.9352	NY	2014	Sliplining	84	268		831.41
231	40.73061	-73.9352	NY	2019	Sliplining	84	150		606
232	40.73061	-73.9352	NY	2012	Sliplining	42	66		469.85
233	40.73061	-73.9352	NY	2012	Sliplining	42	60		357.98
234	40.73061	-73.9352	NY	2015	Sliplining	42	262		291.33
235	40.73061	-73.9352	NY	2013	Sliplining	42	50		413.33
236	40.73061	-73.9352	NY	2014	Sliplining	42	1738		294.87
237	40.73061	-73.9352	NY	2014	Sliplining	42	64		332.56
238	40.73061	-73.9352	NY	2015	Sliplining	42	50		406.13
239	40.73061	-73.9352	NY	2016	Sliplining	42	734		211.86
240	40.73061	-73.9352	NY	2017	Sliplining	42	412		319.49
241	40.73061	-73.9352	NY	2016	Sliplining	42	50		401.25
242	40.73061	-73.9352	NY	2018	Sliplining	42	100		383.7
243	40.73061	-73.9352	NY	2012	Sliplining	48	60		447.48
244	40.73061	-73.9352	NY	2015	Sliplining	48	324		292.41
245	40.73061	-73.9352	NY	2013	Sliplining	48	50		496
246	40.73061	-73.9352	NY	2013	Sliplining	48	700		305.28
247	40.73061	-73.9352	NY	2014	Sliplining	48	854		365.82
248	40.73061	-73.9352	NY	2015	Sliplining	48	50		487.35
249	40.73061	-73.9352	NY	2016	Sliplining	48	380		278.2
250	40.73061	-73.9352	NY	2016	Sliplining	48	50		481.5
251	40.73061	-73.9352	NY	2018	Sliplining	48	164		296.73
252	40.73061	-73.9352	NY	2018	Sliplining	48	100		460.44
253	40.73061	-73.9352	NY	2012	Sliplining	54	244		615.29
254	40.73061	-73.9352	NY	2012	Sliplining	54	60		531.38
255	40.73061	-73.9352	NY	2013	Sliplining	54	472		341.69
256	40.73061	-73.9352	NY	2013	Sliplining	54	123		396.8
257	40.73061	-73.9352	NY	2013	Sliplining	54	50		578.67
258	40.73061	-73.9352	NY	2014	Sliplining	54	250		287.11
259	40.73061	-73.9352	NY	2014	Sliplining	54	166		387.99
260	40.73061	-73.9352	NY	2015	Sliplining	54	50		568.58
261	40.73061	-73.9352	NY	2017	Sliplining	54	22		764.68
262	40.73061	-73.9352	NY	2016	Sliplining	54	50		561.75
263	40.73061	-73.9352	NY	2017	Sliplining	54	123		628.5
264	40.73061	-73.9352	NY	2017	Sliplining	54	676		392.81

265	40.73061	-73.9352	NY	2018	Sliplining	54	448		353
266	40.73061	-73.9352	NY	2018	Sliplining	54	100		537.18
267	40.73061	-73.9352	NY	2014	Sliplining	66	65		554.27
268	40.73061	-73.9352	NY	2016	Sliplining	66	594		535
269	40.73061	-73.9352	NY	2017	Sliplining	66	336		502.8
270	40.73061	-73.9352	NY	2018	Sliplining	66	398		450.21
271	40.73061	-73.9352	NY	2014	Sliplining	42	122		321.48
272	40.73061	-73.9352	NY	2018	Sliplining	42	160		681.45
273	40.73061	-73.9352	NY	2013	Sliplining	48	462		314.13
274	40.73061	-73.9352	NY	2015	Sliplining	48	140		354.25
275	40.73061	-73.9352	NY	2016	Sliplining	48	145		321
276	40.73061	-73.9352	NY	2017	Sliplining	48	110		356.15
277	40.73061	-73.9352	NY	2017	Sliplining	48	368		256.64
278	40.73061	-73.9352	NY	2012	Sliplining	54	90		866.99
279	40.73061	-73.9352	NY	2013	Sliplining	54	699		275.56
280	40.73061	-73.9352	NY	2014	Sliplining	54	765		279.35
281	40.73061	-73.9352	NY	2014	Sliplining	54	162		387.99
282	40.73061	-73.9352	NY	2014	Sliplining	54	538		387.99
283	40.73061	-73.9352	NY	2015	Sliplining	54	250		389.98
284	40.73061	-73.9352	NY	2016	Sliplining	54	90		310.3
285	40.73061	-73.9352	NY	2017	Sliplining	54	247		477.66
286	40.73061	-73.9352	NY	2017	Sliplining	54	440		340.44
287	40.73061	-73.9352	NY	2018	Sliplining	54	145		523.37
288	40.73061	-73.9352	NY	2012	Sliplining	60	60		604.1
289	40.73061	-73.9352	NY	2013	Sliplining	60	1726		380.27
290	40.73061	-73.9352	NY	2013	Sliplining	60	162		391.29
291	40.73061	-73.9352	NY	2013	Sliplining	60	50		661.33
292	40.73061	-73.9352	NY	2014	Sliplining	60	466		321.48
293	40.73061	-73.9352	NY	2014	Sliplining	60	69		554.27
294	40.73061	-73.9352	NY	2014	Sliplining	60	498		432.33
295	40.73061	-73.9352	NY	2015	Sliplining	60	50		649.8
296	40.73061	-73.9352	NY	2016	Sliplining	60	195		304.95
297	40.73061	-73.9352	NY	2016	Sliplining	60	50		642
298	40.73061	-73.9352	NY	2017	Sliplining	60	596		387.58
299	40.73061	-73.9352	NY	2017	Sliplining	60	410		419
300	40.73061	-73.9352	NY	2018	Sliplining	60	100		665.08
301	40.73061	-73.9352	NY	2018	Sliplining	60	15		289.05
302	40.73061	-73.9352	NY	2019	Sliplining	60	452		860

303	40.73061	-73.9352	NY	2012	Sliplining	66	275		671.22
304	40.73061	-73.9352	NY	2013	Sliplining	66	780		456.25
305	40.73061	-73.9352	NY	2016	Sliplining	66	169		642
306	40.73061	-73.9352	NY	2017	Sliplining	66	717		526.89
307	40.73061	-73.9352	NY	2018	Sliplining	66	85		953.11
308	40.73061	-73.9352	NY	2019	Sliplining	72	235		660
309	40.73061	-73.9352	NY	2013	Sliplining	78	245		578.67
310	40.73061	-73.9352	NY	2013	Sliplining	78	258		892.8
311	40.73061	-73.9352	NY	2014	Sliplining	78	340		458.94
312	40.73061	-73.9352	NY	2014	Sliplining	78	173		565.36
313	40.73061	-73.9352	NY	2017	Sliplining	78	12		1047.5
314	40.73061	-73.9352	NY	2013	Sliplining	84	245		578.67
315	40.73061	-73.9352	NY	2013	Sliplining	84	258		892.8
316	40.73061	-73.9352	NY	2014	Sliplining	84	340		458.94
317	40.73061	-73.9352	NY	2014	Sliplining	84	173		565.36
318	40.73061	-73.9352	NY	2017	Sliplining	84	12		1047.5
319	40.73061	-73.9352	NY	2014	Sliplining	90	675		515.47
320	40.73061	-73.9352	NY	2016	Sliplining	90	53		535
321	40.73061	-73.9352	NY	2015	Sliplining	96	1625		649.8
322	40.73061	-73.9352	NY	2017	Sliplining	96	85		885.14
323	40.73061	-73.9352	NY	2018	Sliplining	96	35		1028.32
324	46.7296	-94.6859	MN	2018	CIPP	30	3204		209.45
325	46.7296	-94.6859	MN	2018	CIPP	36	5878		252.51
326	46.7296	-94.6859	MN	2018	CIPP	42	547		307.43
327	46.7296	-94.6859	MN	2018	CIPP	48	1181		472.07
328	46.7296	-94.6859	MN	2018	CIPP	60	314		671.56
329	46.7296	-94.6859	MN	2018	CIPP	108	352		1100
330	46.7296	-94.6859	MN	2018	CIPP	36	346		209.76
331	46.7296	-94.6859	MN	2018	CIPP	48	227		562.76
332	46.7296	-94.6859	MN	2018	CIPP	54	215		332.54
333	46.7296	-94.6859	MN	2018	CIPP	60	243		419.51
334	46.7296	-94.6859	MN	2018	CIPP	66	190		491.14
335	46.7296	-94.6859	MN	2018	CIPP	72	359		547.41
336	46.7296	-94.6859	MN	2018	CIPP	72	93		767.4
337	46.7296	-94.6859	MN	2016	CIPP	84	580		1006.87
338	46.7296	-94.6859	MN	2018	CIPP	30	178		271.15
339	46.7296	-94.6859	MN	2018	CIPP	36	676		199.52
340	46.7296	-94.6859	MN	2019	CIPP	30	169		298

341	46.7296	-94.6859	MN	2019	CIPP	36	234		365
342	46.7296	-94.6859	MN	2019	CIPP	54	187		436
343	46.7296	-94.6859	MN	2019	CIPP	60	340		406
344	46.7296	-94.6859	MN	2010	CIPP	36	84		223.76
345	46.7296	-94.6859	MN	2019	CIPP	30	281		220
346	46.7296	-94.6859	MN	2019	CIPP	36	615		250
347	46.7296	-94.6859	MN	2019	CIPP	42	97		380
348	46.7296	-94.6859	MN	2019	CIPP	48	216		400
349	46.7296	-94.6859	MN	2019	CIPP	54	94		575
350	46.7296	-94.6859	MN	2019	CIPP	60	100		640
351	46.7296	-94.6859	MN	2016	CIPP	30	357		321
352	46.7296	-94.6859	MN	2016	CIPP	36	192		428
353	46.7296	-94.6859	MN	2016	CIPP	48	69		556.4
354	46.7296	-94.6859	MN	2018	SAPL	30	75	1.5	341.17
355	46.7296	-94.6859	MN	2018	SAPL	36	118	1.5	404.43
356	46.7296	-94.6859	MN	2018	SAPL	60	98	2	909.36
357	46.7296	-94.6859	MN	2016	SAPL	84	580	2	1177
358	46.7296	-94.6859	MN	2010	SAPL	36	84	1	294.43
359	46.7296	-94.6859	MN	2018	Sliplining	36	174		202.59
360	46.7296	-94.6859	MN	2018	Sliplining	42	116		427.7
361	46.7296	-94.6859	MN	2015	Sliplining	36	115		162.45
362	46.7296	-94.6859	MN	2015	Sliplining	30	731		238.26
363	46.7296	-94.6859	MN	2015	Sliplining	36	382		303.24
364	46.7296	-94.6859	MN	2015	Sliplining	42	138		422.37
365	46.7296	-94.6859	MN	2015	Sliplining	48	165		471.11
366	46.7296	-94.6859	MN	2015	Sliplining	60	106		785.18
367	46.7296	-94.6859	MN	2015	Sliplining	30	1429		135.38
368	46.7296	-94.6859	MN	2015	Sliplining	36	677		157.04
369	46.7296	-94.6859	MN	2015	Sliplining	42	364		222.02
370	46.7296	-94.6859	MN	2015	Sliplining	48	161		362.81
371	46.7296	-94.6859	MN	2015	Sliplining	54	1291		346.56
372	46.7296	-94.6859	MN	2015	Sliplining	60	1029		384.47
373	46.7296	-94.6859	MN	2015	Sliplining	72	1048		460.28
374	46.7296	-94.6859	MN	2010	Sliplining	36	84		123.66
375	38.9108	-75.5277	DE	2018	SAPL	36	400	1.5	419.51
376	38.9108	-75.5277	DE	2018	SAPL	42	400	1.5	419.51
377	38.9108	-75.5277	DE	2018	SAPL	48	400	1.5	419.51
378	38.9108	-75.5277	DE	2018	SAPL	54	200	2	532.06

379	38.9108	-75.5277	DE	2018	SAPL	60	200	2	532.06
380	27.6648	-81.5158	FL	2017	Sliplining	54	812		942.75
381	27.6648	-81.5158	FL	2017	Sliplining	60	812		942.75
382	27.6648	-81.5158	FL	2019	CIPP	54	1066		296.25
383	27.6648	-81.5158	FL	2019	CIPP	60	186		439.25
384	27.6648	-81.5158	FL	2019	CIPP	42	626		203
385	27.6648	-81.5158	FL	2019	CIPP	36	499		205.85
386	27.6648	-81.5158	FL	2018	CIPP	36	8263		108.25
387	27.6648	-81.5158	FL	2018	CIPP	48	2947		165.68
388	27.6648	-81.5158	FL	2018	CIPP	48	275		184.18
389	27.6648	-81.5158	FL	2018	CIPP	60	24		409.28
390	27.6648	-81.5158	FL	2018	CIPP	72	24		665.08
391	27.6648	-81.5158	FL	2019	CIPP	36	1633		105
392	27.6648	-81.5158	FL	2018	CIPP	36	300		158.6
393	27.6648	-81.5158	FL	2018	CIPP	48	100		230.22
394	27.6648	-81.5158	FL	2018	CIPP	60	100		250.68
395	27.6648	-81.5158	FL	2018	CIPP	72	50		613.92
396	27.6648	-81.5158	FL	2018	CIPP	36	640		118.08
397	27.6648	-81.5158	FL	2019	Sliplining	36	100		180
398	27.6648	-81.5158	FL	2019	Sliplining	48	100		250
399	27.6648	-81.5158	FL	2019	Sliplining	60	50		400
400	27.6648	-81.5158	FL	2019	Sliplining	72	50		750
401	27.6648	-81.5158	FL	2019	SAPL	48	526	1.5	350

Chapter 6

Review the Cured in Place (CIPP) Design Equations

CHAPTER 6 - REVIEW THE CURED IN PLACE (CIPP) DESIGN EQUATIONS

6.1. Introduction

This chapter presents the current design methodologies and their associated equations (where possible) that are used for the design of flexible pipe liners, specifically, CIPP. These include the ASTM F1216 design appendix X1, the WRc Sewerage Rehabilitation Manual, the German Static Calculation for the Rehabilitation of Drains and Sewers Using Lining and Assembly Procedures (ATV-DVWK-M 127 E, Part 2), and the ASTEE 3R2014 Structural Design for Non-Circular Linings Under Groundwater Pressure. It will also offer a brief glimpse of the pending ASCE Manual of Practice for the Design of Flexible Liners.

The current practice of most engineers in North America is to request that cured-in-place-pipes (CIPP) be designed using the non-mandatory design appendix X1 found in the ASTM Standard F1216. This chapter covers the ASTM F1216 design methodology in detail. Originally approved in 1989, the equations found therein are stated as being applicable to circular pipe geometries that have installed ovalities less than 10% at the time of lining. In the case of non-circular shaped pipe geometries such as egg-shaped and ovoid shaped pipes, North American engineers will typically reference the Water Resources Center Sewerage Rehabilitation Manual (WRcSRM) for design guidance (originally introduced in 1983).

6.2. WRc SRM Volume III Sewer Renovation

The WRcSRM contains two design procedures given in its Volume III Sewer Renovation. They are designated as Type I and Type II designs. The type of lining depends on how the lining interacts with the existing pipe as follows:

- Type I – The lining, grout (where present), and existing sewer act as a rigid composite section. A bond is required between the lining and existing sewer (and grout where present),
- Type II – The lining is designed as a flexible pipe and it does not require a bond between the lining, and grout (where present) or the existing sewer.

The design approach given therein states that the existing structure is assessed to be fundamentally sound if the pipework or brickwork is complete and is free from fractures as described in the Manual of Sewer Condition Classification (which follows the NASSCO PACP) without any apparent deformation. It further states that the design procedures of Volume III are generally suitable for sewer sizes less than about 1,800 mm (72 inches).

Worker-entry size linings may be designed as Type I or Type II structures. Two-piece linings (such as GRP panels), designed as Type I linings, are assumed to be jointed at the springline positions.

For non-man entry size flexible sewer linings, the WRcSRM states that they should be designed as Type II structures, as adequate bond to the existing sewer cannot confidently be achieved.

Therefore, with respect to CIPP, Type II lining is the common practice in the UK. The Type II lining thickness is typically calculated based on hydrostatic buckling of the liner due to groundwater pressure. Consideration of any transfer of soil and live loads to the liner is not the norm in the UK.

6.3. German ATV-DVWK-M 127 E, Part 2

This design procedure is purported to consider 1) imperfections with the bedding of the liner in the host pipe, 2) long-term stress detection, 3) contact pressure problems, and 4) necessary non-linear calculations (second order theory due as a rule to concurrent occurrences of thinner wall thicknesses, small elasticity moduli and high longitudinal forces in the liner wall). It should be noted that while the ATV-DVWK-M 127 E, Part 2 is still valid, the Germans have recently advanced (2002) a new design procedure, DWA A 143, Part 2, which is considered more desirable. To this the Germans have added the DWA M 144, Part 3 design advisory leaflet to address a special load case of the Old Pipe Condition II.

The condition of the non-rehabilitated old pipe is divided into two categories:

- Old Pipe Condition I – Soil and traffic loads are taken completely by the old pipe alone. The liner's wall thickness is based only on the groundwater pressure (identified as measured from the invert of the old pipe)
- Old Pipe Condition II – Old pipe-soil system alone capable of bearing the soil and traffic loads (even with longitudinal fractures and small pipe deformation which activates the support of the pipe's bedding (vertically and horizontally). This support is confirmed through long-term observation). The liner's thickness is dictated by the groundwater pressure.
- Old Pipe Condition III – Pipe-soil system in the long-term no longer capable of bearing' significant deformation; compared with Old Pipe Condition II the liner is also stressed by earth and traffic loads.

The load case for Old Pipe Condition I is given as external water pressure only. If there is no groundwater, a virtual groundwater pressure equal to the pipe's diameter plus 4 inches or 5 feet above the invert, whichever is greater, is to be used. The load case for Old Pipe Condition II requires consideration of the external water pressure, soil

load, and traffic load. For the soil load the Germans limit it to 0.75 times the weight of the soil prism directly above the pipe.

The German design procedure uses a classical engineering solution for each pipe condition to arrive at the bending and normal (compressive) stresses generated in the liner. The current leaflet is 84 pages in length with numerous charts, tables and formulae making it impractical to repeat in this report.

As mentioned above, DWA M 144, Part 3 presents design tables for a "special" load case:

- Host pipe state II,
- Local limited pre-strain of 2% of r_L in the invert of circular pipe (normal egg shape profiles: 0.8% of r_{LK}),
- Four-hinge-deformation of 3% of r_L (normal egg shape profiles; in the crown),
- Annular gap of 0.5% r_L (normal egg shape profiles: crown radius),
- Substitute circle for normal egg shape profiles: 0.6 × H (stability proof),

Maletz (2013) discussed the advancement found in the DWA A 143, Part 2. He stated that in State III, even after installation of the liner, the old pipe can get further deformations under load. The liner must adapt to these distortions of the old pipe, because this pipe stiffness is usually lower than the stiffness of the old pipe. In this way, the liner of the old pipe-soil system is affected only marginally. Hence, a lower liner stiffness (reduced wall thickness and/or E-Modulus) may be beneficial in this design case. This shows that the German engineer's statement *"…I calculate only in the host pipe III state, then I get greater wall thicknesses…"* turns out to be wrong. Because by a rise of groundwater and/or a change in the existing pipe-soil-system an increase of frictional effects is possible. This would in turn apply the criteria for design by host pipe state II. Such mixed loading is a compromise between flexibility and stiffness of the liner is important.

It should be noted that the German calculation model for state III consists of a spring system that necessitates the design engineer using Finite Element Analysis.

6.4. ASCE Pipeline Infrastructure Committee

In June 2007, an ASCE Pipeline Infrastructure (PINS) Task Committee published a report entitled Emerging Concepts for the Design of Pipeline Renewal Systems to point out the issues with the ASTM F1216 design appendix and to guide engineers toward a more technically correct design methodology (contained in Part III of the report). Due to a lack of any other design methodology at the time of the writing of ASTM F1216, the simple load/response concept of a conventionally buried flexible pipe prevailed in engineers' minds for a flexible liner installed in a badly deteriorated host pipe (ASCE

Report by PINS Task Committee, 2007). Hence, the Luscher/AWWA design model for the fully deteriorated design condition was adopted.

The PINS Task Committee Report cited experimental research published by Gumbel et al. in 2003 that showed that uniform soil pressure on the liner pipe (as required in the ASTM F 1216 and ASCE Manual of Practice No. 62 on design practice) is improbable and use of the current F1216 design equations for the fully deteriorated design condition is inappropriate. Any soil load transferred to the liner was found to produce bending and small thrust loads for buckling to occur in the liner.

The rigid host pipe-soil structure is the most common soil load bearing resisting structure. This rigid host pipe-soil structure must be assumed to be in a stable equilibrium or capable of attaining such equilibrium with only small deflections of the host pipe for lining to be applicable. Using this rationale, the concept of the host pipe being "fully deteriorated" may become inappropriate. Thus, it is recommended that the liner pipe design should be based on hydrostatic buckling only using the new equations in Part III which recognized this fact. Future vertical deformations should be considered in the hydraulic buckling design analysis (Schrock, Part I of the PINS Task Committee Report).

Currently, an ASCE task group is in the final review stage of its process of developing a new Manual of Practice for the Design of Flexible Liners (MOP) incorporating the information in the PINS Task Committee Report. Using a modified Glock solution for the buckling of flexible liners installed in existing pipes (an encased condition) developed by Olivier Thepot (2000), it can be used for both circular and non-circular geometries making it fit the wide variety of in situ cross-sectional geometries in sanitary sewer, storm sewer, and especially culvert pipes. Thépot's design methodology was codified in France in 2014 as 3R2014 Structural Design for Non-Circular Linings Under Groundwater Pressure. It is an analytical design method applicable to the challenging pipe shapes normally found in sewer and culvert pipes. The current ASCE Task Group has made further advancements to Thépot's work to make sure that they addressed both rigid and flexible host pipe materials in the new MOP.

6.5. The ASTM F1216 Design Appendix X1

ASTM F1216 was first published in 1989 focusing on small diameter sanitary sewer pipe (8 inch through 12-inch diameters). It is an installation practice. However, as there existed no guidance at the time of its writing as to how to design the thickness of these liners in pipes, a non-mandatory appendix on design was included therein (X1. DESIGN CONSIDERATIONS). The standard considers two external load cases for calculating the finished wall thickness of the proposed liner pipe. Figure 6-1 illustrates the partially and fully deteriorated pipe terminologies according to the ASTM F1216 (2016).

- **Partially Deteriorated Pipe Condition (PD)**

In a partially deteriorated pipe condition (PD), there exists a sustained external hydrostatic pressure due to groundwater acting in the annual space between the liner pipe and the host pipe. Even where the permanent groundwater table is below the pipe invert level, the liner must generally be designed to resist a short-term external hydrostatic head which could arise under storm conditions. This is the so-called partially deteriorated pipe condition (PD).

- **Fully Deteriorated Pipe Condition (FD)**

In a fully deteriorated pipe condition, earth and traffic loads will in due course be transferred from the existing pipe-soil structure to the liner pipe. The likelihood of this occurring is assumed to be a function of the condition of the sewer at the time of lining. However, as numerous researchers (Gumbel, 1998, Thepot, 2000, Falter, 2004) have subsequently concluded, in the great majority of practical situations little or no-load transfer ever takes place because the lining process effectively and permanently locks in the existing equilibrium of even quite badly deteriorated sewer structures (rigid pipes) (Gumbel, 1998). The 1994 version of the WRc Manual has recognized this fact in the UK design procedure. In the U.S., lack of understanding in true soil loads (tunnel loads) in liner design has led to an irrationally over-conservative design (Gumbel, 1998).

This excessive conservatism per Gumbel (1998) is particularly acute in the treatment of a fully deteriorated pipe design condition (FD) for two reasons. First, the soil load reaching the liner pipe is overestimated by treating the liner as though it has been directly buried. Whereas the more correct analogy in circumstances where the existing pipe structure may continue to deteriorate after rehabilitation is more like that of a tunnel lining (Schrock & Gumbel, 1997, available at CUIRE website at cuire.uta.edu). Secondly, the formula used to describe liner response to the assumed transferred soil load, and hence calculation of the required wall thickness, has been incorrectly modified from an already conservative theory for direct-bury applications in a way which entails further irrational safety factors (Gumbel, 1998). The design equations for a pipe in fully deteriorated condition were borrowed from the fiberglass pipe industry which has subsequently modified their design equations several times.

X1.1.1 *partially deteriorated pipe* – the original pipe can support the soil and surcharge loads throughout the design life of the rehabilitated pipe. The soil adjacent to the existing pipe must provide adequate side support. The pipe may have longitudinal cracks and up to 10% distortion of the diameter. If the distortion of the diameter is greater than 10%, alternative design methods are required.

X1.1.2 *fully deteriorated pipe* – the original pipe is not structurally sound and cannot support soil and live loads or is expected to reach this condition over the design life of the rehabilitated pipe. This condition is evident when sections of the original pipe are missing, the pipe has lost its original shape, or the pipe has corroded due to the effects of the fluid, atmosphere, soil, or applied loads.

Figure 6-1. Partially and fully deteriorated pipe terminologies according to the ASTM F1216 (2016).

6.5.1. The ASTM Equations for the PD Design Condition

The formula for the hydrostatic buckling of a liner pipe was developed in the UK in 1980s. It is based on the theoretical buckling pressure of a long, perfectly circular, unrestrained flexible pipe material (by Timoshenko). To account for the observed enhancement of this unrestrained buckling pressure in the first experiments in which CIPP liners were inserted in steel casings and subjected to external water pressure, Aggarwal and Cooper (1984) defined a simple empirical factor K applied to the Timoshenko Equation for design purposes. As illustrated in Figure 6-2, it was found that a value of the enhancement factor K = 7 provided a close lower bound to the experimental data, and this value was subsequently recommended as the minimum value to be used where there is full support of the existing pipe. In the ASTM F1216, a minimum value for K of 7 is recommended, while the experimentation found values as high as the low 20's.

In hindsight, there was a major theoretical inconsistency in taking this simple approach. The liner buckling mode assumed involves liner deformations breaching the boundary conditions imposed by the restraining host pipe which obviously cannot occur. Ironically, there was an alternative, non-linear theory consistent with the real-world boundary conditions available at the time that Aggarwal was analyzing his test results (Glock, 1977), but it was missed because it was only available in the German language literature. The unmodified Glock theory, also plotted on the Figure 6-2, follows the trend of the data better. With a shallower slope, the graph illustrates the mean K-factor increases with increasing D/t (e.g., as the liner get thinner the resistance to buckling increases). Neither buckling theory however considered the issue of initial gap imperfections or explained the large, apparently random scatter of Aggarwal's data.

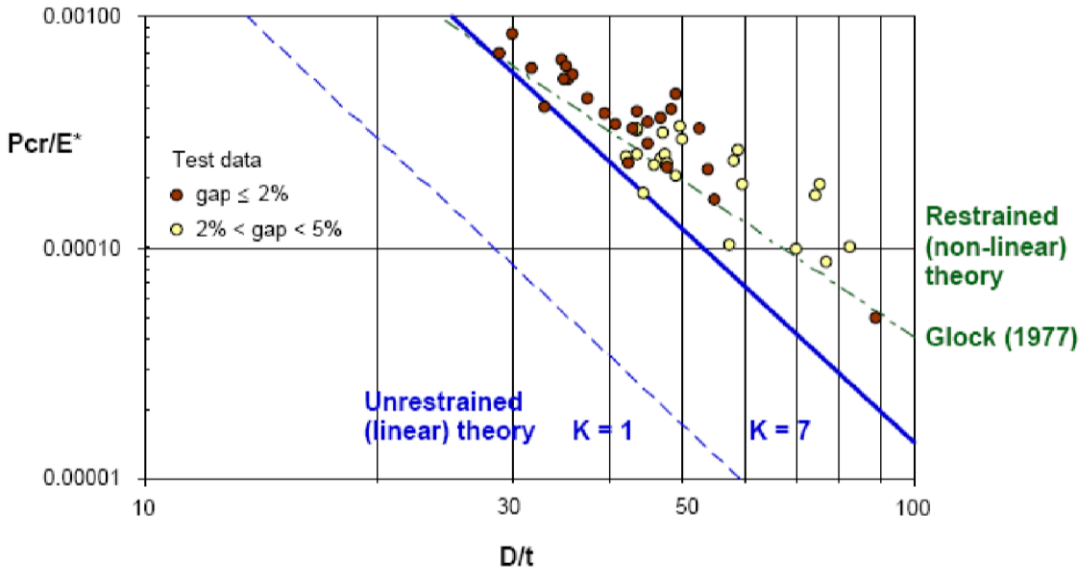


Figure 6-2. Restrained (non-linear) theory, Glock (1977).

The ASTM and WRc equations did from the outset take explicit account of the initial out-of-roundness or ovality due to vertical deformation of the circular pipe being lined. This was accomplished by the insertion of a C-factor into the Timoshenko model. It was a semi-intuitive attempt to account for the local maximum radius of curvature of an elliptically deformed host pipe. Experimental data published by Boot & Welch (1996) suggests that the ASTM C-factor, like the rest of the equation, is conservative. Closer examination of these and other test data (Seeman et al, 2001), as well as theoretical considerations (Boot & Gumbel, 1998), cast doubt on the validity of attempting to isolate the impact of ovality as an independent factor on buckling pressure. The need for an integrated approach to predict the combined effect of ovality, gap, and other imperfections provided a further imperative for updating the current ASTM theoretical model (Gumbel, 1998).

Given the above discussion, to arrive at the required minimum wall thickness to resist external hydrostatic pressure acting on the liner, the ASTM F1216 equation for the partially deteriorated pipe condition takes the actual groundwater pressure as the critical buckling pressure and solves the Eq. 6-1 (Eq. X1.1, ASTM F1216) for t using the ovality reduction factor (C) and safety factor (N).

$$t = \frac{D}{\left[\left(\frac{2 \times K \times E_L \times C}{(1-\nu^2) \times N \times P_{cr}}\right)^{1/3}\right] + 1} \qquad \text{Eq. 6-1}$$

Where,

t thickness of the CIPP, in.

D mean inside diameter of the original pipe, in.

K enhancement factor of the soil-pipe system where there is full support,

E_L long-term (time-corrected) modulus of elasticity for the CIPP, psi,
υ Poisson's ratio of the CIPP (0.3 average for plain felt liners),
N factor of safety,
P_{cr} groundwater load (psi), measured from the invert of the pipe.

Additionally, if the original pipe is oval (no guidance given on how much ovality defines "pipe as oval"), the CIPP design from Eq. X1.1 shall have a minimum thickness as calculated by the Eq. 6-2 (Eq. X1.2, ASTM F1216).

$$1.5\frac{\Delta}{100}\left(1+\frac{\Delta}{100}\right)DR^2-0.5\left(1+\frac{\Delta}{100}\right)DR=\frac{\sigma_L}{PN} \qquad \text{Eq. 6-2}$$

Where,
Δ = percentage ovality of original host pipe,
σ_L = long-term (time-corrected) flexural strength of the CIPP (which is same as initial),
DR = dimension ratio of CIPP (which is D/t).

Thus, the minimum thickness for a PD design condition is the greater of those found by Eq. X1.1 and Eq. X1.2 (if applicable). Lynn Osborn, a long-time engineer with Insituform, has stated that although Insituform wrote the design appendix, they typically didn't use equation X1.2 at all given that equation X1.1 with the conservative ovality factor (C) and enhancement factor (K) produces a sufficiently conservative design thickness on its own.

6.5.2. The Fully Deteriorated (FD) Pipe Design Condition

As stated earlier, the second load case in the ASTM F1216 design appendix supposes that earth and traffic loads will in due course be transferred from the existing pipe-soil structure to the new liner pipe. The design approach therein again is excessively conservative (Gumbel, 1998) for two reasons. First, the soil load reaching the liner pipe is overestimated by treating the liner as though it had been directly buried. Whereas the more correct analogy in circumstances where the existing pipe structure may continue to deteriorate after rehabilitation is more analogous to that of a tunnel lining (Note X1.3 in the design appendix allows this to be done although most engineers are unaware of this). Secondly, the formula used to describe the liner's response to a transferred soil load has been incorrectly modified from an already conservative theory for direct-bury applications in a way which entails further irrational safety factors (Gumbel, 1998).

The equation for the fully deteriorated design condition was from the fiberglass pipe industry in the 1980s which used the Luscher/AWWA design model; and, unfortunately, has not been changed to keep up with the various changes that have been made to the AWWA design model since its placement in the standard. With the lone exception of the change in placement of the ovality reduction factor (C) made in 2007, there have been essentially no changes at all to the F1216 design appendix.

Further, the external hydrostatic head applied to the liner in the FD design condition is given as the height of the water from the top of the pipe to the phreatic surface in this design case, which is incorrect.

The equation X1.3 in the ASTM F1216 pertaining to the fully deteriorated design condition rearranged to solve for the required wall thickness here is presented by Eq. 6-3.

$$t = \left[\frac{(N \times q_{tot})^2 \times D^3 \times 12}{32 \times R_w \times B' \times M_{SN} \times E_L \times C}\right]^{1/3} \quad \text{Eq. 6-3}$$

Where,

t thickness of CIPP, in.
N factor of safety,
q_{tot} total external pressure acting on pipe = $0.433H_w + wHR_w/144 + W_{s'}$, psi,
D mean inside diameter of the original pipe, in.
R_w water buoyancy factor (0.67 min.) = 1- 0.33 (Hw /H),
w soil density, lb/ft3,
B' coefficient of elastic support = 1/(1 + 4e-0.065H), inch-pounds, dimensionless,
M_{SN} constrained soil modulus, psi,
E_L long-term modulus of elasticity of CIPP, psi,
C ovality reduction factor.

In addition to meeting the thickness required by equation X1.3 above, the FD design condition also requires the CIPP to meet the minimum thickness found using equation X1.4. Equation X1.4 came from the flexible pipe manufacturing industry and has to do with the minimum handling stiffness that a pipe must be made to withstand the rigors of handling it during the manufacture, storage, transportation, and subsequent burial of flexible pipes. Something that a CIPP does not ever see. Still, it is quite often this equation that governs the minimum wall thickness of the CIPP. Equation X1.4 of ASTM F1216 is presented here as Eq. 6-4.

$$\frac{EI}{D^3} \geq 0.093 \quad \text{Eq. 6-4}$$

Where,

E initial modulus of elasticity, psi,
I area moment of inertia for unit length of liner, in.^{4}/in.

For the FD design condition, the minimum wall thickness is the greater of the thicknesses found from solving equations X1.1, X1.2, X1.3, and X1.4 in ASTM F1216. In the current version of ASTM F1216, the engineer is directed to not use equations X1.2 and X1.4 in designing CIPP.

6.6. Pending ASCE MOP for Design of Flexible Liners

In the proposed ASCE MOP, there are going to be three design states for the long-term loading on the liner. Those include Design State I, Design State II, and Design State III; with consensus among academia and practicing specialist engineers that Design State I should be sufficient for most gravity sewer and culvert pipes.

Design State I is applied to a host pipe which alone or supported by the surrounding soil (the pipe-soil system) is currently capable of carrying the existing soil overburden and surface live loads without significant deflection in the case of rigid pipes or within permissible deflection in the case of flexible pipes. The existing defects in the pipe have not reduced its structural capacity to the point where it must be reinforced. The pipe is assumed to have sufficient hoop and/or bending stiffness to carry the portion of the external loads transferred to it. Such defects may include cracks and/or fractures with ovality up to 3% in rigid circular pipes and 20% in flexible circular pipes, steel reinforcement corrosion, wearing of surface due to corrosion or abrasion, etc. Design State I is appropriate and sufficient also in cases where a pipe is severely damaged (e.g., corrosion has significantly reduced the pipe wall thickness) if, (1) the pipe-soil system has remained in stable equilibrium for a very long time (many years), and (2) the likelihood of activities nearby causing ground movements that could disrupt the present equilibrium is relatively low. In Design State I external hydrostatic pressure from groundwater is the only external loading on the liner. If the actual groundwater level is less than 1.5 ft above the pipe's crown or 5 ft above the pipe invert, a virtual groundwater level which meets both these criteria is used in the liner's design (understanding that a virtual groundwater level can be raised only to the ground surface).

The MOP uses a modified-Glock formula (Thépot, 2000) for calculating the critical buckling pressure of a proposed flexible liner to fit circular and non-circular shapes, adding corrections for buckling modes and imperfections. Eq. 6-5 presents the Glock-Thépot formula for calculating the critical buckling pressure of a proposed liner.

$$p_{cr} = 2.02 \cdot k^{0.4} \cdot \kappa_p \cdot \frac{1}{1-\nu^2} \cdot \frac{(EI)_L^{0.6} \cdot (EA)_L^{0.4}}{P^{0.4} \cdot R^{1.8}} \qquad \text{Eq. 6-5}$$

Where,

p_{cr} critical buckling pressure, psi,
κ_p reduction factor due to imperfections, dimensionless,
k buckling mode (1: one blister, 2: two blisters), dimensionless (see Figure 6-43)
ν Poisson's ratio for liner material, dimensionless,
A cross-sectional area for unit length of liner, in.^{2}.
I area moment of inertia for unit length, in.^{4}/in.
P perimeter of liner (pipe inside perimeter), in.
R radius of pipe arc where the blister develops, in.

$(EI)_L$ relates to the long-term flexural stiffness of the liner wall,
$(EA)_L$ relates to the long-term compressive stiffness of the liner wall.

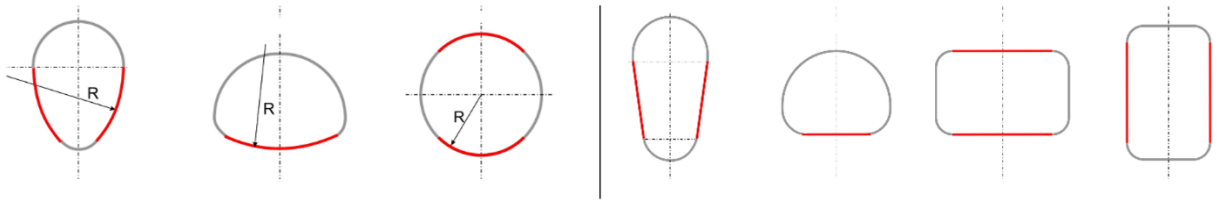


Figure 6-3. Buckling Mode, Thépot (2000).

The critical buckling pressure is used to calculate the critical bending moment and hoop force for a proposed wall thickness. The existing or virtual groundwater pressure is then used to calculate the maximum bending moment, hoop force, flexural stress, hoop stress, and elongation in the proposed liner. The long-term limit states for buckling pressure, material strength, and elongation are then verified using classical engineering solutions not shown herein for reasons of brevity. The calculations incorporate both a factor of safety for wall buckling and the CIPP's material strength. The latter being to account for issues regarding achieving the liner's assumed finished flexural stress strength in the field curing of the liner.

While the MOP covers subcritical shapes (the four shapes on the right in Figure 6-3), it is unlikely that CIPP will be practical for them owing to its relatively low modulus of elasticity and the level of the external hydrostatic design pressure that is required. In these shapes, the MOP will most likely be used for the design thickness of glass-fiber reinforced plastic (GRP) rehabilitation products.

Design State II is applied to a circular rigid pipe that has been subjected to overloading and has developed one or more longitudinal fractures in the crown, invert, and the springlines forming a classical 4-hinge mechanism. This pipe would have deflected more than 3.0% over time but its ovality still remains under 10%. In this design state a pipe is assumed to have lost its bending strength but retains its hoop stiffness; and is presumed capable of carrying the portion of any external loads transferred to it in thrust (compression). Pipe ovality at the time of the liner's installation (or change in radius of the flattest arc element in a non-circular pipe) is treated as an imperfection which obviously decreases the critical buckling pressure the liner can sustain.

Imperfections are classified in the MOP by type; global or local. Global imperfections are distributed around the perimeter either uniformly (an annular gap) or non-uniformly (such as a 4-hinge ovality in fractured and deflected rigid pipes). Local imperfections are distributed on a limited angular sector (local flattening; local intrusion). All imperfections are assumed to be constant in the longitudinal direction as that is the most unfavorable configuration. In the case of corrugated pipes, corrugations are not to be considered as imperfections in the liner design. While the corrugations

may induce wavy deformations in the CIPP, in this case the wavy pattern increases the liner's flexural stiffness.

As post liner installation deformation of the soil-pipe system may occur, which in turn can further decrease the critical buckling pressure, the liner thickness must be verified for more strict limit states (stability and material strength).

In this load case the liner is assumed to receive 60% of the soil prism load acting on the host pipe structure plus any external hydrostatic pressure from any groundwater; plus, any live loading on the surface up to a depth of 10 feet when the span of the pipe is greater than the spread of the live load at the top of the pipe. For pipes with cover depths greater than 10 feet, the soil prism load is taken as 1.0 times the rise of the pipe (analogous to the tunnel loading) or the cover depth; whichever is less. In this design load case, the design analysis estimates the additional deformation that may occur long term and assesses the additional stress and strain induced in the proposed liner's wall section. In this load case the stiffness of the liner is ignored with respect to preventing the future deformation.

Design State III is applied to either a rigid or a flexible circular host pipe which is severely damaged and has lost its hoop and bending stiffness in the case of a rigid host pipe or a severely damaged flexible pipe. A pipe may have holes or missing pieces or eroded to the extent that an invert is gone. In extreme cases there may just be a hole in the soil where the pipe used to be. Carrying all the external loads by the surrounding soil is the only reason that a pipe (or a hole) is still in place. This equilibrium condition is considered to be fragile and likely to fail. Design State III can also be described as a host pipe with 4-hinge ovality progressed further from Design State II, where the pipe segments have now moved relative to each other and no longer contact one another at the fractures. In Design State III, external loads acting on the liner may include all or some of the soil overburden pressure, the groundwater pressure, and any surface live loads.

In this load case the liner is estimated to receive 100% of the soil prism load acting on the host pipe structure plus the groundwater pressure plus any live loading on the surface for pipes up to a depth of 10 feet when the span of the pipe is greater than the spread of the live load at the top of the pipe. For pipes with cover depths greater than 10 feet, the soil prism load is taken as 1.0 times the rise of the pipe (analogous to the tunnel loading) or the cover depth; whichever is less. In this design case the stiffness of the liner is not ignored.

6.7. Dealing with the True Design Condition

Currently the ASTM F1216 design appendix does not distinguish between CIPP installed in rigid host pipes and flexible host pipes. This is problematic given that the

load response behavior of these different classes of host pipe materials is significantly different.

Rigid host pipes can be either badly eroded, cracked, or fractured. This in situ condition at the time of lining has a profound effect on the loads that can be practically expected to be transferred to the liner over the design life period of the liner. In the case of the badly eroded (or corroded) interior wall surface, the host pipe without cracking is obviously capable of the current dead and live loads acting on it. The mere act of lining a rigid pipe in such a condition is taken as protecting the host pipe from any future erosion or corrosion preserving its ability to carry those loads (Gumbel, 1998). Thus, a pipe in this condition should be lined using the wall thickness for the PD condition. Concrete pipes that are cracked should also be designed using the ASTM F1216 PD design condition. Cracked pipes are pipes having a break line visible on the wall surface, while the break is not visibly open, and the pieces of the pipe are still in place (Note: a crack line will occur with a rigid pipe deformation of less than 1%). Cracks can be longitudinal, circumferential, or spirally oriented.

Fractured rigid pipes are, by definition, cracks that have become visibly opened with the pieces of the pipe wall still in place and not able to move due to the support of the soil surround. Fractured pipes meeting this definition are still capable of carrying the loads coming onto them. In the proposed MOP, these pipes could be exhibiting up to a 3% inward deformation of the vertical diametrical dimension. This is because pipes coming to this level of distortion have obviously experienced a redistribution of the loads in the soil-pipe interaction system. Hence, they reached an equilibrium which can support the loads that are coming onto the host pipe. Installing a flexible liner in these pipes, locks in this equilibrium condition. No future deformation should be anticipated as the fractured rigid pipe is carrying its portion of the load in *thrust*.

In broken rigid pipes, the pieces are noticeably displaced and have moved from their original position (e.g., at least ½ t where t = thickness of the pipe wall). Pipes meeting this defined condition have inward deformation of the vertical diametrical dimension exceeding 3% (a conservative assumption). As the deformation increases it is possible that the rigid pipe could have future deformation. It is thus understood that the stability of the deteriorated pipe before and after lining is dependent on the composite action of the soil (intact or deteriorated), the damaged rigid pipe, and the liner within (Law & Moore, 2007). Thus, it is incumbent on the designer to determine what can be inferred from the extent of the damage seen in the CCTV survey; and on the Owner to provide documentation on the soil surround.

Law and Moore (2003) on the kinematics of fractured pipe deformation suggested that fractured rigid pipes respond much like flexible pipes under loading. That changes in the horizontal pipe diameter can be expressed as Eq. 6-6 and Eq. 6-7

$$\frac{\Delta D_H}{OD_{pipe}} = 4\sigma_v(1-K)\frac{(1-v_S)}{(3-2v_S)(1-2v_S)M_S} \approx 1.6\frac{\sigma_v}{M_S} \qquad \text{Eq. 6-6}$$

$$\frac{\Delta D_H}{ID_{pipe}} \approx 1.6 \frac{\sigma_v}{M_s}(1 + \frac{2t_{pipe}}{ID_{pipe}})$$ Eq. 6-7

Where,
σ_v the additional vertical stress after lining takes place, psi,
K the lateral earth pressure ratio,
M_s the constrained soil modulus, psi,
v_s Poisson's ratio of the soil,
ΔD_H change in the horizontal diameter, in.
OD_{pipe} the outside diameter of the pipe, in.
ID_{pipe} the inner diameter of the pipe, in.
t_{pipe} the thickness of the pipe, in.

Where, σv, K, Ms, and Poisson's ratio of the soil all influence the response, and the constant 1.6 is based on K = 0.45, and vs = 0.3. Other combinations of K and vs result in values ranging from 1.4 to 1.7.

The kinematics of pipe deformation can then be further used to provide a relationship between changes in vertical and horizontal diameters that is presented by *Eq. 6-8*:

$$\Delta D_V = -\Delta D_H(1 - \frac{2t_{pipe}}{OD_{pipe}})$$ Eq. 6-8

Where,
ΔD_V the change in the vertical diameter of the pipe, in.

For close-fitting liners in circular pipes, Moore (1998, 2005) indicates that the hydrostatic buckling pressure strength (P_b) in psi can be calculated by Eq. 6-9.

$$P_b = 1.0E_{liner}(\frac{t_{liner}}{D_{liner}})^{2.2} e^{-q/0.18} \times e^{-0.56\Delta/t_{liner}}$$ Eq. 6-9

Where,
E_{liner} the flexural modulus of the liner, psi,
D_{liner} the diameter of the liner, in.
t_{liner} the thickness of the liner, in.

The term Δ in Eq. 6-9 refers to the amplitude of any global wavy imperfection (see Eq. 6-10). The dimensionless ovality q for a fractured rigid circular pipe can be calculated using Eq. 6-10, if the effect of the thickness of the old sewer is neglected (which is conservative).

$$q = \frac{D_H - D_V}{D_H + D_V} \approx \frac{\Delta D_H}{ID}$$ Eq. 6-10

Where,
D_H the horizontal diameter of the old pipe, in.
D_V the vertical diameter of the old pipe, in.
ID the inner diameter of the old pipe, in.

If the liner drapes over the fractured pipe at the invert, then a wavy imperfection results with amplitude, as presented by Eq. 6-11.

$$\Delta_{cr} \approx 0.51 ID \left(\frac{\Delta D_H}{ID}\right)^2 (1 + \frac{2t_{pipe}}{ID})^{-1} \quad \text{Eq. 6-11}$$

Where,
ID the internal diameter (in inches) of the un-fractured pipe. This can be further simplified by ignoring the thickness of the old rigid pipe (providing a conservative approximation).

The reduction in stability because of deformations in the fractured pipe are given in the Figure 6-4 below for a range of liner dimension ratios and fractured pipe deformations, based on expression by Eq. 6-12.

$$e^{-\Delta D_H / 0.18D} e^{-0.28 \frac{D}{t_{liner}} (\frac{\Delta D_H}{D})^2} \quad \text{Eq. 6-12}$$

Figure 6-4 suggests that reductions in stability become significant when the fractured pipe deformation is greater than or equal to 5%. Law and Moore (2003, 2007) suggested that bending strains in the liner can be effectively calculated using the solution for a ring under parallel plate loading as presented by Eq. 6-13.

$$\varepsilon_{cr} = \pm \frac{2.139 \Delta D_V C}{\bar{R}_{liner}^2} \quad \text{Eq. 6-13}$$

Where,
ε_{cr} bending strains in the liner,
$\bar{R}_{liner}$ mid-surface radius of the liner, in.
C the distance from the mid-surface to the extreme fiber responding in tension, in.
ΔD_V the change in vertical pipe diameter.

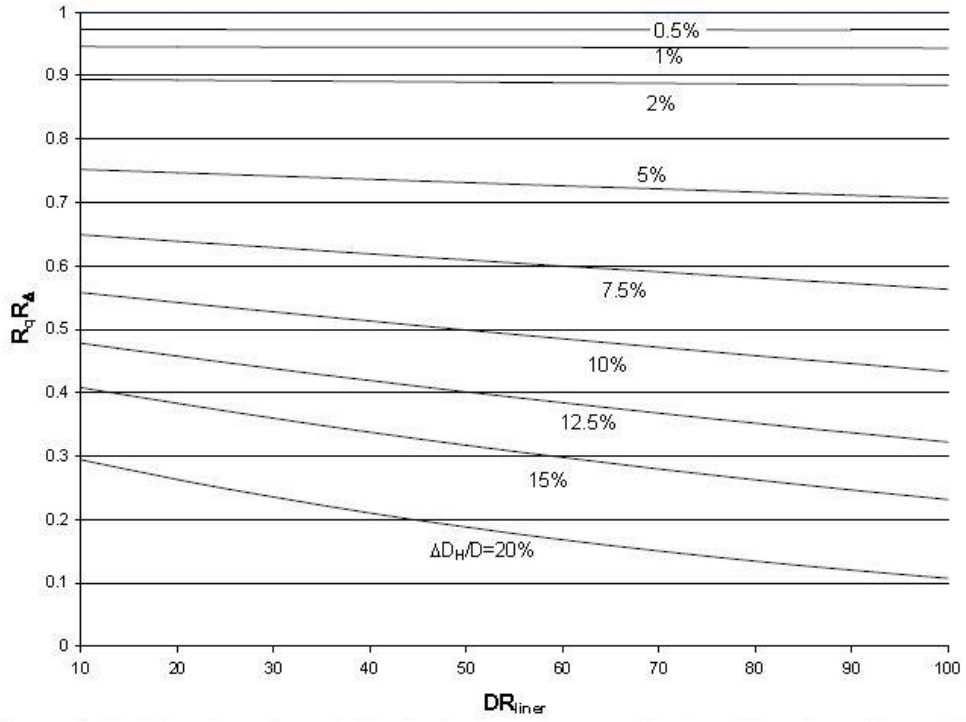


Figure 6-4. Buckling strength reduction for fractured sewer with close fitting liner (Source: Moore, 2008).

As it is illustrated in Figure 6-4, the change in vertical pipe diameter ΔD_V is assumed to take place in some sections of the pipeline after the liner is installed. An implicit assumption here is that the presence of the liner has negligible effect on the amount of vertical diameter decrease. It is a reasonable assumption since the flexural stiffness of the liner is negligible compared to that of the soil surrounding the fractured pipeline. Restoration of the hydraulic integrity of the pipeline should arrest further backfill erosion (assuming erosion results from inflows of groundwater), and it is therefore reasonable to assume that the magnitudes of vertical diameter decrease that are greater than those already observed for the pipeline are unlikely.

Figure 6-5 illustrates how the change in the vertical diameter being considered and the allowable strain for the polymer used in the liner controls the maximum thickness t for a plain wall liner (where t=2c). This bending limit state sets an upper bound to the liner thickness to prevent excessive wall strain. Since greater liner thickness increases the distance to the extreme fiber and thus the maximum bending strains generated for the estimated deformation of the host pipe.

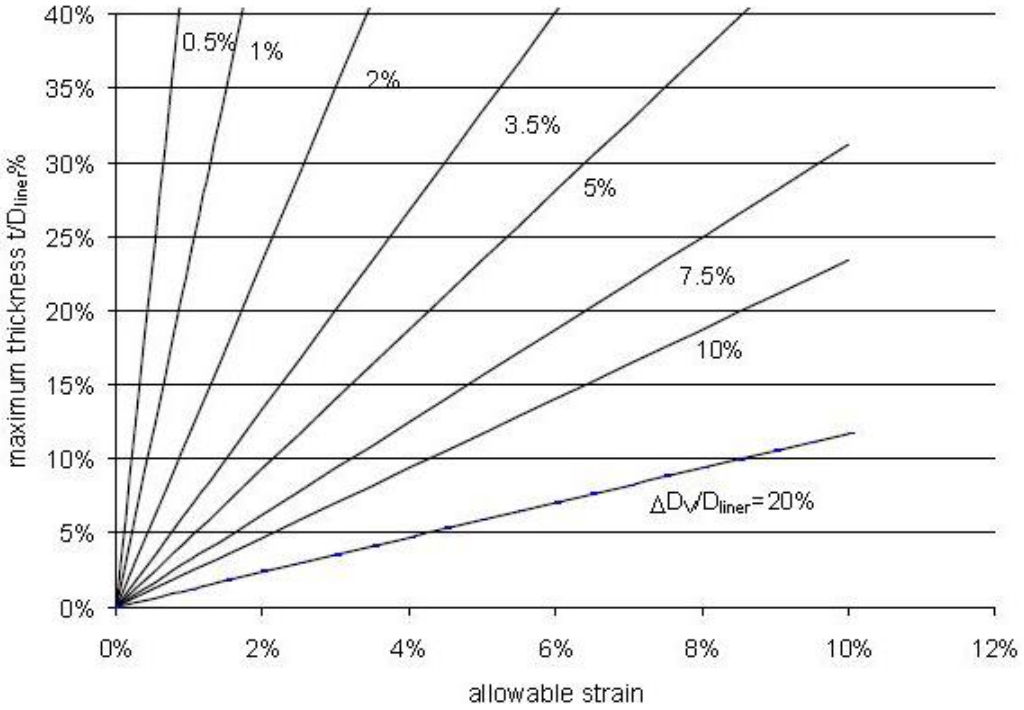


Figure 6-5. Bending limit state (Moore, 2008).

As it is illustrated in Figure 6-5, it is shown that the deflection of the repaired pipeline will be a function of the soil surround's soil modulus. However, determining a suitable value of this modulus may be difficult as many factors, such as material type and method of placement, can alter this modulus significantly. The designer thus can either make use of published data for guidance such as McGrath et al. for M_s (three general classes of soil, SW, ML, and CL at different levels of vertical stress), or using CPT test can measure the in-situ soil's modulus, E_s, and use the relationship expressed by Eq. 6-14 to find $\mathrm{M_s}$. The critical strain for any additional loading coming on to the repaired pipe can then be evaluated using the expression by Eq. 6-15.

$$M_s = \frac{E_s(1-v_s)}{(1+v_s)(1-2v_s)} \qquad \text{Eq. 6-14}$$

$$\varepsilon_{cr} = \pm \frac{17.116\Delta\sigma_V R_{host}(1-k)(1-v_s)^2 c}{\overline{R}^2_{liner}(3-2v_s)(1-2v_s)M_s} \qquad \text{Eq. 6-15}$$

It is understood that applicability of above concept to flexible pipes would not be an issue for a wavy imperfection for fractured pipes.

6.8. Summary

While the non-mandatory design appendix of ASTM F1216 is the design procedure currently specified by North American engineers, it has been found by academicians and specialist engineers as being unrealistic for designing flexible liners like CIPP for a

variety of reasons. While it can be said that it is overly conservative in many aspects, it also has the potential to understate long-term performance in other aspects.

While engineers have thought for years that specifying the FD design condition for CIPP liners is conservative, they inadvertently ended up over designing this class of liners. With excessive thickness comes issues with the installation process as liners go into larger and larger diameter pipes (e.g., full curing throughout the full thickness of the liner). Excessive CIPP thickness may add issues with proper fit and finish issues (e.g., fitting tightly to current shape, wrinkles and fins, etc.). In the case of flexible host pipes like CMP, the dominant structure for resisting the load coming onto the CIPP was the host pipe and/or the surround soil. This meant that knowledge of the current performance properties of the soil surround are critical to the performance of the rehabilitated soil-structure interaction system, which was often given as some arbitrary minimum values in the project specifications.

The only true design methodology existing for non-circular shaped pipe geometries is developed by Olivier Thépot which was subsequently presented in the ASTEE 3R2014 Structural Design for Non-Circular Linings Under Groundwater Pressure.

Except in some rare cases, the loads that will be transferred onto a CIPP liner will come from the deflections that are induced in the host pipe structure from additional soil dead loads, any surface live loads, and any external groundwater loads. Any design procedure used for CIPP must recognize the differences in how rigid pipe structures versus flexible pipe structures will transfer these loads to consider the stresses and strains created in the CIPP liner itself. In reality, CIPP is a reinforcing material as opposed to a standalone structure. If at some point in the future the host pipe will truly be gone, it will be the soil structure that dominates the survival of this hydraulic structure. Therefore, the soil surround must become more important to the engineer who is preparing the plans and specifications for the design of the liner.

This Page Left Intentionally Blank.

Chapter 7

SAPL Field Inspection and Data Collection

CHAPTER 7 - SAPL FIELD INSPECTION AND DATA COLLECTION

7.1. Objectives

The performance of trenchless renewal methods and SAPLs for any project are dependent on quality of the installations. Appropriately designed and properly installed liner systems will generally perform well throughout their design life. Proactive maintenance strategies can be scheduled based on the structural condition and performance assessments of the existing structure through the field inspection and collected data. The objective of this chapter was to conduct field data collections and in-situ inspections of past SAPL projects to expose defects and installation issues as well as making suggestions for development of proper performance construction specifications. The data collected through the field inspection of SAPL projects is used to assess the structural condition and performance of those projects. It should be mentioned that no culverts were inspected with polymeric SAPL, as none were provided by the DOTs to inspect.

7.2 Selection of Culverts

A total of twenty-four culverts that were renewed by the application of SAPL were selected by the CUIRE research team for field evaluation. Culverts were selected from lists of projects provided by seven DOTs across the U.S. including, DelDOT, FDOT, MnDOT, NCDOT, NYSDOT, Ohio DOT and PennDOT. The selection was based on variations in host culvert material (i.e., corrugated metal pipe and reinforced concrete pipe), corrugation profile, pipe diameter, pipe shape, soil cover depth, age, and geographical location. Figure 7-1 illustrates the geographical locations of the selected SAPL culverts from different states (numbered in the order of inspection). A listing of these selected culverts along with their construction and identification details are summarized in Figure 7-1.

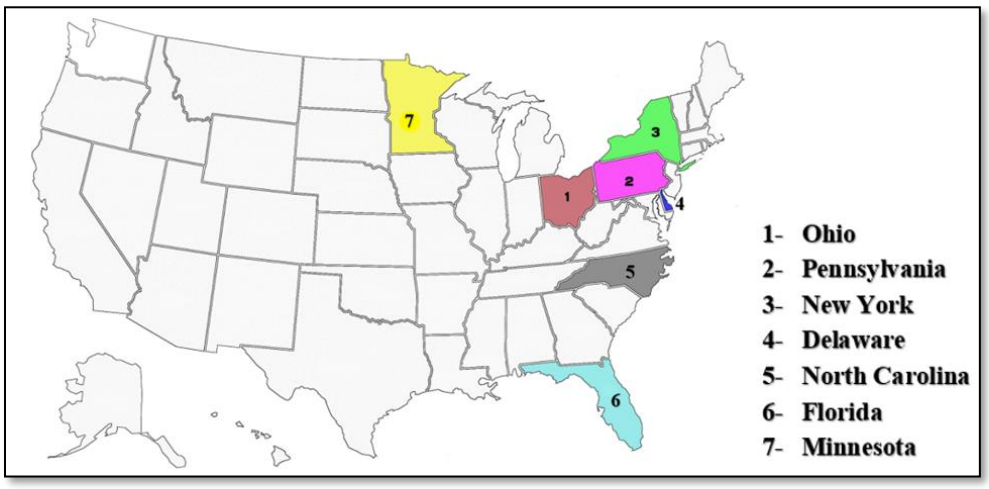


Figure 7-1. Geographical distribution of selected SAPL culverts.

There were five culverts in Ohio, one in Pennsylvania, one in New York, two twin culverts (overall four) in Delaware, eight in North Carolina (including two twin culverts), three in Minnesota and two in Florida (twin culverts are constructed at a very close spacing from each other). Fourteen of the selected culverts were circular shapes and ten of them were arch shapes. Twenty-one culverts or 87.5% of total were CMPs and three or 12.5% of total were RCPs. All culverts were large dimeter and worker-entry sizes, ranging from 54 in. to 156 in. A total of 54% of culverts were lined with reinforced cementitious SAPL material and 46% were lined with geopolymer material. SAPL materials of the inspected culverts were provided by three cementitious vendors (A, B and C) and two geopolymer vendors (X and Y). Overall, six culverts were lined by Vendor A, two lined by Vendor B, nine lined by Vendor C, four lined by Vendor D and three lined by Vendor E. The age range of SAPLs varied from one month to approximately eight years. Depth of soil cover on the culvert varied from one ft to 25 ft and SAPL structural design thicknesses varied from 0.65 in. to 2.5 in.

Table 7-1 List of selected SAPL culverts for field inspection (Cr: Circular, Ar: Arch).

No.	State	Existing Culvert						SAPL		
		Shape	Material	Diameter (in.)	Length (ft)	Soil Cover (ft)	Vendor	Material	Designed Thickness (in.)	Age (Month)
1	Ohio	Cr*	CMP	78	60	4	Y	Geopolymer	1.3	26.9
2	Ohio	Cr	CMP	60	314	15	X	Geopolymer	1	22.2
3	Ohio	Cr	CMP	60	228	12	C	Cementitious	1.5	2.0
4	Ohio	Cr	CMP	54	160	29.15	Y	Cementitious	0.65	26.6
5	Ohio	Cr	CMP	84	194	15	X	Geopolymer	1.5	26.1
6	Pennsylvania	Cr	CMP	68	50	2	A	Cementitious	1	36.0
7	New York	Cr	RCP & CMP	60	167	10	A	Cementitious	1	48.0
8	North Carolina	Cr	CMP	72	43	1	Y	Geopolymer	1.5	1.0
9 10	North Carolina (Twin Culverts)	Cr	CMP	84	71	1	Y	Geopolymer	1.5	1.0
11	North Carolina	Ar*	CMP	72x108	48	1	Y	Geopolymer	1.5	1.0
12	North Carolina	Ar	CMP	72x96	31	1	Y	Geopolymer	1.5	1.0
13 14	North Carolina (Twin Culverts)	Ar	CMP	72x96	40	1	Y	Geopolymer	1.5	1.0
15	North Carolina	Ar	CMP	72x90	45	2	Y	Geopolymer	1.5	1.0
16 17	Delaware (Twin Culverts)	Ar	CMP	81x59	110	3.27	B	Cementitious	2	3.0
18 19	Delaware (Twin Culverts)	Ar	CMP	98x69	125	5.33	B	Cementitious	2	3.0
20	Minnesota	Cr	RCP	84	550	23-24	A	Cementitious	1	36.0
21	Minnesota	Cr	RCP	60 &54	790	2-12	A	Cementitious	1	48.0
22	Minnesota	Cr	RCP	54	652	2-10	A	Cementitious	1	48.0
23	Florida	Cr	CMP	156	100	1-2	A	Cementitious	1	101.3
24	Florida	Ar	CMP	71x103	74	6	C	Cementitious	2	63.4

7.4. Inspection Tools

To measure the SAPL thickness, a nondestructive Olympus ultrasonic thickness measurement device (Model 38DL) was initially used (Olympus 2020). A grinder was used for preparing a smooth surface of liner to be perfectly attached to the ultrasonic transducer and enabled it for wave propagation. However, unlike the preliminary calibration and testing in the laboratory with a cementitious SAPL sample, the device was unable to measure the thickness in the field. SAPLs with lower density material and larger voids resulted in increasing the wave attenuation rate in the material and disabling the device to measure the thickness. In addition, in case of concrete host pipes, the small amount of impedance mismatch between the cementitious or geopolymer SAPL and the host pipe could cause wave transmission rather than wave reflection. Therefore, an alternative mechanical measurement of the SAPL thickness was carried out by drilling into the liner and measuring the depth of the hole by a digital caliper with 0.001 in. accuracy. The drilling was done in a low pace with drill bits that were marked according to the known SAPL design thickness for each location to prevent any probable perforation in the host pipe. The difference in the density of the host pipe (mostly steel) and cementitious SAPL materials resulted in a tangible alteration of drilling speed at the time of reaching the outer surface of the SAPLs which was along with a pop sound. The number of drilling points in this field inspection was limited by DOTs and all drilling holes were patched with a high strength cement mortar. During the inspection, due to the presence of the storm water flow, SAPL thickness measurement using drilling at the invert raised safety issues and was not possible.

Regular tape and laser-distance meter were used for pipe length and inside diameter measurements. The liners conditions were documented systematically in a data collection form specially prepared for this purpose. The data collection form was divided into four sections of project location, host pipe information, SAPL information and SAPL inspection findings. The SAPL inspection findings were documented in a table for each observed defect, it recorded the distance from the inlet of the pipe, a descriptor code, severity, circumferential location, picture number of that defect and any remarks.

7.5. Inspection Procedure

The first step in the inspection procedure was to obtain design documents, such as SAPL previously test results, wall thickness design and installation details for each specific culvert. The research team evaluated construction inspection and any quality control notes to be able to interpret the visual characteristics of SAPL. The selected inspection methodology was to measure thickness of SAPLs and compare with design requirements suggested by vendors and installers. In addition, the research team identified, visualized, and measured all SAPL fractures, deflections, de-bonding, spalling, holes, corrosion, and cracks.

The National Association of Sewer Service Companies' (NASSCO's) Pipeline Assessment & Certification Program (NASSCO 2019) codes were used for recording some of the SAPL defects during field data collection. Some types of defects were observed in the SAPLs that has no defined code in the NASSCO PACP. Therefore, new codes were defined by authors to record them. The observed defects along with their identifying codes are listed in Table 7-2. Any SAPL installation irregularities were documented in proper context. The data obtained in this research can be utilized as a baseline for comparison with future inspections.

Table 7-2 SAPL and existing culvert defects.

SAPL Defects Observed in Field Inspection					
	Defect	**Code**		**Defect**	**Code**
Defined by NASSCO PACP	Circumferential Crack	CC	Defined by Authors	Bolt Heads Visible	BHV
	Longitudinal Crack	CL		Troweling the Liner	LT
	Multiple Cracks	CM		Concrete Patched on the Liner	LCP
	Circumferential Fracture	FC		Nonuniform Liner Thickness	LNT
	Longitudinal Fracture	FL		Low Bond between Liner and Pipe	LB
	Multiple Fracture	FM			
	Infiltration Weeper	IW		Bare Host Pipe	BHP
	Infiltration Runner	IR		Iron Oxidation on the Liner Surface	LIO
	Infiltration Dripper	ID			
	Infiltration Gusher	IG		Efflorescence on the Liner Surface	SLE
	Lining Failure	LF		Irregular Liner Installation	ILI
	Detached Liner	LFD		Heavy and Thick Liner Sagging off	LHS
	Buckled Liner	LFBK			
	Surface Spalling	SSS		Liner Disturbed before Hardening	LHD
	Aggregate Visible (dry)	SAV		Delamination of the Liner	SLD
	Hole	H		Liner Collapse	XL
	Cockroach (V: Vermin)	VC		Frog	VF
	Rat (V: Vermin)	VR		Centipedes and Worm	VW
Existing Culvert Defect Defined by NASSCO PACP					
	Defect	**Code**		**Defect**	**Code**
	Corrosion of Metal Pipe	SCP		Settled Fine Deposits	DSF
	Deformed	D		Settled Hard/Compacted Deposits	DSC
	Joint Offset	JO		Settled Gravel Deposits	DSGV
	Joint Separated	JS		Root	R

7.6. SAPL Issues Due to Lack of Standard

As stated earlier, currently there is no standard design methodology and construction specifications for proper performance of SAPLs. Lack of a standards could be a cause for SAPL defects, as it is presented in Appendix 7-A. Identification and classification of probable SAPL defects can help with preparation of a performance construction specification to avoid and limit those issues. According to the results of

field inspection, the photographs of twelve most common SAPL issues are shown in Figure 7-2.

A summary of field inspection findings of the most common issues along with descriptions are listed in Table 7-3. The existing culverts, in their order of field inspection, along with their length, vendor, age of SAPLs and observed issues after inspection are provided in Table 7-4.



Figure 7-2. Issues found with SAPLs.

Table 7-3 SAPL field inspection findings.

Findings		Description
Cracks and Fractures	• Hairline, circumferential, longitudinal and multiple cracks. • A few circumferential fractures. • Less circumferential cracks in geopolymer SAPLs in comparison with cementitious SAPLs. • Most of circumferential and longitudinal cracks in cementitious SAPLs (including geopolymers) are suspected to be due to shrinkage of materials and movement of CMP in relation to SAPL.	• Hairline cracks are inherent in concrete SAPL linings because of the rigid lining in a flexible CMP. • Hairline cracks typically will heal by efflorescence formation when kept wet. • Insufficient water cement ratio could result in multiple cracks in SAPLs. Some of these cracks might be due to small movement of the host pipe in relation to the SAPL due to seasonal changes. This situation is more in CMP host pipes as well as at the joints in concrete host pipes. Flexible host pipes can and do move slightly while concrete pipes primarily will move at the joints.
Efflorescence	• Efflorescence on SAPL surface mostly along with weepers.	• It was created due to chemical process between cementitious SAPL materials and water (mostly the water coming through the pinholes and weepers). • In some cases, as a remedy, efflorescence blocked the pinholes and stopped it from further leakage.
Rust Staining	• SAPL surface rust staining mostly appeared as a circumferential pattern. • Less effect of rust staining on SAPL surface in corrugated aluminum pipes.	• Rust staining on SAPL surface can be due to corrosion of the existing CMP or corroded rebars of RCP due groundwater or water due to capillary action present as well
Infiltration	• Infiltration weepers and sometimes drippers on SAPL surface.	• Most of them were along with rust stain. Most joints in the host pipe are soil tight only. This implies that water will make its way behind the SAPL liner and it will find the path of least resistance, which will be the nearest crack.
SAPL Thickness	• Inconsistent SAPL thickness. • Most of thick and heavy SAPL materials (Figure 7-2) tended to sag off from both sides of the crown and move towards the springlines. So, the maximum nominal thickness of them were at the crown and around the springlines. • As inspected, hand spray and shotcrete did not provide a consistent thickness of SAPL.	• Installation variabilities and lack of quality control was the most common reasons for inconsistent SAPL thicknesses. • Proper structural design thickness of SAPL and the quality of installation are of the important parameters affecting the SAPL construction performance.

Findings		Description
Installation Issues	• Installation variabilities. • SAPL was disturbed (lack of proper finish) before hardening. • Rough surface SAPL. • Shadowing (non-uniformity of spray nozzle movement, Figure 2) of cementitious SAPL materials caused deeper SAPL valleys at the crown of the culvert and thicker SAPL valleys above the springlines. • Original coating and lining on the CMP at the time of host culvert installation caused detaching SAPL from host pipe.	• Considering the concept of SAPL, it is a centrifugally cast in place rehabilitation methodology for enhancing the structural capacity, improving hydraulic characteristics, abrasion and corrosion protection and sealing of existing culverts. • Shadowing is due to tendency of materials to sag from crown towards the springlines that can be related more to the speed of the installation and/or the direction of the applicator.
Vermin	• Cockroach • Worm • Frog	• Several cockroach and worms with their nests were found on the SAPL surface. • No SAPL defect was observed by vermin.
Deposits	• Settled gravel and fine aggregates were found in a few locations.	

Table 7-4 SAPLs' issues found for each culvert.

Existing Culvert		SAPL			
No.	Length (ft)	Vendor	Age (mo.)	Defects	
1	60	Y	26.9	9 CC, BHV, CM, 3 IW, 3 LIO, CL, SLE, LNT, FC	
2	314	X	22.2	5 CC, LIO, SLE (every 3 ft), 5 IW, SSS, DSGV, LT, VW (along the pipe)	
3	228	C	2.0	CC, VF	
4	160	Y	26.6	LFD, CC (along the pipe), CM, CL	
5	194	X	26.1	CC and LIO (every 3 ft.), VW (along the pipe)	
6	50	A	36.0	3 CC, 2 LIO, CL, 2 CM, SLE, LHD, 2 IW, LNT	
7	20	A	48.0	Aluminum CMP	ILI
	103			RCP	CC and SLE (every 3 ft), 2 ID, 12 LIO, 13 IW, CM
	44			Aluminum CMP	2 LIO, 4 IW, ID, 2 CC, 3 SLE
8	43	Y	1.0	SLD, DSC, DSF	
9	45	Y	1.0	Left from Inlet*	DSGV, JS, LIO, CC
10			1.0	Right from Inlet*	3 FC, 4 CC, LCP, LIO
11	48	Y	1.0	ILI, 2 LB, 2 LHS, BHP	
12	71	Y	1.0	2 CC, 4 SLE, 2 ILI, LIO, LNT, LB	
13	40	Y	1.0	Left from Inlet	2 CC, 2 ILI, SAV
14				Right from Inlet	ILI, LB, 4 CC, 2 IW, LNT, BHP, LHS, SLE
15	31	Y	1.0	LHS, SLD	
16	110	B	3.0	Left from Inlet	3 CM, FM, SAV, 4 CC, FC, 3 IW, SLE, 2 SSS, 3 LIO, LNT
17				Right from Inlet	3 CC, 2 FC, 6 IW, 6 LIO, CL, LCP, ID, LNT
18	125	B	3.0	Left from Inlet	LNT, 3 CL
19				Right from Inlet	LNT, DSC, ILI, 3 CL
20	550	A	36.0	LNT, 12 SLE, 13 LIO, 8 CC, 3 LCP, 7 IW, CM, 2 LT, 3 LHS, 3 ILI	
21	790	A	48.0	FC, ILI, LHS, IW	
22	652	A	48.0	VW, LIO, 3 ILI, 2 CC, IW, 3 SLE	
23	100	A	101.3	20 CC, 7 CM, 2 SLE, 3 LCP, CL, 4 IW, LHS, 2 LIO, 3 FC, LNT	
24	74	C	63.4	12 CC, 12 SLE, LHS, LB, 2 IW, 7 LIO, 2 CL, 3 CM, VZ, VW	

*Twin culverts are constructed in a very close distance from each other. The inspection team entered the culverts from the inlet and distinguished them by left and right culverts from inlet.

7.7. SAPL Thickness

A statistical analysis was performed to compare the SAPL design thickness with the installation. The number of thickness measuring points and drillings was limited by DOTs and the research team was not allowed to drill SAPLs in many locations. Therefore, SAPL thickness for each culvert was measured at springlines and crown in a few locations, mostly at 10-ft intervals and sometimes at 20-ft and 50-ft from upstream locations to avoid any irregularities of inlet and outlet installations. In many cases, aside from the non-uniform thickness and installation issues as illustrated in Figure 7-2, it was observed that the SAPL installation thickness was less than the required design value. This would be a good reason to have a factor of safety added to the design. Due

to the limited numbers of drilling points, it was not possible to measure the SAPL thickness at the same locations with a similar pattern on all pipes. Variation of all arch culverts renewed with cementitious SAPL with 2 in. design thickness at 3 o'clock or springline, 12 o'clock or crown, and 9 o'clock or springline, for instance, are illustrated in Figure 7-3. The upper horizontal continuous line on top and the connection line between the blocks in this figure are representative of 2 in. required design thickness and the average measurement of installed thickness, respectively. For example, as it is shown, the average of installed SAPL thicknesses at 0° (3 o'clock, springline) is 1.5 in. which is 0.5 in. less than the 2 in. design thickness. The horizontal line inside of each block shows the median of measured SAPL thicknesses at that location.

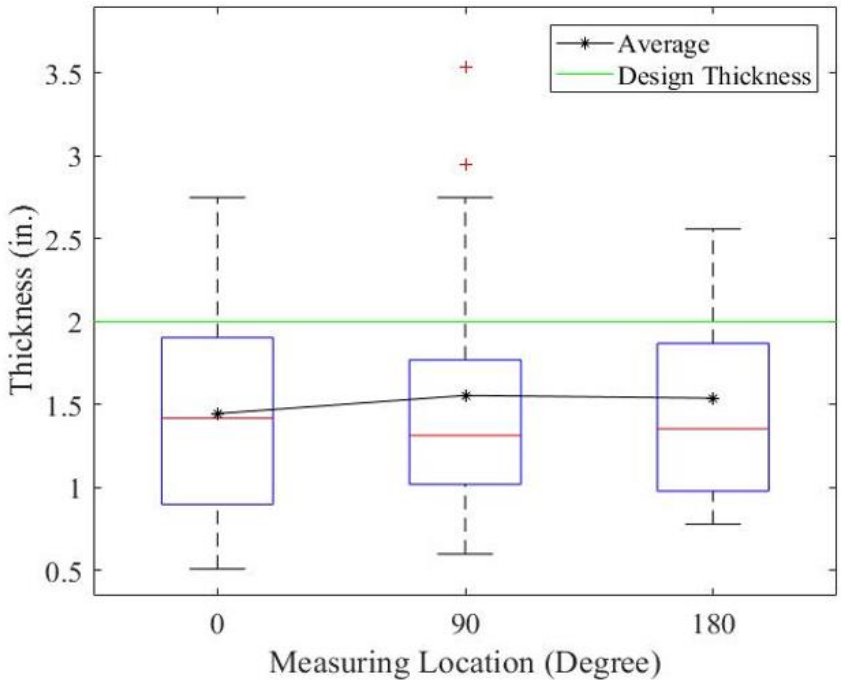


Figure 7-3. SAPL measured thicknesses versus 2 in. design thickness, (arch pipes renewed with cementitious SAPL)

The difference of SAPL design and installed thicknesses for an 84-in. circular CMP, as another example, is illustrated in Figure 7-4. The radius of this polar graph shows the SAPL design thickness and the average of installed thickness along the culvert with blue and red lines, respectively. The average installed thickness at 0°, 30°, 60°, 90°, 120°, 150° and 180° are shown circumferentially in this graph. As it is shown, the installed SAPL thickness (red line) is less than the required 1.5 in. design thickness (blue line) in all circumferential locations along the culvert.

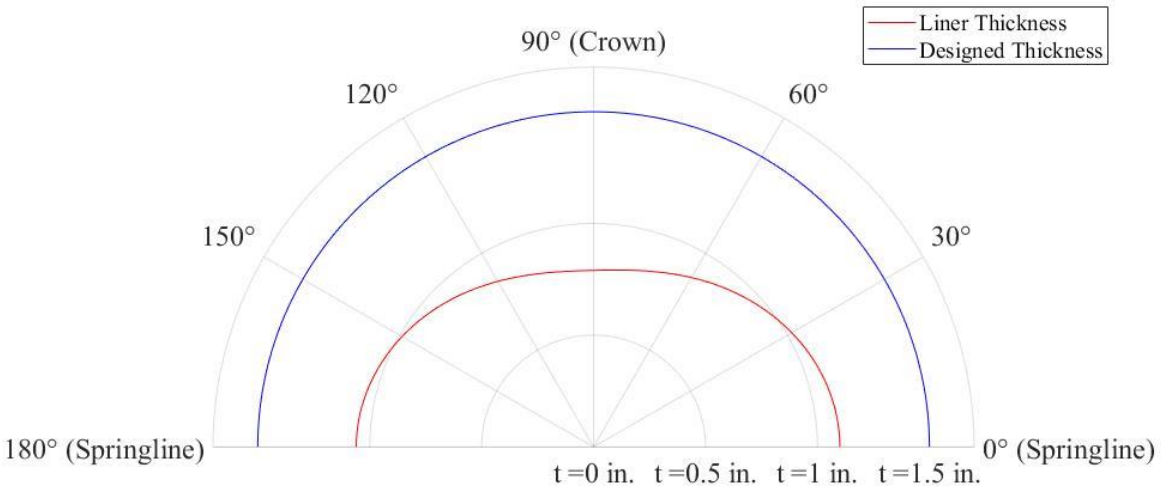


Figure 7-4. SAPL average installed thicknesses versus 1.5 in. design thickness inside an 84-in. diameter circular CMP.

7.8. Rating Systems

To summarize and evaluate the condition of SAPLs, a numerical scale rating system from 0 to 9 was established by the authors to allocate a rating to each liner. Also, eight common issues of the structure were monitored and measured for each site. The numerical rating system (0 to 9) and eight common defects of the structure are summarized in Table 7-5. Rating of "9" (Excellent) indicates a structurally sound and functionally adequate (like-new) with no SAPL defects. Rating numbers decrease with worsening condition up to a rating of "0" (Failed), indicating SAPL failure that directly affects the structural or the functional capacity. SAPLs were given a rating for each issue type and finally an average rating was calculated from Eq. 7-1 for each SAPL.

$$OAR = \frac{\sum Rating}{N} \qquad \text{Eq. 7-1}$$

Where,

OAR	original average rating of the SAPLs, dimensionless,
$\sum Rating$	summation of general material and installation rating for each observed category of defects, dimensionless,
N	number of different categories of defects, dimensionless.

The original average ratings (OAR) of the SAPLs are summarized in tables. In case of a shallow cover culvert in a poor condition of SAPL, the condition of the whole structure is more critical. Therefore, a dimensionless rating modifier (M) based on ratio of soil cover thickness and culvert rise was also used for considering potential risks to public motorists in the case of culvert failure. For example, if a culvert with 4 ft rise and 1 ft of soil cover fails, the impacts of failure on the public will be more compared with failure of a culvert with 4-ft diameter and 12 ft of soil cover. A deeply buried conduit will be more impactful to the public in the sense that it will take longer to

replace with a larger footprint of disturbance. The risk is lower at deeper fills and higher at lower fills. Thus, the original average rating needs to be modified and adjusted to have a rating value for the health of whole structure. The adjusted overall structural health rating (AOR) is given by Eq. 7-2.

$$AOR = M \times OAR \qquad \text{Eq. 7-2}$$

Where,
AOR the adjusted overall structural health rating, dimensionless,
M modifier based on the ratio of soil cover thickness H in ft and culvert rise R in ft, dimensionless.

Masada et al. (2007) provided the rating modifier values. These values are summarized in Table 7-5.

Table 7-5. Rating modifier values (Masada et al. 2007).

Ratio Soil Cover (H) to Rise (R)	Modifier Value (M)
$H/R < 2.5$	0.85
$2.5 < H/R < 5$	0.9
$H/R > 5$	1

Table 7-6 Rating scale to evaluate general conditions of SAPLs.

Rate	Category	Description							
		Crack	Fracture	Efflorescence	Corrosion	Infiltration	Deposits	SAPL Surface	SAPL Thickness
9	Excellent	No	No	No efflorescence	Without rust staining	No leakage	No debris, the flow is not obstructed	New condition; No holes; No discoloration of liner surface; No visible joints or head bolts; No surface damage; No roots	As design thickness
8	Very Good	Hairline crack	No	Circumferential cracks without efflorescence	Without circumferential rust staining	No leakage with circumferential cracks	Very minor deposits; No waterway blockages	Surface in a good condition; Discoloration of concrete; No Spalling or delamination, scaling or softening; surface in good condition	0 - 5% different from design thickness
7	Good	Hairline cracks less than 1/16 in.	Circumferential cracks open less than 1/16 in.	5% of cracks with efflorescence	0%-50% of cracks with minor rust staining	10% of cracks with pinholes	Minor deposits; No waterway blockages	Light scaling on less than 10% of exposed area less than 1/8 in. deep; Delaminated/Spalled area less than 1% of surface area.	5 - 10% different from design thickness
6	Satisfactory	Hairline multiple circumferential cracks less than 1/8 in.	Circumferential cracks open greater than 1/16 in.	10% of cracks with efflorescence	50%-100% of cracks with minor staining	Pinholes	Minor waterway blockages are caused between 0%-5% of the total cross-sectional area of	Scaling on less than 20% of exposed area less than 1/4 in. deep. Minor delamination or spalling areas less than 5% of surface area. Concrete patched on the liner surface.	10 - 15% different from design thickness

Rate	Category	Description							
		Crack	Fracture	Efflorescence	Corrosion	Infiltration	Deposits	SAPL Surface	SAPL Thickness
							culvert. Sediment built up in	Heavy and thick liner sagging off	
5	Fair	Multiple cracks; Circumferential cracks less than 1/8 in., longitudinal cracks less than 1/16 in.	Circumferential cracks open greater than 1/8 in.	25% of cracks with efflorescence	0%-50% of cracks with moderate rust staining	Infiltration weeper	Minor waterway blockages are caused between 5%-10% of the total cross-sectional area of culvert. Sediment built up in channel, tress or bushes growing in the channel.	Scaling on less than 30% of exposed area less than 3/16 in. deep. Total delaminated/ spalled areas less than 15% of surface area. Liner aggregates are visible.	15 - 20% different from design thickness
4	Poor	Extensive cracking with cracks open more than 1/8 in.	Longitudinal cracks open greater than 1/8 in.	50% of cracks with efflorescence	50%-100% of cracks with moderate rust staining	Infiltration dripper	Moderate obstruction is caused due to debris between 10%-45% of the total cross-sectional area of culvert, rock	Spalling at numerous locations; Heavy invert surface scaling greater than 1/2 in.	20 - 25% different from design thickness

Rate	Category	Description							
		Crack	Fracture	Efflorescence	Corrosion	Infiltration	Deposits	SAPL Surface	SAPL Thickness
							settlement causing rock dams, trees or bushes growing into the channel		
3	Serious	Extensive cracking greater than 1/8 in.	Extensive fracture	75% of cracks with efflorescence	0%-50% of cracks with large rust staining	Infiltration runner	Heavy obstructions are caused due to settlement of debris 45%-80% of the total cross-sectional area of culvert is lost	Extensive spalling; minor slabbing; Heavy invert surface scaling; 50% loss of wall thickness at invert	25 - 50% different from design thickness
2	Critical	Full depth holes;	Extensive cracking greater than 1/2 in.	100% of cracks with efflorescence	50%-100% of cracks with large rust staining	Infiltration gusher	Culvert is completely blocked; total loss of hydraulic capacity;	Severe liner slabbing; Heavy invert surface scaling; Total delaminated, spalled, and punky cementitious liner areas are greater than 50% of surface area; Very soft cementitious liner	50 - 75% different from design thickness
1	Imminent Failure	Liner partially collapsed, or collapse is imminent. Holes through cementitious liner; 75% loss of wall thickness at invert; Liner partially collapsed							
0	Failed	Liner is collapsed.							

Rate	Category	Description							
		Crack	Fracture	Efflorescence	Corrosion	Infiltration	Deposits	SAPL Surface	SAPL Thickness
		Liner completely deteriorated at the invert							

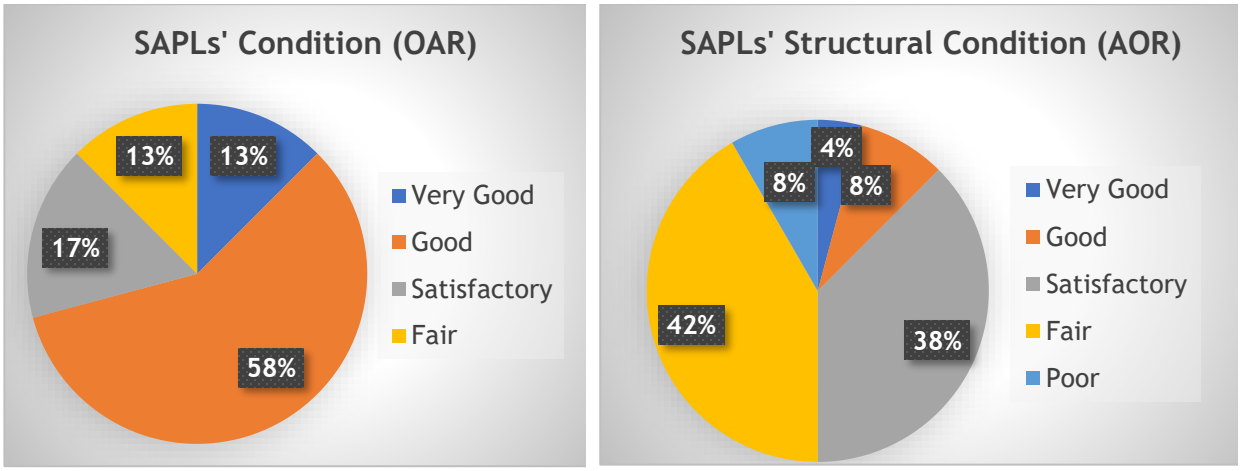
Table 7-7 SAPLs overall average rating score (OAR) and adjusted overall structural rating score (AOR).

Culvert	SAPL				Rating								OAR	M	AOR
	Vendor	Age (m)	H/R	Ave. Thickness	Crack	Fracture	SLE	LIO	Infiltration	Settled Deposit	SAPL Surface	Performed Thickness			
Ohio 1	C	26.9	0.62	1.33	7	7	6	7	5	9	8	5	6.75	0.85	5.74
Ohio 2	B	22.2	3.00	1.48	8	9	2	2	5	8	7	5	5.75	0.9	5.18
Ohio 3	E	2.0	2.40	1.50	8	9	9	9	9	9	9	5	8.38	0.85	7.12
Ohio 4	C	26.6	6.48	1.22	7	9	9	9	9	9	8	4	8.00	1	8.00
Ohio 5	B	26.1	2.14	0.95	8	9	9	7	9	8	8	2	7.50	0.85	6.38
Pen	A	36.0	0.35	1.18	6	9	7	7	5	9	7	6	7.00	0.85	5.95
NY	A	48.0	2.00	1.27	8	9	4.5	5	4.5	9	7	4	6.38	0.85	5.42
NC 1	C	1.0	0.17	0.97	9	9	9	9	9	8	7	2	7.75	0.85	6.59
NC 2-L	C	1.0	0.17	0.98	8	9	9	7	9	8	8	3	7.63	0.85	6.48
NC 2-R	C	1.0	0.17	0.89	8	6	7	6	9	9	7	5	7.13	0.85	6.06
NC 3	C	1.0	0.17	2.01	9	9	9	9	9	9	2	2	7.25	0.85	6.16
NC 4	C	1.0	0.14	0.89	8	9	8	9	9	9	2	3	7.13	0.85	6.06
NC 5-L	C	1.0	0.17	1.63	8	9	9	9	9	9	5	2	7.50	0.85	6.38
NC 5-R	C	1.0	0.17	1.51	8	9	9	9	5	9	2	5	7.00	0.85	5.95
NC 6	C	1.0	0.33	1.29	9	9	9	9	9	9	7	2	7.88	0.85	6.69
Del 1-L	D	3.0	0.67	0.99	5	6	5	7	6	8	5	2	5.50	0.85	4.68
Del 1-R	D	3.0	0.67	1.17	5	6	5	7	4	8	5	2	5.25	0.85	4.46
Del 2-L	D	3.0	0.93	1.39	5	9	8	8	8	8	5	2	6.63	0.85	5.63
Del 2-R	D	3.0	0.93	1.20	5	9	8	8	8	7	5	2	6.50	0.85	5.53
Mn 1	A	36.0	3.57	1.00	6	9	6	5	6	9	7	5	6.63	0.9	5.96
Mn 2	A	48.0	1.56	1.00	8	9	9	9	7	9	8	7	8.25	0.85	7.01
Mn 3	A	48.0	1.33	0.50	7	9	7	8	7	9	8	7	7.75	0.85	6.59
FL 1	A	101.3	0.08	1.62	6	6	7	7	5	9	6	2	6.00	0.85	5.10

FL 2	E	63.4	1.16	2.33	6	9	2	6	7	9	6	4	6.13	0.85	5.21

7.9. Condition Assessment of SAPLs

The overall average rating score (OAR) and the adjusted overall average score (AOR) were used for condition assessment of SAPLs. The condition of SAPL based on OAR are shown in Figure 7-5 (a). According to the rating system definition in this paper, the results indicate that 13% of 24 SAPLs were in a very good condition, 58% in good condition, 17% in satisfactory condition and 13% in fair condition. The adjusted overall average score was used to quantify the structural SAPLs rates according to available data. Similarly, SAPLs structural conditions were evaluated from the AOR. The structural condition of SAPLs from AOR are shown in Figure 7-5 (b). The results indicate 4% of SAPLs were in very good condition, 8% in good condition, 38% in satisfactory condition, 42% in fair condition and 8% in poor condition.



(a) (b)

Figure 7-5. Condition assessment of SAPLs, (a) SAPL original condition given as percent of liner condition, (b) SAPLs structural condition given as percent of liner structural condition.

7.10. Comparative Status of Cementitious and Geopolymer SAPLs.

A comparative analysis of the overall average rating (OAR) scores was conducted on the inspected cementitious and geopolymer SAPLs, as it is presented in table 7-7. Among the twenty-four inspected SAPL renewed culverts, the relative proportions of cementitious and geopolymer liner materials were the same (12 cementitious SAPLs and 12 geopolymer SAPLs). It was observed that 37% of culverts renewed with geopolymer SAPLs and 8% of culverts renewed with cementitious SAPLs were ranked as good condition. Hence, the number of culverts renewed with geopolymer SAPLs in good condition were 29% more than the number of culverts renewed with cementitious SAPLs in the same condition.

Table 7-8 Comparative Status of Cementitious and Geopolymer SAPLs, (According to OAR).

Vendor	SAPLs Conditions (OAR)			
	Very Good (12.6%)	Good (45.8%)	Satisfactory (29.2%)	Fair (12.5%)
A (Cementitious) 25% (6/24)	4.2%	8.3%	12.5%	-
B (Geopolymer) 8% (2/24)	-	4.2%	-	4.2%
C (Geopolymer) 42% (10/24)	4.2%	33.3%	4.2%	-
D (Cementitious) 17% (4/24)	-	-	8.3%	8.3%
E (Cementitious) 8% (2/24)	4.2%	-	4.2%	-

7.11. Numerical Modeling

A multi-variable regression analysis using MATLAB software was performed between the *H*/*R* ratio, the *condition*, *age*, and *thickness* of SAPLs. There is an expected correlation between these parameters. The multi-linear regression analysis on the H/R ratio, age, the average thickness, and structural condition based on AOR of SAPLs results are expressed by Eq. 7-3.

$$AOR = -0.3485 + 1.453\left(H/R\right) + 7.6381(T) - 0.0121(A) - 2.1818\left(H/R\right)(T) + 0.0261\left(H/R\right)(A) - 0.0831(T)(A) + 0.1336\left(H/R\right)^2 - 0.1823(T)^2 + 0.0008(A)^2 \quad \text{Eq. 7-3}$$

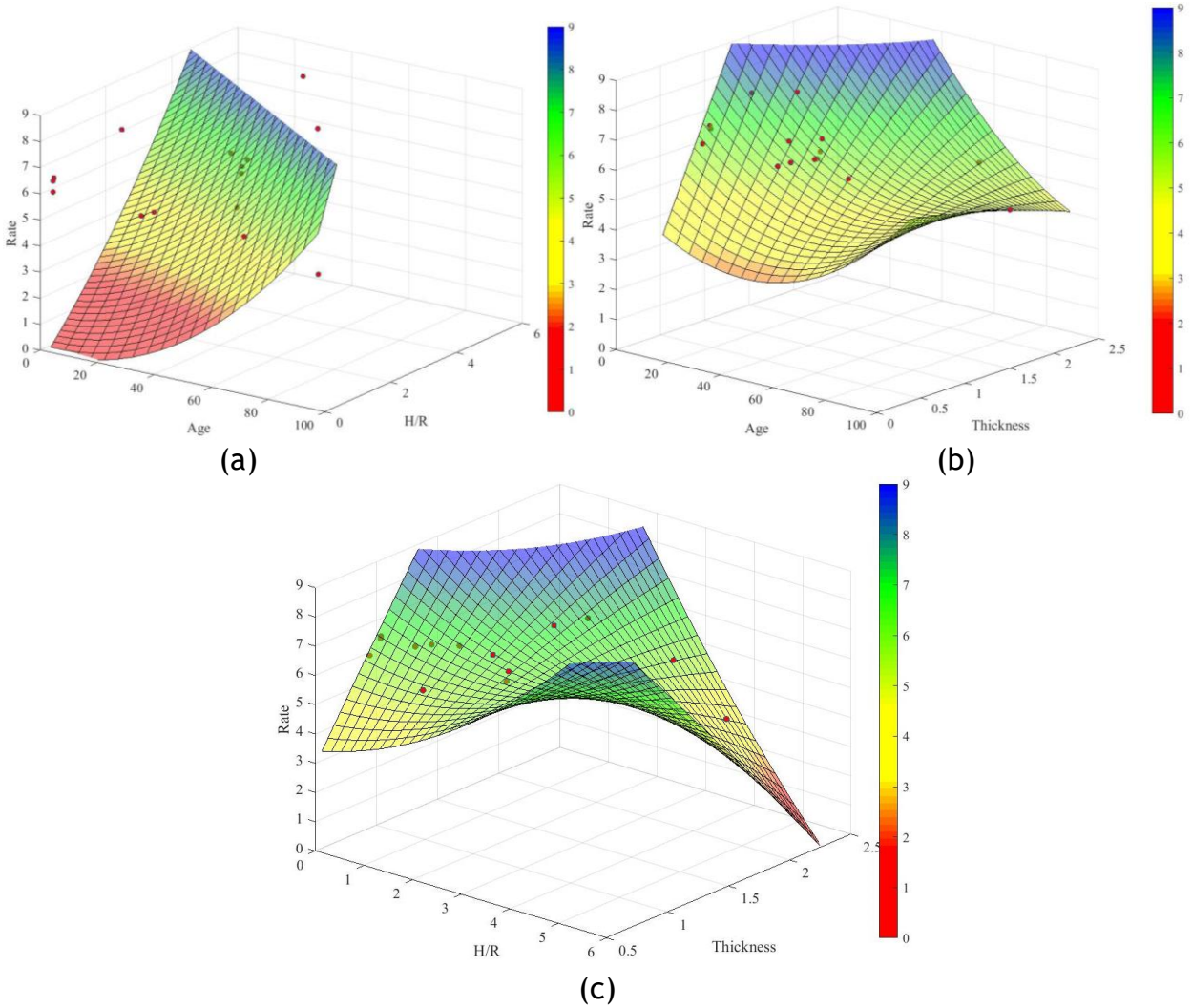
$$r^2 = 77.8\%$$

where,
A SAPL age, month,
T SAPL thickness, in.,
r regression coefficient,
variables *H, R* and *H*/*R* are defined in Eq. 7-2.

r^2 equals to 77.8% indicates that the correlation is good. The relationship of age (*A*), thickness (*T*), *H*/*R* ratio and structural condition of SAPLs (AOR) is plotted in Figure 7-6. A three-dimensional graph is able to illustrate the relationship of three parameters at once. Therefore, three different sets of graphs are used to depict the correlation of *A, T, H*/*R* and AOR. The color counter depicts the SAPL structural condition (AOR), dark blue is SAPL in an excellent structural condition and dark red is a failed SAPL sample. The regression analysis and the graphs show the structural condition of SAPLs are more sensitive to the *H*/*R* ratio. As it is shown in graph (a), the early age SAPLs with a lower number of *H*/*R* show a lower AOR. As it is shown in graph (c), a thicker SAPL not

necessarily behaves better than a thinner sample. There are other parameters such as *H/R*, *age*, quality of material and installation procedure which plays an important role in the final product of the SAPL.

Moreover, variability of SAPL installations were found during the site visit inspection which is mainly due to different design procedures and varied installation practices among DOTs. It was observed that despite using the same material from a specific vendor for some SAPL locations, the condition of the applied SAPLs were not the same, and it was highly impacted by different installers. While SAPL renewal application is favorable practice among some DOTs and it is anticipated to have at least a 50-years design life, it is not probable according to the field inspection data. Thus, there is a strong need of specific design and installation guidelines for these new technologies which is developed in Chapter 8.



(a) (b)

(c)

Figure 7-6. Correlation of Age, H/R, Thickness and AOR of SAPLs, (a) A, H/R and AOR (b) A, T and (AOR), (C) H/R, T and AOR.

7.12. Limitations, Findings and Recommendations

This chapter presents a formula (Eq. 7-3) for relationship of A, T, H/R and AOR of SAPLs for all states in different geographical locations due to lack of enough information in each state. Therefore, it is recommended to have a specific equation for each geographical area.

The SAPL material for all twenty-four culverts in this paper falls into cementitious category, due to lack of any polymeric SAPL site at the time and area of inspection. Therefore, it is recommended to have a specific rating system and sets of equations for polymeric SAPLs as well. A summary of findings and recommendations to improve SAPL performance are presented in Table 7-9.

It is also recommended to have an inspection plan for three different stages: pre-installation inspection, installation inspection and post-installation inspection, as it is presented in Table 7-10. In addition, Chapter 9 presents SAPL performance construction specifications.

Table 7-9 Summary of findings and recommendations.

Summary of Findings	Recommendations
Cracks	• Hairline cracks are not a reason for concern unless they produce spalls or cause loosening of the lining material.
	• ASTM standard C1090 is recommended for measuring changes in height of cylindrical specimens of hydraulic-cement grout during a stipulated testing period of 28 days. • According to the ASTM A979, the water cement ratio shall not exceed 0.5 by weight. • According to the ASTM A849, only potable water shall be used.
Efflorescence	• Pressure washing along with brushing and rinsing the surface with water may help eliminate it in early age of formation or ameliorate it.
Rust Staining	• Corroded areas, areas with any leakage or water seepage, any holes and voids shall be sealed off (with polyurethane or similar grout) before the SAPL application.
Infiltration	• Point repair and invert repair (paving the invert as per ASTM A849) shall be done prior to the SAPL application. • An installation inspection is recommended to do visual inspection and verify the SAPL is leak free with low probability of rust staining formation.
Issues with SAPL Thickness	• The SAPL design thickness recommends being calculated based upon the compressive strength of the SAPL material, the flexural bending strength of the SAPL material and the AASHTO truck loading for culvert pipes based upon the type of the soil used [(1)]. • It is recommended the SAPL thickness shall follow the design thickness and be applied uniformly by spin caster along the pipe according to the ASTM A979.

Installation	• According to ASTM A979, the SAPL must be placed in one or more passes/coats/lifts to reach the design thickness. Applied SAPL material over the pipe surface should provide a uniform thickness. The SAPL must exhibit an even application both longitudinally and circumferentially with no signs of uncured product. • According to ASTM A849, troweled surface finishes that do not have an acceptable level of smoothness are not acceptable. • According to the ASTM A849, a clean inside surface of the culvert can provide a good adherence between the pipe and the liner and directly impact the performance of the final product of SAPL. • According to ASTM A849, curing operations must begin immediately after SAPL installation and continue for at least 72 hrs. The pipe ends shall be closed with airtight covers and the cementitious SAPL kept wet via an intermediate water source or a liquid membrane-forming compound conforming to ASTM C309. • Cleaning and surface preparation shall be done before SAPL application. • Before the SAPL application, all the debris must be removed from the culvert and its interior surface should be cleaned with high pressurized waterblast to remove all the remaining dirt. • SAPL waste material: As the SAPL application is environmentally friendly, by the end of SAPL installation, having a waste management plan by installer according to the ASTM E3073-17 is recommended.

(1) The compressive and flexural strength of the SAPL material can be achieved according to the ASTM C109 (standard test method for compressive strength of hydraulic cement mortars) and ASTM C1609 (standard test method for flexural performance of fiber-reinforced concrete using beam with third-point loading) respectively.

It is also recommended to have an inspection plan for three different stages: pre-installation inspection, installation inspection and post-installation inspection, as it is presented in Table 7-10.

Table 7-10 Inspection plan.

Inspection	
Pre-Installation Inspection	• Proper cleaning and surface preparation must be done before SAPL application. Surface preparation include stoppage of water through the joints of the host conduit.
Installation Inspection	• A minimum of three test specimens of the SAPL material randomly must be taken to verify the required compressive and flexural strengths. • At least 6 random samples (3 in the valleys of the corrugations and 3 over the crest) must be taken for thickness verification in accordance with ASTM D1005 or ASTM D7091.
Post-installation Inspection	• Routine inspections are suggested to be conducted on a defined (5 years) frequency. • Visual and nondestructive condition assessment.

7.13. Summary and Conclusions

Spray applied pipe linings (SAPLs) structurally renew existing pipes and provide a protective interior coating, thus inhibiting further deterioration of the interior of culverts and drainage pipes. Currently no standard design methodology and performance construction specification exist for SAPLs. Vendors have their own design approaches and installation procedures which highly impact the performance of the applied SAPL. SAPL field data collection presented in this chapter identified and addressed the existing issues with the applied liner on the interior surface of the culverts which highlights the needs for comprehensive performance construction specifications to satisfy the liner design requirements. The common cementitious/geopolymer SAPL issues (due to lack of any standard) identified in this chapter includes circumferential crack, fracture, infiltration weeper, efflorescence, rust staining and non-uniform thickness. The condition of inspected SAPLs summarized and evaluated using an established numerical scale rating system from 0 (Failed) to 9 (Excellent). This chapter depicted that besides the design, liner installation process is a main key to reach a uniform thickness of SAPL and to achieve its structural application. It was observed that the corrugated aluminum pipes experienced less effect of corrosion on the surface of SAPL compared with the corrugated steel pipes. It implies that corrugated aluminum performs better in locations with high levels of corrosive environments. Due to different crack patterns in cementitious and geopolymers, it is recommended to select the type of SAPL materials in accordance with the deteriorated culvert's condition, geographical and weather conditions (freeze/thaw), cover depth and skew angle of culvert with the road for each location. Refer to Chapter 9 – Performance Specifications for more information. Finally, authors used the available ASTM and AASHTO standards for other purposes and provided recommendations (Table 7-9) for proper SAPL installation to address the issues as well as having a robust quality control and inspection plans for stages of pre-installation, installation and post-installation.

Appendix 7-A: Inspected SAPL Projects

Table 7-A 1. Ohio DOT, Site 1, SAPL Inspection Information and Photos (39.296586, -84.209197).

Ohio, Site 1: Warren County		
 Bolt Heads Are Visible	 Circumferential Crack	 Iron Oxidation, Longitudinal and Circumferential Crack
 Circumferential Crack Through the Invert Iron Oxidation	 Efflorescence Circumferential Crack	 Multiple Hairline Cracks

Table 7-A 2. Ohio DOT, Site 2, SAPL Inspection Information and Photos (39.947090, -82.53195).

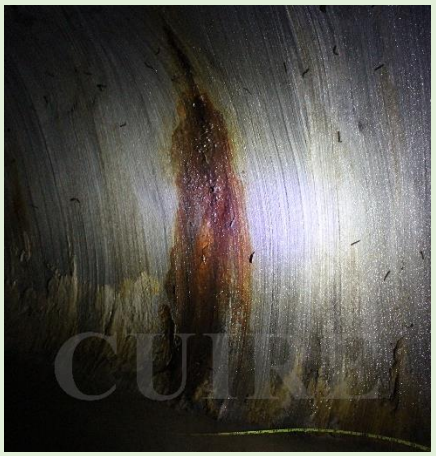
Ohio Site 2: Muskingum County, Ohio		
 Inconsistent Thickness Concrete Patching on the Liner Surface	 Corrosion of Metal pipe with Iron Oxidation on Liner Surface	 Aggregate Deposits
 Corrosion of Metal pipe with Iron Oxidation on Liner Surface, Aggregate Deposits at Invert	 Worms on the Liner Surface (Vermin)	 Circumferential Crack

Table 7-A 3. Ohio DOT, Site 3, SAPL Inspection Information and Photos (39.93299, -81. 53146).

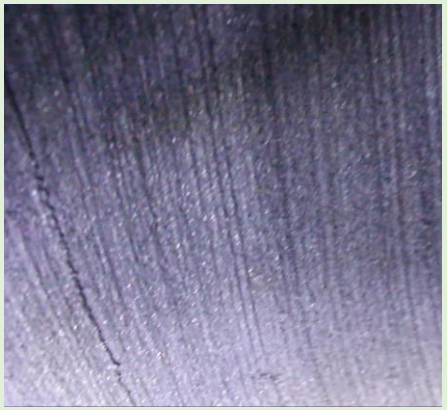
Ohio Site 3: Guernsey County, Ohio		
 Hand Spray Application with Troweling	 Vermin (Frog)	 Circumferential Crack

Table 7-A 4. Ohio DOT, Site 4, SAPL Inspection Information and Photos (39.993314, -81. 549682).

Ohio, Site 4: Guernsey County, Ohio		
 Multiple Cracks	 Circumferential Crack through the Invert	 CMP Coating

Table 7-A 5. Ohio DOT, Site 5, SAPL Inspection Information and Photos (39.296586, -84.209197).

Ohio, Site 5: Warren County		
 **Shadowing**	 **Longitudinal Crack**	 **Deep Corrugation at The Crown and Thicker Thickness in the Valleys Above Springline**
 **Corrosion of Metal pipe with Iron Oxidation on SAPL Surface**	 **Aggregate Deposits at Invert**	 **Circumferential Crack**

Table 7-A 6. PennDOT, Site 6, SAPL Inspection Information and Photos (39.296586, -84.209197).

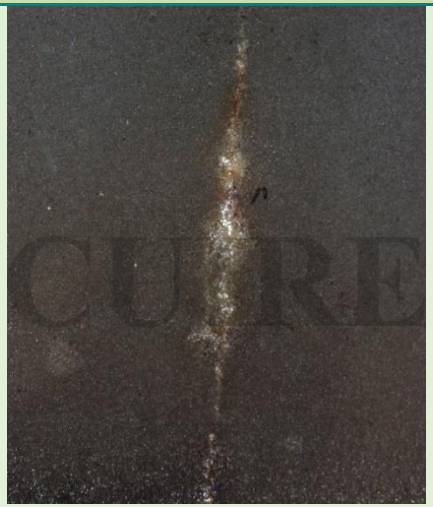
Pennsylvania, Site 6: Warren County		
  **SAPL Irregularities at the Crown, Iron Oxidation on SAPL Surface below the Springline**	 **Circumferential Crack**	 **Multiple Cracks**
 **Disturbed SAPL Surface**	 **SAPL Irregularities (Problem with Application Process)**	 **Invert Problem (Installation Problem)**

Table 7-A 7. NYSDOT, Site 7, SAPL Inspection Information and Photos (39.296586, -84.209197).

New York, Site 7: Warren County		
 **Active Leakage from Pinhole Iron Oxidation on SAPL Surface**	 **Circumferential Shrinkage Cracks Efflorescence**	 **Infiltration Dripper**
 **SAPL Irregularities**	 **SAPL Irregularities**	 **360 degrees Infiltration Dripper Efflorescence, Iron Oxidation**

Table 7-A 8. DelDOT, Site 8, SAPL Inspection Information and Photos (39.693453, -75.709608).

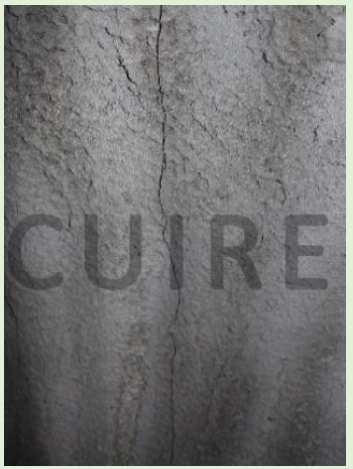
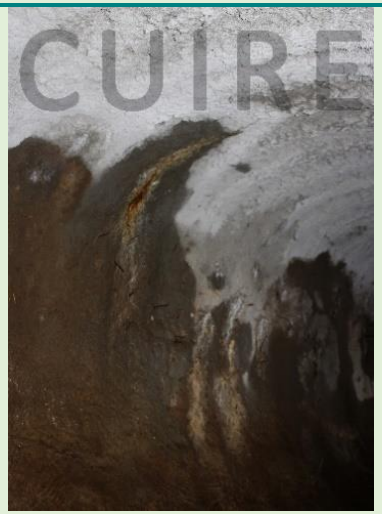
Delaware, Site 8: New Castle County		
 **Multiple Cracks** **Active Leakage**	 **Infiltration Dripper** **Circumferential Crack**	 **Circumferential Fracture**
 **Multiple Cracks** **Iron Oxidation, Efflorescence**	 **Circumferential Crack** **Iron Oxidation, Efflorescence**	 **Multiple Cracks** **Iron Oxidation**

Table 7-A 9. DelDOT, Site 9, SAPL Inspection Information and Photos (39.693589, -75.708805).

Delaware, Site 9: New Castle County	
 Invert Repair	 Longitudinal Shrinkage Crack
 The Liner Material Started Moving Down	 Multiple Cracks

Table 7-A 10. NCDOT, Site 10, SAPL Inspection Information and Photos (35.51417, -82.6048).

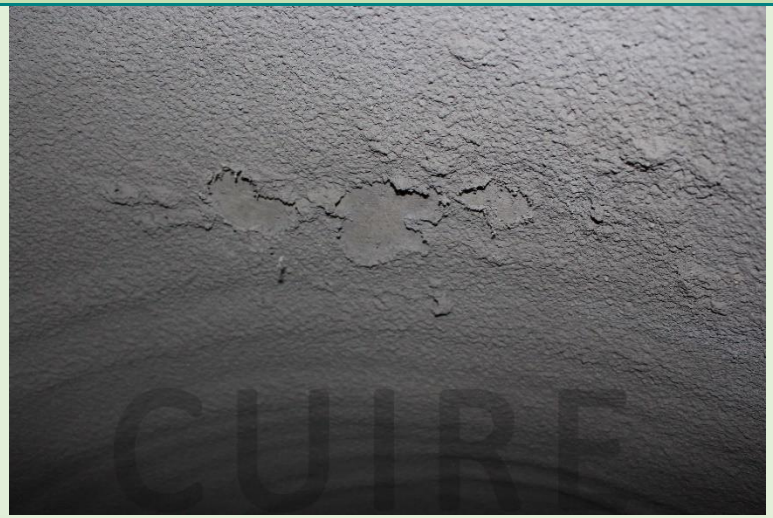
North Carolina, Site 10: Buncombe County, SR 3479 Pole Creasman Rd	
	
Delamination at the Crown	**Settled Deposits (Hard/Compacted)**

Table 7-A 11. NCDOT, Site 11, SAPL Inspection Information and Photos (35.56486, -82.6712).

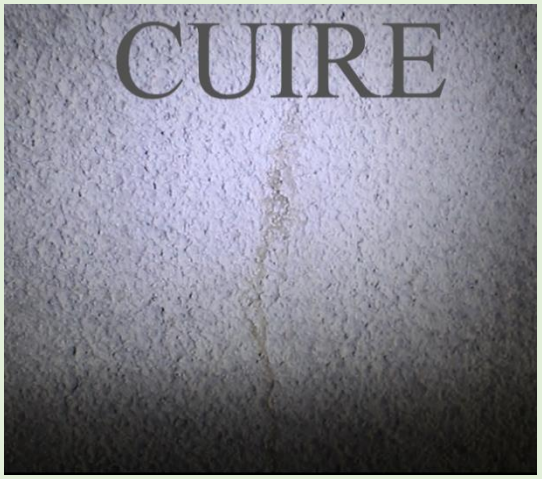
North Carolina, Site 11: Buncombe County	
 **Patched Concrete at the Crown**	 **Circumferential Fracture**
 **Open Joint in CMP**	 **Iron Oxidation Pinhole**

Table 7-A 12. NCDOT, Site 12, SAPL Inspection Information and Photos (35.48614, -82.6917).

North Carolina, Site 12: Buncombe County		
 Irregular Installation	 The Bolts are not Completely Covered	 The Material is not Bonded Completely
 Irregular Installation	 The Bolts are not Completely Covered	 The Material is not Bonded Completely

Table 7-A 13. NCDOT, Site 13, SAPL Inspection Information and Photos (35.54256, -82.7008).

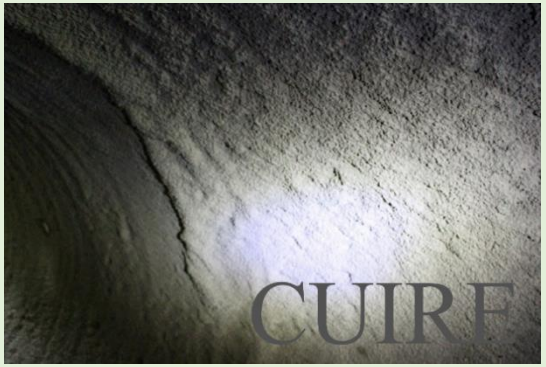
North Carolina, Site 13: Buncombe County		
		
Inconsistent Filling of Corrugation	**Efflorescence from Pinhole, Iron Oxidation**	**The Material is not well Bonded**

Table 7-A 14. NCDOT, Site 14, SAPL Inspection Information and Photos (35.75733, -82.4041).

North Carolina, Site 14: Buncombe County	
	
The Liner Material Seems Dry	Bare CMP Invert without any Liner
	
The Liner Material is not Well Bonded	Hanged Liner Material from the Crown

Table 7-A 15. NCDOT, Site 15, SAPL Inspection Information and Photos (35.53696, -82.7417).

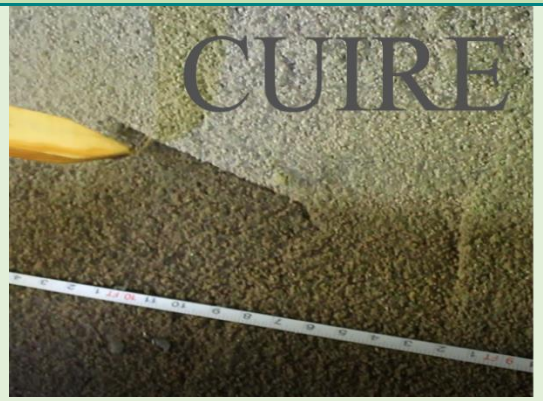
North Carolina, Site 15: Buncombe County		
 Heavy Material Rolling Down on SAPL Surface	 Patched Concrete on SAPL Surface	 Patched Concrete on SAPL Surface
 Delamination	 A Lift over SAPL Material	 Separated Layer of SAPL Material

Table 7-A 16. MnDOT, Site 16, SAPL Inspection Information and Photos (45.0252992601, -93.0906454079).

Minnesota, Site 16: Ramsey County		
 Multiple Cracks	 Circumferential Crack through the Invert Iron Oxidation, Efflorescence	 Inconsistent SAPL Thickness On RCP
 Ron Oxidation Efflorescence	 Heavy and Rough Material at the Crown	 Inconsistent SAPL Thickness both Sides of RCP Joint

Table 7-A 17. MnDOT, Site 17, SAPL Inspection Information and Photos (44.94813056, -92.86611111).

Minnesota, Site 17: Washington County	
 SAPL Irregularity at Pipe Joint	 Irregular SPL Surface at Host Pipe Transition from 60 in. to 54 in.
 Circumferential Fracture at Inlet	 SAPL Irregularity

Table 7-A 18. MnDOT, Site 18, SAPL Inspection Information and Photos (39.296586, -84.209197).

Minnesota, Site 18: Warren County		
 SAPL Irregularity	 Efflorescence	 Iron Oxidation on SAPL Surface
 SAPL Irregularity	 SAPL Irregularity	 Vermin

Table 7-A 19. FLDOT, Site 19, SAPL Inspection Information and Photos (39.296586, -84.209197).

Florida, Site 19: Clay County		
 Hand Patched Concrete on Circumferential Cracks	 Circumferential Crack at Crown	 Pinholes with Active Leakage Circumferential Cracks
 Vermin Nest on SAPL Surface	 Multiple Cracks below the Springline	 Circumferential Crack at Crown

Table 7-A 20. FLDOT, Site 20, SAPL Inspection Information and Photos (39.296586, -84.209197).

Florida, Site 20: Leon County	
 Efflorescence and Iron Oxidation on SAPL Surface	 Rough and Inconsistent SAPL Thickness
 Multiple Cracks	 Vermin (Spider)

This Page Left Intentionally Blank.

Chapter 8

SAPL Design Equations

CHAPTER 8 - DEVELOPMENT OF STRUCTURAL DESIGN EQUATIONS

This chapter discusses the development of a set of design equations for the two types of spray in place liner systems (cementitious and polymeric) using the data from the soil box testing on this project along with other applicable published research. The equations are desired to address both circular and arch pipe geometries. Existing design standards were evaluated to determine if they fit the results of the soil box testing conducted on this project. The details of some of these evaluations and the conclusions reached are covered extensively in Chapter 11. It should be noted that the backfill used in the soil box was placed and compacted to approximately 85% of the standard proctor density.

The project team was instructed to develop design equations consistent with AASHTO LRFD Bridge Design Specifications (BDS). The following is the result of that effort.

8.1. Live and Dead Loads Used for Liner Designs

The first step in the design process is to estimate the vehicular and earth loads that will come onto the liner (pipe) after the rehabilitation work is completed. In the 9th Edition of the AASHTO Bridge Design Specifications (BDS) it is written that loads from wheel pairs on the ground surface attenuate with depth based on a Live Load Distribution Factor (LLDF). For concrete pipes with diameters of 2.0 feet or less use 1.15 (for cover depths 2.0 feet or less) to 1.75 for concrete pipes 8 feet in diameter and larger. The designer is to interpolate the LLDF for diameters between the 2.0 feet and 8 feet. For all other pipe materials, it recommends 1.15 for coarse grained soils (SC1 and SC2) and 1.00 in other backfill materials. Given the semi-rigid performance of the cementitious SAPL it is recommended to use the distribution factor for a concrete pipe. For the flexible polymeric SAPL use the 1.15 LLDF.

Using Article 3.6.1.2.6 of the BDS, distributed service live load calculations are made considering a single-axle truck (the AASHTO Design Truck, Figure 3.6.1.2.2-1 of the BDS) travelling perpendicular to the pipe (parallel to the span) on an unpaved surface or a roadway with a flexible pavement. The distributed service live load applied to the pipe includes a dynamic load allowance factor and a multiple presence factor (M_p). Vehicular live loading for culverts under roadways designated as HL-93 shall be calculated as the larger of:

- The design truck or design tandem, and
- The design lane load (0.64 kips per linear ft uniformly distributed over a 10.0-ft width).

Only the axle loads of the design truck or design tandem are to be applied as the live load on culverts per the Articles 3.6.1.2.2 and 3.6.1.2.3 in AASHTO LRFD BDS

The live load (P_L) is calculated using the following expression:

$$P_L = \frac{M_p P I_f}{l_w w_w} \quad \text{Eq. 8-1}$$

Where,
P_L live load on pipe, psi,
M_p multiple presence factor, typically equal to 1.2,
P Load, lbs. (based on depth of culvert, h_{int} and size of pipe),
I_f dynamic load allowance factor = 1 + 0.33 [(96 – h)/96] ≥ 1.0,
l_w live load patch width, in., at depth h
w_w Live load width, in., at depth h
h depth of cover over culvert, in.,

As the depth of cover on the pipe increases the load widths increase. For live load distribution transverse or parallel to the culvert span, the wheel/axle load interaction depth shall be determined as:

For live load transverse to culvert span:

$$H_{int-t} = \frac{s_w - w_t - 0.06D_i}{LLDF} \quad \text{Eq. 8-2}$$

Where $h < H_{int\text{-}t}$:

$$w_w = w_t + LLDF\ (h) + 0.06D_i \quad \text{Eq. 8-3}$$

Where $h \geq H_{int\text{-}t}$:

$$w_w = w_t + s_w + LLDF\ (h) + 0.06D_i \quad \text{Eq. 8-4}$$

For live load distribution parallel to culvert span:

$$H_{int-p} = \frac{s_a - l_t}{LLDF} \quad \text{Eq. 8-5}$$

Where $H < H_{int\text{-}p}$:

$$l_w = l_t + LLDF(h) \quad \text{Eq. 8-6}$$

Where $h \geq H_{int\text{-}p}$:

$$l_w = l_t + s_a + LLDF(h) \quad \text{Eq. 8-7}$$

Where,

s_a axle spacing, inches.
s_w spacing between the wheel pairs on the axle, inches.
D_i inside diameter or clear span of culvert, in.
l_t tire patch length, 10 inches
w_t tire patch width, 20 inches
LLDF live load distribution factor
$H_{int\text{-}t}$ wheel interaction depth transverse to culvert span, inches
$H_{int\text{-}p}$ wheel interaction depth parallel to culvert span, inches

Per 3.6.1.2.6a, for single span culverts, the effects of live load may be neglected where the depth of fill (cover) to the top of the pipe is more than 8.0 feet and exceeds the span length. For multiple span culverts, the effects may be neglected where the depth of fill exceeds the distance between inside faces of end walls. This allowance should be applicable to standalone liner designs.

Given that lining takes place in an existing pipe with an existing pavement structure in place, it is important to note that rigid pavements will dramatically reduce any live load effects on buried pipes. This is given in the Portland Cement Association's calculation method to consider loads transmitted through concrete pavements (*Vertical Pressure on Concrete Culverts Under Wheel Loads on Concrete Pavement Slabs*, Portland Cement Association, Publication ST-65, 1951) that is still in use today and is suitable for computing live loads on liners under rigid pavements. (The same method is also presented in the *Concrete Pipe Design Manual*, published by the American Concrete Pipe Association if one cannot find access to the referenced report.) It is recommended that given the liner is being designed for the site-specific conditions at the time of its installation that this reduction in live load be considered for all liners installed in pipes below a rigid pavement.

In calculating the earth loads to be supported by the liner it is understood that before the culvert is lined, the earth loads are already being supported by the existing deteriorated structure and the surrounding soil structure; and that for deeply buried culverts it would be excessively conservative to design liners to support the weight of the entire soil column above it (i.e., soil prism load). In Article 12.13.2.1 of the BDS, the earth pressure at the crown of a steel tunnel liner is calculated using a load coefficient times the unit weight of the soil times the span of the structure. Figure 12.13.2.1-2 in the BDS provides values of this load coefficient as a function of the surrounding soil type (granular soil, saturated silt and clay, and saturated clay) versus the ratio of the overburden depth to the span of the liner. For a granular soil, the maximum value of the coefficient is approximately 1.6. This is consistent with the position that most engineers have of using a value of 2.0 as a conservative value for this coefficient (Moore, 2016). However, given that this figure is based upon a corrugated metal tunnel liner which is flexible, it was thought to look at the ASCE Manual of Practice 60 for Gravity Sanitary Sewer Design and Construction which is more

detailed in its values for the coefficient for tunneled pipe installation in undisturbed soil and will provide the designer with the best estimate of the soil loading likely to come onto the liner.

In section 9.2.2.7.2 of the ASCE MOP 60, the earth load on a pipe (in our case a liner) is computed by the equation shown below:

$$W_t = C_t B_c(\delta_{soil} B_c - 2c) \qquad \text{Eq. 8-8}$$

Where,
W_t earth load (lb/ft of pipe),
δ_{soil} soil unit weight (pcf),
B_c O.D. or outside span length of the liner (ft),
c soil cohesion (lb/ft^2).

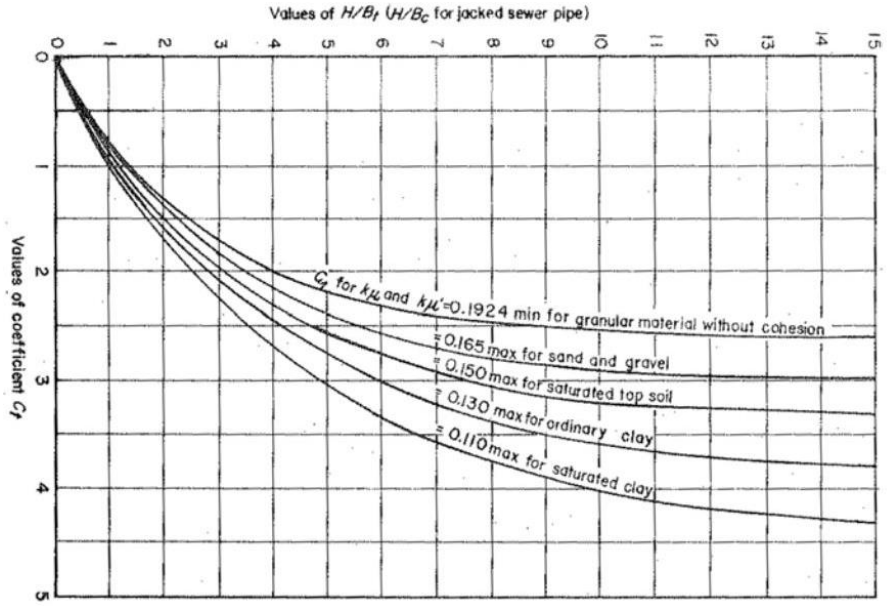


Figure 8-1 Diagram for coefficient Ct (Figure 9-13 in ASCE MOP 60).

The value of H used in the above Figure 8-1 is the cover depth in feet measured from the top of the ground or roadway surface to the top of the pipe.

In lieu of actual testing for the value of cohesion in the surrounding soil, Table 9-2 in the ASCE MOP 60 gives recommended conservative safe values for the coefficient of cohesion for various soils. It is repeated below as Table 8-1.

Table 8-1 Recommended Safe Values of Cohesion

Material	lb/ft^2
Clay, very soft	40
Clay, medium	250
Clay, hard	1,000
Sand, loose dry	0
Sand, silty	100
Sand, dense	300

Per the ASCE MOP 60, an analysis of the Figure 8-1 for computing C_t indicates that for very high values of H/B_c, the coefficient C_t approaches the limiting value of $1/(2K\mu')$. K being the ratio of the active horizontal pressure at any point in the fill to the vertical pressure which causes the active horizontal pressure, and μ' being the coefficient of sliding friction between the fill material and the sides of the ditch. The MOP 60 states that when the tunnel (culvert being lined) is very deep and the size of the liner relatively small, the load on the tunnel can be calculated readily by using this limiting value of C_t. Therefore, the maximum earth load that the liner is likely to experience over its service life, P_E, is estimated to be as follows:

$$C_t = \frac{1-e^{-2K\mu'\frac{H}{B_c}}}{2K\mu'} \qquad \text{Eq. 8-9}$$

$$P_E = C_t(\delta_{soil}B_c - 2c)/144 \qquad \text{Eq. 8-10}$$

Where,

P_E earth load acting on the horizontal soil plane at the top of the pipe (psi).

B_c substitute H for B_c when it is less than the span of the culvert (ft)

When the groundwater is above the top of the culvert, the portion of the cover that is below the phreatic surface (water table) will need to be adjusted to reflect the buoyant weight of the soil rather than its dry density. And the external hydrostatic pressure (P_W) is then separately added to the culvert's dead load (P_D).

$$P_E = [(C_tB_c - H_w)\delta_{soil} + H_w(\delta_{soil} - 62.4)]/144 \qquad \text{Eq. 8-11}$$

$$P_w = 0.433\ (H_w + H_r) \qquad \text{Eq. 8-12}$$

$$P_D = P_E + P_W \qquad \text{Eq. 8-13}$$

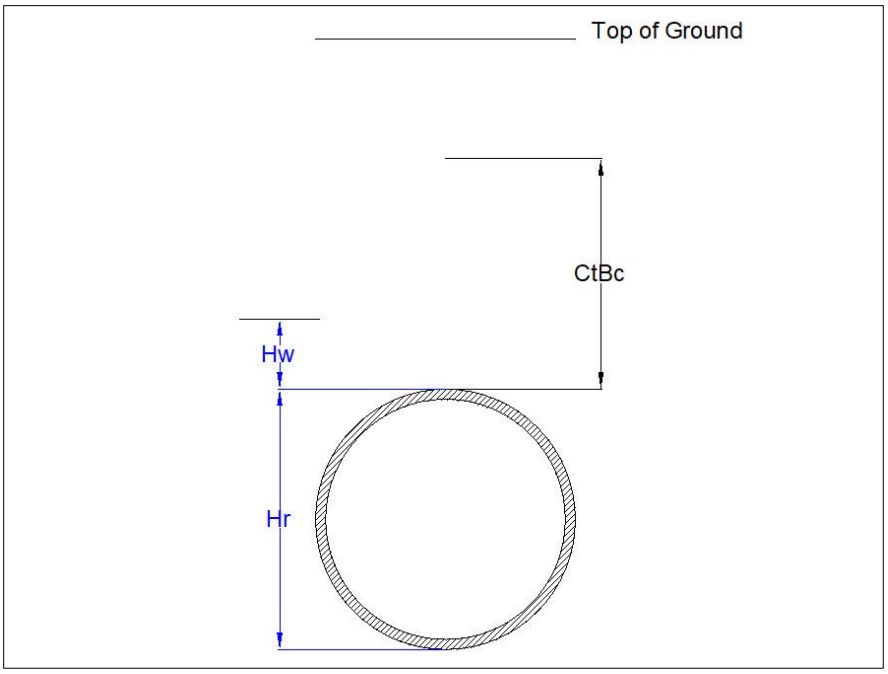


Figure 8-2 Dead loads acting on pipe.

P_w external hydrostatic pressure acting on the pipe (psi),
H_w height of the groundwater above the top of the pipe (ft),
H_r height of the vertical dimension of the pipe (ft).
C_tB_c height of soil prism acting on liner (ft).

Note that when the water table is below the bottom of the pipe both H_w and H_r are set to zero. If the water table is at the top of the pipe, H_r is set to the vertical height of the pipe.

8.2. Design for Liner Thickness Using Polymeric and Cementitious Materials

Any proposed design methodology for a rigid, cementitious material or a flexible, polymeric material to produce a pipe within a pipe to be fully structural on its own requires recognizing the current state of the stresses in the existing soil-structure interaction system, the differences in the types of loading that can come onto the new liner, and the liner's load response behavior.

Moore (2013) established in his study of cementitious liners that the mode of failure is brittle fracturing due to circumferential bending and stated that they are not susceptible to buckling. He did not say that the liner had to perform as a rigid structure. He showed both a rigid structure design and a semi-rigid structure design using cementitious materials. The semi-rigid structure carried significantly more load before fracturing and was substantially thinner. It is recommended that this semi-rigid design approach be taken. Designing for the thinnest wall section that offers the needed structural performance will yield such a structure that has some ductility to it.

The maximum pipe span in the current study was 71 inches. Existing installations of cementitious SAPL's up to 156 inches in diameter in highway and railway live load applications have been in the ground for up to ten years at present and are performing satisfactorily. The latter installations have even been validated by third-party engineering firms with FEM design and follow-up field measurements using a version of the equations for a thin wall buried ring structure herein. The equations were found to be conservative. There is no such information found on the polymeric structures. Therefore, early adopters of the equations presented herein should consider backing up these equations with FEM when designing for pipes above 120 inches in diameter until they have confirmed the reliability of the calculations in further research.

8.2.1. Cementitious Spray Applied Liner Design Procedure

For the cementitious materials there was no design method given in the AASHTO LRFD Bridge Design Specification that could be easily taken and adapted for this project. Darabnoush Tehrani (2020) found that a modified Iowa equation for deflection of buried pipes gave a suitable enough solution to be used for circular pipe shapes. Limiting the predicted deflection to 1.0 percent or less he stated provided a safe estimate against cracking of the cementitious liner. This equation (the modified Iowa equation) will not accommodate pipe-arch shapes. Therefore, a mechanical analysis of a thin-walled ring structure was formulated to analyze the critical top curved beam element to the load coming onto the circular pipe structure, along with the bottom curved beam element for pipe arch culverts. This analysis zooms in on the critical crown or invert locations identifying the impact of thrust and bending stresses generated by the dead and live loading conditions acting thereon based upon the distributional effects of the live loading at the surface and the depth of cover.

The following design procedure is recommended for cementitious liner systems with the intent to replace the structural performance offered by the existing culvert pipe material for the site-specific conditions of a new pipe within a pipe (liner) installed without excavation. The solution, further described in the design example section and validated with the soil box testing, requires beginning with an initial assumed wall thickness and using the equations below solving for the stress at the crown or invert of the liner. If the solution does not meet the requirement of Eq. 8-15, a new estimated wall thickness is tried. The process is repeated until the stress in the crown or invert meets the requirements in Eq. 8-15. For cementitious liners, this will be either its compressive strength or its flexural strength.

Step 1.

Choose an initial wall thickness to begin the analysis. It is suggested that the minimum wall thickness be 1.00 inch. It is further recommended that on host pipes that have internal projections, such as fasteners in a steel plate corrugated metal pipe, that the minimum wall thickness be chosen to provide a minimum cover over these projections (i.e., the bolts or fasteners) of 0.50 inches (equation 8-14). Typically, it has been found that the bolts used to join the 6"x2" corrugated metal pipe shapes protrude

between 1.00 and 1.25 inches. The initial wall thickness at the start of the iterative design process shall be the greater of these two values.

$$t_{initial} = h_{projection} + 0.50 \quad \text{, 1.0 inch minimum} \qquad \text{Eq. 8-14}$$

Step 2.

Using the starting thickness from Step 1, calculate the maximum stress for the liner in the circular or pipe-arch geometry using the AASHTO LRFD service limit state for the live loading specified on the project. The negative sign for the thrust represents compression in the liner and the positive sign on the moment portion of the equation reflects tension. The net stress at the crown must satisfy Eq. 8-15. Eq. 8-16 is for thin-walled rings where the ratio of $r/t \geq 10$. Eq. 8- and Eq. Eq. 8-18 estimate the thrust and bending moment at the center of the circular arc under investigation. These two equations are for arc elements modeled as a circular beam element with the ends being pinned as opposed to fixed. By focusing a critical arc element this solution is suitable for circular or pipe-arch shaped culverts.

$$\sigma_{CS} \leq \sigma_{crown} \leq \sigma_{flex} \qquad \text{Eq. 8-15}$$

Where,

$$\sigma_{crown} = -\frac{T}{A} + \frac{M \cdot c}{I_{SAPL}} \qquad \text{Eq. 8-16}$$

$$T_{service} = 0.8323(\gamma_{EV} P_E + C_L \gamma_{LL} P_L) r + P_W \qquad \text{Eq. 8-17a}$$

$$T_{strength} = 0.8323(\gamma_{EV} \eta_{EV} \eta_R P_E + C_L \gamma_{LL} \eta_{LL} \eta_R P_L) r + \gamma_{WA} P_W \qquad \text{Eq. 8-17b}$$

$$M_{service} = 0.0062 C_L \gamma_{LL} P_L r^2 \qquad \text{Eq. 8-18a}$$

$$M_{strength} = 0.0062 C_L \gamma_{LL} \eta_{LL} \eta_R P_L r^2 \qquad \text{Eq. 8-18b}$$

Where,

σ_{crown} the normal stress (psi),
σ_{CS} the compressive stress strength of the liner material (psi),
σ_{flex} the flexural stress strength (modulus of rupture) of the liner material (psi),
T thrust in liner (lb/in.),
M moment (in.-lb/in.),
I_{SAPL} area moment of inertia of the liner wall section ($in.^4/in.$),
c distance from the centroid of the liner pipe wall profile to the interior wall surface (in.),
P the vertical pressure being applied to the horizontal soil plane at the top of the pipe as a result of the live load and earth loads (psi)
r the top radius of the liner structure measured to the centroid of the liner's profile (in.),

t wall thickness of the liner (in.),
A area of the cross-section of the proposed liner per linear inch (in.^{2}/in.),
C_L live load distribution coefficient (in.), is equal to l_w / $S \leq 1.0$,
γ_{EV} load factor for soil prism load, 1.30,
γ_{WA} load factor for groundwater load, 1.0
γ_{LL} load factor for live load, 1.00 for service and 1.75 for strength
η_{EV} load modifier for soil prism load, use 1.0 per Article 1.3.2 of the BDS,
η_R load modifier for redundancy, 1.0 for strength limit state under live loads
η_{LL} load modifier for live load, use 1.0 per Article 1.3.2 of the BDS.

When the profile of the liner follows the corrugation profile of the host pipe, the moment of inertia of the SAPL, I_{SAPL}, can be calculated using Eq. 8-19 below for the designer's estimated geometry of the finished liner. Alternatively, the moment of inertia can be estimated by filling the valleys of the corrugations and then adding the proposed design wall thickness above the crests of the corrugations without taking credit for the filling of the corrugations. This latter alternative can be treated as a uniform wall thickness where the moment of inertia would be $t^3/12$ (with t being the height of the liner above the crests of the corrugations) and is the most conservative value for I.

The moment of inertia for a corrugated profile (Blodgett, 1934) where the liner will follow the profile of the pipe can be estimated using the Eq. 8-19. This equation is not used for designs where the liner material is used to first fill the valleys of the corrugations and then a specified thickness is applied above the crests of the corrugations. Figure 8-3 illustrates cross-section of 1.0-inch-thick SAPL in soil box testing.

$$I = C_5 \cdot b \cdot t^3 + C_6 \cdot b \cdot d^2 \cdot t \qquad \text{Eq. 8-19}$$

Where:
b *width of one cycle of the corrugation profile, in.*
d *depth of the corrugation, in.*
t *thickness of the liner, in.*
K *e/d,*
e *pitch of the corrugation (distance from ridge to ridge), in.*
a the acute angle which the tangent makes with the neutral axis, radians,
C_5 $= \frac{(6\cdot\alpha+3\cdot\sin 2\alpha+8\cdot\sin\alpha)g^2+4\cdot\sin\alpha}{12K}$, a constant,
C_6 $= \frac{(K\cdot\tan\alpha-2)}{4\cdot exsec\,\alpha}$, a constant.

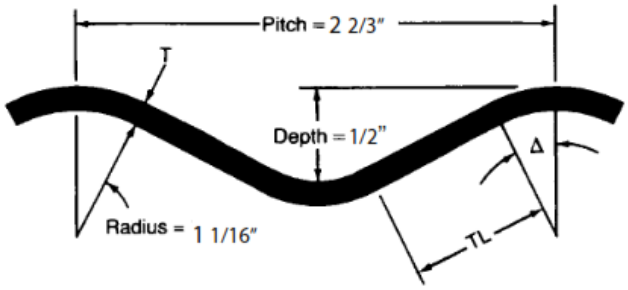


Figure 8-3 Typical corrugation profile showing tangent angle.

The tangent angle α is in radians. The tangent angle, Δ, shown in Figure 8-3, is in degrees (Corrugated Metal Pipe Handbook).

8.2.2. Sample Calculations of a Cementitious Liner

To demonstrate the design procedure and compare the results to the testing done in the soil box, an example is given below for an existing 60-inch diameter circular corrugated metal pipe having a corrugation profile of 2 – 2/3 by 1/2. The cover over the pipe is 2.0 feet. At this cover depth, the liner is subject to the AASHTO design truck moving transverse to the span of the culvert. This example will also use the 85% standard proctor density of the soil (assumed to be 120 lb/bf) without groundwater as was done in the soil box testing. The sandy material is cohesionless.

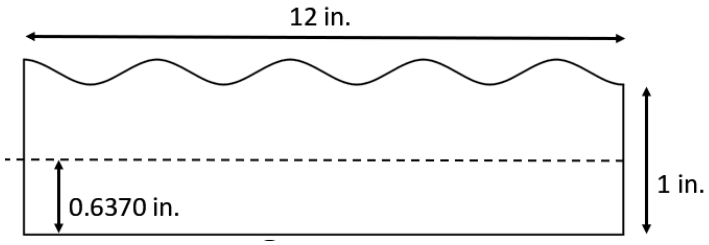


Figure 8-4 Cross-section on 1.0-inch-thick liner in soil box testing.

Following the guidance given in step 1 of the proposed design procedure, an initial wall thickness of 1.00 inch after corrugations were filled was chosen to begin the analysis. The shape of the liner geometry in the soil box testing is shown in Figure 8-4. Using CAD to graphically solve for the location of the centroid of the profile was shown to be 0.6370 in. from the inside face of the lined pipe. The graphically determined moment of inertia was found to be 0.1814 $in.^4$ /in. (see Appendix A)

The modulus of elasticity of the Standard Cement geopolymer concrete used in this example determined by ASTM C469 is given to be 3,690,000 psi. The compressive strength, σ_{cs}, is 8,390 psi, and the modulus of rupture (or flexural strength, σ_{flex}) is 1,665 psi. These values were provided by Standard Cement from their third-party testing results. When calculations are being made before a material supplier is known it is recommended to use 3,600,000 psi for the modulus of elasticity, and 8,000 psi for

the compressive strength, and 1,200 psi for the flexural strength, respectively in the calculations.

At 2.0 feet of cover, l_w is equal to 37.6 inches (10 + 1.15 ·24) and w_w calculates to be 51.2 inches (20+1.15·(24)+(0.06·60)). The ASSHTO truck service live load calculated using Eq. 8-1 is 12.4 psi.

Using Eq. 8-10 and a C_t value of 0.4 obtained from Figure 8-1:

$$P_E = \frac{C_t(\delta_{soil}B_c - 2c)}{144} = \frac{0.4(120 \cdot 2 - 2 \cdot 0)}{144} = 0.67\ psi \qquad \text{Eq. 8-10}$$

$T_{service}$ and $M_{service}$ are then calculated as follows:

$$T_{service} = 0.8323(\gamma_{EV}P_E + C_L\gamma_{LL}P_L)r + P_W = 0.8323\left(1.0 \cdot 0.67 + \left(\frac{37.6}{60} \cdot 1.0 \cdot 12.4\right)\right)30 = 210.8\ Lbs \qquad \text{Eq.8-17a}$$

$$M_{service} = 0.0062C_L\gamma_{LL}P_L r^2 = 0.0062\left(\frac{37.6}{60}\right) \cdot 1.0 \cdot 12.4 \cdot 30^2 = 43.4\ in - lbs \qquad \text{Eq.8-18a}$$

Substituting into equation 8-16 for the 1.00-inch liner, the service load stress is:

$$\sigma_{crown} = -\frac{210.8}{1.0} + \frac{43.4 \cdot 0.637}{0.1814} = -58.5\ psi \qquad \text{Eq. 8-16}$$

This net stress level satisfies equation 8-12 for the service condition as is shown below. Therefore, the 1.00" thick liner is sufficient for the service condition as no cracking should occur if the net inner stress level is compressive.

$$-8390\ psi \leq -58.5\ psi \leq 1665\ psi \qquad \text{Eq. 8-15}$$

The above resultant negative stress level indicates that the inner wall surface of the liner is in compression at the total applied service loading of 13.3 psi at the top of the pipe. The data obtained from the soil box testing presented below in Table 8-4 shows that at 13.3 psi vertical pressure on the top of the host pipe showed the stress in the crown of the liner was -15.4 psi (calculated from the strain measurements) which is in agreement with the above solution; both in the relative magnitude of the stress level and the lack of a significant moment at that point.

Checking the proposed 1.00-inch liner thickness for the strength design condition:

$$T_{strength} = 0.8323(\gamma_{EV}\eta_{EV}\eta_R P_E + C_L\gamma_{LL}\eta_{LL}\eta_R P_L)r + \gamma_{WA}P_W = 0.8323\left((1.3 \cdot 1.0 \cdot 1.05 \cdot 0.67) + \left(\frac{37.6}{60} \cdot 1.75 \cdot 1.0 \cdot 1.0 \cdot 12.4\right)\right)30 + 0 = 362.4 \text{ lb} \quad \text{Eq. 8-17b}$$

$$M_{strength} = 0.0062C_L\gamma_{LL}\eta_{LL}\eta_R P_L r^2 = 0.0062\left(\frac{37.6}{60}\right)1.75 \cdot 1.0 \cdot 1.00 \cdot 12.4 \cdot 30^2 = 75.9\ in.-lb \quad \text{Eq. 8-18b}$$

$$\sigma_{crown} = -\frac{T}{A} + \frac{M \cdot c}{I_{SAPL}} = -\frac{362.4}{1.0} + \frac{75.9 \cdot 0.637}{0.1814} = -95.9\ psi \quad \text{Eq. 8-16}$$

$$-8390\ psi \leq -95.9\ psi \leq 1665\ psi \quad \text{Eq. 8-15}$$

Thus, the 1.00-inch-thick liner also meets the strength design condition. Its net stress level of -98 psi is in reasonable agreement with the -61.6 psi value given below in Tables 8-2 through 8-4 for the fully factored load of 23.4 psi at the top of the pipe.

Table 8-2 Soil Box Pipe Deformation (in.)
(+ means outward and – means inward movement).

Type		(Springline) 90°	(Crown) 180°	(Invert) 0°
60" Circular	13.3 psi vertical pressure at top of pipe			
	Host Pipe	+0.45	-3.46	0
	1.00" Cementitious	+0.07	-0.1902	0
	2.00" Cementitious	+0.0975	-0.186	0
	3.00" Cementitious	-0.027	-0.066	0
47"x71" Arch	Host Pipe	+0.11	-3.500	+0.800
	1.00" Cementitious	+0.11	-0.4127	+0.11
	2.00" Cementitious	+0.26	-0.722	+0.02
	3.00" Cementitious	0.00	-0.44	0.00
60" Circular	23.4 psi vertical pressure at top of pipe			
	Host Pipe	+0.31	-4.171	0.00
	1.00" Cementitious	+0.1874	-0.47	0.00
	2.00" Cementitious	+0.1940	-0.400	0.00
	3.00" Cementitious	+0.070	-0.200	0.00
47"x71" Arch	Host Pipe	Did not reach	Did not reach	Did not reach
	1.00" Cementitious	+0.189	-0.7039	+0.340
	2.00" Cementitious	+0.050	-1.166	+0.04
	3.00" Cementitious	+0.48	-0.6582	+0.00

Table 8-3 Soil Box Hoop Strain Measurements,
(+ means tension and – mean compression)

Type		(Springline) 90°	(Crown) 180°	(Springline) 270°
60" Circular	13.3 psi vertical pressure at top of pipe			
	Host Pipe	0.000049	-0.000350	-0.000017
	1.00" Cementitious	-0.000096	-0.000004	-0.000048
	Host Pipe	-0.000015	-0.000586	+0.000270
	2.00" Cementitious	-0.000090	+0.000032	+0.000082
	Host Pipe	-	-	+0.000082
	3.00" Cementitious	-0.000130	+0.000042	-0.000094
47x71" Arch	Host Pipe	+0.000323	-0.000685	-0.000051
	1.00" Cementitious	-0.002490	+0.000054	-0.000431
	Host Pipe	+0.000123	-0.000959	+0.000505
	2.00" Cementitious	-0.000177	+0.000123	-0.000197
	Host Pipe	-	-	+0.000143
	3.00" Cementitious	-0.000284	+0.000068	-0.000183
60" Circular	23.4 psi vertical pressure at top of pipe			
	Host Pipe	+0.000151	-0.000800	-0.000129
	1.00" Cementitious	-0.000348	-0.000016	-0.000198
	Host Pipe	+0.000123	-0.000959	+0.000505
	2.00" Cementitious	-0.000177	+0.000123	-0.000197
	Host Pipe	-	-	+0.000143
	3.00" Cementitious	-0.000284	+0.000068	-0.000844
47"x71" Arch	Host Pipe	+0.000473	-0.000071	-0.000129
	1.00" Cementitious	-0.002092	+0.000071	-0.000844
	Host Pipe	+0.000103	-0.001213	+0.000451
	2.00" Cementitious	-0.001005	+0.000009	-0.000761
	Host Pipe	+0.000088	-0.001000	+0.000278
	3.00" Cementitious	-0.000215	+0.000019	-0.000890

Table 8-4 Soil Box Hoop Stress Measurements (psi),
(+ means tension and – mean compression)

Type		(Springline) 90°	(Crown) 180°	(Springline) 270°
60" Circular	13.3 psi vertical pressure at top of pipe			
	Host Pipe	1421	-10150	-493
	1.00" Cementitious	-369.6	-15.4	-184.8
	Host Pipe	-435	-16994	7830
	2.00" Cementitious	-346.5	123.2	315.7
	Host Pipe	-	-	2378
	3.00" Cementitious	-500.5	161.7	-361.9
47x71" Arch	Host Pipe	9367	-19865	-1479
	1.00" Cementitious	-9586.5	207.9	-1659.35
	Host Pipe	3567	-27811	14645
	2.00" Cementitious	-681.45	473.55	-758.45
	Host Pipe	-	-	4147
	3.00" Cementitious	-1093.4	261.8	-704.55
60" Circular	23.4 psi vertical pressure at top of pipe			
	Host Pipe	4379	-23200	-3741
	1.00" Cementitious	-1339.8	-61.6	-762.3
	Host Pipe	3567	-27811	14645
	2.00" Cementitious	-681.45	473.55	-758.45
	Host Pipe	-	-	4147
	3.00" Cementitious	-1093.4	261.8	-3249.4
47"x71" Arch	Host Pipe	13717	-2059	-3741
	1.00" Cementitious	-8054.2	273.35	-3249.4
	Host Pipe	2987	-35177	13079
	2.00" Cementitious	-3869.25	34.65	-2929.85
	Host Pipe	2552	-29000	8062
	3.00" Cementitious	-827.75	73.15	-3426.5

Table 8-5 Soil Box Hoop Strain Measurements,
(+ means tension and – mean compression)

Type		(Springline) 90°	(Crown) 180°	(Springline) 270°
60" Circular	13.3 psi vertical pressure at top of pipe			
	Host Pipe	0.0000510	-0.0008380	-
	0.25" Polymeric	-0.0000550	0.0000800	-
	Host Pipe	-	-0.0000060	-0.0000030
	0.50" Polymeric	-0.0000460	0.0001860	0.0000310

Type		(Springline) 90°	(Crown) 180°	(Springline) 270°
	Host Pipe	0.0000380	-0.0006810	-
	1.00" Polymeric	-0.0000430	0.0006670	-
47x71" Arch	Host Pipe	-	-0.0001700	-
	0.25" Polymeric	0.0000280	0.0001380	-0.0000040
	Host Pipe	0.0001220	-	0.0000010
	0.50" Polymeric	0.0001030	0.0020490	0.0002330
	Host Pipe	-0.0000010	-0.0003900	-0.0000350
	1.00" Polymeric	0.0000340	0.0009060	0.0000270
60" Circular	23.4 psi vertical pressure at top of pipe			
	Host Pipe	0.0002070	-0.0019170	-
	0.25" Polymeric	-0.0000920	0.0001960	-
	Host Pipe	-	-0.0000180	-0.0000080
	0.50" Polymeric	-0.0001480	0.0003370	0.0000360
	Host Pipe	0.0001030	-0.0013340	-
	1.00" Polymeric	-0.0001550	0.0014090	-
47"x71" Arch	Host Pipe	-	-0.0007680	-
	0.25" Polymeric	-0.0003140	0.0004070	-0.0000030
	Host Pipe	0.0003440	-	0.0001700
	0.50" Polymeric	0.0001810	-0.0004690	0.0002070
	Host Pipe	0.0000480	-0.0009230	-0.0000530
	1.00" Polymeric	0.0000410	0.0019330	0.0000680

Table 8-6 Soil Box Hoop Stress Measurements (psi)
(+ means tension and – mean compression)

Type		(Springline) 90°	(Crown) 180°	(Springline) 270°
60" Circular	13.3 psi vertical pressure at top of pipe			
	Host Pipe	1479	-24302	-
	0.25" Polymeric	-18.1065445	26.336792	-
	Host Pipe	-	-174	-87
	0.50" Polymeric	-15.1436554	61.2330414	10.2055069
	Host Pipe	1102	-19749	-
	1.00" Polymeric	-14.1560257	219.5830033	-
47x71" Arch	Host Pipe	-	-4930	-
	0.25" Polymeric	9.2178772	45.4309662	-1.3168396
	Host Pipe	3538	-	29
	0.50" Polymeric	33.9086197	674.5510851	76.7059067
	Host Pipe	-29	-11310	-1015
	1.00" Polymeric	11.1931366	298.2641694	8.8886673
	23.4 psi vertical pressure at top of pipe			

Type		(Springline) 90°	(Crown) 180°	(Springline) 270°
60" Circular	Host Pipe	6003	-55593	-
	0.25" Polymeric	-30.2873108	64.5251404	-
	Host Pipe	-	-522	-232
	0.50" Polymeric	-48.7230652	110.9437363	11.8515564
	Host Pipe	2987	-38686	-
	1.00" Polymeric	-51.0275345	463.8567491	-
47"x71" Arch	Host Pipe	-	-22272	-
	0.25" Polymeric	-103.3719086	133.9884293	-0.9876297
	Host Pipe	9976	-	4930
	0.50" Polymeric	59.5869919	-154.3994431	68.1464493
	Host Pipe	1392	-26767	-1537
	1.00" Polymeric	13.4976059	636.3627367	22.3862732

A second example of the design of a 1.0-inch-thick cementitious liner was made for the same 60-inch diameter pipe for a depth of cover equal to 12 feet to demonstrate the reduction in the soil prism loading due to what is in effect a tunnel loading for the liner. The density of the surrounding soil, a silty sand, determined through testing by the DOT to be 95% (standard proctor density). It measured 120 pcf. The soil shall be considered cohesionless. The water table is assumed to be below the pipe.

For single culverts, the effects of live load may be neglected where the depth of fill (cover) to the top of the pipe is more than 8.0 feet of cover and exceeds the span length (Article 3.6.1.2.6a).

Using Figure 8-1 and the ratio of H/B_t of 2.4 (12/5), C_t for a sand or gravel is found to be 1.6. The soil load at the top of the pipe is then calculated as:

$$P_E = \frac{C_t(\delta_{soil} B_c - 2c)}{144} = \frac{1.6(120 \cdot 5 - 2 \cdot 0)}{144} = 6.7\ psi \qquad \text{Eq.8-10}$$

$T_{service}$ and $M_{service}$ are then calculated as follows:

$$T_{service} = 0.8323(\gamma_{EV} P_E + C_L \gamma_{LL} P_L) r + P_W = 0.8323(1.0 \cdot 6.7 + 0)30 + 0 = 166\ Lbs \qquad \text{Eq.8-17a}$$

$$M_{service} = 0.0062 C_L \gamma_{LL} P_L r^2 = 0\ in - lbs \qquad \text{Eq.8-18a}$$

Substituting into equation 8-16 for the 1.00-inch liner:

$$\sigma_{crown} = -\frac{T}{A} + \frac{M \cdot c}{I_{SAPL}} = -\frac{-166}{1.0} + 0 = -166\ psi \qquad \text{Eq. 8-16}$$

$-8{,}390\ psi \leq -166\ psi \leq 1{,}665\ psi$, therefore Eq. 8-15 is satisfied for the service condition.

Checking the 1.00-inch thickness for the strength condition:

$T_{strength} = 0.8323(\gamma_{EV}\eta_{EV}\eta_R P_E + C_L\gamma_{LL}\eta_{LL}\eta_R P_L)r + \gamma_{WA}P_W = 0.8323(1.3 \cdot 1.0 \cdot 1.05 \cdot 6.7 + 0)30 + 0 = 228$ lb Eq. 8-17b

Substituting into equation 8-16 for the 1.00-inch liner:

$\sigma_{crown} = -\frac{T}{A} + \frac{M \cdot c}{I_{SAPL}} = -\frac{228}{1.0} = -228\ psi$ Eq. 8-16

$-8390\ psi \leq -228\ psi \leq 1665\ psi$, therefore Eq. 8-15 is satisfied for the strength condition.

The 1.00-inch-thick liner is acceptable for the 60-inch diameter CMP having a depth of cover equal to 12 feet.

Design example for cementitious liner in a 47" x 71" CMPA.

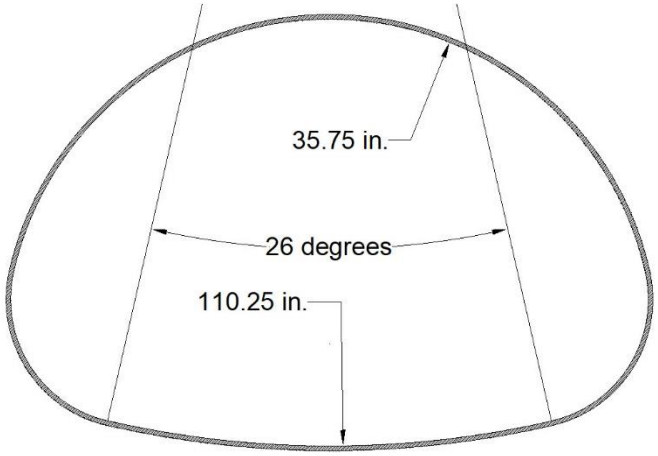


Figure 8-5 Key Dimensions of 47"x71" Pipe-arch

For a pipe-arch culvert the stress at both the top and bottom of the structure require analysis. The soil load and the live load calculated to be acting on the crown arc element of the pipe are reduced by the ratio of the radius of the top arc element divided by the radius of the bottom arc element. For the 47x71" pipe arch in the soil box testing these two radii are 35.75" and 110.25", respectively, and the resultant ratio is equal to 0.324 (35.75/110.25). In the case where the culvert is below the groundwater, the external hydrostatic head is not reduced by the ratio of the top radius to the bottom radius.

The same installation conditions (2.0 feet cover, no groundwater, AASHTO live load, etc.) will be used as that for the earlier 60-inch diameter pipe to show a comparison with the soil box test results.

Using Eq. 8-10 and a C_t value of 0.3 obtained from Figure 8-1:

$$P_E = \frac{C_t(\delta_{soil}B_c - 2c)}{144} = \frac{0.3(120 \cdot 2 - 2 \cdot 0)}{144} = 0.5\ psi \qquad \text{Eq. 8-10}$$

The service live loading on the subject liner is estimated to be 12.4 psi applied over a 37.6-inch length (i.e., L_w) as given in the earlier sample calculation above.

$T_{service}$ and $M_{service}$ are then calculated as follows:

Analyzing the 47x71" pipe arch at 2.0 feet of cover is done as follows:

Top Radius:

$$T_{service} = 0.8323(\gamma_{EV}P_E + C_L\gamma_{LL}P_L)r + P_W = 0.8323\left(1.0 \cdot 0.5 + \left(\frac{37.6}{71} \cdot 1.0 \cdot 12.3\right)\right)35.75 = 209\ Lbs \qquad \text{Eq. 8-17a}$$

$$M_{service} = 0.0062C_L\gamma_{LL}P_L r^2 = 0.0062\left(\frac{37.6}{71}\right) \cdot 1.0 \cdot 12.3 \cdot 35.75^2 = 51\ in - lbs \qquad \text{Eq. 8-18a}$$

Substituting into equation 8-16 for the 1.00-inch liner, the service load stress is:

$$\sigma_{crown} = -\frac{T}{A} + \frac{M \cdot c}{I_{SAPL}} = -\frac{209}{1.0} + \frac{51 \cdot 0.637}{0.1814} = -29.9\ psi \qquad \text{Eq. 8-16}$$

This net stress level satisfies equation 8-15 for the service condition as is shown below. Therefore, the 1.00" thick liner is sufficient for the service condition as no cracking should occur with the tensile net inner stress level being so small.

$$-8390\ psi \leq -29.9\ psi \leq 1665\ psi \qquad \text{Eq. 8-15}$$

Checking the strength condition in the top radius:

$$T_{strength} = 0.8323(\gamma_{EV}\eta_{EV}\eta_R P_E + C_L\gamma_{LL}\eta_{LL}\eta_R P_L)r) + \gamma_{WA}P_W = 0.8323\left((1.3 \cdot 1.0 \cdot 1.05 \cdot 0.5) + \left(\frac{37.6}{71} \cdot 1.75 \cdot 1.0 \cdot 1.0 \cdot 12.3\right)\right)35.75 + 0 = 359.7\ \text{lb} \qquad \text{Eq. 8-17b}$$

$$M_{strength} = 0.0062 C_L \gamma_{LL} \eta_{LL} \eta_R P_L r^2 = 0.0062 \left(\frac{37.6}{71}\right) 1.75 \cdot 1.0 \cdot 1.00 \cdot 12.3 \cdot 35.75^2 = 89.8\ in - lbs$$ Eq. 8-18b

$$\sigma_{invert} = -\frac{T}{A} + \frac{M \cdot c}{I_{SAPL}} = -\frac{359.7}{1.0} + \frac{89.8 \cdot 0.637}{0.1814} = -44.4\ psi$$ Eq. 8-16

$$-8390\ psi \leq -44.4\ psi \leq 1665\ psi$$ Eq. 8-15

The net stress strength in the top radius is compressive. Eq. 8-15 is satisfied for the strength condition in the top radius.

Bottom radius:

While it is not necessary for this example calculation, it is good practice to check the stress condition in the bottom radius of the arch as well. This requires adjusting the soil and live loads at the top of the pipe by the ratio of the top radius to the bottom radius (in this case 0.324). Also, the span divided by 2 will be substituted in the equations for *r*. Using the load ratio of 0.324, check the proposed 1.00-inch liner thickness for the strength design condition:

$$T_{strength} = 0.324 \cdot 0.8323(\gamma_{EV} \eta_{EV} \eta_R P_E + C_L \gamma_{LL} \eta_{LL} \eta_R P_L) r) + \gamma_{WA} P_W = 0.324 \cdot 0.8323 \left((1.3 \cdot 1.0 \cdot 1.05 \cdot 0.5) + \left(\frac{37.6}{71} \cdot 1.75 \cdot 1.0 \cdot 1.0 \cdot 12.3\right)\right) 35.5 + 0 = 116.5\ pounds$$ Eq. 8-17b

$$M_{strength} = 0.0062 C_L \gamma_{LL} \eta_{LL} \eta_R P_L r^2 = 0.324 \cdot 0.0062 \left(\frac{37.6}{71}\right) 1.75 \cdot 1.0 \cdot 1.05 \cdot 12.3 \cdot 35.5^2 = 30.2\ in - lbs$$ Eq. 8-18b

$$\sigma_{invert} = -\frac{T}{A} + \frac{M \cdot c}{I_{SAPL}} = -\frac{116.5}{1.0} + \frac{30.2 \cdot 0.637}{0.1814} = -10.3\ psi$$ Eq. 8-16

$$-8390\ psi \leq -10.3\ psi \leq 1665\ psi$$ Eq. 8-15

This net stress level of -10.3 psi satisfies equation 8-15 for the strength condition. Therefore, the 1.00" thick liner is sufficient for the strength condition as no cracking should occur if the net inner stress level is compressive.

In Table 8-3 the stress in the crown of the 47"x71" pipe-arch at the service loading of 13.3 psi was calculated from the strain measurement of +0.000054 in the soil box testing to be 208 psi: slightly in tension. No measurements were made on the invert of the pipe. For the limited testing that was performed in the soil box testing of both the circular and the pipe-arch shapes, it appears that the proposed equations agree with the measured stresses. More study, however, is recommended to refine Eq. 8-16, 8-17, and 8-18 over a larger database.

8.2.3. Development of Proposed Design Equations for Flexible Polymeric Materials

The above proposed equations are not being proposed for the flexible polymeric materials due to the viscoelastic behavior of these materials and the need to have the design model evaluate the effects of creep under long-term loading conditions.

The design equations presently in use for (thermoset) polymeric materials found in the ASTM F1216 design appendix X1 for the fully deteriorated design case (standalone pipe) follow a design for the installation of fiberglass pipe developed by the AWWA Committee C950 in 1980s. The F1216 design appendix was written for cured in placed pipe (CIPP). This equation was the predecessor to Eq. 8-26 below.

As the AWWA committee evolved and the fiberglass pipe design was put into a Manual of Practice (M45), it has undergone numerous improvements over the years; with today's version of this manual of practice (third edition, 2014) reflecting the state of the art for these pipe installations. Articles 12.12 and 12.15 of the AASHTO Design Manual already contain much of this latest iteration of the AWWA M45 design method. The project team simply needed to bring the updates to this report reflecting the liner being a pipe installed without excavation into the site-specific conditions of the host pipe it is meant to replace, and what loads are probable to come onto the new pipe (liner) after its installation.

It should be noted that the equations of Articles 12.12 and 12.15 do not address non-circular pipe shapes. Currently these liners would need to be designed using 3R2014 (Structural Design for Non-Circular Linings under Groundwater Pressure), which is the precursor to the ASCE Manual of Practice of Flexible Liners that is currently in pre-publication editing. While its focus is on the external hydrostatic load acting on the liner, the live and dead loads can be added as an equivalent external hydrostatic head acting on the liner. This design method looks at the long-term effects of the axial compression taken on by the liner, the circumferential shortening that will occur due to creep in these materials, and the stability against buckling of the liner in the area of the largest radius.

Given that sprayed in place polymeric liners will typically follow the corrugation profile, one will need to calculate the moment of inertia to use in the design equations presented herein. As presented earlier, the moment of inertia for a corrugated profile (Blodgett, 1934) where the liner will follow the profile of the pipe can be estimated using Eq. 8-19.

$$I = C_5 \cdot b \cdot t^3 + C_6 \cdot b \cdot d^2 \cdot t \qquad \text{Eq. 8-19}$$

Where:

b *width of one cycle of the corrugation profile, in.*

d *depth of the corrugation, in.*

t *thickness of the liner, in.*

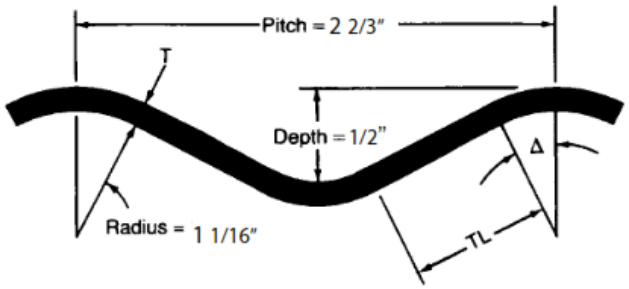


Figure 8-3 Typical corrugation profile showing tangent angle.

K *e/d,*

e *pitch of the corrugation (distance from ridge to ridge), in.*

a the acute angle which the tangent makes with the neutral axis, radians,

C_5 $= \frac{(6\cdot\alpha+3\cdot\sin 2\alpha+8\cdot\sin\alpha)g^2+4\cdot\sin\alpha}{12K}$, a constant,

C_6 $= \frac{(K\cdot\tan\alpha-2)}{4\cdot exsec\,\alpha}$, a constant.

The tangent angle α is in radians. The tangent angle, ∆, is given in the Corrugated Metal Pipe Handbook in degrees.

8.2.3.1 Circular Shapes

The equations below are the project team's refinements of the current M45 design method as it pertains to a liner installation in a circular pipe. As with new pipe installations, the allowable maximum localized distortion (i.e., deflection) of the liner (pipe) after its installation is to be limited based on the service requirements and overall stability of the soil-structure interaction system. Deflection must be within the material's limits (typically 5% of the diameter of the pipe), and at shallow bury depth the proper supporting of the surface improvements.

The recommended design for polymeric liner materials in a circular pipe is as follows:

Step 1.

Choose an initial wall thickness to begin the analysis. This shall be done using the following equations. The first equation represents a minimum dimension ratio of 50. The second equation is used on pipes that have projections, such a steel plate corrugated metal pipe. The intent is to have a minimum cover over the projection (bolt) of 0.50 inches. Use the greater of Eq. 8-18 and 8-19.

$$t_{initial} = D_i/50 \quad \text{Eq. 8-20}$$

Or

$$t_{initial} = h_{projection} + 0.50 \quad \text{Eq. 8-21}$$

Step 2.

Using the starting thickness from Step 1, calculate the maximum deflection for the liner using the AASHTO LRFD service condition for the live loading specified on the project.

$$\Delta_t \leq \Delta_A = 0.05 \cdot D_i \quad \text{Eq. 8-22}$$

$$\Delta_t = \frac{K_B(D_L.P_E + C_L \cdot P_L)D_o}{1000\left((E_{SAPL} \cdot I_{SAPL}/R^3) + 0.061M_s\right)} \quad \text{Eq. 8-23}$$

Where,

Δ_t total deflection of the pipe, expressed as a reduction of the vertical diameter (in.),
Δ_A total allowable deflection of liner, reduction in vertical diameter (in.)
D_i inner diameter of the liner (in.),
D_L deflection lag factor, a value of 1.0 is recommended for rehabilitation lining,
K_B bedding coefficient, a value of 0.083 is recommended for rehabilitation lining,
P_E Soil prism pressure (psi), use Eq. 8-10 above,
C_L live load distribution coefficient (in.), is equal to $l_w/S \leq 1.0$,
P_L service live load pressure as specified in Article 12.12.3.9 (psi),
D_o outside diameter of liner (in.),
E_{SAPL} short-term circumferential flexural modulus of liner material (ksi),
I_{SAPL} moment of inertia of liner profile per unit length of liner ($in.^4/in.$),
R radius of liner measured to the centroid of liner profile (in.),
M_s secant constrained soil modulus, as specified in Article 12.12.3.5 (ksi).

The deflection lag factor is recommended to be set at 1.0 because the long-term consolidation of the backfill has already occurred at the point in time that the liner is being installed and the likelihood of additional settlement in the pipe embedment zone is minimal going forward.

The value recommended for the bedding coefficient, K, is 0.083. This is the bedding coefficient for a pipe with bedding installed to the springline. It is recommended that further study be carried out to find if a lower value is warranted given the age of the installation and the surrounding soil being to the top of the pipe.

Equation 8-23 above is from the BDS Article 12.15.5.2. It is equation 12.15.5.2-1 therein. Equation 8-22 has been generated to show the recommended limit state of 5% deflection.

Note: If the existing host pipe has an existing ovality greater than 3% it is recommended that the design be based on the non-circular shaped pipe design to properly account for the buckling potential of the liner under the required design loading. Also, from a technical standpoint, the modulus of elasticity of the material used in equation 8-23 for the analysis should be the long-term modulus for the dead load and the short-term modulus for the live load. The long-term modulus of the proposed material is determined per flexural testing conducted over a minimum of 10,000 hours per ASTM D2990. If third-party testing is not available for a proposed material, a maximum value of 50% of the short-term value per D790 may be used. Equation 8-23 can be split up into two components to calculate the true net deflection when the live load is applied.

Step 3. Strength limit state for flexure

The long-term strain due to flexure (bending) shall satisfy:

$$\varepsilon_f \leq \phi_f S_b \qquad \text{Eq. 8-24}$$

$$\varepsilon_f = \gamma_{EV} D_f \left(\frac{t_t}{D}\right)\left(\frac{\Delta_A}{D}\right) \qquad \text{Eq. 8-25}$$

Where,

ε_f factored long-term strain due to flexure,
ϕ_f resistance factor for flexure, 0.90 (Table 12.5.5-1, BDS),
S_b long-term ring-bending strain for product under design per the manufacturer's testing (ASTM D5365),
γ_{EV} load factor for vertical pressure from dead load of earth fill, recommend 1.30 for rehab,
D_f shape factor (dimensionless) as specified in Table 12.12.3.10.2b-1 of the BDS,
t_t total wall thickness (in.),
D diameter to centroid of liner profile (in.),
Δ_A total allowable deflection of liner, reduction in vertical diameter (in.).

Note: The pipe stiffness needed to find the shape factor in Table 12.12.3.10.2b-1 is equal to 6.72 EI/r3.

Step 4. Strength limit state for global buckling

Factored buckling strain (in thrust) shall satisfy the following:

$$\varepsilon_{fb} \leq \phi_{bck} \varepsilon_{bck} \qquad \text{Eq. 8-26}$$

In which:

$$\varepsilon_{fb} = \frac{(\gamma_{WA}\eta_{EV}H_w\gamma_w+\gamma_{EV}\eta_{EV}P_ER_w+\gamma_{LL}\eta_{LL}C_LP_L)R}{1000E_{SAPL}A_g} \quad \text{Eq. 8-27}$$

$$\varepsilon_{bck} = \frac{1.2C_n(E_{SAPL}I_{SAPL})^{1/3}}{A_g \cdot E_{SAPL}}\left[\frac{\phi_s M_s(1-2v)}{(1-v)^2}\right]^{2/3} R_h \quad \text{Eq. 8-28}$$

In which:

$$R_h = \frac{11.4}{11+\frac{D}{12H}} \quad \text{Eq. 8-29}$$

Where:

ε_{fb} factored buckling strain demand (in./in.),
ϕ_{bck} resistance factor for global buckling as defined in Table 12.5.5-1, use 0.70
ε_{bck} nominal strain capacity for buckling (in./in.),
C_L live load distribution coefficient as specified in Article 12.12.3.7 (psi),
P_L live load pressure (psi),
R_w water buoyancy factor (0.67 minimum) = 1-0.33 (H_W/H),
η_{EV} load modifier for vertical pressure from dead load of earth fill on a buried structure per Article 1.3.2, recommend 1.0 for rehab,
γ_{EV} load factor for vertical pressure from dead load of earth fill, recommend 1.3 for rehab,
γ_w density of water per vertical foot of water, 0.433
γ_{WA} load factor for hydrostatic pressure, as per Article 3.4.1, 1.0
η_{LL} load modifier as specified in Article 1.3.2, as they apply to live loads on culverts,
γ_{LL} load factor for live load, as specified in Article 3.4.1,
R radius of liner to centroid of liner wall (in.),
C_n scalar calibration factor, 0.55,
ϕ_s resistance factor of the soil to account for variability, 0.9,
E_{SAPL} long-term circumferential flexural modulus (ksi),
A_g area of liner wall (in.^{2}/in.),
M_s constrained soil modulus as specified in Table 12.12.3.5-1 (ksi),
v Poisson's ratio of the soil, 0.3
H depth of fill over top of pipe (ft), maximum of two times the OD of the pipe,
H_w height of the groundwater measured from the top of pipe (ft).

It is suggested that the deflection limit typically be held to a five percent reduction of the vertical diameter which is common industry practice for flexible liners and in keeping with Article 12.15.4 of the BDS. However, if the pipe material manufacturer has third-party testing suggesting otherwise, the manufacturer's testing should govern. In the soil box testing, the polyurethane material placed in the 60-inch circular CMP exhibited initial cracking at 4.00%, 2.92%, and 3.53% for the 0.25-inch, 0.50 inch, and 1.00-inch-thick liners, respectively. In consultation with the tested

material manufacturer's engineering team, it was confirmed that they recommend a 5.0% deflection limit for their product. More study is required to determine if there was bonding between the host pipe and the liner which could have led to this failure of the liner prior to the manufacturer's recommended 5%.

One of the assumptions that must be made to use the above equations is that there is no bond between the liner and the host pipe. The desired design condition where the host pipe is no longer present would meet this criterion. The above equations for circular polymeric pipes have a long performance history with refinements being made as new lessons are learned in the field.

8.2.3.2. Non-Circular Pipe Shapes

Currently flexible liners of these types of materials are being designed using the French ASTEE 3R2014: Structural Design for Non-Circular Linings under Groundwater Pressure. This limit state design model evaluates the time dependent response of the polymeric liner to the loading using the current radii of the existing structure being lined. Most importantly, the design model looks at the long-term effects of the axial compression in the liner, the circumferential shortening that will likely occur due to creep, and the final buckling of the liner in the area of the largest radius (flattest arc element). This design model developed by Olivier Thepot is the result of empirical testing (research) and has been endorsed by John Gumbel, J C Boot, and Ian Moore, all pioneering researchers in the design of flexible close fit liners. Liners under a constant external hydrostatic loading are typically evaluated using the long-term modulus of the SAPL material while the short-term live loading condition is modeled using the short-term modulus of the SAPL material. It is proposed that live and dead loads other than groundwater can be treated as additional external hydrostatic loads. This design approach will be conservative.

A flexible liner inside a host pipe and exposed to external groundwater pressure can fail in two different ways. The first is by a material strength failure. The second, and more likely failure mechanism is buckling (i.e., excessive localized deflection). In this project the polymeric liner failed by a strength failure due to the deflection that occurred in the crown area due to the live loading applied. Therefore, it is recommended that the proposed liner be checked first for deflection performance followed by the design for buckling performance.

Checking for deflection performance:

$$\Delta_t \leq \Delta_A = 0.05 \cdot R_{top} \qquad \text{Eq. 8-30}$$

$$\Delta_t = \frac{P_L {R_{top}}^4}{384 \cdot E_{SAPL} \cdot I_{SAPL}} \qquad \text{Eq. 8-31}$$

Where:
R_{top} top radius of pipe, inches

If Eq. 8-22 is satisfied for the proposed wall thickness, the design can proceed for buckling performance.

While all circular pipes have what is called critical shape, not all non-circular pipes are of a critical shape. To use the equations proposed below, an existing structure's shape must first be checked to confirm it is critical (i.e., that failure will be by buckling).

Step 1. Non-circular pipe shape liner design

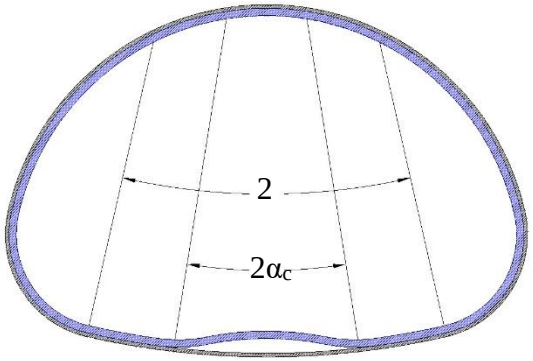


Figure 8-6 Pipe arch shape showing bottom arc angle.

The design of a non-circular shape pipe liner begins with selecting a liner thickness using either Eq. 8-20 or 8-21 above; whichever is greater. Following an initial wall thickness estimate, the designer must confirm that the existing pipe shape is a critical pipe shape. In the case of a pipe arch shaped culvert, Figure 8-6 shows the angle subtended by the bottom radius of the pipe arch as 2α. The critical angle α_{cr} equals half of the "blister" (i.e., lift) that forms just before buckling occurs. The critical angle is calculated as follows:

$$\alpha_{cr} = 1.55\Gamma_{\alpha,g}\frac{1}{k^{1/5}}\frac{t^{2/5}P^{1/5}}{R^{3/5}} \qquad \text{Eq. 8-32}$$

Where:

a half arc angle where blister develops, radians
a_{cr} calculated half blister angle just before buckling occurs, radians.
k deformation mode, *k* = 1 for a pipe arch shape
$\Gamma_{\alpha,g}$ amplification factor for the critical angle due to initial gap, for SAPL = 1
P perimeter of the lining, in.
t thickness of the liner, in.
R radius of the arc where the blister develops, in.

$$\frac{\alpha_{cr}}{\alpha} \leq 1.5 \qquad \text{Eq. 8-33}$$

If Eq. 8-29 is not verified, the lining will be sub-critical, and another method must be used such as finite element analysis to design the liner.

Step 2. Calculation of the design pressure p

The design pressure equals the external pressure exerted on the center of the blister on the bottom of the liner. This consists of the pressure of any groundwater and the soil and live loads acting on the top of the liner adjusted by the ratio of the top radius to the bottom radius of the pipe arch as shown before in the cementitious design calculations.

$$p = (0.433 \cdot H_w) + \frac{R_{top}}{R_{bottom}}(P_E + C_L \cdot P_L) \quad \text{Eq. 8-34}$$

Step 3. Calculation of the critical buckling pressure and deflection

The buckling pressure of a critical lining for an initial gap of 0 in. for a spray applied liner is given by the following equation:

$$p_{cr} = 0.60 E_{SAPL} \frac{t^{2.2}}{P^{2/5} R_{bottom}{}^{9/5}} \quad \text{Eq. 8-35}$$

Where:

H	height of cover above the top of the pipe, ft
H_w	height of any groundwater above the pipe invert, ft
R_{top}	top radius of the pipe arch, in.
R_{bottom}	bottom radius of the pipe arch, in.
δ_{soil}	density of the soil, lb/ft^3
C_L	live load distribution coefficient (in.), is equal to $l_w/S \leq 1.0$,
P_L	service live load pressure as specified in Article 12.12.3.9 (psi),
p_{cr}	buckling pressure of a critical lining, psi.
E_{SAPL}	modulus of the lining material, psi
P	perimeter of the lining, in.
t	thickness of liner, in.

Given the time dependent response of a flexible polymeric liner, the modulus, E_{SAPL}, is the long-term value for considering a continuous external hydrostatic pressure acting on the liner; but should be the short-term value when considering the live loading condition given its short duration.

The critical deflection d_{cr} equals the maximum deflection at the middle of the blister just before buckling. It is calculated as follows:

$$d_{cr} = 0.5\Gamma_{d,g} \frac{R_{bottom}}{k^{2/5}} \left(\frac{t^2 P}{(R_{bottom})^3}\right)^{2/5} \quad \text{Eq. 8-36}$$

Where:

$\Gamma_{d,g}$ amplification factor for the critical deflection due to initial gap, for SAPL = 1

Step 4. Calculation of the critical bending moment and the critical axial force

The critical bending moment is the maximum moment at the middle of the blister just before buckling.

$$M_{cr} = 0.1\Gamma_{M,g}\frac{E_{SAPL}(t)^3}{R_{bottom}} \quad \text{Eq. 8-37}$$

$$N_{cr} = 1.26 p_{cr} R_{bottom} \quad \text{Eq. 8-38}$$

Where:

$\Gamma_{M,g}$ amplification factor for the critical moment due to initial gap, for SAPL = 1

Step 5. Calculation of the maximum bending moment, axial force, and deflection under the design conditions

The bending moment is maximum at the middle of the blister and is calculated as follows:

$$M_u = \frac{m_b(p/p_{cr})M_{cr}}{1-(1-m_b)(p/p_{cr})^2} \quad \text{Eq. 8-39}$$

Where:

$$m_b = \frac{2.56(\alpha/\alpha_{cr})^2}{1+4.35(\alpha/\alpha_{cr})^5} \quad \text{Eq. 8-40}$$

$$N_u = \frac{p}{p_{cr}}N_{cr} \quad \text{Eq. 8-41}$$

and

$$d_s = d_{cr}\left[1 - \left(1 - \frac{p}{p_{cr}}\right)^{0.5}\right] \quad \text{Eq. 8-42}$$

Step 6. Check evaluated wall thickness for the limit state of stability.

The following condition must be verified:

$$p \leq \phi_{bck} p_{cr} \quad \text{Eq. 8-43}$$

Where:

ϕ_{bck} resistance factor to buckling, 0.5 is recommended.

The resistance factor of 0.5 is consistent with current industry practice using this design model to have a safety factor of 2.0.

Step 7. Check evaluated wall thickness for the limit state of strength.

The following condition must be verified:

$$\sigma_u \leq \phi_M \sigma_R \quad \text{Eq. 8-44}$$

$$\sigma_u = \sigma_{u,b} + \sigma_{u,d} \quad \text{Eq. 8-45}$$

Where,

$$\sigma_{u,b} = \frac{6M_u}{t^2} \quad \text{Eq. 8-46}$$

$$\sigma_{u,d} = \frac{N_u}{A} \quad \text{Eq. 8-47}$$

Where:

σ_R stress strength of material corresponding to 95% lower confidence limit, psi,

ϕ_M strength resistance factor for material, use 0.67 in absence of testing.

Step 8. Check evaluated wall thickness for the limit state of deflection.

The maximum long-term deflection must be less than the permissible long-term deflection. As this is a serviceability requirement, no resistance factor is applied. It is suggested that the permissible deflection for flexible polymeric liners be less than 3% of the straight section (flattest arc element). However, a different value may be used at the engineer's discretion. The check per Eq. 8-48 is as follows setting d_L equal to the value found by Eq. 8-49:

$$d_s \leq d_L \quad \text{Eq. 8-48}$$

$$d_{3.0\%} = \alpha \cdot R \cdot 0.03 \quad \text{Eq. 8-49}$$

8.2.4. Sample Calculations of a Flexible Polymeric Liner

8.2.4.1 Circular Polymeric Pipe Liner Example

To demonstrate the recommended design procedure for a circular pipe lining an example is given below for an existing 60-inch diameter circular corrugated metal pipe having a corrugation profile of 2 – 2/3 by 1/2. The cover over the pipe is 2.0 feet. The liner is subject to a highway live load. Using equation 8-20, an initial guess as to the minimum wall thickness of the liner calculates to be 1.20 inches (D_i / 50). Assuming the

material is sprayed on to follow the corrugation profile of the host pipe, the moment of inertia of the liner found graphically will be taken as approximately 0.0456.

The manufacturer of the polyurethane material used in this design has indicated in the past that it wants to limit the deflection to 5.0% (3.00 in.). The short-term flexural modulus is 735 ksi; and the long-term modulus is 529 ksi.

Because of the shallow cover depth, the constrained soil modulus value will be taken from the 85-Sn column for a soil Class I and Class II at 85% SPD. At 4.5 feet of depth (location of the springline), the value is 0.503 ksi.

Using equation Eq. 8-23:

Checking for deflection performance once the existing pipe is gone:

Using Eq. 8-10 and a C_t value of 0.4 obtained from Figure 8-1:

$$P_E = \frac{C_t(\delta_{soil}B_c - 2c)}{144} = \frac{0.4(120\cdot 2 - 2\cdot 0)}{144} = 0.7\ psi$$ Eq. 8-10

$\Delta_t = \frac{K_B(D_L\cdot P_E + C_L\cdot P_L)D_o}{1000\left((E_{SAPL}\cdot I_{SAPL}/R^3) + 0.061M_s\right)} = \frac{0.083\ (1.0\cdot(0.7) + (\frac{37.6}{60}\cdot 12.4))\cdot 60}{1000(\left(735\cdot\frac{0.0456}{29.4^3}\right) + (0.061\cdot 0.503))} = 1.3\ in.$, which is a deflection of 2.2%.

The short-term modulus was used in the above deflection check because the live load is a quick on and off-loading condition.

Therefore the 1.20 in. thickness is OK in the service check for deflection.

Checking the long-term strain due to flexure (bending):

$$\varepsilon_f = \gamma_{EV}D_f\left(\frac{t_t}{D}\right)\left(\frac{\Delta_A}{D}\right) = 1.3\cdot 5.5\left(\frac{1.2}{60}\right)\left(\frac{3}{60}\right) = 0.007$$ Eq. 8-25

$$\varepsilon_f \le \phi_f S_b = 0.9\cdot 0.013 = 0.012$$ Eq. 8-24

Therefore, the long-term strain due to the estimated deflection is acceptable.

Checking the 1.20-inch-thick liner for buckling at 2.0 feet of cover:

$$\varepsilon_{fb} = \frac{(\gamma_{WA}\eta_{EV}H_w\gamma_w + \gamma_{EV}\eta_{EV}P_ER_w + \gamma_{LL}\eta_{LL}C_LP_L)R}{1000E_{SAPL}A_g} = \frac{\left(0 + 1.30\cdot 1.0\cdot 0.7\cdot 1.0 + 1.75\cdot 1.0\cdot\frac{37.6}{60}\cdot 12.4\right)29.4}{1000\cdot 529\cdot 1.2} = 0.0007$$ Eq. 8-27

$$\varepsilon_{bck} = \frac{1.2C_n(E_{SAPL}I_{SAPL})^{1/3}}{A_{eff}E_{SAPL}}\left[\frac{\phi_s M_s(1-2v)}{(1-v)^2}\right]^{2/3} R_h =$$

$$\frac{1.2\cdot 0.55(529\cdot 0.0456)^{1/3}}{1.2\cdot 529}\left[\frac{0.9\cdot 0.503(1-2\cdot 0.3)}{(1-0.3)^2}\right]^{2/3}\left(\frac{11.4}{11+\frac{60}{12\cdot 2.0}}\right) = 0.0013\ in.per\ in. \qquad \text{Eq. 8-28}$$

Checking to see if Eq. 8-26 is satisfied:

$$\varepsilon_{fb} \le \phi_{bck}\varepsilon_{bck} \qquad \rightarrow \qquad 0.0007 \le 0.70 \cdot 0.0013 = 0.0009 \qquad \text{Eq. 8-26}$$

Therefore, the strength buckling limit state of Eq. 8-26 is satisfied by the 1.2-inch-thick liner.

8.2.4.2. Non-Circular Shape Pipe Design Example

To demonstrate the proposed non-circular design procedure for a pipe arch shape, an example is given below for an existing 47 x 71" corrugated metal pipe arch having a corrugation profile of 2 – 2/3 by 1/2. The cover over the pipe is 2.0 feet. The liner is subject to a highway live load (HL-93). There is no groundwater for this example. An initial estimate as to the minimum wall thickness of the liner was made of 1.0 inches. Assuming the material is sprayed on to follow the corrugation profile of the host pipe, the moment of inertia of the liner was calculated to be approximately 0.0456 in.^{4}/in.

Beginning with the check for deflection performance:

$$\Delta_t = \frac{P_L\cdot R_{top}^4}{384\cdot E_{SAPL}\cdot I_{SAPL}} = \frac{12.3\cdot 35.75^4}{384\cdot 735{,}000\cdot 0.0456} = 1.56\ inches \qquad \text{Eq. 8-31}$$

$$\Delta_t \le \Delta_A = 0.05 \cdot R_{top} = 0.05 \cdot 35.75 = 1.78\ inches \qquad \text{Eq. 8-30}$$

Therefore, the 1.0-in. thickness is good for the deflection performance.

The bottom radius arc element subtends an arc of 26.0°; α= 13.0°. The interior perimeter of the pipe-arch is 188.50 in. The bottom radius is 110.25 in., and the top radius is 35.6 in. Using Eq. 8-32 to solve for α_{cr}:

$$\alpha_{cr} = 1.55\Gamma_{\alpha,g}\frac{1}{k^{1/5}}\frac{t^{2/5}P^{1/5}}{R^{3/5}} = 1.55\cdot 1.0\frac{1}{1^{1/5}}\frac{1.0^{2/5}\cdot 188.5^{1/5}}{110.25^{3/5}} = 0.263\ rad.\ (15.0^\circ) \qquad \text{Eq. 8-32}$$

$\frac{\alpha_{cr}}{\alpha} = \frac{15.0}{13.0} = 1.2 \le 1.5$, therefore Eq. 8-33 is satisfied.

The loading on the bottom arc element is as follows:

$$p = (0.433\cdot H_w) + \frac{R_{top}}{R_{bottom}}(P_E + C_L\cdot P_L) = (0.433\cdot 0) + \frac{35.6}{110.25}\left(0.7 + \frac{37.6}{71}\cdot 12.3\right) = 2.3psi$$

Eq. 8-34

The critical pressure and deflection are as follows:

$$p_{cr} = 0.60 \cdot 735{,}000 \frac{1.0^{11/5}}{(188.5)^{2/5} \cdot (110.25)^{9/5}} = 11.5\ psi$$ Eq. 8-35

The short-term modulus was used in the above equation because the dominant load acting on the liner is the live load which is a short-term loading condition.

$$d_{cr} = 0.5\Gamma_{d,g} \frac{R_{bottom}}{k^{2/5}} \left(\frac{t^2 P}{(R_{bottom})^3} \right)^{2/5} = 0.5 \cdot 1.0 \frac{110.2}{1^{2/5}} \left(\frac{1.0^2 \cdot 188.5}{(110.25)^3} \right)^{2/5} = 1.6\ in.$$ Eq. 8-36

Calculating the critical bending moment and critical axial force:

$$M_{cr} = 0.1\Gamma_{M,g} \frac{E_{SAPL}(t)^3}{R_{bottom}} = 0.1 \cdot 1.0 \frac{735000 \cdot 1^3}{110.25} = 666.7 \text{ in.-lb}$$ Eq. 8-37

$$N_{cr} = 1.26 p_{cr} R_{bottom} = 1.26 \cdot 11.5 \cdot 110.25 = 1597.5\ lb.per\ in.$$ Eq. 8-38

Calculating the maximum bending moment and maximum axial force:

$$M_u = \frac{m_b (p/p_{cr}) M_{cr}}{1-(1-m_b)(p/p_{cr})^2} = \frac{0.62(2.3/11.5)666.7}{1-(1-0.62)(2.3/11.5)^2} = 83.9\ in.-lb$$ Eq. 8-39

$$m_b = \frac{2.56(\alpha/\alpha_{cr})^2}{1+4.35(\alpha/\alpha_{cr})^5} = \frac{2.56(13/15.0)^2}{1+4.35(13/15.0)^5} = 0.62$$ Eq. 8-40

$$N_u = \frac{p}{p_{cr}} N_{cr} = \frac{2.3}{11.5} 1597.5 = 319.5\ lb.per\ in.$$ Eq. 8-41

Checking for the limit state of stability (Eq. 8-43):

$p \le \phi_{bck} p_{cr} \rightarrow 2.3 \le 0.5 \cdot 11.5 = 5.75\ psi$ Therefore, the condition of stability is verified.

Checking for the limit state of strength (Eq. 8-44):

$$\sigma_{u,b} = \frac{6M_u}{t^2} = \frac{6 \cdot 83.9}{1.0^2} = 503.7\ psi$$ Eq. 8-46

$$\sigma_{u,d} = \frac{N_u}{A} = \frac{319.5}{1} = 319.5\ psi$$ Eq. 8-47

$$\sigma_u = \sigma_{u,b} + \sigma_{u,d} = 503.7 + 319.5 = 823.2 \text{ psi}$$ Eq. 8-45

$\sigma_u \le \phi_M \sigma_R \rightarrow 823.2 \le 0.67 \cdot 14000 = 9333\ psi$ Therefore, the condition of strength is verified per Eq. 8-44.

Checking for the limit state of deflection (Eq. 8-48):

$$d_{cr} = 0.5\Gamma_{d,g}\frac{R_{bottom}}{k^{2/5}}\left(\frac{t^2 P}{(R_{bottom})^3}\right)^{2/5} = 0.5 \cdot 1.0 \cdot \frac{110.25}{1^{2/5}}\left(\frac{1.0^2 \cdot 188.5}{(110.25)^3}\right)^{2/5} = 1.6\ in. \quad \text{Eq. 8-36}$$

$$d_s = d_{cr}\left[1 - \left(1 - \frac{p}{p_{cr}}\right)^{0.5}\right] = 1.6\left[1 - \left(1 - \frac{2.3}{11.5}\right)^{0.5}\right] = 0.17\ in. \quad \text{Eq. 8-42}$$

$$d_{3.0\%} = \alpha \cdot R \cdot 0.03 = 0.227 \cdot 110.25 \cdot 0.03 = 0.75\ in. \quad \text{Eq. 8-49}$$

$d_s \leq d_L \quad \rightarrow \quad 0.17 \leq 0.75$, deflection is within the suggested limit of 3% Eq. 8-48

The proposed 1.00-inch-thick liner is acceptable for the design conditions given for this example. The designer could choose a thinner liner thickness and rerun the calculations to find the optimal thickness for the lining.

The soil box testing on this project did not directly capture the stress (or strain) on the bottom arc elements of the lined culverts. Therefore, the above calculated stresses in the liner on the bottom of the pipe will require more study to confirm the accuracy of the calculated stresses. However, given that the soil and live loads were shown as additional external hydrostatic loads for purposes of using the proposed design equations, the calculated stresses should be conservative.

8.3. Summary and Recommendations

The objective of this portion of the project was to develop a set of equations for sprayed in place flexible, polymeric materials and a set of equations for sprayed in place cementitious materials. These sets of equations are for installing spray applied liners within the existing pipes given their current in situ conditions to perform, after lining, as standalone pipes in the site-specific embedment soil.

The design method presently in use for polymeric materials consists of following the design appendix X1 of the ASTM Standard F1216. The fully deteriorated design case (standalone pipe) follows an old design used for the installation of fiberglass pipe by the AWWA Committee C950 in 1987. It calculated the allowable buckling strength of the liner. It did not address the liner providing any resistance to bending (deflection) as some may have thought. The resistance to bending would come in equation 8-24 given above, which is the Spangler or modified Iowa equation. As the AWWA committee evolved and the fiberglass pipe design was put into a Manual of Practice (M45), it has undergone numerous improvements over the years and has become the state of the art for these type of pipe installations.

For the flexible, polymeric materials it was found that Articles 12.12 and 12.15 of the AASHTO Bridge Design Construction Specifications already contained much of the latest iteration of the AWWA M45 design method for thermoset plastic materials. However, as it has been drafted from the standpoint of an open cut excavation installation, it needed to be streamlined and defined in terms required to address a

pipe being installed using a trenchless method into the site-specific conditions of an existing pipe; and what loads were probable to come onto the new pipe (liner) after its installation. This mission was accomplished by showing the relevant current M45 design equations in this document along with definitions of the variables with changes given that would be appropriate to the lining process over a new direct bury process. More study is needed to determine a more accurate bedding coefficient for a mature soil-structure interaction system. Using the 0.083 herein will be conservative.

Unlike the design equations presented herein for the cementitious liners, the equations of Articles 12.12 and 12.15 cannot be readily adapted to address non-circular pipe shapes such as pipe arches. Further, the single size testing of the pipe arch in the current project did not provide enough information to predict the compressive performance of a thermoset resin as a standalone pipe in this geometry. Currently flexible liners of these materials are being designed using the French ASTEE 3R2014: Structural Design for Non-Circular Linings under Groundwater Pressure. The proposed design equations in this document have conservatively assumed that the soil and live loads can be considered as additional external hydrostatic loads to predict the stresses and deflection that will occur in the critical arc element.

For the cementitious materials there was no design method given in the AASHTO Design Manual that could be easily taken and adapted by the research team. Darabnoush Tehrani (2020) found that a modified Iowa equation for deflection of buried pipes gave a suitable enough solution to be used for circular pipe shapes. Limiting the predicted deflection to 1.0 percent or less he stated provided a safe estimate against cracking of the cementitious liner. Again, this equation (the modified Iowa equation) will not accommodate pipe-arch shapes. Therefore, a mechanical analysis of a thin-walled ring structure was formulated to analyze the critical top curved beam element to the load coming onto the circular pipe structure, along with the bottom curved beam element for pipe arch culverts. This analysis zooms in on the critical crown location identifying the impact of thrust and bending stresses generated by the dead and live loading conditions acting thereon based upon the distributional effects of the live loading at the surface and the depth of cover. The 60-inch circular pipe example using the equation presented herein appeared to agree well with the experimental testing contained within this project as stated earlier. The predicted stress level in the liner corresponded well with the strain measurements in the soil box testing.

While the constraints of this project (corrugation profile) and additional testing did not allow the project team to present scientific evidence that the best approach to applying these liners is to fill the valleys in corrugated pipes first and then calculate a minimum liner thickness above the crests of the corrugation profile, it must be stressed that a wall thickness design is useless if the geometry of the finished liner used in the design phase cannot be practically constructed by the contractor in the field and verified by the construction observation personnel. Uniformity of the liner's thickness around the circumference is necessary to ensure the in-ground performance of the liner is achieved. In Chapter 4 it was presented that as the corrugation profile becomes larger, the ability of the contractor to apply a uniform thickness, either mechanically

or by hand spraying, becomes challenging. And the field verification of the liner thickness on the corrugated profile becomes even more challenging. This issue was clearly demonstrated by the results the Delaware DOT obtained on their project which were measured by the project team in Chapter 7. The contractor claimed to have applied 2.0 inches when, in fact, he had applied only about half of that amount.

Further, it can be seen herein that filling the valley of the corrugations and then applying the calculated thickness of the liner increases the moment of inertia of the cross-section which in turn diminishes the magnitude of the bending moment induced in the liner by the live loading. In the example calculation presented the thrust (compression) in the liner became the dominant stress at the interior wall surface of the liner.

More testing is recommended to further confirm the validity of the equations for the cementitious liners proposed herein over a much larger number of installations. It is also recommended that this testing be conducted on existing installations to reflect the actual support provided by the surrounding soil (constrained soil modulus).

Appendix 8-A: Moment of Inertia Calculation

Table 8-A 1. Moment of inertia (3.0 in. cementitious SAPL – corrugation filled).

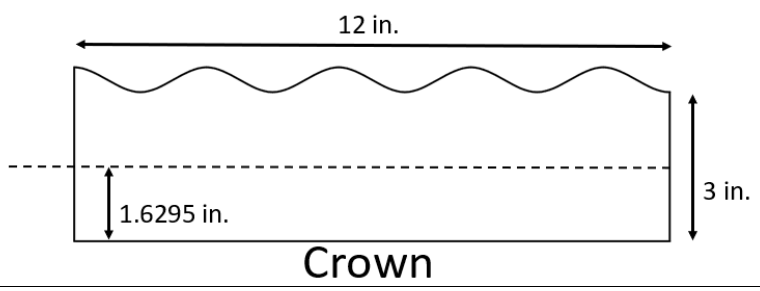
3.0 in. Cementitious SAPL	
---------- REGIONS ----------	
Area	38.9963
Perimeter	31.4585
Bounding box	X: -5.9974 -- 6.0026, Y: -1.6295 -- 1.8705
Centroid	X: 0.0000, Y: 0.0000
Moments of inertia	X: 34.9097, Y: 467.9166
Product of inertia	XY: 0.1613
Principal moments and X-Y directions about centroid:	I: 34.9096 along [1.0000 -0.0004] J: 467.9167 along [0.0004 1.0000]
Moment of Inertia (in.^{4}/in.): 2.9	

Table 8-A 2. Moment of inertia (2.0 in. cementitious SAPL – corrugation filled).

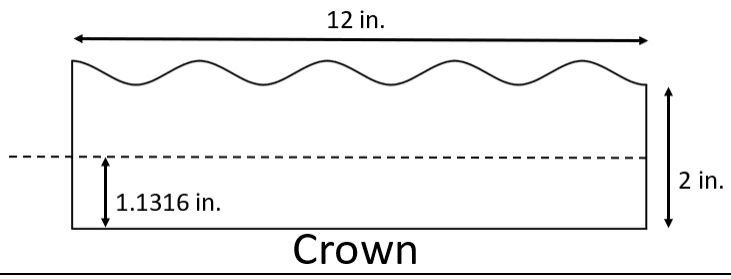
2.0 in. Cementitious SAPL	
---------- REGIONS ----------	
Area	26.9963
Perimeter	29.4585
Bounding box	X: -5.9963 -- 6.0037 Y: -1.1316 -- 1.3684
Centroid	X: 0.0000 Y: 0.0000
Moments of inertia	X: 11.7947 Y: 323.9165
Product of inertia	XY: 0.1112
Radii of gyration	X: 0.6610 Y: 3.4639
Principal moments and X-Y directions about centroid:	I: 11.7946 along [1.0000 -0.0004] J: 323.9166 along [0.0004 1.0000]
Moment of Inertia (in.^{4}/in.): 0.982	

Table 8-A 3. Moment of inertia (1.0-in. cementitious SAPL – corrugation filled).

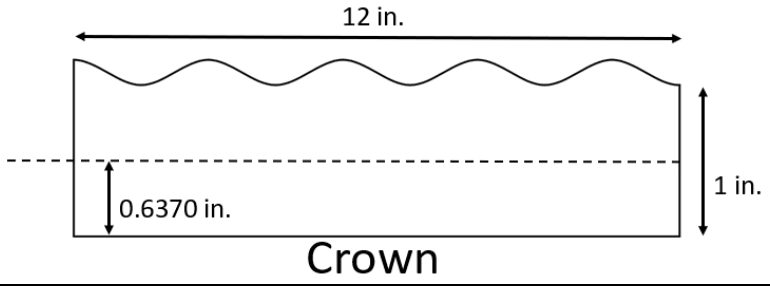
1.0 in. Cementitious SAPL		
---------- REGIONS ----------		
Area	14.9963	
Perimeter	27.4585	
Bounding box	X: -5.9933 -- 6.0067	Y: -0.6370 -- 0.8630
Centroid	X: 0.0000	Y: 0.0000
Moments of inertia	X: 2.1772	Y: 179.9162
Product of inertia	XY: 0.0607	
Radii of gyration	X: 0.3810	Y: 3.4637
Principal moments and X-Y directions about centroid:	I: 2.1772 along [1.0000 -0.0003] J: 179.9162 along [0.0003 1.0000]	
Moment of Inertia (in.^{4}/in.): 0.1814		

Table 8-A 4. Typical moment of inertia values for a corrugated profile to be considered for different SAPL thicknesses

t = SAPL Thickness (in.)	I = Moment of Inertia (in.^{3}/12)
0.25	0.0091125
0.5	0.018225
0.75	0.0273375
1.0	0.03645
1.25	0.0455625
1.5	0.054675
1.75	0.0637875
2.0	0.0729

Chapter 9

Performance Construction Specifications

CHAPTER 9 - PERFORMANCE CONSTRUCTION SPECIFICATIONS
9.1. POLYMERIC SPRAY APPLIED PIPE LINING

9.1.1 - GENERAL

9.1.1.1 Summary

A. Description. This work consists of conduit lining with spray applied, polymeric (epoxy or polyurethane based) material designed to withstand all live, dead and hydrostatic loads. Spray apply the polymeric material by centrifugally casting or hand spray. The term “host conduit” refers to the conduit being renewed with the spray applied structural liner system. This section defines inspecting, cleaning, and preparing existing stormwater gravity conduits, and lining them with cured-in-place polymeric materials with the spray on method.

9.1.1.2 Reference Standards

A. AASHTO:

1. LRFD Bridge Design Specifications.

B. ASTM International:

1. ASTM C1157/C1157M: Standard Performance Specification for Hydraulic Cement.
2. ASTM D624: Standard Test Method for Tear Strength of Conventional Vulcanized Rubber and Thermoplastic Elastomers.
3. ASTM D638: Standard Test Method for Tensile Properties of Plastics.
4. ASTM D695: Standard Test Method for Compressive Properties of Rigid Plastics.
5. ASTM D790: Standard Test Methods for Flexural Properties of Unreinforced and Reinforced Plastics and Electrical Insulating Materials.
6. ASTM D792: Standard Test Methods for Density and Specific Gravity (Relative Density) of Plastics by Displacement.
7. ASTM D2240: Standard Test Method for Rubber Property—Durometer Hardness.
8. ASTM D2990-17: Standard Test Methods for Tensile, Compressive, and Flexural Creep and Creep-Rupture of Plastics.
9. ASTM D4060: Standard Test Method for Abrasion Resistance of Organic Coatings by the Taber Abraser.
10. ASTM D4541: Standard Test Method for Pull-Off Strength of Coatings Using Portable Adhesion Testers.
11. ASTM D4787: Standard Practice of Continuity Verification of Liquid or Sheet Linings Applied to Concrete Substrates.

12. ASTM D6132: Standard Test Method for Nondestructive Measurement of Dry Film Thickness of Applied Organic Coatings Using an Ultrasonic Coating Thickness Gage.
13. ASTM D7234: Standard Test Method for Pull-Off Adhesion Strength of Coatings on Concrete Using Portable Pull-Off adhesion Testers.
14. ASTM E96/E96M: Standard Test Methods for Water Vapor Transmission of Materials.
15. ASTM E1252 Standard Practice for General Techniques for Obtaining Infrared Spectra for Qualitative Analysis.
16. ASTM G62: Standard Test Methods for Holiday Detection in Pipeline Coatings.

C. NASSCO:

1. Pipeline Assessment Certification Program (PACP), Version 7.0.4.

D. American Concrete Institute (ACI)

1. Guide for Cast-in-Place Low-Density Concrete, ACI 523.1R-06, Section 7.3 Pipeline and Culvert Fills. 2006

E. Specifics for ASTM Tests:

For ASTM tests not listed in the NTPEP Work Plan.

Standard Test	Test Specifics
ASTM C1157/C1157M: Standard Performance Specification for Hydraulic Cement	Cement for General Applications
ASTM D2990: Standard Test Methods for Tensile, Compressive, and Flexural Creep and Creep-Rupture of Plastics	For flexural creep, use flexural stress specimen load equal to 0.25% of short-term modulus.
ASTM D4787: Standard Practice of Continuity Verification of Liquid or Sheet Linings Applied to Concrete Substrates.	Holiday detection for concrete substrates.
ASTM D6132: Standard Test Method for Nondestructive Measurement of Dry Film Thickness of Applied Organic Coatings Using an Ultrasonic Coating Thickness Gage.	For substrates of dissimilar material than the lining material. Homogeneous lining polymers only.
ASTM G62: Standard Test Methods for Holiday Detection in Pipeline Coatings	Method B

9.1.1.3 Pre-Construction Meeting

A. As required by the Owner, convene a pre-construction meeting at a minimum of one (1) week prior to commencing work of this Section.

B. Discuss the installation plan including:

1. Flow control/bypass, if necessary.
2. Access to the host conduit.
3. Major work items including:
    a. Method and materials to stop infiltration (Paragraph 9.1.2.2), why the material is appropriate for the application and a back-up plan, if needed.
    b. Method and materials to fill voids and gaps (Paragraph 9.1.2.2).
4. Thickness measurements locations, frequency, and method (Paragraph 9.1.3.4).
5. The safety plan (Paragraph 9.1.1.4.D), specifically confined space requirements and procedures, as necessary.
6. The quality assurance/control plan (Paragraph 9.1.1.4.D).

9.1.1.4 Submittals

A. Product Data: Submit Manufacturer's information on all liner materials including Safety Data Sheets (SDS).

B. Inspection Records:

1. Submit a pre-installation video recording of the host conduit (Paragraph 9.1.3.2).
2. Submit a post-installation video recording of the rehabilitated conduit (Paragraph 9.1.3.4).

C. Manufacturer's Certificate: Certify that products supplied meet or exceed the requirements of this specification.

D. Liner Design and Installation: Submit a written installation plan for the host conduit rehabilitation to the Owner. Include the following information:

1. Structural design calculations and drawings for liner thicknesses performed and stamped by a registered professional engineer including all assumptions and the information in Tables 9-1 and 9-2 of this Section and in accordance with UTA/CUIRE SAPL Study equations available on Ohio DOT website: www.dot.state.oh.us/research
2. Methods of cleaning the host conduit.

3. Verify host conduit inside dimensions and length measurements prior to equipment fabrication, if applicable. Indicate measurements on submittals.
4. Methods of surface preparation.
5. Methods of water infiltration stoppage.
6. Plan to bypass or divert flow around the host conduit, if applicable.
7. The location of gaps or where a portion of the host conduit is missing.
8. The location of deformities that may affect liner design and the plan to mitigate these deformities in the design and during construction.
9. Method to verify applied thickness during and after installation (Paragraph 9.1.3.4).
10. Method to prepare test panels.
11. Site specific health and safety plan.
12. Quality Assurance/Control Plan to include testing and measurements during and after product installation.

E. Perform AASHTO NTPEP physical testing and submit test data on physical/mechanical properties listed in Table 9-1. Or, submit the latest NTPEP test results if the testing was completed within the current acceptable NTPEP testing frequency. Third party testing results are acceptable for any tests not covered in AASHTO NTPEP.
F. Based on NTPEP physical testing, provide physical properties to be used in design (Table 9-1).
G. Manufacturer requirements for receiving, handling, and storage of materials.

9.1.1.5 Qualifications

A. Submit qualifications for Manufacturer, Installer and Licensed Professional.
    1. Manufacturer: Company providing liner materials. Provide a minimum of three (3) installations using materials for a spray applied pipe liner. Include contact names and information.
    2. Installer: Company specializing in performing work of this Section. Submit a minimum of five (5) similar projects in installation of liner materials and licensed or certified by Manufacturer. Submit a minimum of three (3) similar projects supervised by the Foreman to be assigned for the work in this Section.
    3. Licensed Professional: Professional engineer experienced in design of the specified work in this Section and licensed in the project location.
B. Submit certification letter from the Manufacturer stating that the contractor is an approved Installer of the material.

9.1.1.6 Delivery, Storage, and Handling

A. Inspection: Accept materials onsite in Manufacturer's original packaging and inspect for damage. Do not use material from defective, punctured or damaged containers. Ensure that each container is labeled with a batch or lot number and with an expiration or use-by date. Do not use material that exceeds the expiration or use-by date. Accept only materials in conformance with product data submittals listed in Paragraph 9.1.1.4.

B. Store liner material according to Manufacturer instructions.

9.1.1.7 Warranty

A. Warrant the liner material, installation and finished product, including repaired defects, as required by the Owner's specifications with one (1) year being the minimum.

9.1.2 - PRODUCTS

9.1.2.1 Design Objectives

1. Design liner product to withstand all live, dead and hydrostatic loads for a design and service life determined by the Owner with a minimum service life of 50 years. Assume the existing conduit cannot share loading or contribute to structural integrity of liner.

9.1.2.2 Materials

A. Chemical Grout:

1. Use materials, additives, mixture ratios, and procedures for the grouting process in accordance with Manufacturer's recommendations.
2. Use chemical grout to stop infiltration of water.

B. Hydraulic Cement:

1. Use hydraulic cement in accordance with ASTM C1157.
2. Use hydraulic cement to stop infiltration of water.
3. Patch holes and gaps in the host conduit with hydraulic cement or other acceptable material.

C. Polymeric Grout:

1. Use non-shrink grouts formulated from epoxy or polyurethane thermoset polymers.
2. Can be thickened with sand or other admixtures for desired consistency.
3. Patch holes and gaps in the host conduit with polymeric grout or other acceptable material.

D. Controlled Low Strength Material (CLSM):

1. Use CLSM in accordance with ACI 523.1R-06, Section 7.3 Pipeline and Culvert Fills.
2. Fill voids surrounding the host pipe with CLSM.

E. Liner Material:

1. Use polymer materials, additives, mixture ratios, and procedures in accordance with Manufacturer's recommendations.

9.1.2.3 Design Criteria

See Chapter 8 of the UTA/CUIRE SAPL Study equations specifically Equation 8-8 for soil loads available on Ohio DOT website: www.dot.state.oh.us/research

A. Design liner material to provide a jointless, continuous, and structurally sound finished product.

B. Provide the liner material physical properties to be used in design where the Minimum Requirements column is shown as "Declared Value" in Table 9-1. Confirm with NTPEP physical testing (Paragraph 9.1.1.4 E and F).

Table 9-1: Polymeric Based Structural Liner Properties

Property	Test Method	Minimum Requirements
Flexural Strength Flexural Modulus Flexural Creep	ASTM D790-17 ASTM D790-17 ASTM D2990-17	Declared Value, but not less than 10,000 psi Declared Value, but not less than 250,000 psi Declared Value – Qualification Test by 3rd Party
Compressive Strength Compressive Modulus Compressive Creep	ASTM D695-15 ASTM D695-15 ASTM D2990-17	Declared Value, but not less than 8,000 psi Declared Value, but not less than 300,000 psi Declared Value – Qualification Test by 3rd Party

C. Use the following variables for fully deteriorated gravity conduit design:

Table 9-2: Polymeric Based Structural Liner Variables

Variable	Value	Units	Source
Groundwater Level	At the top of conduit (minimum) or the average high seasonal groundwater level (maximum), whichever is higher	ft	
Soil Density	120 minimum	lb/cf	
Soil Modulus of Reaction	2,000 maximum	psi	AASHTO
Thickness	As designed but not less than 0.5	in.	

9.1.3 - EXECUTION

9.1.3.1 Submittals

A. Begin no work until the submittals have been accepted.

B. Resubmit any changes or deviations from the accepted submittals.

9.1.3.2 Cleaning, Inspection and Preparation

A. Cleaning: Remove all debris from the host conduit, typically with a water-blast sufficient to remove all laitance and loose material. Flush debris from the conduit. Remove all coatings, corrosion and other surface materials to the satisfaction of Owner. Remove all debris and obstructions that may impede the placement of the lining material. Perform final cleaning and preparation of the host conduit surface in accordance with the Manufacturer's recommendations.

B. Pre-installation Video Inspection:

1. Conduct a video inspection of the host conduit prior to liner installation using NASSCO certified personnel experienced in making closed-circuit television (CCTV) condition surveys or hand-held camera surveys when the host conduit is of the size that requires a worker-entry condition survey.
2. Determine condition of existing conduit, joints, and location of any branch connections after cleaning, surface prep, and water infiltration stoppage prior to application of the liner.
3. Record obstacles, major defects (hole, missing invert, etc.), and any variations to the conduit.

C. Preparation:

1. Completely seal active leaks and stop any groundwater intrusion with quick setting chemical grout or hydraulic cement prior to application of liner material.
2. Repair missing invert with hydraulic cement, polymeric grout or concrete.
3. Patch gaps or where a portion of the host conduit is missing with hydraulic cement, polymeric grout or other acceptable material to provide a solid continuous surface on which to spray.
4. Fill voids surrounding the host pipe with controlled low strength material (CLSM) in accordance with Guide for Cast-in-Place Low-Density Concrete, ACI 523.1R-06, Section 7.3 Pipeline and Culvert Fills.
5. Prepare host conduit surface in accordance with Manufacturer's recommendations.
6. Prepare branch connections to the host conduit according to the Manufacturer's recommendations.

9.1.3.3 Installation

A. Bypassing Flow/Draining Pooled Water:

1. Where required, bypass or divert flows to isolate each section of host conduit for lining.
2. Remove pools of water from within the conduit. Refer to liner material Manufacturer's host conduit preparation instructions to determine surface dryness required for application.
3. Prevent the accumulation and flow of water through the host conduit and liner until after the work is complete and the liner material is cured.
4. Maintain bypass operation until the lining process is complete and as required by the Manufacturer.
5. Obtain any required environmental permits for discharge of the bypass flow.

B. Spray Applied Polymeric Liner:

1. Prepare liner material according to Manufacturer's recommendations.
2. Protect walls, surfaces, streambed and plants at the entrance and exit of the host conduit from overspray. Apply the material to the prepared surface using methods that provide a uniform surface. Use only equipment recommended by the Manufacturer to perform the spray lining. Record the batch or lot number from the material containers used each day.
3. Install liner material in accordance with Manufacturer's recommendations at the design thickness. Cure and finish the liner material in accordance with Manufacturer's recommendations.
4. Verify the applied thickness, as submitted in Paragraph 9.1.1.4, at various, random perimeter locations at least once every 10 feet to the satisfaction of the Owner. Apply additional material to any areas found to be less than the design thickness.
5. Reinstate branch connections to the host conduit according to Manufacturer's recommendations.
6. Prepare at least two (2) test panels and transport the test panels to an accredited third-party laboratory.
7. Contain, collect, characterize and legally dispose of all waste generated during the work.
8. Restrict flow and personnel entry into the conduit until the spray applied material has cured.

9.1.3.4 Field Quality Assurance/Control

A. General:

1. Conduct a post-installation video recording of the rehabilitated conduit by NASSCO certified personnel experienced in making closed-circuit television (CCTV) condition surveys or hand-held camera surveys when the lined host conduit is of the size that requires a worker-entry condition survey.
    a. Code defects on the inspection log in accordance with the NASSCO PACP standard.
    b. Measure any cracks or other deficiencies in the liner.
2. Repair all defects affecting the structural capability, longevity or hydraulics of the installed liner. Submit certification from the Licensed Professional and Manufacturer that all liner repairs have been completed as recommended by the Manufacturer.
3. Include the following defects. Code defects on the inspection log in accordance with the PACP standard.
    a. Crack: longitudinal, circumferential and multiple.
    b. Fracture: longitudinal, circumferential and multiple.
    c. Infiltration: weeper, dripper, runner and gusher.
    d. Exfiltration.
    e. Detached liner.
    f. Delaminated liner.
    g. Shadowing.
    h. Irregularities.
    i. Pinholes.
    j. Thickness variations.
    k. Bubbles.
    l. Foreign inclusions.
    m. Roughness.
    n. Dry spots.
4. Complete any repairs involving cutting, sealing, removing or joining portions of the liner in strict compliance with the Manufacturer's recommendations. This includes stopping active infiltration, properly preparing the surface to be repaired, mixing the polymer components and applying the polymer used in the repair procedure.

B. Required Testing

1. Thickness. Verify the applied thickness as submitted in Paragraph 9.1.1.4, at various perimeter locations, including the host conduit crown at least once every 10 ft. Optional methods include:
    a. Ultrasonic measurements in accordance with ASTM D6132.

b. Measure the cylindrical coupon removed by performing the adhesion test, ASTM D7234. Repair the hole as recommended by the manufacturer.

2. Prepare test panels as recommended by the Manufacturer. Transport the test panels to an accredited third-party laboratory and test for physical properties as shown in Table 9-1.

C. Basis of Acceptance:

3. The liner is continuous over the entire length of the host conduit.
4. No visual defects, including foreign inclusions, dry spots, pinholes, cracks, or delaminations. Identified defects have been properly repaired.
5. Thicknesses measured are equal to or greater than the minimum design thickness.
6. All test results pass specified or declared values as shown in Table 9-1 and submitted.
7. No infiltration of water through the liner.

9.2 Cementitious Spray Applied Pipe Lining

9.2.1 – GENERAL

9.2.1.1 Summary

A. Description. This work consists of conduit lining with spray applied, factory blended cementitious or geopolymer material designed to withstand all live, dead and hydrostatic loads. Spray apply the cementitious or geopolymer material by centrifugally casting. The term “host conduit” refers to the pipe being renewed with the spray applied structural liner system. Includes inspecting, cleaning and preparing existing stormwater gravity conduits and spray applying cementitious or geopolymer material.

9.2.1.2 Reference Standards

A. AASHTO:

1. T 358 – Standard Method of Test for Surface Resistivity Indication of Concrete’s Ability to Resist Chloride Ion Penetration.
2. LRFD Bridge Design Specifications.

B. ASTM International:

1. ASTM C109 – Standard Test method for Compressive Strength of Hydraulic Cement Mortars (Using 2-in Cube Specimens).
2. ASTM C266 – Standard Test Method for Time of Setting of Hydraulic-Cement Paste by Gillmore Needles.

3. ASTM C469 – Standard Test Method for Static Modulus of Elasticity and Poisson's Ratio of Concrete in Compression.
4. ASTM C496 – Standard Test Method for Splitting Tensile Strength of Cylindrical Concrete Specimens.
5. ASTM C418 - Standard Test Method for Abrasion Resistance of Concrete by Sand Blasting
6. ASTM C666 – Standard Test Method for Resistance of Concrete to Rapid Freezing and Thawing.
7. ASTM C1090 – Standard Test Method for measuring Changes in Height of Cylindrical Specimens of Hydraulic-Cement Grout.
8. ASTM C1157 – Standard Performance Specification for Hydraulic Cement
9. ASTM C1583 Standard Test Method for Tensile Strength of Concrete Surfaces and the Bond Strength or Tensile Strength of Concrete Repair and Overlay Materials by Direct Tension (Pull-Off Method)
10. ASTM C1609 – Standard Test Method for Flexural Performance of Fiber-Reinforced Concrete (Using Beam with Third-Point Loading)
11. ASTM C 1872 Standard Test Method for Thermogravimetric Analysis of Hydraulic Cement

C. NASSCO:

1. Pipeline Assessment Certification Program (PACP), Version 7.0.4.

D. American Concrete Institute (ACI):

1. Guide for Cast-in-Place Low-Density Concrete, ACI 523.1R-06, Section 7.3 Pipeline and Culvert Fills. 2006

E. Specifics for ASTM Tests

For ASTM tests not listed in the NTPEP Work Plan.

Standard Test	Test Specifics
ASTM C1157/C1157M: Standard Performance Specification for Hydraulic Cement	Cement for General Applications

9.2.1.3 Pre-Construction Meeting

A. As required by the Owner, convene a pre-construction meeting a minimum of one (1) week prior to commencing work of this Section.

B. Discuss the installation plan including:

1. Flow control/bypass, if necessary
2. Access to the host conduit

3. Major work items including:
    a. Method and materials to stop infiltration (Paragraph 9.2.2.2), why the material is appropriate for the application and a back-up plan, if needed.
    b. Method and materials to fill voids and gaps (Paragraph 9.2.2.2)
4. Thickness measurements locations, frequency and method (Paragraph 9.2.3.4).
5. The safety plan (Paragraph 9.2.1.4.D), specifically confined space requirements and procedures as necessary
6. The quality assurance/control plan (Paragraph 9.2.1.4.D)

9.2.1.4 Submittals

A. Product Data: Submit Manufacturer's information on all liner materials including Safety Data Sheets (SDS).

B. Inspection Records:
    1. Submit a pre-installation video recording of the host conduit (Paragraph 9.2.3.2).
    2. Submit a post-installation video recording of the rehabilitated conduit (Paragraph 9.2.3.4).

C. Manufacturer's Certificate: Certify that products supplied meet or exceed the requirements of this specification.

D. Liner Design and Installation: Submit a written installation plan for the host conduit rehabilitation to the Owner. Include the following information:
    1. Structural Design calculations for liner thicknesses performed and stamped by a registered professional engineer including all assumptions and the information in Tables 9-3 and 9-4 of this Section and in accordance with UTA/CUIRE SAPL study equations.
    2. Methods of cleaning the host conduit.
    3. Verify host conduit inside dimensions and length measurements prior to equipment fabrication, if applicable. Indicate measurements on submittals.
    4. Methods of surface preparation required.
    5. Methods of water infiltration stoppage.
    6. Plan to bypass or divert flow around the host conduit, if applicable.
    7. The location of gaps or where a portion of the host conduit is missing.
    8. The location of deformities that may affect liner design and the plan to mitigate these deformities in the design and during construction.

9. Use spin casting unless the Owner approves hand application. Submit justification for hand application, if necessary.
10. Method to verify applied thickness during and after installation for the types of host conduit materials on the project (metal or concrete). See Paragraph 9.2.3.4.
11. Control of temperature and humidity in the host conduit as recommended by the Manufacturer.
12. Site specific health and safety plan.
13. Quality assurance/control plan to include testing and measurements during and after product installation.

E. Perform AASHTO NTPEP physical testing and submit test data on physical/mechanical properties as indicated in Table 9-3. Or, submit the latest NTPEP test results if the testing was completed within the current acceptable NTPEP testing frequency. Third party testing results are acceptable for any tests not covered in AASHTO NTPEP.

F. Based on NTPEP physical testing, provide physical properties to be used in design (see Table 9-3).

G. Manufacturer's requirements for receiving, handling and storage of materials.

9.2.1.5 Minimum Qualifications

A. Submit qualifications for Manufacturer, Installer and Licensed Professional.

1. Manufacturer: Company providing liner materials. Provide a minimum of three (3) installations using materials for a spray applied pipe liner. Include contact names and information.
2. Installer: Company specializing in performing work of this Section. Submit a minimum of five (5) similar projects in installation of liner materials and licensed or certified by Manufacturer. Submit a minimum of three (3) similar projects supervised by the Foreman to be assigned for the work in this Section.
3. Licensed Professional: Professional engineer experienced in design of the specified work in this Section and licensed in the project location.

B. Submit certification letter from the Manufacturer stating that the contractor is an approved Installer of the material.

9.2.1.6 Delivery, Storage, and Handling

A. Inspection: Accept materials onsite in Manufacturer's original packaging and inspect for damage. Do not use material from defective, punctured or damaged containers. Ensure that each container is labeled with a batch or lot number. Accept only materials in conformance with product data submittals listed in Paragraph 9.2.1.4.

B. Store liner material according to Manufacturer's instructions.

9.2.1.7 Warranty

A. Warrant the liner material, installation and finished product, including repaired defects, as required by the Owner's specifications with one (1) year being the minimum.

9.2.2 - PRODUCTS

9.2.2.1 Design Objectives

A. Design liner product to withstand all live, dead and hydrostatic loads for a design and service life determined by the Owner with a minimum service life of 50 years. Assume the existing conduit cannot share loading or contribute to structural integrity of liner.

9.2.2.2 Materials

A. Chemical Grout:

1. Use materials, additives, mixture ratios, and procedures for the grouting process in accordance with Manufacturer's recommendations.
2. Use chemical grout to stop infiltration of water.

B. Hydraulic Cement:

1. Use hydraulic cement in accordance with ASTM C1157.
2. Use hydraulic cement to stop infiltration of water.
3. Patch holes and gaps in the host conduit with hydraulic cement, concrete or the same cementitious or geopolymer based material to be used for the liner.

C. Controlled Low Strength Material (CLSM)

1. Use CLSM in accordance with ACI 523.1R-06, Section 7.3 Pipeline and Culvert Fills.
2. Fill voids surrounding the host pipe with CLSM.

D. Liner Material:

1. Use cementitious or geopolymer materials, additives, mixture ratios, and procedures in accordance with Manufacturer's recommendations.

9.2.2.3 Design Criteria

A. See Chapter 8, of the UTA SAPL Study equations specifically Equation 8-8 for soil loads available on Ohio DOT website: www.dot.state.oh.us/research

B. Design liner material to provide a jointless, continuous, and structurally sound finished product.

C. Provide the liner material physical properties to be used in design where the Minimum Requirements column is shown as "Declared Value" in Table 9-3. Confirm with NTPEP physical testing (Paragraphs 9.2.1.4.E and F).

Table 9-3: Cementitious Based Structural Liner Properties.

Property	Test Method	Duration	Minimum Requirements
Compressive Strength	ASTM C109 (2.0-inch cubes)	28 day (min)	Declared Value, but not less than 8,000 psi
Flexural Strength (Modulus of Rupture)	ASTM C 1609	28 days (min)	Declared Value, but not less than 1,000 psi
Compressive Modulus of Elasticity	ASTM C 469	28 days (min)	Declared Value, but not less than 3,500,000 psi

D. Use the following variables for fully deteriorated gravity pipe design:

Table 9-4: Cementitious Based Structural Liner Variables.

Variable	Value	Units	Source
Groundwater Height	At the top of conduit (minimum) or the average high seasonal groundwater level (maximum), whichever is higher	ft	
Soil Density	120 minimum	lb/cf	
Soil Modulus of Reaction	2,000 maximum	psi	AASHTO LRFD
Thickness (above the crest of the corrugations for CMP)	As designed but not less than 1.0 in. over crest for all diameters	in.	

9.2.3 - EXECUTION

9.2.3.1 Submittals

A. Begin no work until the submittals have been accepted.

B. Resubmit any changes or deviations from the accepted submittals.

9.2.3.2 Cleaning, Inspection and Preparation

A. Cleaning: Remove all debris from the host conduit, typically with a water-blast sufficient to remove all laitance and loose material. Flush debris from the conduit. Remove all coatings, corrosion and other surface materials to the satisfaction of the owner. Remove all debris and obstructions that may impede the placement of the lining material. Perform final cleaning and preparation of the host conduit surface in accordance with the Manufacturer's lining recommendations.

B. Pre-Installation Video Inspection:

1. Conduct a video inspection of the host conduit prior to liner installation, but after cleaning, using NASSCO certified personnel experienced in making closed-circuit television (CCTV) condition surveys or hand-held camera surveys when the host conduit is of the size that requires a worker-entry condition survey.
2. Determine condition of host conduit, joints, and location of any branch connections after cleaning, surface prep, and water infiltration stoppage prior to application of the liner.
3. Record obstacles, major defects (holes, missing invert, etc.), and any variations to the conduit.

C. Preparation:

1. Completely seal active leaks and stop any groundwater intrusion with chemical grout or hydraulic cement prior to application of liner material.
2. Repair missing invert with hydraulic cement, concrete or the cementitious or geopolymer lining material to be used.
3. Patch gaps or where a portion of the host conduit is missing with hydraulic cement, concrete or the same cementitious or geopolymer based material to be used for the liner to provide a solid continuous surface on which to spray.
4. Fill voids surrounding the host pipe with controlled low strength material (CLSM) in accordance with Guide for Cast-in-Place Low-Density Concrete, ACI 523.1R-06, Section 7.3 Pipeline and Culvert Fills.
5. Prepare host conduit surface in accordance with Manufacturer's recommendations.
6. For aluminum or aluminized steel host conduits, apply a coating to the cleaned metal surface to provide a reaction barrier between the aluminum and the cementitious alkalis. Coating options are:
    a. Two coats of a bituminous paint with a total thickness of at least 16 mils.
    b. A polyvinyl acetate bonding agent, Weld-Crete or equal.
7. Prepare branch connections to the host conduit according to the Manufacturer's recommendations.

9.2.3.3 Installation

A. Bypassing Flow/Draining Pooled Water

1. Where required, bypass or divert flows to isolate each section of the host conduit for lining.
2. Remove pools of water from within the conduit. Refer to liner material Manufacturer's host conduit preparation instructions to determine surface dryness required for application.
3. Prevent the accumulation and flow of water through the host conduit and liner until after the work is complete and the liner material has hardened.
4. Maintain bypass operation until lining is totally formed and lining process is complete and as required by the Manufacturer.
5. Obtain any required environmental permits for discharge of the bypass flow.

B. Spray Applied Cementitious Liner:

1. Prepare liner material according to Manufacturer's recommendations.
2. Control the temperature and humidity in the host conduit according to the Manufacturer's recommendations.
3. Protect walls, surfaces, streambed and plants at the entrance and exit of the host conduit from overspray. Apply the material to the prepared surface using methods that provide a uniform surface. Use only equipment and processes recommended by the Manufacturer to perform the spray lining. Record the batch or lot number from the material containers used each day.
4. When host conduit has corrugations, fill corrugations and then add design liner thickness.
5. Install liner material in accordance with Manufacturer's recommendations at the design thickness. Cure and finish the liner material in accordance with Manufacturer's recommendations.
6. Limit application passes to 0.5 inch.
7. Verify the applied thickness (above the crest of the corrugations for CMP, see Chapter 4 of the UTA/CUIRE SAPL study available on Ohio DOT website www.dot.state.oh.us/research as submitted in Paragraph 9.2.1.4, at various, random perimeter locations at least once every 10 feet to the satisfaction of the Owner. Apply additional material to any areas found to be less than the design thickness.
8. Reinstate branch connections to the host conduit according to Manufacturer's recommendations.
9. Contain, collect, characterize and legally dispose of all waste generated during the work.

10. Restrict flow and personnel entry into the conduit until the spray applied material has hardened.

11. ~~Prevent the escape of any rinse water from the lined pipe or otherwise capture the water until (1) the water can be pumped to a container for proper transportation and off-site disposal; or (2) monitor the pH of the rinse water continuously until the pH is less than 9 whereupon the rinse water may be released.~~

9.2.3.4 Field Quality Assurance/Control

A. General:

1. Conduct a post-installation video recording of the rehabilitated conduit by NASSCO certified personnel experienced in making closed-circuit television (CCTV) condition surveys or hand-held camera surveys when the lined host conduit is of the size that requires a worker-entry condition survey.
    a. Perform video a minimum of 30 days after installation is complete.
    b. Code defects on the inspection log in accordance with the NASSCO PACP standard.
    c. Measure any cracks or other deficiencies in the liner.
2. Repair all defects affecting the structural capability, longevity or hydraulics of the installed liner. Submit certification from the Licensed Professional and Manufacturer that all liner repairs have been completed as recommended by the Manufacturer.
3. Include the following defects.
    a. Crack: longitudinal, circumferential, and multiple. Larger than 0.01 inch
    b. Fracture: longitudinal, circumferential, and multiple
    c. Infiltration: weeper, dripper, runner, and gusher
    d. Exfiltration
    e. Surface Spalling
    f. Detached liner
    g. Delaminated liner
    h. Efflorescence
    i. Shadowing
    j. Irregularities
    k. Pinholes
    l. Thickness variations
    m. Foreign inclusions
    n. Roughness
    o. Deformation
    p. Dry spots

B. Required Testing

1. Thickness (above the crest of the corrugations for CMP). Verify the applied thickness, as submitted in Paragraph 9.2.1.4, at various, random perimeter locations, including the host conduit crown, at least once every 10 feet. Apply additional material to any areas found to be less than the design thickness. Optional methods include:
    a. For metal host conduits, utilize a non-destructive thickness testing device to verify thickness. Use Hilti PS 200 S Ferroscan, or equal, configured to measure concrete cover depths up to 6.25 inches. Validate non-destructive testing by measuring the liner thickness at the inlet or outlet end of the conduit where the liner thickness is readily apparent or by comparing to core samples.
    b. Install depth gauges that protrude from the host conduit wall a distance equal to the final liner thickness. Install gauges at the 12 o'clock position at least every 10 feet along the length.
    c. Collect core samples where core diameter is at least twice the liner thickness. Repair cored area with liner material.
2. Compressive Strength. Prepare test specimens as required per ASTM C109 utilizing ACI certified level one sample technicians to properly obtain and transport the test specimens to an accredited third-party laboratory. Test compressive strength (ASTM C109) as shown in Table 9-3.
3. Conduct all thickness testing in the presence of the Owner or Owner's representative.
4. Field Quality Assurance /Control Submittals
    a. Thickness measurements/verification during and after installation.
    b. Temperature and humidity in the host conduit.
    c. Compressive strength.

C. Basis of Acceptance:
1. The liner is continuous over the entire length of the host conduit.
2. No visual defects, such as foreign inclusions, holes and cracks no larger than 0.01 inches wide, and no waviness when rehabilitating concrete conduits. Identified defects have been properly repaired.
3. Thicknesses measured are equal to or greater than the minimum design thickness.
4. All test results pass specified or declared values as shown in Table 9.3 and submitted.
5. No infiltration of water through the liner.

Chapter 10

Finite Element Modeling of SAPL Renewed Corrugated Metal Pipes Tested in a Soil Box

CHAPTER 10 - FINITE ELEMENT MODELING OF SAPL RENEWED CORRUGATED METAL PIPES TESTED IN A SOIL BOX

10.1. Finite Element Modeling of Soil Box Tests of CMPs

This chapter summarizes the finite element method (FEM) simulations of the soil box tests performed at CURIE. This Chapter was prepared when only the soil box results for polymeric SAPL were available and the soil box tests on cementitious SAPL were not completed yet Therefore, this report mainly focuses on the FEM simulations of the CMPs repaired with polymeric SAPL along with the additional parametric study performed on CMPs repaired with polymeric SAPL based on the request for the development of the design equation. The FEM work for the parametric studies is presented in Appendix E. Later FEM simulations of the invert-cut circular CMP repaired with cementitious SAPL were performed when the soil box results were available. For the cementitious SAPL FEM model, models were developed for the circular invert-cut CMPs lined with 1-in., 2-in., and 3-in. thicknesses. The results were added in Appendix F. The parametric studies for the cementitious SAPL were not performed.

ABAQUS was used to perform FEM simulations and analyses. The simulations include three CMP pipes without linings, three invert-removed circular CMP lined with a polymeric SAPL, and three invert-removed arch CMP lined with a polymeric SAPL in details. The three CMP pipes without linings are one bare intact circular CMP, one bare invert-cut circular CMP, and one bare invert-cut arch CMP. These three CMP pipes were used as the control tests to provide baseline results of the CMP pipes before lining. The polymeric SAPL liner was applied at three thicknesses, 0.25, 0.5, and 1 inch, respectively. The intact circular CMP pipe test was first simulated to develop a calibrated FEM model of the bare intact circular CMP pipe. FEM models for the invert-cut bare circular and arch CMP pipes were also developed. However, the simulated load-displacement curves show significant differences from the measured ones. The cover soil collapsed when the invert was removed entirely during the tests for the bare circular and arch pipes. Settlements in the magnitude of 5-6 inches were observed. The FEM models were not capable of modeling the soil collapse and the associated soil behavior and pipe and soil interactions. The invert-removal process was modified to keep the bolt supports at each end for the lined circular and arch pipes during the lining process. No soil collapse was observed for the liner pipes when the supports were removed after the liner was cured and ready for the load test. Each lined circular and arch CMP pipe was modeled in ABAQUS and verified against the measured results. Both the lined circular and arch CMP pipes were modeled with three additional liner thickness to evaluate the thickness effects on the lined CMP pipes.

10.1.1. Model Setup

A three-dimensional FEM model was adopted for all the pipe tests. The model includes three solid parts: soil, CMP pipe, and liner (for lined pipes). The geometry of the corrugated pipe is complex and difficult to be modeled in ABAQUS. Therefore, all the solid parts were generated in CAD software and imported into ABAQUS for meshing and modeling. Since three liner thicknesses were used for the lined pipes, the model

for each liner needed to be re-created in the CAD software. All the FEM simulations were carried on the full-size model of the soil box except for the intact circular CMP.

10.1.2. Boundary Condition and Loading

Boundary conditions are critical to the FEM modeling of the CMP pipe tests in the soil box. The boundary conditions in the models were defined according to the experimental setup. All the vertical soil faces were defined as restricted in their normal directions and free in their tangential directions. The vertical movement of the soil was restricted on the bottom surface. The boundary conditions are shown in Figure 10-1.

A rigid steel pad connected to a hydraulic jack was used for loading. In the FEM model, the load was applied on the top surface area corresponding to the load pad using a master node located in the centroid. The master node constrained all the nodes in the loading area through the equation constraint. This equation definition ensured a simultaneous movement of all loaded nodes the same as the master node (simulating load transfer from rigid load pad), such that any movement in the central node was mirrored by all the nodes with the equation constraint. The load was applied by providing the displacement of the master soil node located in the centroid of the load pad.

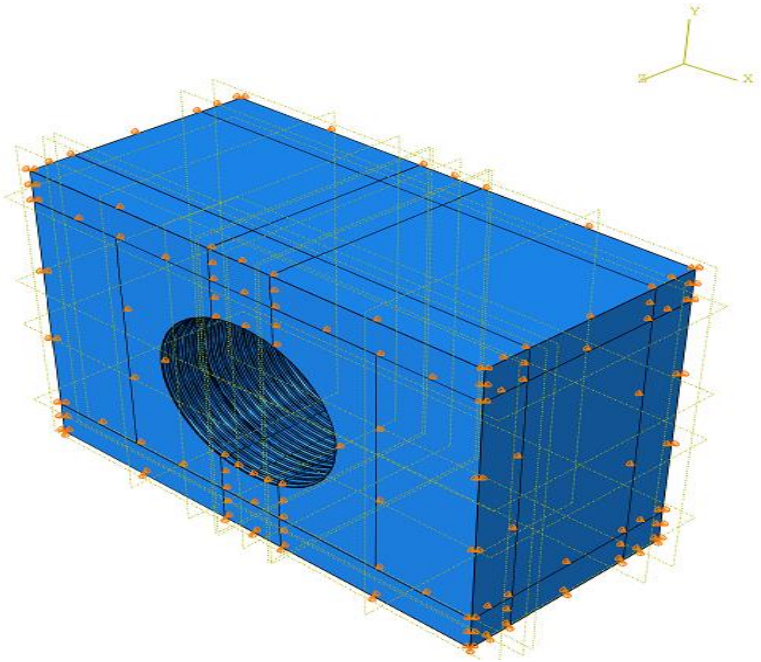


Figure 10-1. FE model of the soil-pipe-liner system.

10.1.3. Material Model

10.1.3.1 Soil Properties

Three types of soil: poorly graded sand (SP), poorly graded gravel (GP), and TxDOT specified grade D sub-base layer classified according to ASTM D -2487 were considered as the backfill and cover soils, respectively in the experiment. For the first control test on the intact bare CMP pipe, the gravel classified as GP was used as the

cover soil, but it was later replaced by the TxDOT Grade D sub-base layer (RCA) for the rest of the soil box tests. All the soils were modeled using the Drucker Prager Model available in the ABAQUS material model library. The material properties used in the FEM model are listed in Table 10-1.

Drucker Prager Model is a three-dimensional pressure-dependent model through which the strength properties of the soil increase with the intermediate principal stress (SIMULIA, 2014). The property of the poorly graded sand was taken from the laboratory experiment carried at the UTA Geotech Lab, while the property of the poorly graded gravel (GP) was taken from CUIRE (2012) final report. The properties for the RCA soils were chosen from Arulrajah et al. (2012). All the soil properties were chosen as the representative soil properties that can be achieved for the selected soils in the soil box. The density used for the model was reduced to match the 85% compaction of the maximum dry density of the soil. Also, the soil Young's moduli were chosen according to the ASTM D-3839-14, considering the depth dependency of Young's moduli. In the calibration process, the internal friction angle of the sand and gravel was slightly adjusted to match the experimental results better. The properties shown in Table *10-1* are the finalized values after the calibration process.

Table 10-1. Soil properties.

Soil Parameters	Sand	Gravel	RCA
Density (pcf) (Max. dry density)	115	130	130
Young's Modulus (psi)	510	1,000	1,100
Poisson Ratio	0.3	0.28	0.3
Angle of Friction (°)	32.0	37.5	39
Dilation Angle (°)	1	2	1

10.1.3.2 CMP Properties

The intact circular CMP is made of corrugated steel sheets conforming to ASTM 929 with yield strength 33 ksi and ultimate strength 45 ksi. The modulus of elasticity of the steel is 29,000 ksi. The elastic-plastic model available in ABAQUS was used to model the behavior of CMP steel. The properties are listed below in Table 10-2.

Table 10-2. Properties of steel.

Property	Value
Density (lb/in.^{3})	0.284
Elastic Modulus (psi)	29,000,000
Poisson's Ratio	0.3
Yield Stress (psi)	33,000
Ultimate Stress (psi)	45,000

10.1.3.3 Polymeric SAPL Properties

The liner properties were initially taken from the lab test performed by the CUIRE laboratory and later optimized to best match the test results. The liner test report suggested a brittle behavior with a small plastic zone with only 0.22% of strain increase from the yield and breaking strain. A simple elastic-plastic model was used to model the SAPL liner. In the FE model, the occurrence of a crack in the liner was identified by observing its plastic strain. The appearance of plastic strain is assumed to be a crack in the FE model. The optimized properties of the material are given in Table 10-3.

Table 10-3. Properties of polymeric liner material used in FEM models.

Property	Value
Density (lb./in3)	0.00014
Elastic Modulus (psi)	850,000
Poisson's Ratio	0.3
Tensile Yield Stress (psi)	7,482
Tensile Break Strength (psi)	8,821

10.1.4. Soil-CMP and Liner-CMP Interaction

Soil-pipe interaction is critical to the modeling of buried pipes. ABAQUS allows the user to define different interaction models for the interface between the pipe and soil, such as tie interaction and surface to surface interaction. In this soil box model, the interaction between the pipe and soil interface was modeled by the surface-to-surface contact model, where the pipe was treated as the master surface, and the soil was treated as the slave surface. Considering the corrugated surface of the CMP, a rough friction coefficient of 0.5 was defined between the CMP and soil, and the contact was defined as a hard contact, i.e., the pipe does not "pierce" the soil but displaces it. This friction coefficient was the optimized value by the calibration of the FE model with the intact CMP test.

The same contact model was used to model the CMP and liner interactions, but a larger friction coefficient of 1.0 was used to represent a stronger tangential bonding. No normal bonding was considered, and normal detachment was allowed as a complete separation between the SAPL liner and the CMP pipe was observed from the soil box tests.

10.1.5. Elements

A. Soil

The soil was modeled as solid elements in all the FE model. The soil was meshed as solid linear C3D8R elements, which is 8 noded linear brick, reduced integration with control in the hourglass. The mesh size of the soil was optimized to be 2.4 in. through

mesh sensitivity analysis. Figure 10-2 shows the distribution of the mesh around the soil.

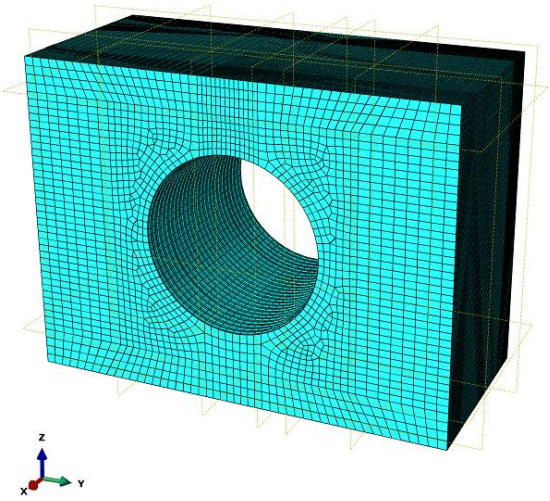


Figure 10-2. Soil model in FE with 2.4 in. mesh size.

B. CMP

The CMP was also modeled using solid linear hexagonal C3D8R elements. The mesh size of the CMP used was 1.8 in. Figure 10-3 shows the distribution of the mesh around CMP.

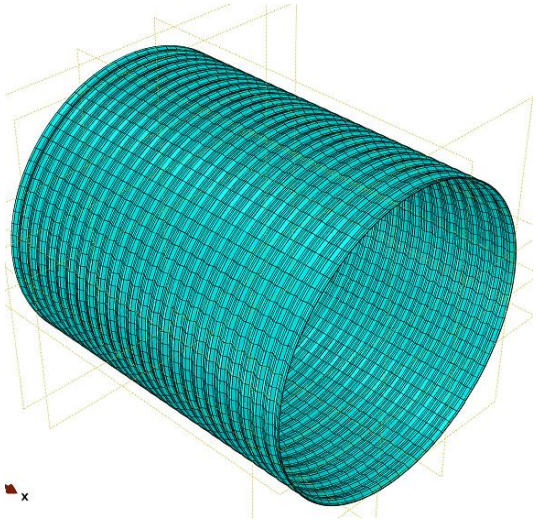


Figure 10-3. CMP model in FE.

C. Liner

All liners of three different thicknesses were modeled as solid linear hexagonal C3D8R element type with a mesh size of 1.8 in, the same size as the CMP, and its distribution is shown in Figure 10-4.

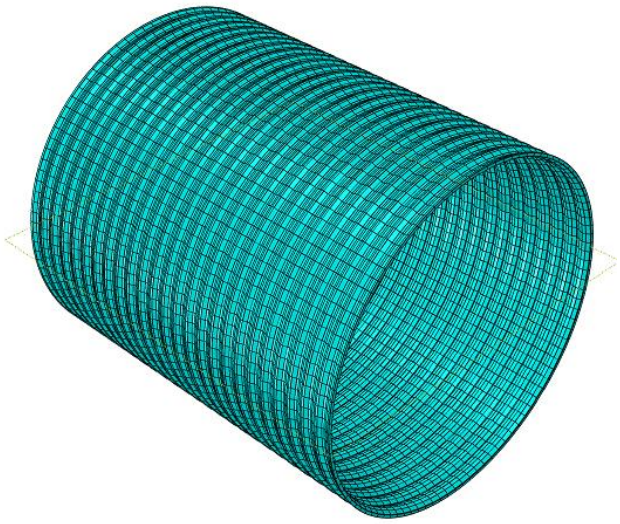


Figure 10-4. 1 in. liner model in FE.

10.1.6. Mesh Size Analyses

FEM provides approximate solutions of unknown functions over the solution domain. The domain is divided into small elements represented by the element nodes. The number of elements, i.e., element size, for the modeling domain affects the accuracy of the solution. With coarser mesh or larger elements, the model could behave stiffer and yield inaccurate results, while finer mesh leads to more accurate results with the cost of increased computation time. Hence selecting the proper mesh size is one of the essential steps in the FEM analysis to make the model independent of the mesh size.

To determine the mesh sensitivity of the model, total energy, load-displacement for soil and pipe, and the Von Mises stress for the pipe were compared for the mesh sizes of 3.4, 3, 2.4 inches. For the soil, load-displacement does not vary by a significant amount for mesh sizes 3.4, 3, 2.4 (Figure 10-5). Thus, the mesh size of 2.4 was chosen, and its distribution is shown in Figure 10-6.

Table 10-4. Run time for different mesh sizes.

Mesh Size (in.)		Run Time
Pipe	**Soil**	**(hrs.)**
3.4	3.4	0.5
3	3	1
2.4	2.4	4
1.75	**2.4**	**6**
1.5	2.4	20
1	2.4	25
0.75	2.4	96

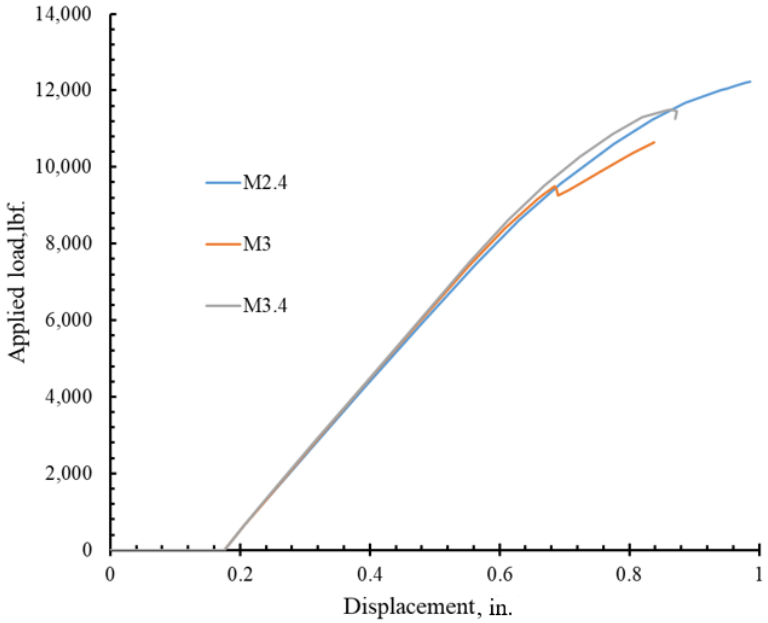


Figure 10-5. Load displacement plot for the soil (Chimauriya, 2019).

Figure 10-7 shows the vertical displacement of the CMP's crown, and Figure 10-8 shows the von Mises stress taken at the crown of the pipe. The plots were generated for the mesh size ranging from 2.4 in. to 0.75 in. After the mesh size of the pipe was reduced to 1.75 in., no significant change in the plots was observed. Thus, the CMP mesh size of 1.8 was chosen for all the models. Since the liner is in complete contact with the CMP, it has the same mesh size as the CMP. Also, comparing the run time and mesh size of pipe and liner, the model with the mesh size smaller than 1.8 was taking a considerable amount of the computational time (Table 10-4). Thus, the mesh size of 1.8 was chosen for the CMP and the liner. The soil mesh size was taken as 2.4 in. in the vicinity of the pipe and the loading zone and 4.0 in. in the rest of the domain.

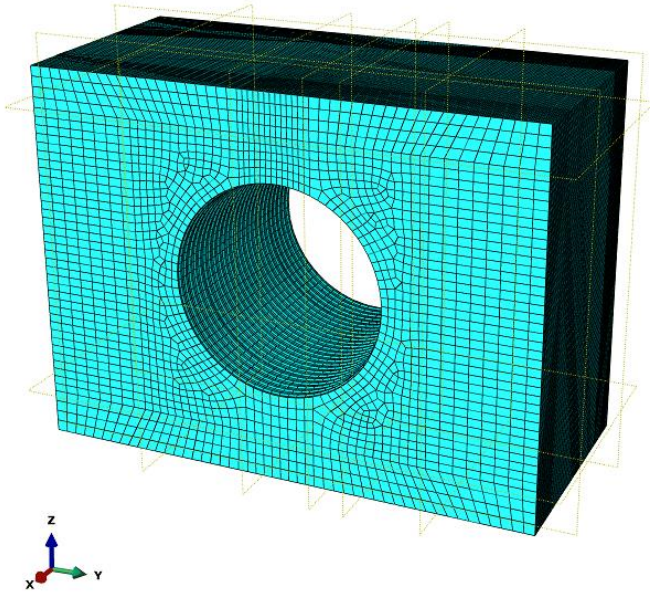


Figure 10-6. Mesh size distribution in the soil.

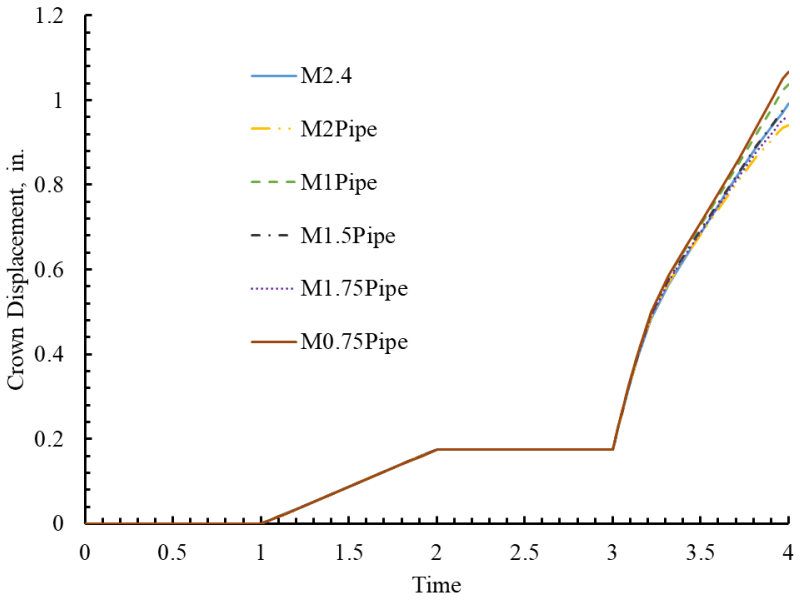


Figure 10-7. Load displacement plot for the pipe at the crown.

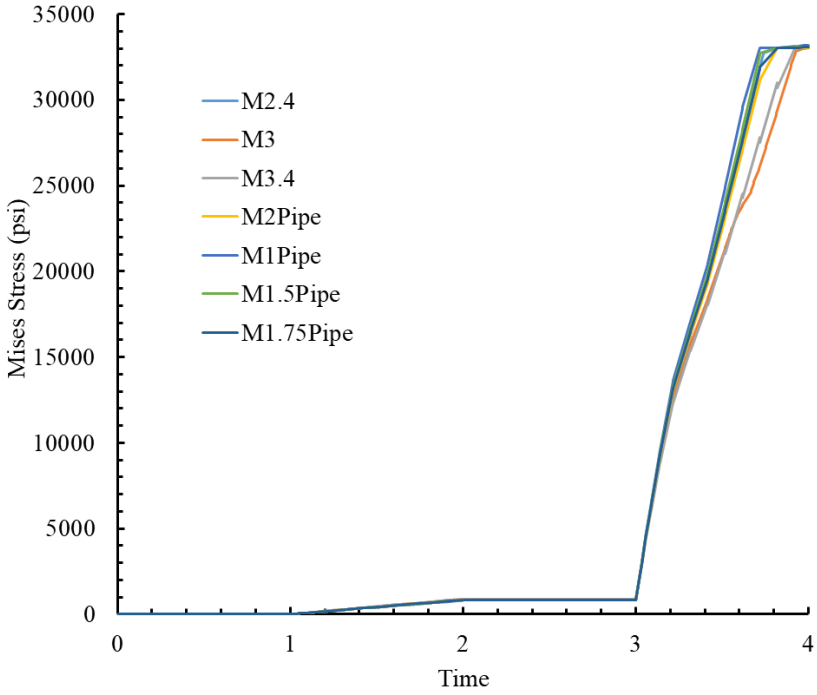


Figure 10-8. Von Mises Stress in the pipe.

10.1.7. Modeling Steps

The following steps were used to simulate the soil box tests of CMP pipes:

STEP-1 Geostatic: Geostatic step was used to model the soil stress field. In this step, only the soil domain was activated, and the inward tunnel surface of the soil was fixed. Geostatic (in-situ) stresses, including vertical and horizontal stress, were

established for the soil domain without considering the CMP pipe. The vertical stresses were defined according to equation 10-1 below, while the lateral stress was defined according to equation 10-2.

$$\sigma = \gamma H \qquad \text{Eq. } 10-1$$

$$\sigma_h = (1 - sin\varphi)\gamma H \qquad \text{Eq. } 10-2$$

STEP-2 Installation of CMP:

The CMP domain was activated. In this step, the gravity load of the pipe was activated, and pipe soil interaction was established by removing the restrictions applied to the inner tunnel surface of the soil.

STEP-3 Removal of the invert:

After the establishment of the pipe load, the invert of the CMP was removed through the process of model change in which the invert part was removed (only applicable to the invert- removed CMPs).

STEP-4 Installation of the liner:

The liner model was activated, and the pipe-liner contact was activated to establish the liner-CMP interaction (only applicable to the invert-removed CMPs with liners).

STEP 5 Load application:

Application of the load on top of the 1 ft cover was initiated by defining the loading displacement.

10.2. Simulation Results of the Control Test

All the results obtained from the FEM models were plotted along with their respective lab test counterparts. The test results obtained from the FE analysis for the intact CMP are discussed below.

10.2.1. Intact CMP Loaded with a 10x20 in.^{2} Load Pad

In the test of the intact CMP, the soil box was loaded using the load pad size of the 10x20 in.^{2}. With the smaller load pad, it was observed that the failure of soil occurred prematurely before any significant deformation in the CMP. During the control test, the soil failed at 21 kips of the load with about 5 in. displacement of soil. After the soil failure, the load continued to increase with more load transferred to the pipe. The maximum capacity of the system was 25 kips with 10 in. displacement of soil. The cover soil failed as the result of bearing capacity failure. Similar to the observation in the lab test, the FEM model also predicted the failure of the soil before any significant deformation in the CMP. However, the FE model did not provide a converged solution after the bearing capacity failure of the intact CMP. Thus, the soil could not be displaced by more than 5 in. The development of the significant plastic strain in the loaded area could be seen in the model before the significant deflection in the pipe (Figure 10-9, Figure 10-11).

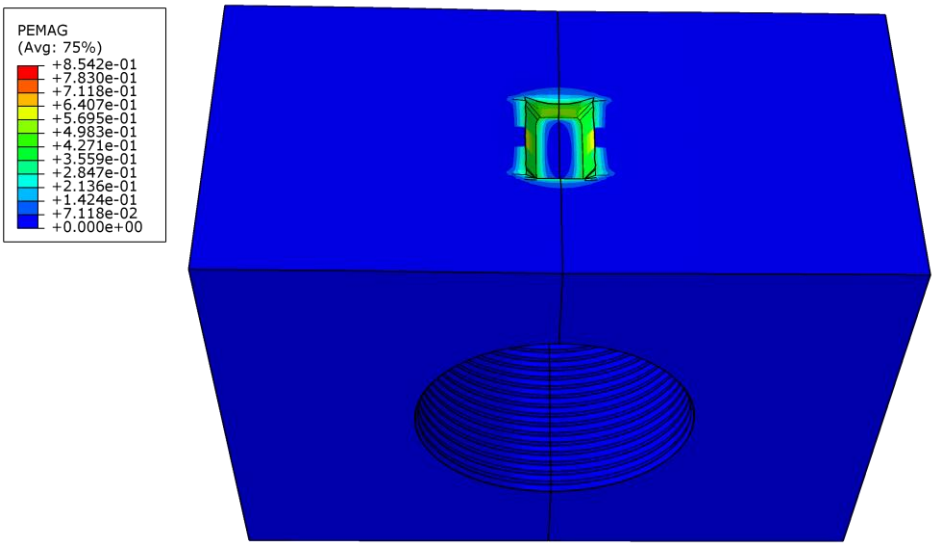


Figure 10-9. Plastic strain due to the soil failure in the loaded area at 5-inch settlement.

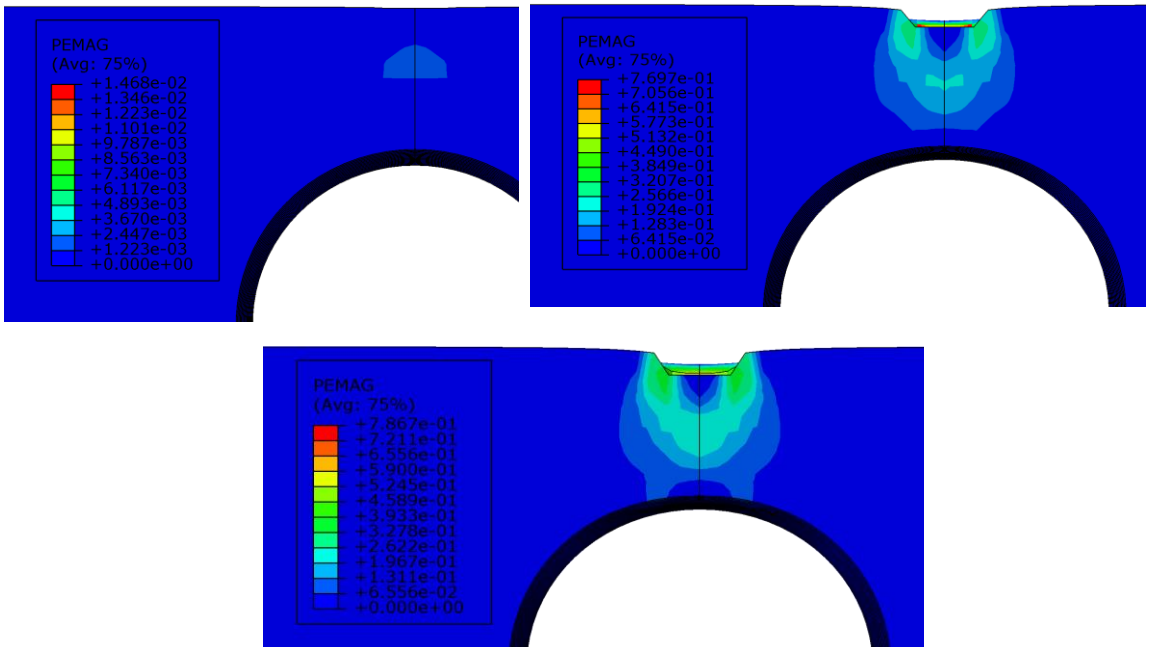


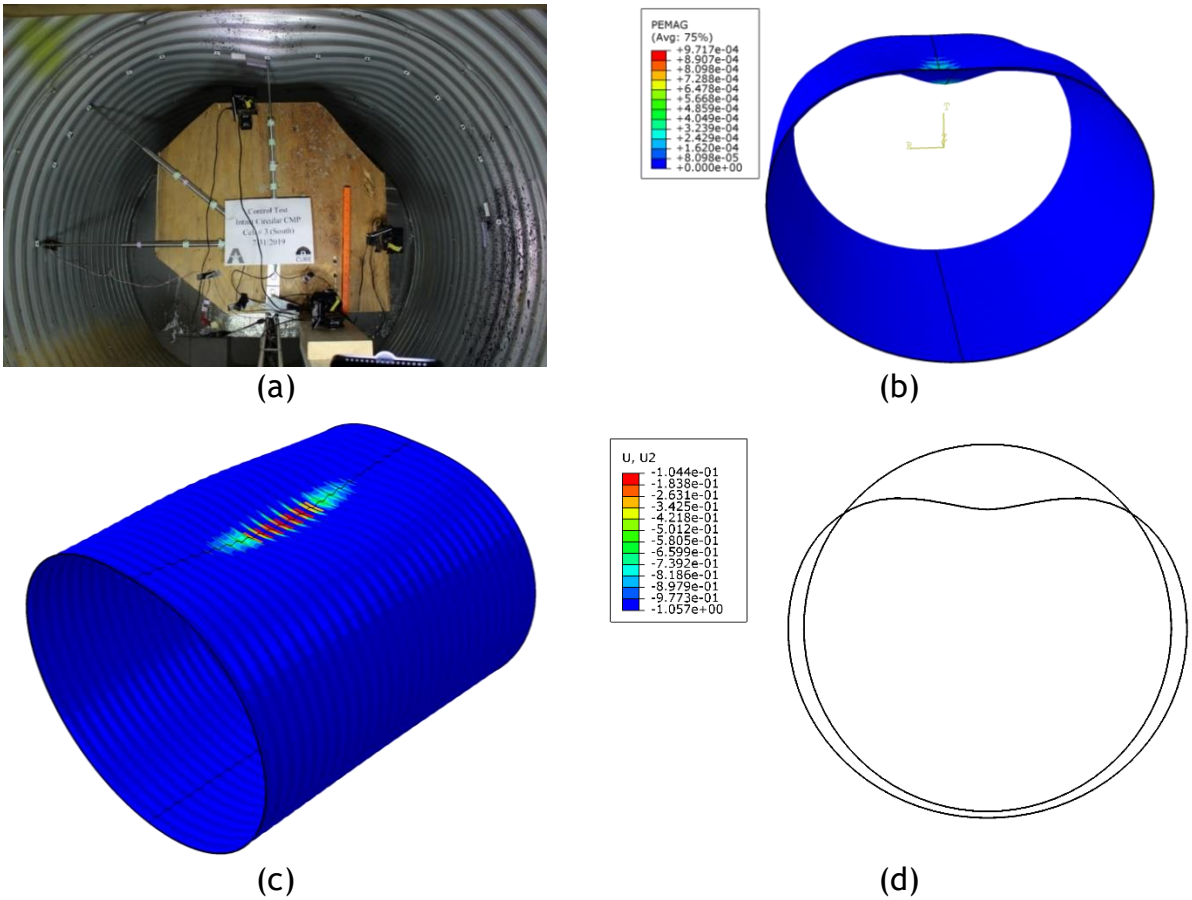
Figure 10-10. Progression of plastic strain under the load pad in soil ((a) at 1 in. settlement, (b) at 4 in. settlement (c) at 5 in. settlement

The FEM model can adequately predict the behavior of the CMP before soil failure, as observed in the lab experiment. As shown in Figure 10-11(a), the deformation of the CMP is pronounced at the crown below the load pad. The deformed shape of the CMP model showed a similar deformation pattern just below the load pad when the deformation was scaled up, as shown in Figure 10-11.

Load displacement plot

Load-displacement curves were determined from the FEM results at the load pad and the CMP crown. In the load-displacement curves, only the incremental displacement caused by the applied load was included. For intact CMP, two load-displacement curves were compared. The first load-displacement curve is obtained for the displacement of the crown at the center of the CMP, which represents the result from the LVDTs placed to read the displacement of the crown in the experiment. The other load-displacement curve was obtained for the soil settlement during the application of the load from the actuator (Figure 10-13). The FE plot was obtained for the 5 in. displacement of the soil.

The load was continued after the bearing failure of the soil. As the load was predominantly transferred to the CMP, the load-displacement curve rose again and then dropped after the local bending failure of the CMP. However, this post soil failure behavior could not be modeled in FEM as the model did not converge in implicit analyses for large and localized deformation. Thus, the comparison between the FE model and the lab test was made for soil displacement less than 5 in.



(a) (b)

(c) (d)

Figure 10-11. Plastic strain and deflection pattern in CMP (a) Experimental Result (b), (c) and (d)FEM Result (scaled up by 5 times).

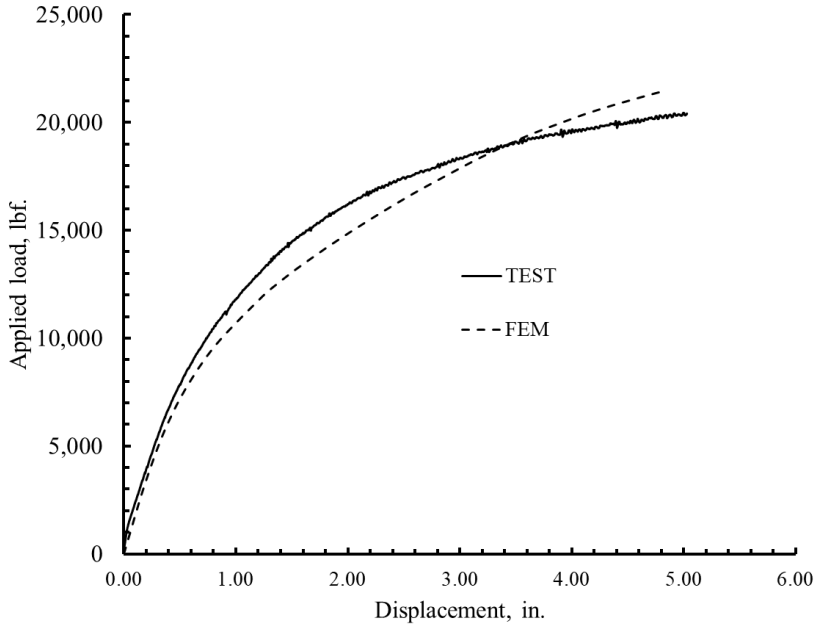


Figure 10-12. Load displacement curve for soil at 5-in. displacement of soil of intact CMP.

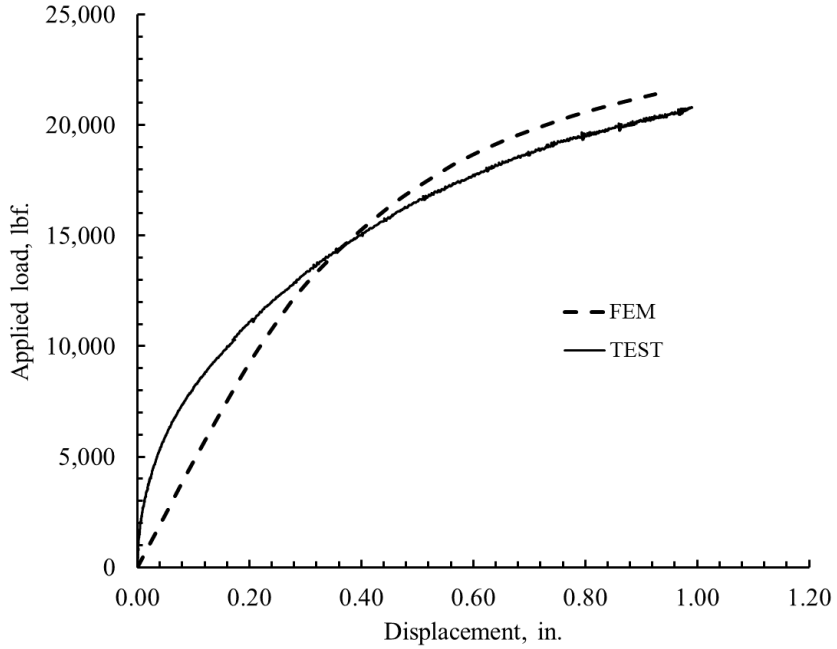


Figure 10-13. Load displacement curve for the crown at 5-in. displacement of the soil of intact CMP.

The load vs. displacement plot shows a good match between the experimental and FEM results. The discrepancy between the load at the 5 in. displacement of soil for the experiment and FEM is about 5 %, while the discrepancy between the pipe crown displacement in the experiment and FEM is about only 1.5 % (Figure 10-13). The results are summarized in Table 10-5.

Table 10-5. Comparison of the results from FEM and experiment.

Model	Applied Displacement of soil (in.)	Maximum Applied Load (kips)	Max. vertical displacement of pipe at the crown (in.)	Discrepancy in displacement (%)	Discrepancy in load (%)
Experimental	5	20.43	0.93	0.0	0.0
FEM	5	21.4	0.92	1.08	4.75

Earth Pressure Distribution

Among the earth pressure cells installed near the top, springline, and invert, only the earth pressure near the top greatly increased with the increase of applied load. Therefore, the FEM comparison was made only for the earth pressure above the crown. The earth pressure variation at the top of CMP was obtained from experimental results, and the FE model at a similar location followed a similar trend (Figure 10-14). It is observed that (Figure 10-14) the simulated earth pressure is less than the measurement at the initial loading and converges to the measurement when it approaches the failure settlement.

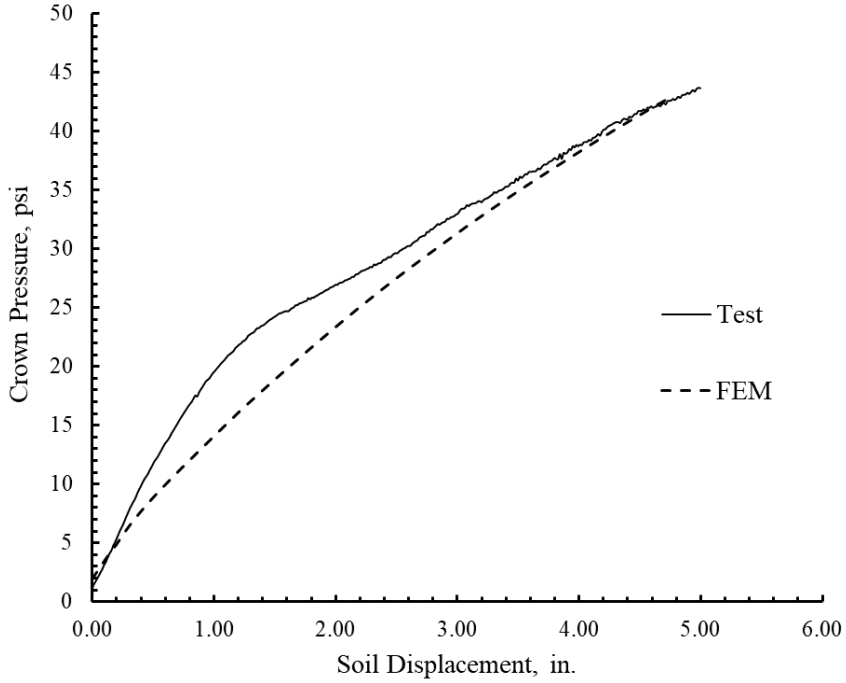


Figure 10-14 Earth pressure distribution just above the crown of the pipe of the intact pipe.

10.2.2. Intact CMP (20x40 in.^{2} load pad)

The first control test of the intact circular CMP with the 10x20 in.^{2} load pad showed a bearing capacity failure of the soil before any significant deformation in the CMP. This was not the desired situation as the failure of the CMP was expected before the bearing capacity failure of the soil. A bigger load pad of 20x40 in.^{2} was used for the

rest of the pipe tests to delay the bearing capacity failure of soil. In addition, a TxDOT Grade D gravel for sub-base layer RCA was used as the top 1 ft cover soil for the rehabilitated invert-cut CMP tests. All these changed conditions were incorporated for the intact CMP FE model, and the results were obtained as the baseline model for the rehabilitated CMP pipe tests.

When loaded with the larger load pad, the CMP pipe reached 5% pipe diameter deflection, the failure criterion for the pipe, before the failure of the soil. The bending failure at the crown (Figure 10-15) extended to both ends of the pipe rather than a more localized one seen in the test with the small load pad.

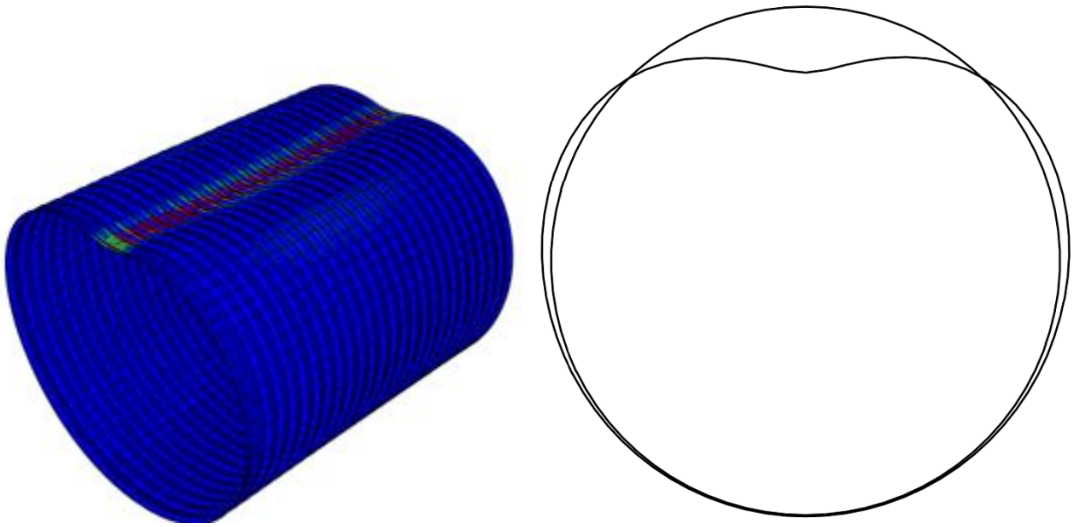


Figure 10-15. Plastic strain and the deformation of the pipe loaded under the 20x40 in.^{2} load pad.

Load Displacement Plots

The load-displacement graphs were plotted from the FEM results against the applied load for movement of soil just below the load pad and the displacement of the crown at the center of the CMP. From the load-displacement graphs, it was found that the crown of the CMP was displaced by more than 4.2 in. i.e., 6.67 % of the diameter of the CMP at the peak load condition while the displacement of the soil at peak load was 5.9 in. Since flexible pipes have the 5% deflection criteria as its failure criteria, the CMP failed before the failure of the soil (Figure 10-16 and Figure 10-17). The result suggests that the use of the bigger load pad avoids the failure of the soil through punching, which was observed in the control test for the intact CMP. With the use of the bigger load pad configuration, the CMP carried nearly double the load as compared with the load-carrying capacity of the smaller load pad configuration. The results and the comparison are summarized in Table 10-6.

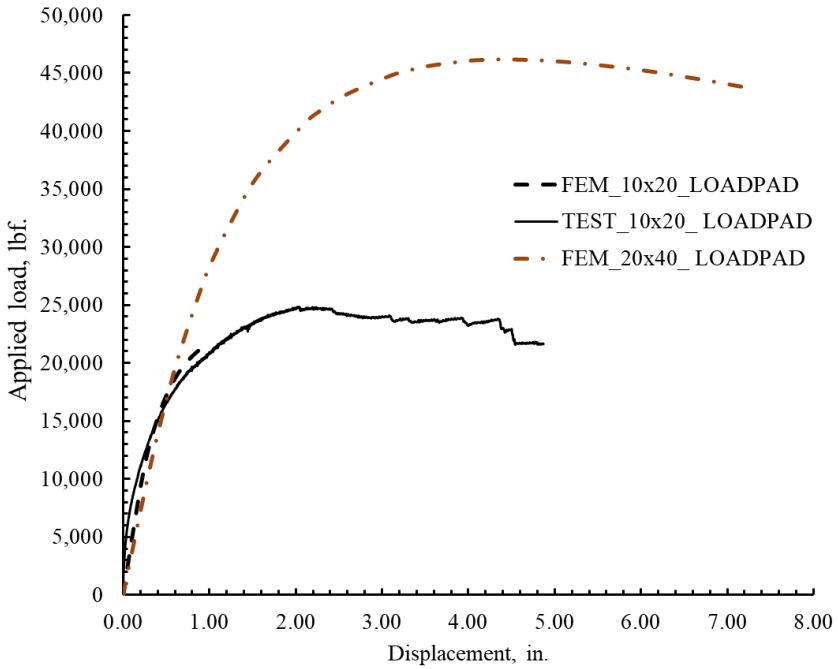


Figure 10-16. Effect of load pad size on the load-displacement at the crown.

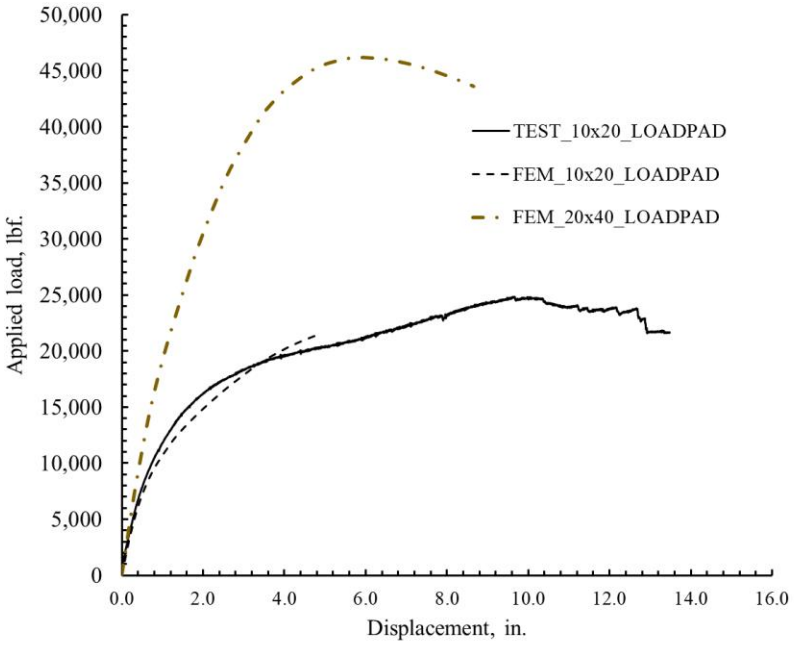


Figure 10-17. Effect of load pad size on the load- soil settlement under the load.

Table 10-6. Comparison of the results for the intact CMP for smaller and bigger load conditions.

Description (At Failure of Soil)	**10x20 in.^{2} Load Pad**	**20x40 in.^{2} Load Pad**
Ultimate load (kips)	21.01	46.05
Crown Displacement (in.)	1.3	4.26
Soil Displacement (in.)	5.0	5.99

Earth Pressure Distribution

The earth pressure at 4 in. above the crown for the bigger load pad region was plotted against the soil displacement and was compared with the earth pressure at the same location for the smaller load pad. The earth pressures for both load pads exhibit similar pressure-displacement behavior for soil displacement less than 4 in. The soil pressure for the large load pad quickly peaks and decreases while the soil pressure for the small load pad continues to increase until failure, as shown in Figure 10-18. The use of the large load pad can delay soil failure and allow the pipe to fail first.

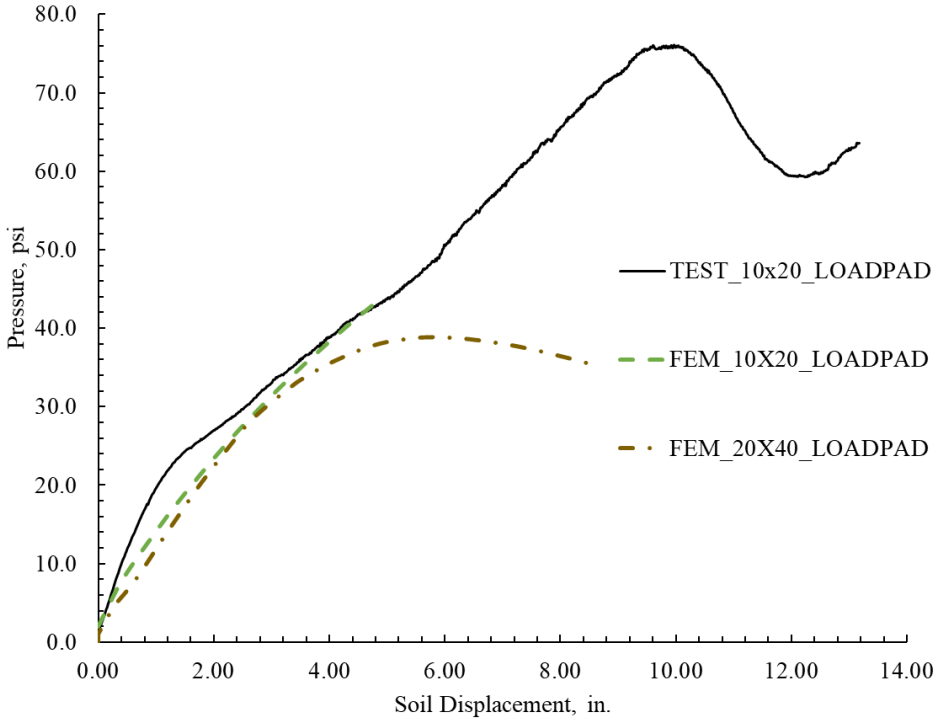


Figure 10-18. Earth pressure comparison for the bigger and smaller load pad conditions.

10.2.3. Invert-Cut CMP

The calibrated FEM model for the intact CMP was modified for modeling the invert-removed CMP. The only modification was the invert-removal from the intact-CMP model. By implementing the model change function in ABAQUS, the invert was removed from the FEM model after the geo-static step. In the lab test, significant movements of the cover soil and the CMP were observed immediately after the invert removal. A gap above the top was found between the soil and the pipe. The FEM model was capable of simulating the invert removal from the intact CMP. However, the FE model was not able to simulate the collapse behavior of the soil as observed in the experiment. The observed cover soil settlement was more than 6 in. on the top surface while the FE model predicted only about 1 in. settlement. After the invert was removed, the CMP moved downward, and the invert-gap was reduced. The CMP

deformation is reported in Figure 10-19 (b) (Darabnoush Tehrani, et al., 2020). The following was observed from the experiment. After removal of the invert, the gap at the invert was reduced by 3 inches on each side of the invert. The crown moved 3.1 inches vertically downward. Also, the edges of the gap moved slightly into the soil. The crown of the CMP had 5 in. downward movement. The following was observed from the FEM simulation results. From the FE results, it was obtained that after the invert removal, the CMP invert edges moved by 2.4 in. from both sides resulting in the reduction of 4.8 inches of the gap (Figure 10-19(a), (c)). The test result for the invert removal case was reported by (Darabnoush Tehrani, et al., 2020). The results after the invert removal are summarized in Table 10-7.

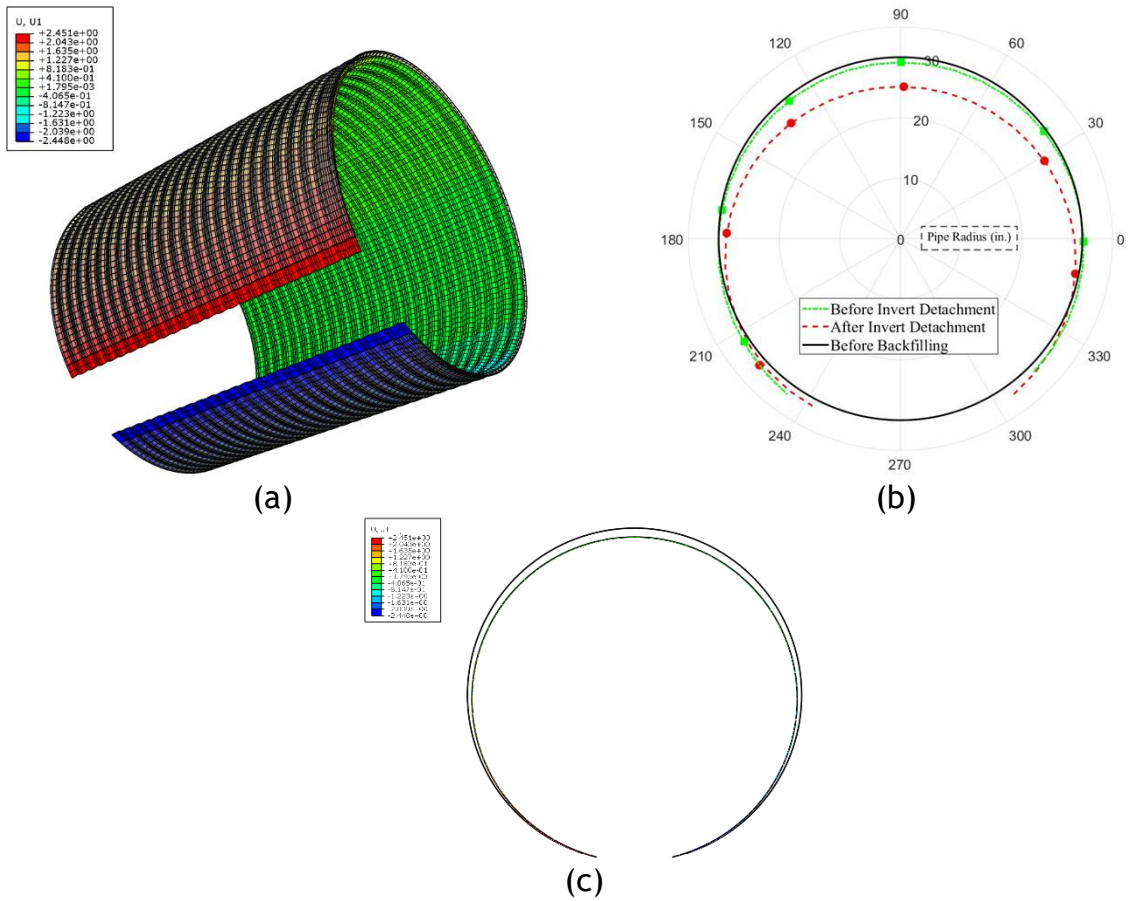


Figure 10-19. (a) Reduction in the invert gap from FEM (b) Experimental recording of the reduction in invert gap by Digital Image Processing (Darabnoush Tehrani, et al., 2020) (c) Vertical diameter change from FEM after invert removal.

Table 10-7. Comparison of the change in dimension of the pipe after the removal of the invert.

Description	FEM	TEST
Reduction in the 18 in. invert gap (in.)	2.4	3
Reduction in vertical diameter (in.)	2.25	3.1
Soil movement (in.)	1.0	6.5

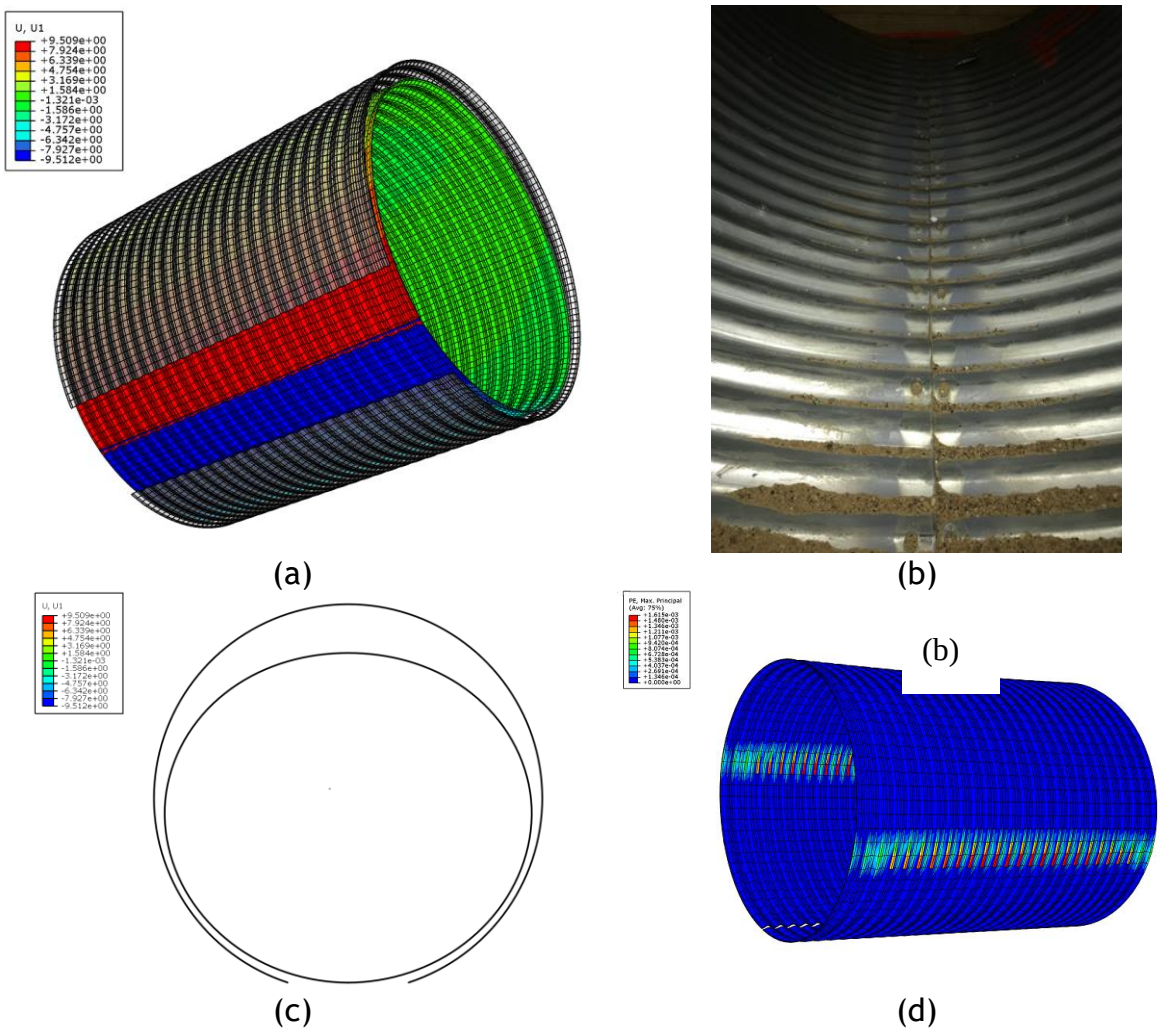


Figure 10-20. Complete closure of the invert after loading (a), (c) from FEM (b) closure of invert seen in the Experiment (d) plastic strain at the spring line area.

Summary of the invert-cut FE model

Comparing the FE results and the experimental results from the invert-cut CMP, the model over-predicts the load by about 145% at the time when the two invert edges meet. Also, the FE model could not predict the collapse of the soil as it was in the experiment condition. When the loading on the load pad started, the invert-gap was closing rapidly, and the invert edges were in contact at 8 kips load. In the FEM simulation, the edges closed at 22 kips load. The closing of the invert during the application of load is seen in

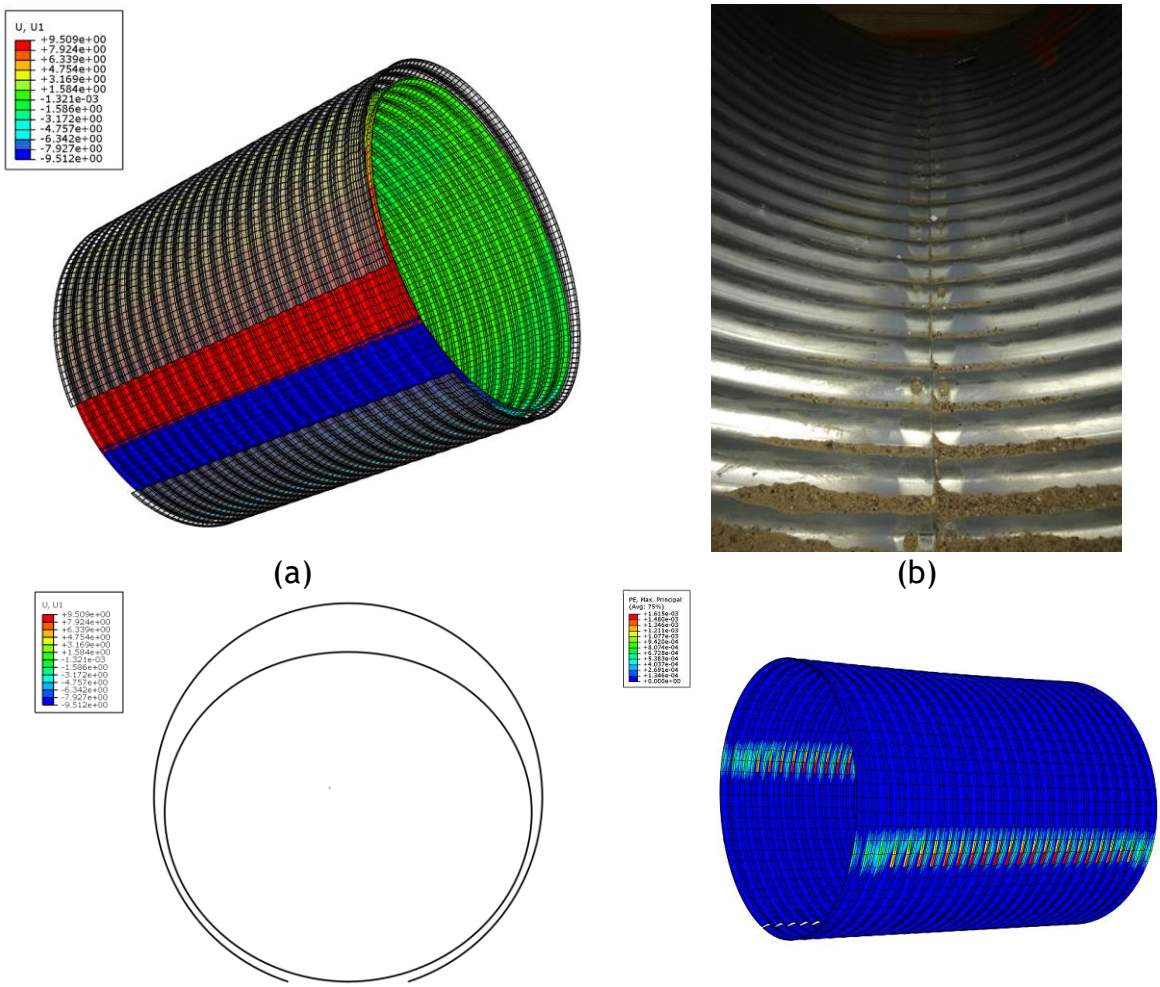


Figure 10-20. FEM exhibited a stiffer response and significantly overt predict the load-bearing capacity. The load-displacement comparison for the invert-cut CMPs can be found in Appendix 10-A.

10.3. Results from Circular polymeric SAPL Lined CMPs

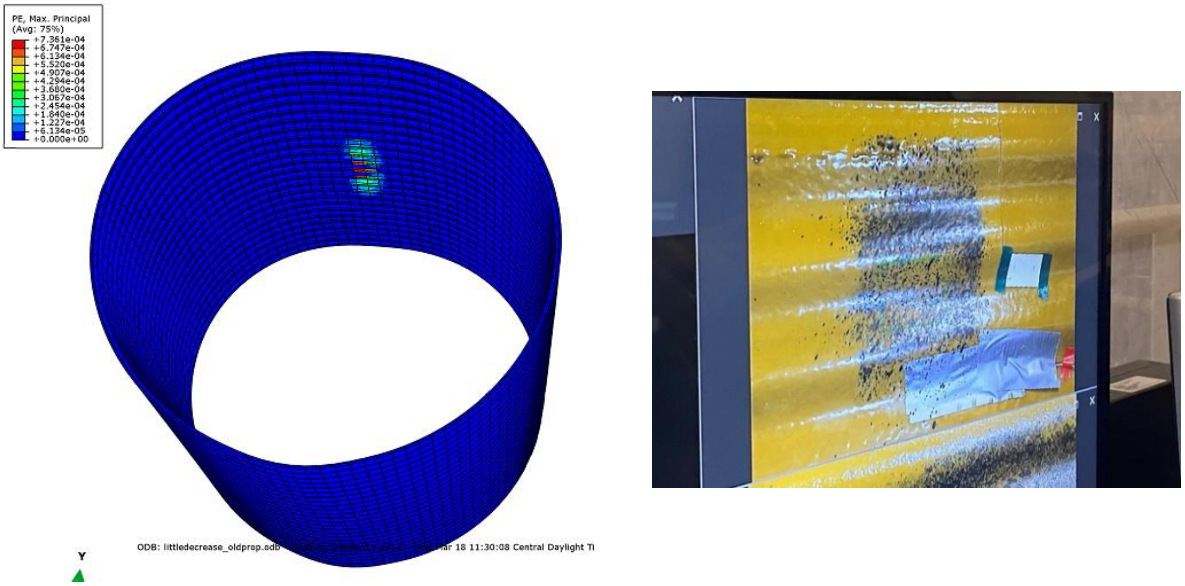
For the tests of the CMP rehabilitated by spray-applied pipe liner, the process of the invert removal was changed. At first, the mid-section of the invert was removed while 1 in. strips on the two ends of the invert was left in place. With the 1 in. end strip maintaining the ring stiffness in the CMP, the liner was applied. After the liner was set, the remaining end strips were removed. This time, no noticeable movement in the soil or the pipe was observed. The collapse of the soil was prevented, and the calibrated intact-circular CMP pipe model could be modified to model the rehabilitated CMPs. The invert removal was initiated before the activation of the geo-static stress of the soil. The liner and CMP were activated simultaneously to take the geo-static stress of the soil.

The tensile strength test of liners performed at CURIE suggests that the liner demonstrates mostly linear elastic behavior with brittle failure. Therefore, the liner was modeled using an elastic-plastic model and the plastic strain in the liner is

considered as the crack strain in the liner. Thus, the appearance of the 1st crack in the experiment was related to the appearance of the first plastic strain in the liner model. The results for the circular lined CMPs are discussed in detail for the 0.25-in. thick liner while for the remaining liner thickness, only a brief description is presented in this section, and all detailed graphs are placed in Appendix 10-B.

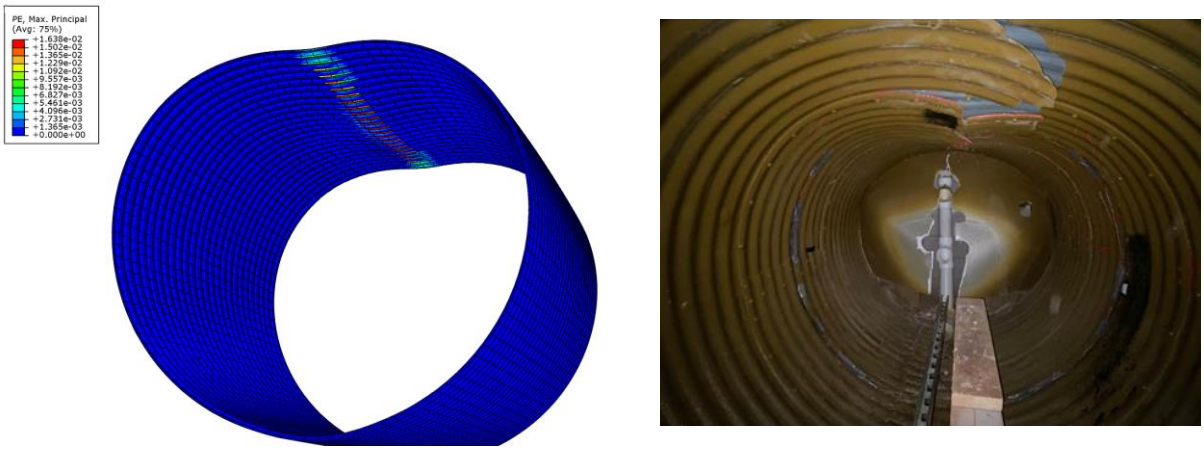
10.3.1. 0.25-in. thick polymeric SAPL

The FE model for 0.25 in. liner compared well with the experimental results. In the test, it was observed that the first crack occurred right at the center of the CMP at the crown region. In the FEM model also, the 1st plastic strain was seen in the center of the CMP in the crown region (Figure 10-21). The plastic strain seen in the crown propagated longitudinally along the crown of CMP in the FE model, which matches fairly well with the propagation of the crack in the experimental results. (Figure 10-22). The deformation of the liner during the time of the first crack and at ultimate load condition is shown in Figure 10-23, Figure 10-24. The comparison of the other results is further discussed in this section:



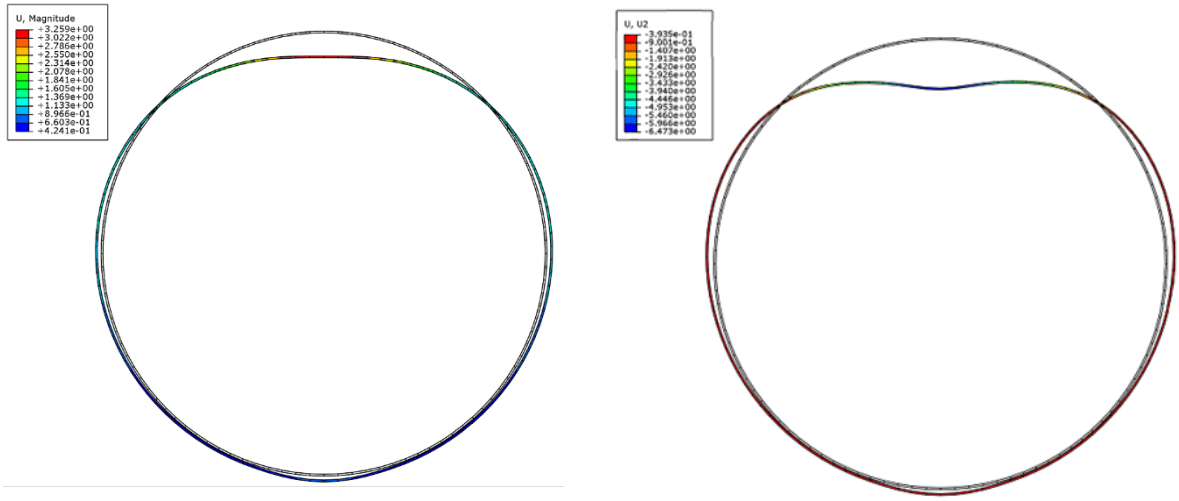
(a) (b)

Figure 10-21. (a) 1st plastic strain in the CMP (b) 1st crack in the model for 0.25 in. thick polymeric SAPL



(a) (b)

Figure 10-22. (a) Plastic strain at the ultimate load in the FE model (b) Crack in the model at the end of the test for 0.25 in. thick polymeric SAPL



(a) (b)

Figure 10-23. (a) Deformation of CMP at the time of the 1st plastic strain, and (b) Deformation of CMP at the ultimate load condition for 0.25 in. thick polymeric SAPL

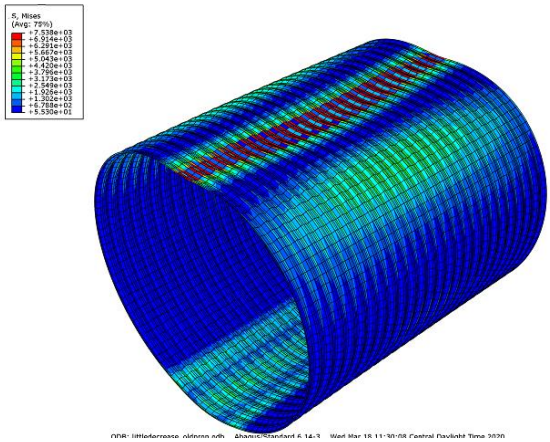


Figure 10-24. Stress distribution in the pipe at the ultimate load conditions for 0.25-in. thick polymeric SAPL.

Load Displacement Plots

The displacement of the CMP and the liner was monitored at the crown using the LVDT readings in the experiment. The load-displacement curve was plotted for the FE results at the same location (Figure 10-25). The comparison showed very similar results, and the predictions of the crack load, ultimate load, and the displacement of the pipe were within the accuracy of 8 % (Table 10-8).

Initially, the measured curve shows a stiffer response than the FEM model. This is attributed to the fact that the liner was adhered to the wall due to the over spraying of the liner, which was not included in the FE model. The over spraying of the liner to the end wall caused the rehabilitated CMP to be stiffer. During the test, a slight drop in the load was observed at the appearance of the first plastic strain while no such drop was observed in the simulated curve. The liner remains its strength in the FEM model when plastic is developed. However, the cracked liner lost its strength in the experiment. The FE results showed the first plastic strain at 44 kips of the load, and this load for the appearance of first plastic strain in the model matches closely with the load at the appearance of the first crack from the experiment. The displacement of the liner at the first crack load in the experiment and the first plastic strain also showed a discrepancy of 6% only. The liner pipe system took peak load of 46 kips in the test, which was predicted to the accuracy of 2 % by the FE model. Overall, the FE model predicted the load and the displacement at the different locations with enough accuracy, as shown in Figure 10-25.

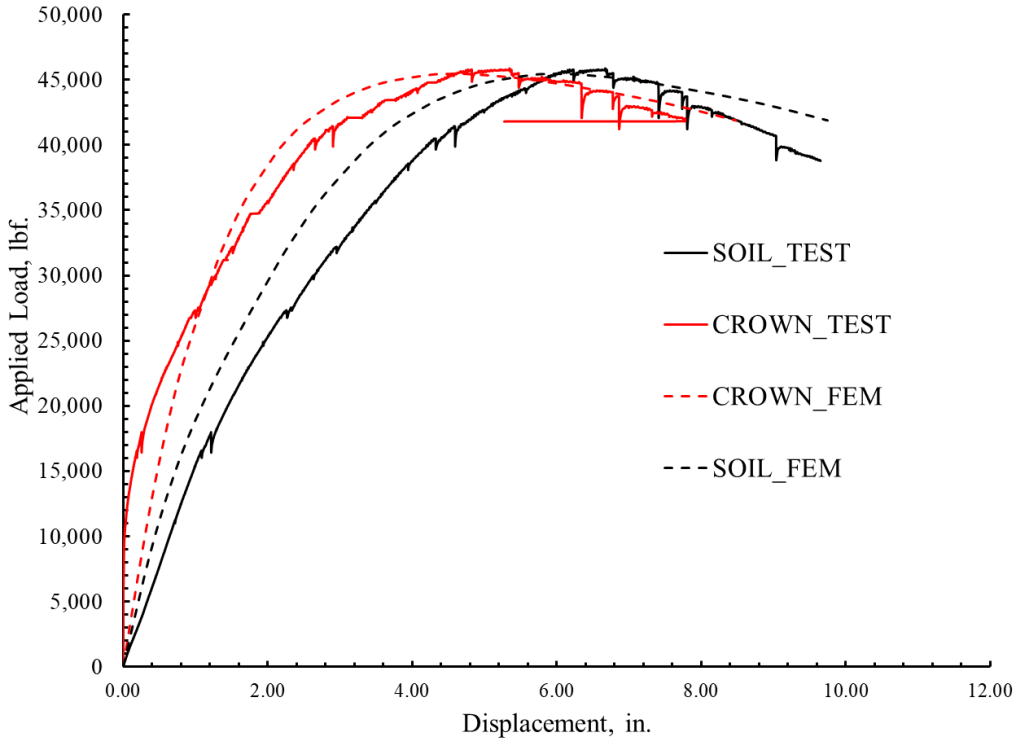


Figure 10-25. Comparison of the liner displacement at crown for 0.25 in. thick polymeric SAPL between experiment and FEM results.

Table 10-8. Comparison of the load-displacement between FE model and the experimental results for 0.25-in. thick polymeric SAPL.

Description	1st plastic strain	1st crack	Discrepancy Test vs. FEM (%)	Ultimate Load		Discrepancy Test vs. FEM (%)
	FEM	Test		FEM	Test	
Crown Displacement (in.)	3.13	2.92	6.7	4.98	5.23	5.0
Soil Displacement (in.)	4.79	4.64	3.1	6.48	6.49	0.5
Load (kips)	44.40	41.3	6.9	46.37	45.78	1.2
Spring line disp. (in.)	0.68	0.86	26.4	0.85	1.14	25.4

Earth Pressure Distribution

Besides the load-displacement comparison, the comparison of the earth pressure obtained from the experiment and the FE model was also made. The comparison of the earth pressure is made for only the pressure obtained at the crown as the measured earth pressure at the springline and invert are low and doesn't increase much with the increase of the applied load measured. The pressure plot showed a similar pattern between the experimental and the FE model results (Figure 10-26, Figure 10-27). The earth pressure at the time of the first crack and the first plastic strain of the liner is nearly equal. The earth pressure at the 1st crack is 36.42 psi (at 2.92 in. liner displacement in the experiment), while in the FE model at the time of 1st plastic strain, the earth pressure was 36.16 psi (at 3.13 in. liner displacement). The ultimate crown pressure showed a discrepancy of about 7% between the experimental and FE model results.

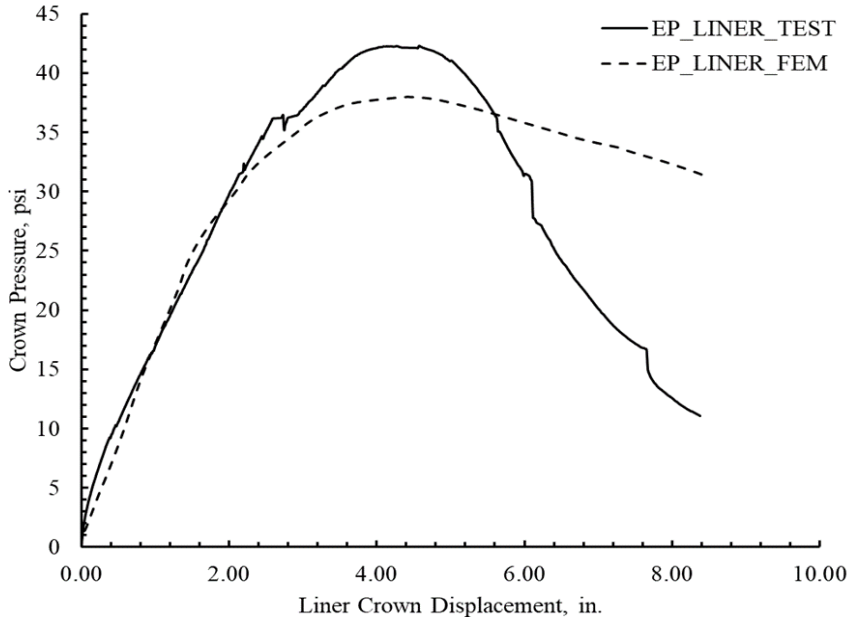


Figure 10-26. Comparison of the earth pressure at crown plotted against the liner displacement for 0.25 in thick polymeric SAPL

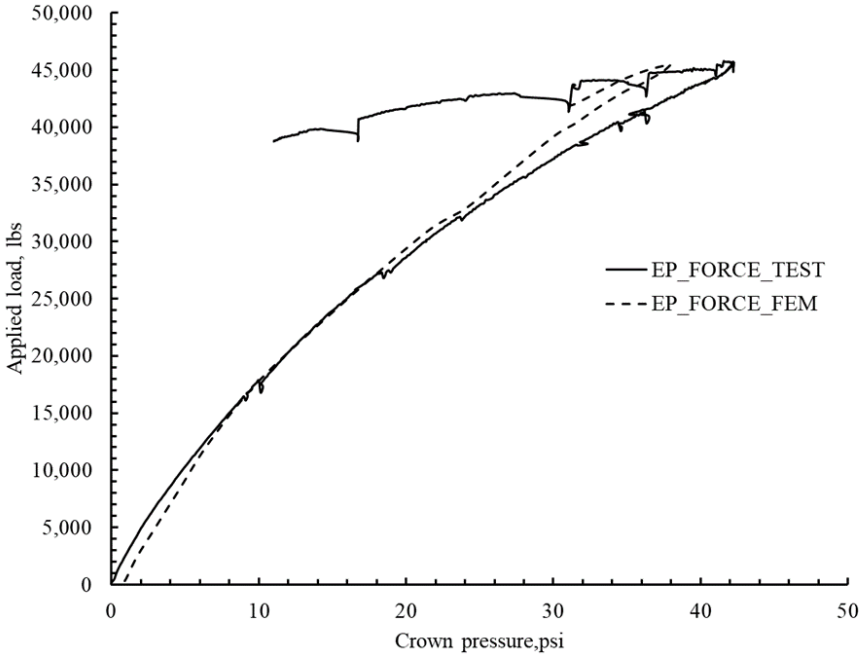


Figure 10-27. Comparison of the earth pressure at crown plotted against the applied load for 0.25 in. thick polymeric SAPL

10.3.2. 0.5-in. thick polymeric SAPL

The FE model for 0.5-in. thick SAPL also compares well with the experimental results. Like the test on 0.25-in. thick SAPL, it was also observed that the first crack occurred at the center of the CMP at the crown region (Figure 10-28). In the FEM model also the first plastic strain was seen in the center of the CMP in the crown region. The plastic strain propagated longitudinally along with the crown in the FE model, which matches the observed propagation of the crack during the lab test. The detailed graphs of the load-displacement for 0.5-in. thick liner is presented in Appendix B. Table 10-9 shows the comparison of the load and displacement at the crack and ultimate load for 0.5 in. thick liner.

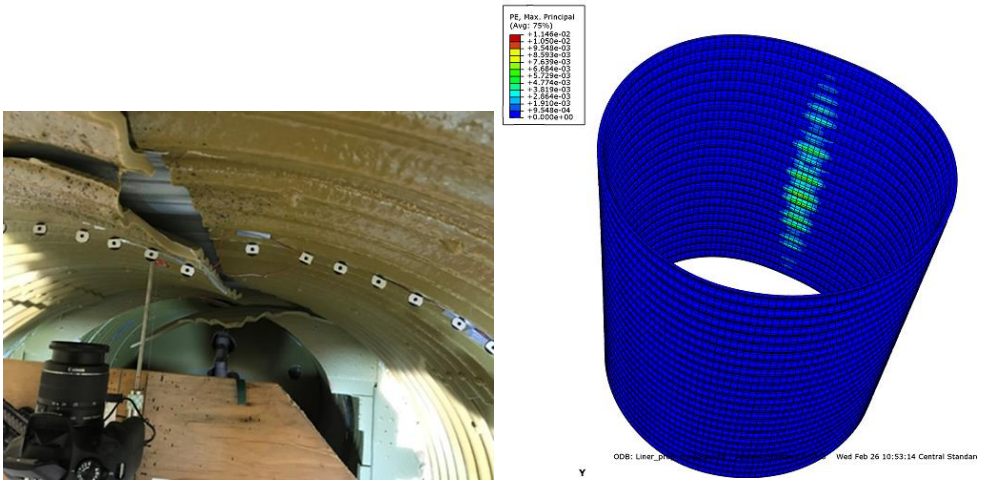


Figure 10-28. Crack in the CMP (Left) Plastic strain in the crown from FE model (Right) of the CMP at the ultimate load conditions for 0.5 in. thick polymeric SAPL.

Table 10-9. Comparison of the load and displacement at the crack and ultimate load conditions for 0.5-in. thick polymeric SAPL.

Description	1st plastic strain	1st crack	Discrepancy Test vs. FEM (%)	Ultimate Load		Discrepancy Test vs. FEM (%)
	FEM	Test		FEM	Test	
Crown Displacement (in.)	2.01	2.18	8.01	5.08	4.74	6.00
Soil Displacement (in.)	3.45	3.02	12.00	7.17	6.09	15.06
Load (kips)	43.11	42.59	1.20	52.09	52.24	0.20
Spring line disp. (in.)	0.64	0.60	6.25	0.99	1.15	15.00

10.3.3. 1-in. thick polymeric SAPL

Like the test on 0.25 in. thick SAPL and 0.5 in. thick SAPL, in this test also it was observed that the first crack occurred right at the center of the CMP at the crown region. In the FEM model also the 1st plastic strain was seen in the center of the CMP at the crown region. After that in the FE model the plastic strain propagated along the centerline in the FEM, which was like the experiment results (Figure 10-29). The pipe did not deflect much after the crack in the ultimate load conditions, unlike the other thickness liner.

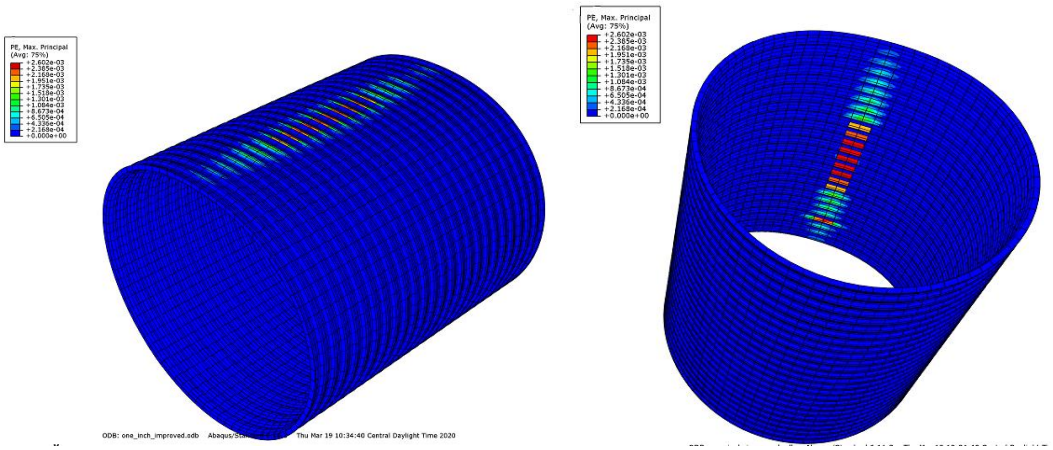


Figure 10-29. Plastic strain in the inside and outside the liner for 1 in. thick polymeric SAPL.

Like previous comparisons, for 1 in. thick SAPL also the load-displacement comparison was made for the displacement of the crown, spring line, shoulder of the liner, and settlement of the soil. This FE model showed similar results, and the prediction of the crack load, ultimate load, and the displacement of the pipe were within the discrepancy of less than 2% for most of the cases (Table 10-10). The details of the comparison for the different parameters are presented in Appendix 10-B.

Table 10-10. Comparison of the load and displacement at crack and ultimate load conditions for 1-in. thick polymeric liner.

Description	1st plastic strain	1st crack	Discrepancy Test vs. FEM (%)	Ultimate Load		Discrepancy Test vs. FEM (%)
	FEM	Test		FEM	Test	
Crown Displacement (in.)	3.05	2.36	22	3.85	4.16	12
Soil Displacement (in.)	5.42	4.9	10.90	8.0	7.4	17
Load (kips)	64.97	66.26	2	73.27	72.17	4
Spring line disp. (in.)	0.88	0.70	12.63	1.08	1.02	5.55

Summary

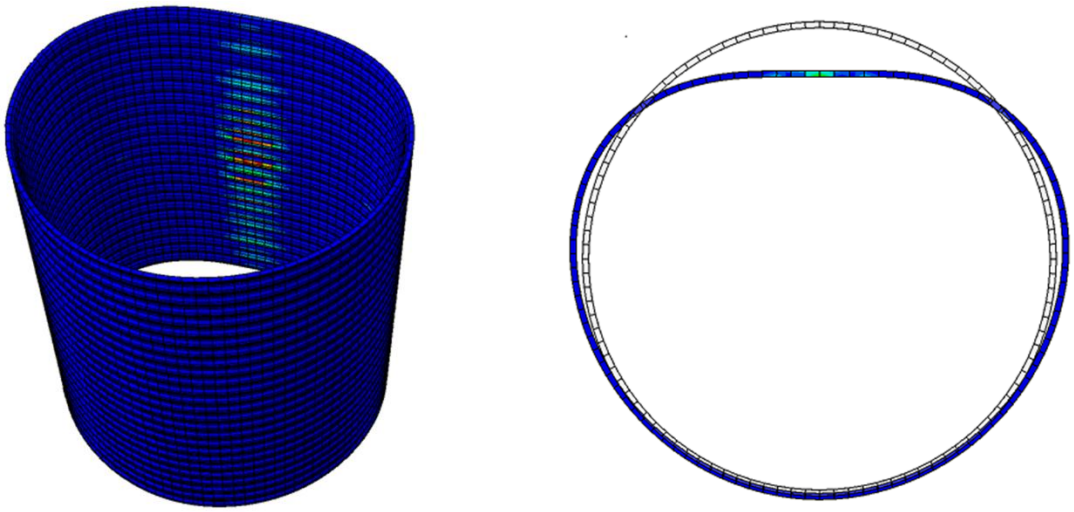
The FE analyses of the invert removed-circular CMPs rehabilitated by the polymeric Spray Applied Pipe Liner (SAPL) show the FEM results agree with the test result. The load-displacement plots were compared for the soil at the top and displacement of the pipe crown. The soil pressure was compared at the location 4 in. above the crown. The crack load was also predicted by the plastic strain in the liner. The results are predicted with a discrepancy of around 10%. Also, the assumption of the 1st plastic strain as the 1st crack predicts the crack and the crack pattern in the CMP well. From both the test and FEM results it is seen that the rigidity of the pipe is increased with the increase in the thickness of the liner. The drop in the load after the ultimate load is not predicted by the FE analysis as the FEM model was implicit and was not modeled for the -post-failure analysis of the liner. Although predicting the ultimate load for the thinner liner thickness was not a problem as the load-displacement curve first flatten and then only the drop was seen in test, and the FEM was able to predict the flatten curve for 0.25 in. thick liner and 0.5 in. thick liner. But for 1 in. thick liner, there was no flattening of the curve before the drop in the load, so the ultimate load was obtained by providing the ultimate displacement to the soil, after which the FE model fails to converge.

10.4. Parametric Analysis on Lined Invert-Removed Circular CMP pipe

After the calibration of the lined invert-removed circular CMP models, a parametric analysis was performed for different liner thicknesses. The chosen liner thicknesses for the parametric analysis are: 0.75-in., 1.5-in., and 2-in. All the above models were performed for CMP lined by following the corrugations. Another lining method is to fill the corrugations first and then spray the entire pipe. One representative FEM model with 0.25 in. liner was developed for CMPs repaired with filled corrugations. The highlights of the FEM simulations are presented in this section, and the load-displacement plots for each case are provided in Appendix 10-B.

10.4.1. 0.75-in thick polymeric SAPL

For 0.75-in thick SAPL also the first crack and the following cracks would occur right at the crown (Figure 10-30).



(a) (b)

Figure 10-30. (a) Development of plastic strain in the inside polymeric liner for 0.75 in. thickness, and (b) Deformation pattern of the polymeric liner.

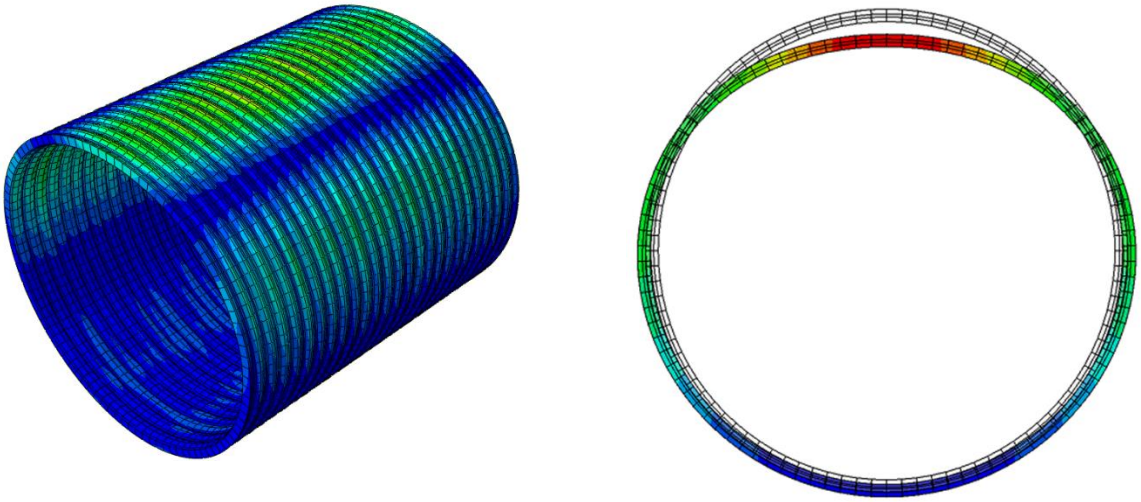
The liner and the CMP system would take the ultimate load of 65 kips while the load at the first crack is 53 kips. The first plastic strain in the liner appears after 2.6 in. displacement of the liner. The results are summarized in Table 10-11.

Table 10-11. Predicted crack and ultimate load and displacement for 0.75-in. thick polymeric SAPL.

Description	Predicted 1st crack condition	Ultimate Load
	FEM	FEM
Crown Displacement (in.)	2.6	5.77
Soil Displacement (in.)	4.91	9.7
Load (kips)	52.47	65.37

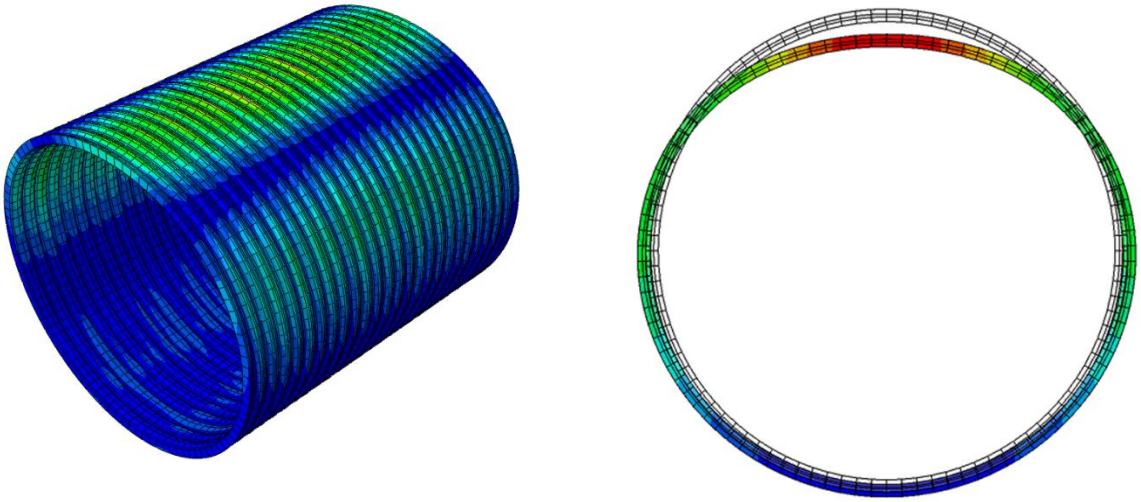
10.4.2. 1.5-in. thick polymeric SAPL

A very stiff response of the liner was observed for 1.5-in thick SAPL, and no plastic strain was observed in the model till the FE model failed to converge. Since the load taken by the system was more than 79 kips the failure of the soil occurred before any strain could be seen in the model, thus causing convergence error in the model. The displacement of the circular CMP was also only around 2.76 inches at these ultimate load conditions. Von Mises stress at the ultimate load and deformation of the liner at 79 kips of load is shown in



(a) (b)

Figure 10-31.



(a) (b)

Figure 10-31. (a) Ultimate von Mises stress distribution around the liner and (b) Deformation pattern for 1.5- in. thick polymeric SAPL.

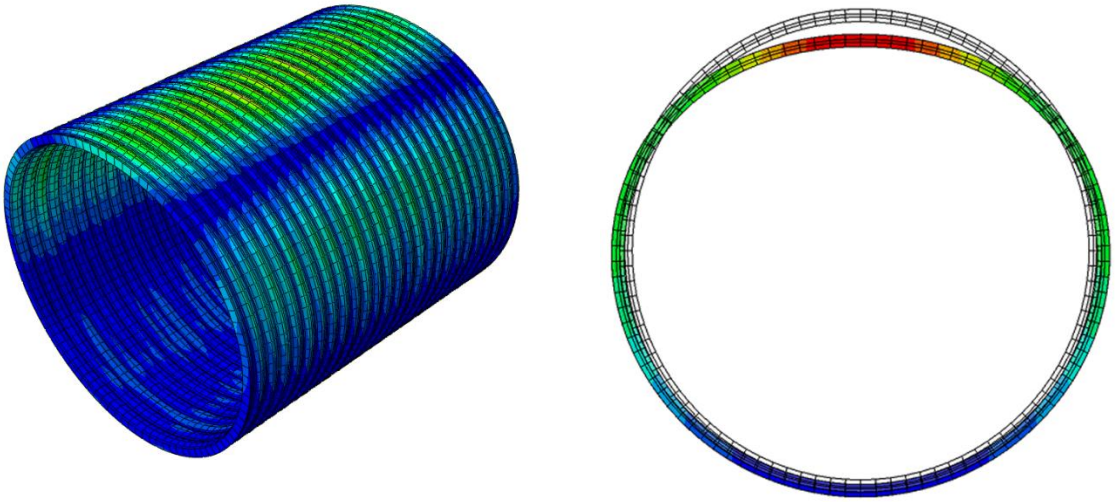
The displacement of the liner at 79 kips of the load was 2.75 in. The load-displacement graphs are presented in Appendix 10-B. The results are summarized in Table 10-12.

Table 10-12. Predicted crack and ultimate load for 1.5-in. thick polymeric SAPL.

Description	Predicted 1st crack load conditions	Ultimate Load
	FEM	FEM
Crown Displacement (in.)	2.76	2.76
Soil Displacement (in.)	7.47	7.47
Load (kips)	78.98	78.98

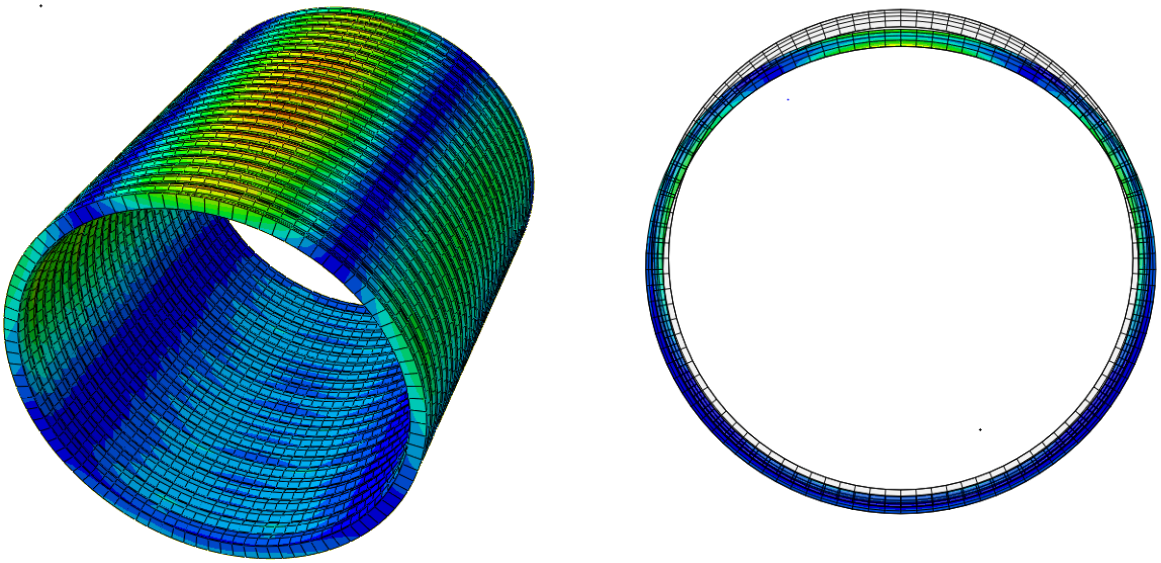
10.4.3. 2-in. thick polymeric SAPL

For 2-in. thick SAPL also a very stiff response of the liner was observed, and no plastic strain was observed in the model until the FE model failed to converge and reach the ultimate load. Since the load taken by the system was more than 80 kips the failure of the soil occurred before any plastic strain could be seen in the model, thus causing convergence error in the model. The displacement of the circular CMP was also only around 2.06 inches at this ultimate load condition. Von Mises stress at the ultimate load and deformation of the liner at 79 kips of load are shown in Figures 10-31 and 10-32.



(a) (b)

Figure 10-31. (a) Development of plastic strain and (b) Deformation pattern for 2- in. thick polymeric SAPL.



(a) (b)

Figure 10-32. (a) Development of plastic strain and (b) Deformation pattern for 2- in. thick polymeric SAPL.

The ultimate load for 2-in. polymeric thick liner would be 80 kips and the crack in the model would occur only after the failure of the soil. The displacement of the liner at the ultimate load was around 2.76 in. The results are summarized in Table 10-13.

Table 10-13. Predicted crack and ultimate load for 2-in. thick polymeric SAPL.

Description	Predicted 1st Crack Condition	Ultimate Load
	FEM	FEM
Crown Displacement (in.)	2.06	2.06
Soil Displacement (in.)	6.91	6.91
Load (kips)	80.50	80.50

10.4.4. 0.25-in thick (over the Crest) polymeric SAPL (Filled Corrugation)

All the results presented above represent the rehabilitation techniques that follow the corrugation profile. Other techniques of the rehabilitation would be filling the corrugation with the same material and then applying the SAPL. FEM was employed to obtain the results for the 0.25-in thick SAPL with filled corrugation. The appearance of the plastic strain or the predicted crack was right at the center, and it propagated along with the crown as it approached the ultimate load. The load-deformation and appearance of plastic strain are shown in Figure 10-33.

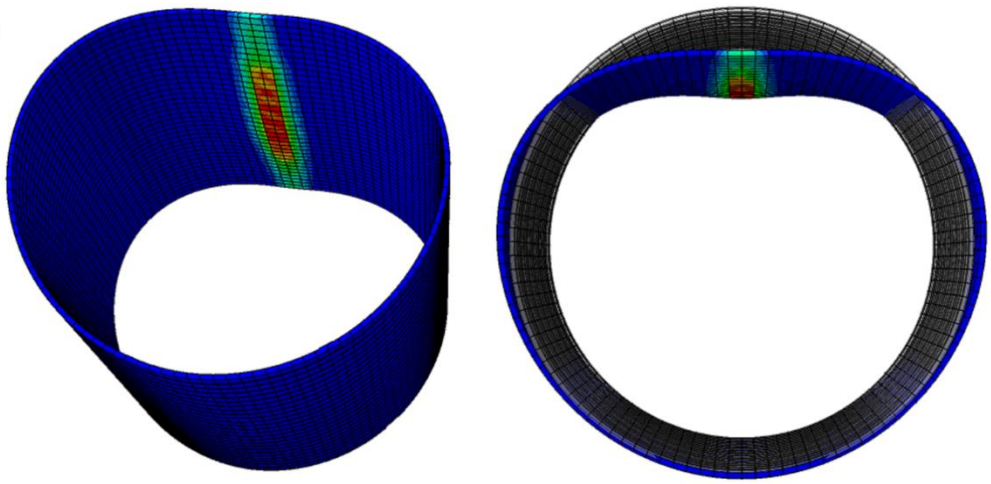


Figure 10-33. (a) Development of plastic strain (b) Deformation pattern for 0.25-in thick polymeric SAPL with filled corrugation.

Load Displacement Plots

A load-displacement curve was plotted for the 0.25-in. thick polymeric SAPL (over the crest). The results are summarized in Table 10-14.

The load-displacement curve shows the displacement of the liner and the soil under the application of the load. From Figure 10-34 it is observed that the liner and the CMP system would take 58 kips of the ultimate load while the first crack would occur after 51 kips of load. The ultimate load and the crack load lie between the results obtained from 0.5-in. thick SAPL and 0.75-in. thick SAPL. The displacement of the liner at the ultimate load was around 2.73 in. The results are summarized in Table 10-14.

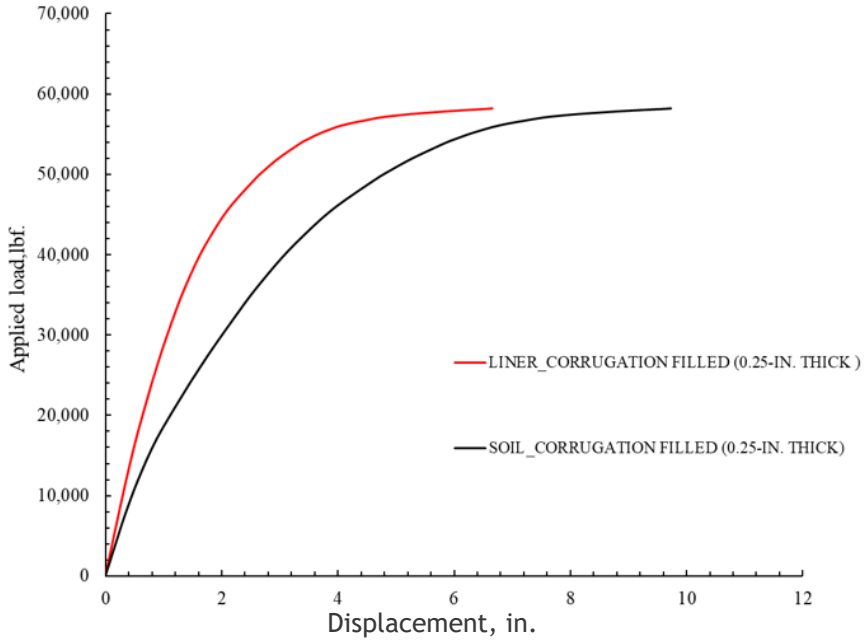


Figure 10-34. Load displacement plot for the liner displacement at crown and settlement of soil from FE analysis for 0.25-in. thick (filled over the crest) polymeric SAPL.

Table 10-14. Prediction of crack and ultimate load for 0.25-in. thick filled corrugated polymeric SAPL CMP.

Description	Predicted 1st crack condition	Ultimate Load
	FEM	FEM
Crown Displacement (in.)	2.73	5.6
Soil Displacement (in.)	4.91	9.0
Load (kips)	50.08	58.25

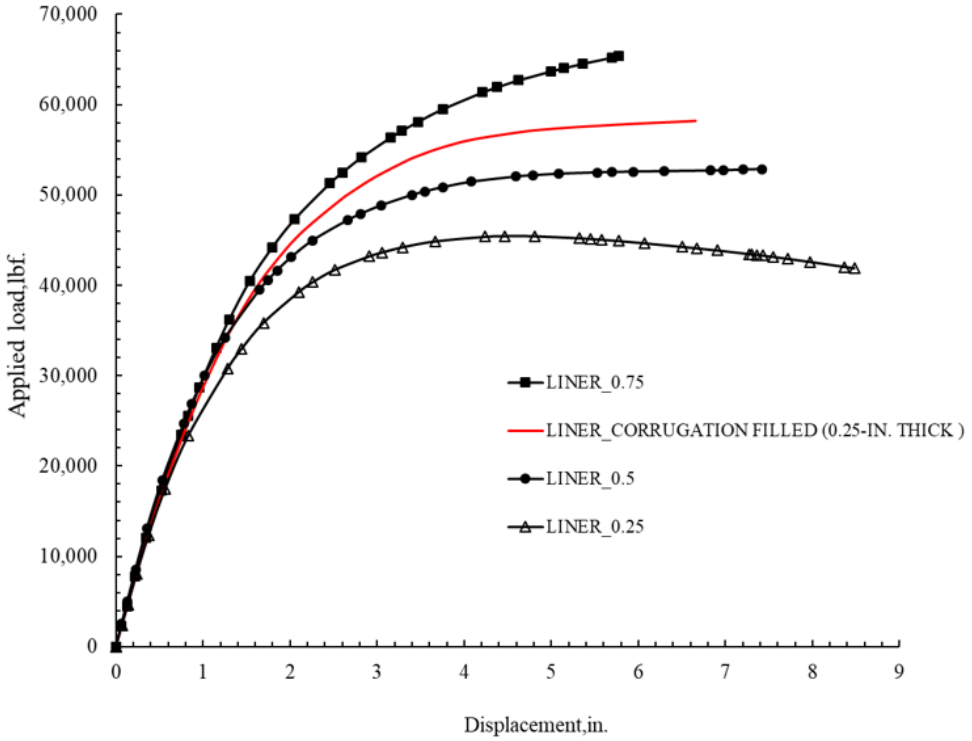


Figure 10-35. Load displacement plot from FE analysis for 0.25-in. thick (over the crest) polymeric SAPL.

The comparison of the filled corrugation results with the results from the following the corrugation are shown in Figure 10-35 and is summarized in Table 10-15. The results suggest that the performance of 0.25-in. thick polymeric filled corrugation lies between the performance of the liner with 0.5-in. thick and 0.75-in. thick polymeric SAPL following the corrugation.

Table 10-15. Comparison of the result for filling the corrugations and following the corrugations.

Description	Reduction in Vertical Diameter (in.) at Crack	Reduction in Vertical Diameter (in.) at Ultimate Load	Load at Crack (kips)	Ultimate Load (kips)	Increase/ Decrease (%)
0.25 in. thick liner (following corrugation)	3.29	4.81	44.21	45.63	-22
0.5 in. thick liner (following corrugation)	2.01	5.08	43.11	52.63	-10
0.75 in. thick liner (following corrugation)	2.6	5.77	52.47	65.22	+12
0.25 in. thick corrugation filled liner	2.73	6.65	50.58	58.20	0

10.5. Polymeric SAPL Performance Comparison

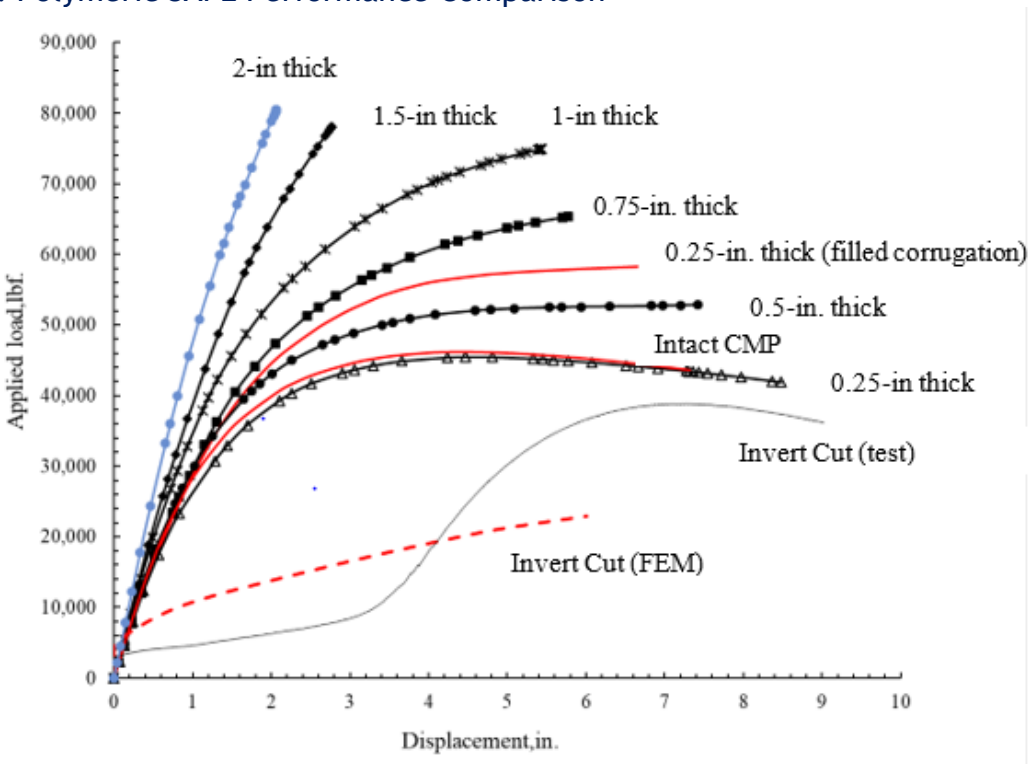


Figure 10-36. Comparison of the load-displacement plot at the crown obtained from all the FE results.

The overall comparison of the intact CMP, invert removed CMP, and the rehabilitated invert removed CMP is shown in Table 10-16 and Figure 10-36. The

comparison shows that the introduction of the liner will be able to bring back the structural capacity of the CMP whose inverts are removed. It is seen that the 0.25 in. thick liner will restore the structural capacity of the CMP almost the same as the intact CMP. The 0.5 in. thick liner surpasses the ultimate structural load carried by the intact CMP by about 10%, while for 1 in. thick liner, the ultimate load in the similar burial configuration and loading condition is about 52% higher than the intact CMP. 1.5-in. thick and 2-in. thick SAPLs showed that failure of the soil occurs before any appearance of the crack and it would take 80% more load than the intact CMP.

Table 10-16 Comparison of the reduction in diameter and the ultimate load obtained from FEM.

Description	Reduction in Vertical Diameter (in.) at the Crack	Reduction in Vertical Diameter (in.) at Ultimate Load	Load at Crack (kips)	Ultimate Load (kips)	Increase/ Decrease (%)
Intact Pipe		4.83		46.17	-
Invert Cut Pipe		6.01		10.28	-78
0.25 in. thick liner	3.29	4.81	44.21	45.63	-1.5
0.5 in. thick liner	2.01	5.08	43.11	52.63	+14
0.75 in. thick liner	2.6	5.77	52.47	65.22	+42
1 in. thick liner	3.19	4.76	64.97	73.27	+59
1.5 in. thick liner	3.00	3.00	78.04	78.04	+70
2.0 in. thick liner	2.06	2.06	80.04	80.04	+80
0.25 in. thick filled liner	2.73	6.65	50.58	58.20	+26

10.6. Results for Arch Control Test

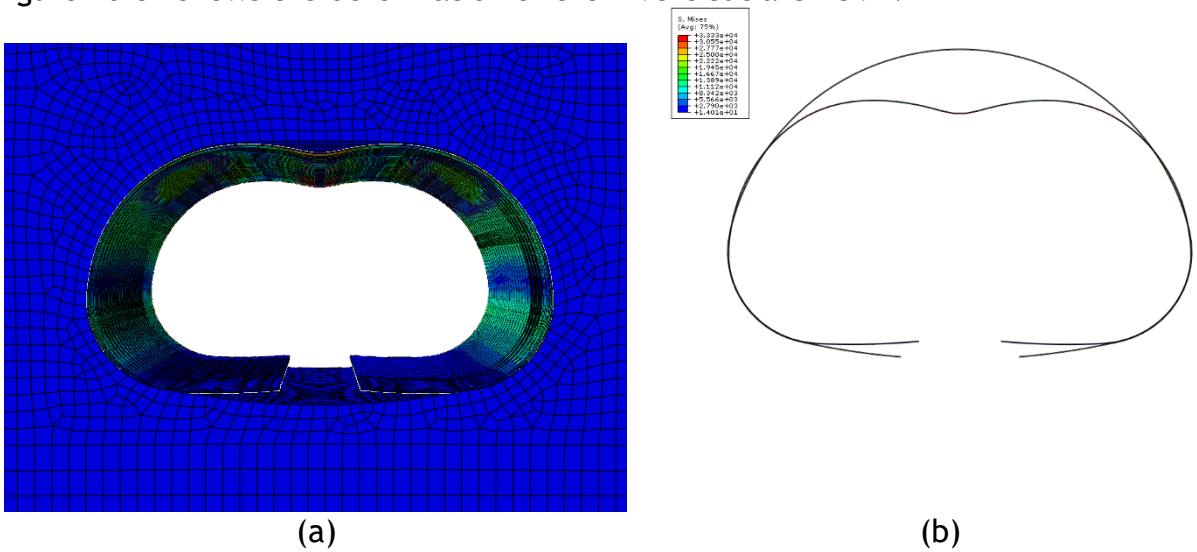
Another setup of soil box test was performed to study the performance of arch CMPs rehabilitated with SAPLs. Like circular CMP control test for arch CMP a control test was carried on the invert-cut arch CMP too. No control test was carried for the intact arch CMP.

For the arch structure also the boundary conditions, mesh sizes, element types, loading conditions, and interaction factors were kept consistent with the circular CMPs. The test results obtained from the FE analysis for the intact CMP are discussed in below section.

10.6.1. Invert-Cut Arch CMP

The control test for the arch CMP was performed under the 20x40 in.^{2} load pad. During the removal of the invert, significant movement in the soil and the pipe was observed in the experiment. A gap between the soil, and the CMP pipe was observed near the invert. This observance was like the invert removal process of the invert-cut circular CMP. A FEM model of the invert-removed arch CMP was developed to simulate the invert-removal process. However, the FE model was not able to predict the collapse behavior of the soil. The cover soil settled more than 6 in. immediately following the removal of the invert in the experiment; however, the simulation predicted only about 1 in. settlement of the cover soil. Also, the horizontal movement of the CMP at the springline was about 2.5 inches from either side in the experiment, but the FE model predicted only about 0.7 in. movement at the spring lines.

Although the FE model could not replicate the invert removal process, the behavior of the CMP during loading was well predicted. Figure 10-37 (a) shows the raising of the invert after the ultimate load conditions in the CMP. At the end of the loading condition in the FE model, the model predicted the 3 in. rise of the cut invert along with the inward movement, which is like the phenomena observed in the test. Figure 10-37 shows the deformation of the invert cut arch CMP.



(a) (b)

Figure 10-37. (a) Bending of the arch CMP along the crown after complete loading (b) Vertical diameter change from FEM after complete loading.

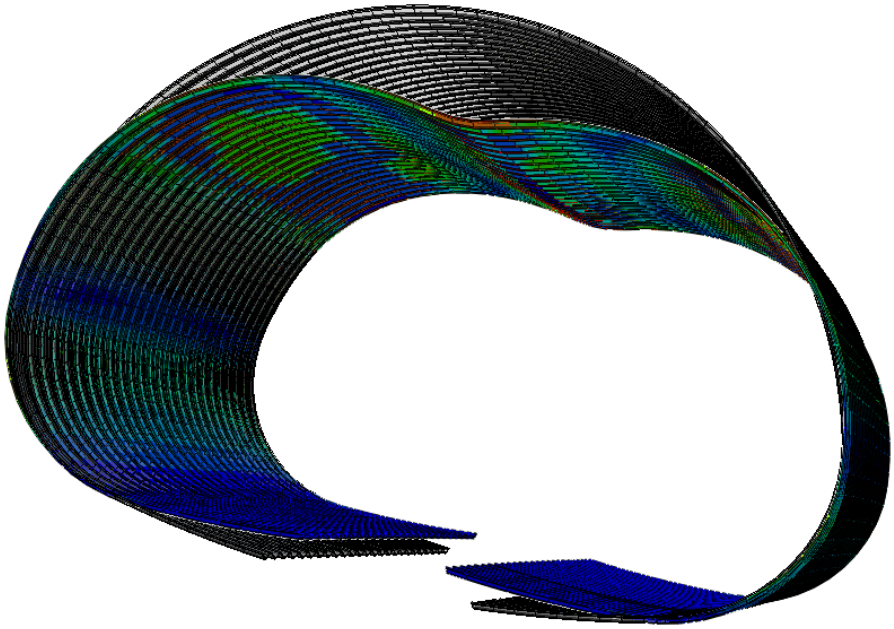


Figure 10-38. Deformation of the invert cut arch CMP from the FE model.

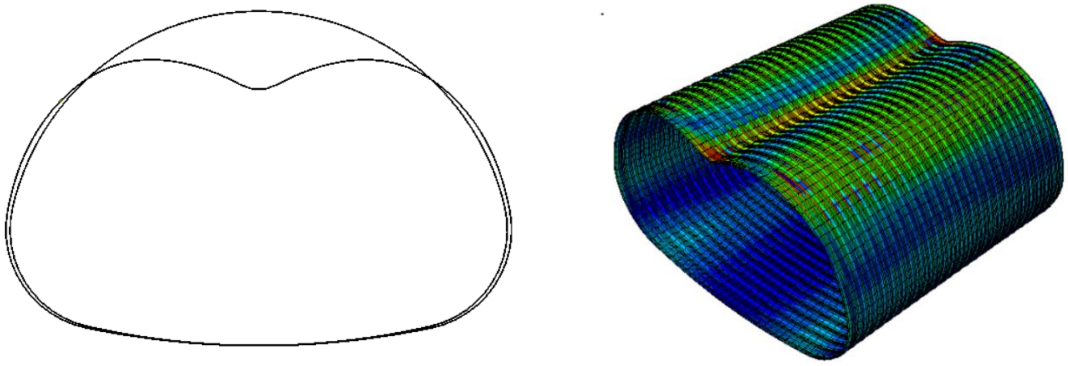
The load displacement graph of the invert cut arch CMP is provided in the Appendix 10-C. The comparison of the test results and FEM are shown in Table 10-17.

Table 10-17. Comparison of load and displacement for invert cut arch CMP.

Ultimate Conditions	FEM	TEST	Discrepancy (%)
Load (kips)	30.5	27.15	12.33
Vertical displacement of CMP (in.)	6.02	4.69	28.35
Soil settlement (in.)	6.84	6.69	2.30

10.6.2. Intact Arch CMP

Since no control test was performed for the intact arch CMP, the FEM model was employed to get the load-deformation curve and earth pressure. The obtained results were used to establish the base model for the comparison with the invert removed arch CMP repaired with liner. Figure 10-39 shows the deformation of the CMP at the ultimate load conditions. The failure pattern was like circular intact CMP with the local bending observed along with the crown.



(a) (b)

Figure 10-39. (a) Vertical diameter change from FEM after complete loading, and (b) ultimate Mises stress in around the arch CMP.

The load-displacement plot shows that the intact CMP would take 36 kips of the peak load. The FE model shows that upon removal of the invert, the arch pipe would lose 20% of its load capacity. The arch CMP was deflected by more than 5% of the vertical dimension at peak load Figure 10-40.

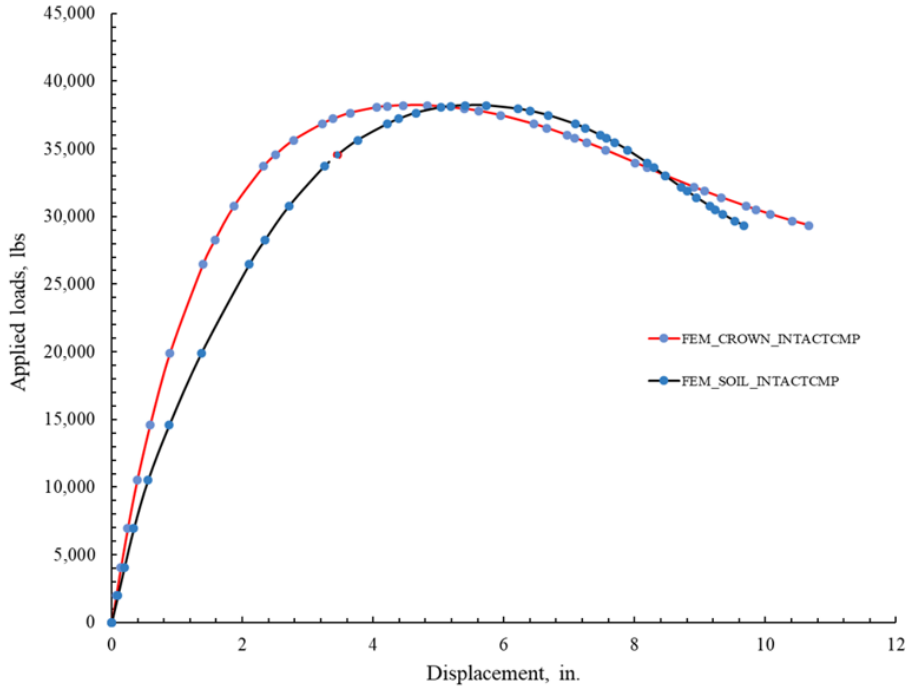


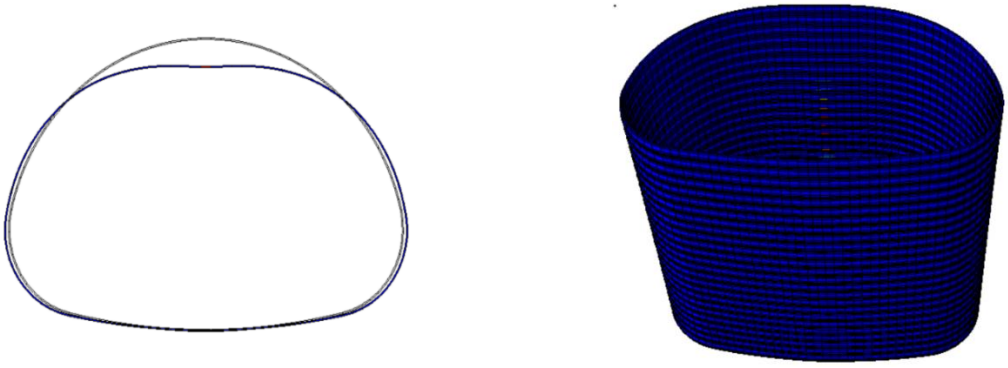
Figure 10-40. Load displacement plot for intact arch CMP.

10.7. Results from invert removed arch CMPs lined with polymeric SAPL

Similar to circular CMP, the liner is modeled using the simple elastic-plastic model, and the plastic strain in the liner is considered as the crack in the liner. This section presents the detailed modeling results and comparison for 0.25-in. thick polymeric SAPL, and for the rest of the results, only the brief results are discussed. The comparison graphs could be found in Appendix D.

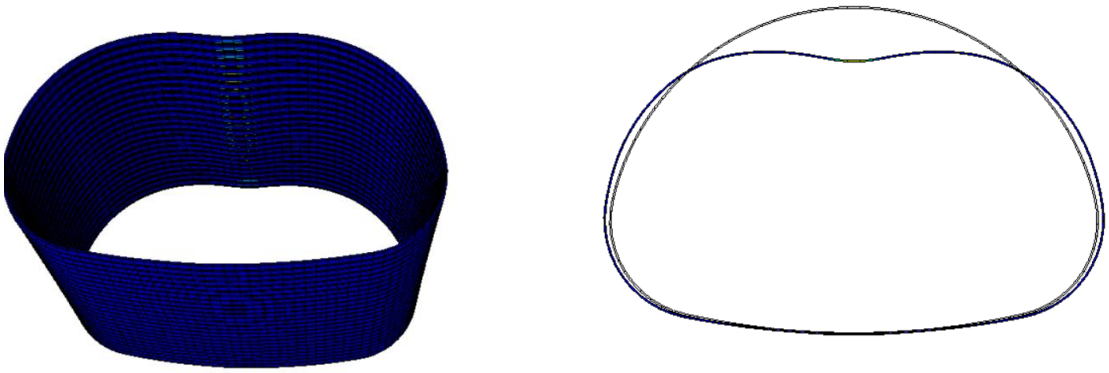
10.7.1. 0.25-in. thick Arch polymeric SAPL

The FE model for 0.25 in. liner compared well with the experimental results. In the test, it was observed that the first crack occurred right at the center of the CMP at the crown region. In the FEM model also, the 1st plastic strain was seen in the center of the CMP at the crown region (Figure 10-41). The plastic strain seen in the crown propagated longitudinally along with the crown of CMP, which matches fairly well with the propagation of the crack in the experimental results, as shown in Figure 10-42. The stress in around the soil at peak load is seen concentrated in the load pad zone and around haunch and springline areas. The distribution of the stress is shown in Figure 10-43.



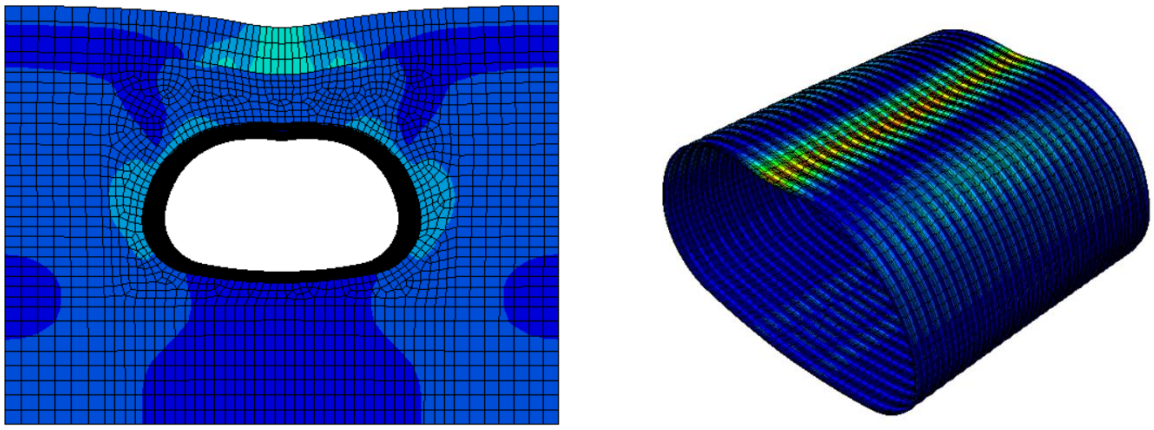
(a) (b)

Figure 10-41. (a) Deformation of arch CMP at 1st plastic strain in the 0.25-in. thick arch liner, and (b) 1st plastic strain in 0.25-in. thick polymeric SAPL.



(a) (b)

Figure 10-42. Deformation of the CMP at ultimate load condition for 0.25-in thick polymeric SAPL.



(a) (b)

Figure 10-43. Stress Distribution (a) Soil (b) in the SAPL at the ultimate load conditions for 0.25 in. thick arch polymeric SAPL.

Load Displacement Plots

The load-displacement curve showed a similar trend to the experimental results, but the prediction of the ultimate load and the crack load is higher by around 20%, as seen in Figure 10-44. In the FE model, the liner thickness was uniform all around the CMP, but the thickness varied during the application of the liner in the experiment. Due to the small thickness, the liner could not completely cover the seams in CMP, thus creating the discontinuation in the liner. This might be the cause of the lower peak load in the experiment than in the FE model. The comparison is summarized in Table 10-18.

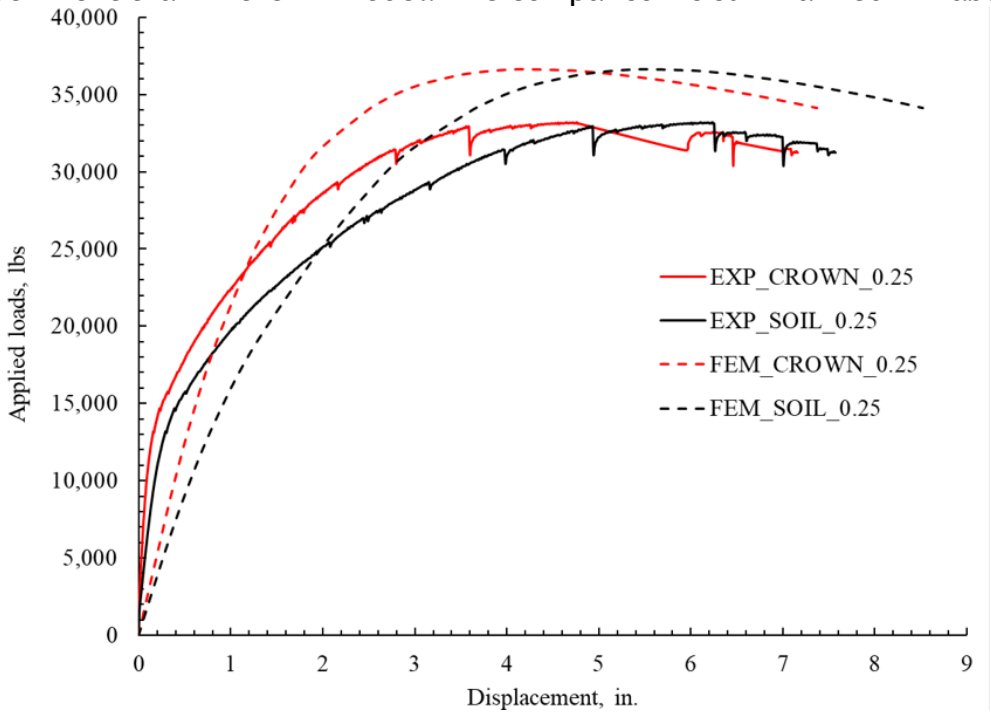


Figure 10-44. Comparison of the liner displacement at crown and soil settlement for 0.25 in. thick arch polymeric SAPL between Experiment and FEM results.

Table 10-18. Comparison of the load and displacement between the FE model and the experimental results for 0.25 in. thick arch polymeric SAPL.

Description	1st Plastic Strain	1st Crack	Discrepancy Test vs. FEM (%)	Ultimate Load		Discrepancy Test vs. FEM (%)
	FEM	Test		FEM	Test	
Crown Displacement (in.)	3.82	2.18	42.93	4.15	4.75	14.45
Soil Displacement (in.)	5.13	3.16	38.40	5.48	6.24	13.86
Load (kips)	36.5	29.05	20.41	36.61	33.12	9.53

Earth Pressure Distribution

Like the circular CMP results, maximum earth pressure in soil was observed at the crown level of CMP and the comparison is made accordingly... FEM earth pressure distribution at the crown area was plotted and compared with the experimental results and the graph (Figure 10-45 and Figure 10-46) shows that the earth pressure distribution follows the similar trend between FEM and experimental results. The ultimate pressure from FEM and experimental is close.

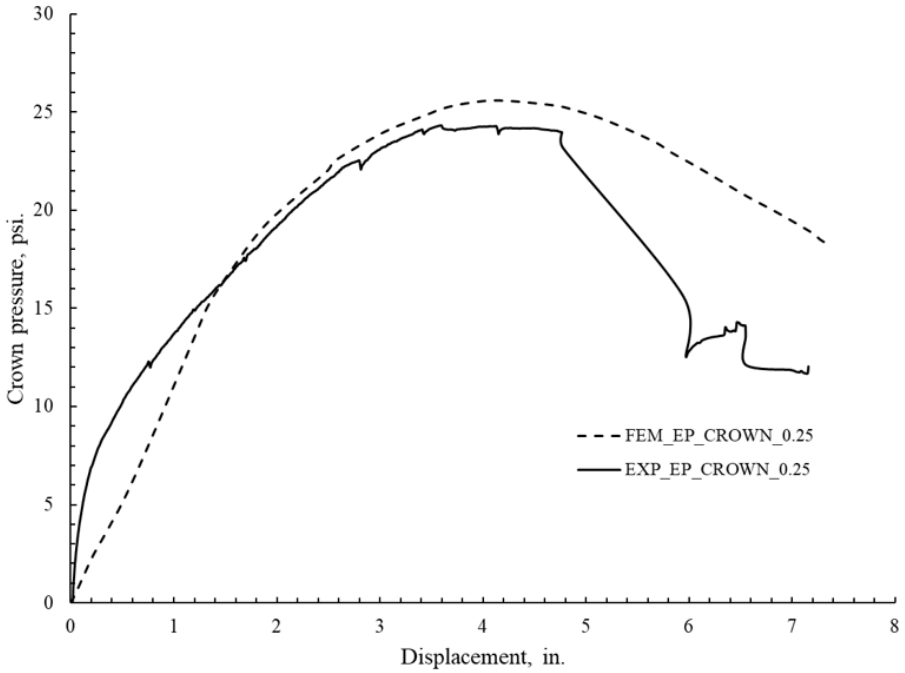


Figure 10-45. Comparison of the earth pressure at crown plotted against the soil displacement for 0.25-in. thick arch polymeric SAPL.

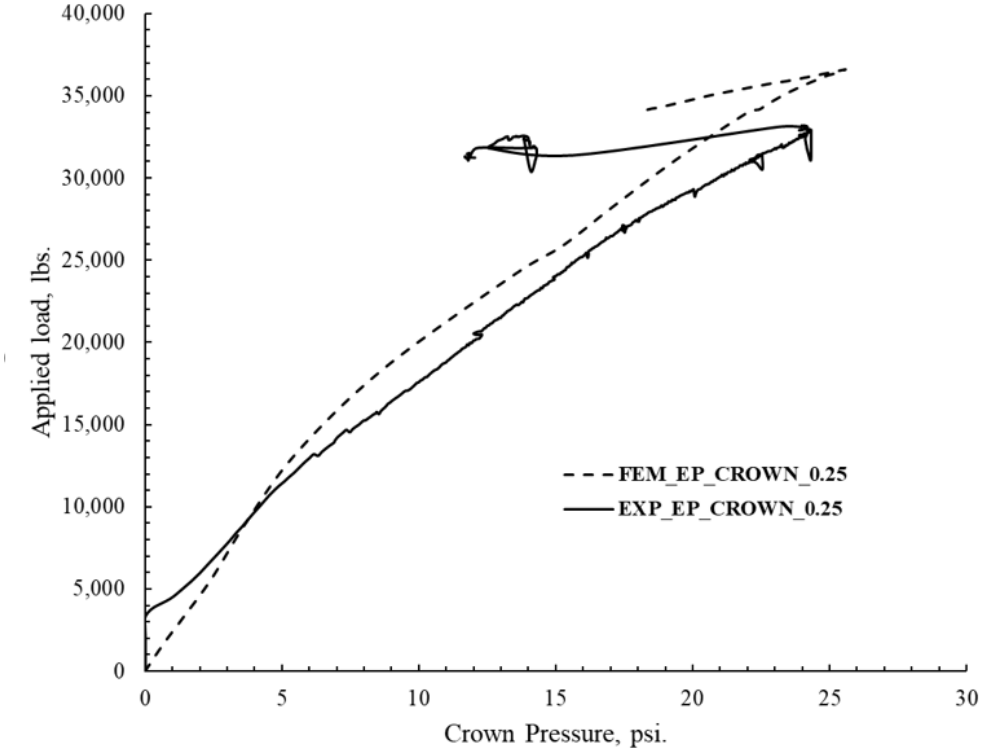


Figure 10-46. Comparison of the earth pressure at crown plotted against the applied load for 0.25-in. thick arch polymeric SAPL.

10.7.2. 0.5-in. thick polymeric SAPL

The behavior of the FE model and the experimental results were also similar for this thickness liner. The FE model shows that the first plastic strain will occur right at the center of the liner, and the crack propagates along the crown. Here also the peak load was predicted 10% higher than the experimental results. The liner showed the circumferential crack at the end parts of the CMP before the load was applied to it, which might have reduced in the peak load in the test.

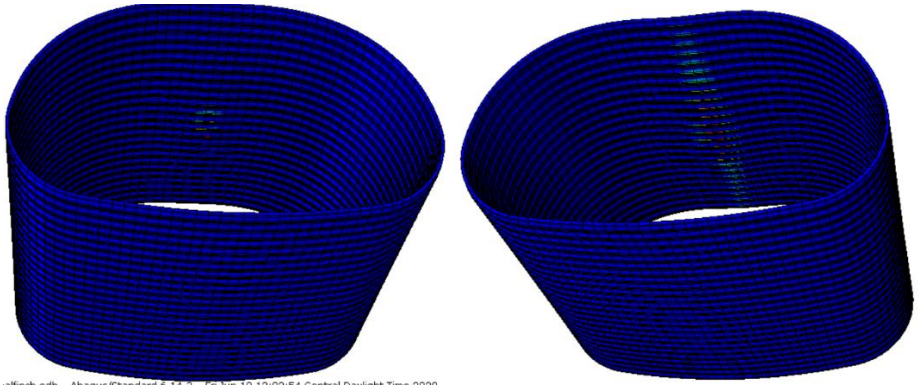


Figure 10-47. First plastic strain from FE model for 0.5-in. thick arch polymeric SAPL.

The details of the load-displacement and the earth pressure distribution graphs are presented in Appendix D for this liner thickness. The comparison chart is presented in Table 10-19. In the experiment, the liner cracked circumferential near to the ends prior to loading. The ultimate load conditions for this thickness liner was predicted with a discrepancy of less than 10%.

Table 10-19. Comparison for the load-displacement plots from the FE model and test for 0.5 in. thick arch polymeric SAPL.

Description	1st Plastic Strain	1st Crack	Discrepancy Test vs. FEM (%)	Ultimate Load		Discrepancy Test vs. FEM (%)
	FEM	Test		FEM	Test	
Crown Displacement (in.)	4.57	0.83	80.05	6.13	6.43	4.89
Soil Displacement (in.)	6.13	1.77	71.1	6.98	7.28	4.29
Load (kips)	39.68	26.27	33.79	39.98	36.08	9.75

10.7.3. 1-in. thick polymeric SAPL

The FE model shows that the first plastic strain will occur right at the center of the liner, and the crack propagates along the crown Figure 10-48 and Figure 10-49. The FE model shows that significant displacement of the liner is required for the first plastic strain to appear (about 6 in.), but the experimental results show that the first crack occurs within the small displacement of the liner (about 0.32 in.). The ultimate load for this thickness liner was predicted with a discrepancy of less than 1% (Table 10-20). Although the ultimate load of the system was predicted with more than 95% accuracy, the load-displacement curve showed a different response. The experimental results showed a very stiff response, while the FE model showed a flexible response. Details of the load-displacement and earth pressure comparison are presented in Appendix D.

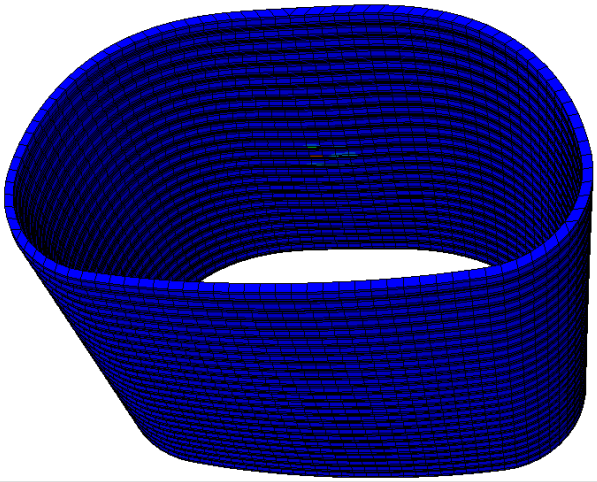


Figure 10-48.1st plastic strain in the liner for 1-in. thick arch polymeric SAPL.

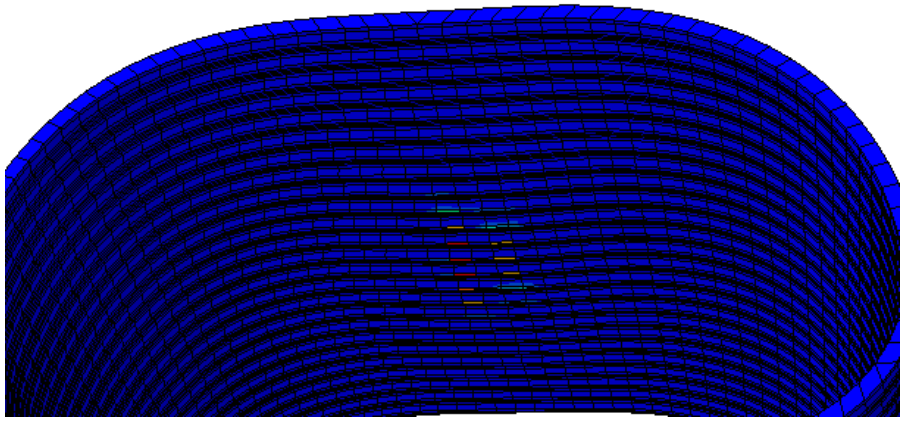


Figure 10-49. Development of the plastic strain in 1-in. thick arch polymeric SAPL along the crown.

Table 10-20. Comparison of the test and FE model results for 1-in. thick arch polymeric SAPL

Description	1st Plastic Strain	1st Crack	Discrepancy Test vs. FEM (%)	Ultimate Load		Discrepancy Test vs. FEM (%)
	FEM	Test		FEM	Test	
Crown Displacement (in.)	6.08	0.32		7.2	5.33	25.97
Soil Displacement (in.)	8.3	1.22		9.66	7.71	20.18
Load (kips)	53.3	41.08		54.78	53.83	0.08

10.7.4 Reasons for discrepancy between FEM and Experiment

The test results show a stiffer response as compared to the FE model. For the rehabilitated CMP with liner, in all the cases, the FE model predicted the incidence of the first plastic strain, which was supposed to be a crack in test condition, when it reached the ultimate load conditions. This behavior was not observed in the test where the cracks occurred at a lower load than the ultimate load. The reasons for these discrepancies are:

a. Exclusion of the attachment of the CMP and the liner to the boundary wall in FEM due to over spraying during the application of the liner.
b. Cracks occurred in the liner prior to loading.
c. The earth pressure comparison from FEM and experiment showed close match for 0.25-in. thick SAPL and 0.5-in. thick SAPL which shows that the transfer of load from load pad to crown of CMP was same between experiment and FEM. The earth pressure comparison could be found at Appendix E.
d. Since the stress to reach the breaking point for the liner required large displacement in the FE model, this suggests that the stiffness value used in the model might be less compared to the test results.

e. The geometry of the arch is complex compared to the circular CMP, and as for circular CMP, FE models are performing well with similar properties; the difference in the standard and manufactured geometry of the CMP could be one of the reasons for the mismatch between the test and FE results.
f. The FE model considers the same value for the soil stiffness all around the embedment but might not be the case for the test.

The attachment of the liner to the wall was studied through FEM. A FEM model was run restricting the vertical movement of liner ends as shown in

Figure *10-50*. Although the FEM would not simulate the separation of liner as in experiment, but it would give us the initial condition of the experiment. The FEM was run for all the thicknesses.

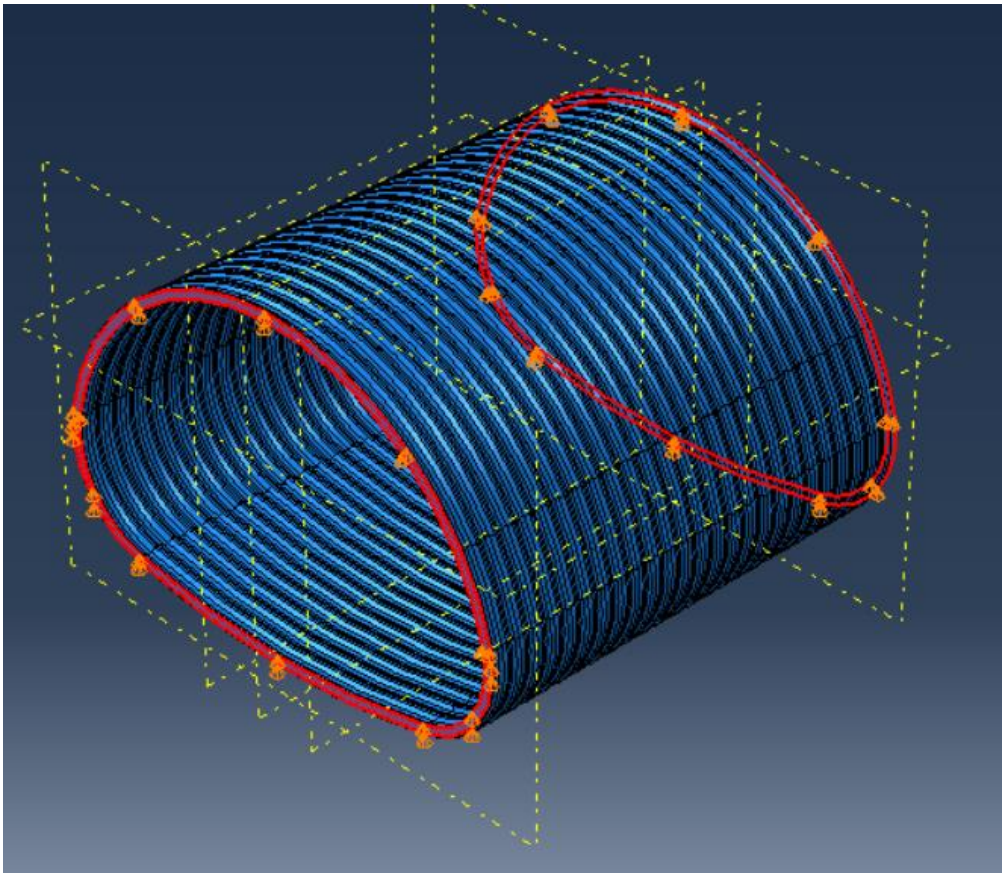


Figure 10-50. 1-in. thick polymeric SAPL liner showing the restriction of the vertical movement at two ends.

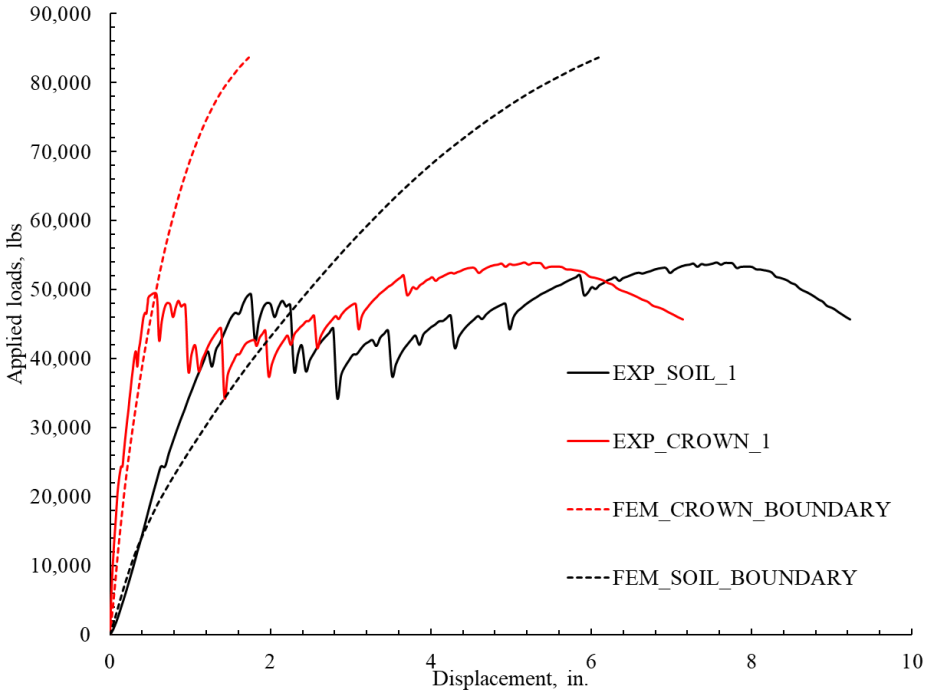


Figure 10-51. Load displacement curve comparison between FEM and Experiment for 1-in. thick SAPL with the boundary conditions at the end.

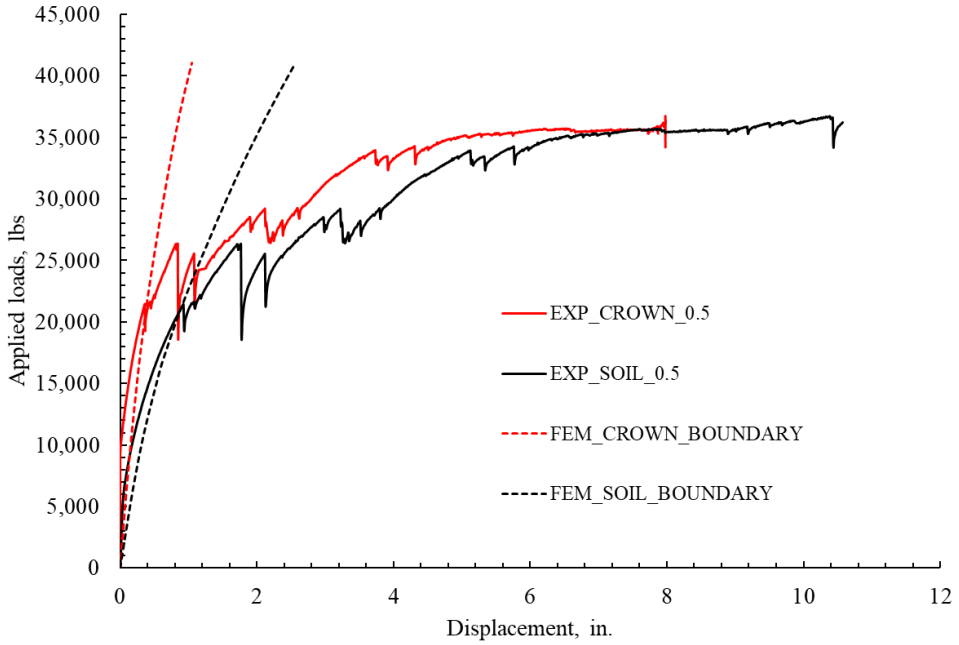


Figure 10-52. Load displacement curve comparison between FEM and Experiment for 0.5-in. thick polymeric SAPL with the boundary conditions at the end.

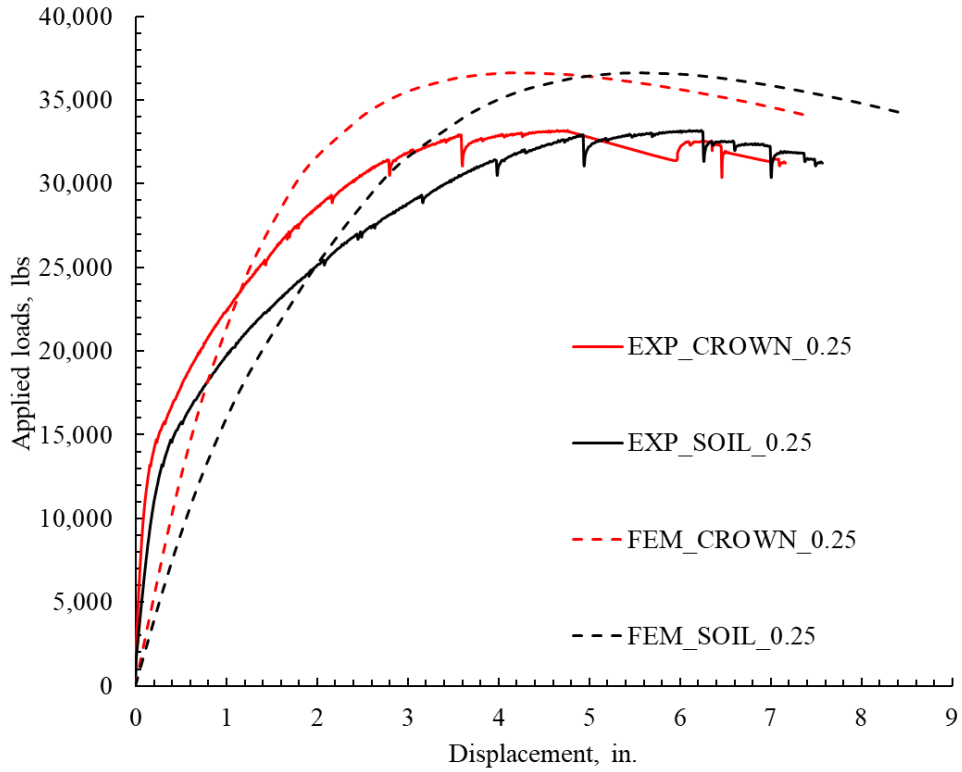


Figure 10-53. Load displacement curve comparison between FEM and Experiment for 0.5-in. thick polymeric SAPL with the boundary conditions at the end.

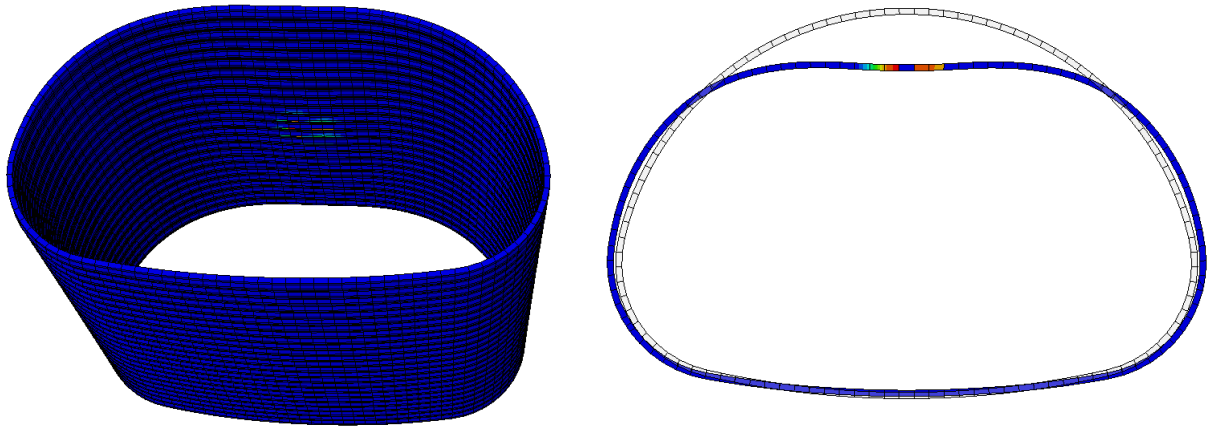
Findings:
The FEM results obtained with the movement of restriction at the ends showed the close resemblance for the initial graph between the experiment and FEM (Figure 10-51, Figure 10-52, Figure 10-53). It shows that the effect of the attachment of liners to the boundary wall should be taken into consideration to get close results between experiment and FEM. It was also seen that the effect was more prominent with the increase in the thickness of liner.
Even though the attachment to the boundary wall is causing the stiff behavior of the system but the ultimate load obtained from the FEM and experimental have the discrepancies within 10%. Thus, the FEM model without the attachment to the boundary wall could be used to evaluate the ultimate load carrying capacity of the polymeric lined invert removed arch CMPs.

10.7.4. 0.75-in. thick polymeric SAPL

Using occurrence of plastic strain as the initiation of crack, the above FEM models of arch CMP repaired with SAPLs over-predicted the load and displacement for the 1st crack. However, the ultimate load and ultimate liner displacement were predicted with discrepancies of less than 10% and 20%, respectively. Therefore, the FEM models could

be used to predict the ultimate load for other thickness of the liner which were not tested in the soil box tests.

The first liner thickness investigated was 0.75 in. thick, which was applied following the corrugations. Like previous FE models, 1st plastic strain occurred when the system was nearing the ultimate stage, as shown in Figure 10-54.



(a) (b)

Figure 10-54. (a) Development of plastic strain in the inside liner for 0.75 in. thick arch liner (b) Deformation pattern of 0.75-in. thick arch polymeric SAPL.

The load-displacement curve is presented in the Appendix D. It is observed that the liner and the CMP system would take 43 kips of the ultimate load while the load at the first 1st plastic strain would be 42.9 kips. The results are summarized in Table 10-21.

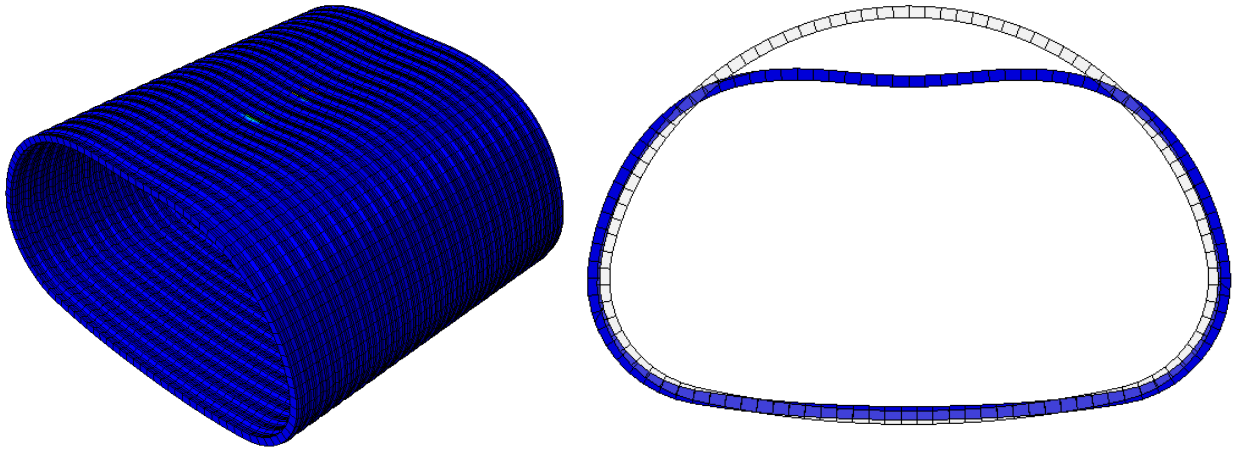
Table 10-21. Crack and Ultimate load prediction for 0.75-in. thick arch polymeric SAPL.

Description	Predicted 1st Crack Condition	Ultimate Load
	FEM	FEM
Crown Displacement (in.)	6.08	6.54
Soil Displacement (in.)	8.19	8.66
Load (kips)	42.93	43.08

10.7.5. 1.5-in. thick polymeric SAPL

The second thickness under consideration was 1.5 in. thick following the corrugations. For 0.75-in. thick SAPL also the first crack and the following cracks

occurred at the crown (Figure 10-55). Like the previous FE models, plastic strain occurred when the system was nearing the ultimate stage.



(a) (b)

Figure 10-55. (a) Development of plastic strain in the inside liner for 1.5 in. thick arch SAPL, and (b) Deformation pattern for 1.5- in. thick arch polymeric liner.

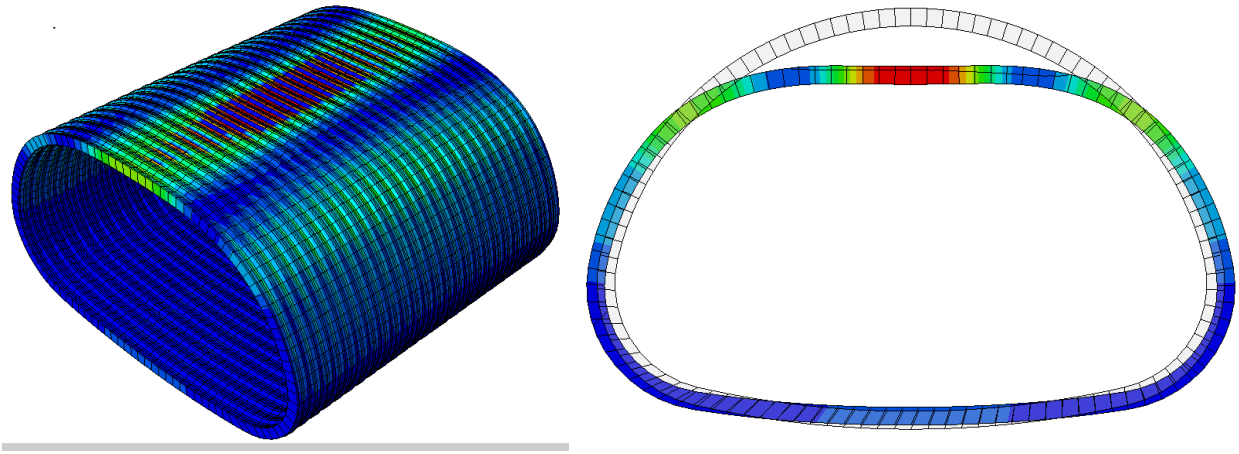
The liner and the CMP system took 52 kips of load for the first crack to occur and simultaneously the system achieved the ultimate load conditions. This liner took a smaller load compared to the 1-in. thick SAPL. The results are summarized in Table 10-22.

Table 10-22. Crack and Ultimate load prediction for 1.5-in. thick arch polymeric SAPL.

Description	Predicted load at 1st Crack	Ultimate Load
	FEM	FEM
Crown Displacement (in.)	7.5	7.5
Soil Displacement (in.)	9.66	9.66
Load (kips)	52	52

10.7.6. 2-in. thick polymeric SAPL

For 2-in. thick polymeric SAPL, no plastic strain was observed even after the displacement of the soil beyond 10 in. The 2-in. thick SAPL took ultimate load of around 67 kips. The Mises stress and the deformation pattern are shown in Figure 10-56.



(a) (b)

Figure 10-56. (a) Development of mises stress, and (b) Deformation pattern for 2- in. thick arch polymeric SAPL.

The results are summarized in Table 10-23.

Table 10-23. Crack and ultimate load prediction for 2-in. thick arch polymeric SAPL.

Description	Ultimate Load
	FEM
Crown Displacement (in.)	6.11
Soil Displacement (in.)	9.66
Load (kips)	66.87

10.7.7. 0.25 in. thick filled (over the corrugation) polymeric SAPL

Like polymeric SAPL rehabilitated invert-cut circular CMP, a FEM model for the polymeric SAPL rehabilitated invert-cut arch was analyzed considering the filled corrugated condition. The thickness of the polymeric SAPL over the corrugation was 0.25-in. thick. The performance of this SAPL in terms of load-carrying capacity is between the load-carrying capacity of 0.5-in. thick SAPL (following the corrugation) and 0.75-in. thick SAPL (following the corrugation).

A load-displacement curve was plotted for the 0.25-in. thick SAPL (over the crest). The load-displacement curve shows the displacement of the liner and the soil under the application of the load. From Figure 10-57 it is observed that the liner and the CMP system would take 43 kips of ultimate load while the first crack would occur after 42.5 kips. The ultimate load and the crack load lie between the results obtained from 0.5-in. thick polymeric SAPL and 0.75-in. thick polymeric SAPL following the corrugations, as shown in Figure 10-58.

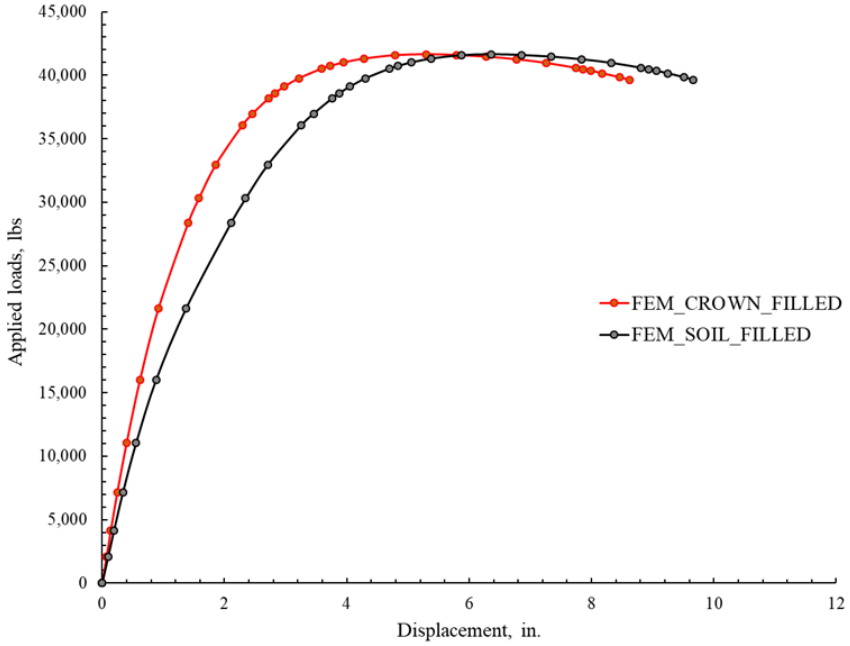


Figure 10-57. Load displacement curve for 0.25-in. thick polymeric SAPL (filled corrugations).

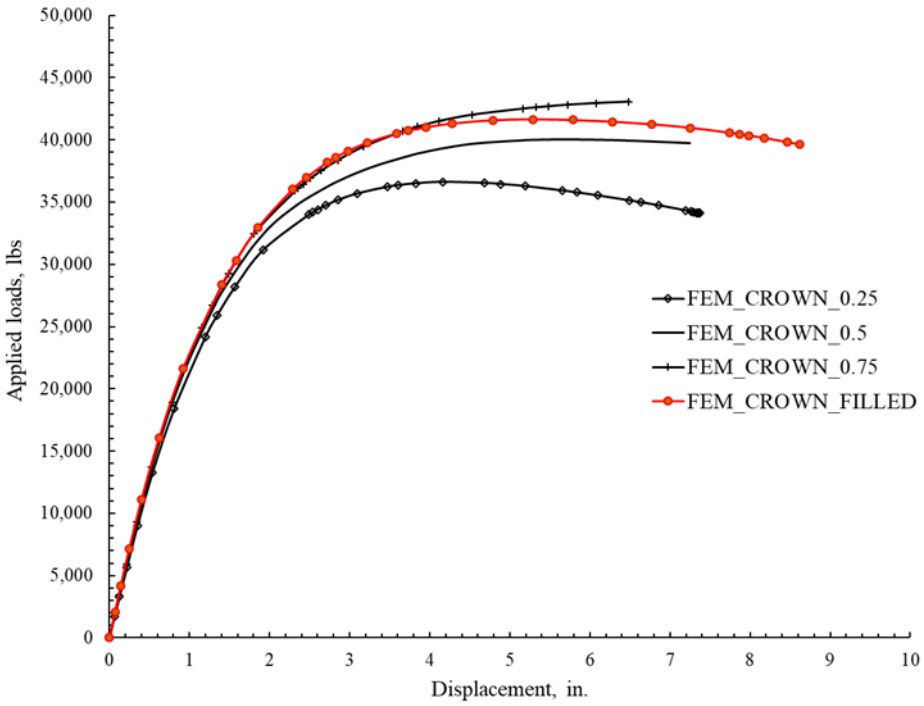


Figure 10-58. Comparison of the performance of 0.25-in. thick filled corrugated polymeric SAPL for arch with liner thickness following the corrugation.

10.7.8. Comparison of Liner Performance

Load Displacement Comparison

The overall comparison of the intact CMP, invert removed CMP, and the rehabilitated invert removed CMP is shown in Table 10-24 and Figure 10-59. The comparison shows that the introduction of the liner will restore the structural capacity of the CMP where the invert is removed. It can be seen that 0.25-in. thick liner will return the structural capacity of the CMP to very nearly the same as the intact CMP. The 0.5-in. thick liner surpasses the ultimate structural load carried by the intact CMP by about 10%, while for 1-in. thick liner the ultimate load in the similar burial configuration and loading condition is about 48.23% higher than the intact CMP. The 2-in. thick SAPL increased the capacity by 80%.

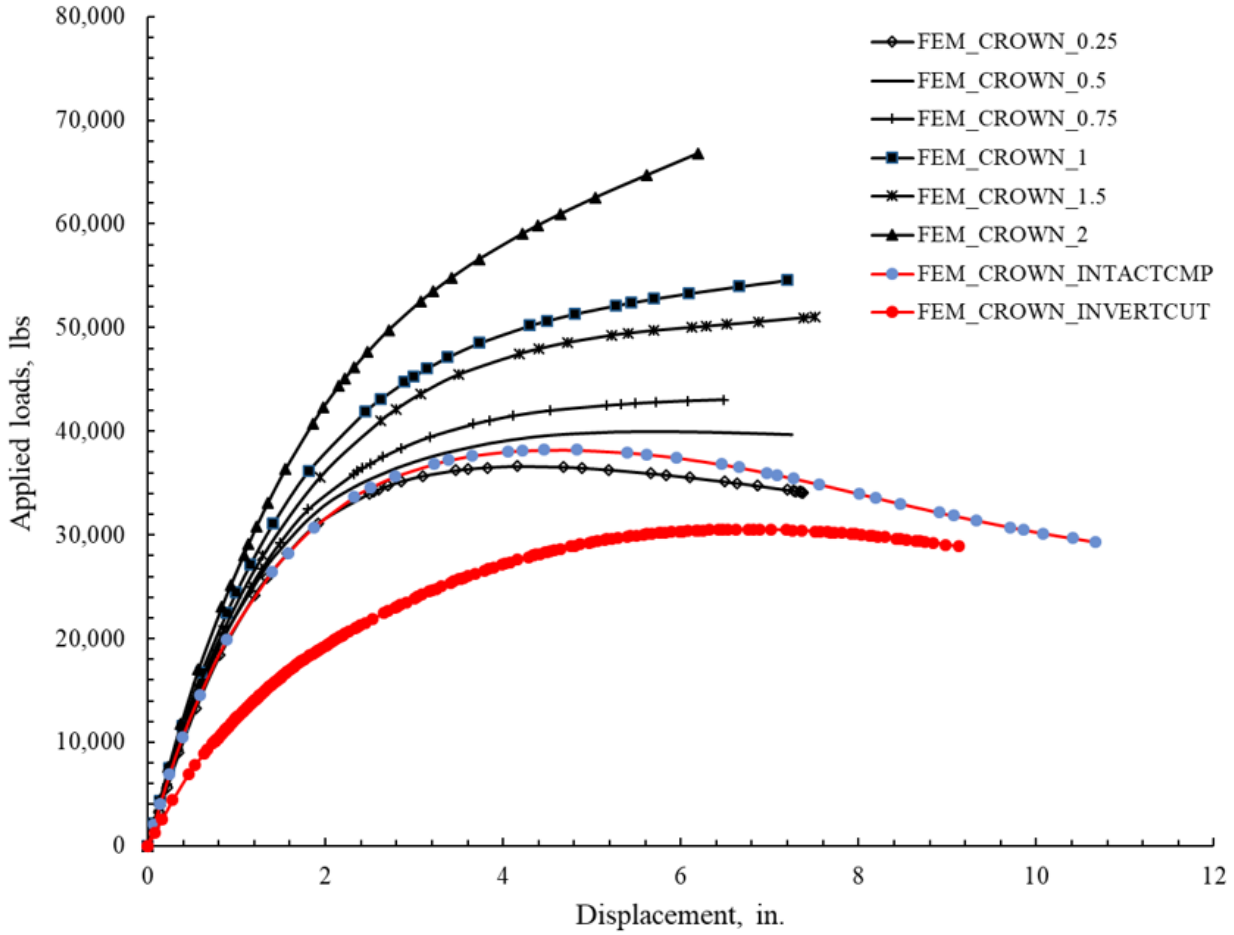


Figure 10-59. Comparison of the load-displacement plot at the crown obtained from all the FE results for arch CMP lined with polymeric SAPL.

Table 10-24. Comparison of the reduction in the diameter and the ultimate load obtained from FEM for arch CMP lined with polymeric SAPL.

Description	Load at the Crack (kips)	Ultimate Load (kips)	Increase/Decrease in Ultimate Load Capacity (%)
Intact Pipe	-	36.82	-
Invert Cut Pipe	-	30.52	-17
0.25 in. thick liner	36.5	36.62	0.54
0.5 in. thick liner	39.68	39.98	+8.58
0.75 in. thick liner	42.93	43.08	+17.00
1 in. thick liner	52.79	54.58	+48.23
1.5 in. thick liner	51	51	+41.22
2 in. thick liner	-	66.80	+80.42

10.8. Summary and Conclusions

3D FEM models were developed in ABAQUS and solved using an implicit scheme to simulate the soil box tests on CMPs performed at CUIRE. The boundary conditions were defined similarly to the experimental setup. C3D8R elements were used to model the soils, CMPs, and liners. The mesh sensitivity of the model was analyzed in terms of total energy, load-displacement for soil-CMP, and the Von Mises stress for the CMP. The soil was modeled using Drucker Prager Model, which represents the pressure-dependent soil model while CMP was represented by a non-linear elastic-plastic model. The interaction between the soil and the pipe was defined as surface-to-surface contact with a friction coefficient of 0.5. The interaction did not allow the slippage between the soil and CMP surface. The liner and CMP interaction were also defined as surface-to-surface contact with friction coefficient of 1. For both interactions, a hard contact was used.

The properties of the polymeric SAPL as reported from CUIRE suggested a brittle material with a small plastic region. Since the FEM model was the implicit solver, post-cracking behavior was not simulated in the FE models. However, the FEM models can predict the crack load and ultimate load for models with lab test counterparts. The crack in the liner model was represented by the plastic strain developed in the liner. As the plastic region of the liner was very small, the appearance of the first plastic strain in the FE model was compared with the appearance of the first crack in the test.

The following conclusions are drawn from the simulations of each type of CMPs lined with polymeric SAPL.

10.8.1. Circular CMPs lined with polymeric SAPL

1. Prediction of different parameters by the FE model showed reasonable accuracy for all cases except for the control test on the invert-cut CMP.
2. Intact pipe FEM results for load-displacement, earth pressure at the crown, strains, and bending moments compares well with the test results with a discrepancy of less than 5%.
3. When the load pad size was increased from 10x20 $in.^2$ to 20x40 $in.^2$, the load-carrying capacity of the intact CMP soil-box system increased by about 90%, and the bearing failure of the soil was not observed before the pipe failures.
4. For invert cut pipe, the FE model over predicts the load by about 145% before the invert edges meet. The FEM over-prediction is caused by the soil model's limitation to replicate the collapse behavior of the soil during the invert removal process.
5. FE analyses of the invert-removed CMPs with liners predict load -displacement, earth pressure curves and ultimate load with less than 10% discrepancy with the measured values.
6. Also, the prediction of the first crack, which was represented by the appearance of the first plastic strain in FE model matches the test results with less than 10% discrepancy.
7. The lost load capacity of intact CMP due to the complete removal of invert from the CMP could be restored with the application of only 0.25-in. thick polymeric liner. With the liner thickness of 0.5-in. thick the load capacity of the invert cut CMP increased by 10% compared to its intact capacity.
8. The parametric analysis for the rehabilitated invert removed circular CMP showed that thickness and the capacity of the liner have a linear relationship.
9. The FE analysis for the filled corrugation with 0.25-in thick over the crest provided the load capacity in between the load capacity for 0.5-in. thick and 0.75-in. thick liner that was applied by following the corrugation.
10. In addition, through parametric analysis, FE model clearly shows the increase in the rigidity of the circular CMP pipe with the increase in the thickness in the liner as we can see the reduction in the deformation of the liner at first plastic strain condition and ultimate load condition.

10.8.2. Arch CMP lined with polymeric SAPL

1. The FE analysis shows that the load-carrying capacity of the intact arch CMP is 20% less than the equivalent intact circular CMP.
2. Like the invert removed circular CMP, the invert removed arch FE model also could not predict the collapse behavior of soil during the invert removal process. Although the FEM could not predict the collapse behavior, the ultimate load and displacement results were predicted within the discrepancies of 20%. Also, the load-displacement curve comparison between the test and FE simulation showed a similar response.
3. For the polymeric lined invert cut arch CMPs, the FE model predicted the ultimate load and the displacement with discrepancies of less than 10% for all the tests. During the test, there were circumferential cracks present in the liner before

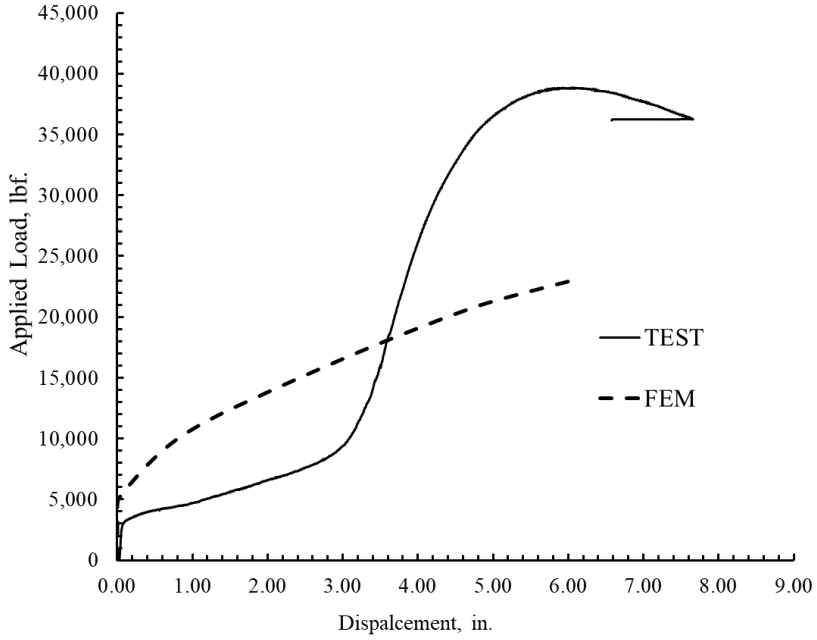
loading, which could have resulted in less load carrying capacity of the system. Also, the FE model did not account for the attachment of the liner to the boundary wall due to over-spraying.

4. The response of the liner in the test was stiffer than the response of the liner from the FE model before the occurrence of the major crack.
5. From parametric and calibration of FE models, it was found that the plastic strain on the CMP appeared when the system is near the ultimate load conditions.
6. Like the lined invert cut circular CMPs the FE model also predicted that the 0.25-in. thick SAPL was enough to re-establish the lost capacity of the CMP through invert removal. While 0.5-in. thick SAPL and 0.75-in. thick SAPL, when compared to intact arch CMP capacity, increased the capacity by 9% and 18%, respectively. The 1-in. thick SAPL and 2-in. thick SAPL increased the load capacity by nearly 50% and 80%, respectively.
7. The load-carrying capacity of the renewed invert-cut circular CMPs is greater than the load-carrying capacity of renewed invert-cut arch CMPs for the same thickness of the liner.

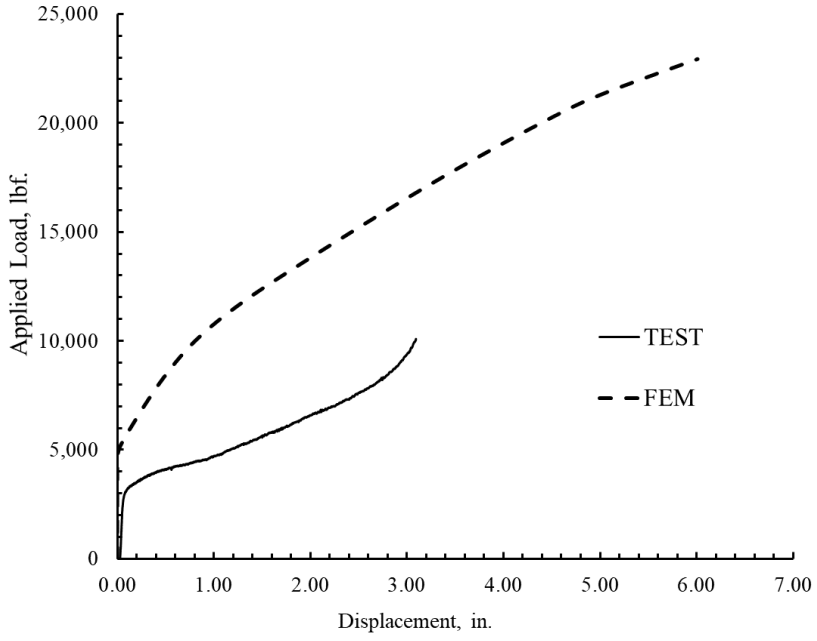
10.8.3. Limitations

1. The FE model was implicit and thus could not predict the load drop after the ultimate load.
2. The Drucker Prager model is not suitable for modeling the soil collapse behavior observed in the test of the invert-removed circular CMP pipe.
3. Since the brittle polymeric material of the liner was modeled using the simple elastic-plastic model instead of crack models, a drop in load at first crack was not observed in the FE model.
4. FEM models for the CMP pipes and liners were based on the nominal geometry specified in the design. Actual geometry discrepancies were not evaluated in the FEM models.

The load-displacement results exclude all the displacement before the loading at the loading plate for lab tests and FEM results.

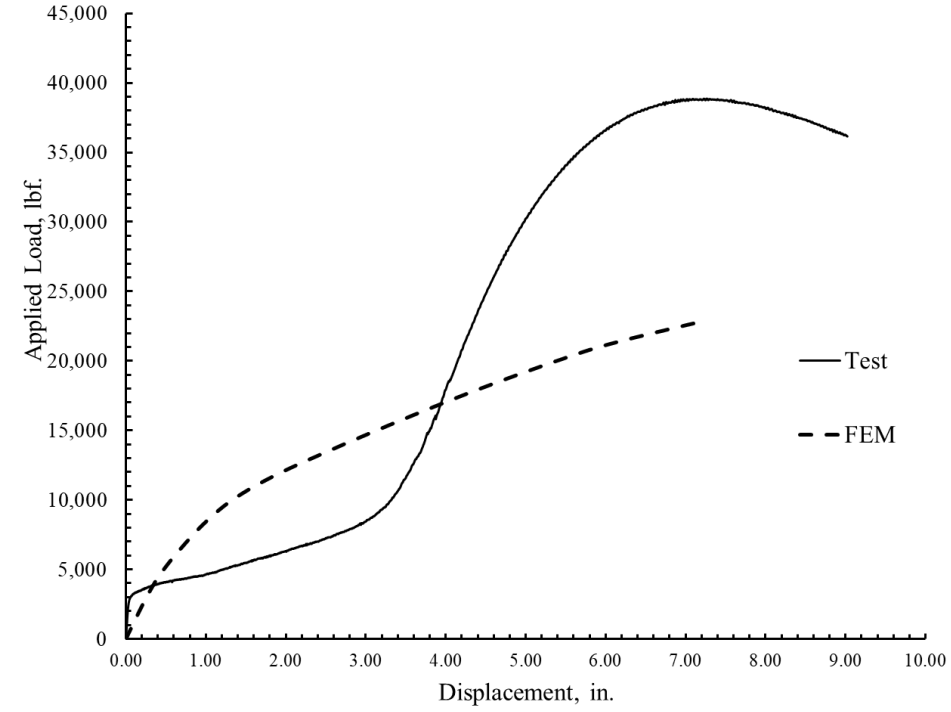


(a)

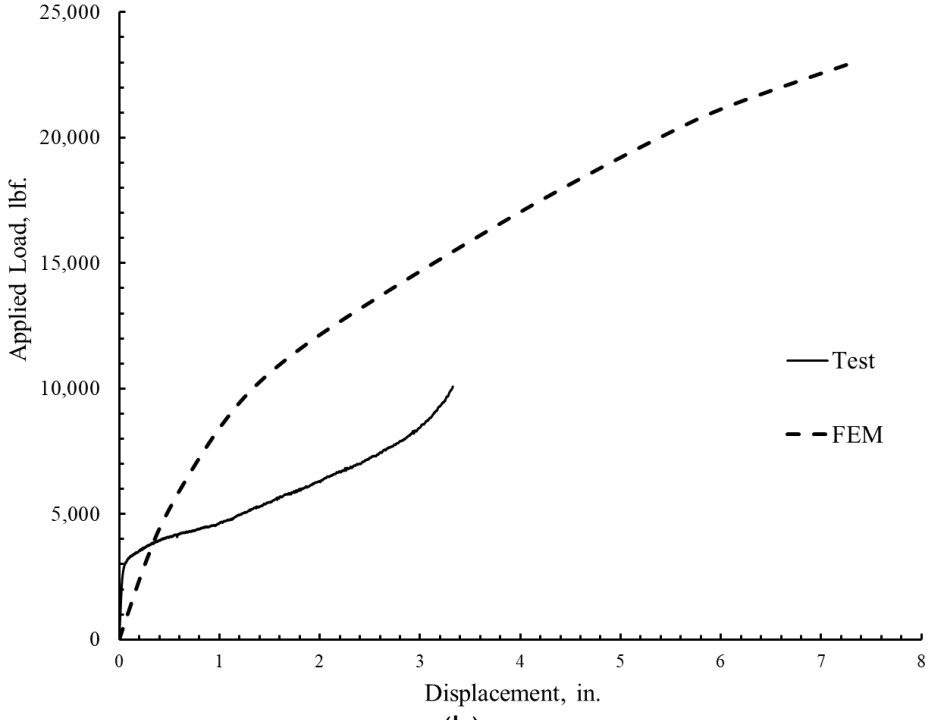


(b)

Figure 10A- 1. Load displacement plot for the movement of CMP's crown (a) Comparison at the ultimate conditions, and (b) Comparison when the inverts just meet.



(a)



(b)

Figure 10A- 2. Load displacement for the soil movement just beneath the load pad (a) Comparison at the ultimate conditions, and (b) Comparison when the inverts just meet.

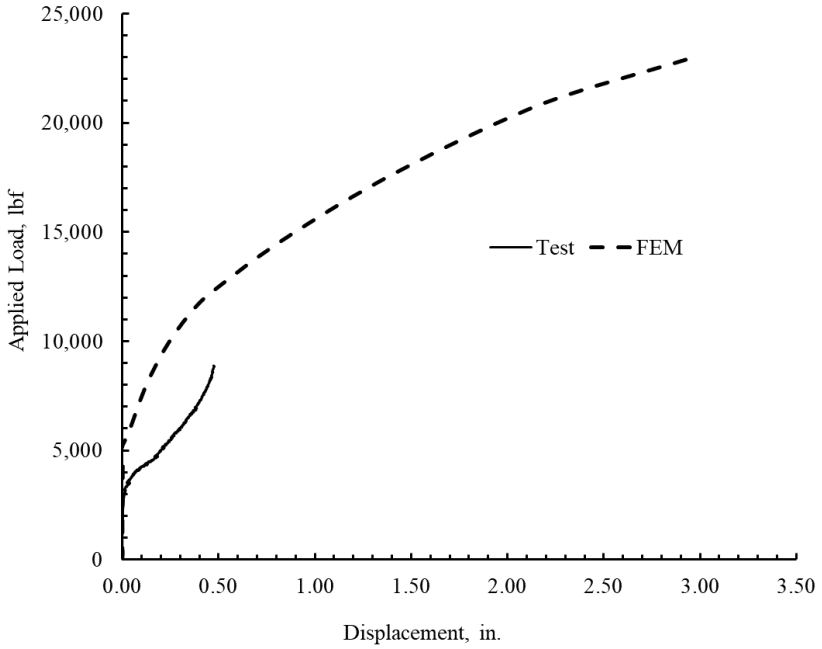
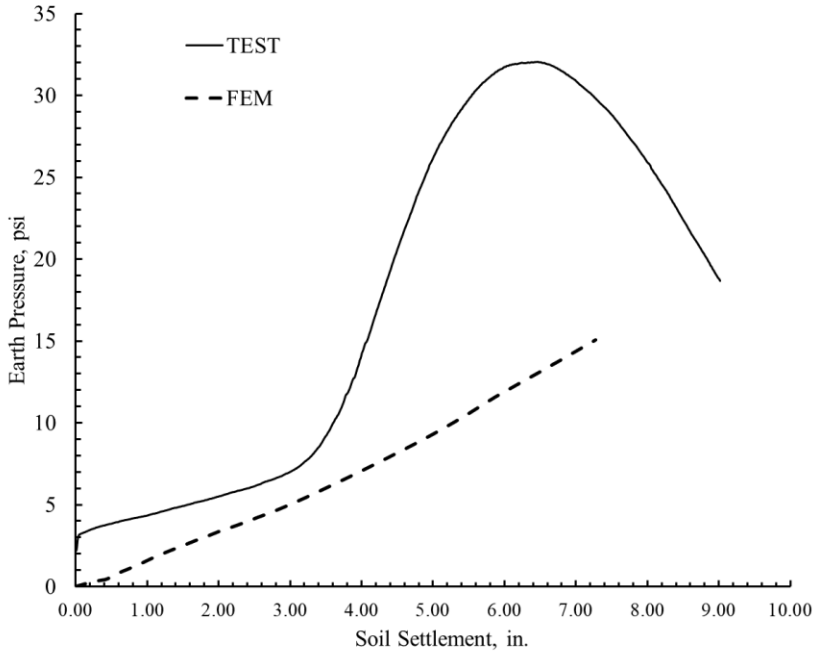
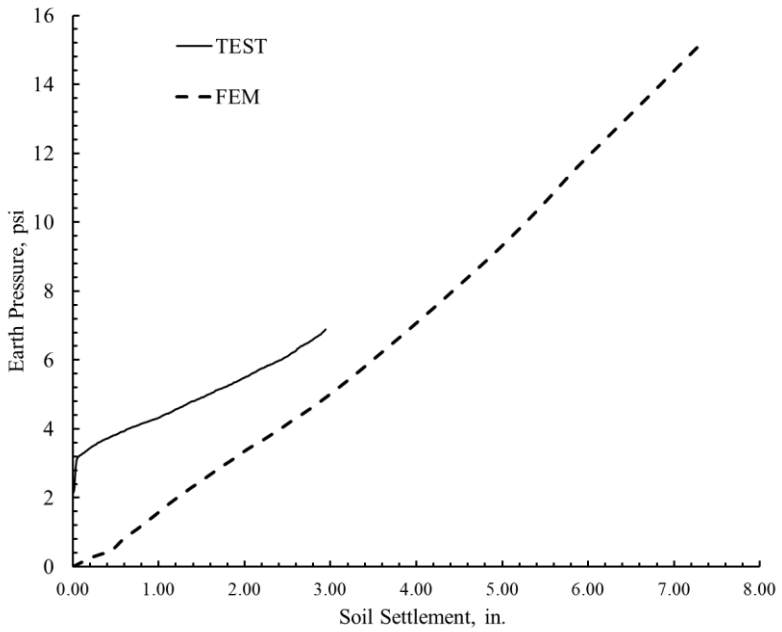


Figure 10A- 3. Movement of the spring line for FEM and TEST just before the meeting of the invert edges.



(a)

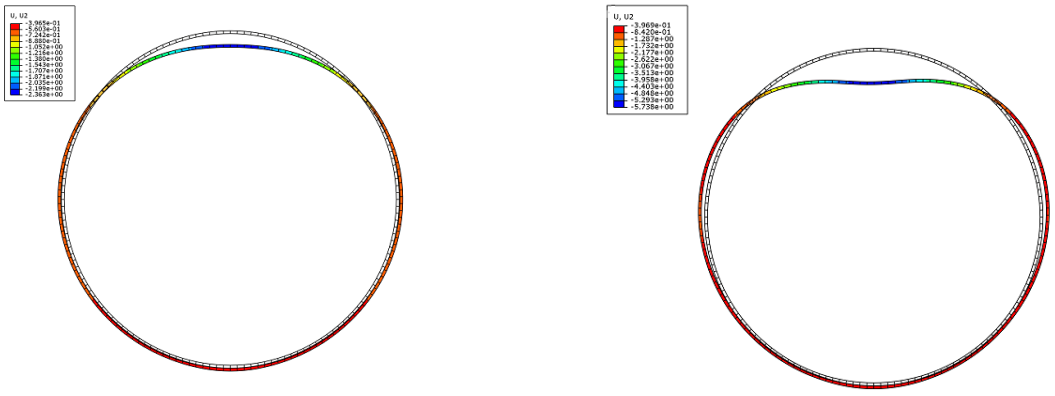


(b)

Figure 10A- 4. Earth Pressure Comparison: (a) Comparison at the ultimate conditions, and (b) Comparison when the inverts just meet.

Appendix 10-B: Invert-cut circular CMP with polymeric SAPL

0.5 in. thick polymeric SAPL



(a) (b)

Figure 10B- 1. (a) Deformation of the liner at the appearance of the first plastic strain, and (b) Deformation of the liner at the ultimate load for 0.5 in. thick polymeric circular SAPL.

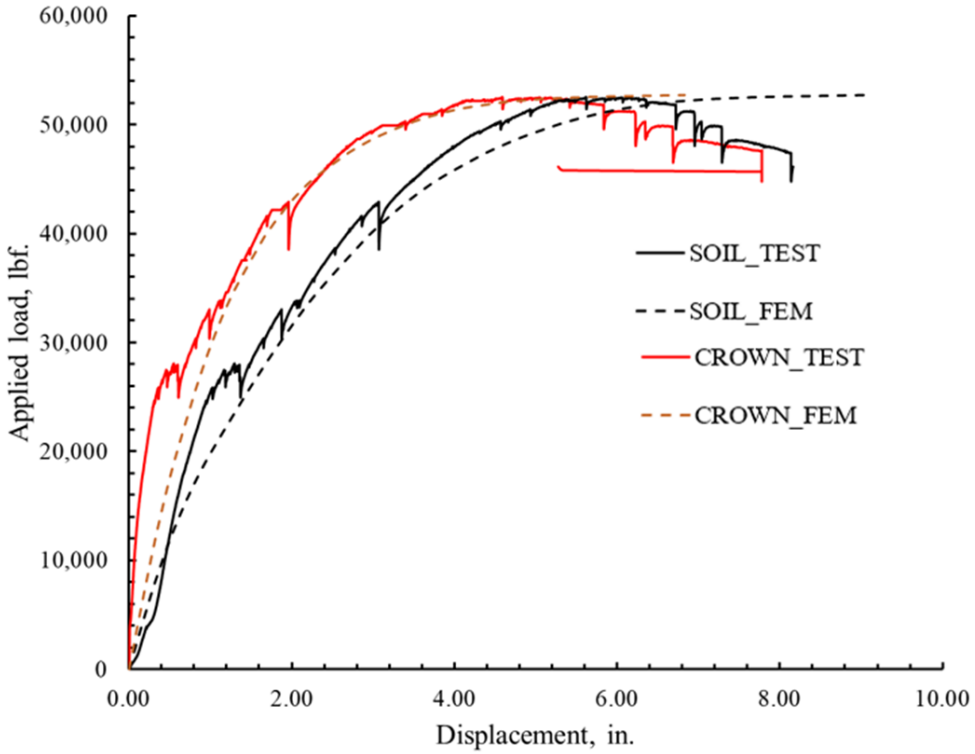


Figure 10B- 2. Comparison of load-displacement plot for the 0.5 in. thick polymeric circular liner.

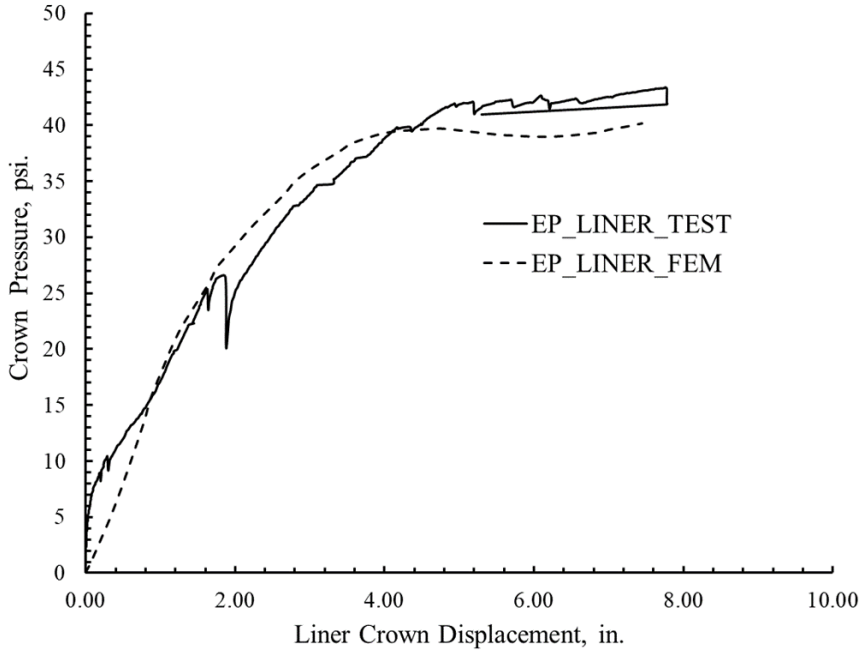


Figure 10B- 3. Comparison of the earth pressure with liner displacement at crown for 0.5 in. thick polymeric circular liner.

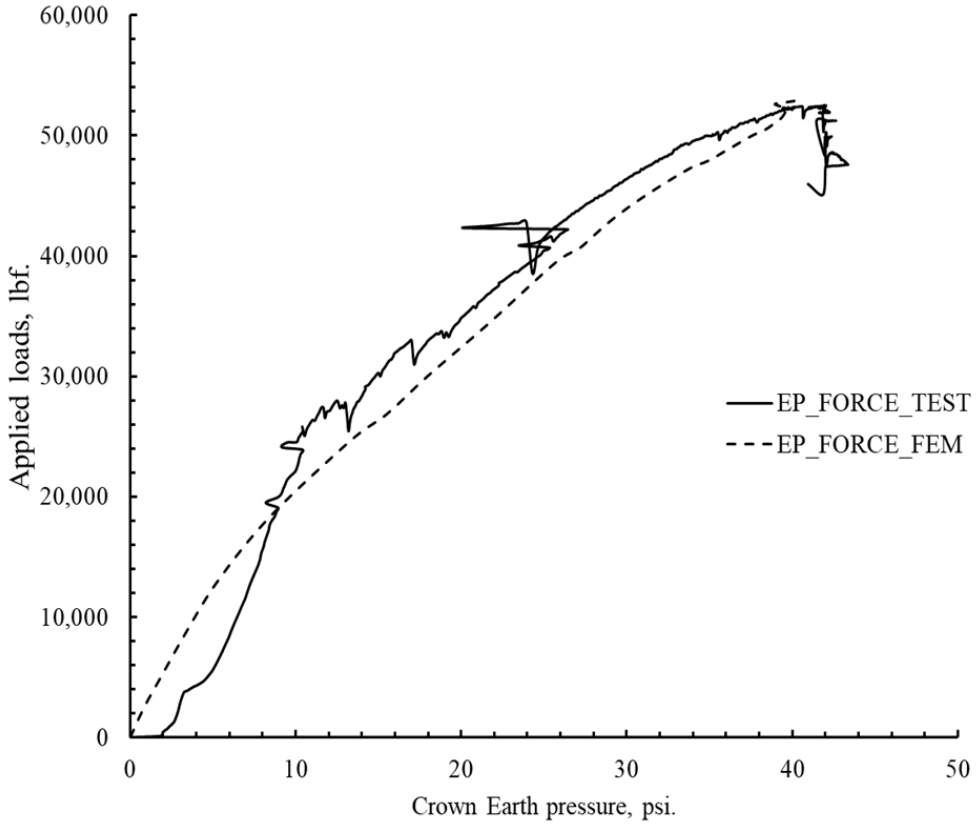
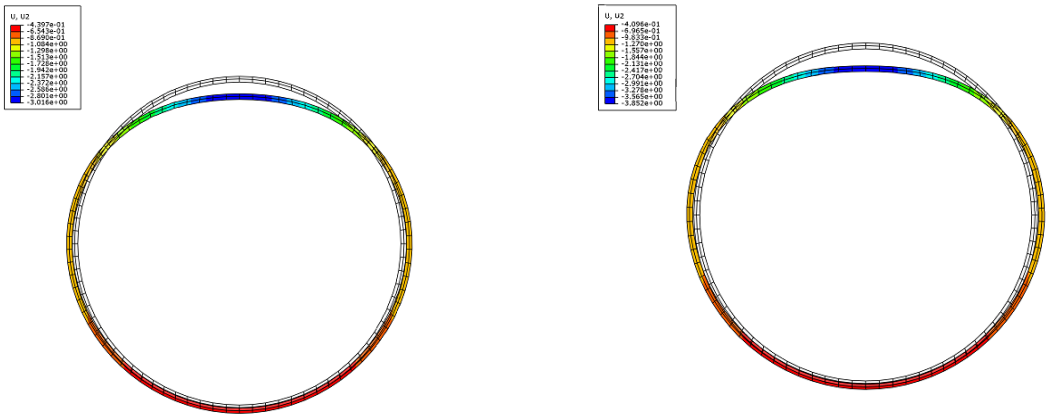


Figure 10B- 4. Comparison of the earth pressure with the applied load for 0.5 in. thick polymeric circular liner.

1-in. thick polymeric SAPL



(a) (b)

Figure 10B- 5. Deformation of the liner at (a) 1st plastic strain (b) at ultimate load conditions for 1-in. thick polymeric circular liner.

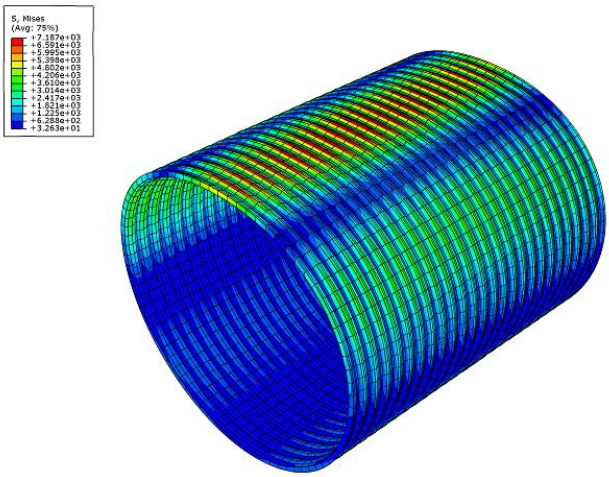


Figure 10B- 6. Von Mises stress around the liner at the ultimate load conditions for 1 in. thick polymeric circular liner.

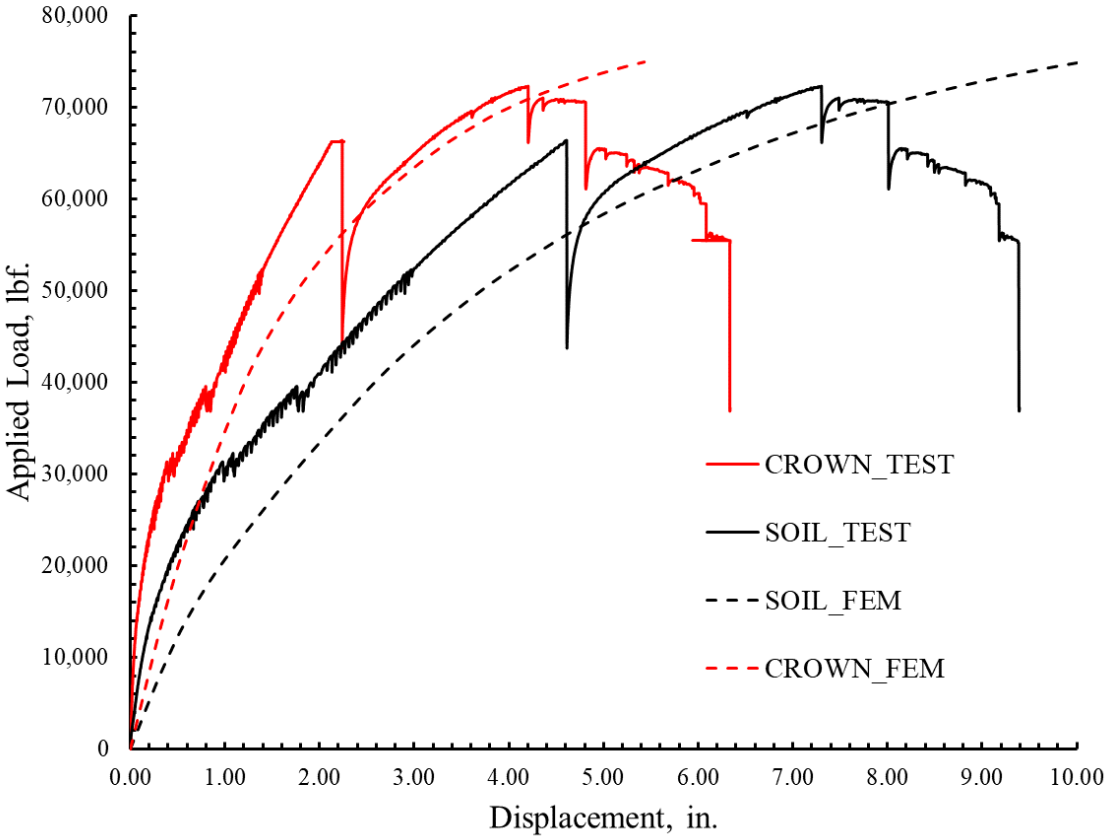


Figure 10B- 7. Load displacement comparison for FE and test results for 1-in. thick polymeric circular liner.

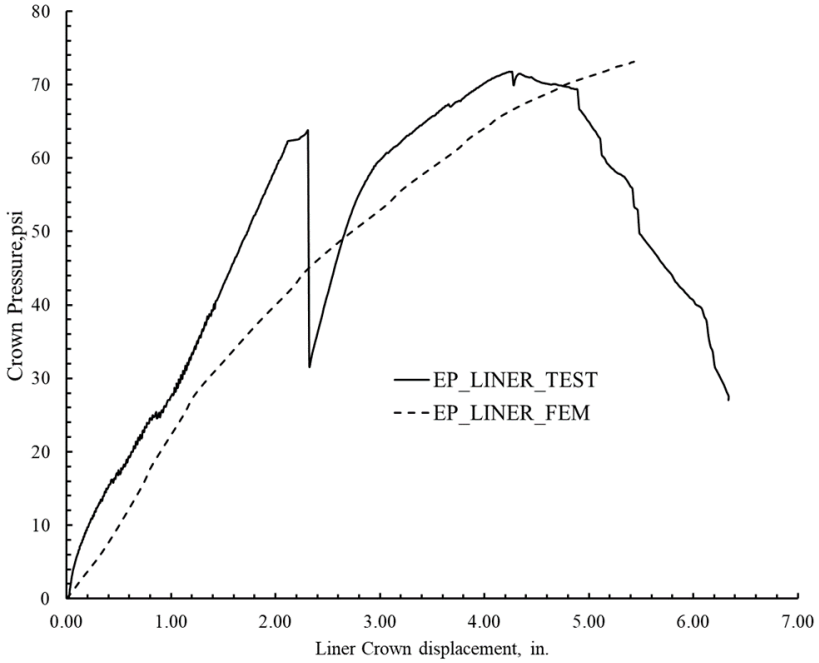


Figure 10B- 8. Comparison of the earth pressure with liner's crown disp., for 1-in. thick polymeric circular liner.

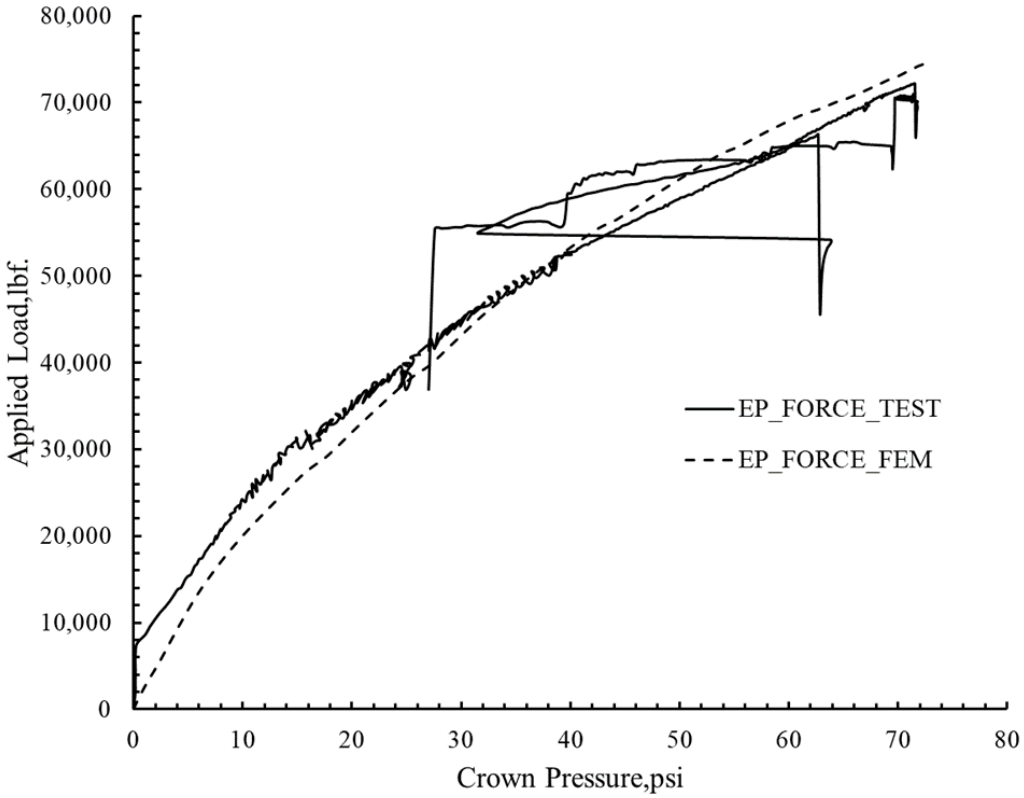
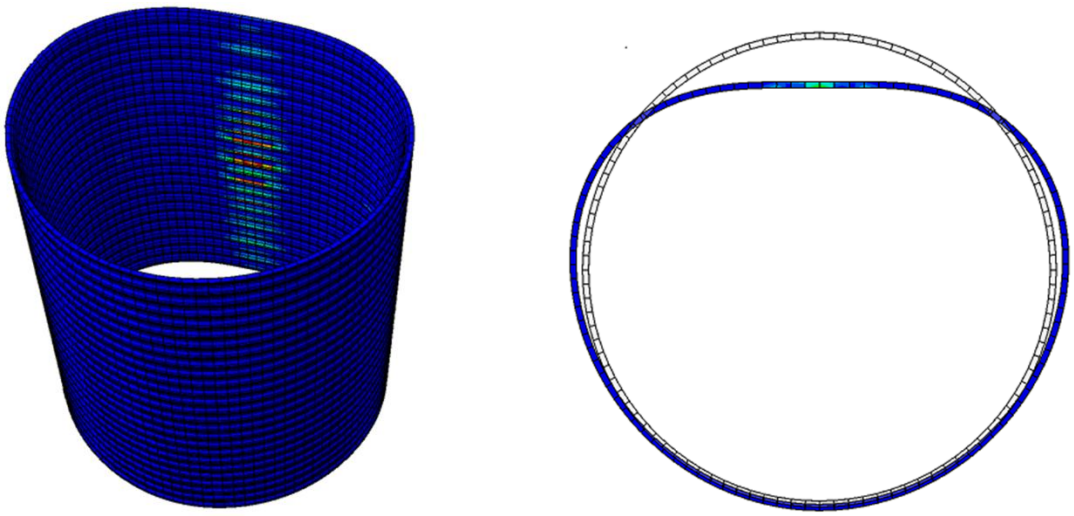


Figure 10B- 9. Comparison of the Earth pressure with applied load, for 1-in. thick polymeric circular liner.

0.75-in. thick polymeric SAPL



(a) (b)

Figure 10B- 10. (a) Development of plastic strain in the inside liner for 0.75-in. thickness polymeric circular liner and
(b) Deformation pattern of the polymeric circular liner.

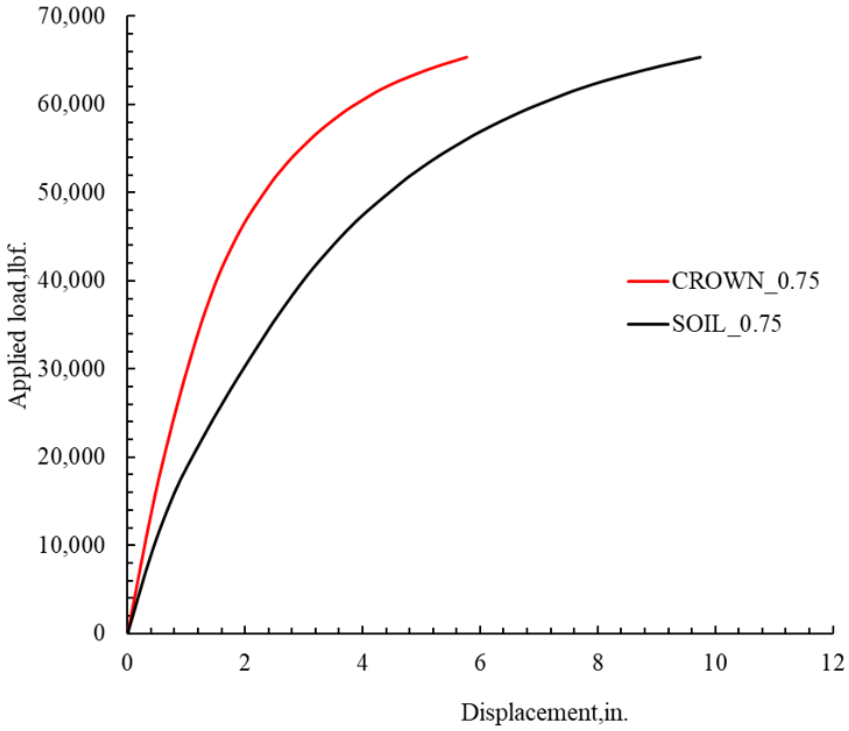


Figure 10B- 11. Load displacement plot from FE analysis for 0.75-in. thick polymeric circular liner.

1.5-in. thick polymeric SAPL

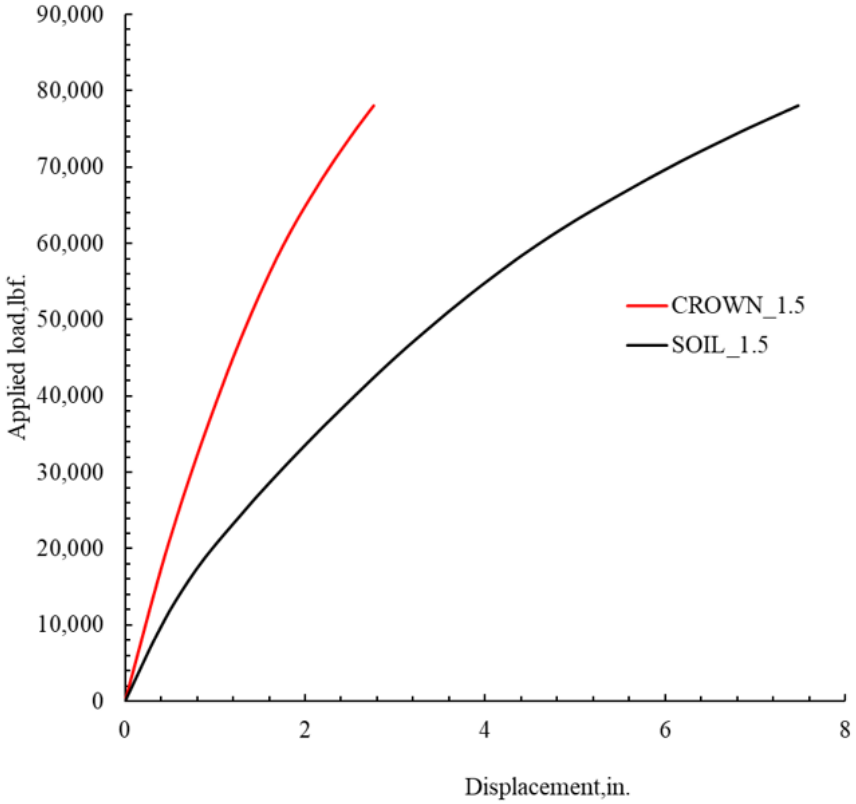
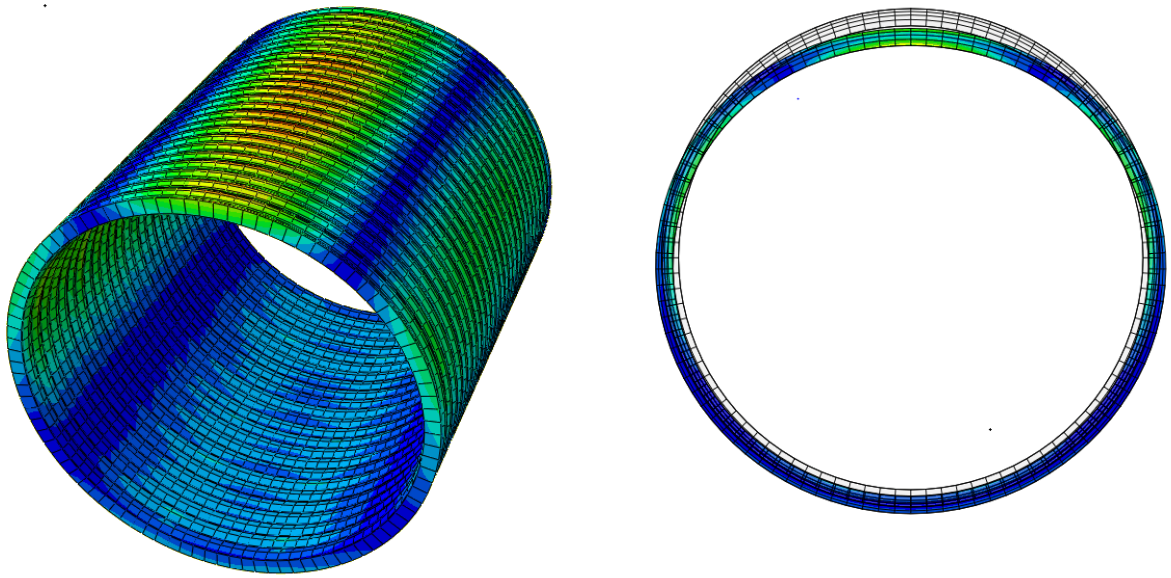


Figure 10B- 12. Load displacement curve for 1.5-in. thick polymeric circular liner.

2.0-in. thick polymeric SAPL



(a) (b)

Figure 10B- 13. (a) Development of plastic strain, and (b) Deformation pattern for 2-in. thick polymeric circular liner.

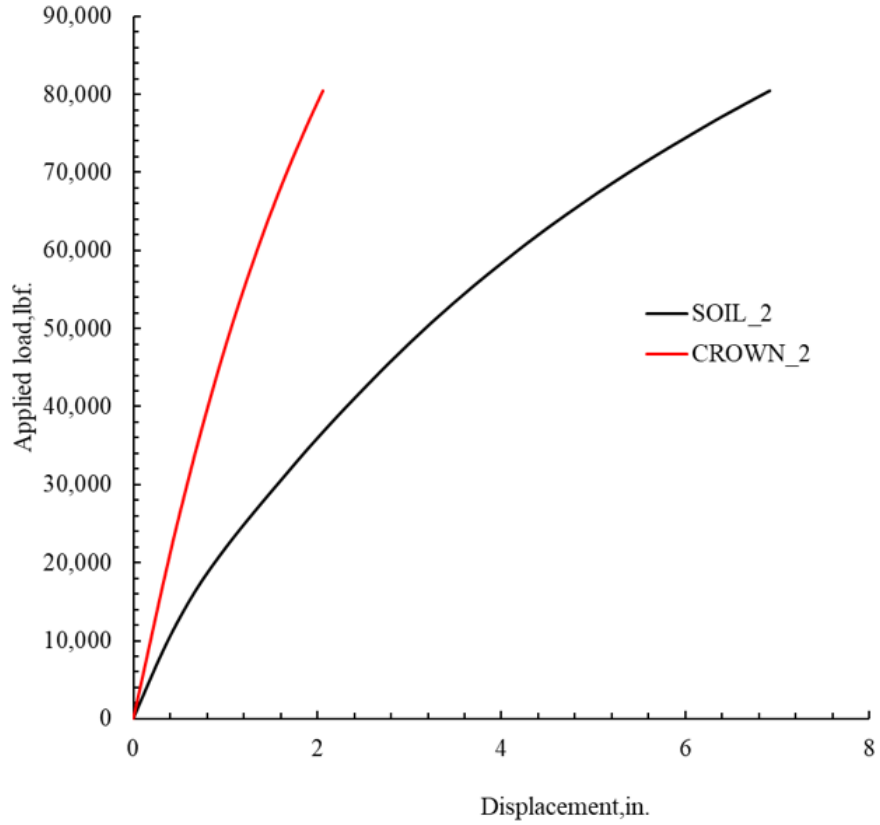


Figure 10B- 14. Load displacement plot from FE analysis for 2-in. thick polymeric circular liner.

Appendix 10-C: Invert-cut Arch CMP

The load-displacement results exclude all the displacement before the loading of the system for both test and FEM results. The load-displacement curve for the invert-cut CMP showed the similar trend to test results. The FEM predicted the load displacement curve to be less stiff than the test results. The FE model predicted the ultimate load to be at around 30 kips while the test results showed the ultimate load to be around 27 kips of load. The displacement of the soil and the CMP was similar at the ultimate load condition.

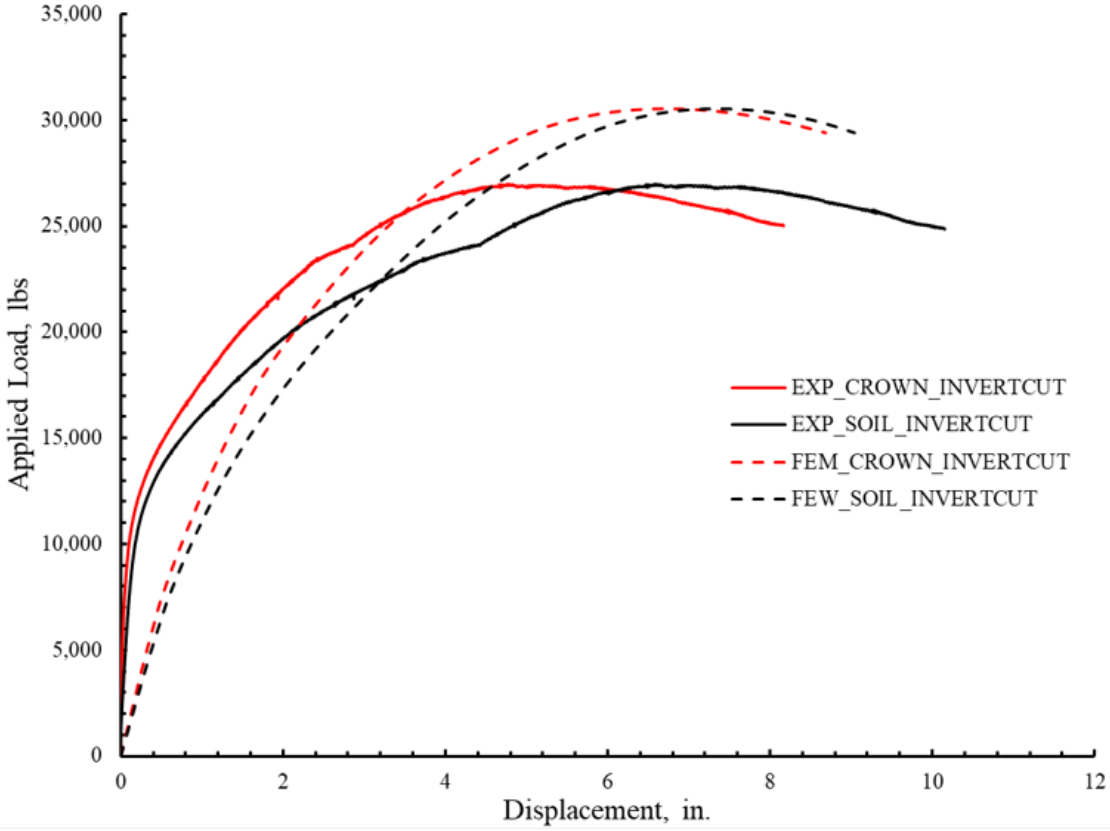


Figure 10C- 1. Load displacement plot for the movement of arch CMP's crown and settlement below load pad for invert cut arch CMP.

Appendix 10-D: Parametric Study of Invert-cut Circular CMPs Repaired with polymeric SAPL

This section presents a parametric study performed on circular pipes with various diameters, cover thickness, and liner thickness. Soil box tests were performed on 60 in. diameter CMP with 2 ft cover. This parametric study investigates the effect of cover thickness and the pipe diameter on the structural capacity of the invert-cut CMP repaired with polymeric liners. All the pipes were simulated with three liner thickness 0.25, 0.5, and 1 in., which were the thickness applied in the soil box tests. The used FEM models were modified from the FEM model verified with the experimental results, as shown in previous sections. The tested CMP pipes were 60 in. diameter with 2-ft cover, lined with 0.25-in., 0.5-in., and 1-in. thick polymeric liner. The only changes made in these models are cover thickness and pipe diameter. The FEM results of the parametric study are presented in the form of tables and graphs. The legend 0.25_3_60 stands for 0.25-in. thick liner with 3-ft cover depth for 60-in. diameter pipe. A similar notation is followed for all the graphs.

Invert-cut circular 60-in. CMPs with 3-ft Cover and 0.25-, 0.5-, and 1-in. thick polymeric Liner

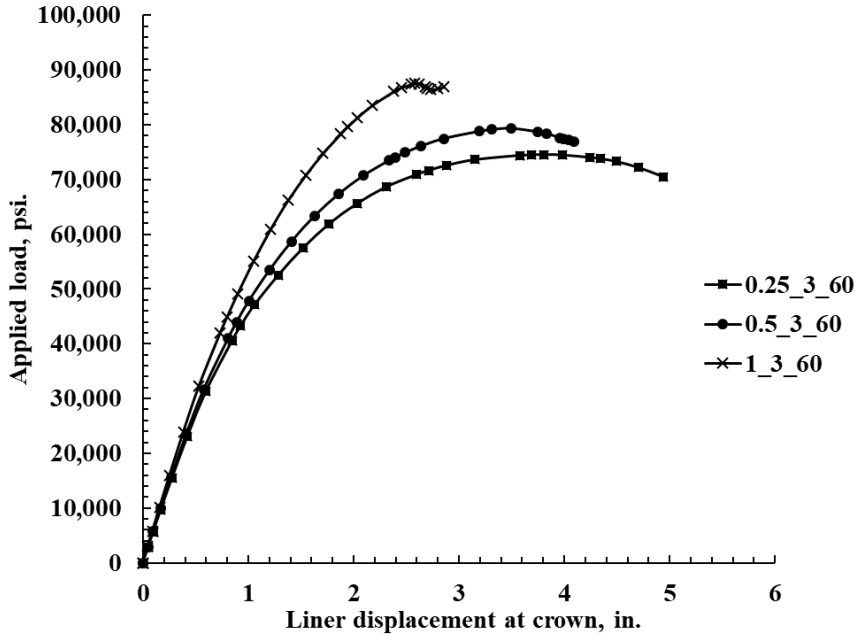


Figure 10D-1. Load displacement plot for 60-in. invert-cut circular CMP with 3 ft cover and 0.25-, 0.5-, and 1-in. thick polymeric circular liner.

Table 10D-1: Comparison of applied load, displacement, and earth pressure at the first crack point and ultimate point for 60 in. invert-cut circular CMP with 3-ft cover.

Polymeric Liner Thickness	1st crack point			Ultimate load		
	Load (kips)	Crown Disp. (in.)	Earth Pressure (psi)	Load (kips)	Crown Disp. (in.)	Earth Pressure (psi)
0.25	71.63	2.61	34	74.5	3.98	39.3
0.5	73.45	2.25	38	79.4	3.49	48.75
1	87.5	2.63	58	87.5	2.85	58.58

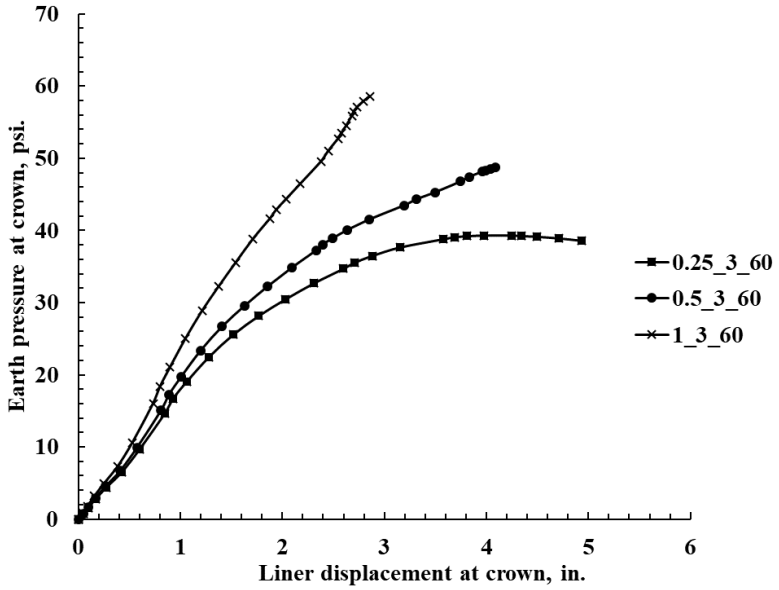


Figure 10D-2. Earth pressure at 4 in. above the crown vs. crown displacement for 60-in. invert-cut circular CMP with 3-ft cover and 0.25-, 0.5-, and 1-in. polymeric circular thick liner.

Invert-cut circular 60 in. CMPs with 1-ft cover and 0.25-, 0.5-, and 1-in. thick polymeric circular liner

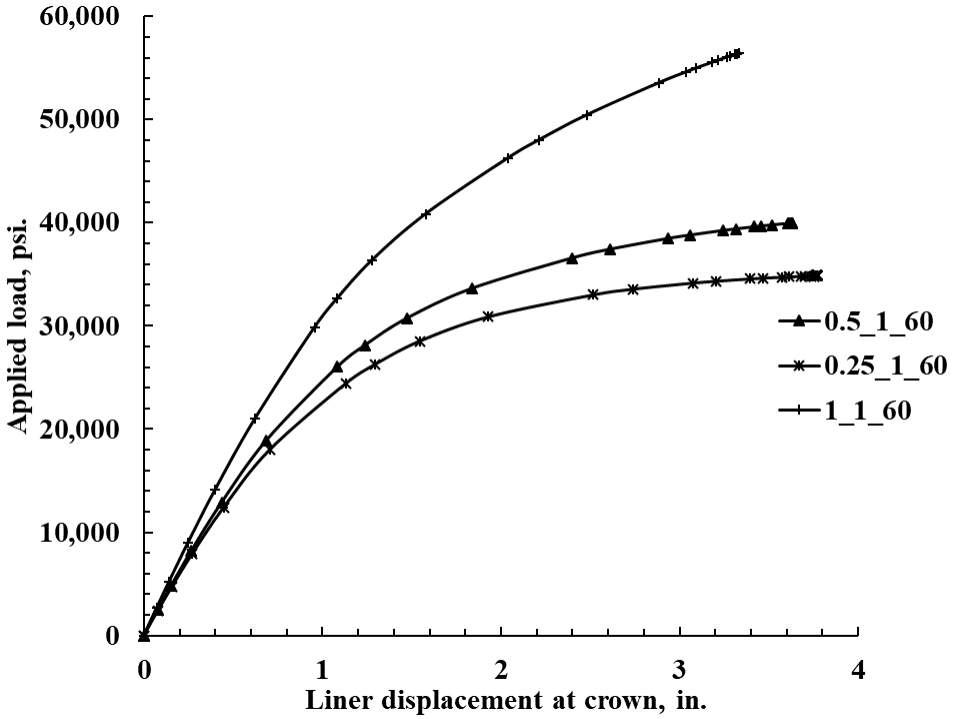


Figure 10D-3. Load displacement plot for 60-in. invert-cut circular CMP with 1-ft cover and 0.25-, 0.5-, and 1-in. thick polymeric circular liner.

Table 10D-2. Comparison of applied load, displacement, and earth pressure at the first crack point and ultimate point for 60-in. invert-cut circular CMP with 1-ft cover and 0.25-, 0.5-, and 1-in. thick polymeric circular liner.

Liner Thickness	1st Crack Point			Ultimate Load		
	Load (kips)	Crown Disp. (in.)	Earth Pressure (psi)	Load (kips)	Crown Disp. (in.)	Earth Pressure (psi)
0.25	34.73	2.73	20.34	34.84	3.76	20.34
0.5	33.63	1.83	28.56	39.94	3.60	32.20
1	53.54	2.47	60.03	56.36	3.21	68.98

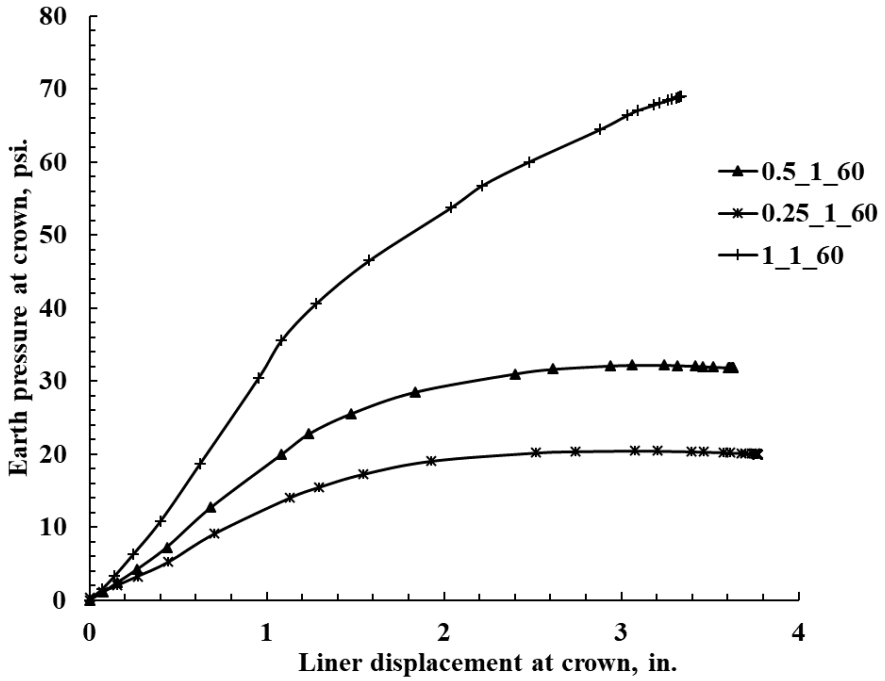
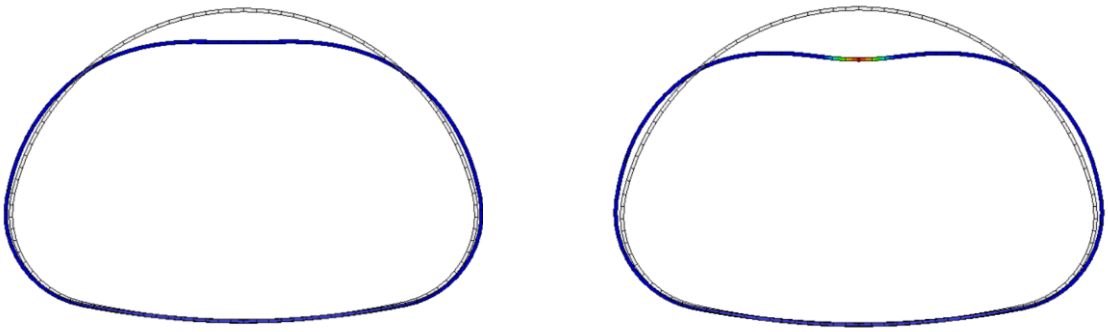


Figure 10D-4. Earth pressure at 4 in. above the crown vs. crown displacement for 60-in. invert-cut circular CMP with 1-ft cover and 0.25-, 0.5-, and 1-in. polymeric circular thick liner.

Appendix 10E: Invert-cut Arch CMP with polymeric Liners

0.5-in. thick polymeric SAPL



(a) (b)

Figure 10E- 1. Deformation pattern at the first crack (a) and at ultimate crack, and (b) 0.5 in. thick arch polymeric liner.

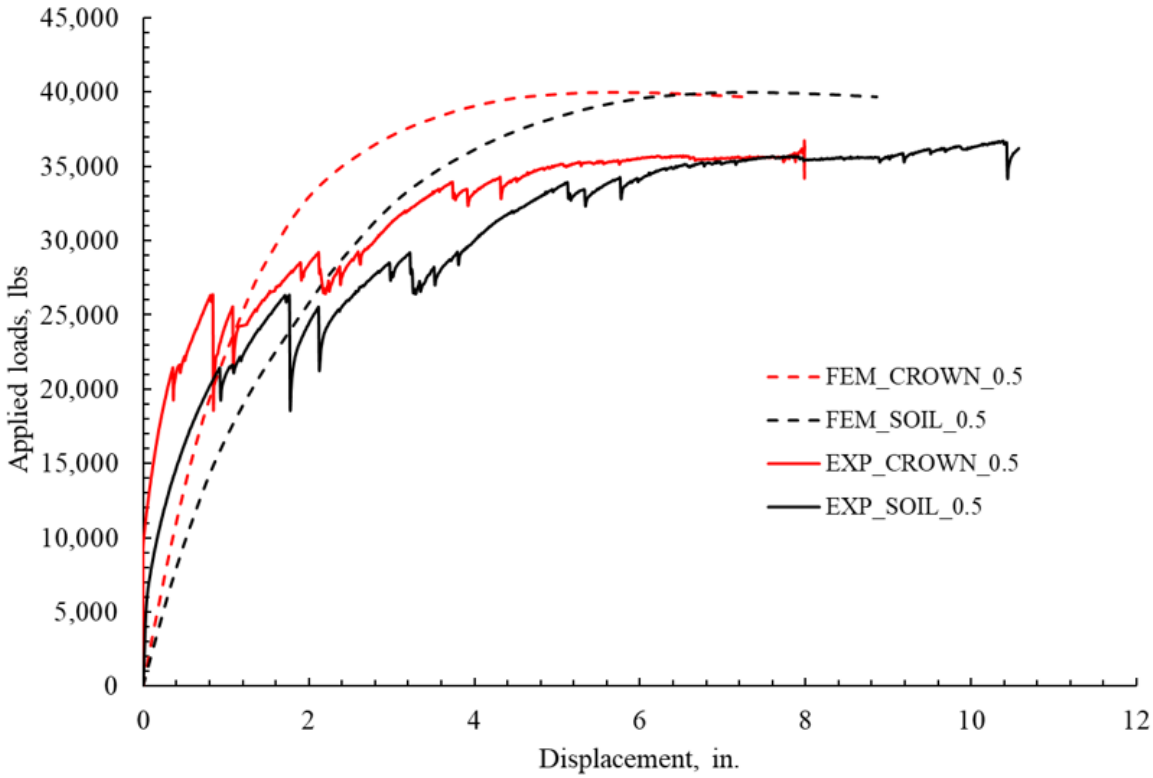


Figure 10E- 2. Comparison of load displacement plot for the 0.5-in. thick arch polymeric liner.

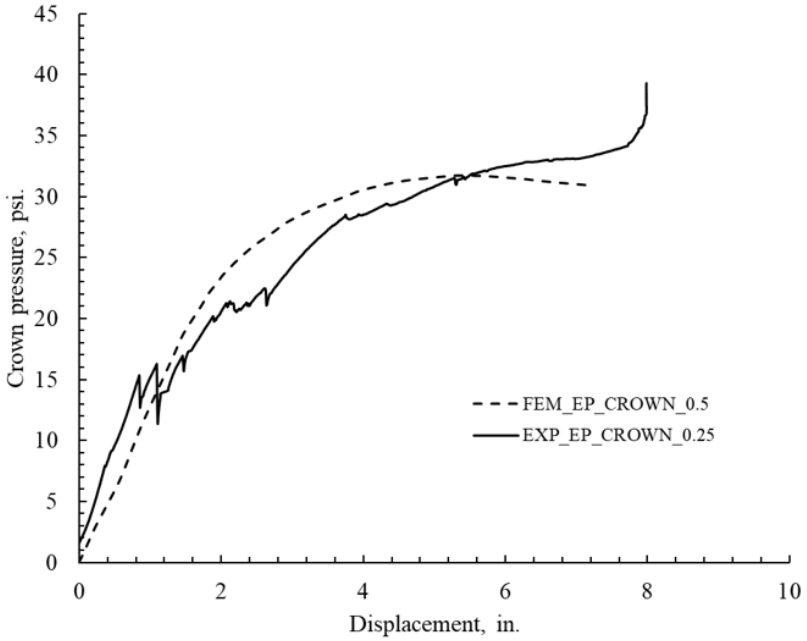


Figure 10E-3. Comparison of the earth pressure with liner displacement at crown for 0.5-in. thick arch polymeric liner.

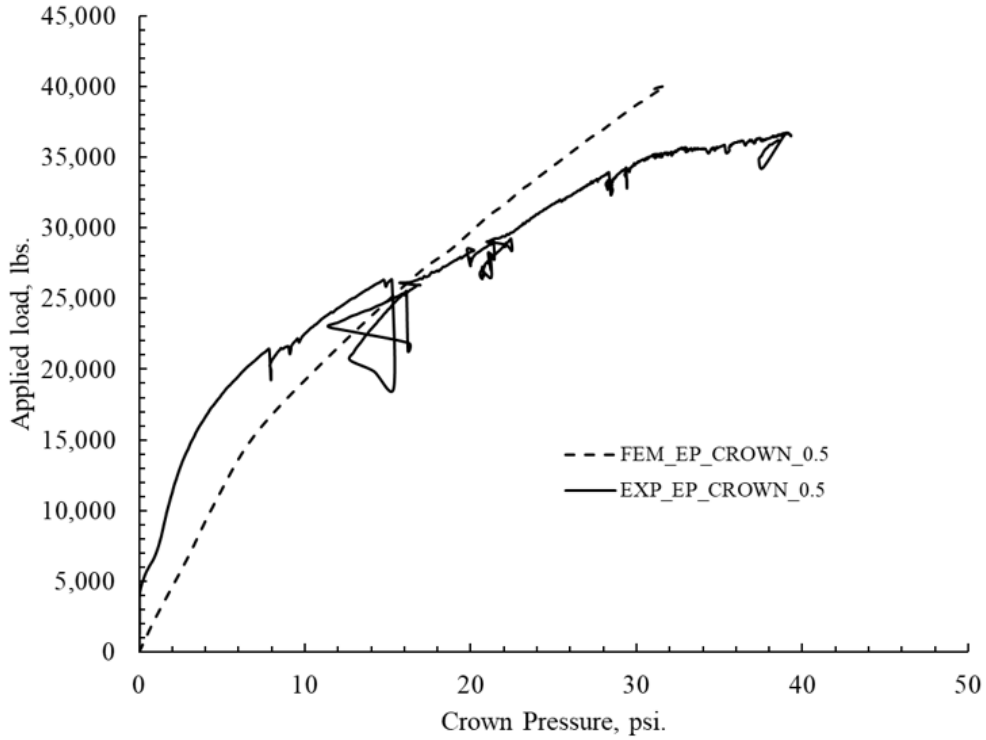
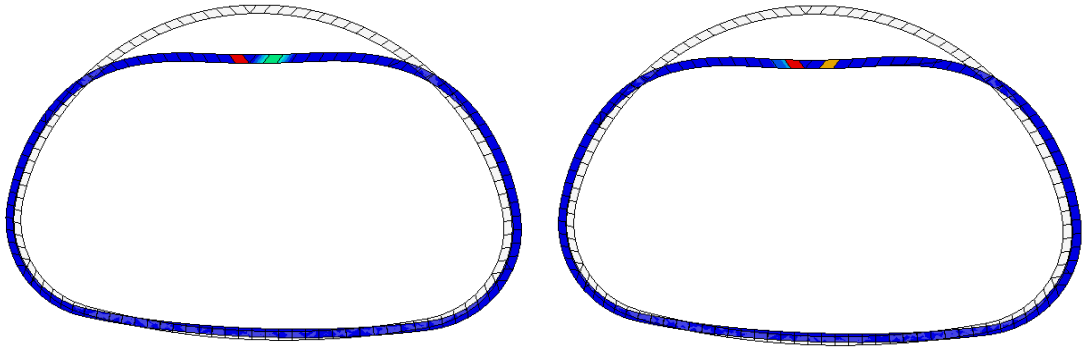


Figure 10E-4. Comparison of the earth pressure with the applied load for 0.5-in. thick arch polymeric liner.

1-in. thick polymeric SAPL



(a) (b)

Figure 10E-5. Deformation of the liner at (a) 1st plastic strain (b) at ultimate load conditions for 1-in. thick arch polymeric liner.

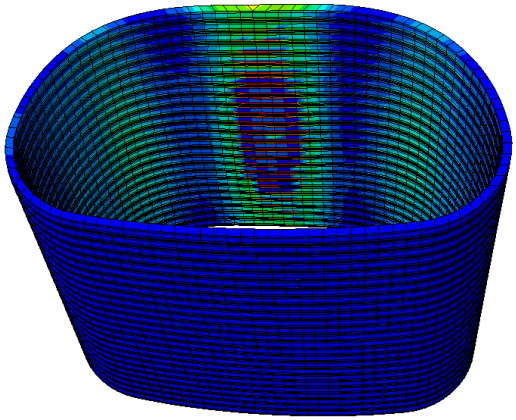


Figure 10E-6. Ultimate Von Mises stress around the liner at the ultimate load conditions for 1 in. thick arch polymeric liner.

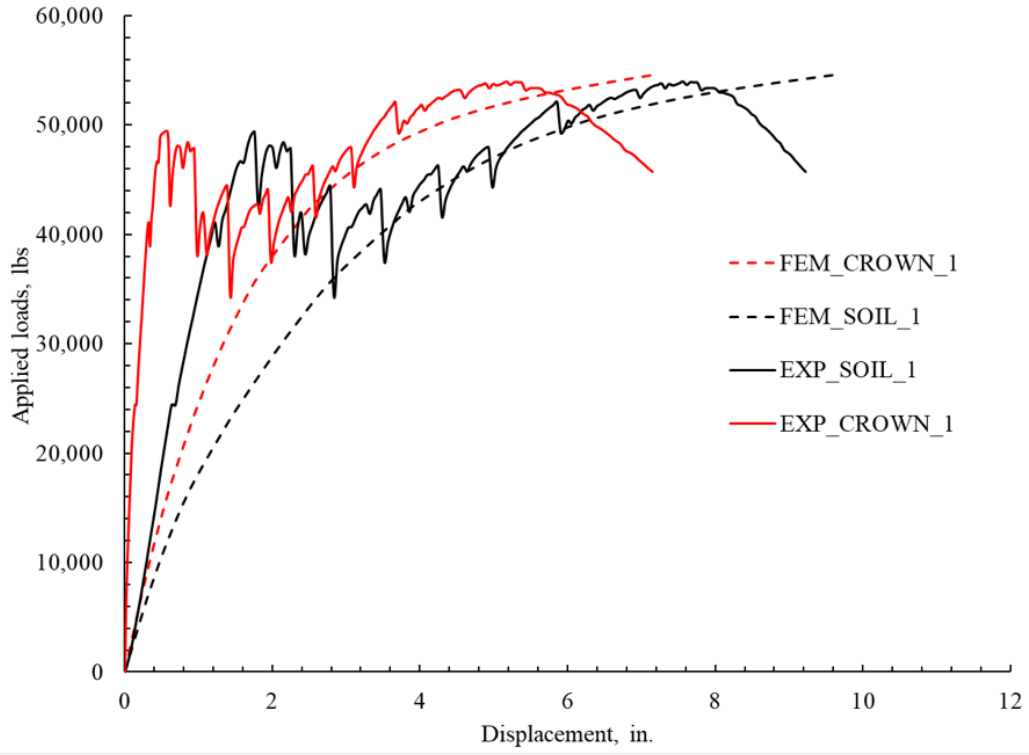


Figure 10E-7. Load displacement plot at the crown and settlement of soil below load pad for 1-in. thick arch polymeric liner.

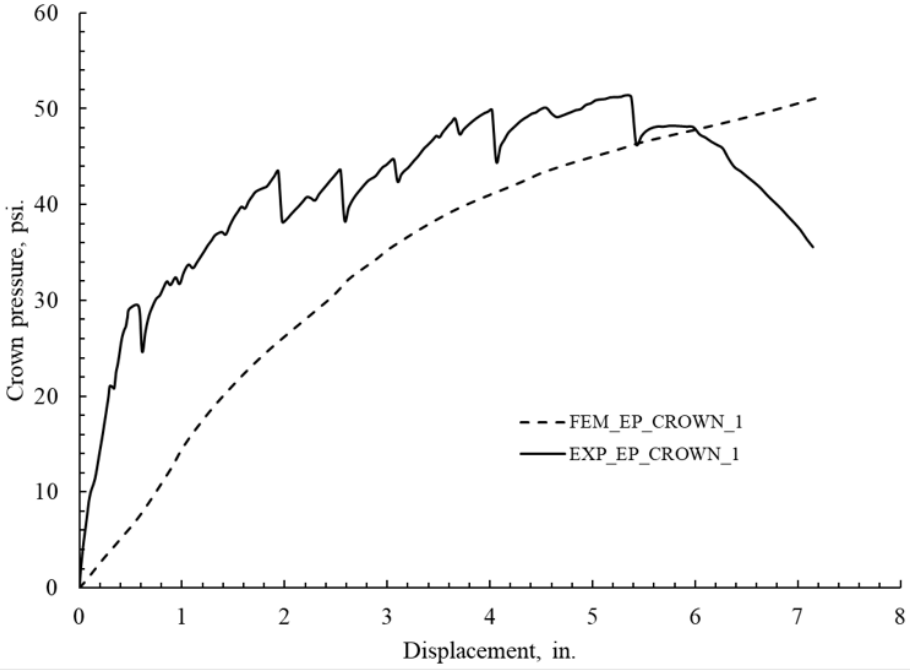


Figure 10E-8. Comparison of the Earth pressure with polymeric liner's crown disp., for 1-in. thick arch polymeric liner.

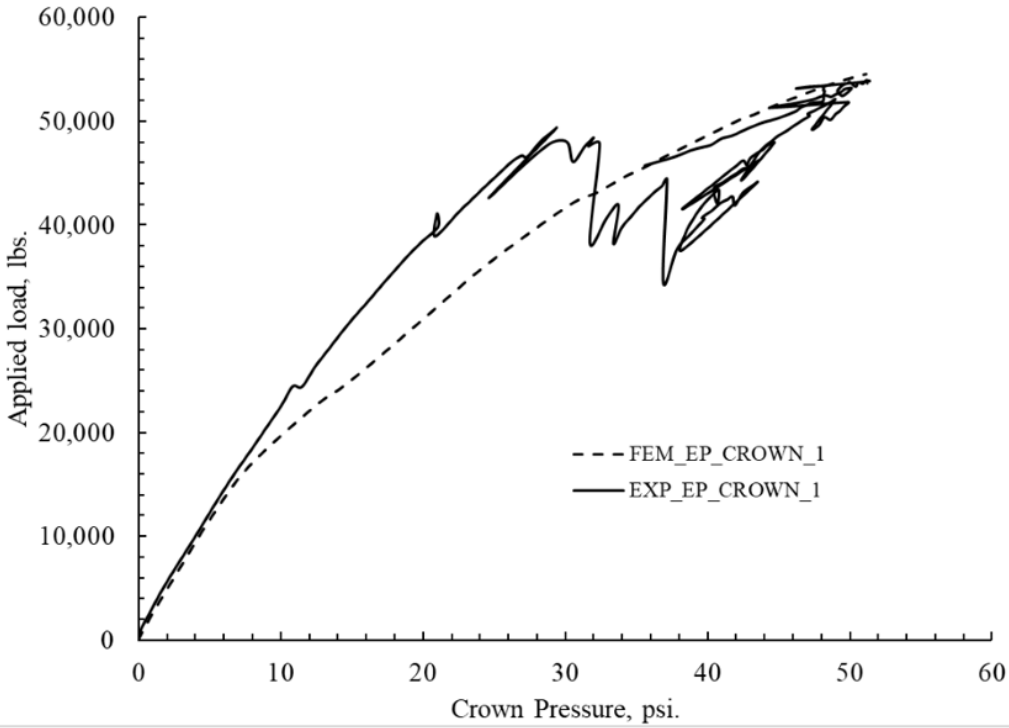


Figure 10E-9. Comparison of the earth pressure with applied load for 1-in. thick arch polymeric liner.

0.75-in. thick polymeric SAPL

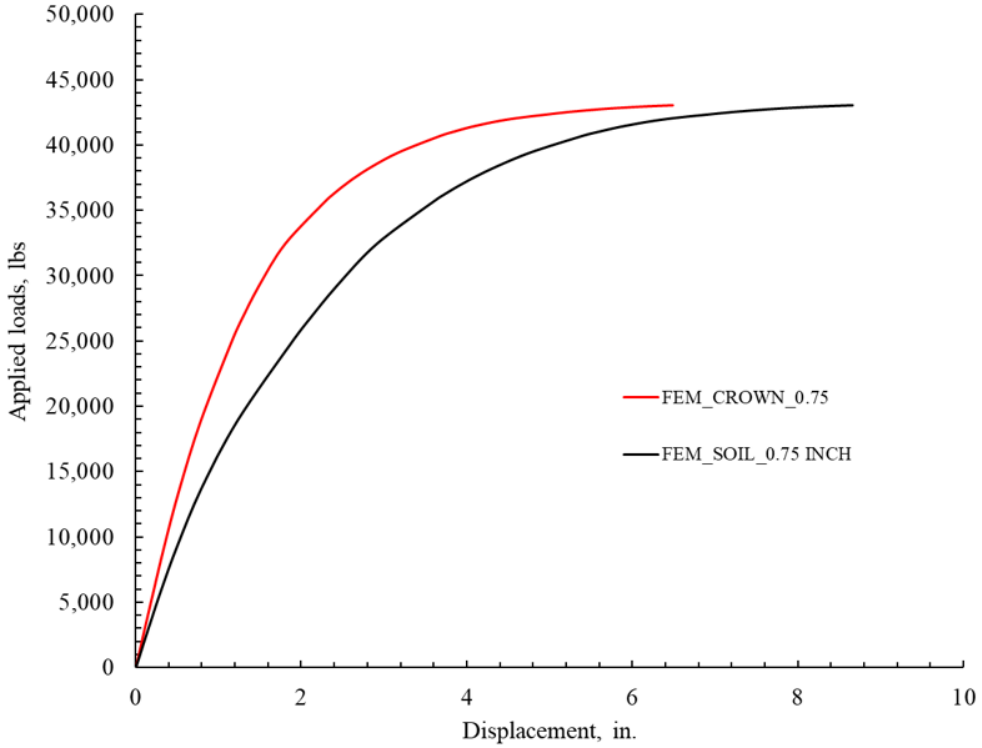


Figure 10E-10. Load displacement plot of crown displacement and soil settlement from FE analysis for 0.75-in. thick arch polymeric liner.

1.5-in. thick polymeric SAPL

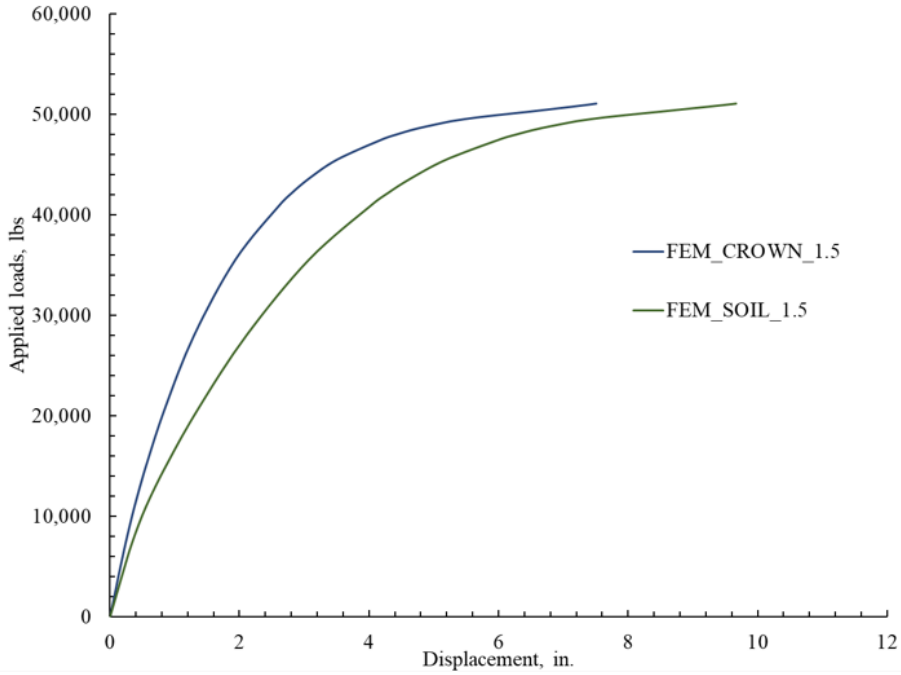


Figure 10E-11. Load displacement plot of crown displacement and soil settlement from FE analysis for 1.5-in. thick arch polymeric liner.

2.0-in. thick polymeric SAPL

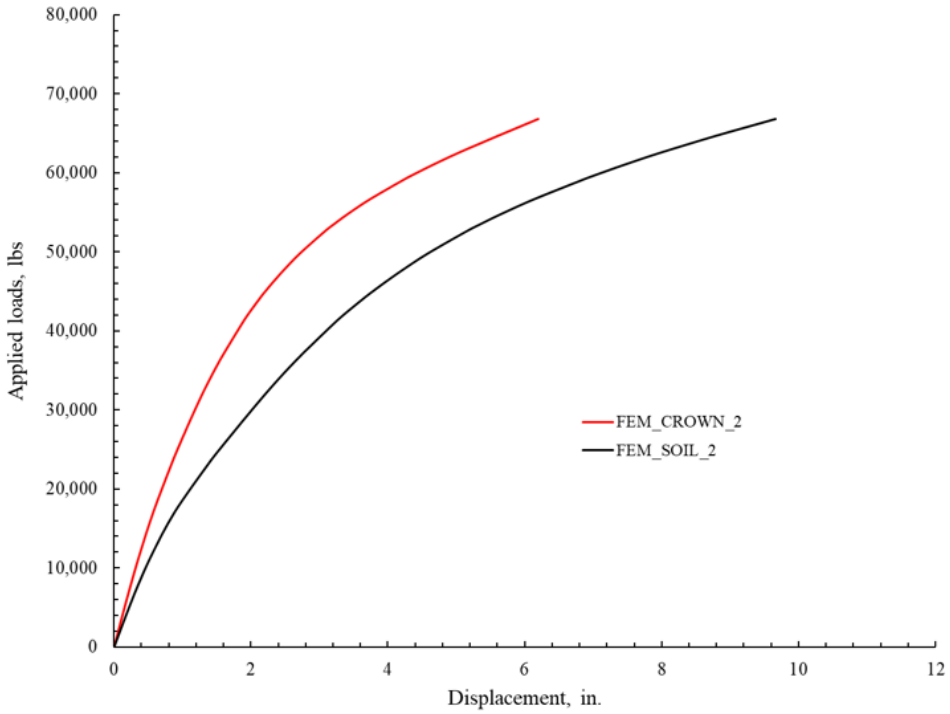


Figure 10E-12. Load displacement plot of crown displacement and soil settlement from FE analysis for 2.0- in. thick arch polymeric liner.

Invert-cut Circular 48 in. CMPs with 3 ft cover and 0.25, 0.5, and 1 in. thick polymeric Liner

Table 10E-3. Comparison of the applied load, displacement, and earth pressure at the first crack and ultimate load for 48 in. invert-cut circular CMP with 3 ft cover and 0.25, 0.5, and 1 in. thick polymeric liner.

Liner thickness	1st crack point			Ultimate load		
	Load (kips)	Crown disp. (in.)	Earth pressure (psi)	Load (kips)	Crown disp. (in.)	Earth pressure (psi)
0.25	42.86	1.13	16.25	64.24	3.72	34.38
0.5	56.63	1.98	26.08	65.87	3.4	37.26
1	67.89	2.16	42.24	70.08	3.21	42.24

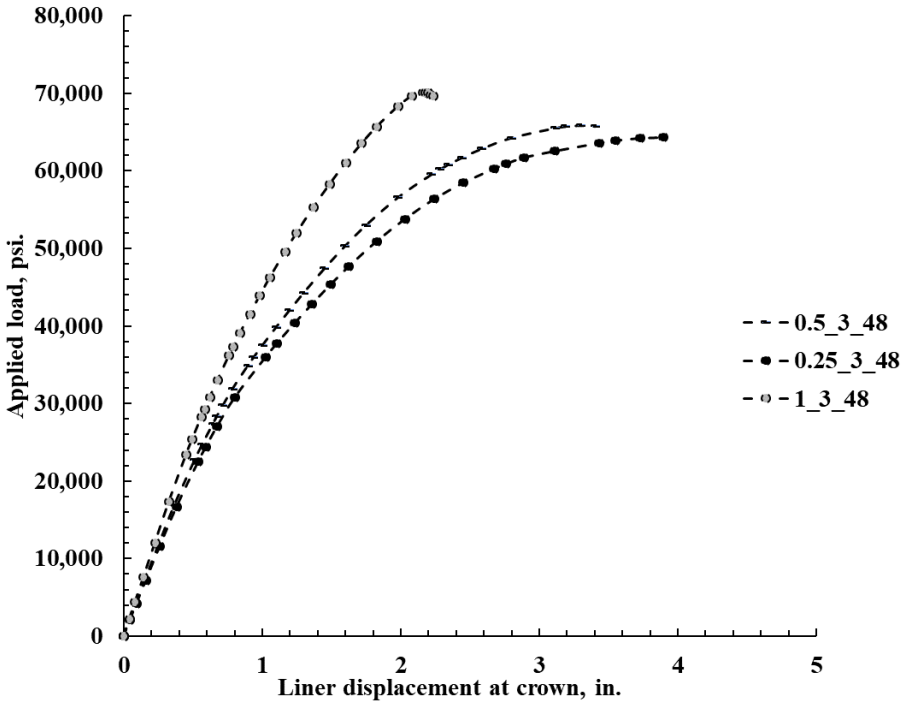


Figure 10E-13. Load displacement plot for 48 in. invert-cut circular CMPs with 3 ft cover and 0.25, 0.5, and 1 in. thick polymeric liner.

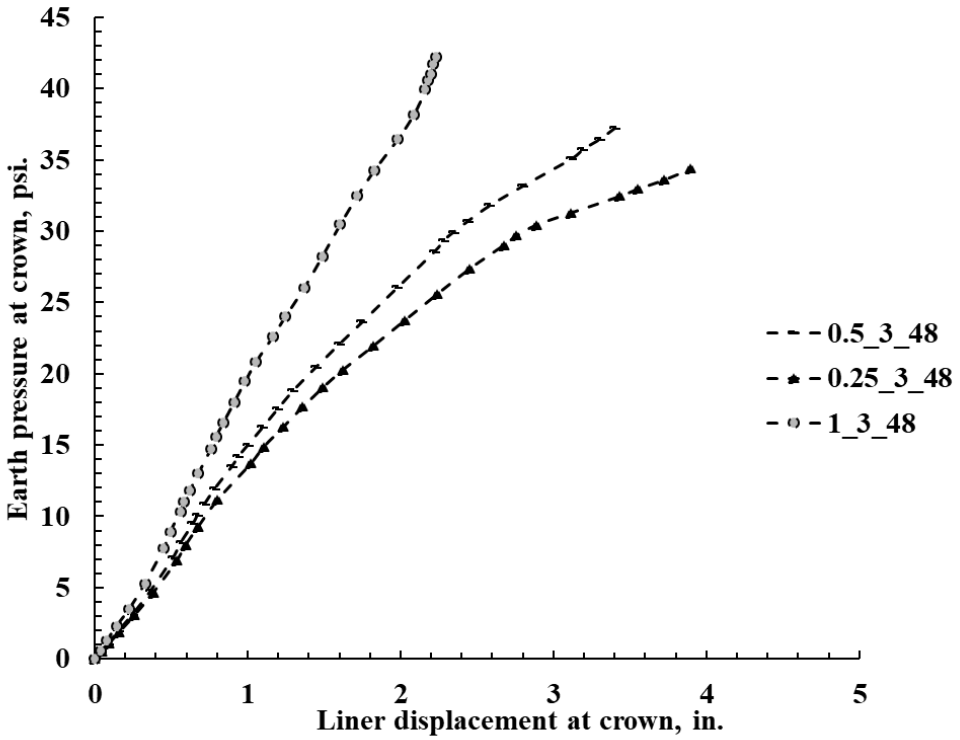


Figure 10E-14. Earth pressure at 4 in. above the crown vs. crown displacement for 48 in. invert-cut circular CMPs with 3 ft cover and 0.25, 0.5, and 1 in. thick polymeric liner.

Invert-cut Circular 48 in. CMPs with 2 ft. cover and 0.25, 0.5, and 1 in. thick polymeric liner

Table 10E-4. Comparison of applied load, displacement, and earth pressure at the first crack and ultimate load for Invert-cut Circular 48 in. CMPs with 2 ft cover and 0.25, 0.5, and 1 in. thick polymeric liner.

Liner Thickness	1st Crack point			Ultimate Load		
	Load (kips)	Crown Disp. (in.)	Earth Pressure (psi)	Load (kips)	Crown Dsp. (in.)	Earth Pressure (psi)
0.25	41.60	1.98	30.69	53.0	5.13	47.51
0.5	42.99	1.84	31.36	56.34	4.60	49.43
1	65.91	2.58	59.72	73.29	3.45	75.61

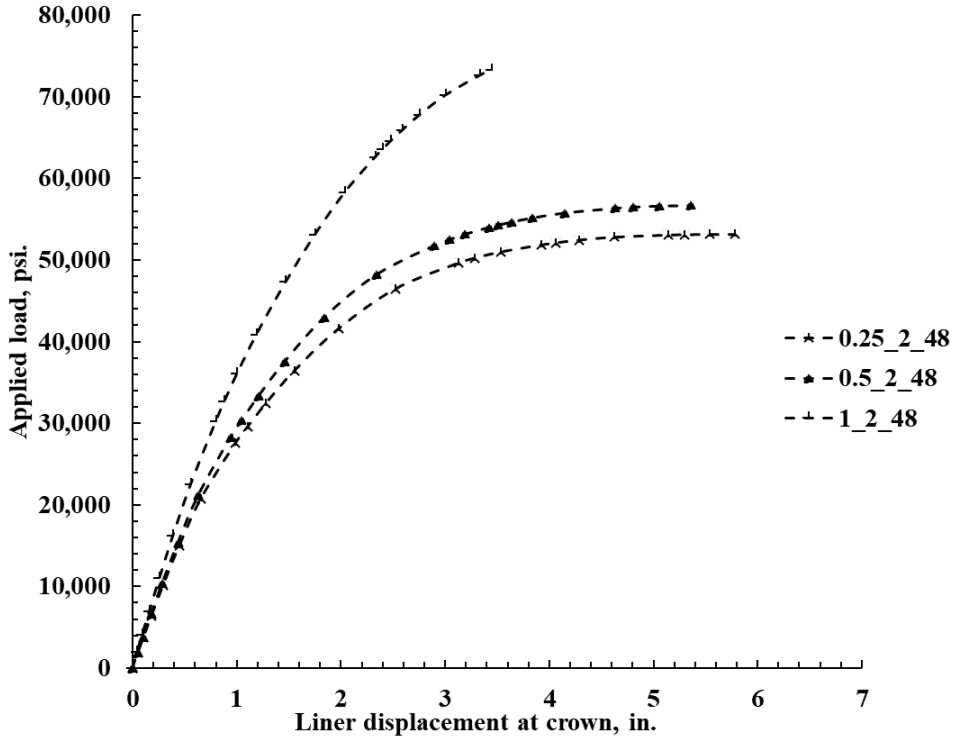


Figure 10E-15. Load displacement plot for Invert-cut Circular 48 in. CMPs with 2 ft cover and 0.25, 0.5, and 1 in. thick polymeric liner.

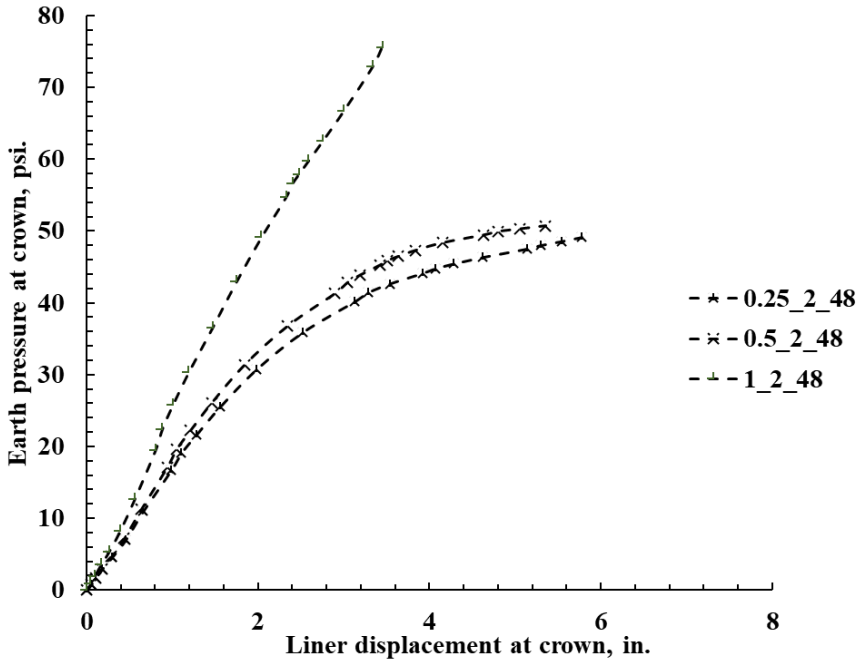


Figure 10E-16. Earth pressure at 4 in. above the crown vs. crown displacement for Invert-cut Circular 48 in. CMPs with 2 ft cover and 0.25, 0.5, and 1 in. thick polymeric liner.

Invert-cut Circular 48 in. CMPs with 1 ft cover and 0.25, 0.5, and 1 in. thick Liner

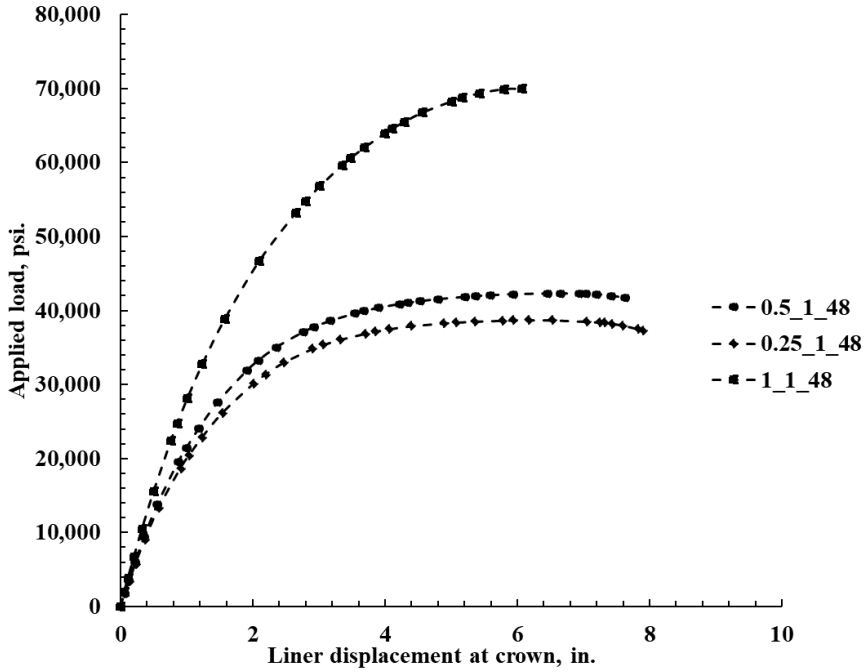


Figure 10E-17. Load displacement plot for Invert-cut circular 48 in. CMPs with 1 ft cover and 0.25, 0.5, and 1 in. thick polymeric liner.

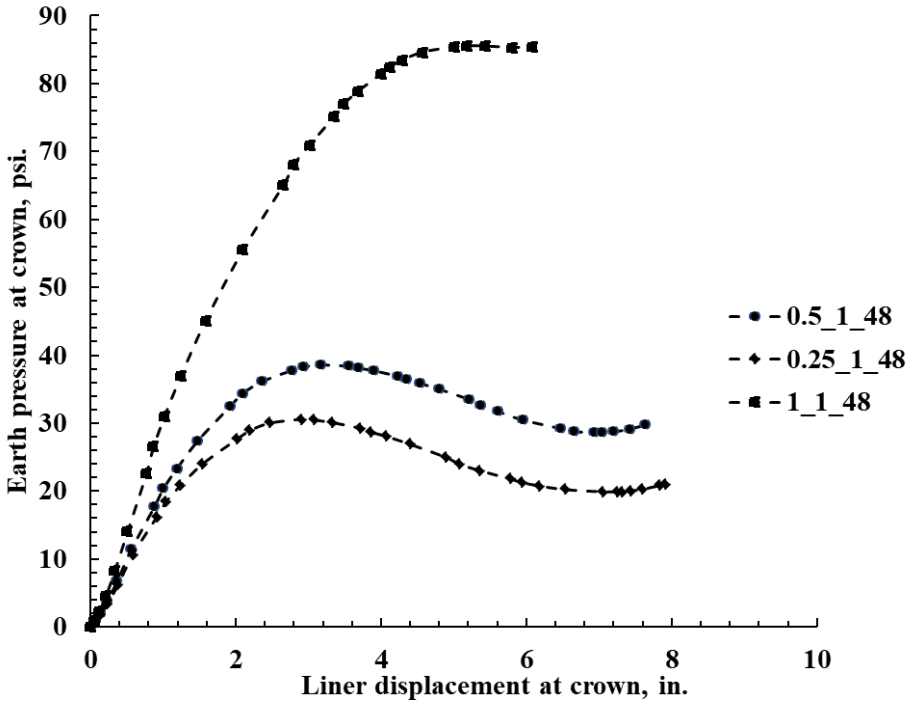


Figure 10E-18. Earth pressure at 4 in. above the crown vs. crown displacement for Invert-cut circular 48 in. CMPs with 1 ft cover and 0.25, 0.5, and 1 in. thick polymeric liner.

Table 10E-5. Comparison of applied load, displacement, and earth pressure at the first crack and ultimate load for Invert-cut Circular 48 in. CMPs with 1 ft cover and 0.25, 0.5, and 1 in. thick polymeric liner.

Liner thickness	1st crack point			Ultimate load		
	Load (kips)	Crown disp. (in.)	Earth pressure (psi)	Load (kips)	Crown disp. (in.)	Earth pressure (psi)
0.25	31.36	2.19	28.95	38.70	6.50	30.50
0.5	31.87	1.91	32.52	42.85	6.40	38.33
1	46.66	2.09	55.53	69.91	5.80	85.28

Invert-cut Circular 36 in. CMPs with 3-ft cover and 0.25, 0.5, and 1 in. thick polymeric Liner

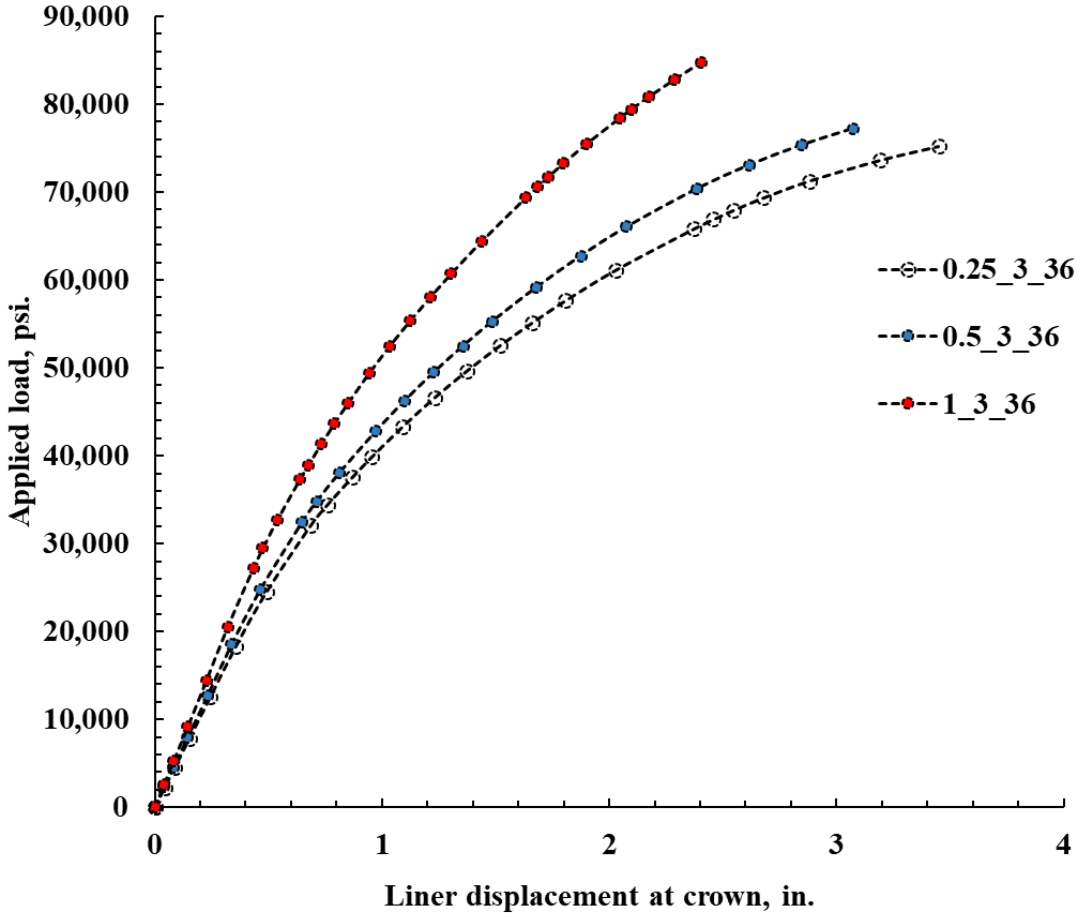


Figure 10E-19. Load displacement plot for invert-cut circular 36 in. CMPs with 3 ft cover and 0.25, 0.5, and 1 in. thick polymeric liner.

Table 10E-6. Comparison of applied load, displacement, and earth pressure at the first crack and ultimate load for invert-cut circular 36 in. CMPs with 3 ft cover and 0.25, 0.5, and 1 in. thick polymeric liner.

Liner Thickness	1st crack point			Ultimate load		
	Load (kips)	Crown Disp. (in.)	Earth Pressure (psi)	Load (kips)	Crown Disp. (in.)	Earth Pressure (psi)
0.25	55.15	1.67	23.25	75.23	3.45	39.73
0.5	55.27	1.48	21.25	77.23	3.07	38.19
1	84.80	2.40	45.87	84.81	2.40	45.87

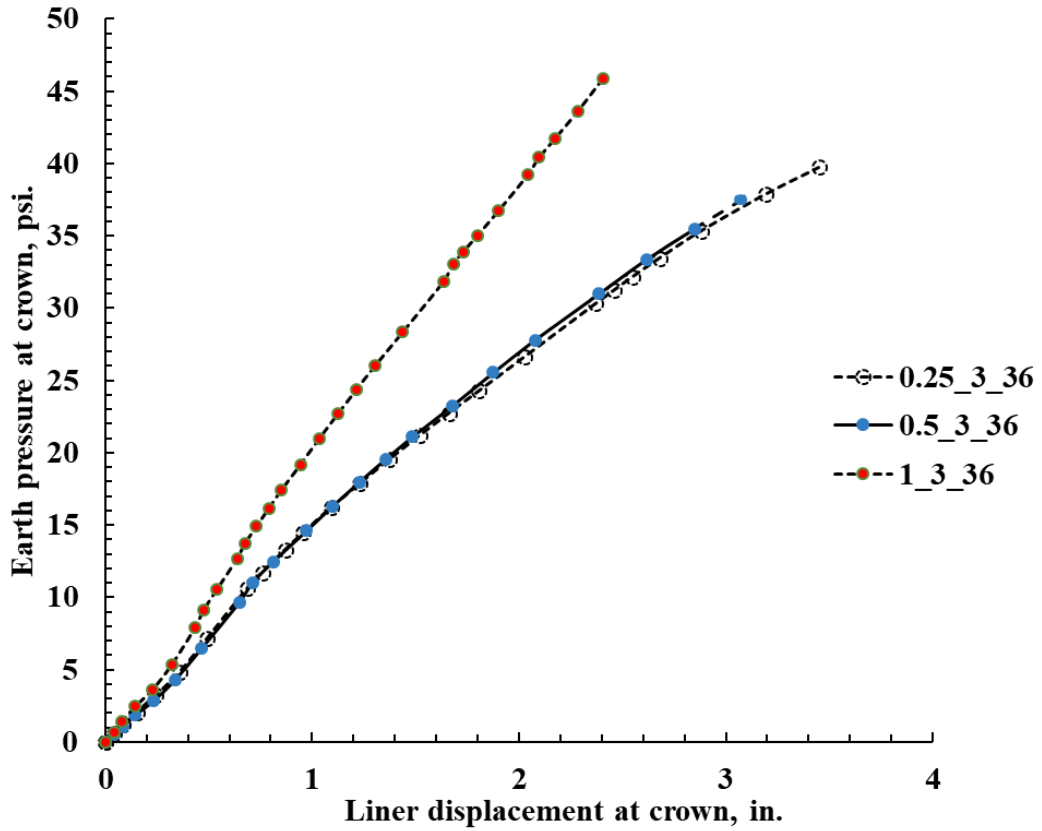


Figure 10E-20. Earth pressure at 4 in. above the crown vs. crown displacement for Invert-cut circular 36 in. CMPs with 3 ft cover and 0.25, 0.5, and 1 in. thick polymeric liner.

Invert-cut Circular 36 in. CMPs with 2 ft cover and 0.25, 0.5, and 1 in. thick polymeric liner

Table 10E-7. Comparison of applied load, displacement, and earth pressure at the first crack point and ultimate load for invert-cut circular 36 in. CMPs with 2 ft cover and 0.25, 0.5, and 1 in. thick polymeric liner.

Liner thickness	1st crack point			Ultimate load		
	Load (kips)	Crown disp. (in.)	Earth pressure (psi)	Load (kips)	Crown disp. (in.)	Earth pressure (psi)
0.25	38.63	1.46	24.82	63.58	5.35	53.53
0.5	39.80	1.36	25.30	67.78	4.90	54.72
1	78.26	2.94	65.30	90.51	3.92	85.41

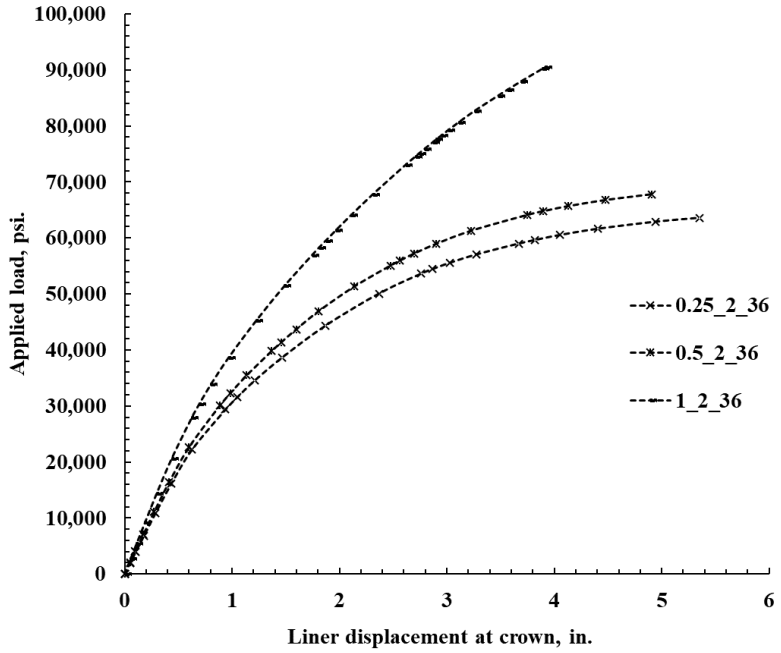


Figure 10E-21. Load displacement plot for invert-cut circular 36 in. CMPs with 2 ft cover and 0.25, 0.5, and 1 in. thick polymeric liner.

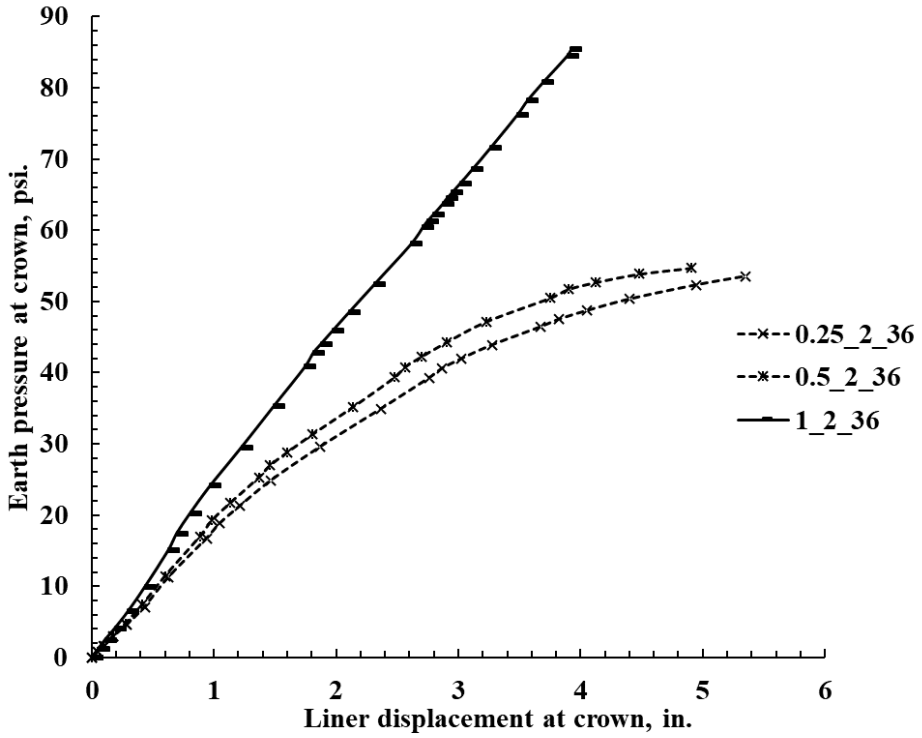


Figure 10E-22 Earth pressure at 4 in. above the crown vs. crown displacement for invert-cut circular 36 in. CMPs with 2 ft cover and 0.25, 0.5, and 1 in. thick polymeric liner.

Invert-cut Circular 36 in. CMPs with 1 ft cover and 0.25, 0.5, and 1 in. thick polymeric liner

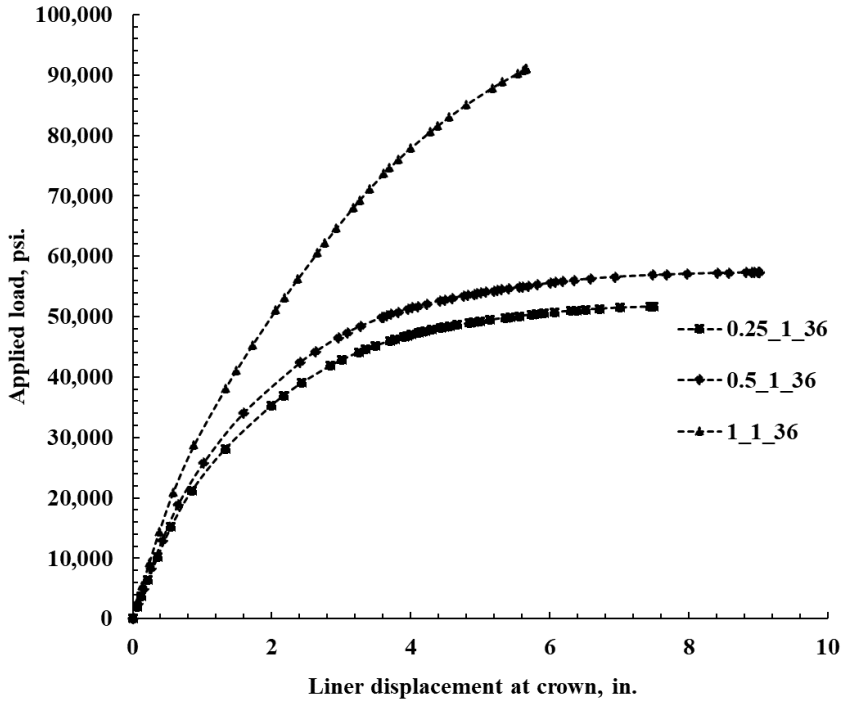


Figure 10E-23. Load displacement plot for invert-cut circular 36 in. CMPs with 1 ft cover and 0.25, 0.5, and 1 in. thick polymeric liner.

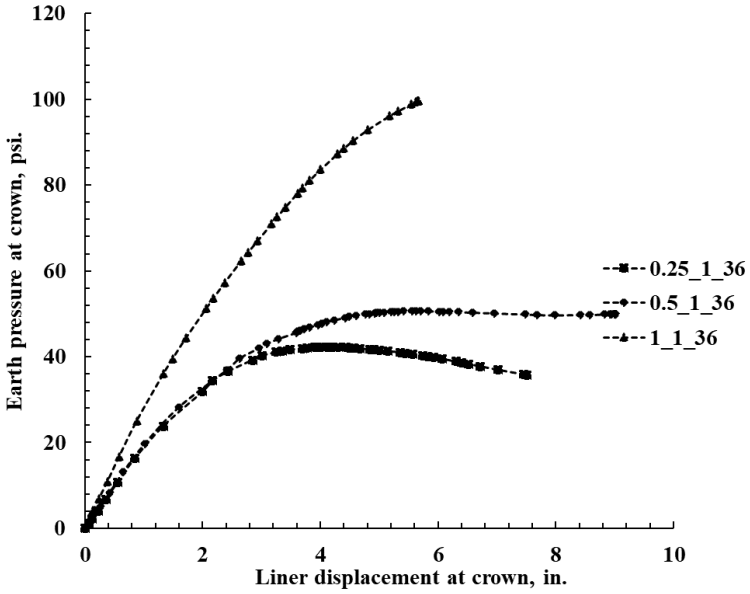


Figure 10E-24. Earth pressure 4 in. above the crown vs. crown displacement for invert-cut circular 36 in. CMPs with 1 ft cover and 0.25, 0.5, and 1 in. thick polymeric liner.

Table 10E-8. Comparison of applied load, displacement, and earth pressure at the first crack and ultimate load for invert-cut circular 36 in. CMPs with 1 ft cover and 0.25, 0.5, and 1 in. thick polymeric liner.

Liner thickness	1st crack point			Ultimate load		
	Load (kips)	Crown disp. (in.)	Earth pressure (psi)	Load (kips)	Crown disp. (in.)	Earth pressure (psi)
0.25	36.87	2.17	34.30	51.63	7.50	42.20
0.5	42.38	2.41	36.95	56.86	7.48	50.58
1	53.15	2.18	53.62	90.77	5.62	99.40

Appendix 10-F: Invert-cut Circular CMPs Repaired with Cementitious Liner

This section presents the FEM study of invert-cut circular CMPs renewed with cementitious liner. The laboratory tests are presented in Chapter 11. The details of the test results are not repeated here. The circular CMPs are modeled the same as shown in the FEM models for invert-cut circular CMPs repaired with polymeric liner. The only change made is the liner material, which was replaced with the cementitious material.

Material Model

The liner properties were initially taken from the lab test performed by the CUIRE laboratory and later optimized to best match the test results. A simple elastic-plastic model was used to model the cementitious liner. In the FE model, the occurrence of a crack in the liner was identified by observing its plastic strain. The appearance of plastic strain is assumed to be a crack in the FE model. The optimized properties of the material are given in Table 10F-.

Table 10F-1. Properties of cementitious liner material used in the FEM models.

Property	Value
Density (lb./in3)	0.00024
Elastic Modulus (psi)	369,000
Poisson's Ratio	0.3
Tensile break strength (psi)	685
Compressive Strength (psi)	8,390

The properties of soil and the CMP are consistent with the one used with the polymeric liner.

Soil and CMP interaction

Soil-pipe interaction is critical to the modeling of buried pipes. ABAQUS allows the user to define different interaction models for the interface between the pipe and soil, such as tie interaction and surface-to-face interaction. In this soil box model, the interaction between the pipe and soil interface was modeled by the surface-to-surface contact model, where the pipe was treated as the master surface, and the soil was treated as the slave surface. Considering the corrugated surface of the CMP, a rough friction coefficient of 0.5 was defined between the CMP and soil, and the contact was defined as a hard contact, i.e., the pipe does not "pierce" the soil but displaces it. This friction coefficient was the optimized value by the calibration of the FE model with the intact CMP test. Tie connection was used to establish the interaction between the cementitious liner and the CMP, which is believed to have a tie bond without relative movements.

Results and discussion

The comparison of the experimental results and the FEM results is discussed in tables and graphs. The comparison shows that the experimental result and the FEM results of the load-displacement agree for the occurrence of the first crack but are not in agreement for the ultimate load conditions. Also, the FEM prediction of cracks on the crown, invert, and shoulder portions of the cementitious liner matched the crack pattern that occurred during the experiment. The FEM results show that the simple elastic-plastic model didn't yield a soil pressure close to the experiment measurement.

1-in. thick liner

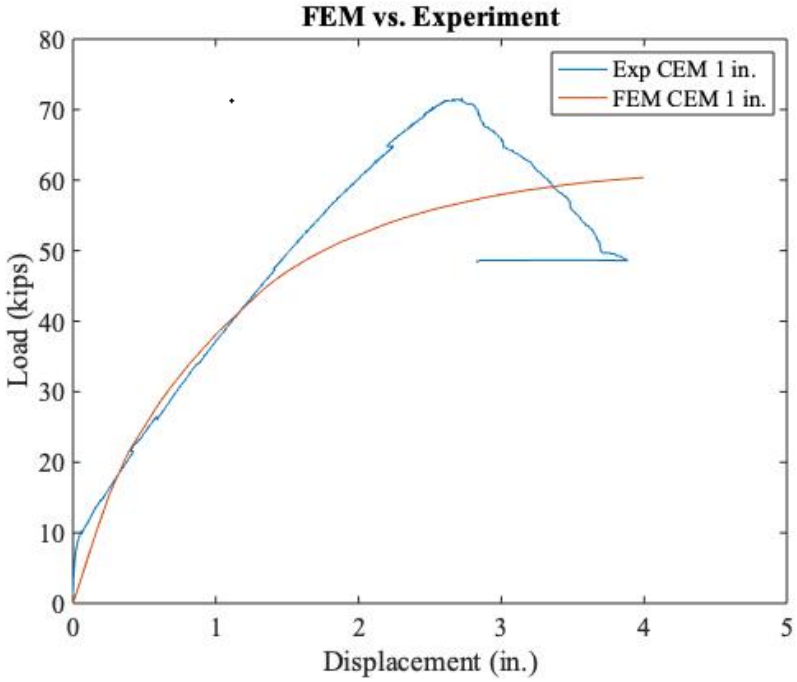


Figure 10F-1. Load displacement plot for 1-in. thick cementitious liner.

Table 10F-2. Comparison of experimental and FEM results for 1-in. thick cementitious liner.

Model	1st crack point			Ultimate load		
	Load (kips)	Crown Disp. (in.)	Earth Pressure (psi)	Load (kips)	Crown Disp. (in.)	Earth Pressure (psi)
FEM	10.25	0.4	18.89	60.38	4.09	60.24
Experimental	10.0	0.2	14	71.76	2.4	100.1

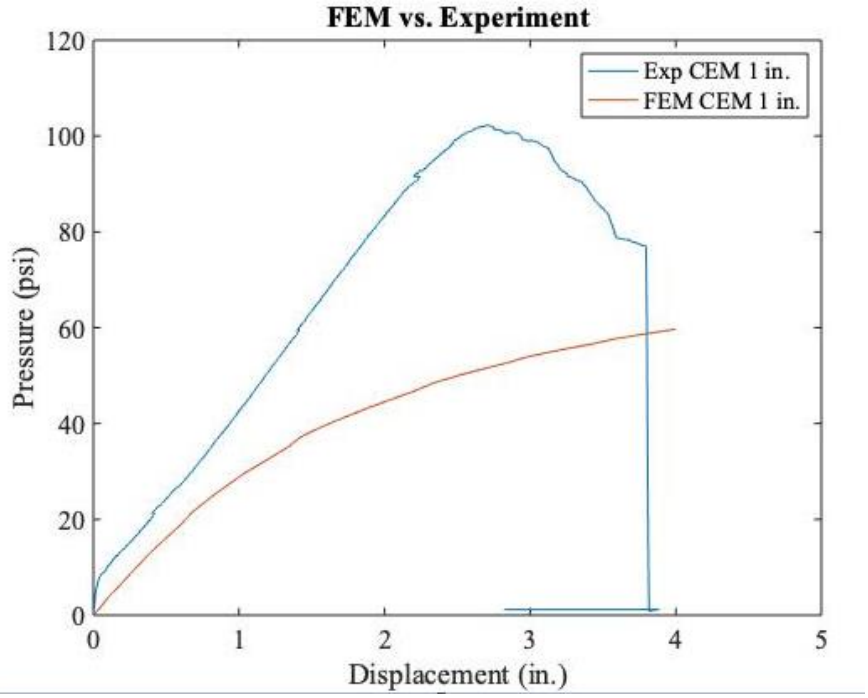
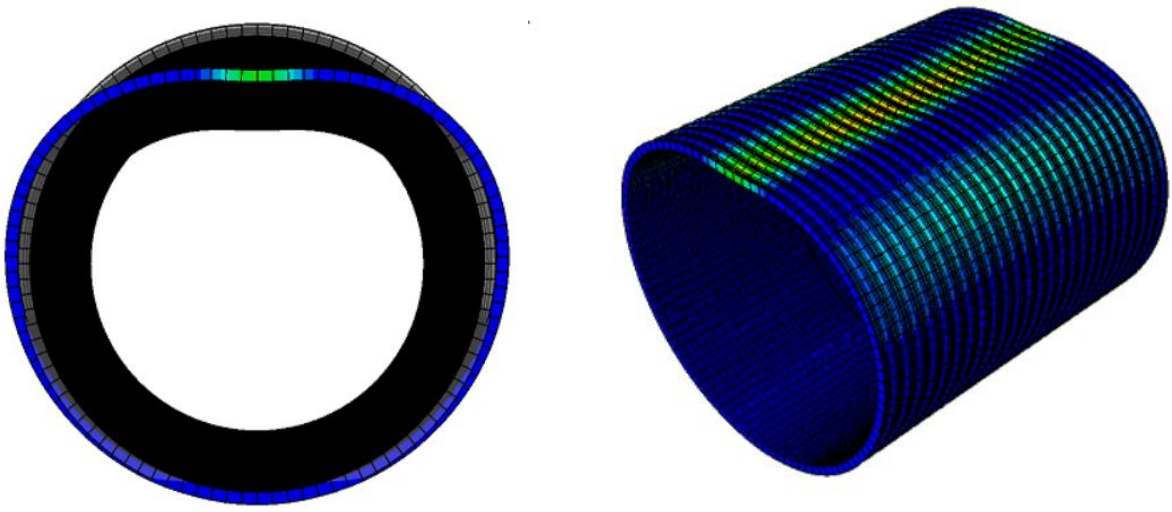


Figure 10F-2. Earth pressure at 4 in. above the crown vs. crown displacement for 1-in. thick cementitious liner.



(a) (b)

Figure 10F-3. (a) Deformation if 1-in. thick cementitious liner under ultimate load and (b) crack location in 1-in. thick cementitious liner.

2-in. thick liner

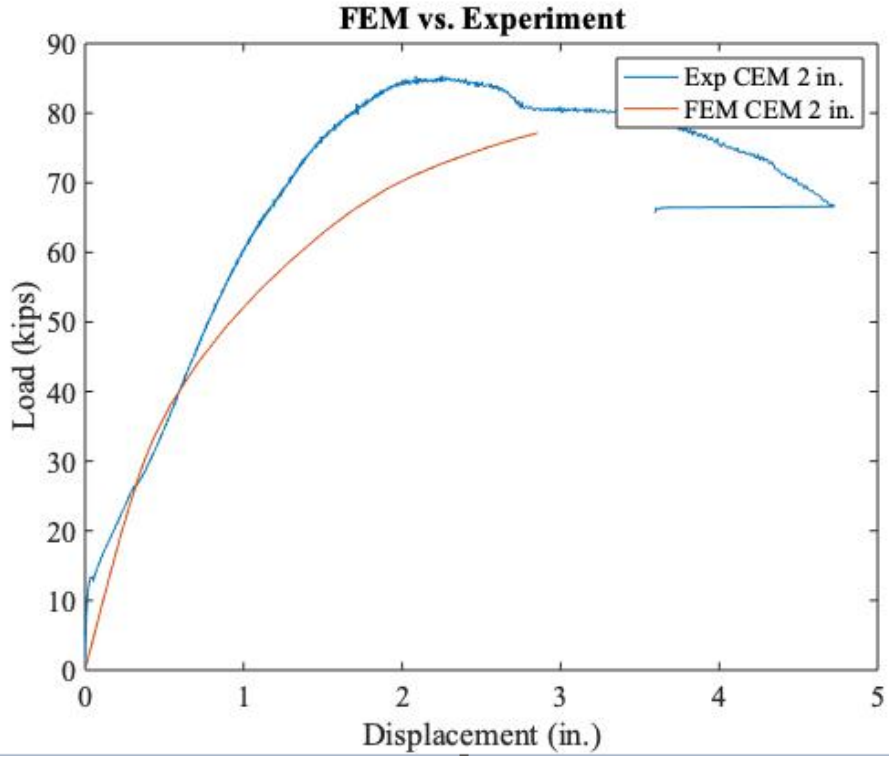


Figure 10F-4. Load displacement plot for 2-in. thick cementitious liner.

Table 10F-3. Comparison of experimental and FEM results for 2 in. thick cementitious liner.

Model	1st crack point			Ultimate load		
	Load (kips)	Crown Disp. (in.)	Earth Pressure (psi)	Load (kips)	Crown Disp. (in.)	Earth Pressure (psi)
FEM	14.14	0.43	24.64	76.5	2.74	79.73
Experimental	14.0	0.2	20.0	85.42	2.2	116.3

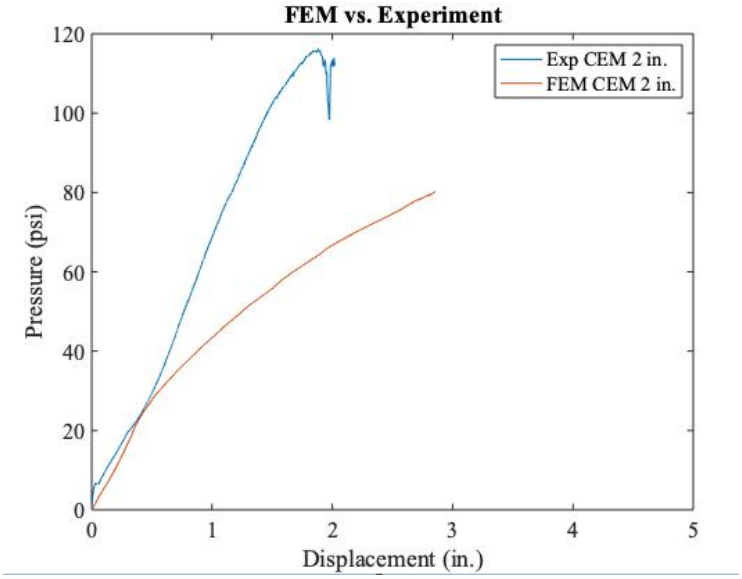
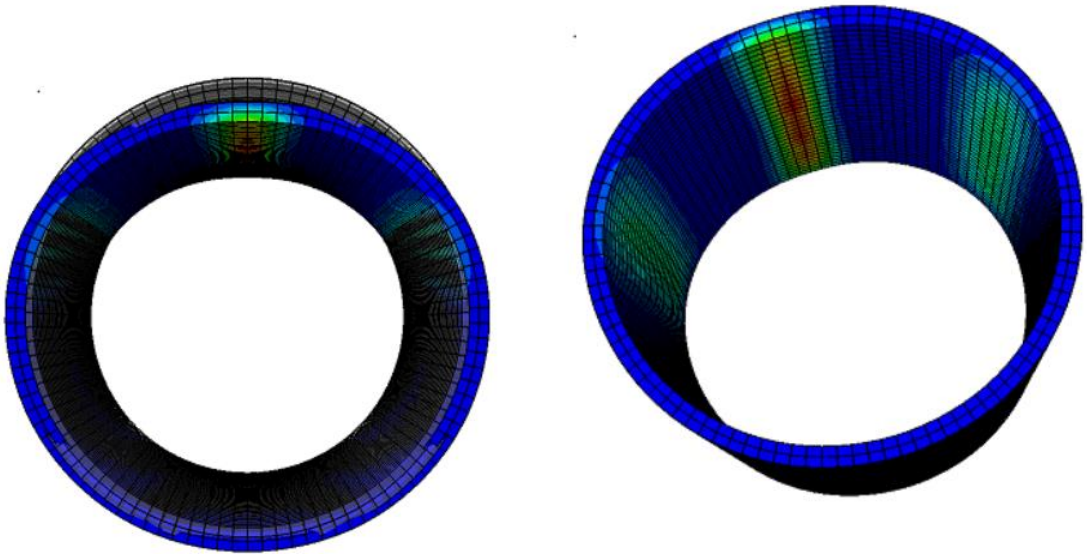


Figure 10F-5. Earth pressure 4 in. above the crown vs. crown displacement for 2-in. thick cementitious liner.



(a) (b)

Figure 10F-6. (a) Deformation of 2 in. thick cementitious liner under ultimate load, and (b) crack location in 2-in. thick cementitious liner.

3-in. thick liner

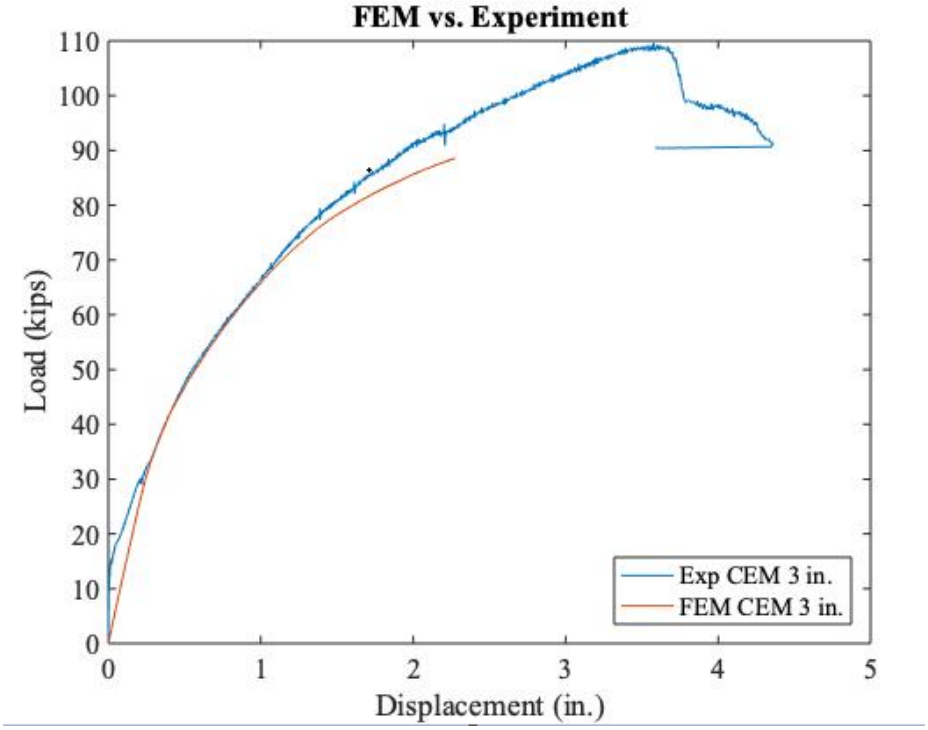


Figure 10F-7. Load displacement plot for 3-in. thick cementitious liner.

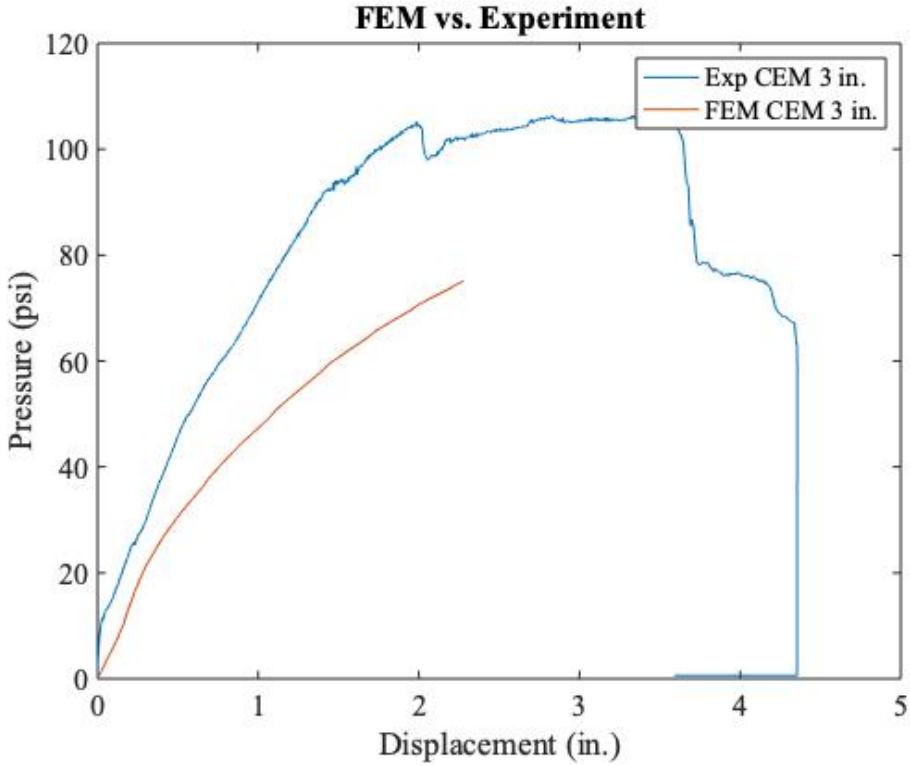
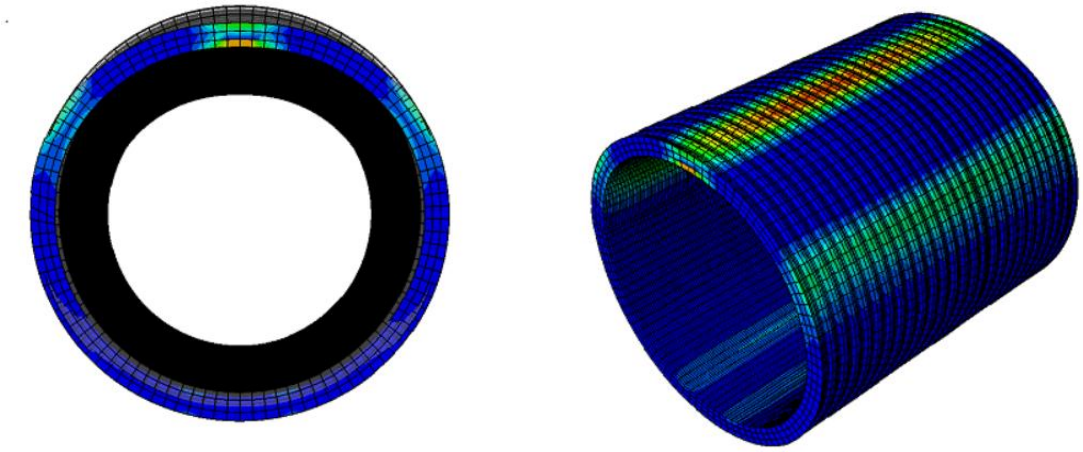


Figure 10F-8. Deformation of 3-in. thick cementitious liner under ultimate load.



(a) (b)

Figure 10F-9. (a) Deformation of 3 in. thick cementitious liner under ultimate load, and (b) crack location in 3 in. thick cementitious liner.

Table 10F-4. Comparison of experimental and FEM results for 3-in. thick cementitious liner.

Model	1st crack point			Ultimate load		
	Load (kips)	Crown Disp. (in.)	Earth Pressure (psi)	Load (kips)	Crown Disp. (in.)	Earth Pressure (psi)
FEM	22.58	0.33	26.78	88.56	2.27	74.4
Experimental	18.71	0.2	22.0	109.7	3.7	106.8

A simple elastic-plastic model was used to model the cementitious liner. This model is limited to the prediction of the ultimate load. The FEM model of the invert-cut CMPs repaired with cementitious liner can generally predict the first crack load reasonably well but under-estimated the ultimate load. It is suspected that the liner thickness may not be as uniform as in the FEM model, which can significantly impact the FEM results. Besides, the material uncertainties of the soil and the cementitious liner can be better accounted for optimizing the FEM results.

Chapter 11

Laboratory Testing

CHAPTER 11 - LABORATORY TESTING

11.1 OVERVIEW

The laboratory testing of this study was designed to include both structural and material evaluations. The Tests were conducted at the Center for Underground Infrastructure Research and Education (CUIRE) laboratory facility located at the University of Texas at Arlington (UTA), as shown in Figure 11-1 and Figure 11-2. The CUIRE soil box is 25 ft long 12 ft wide and 10 ft deep. CUIRE's soil box has access with a truck passing door. The soil box is equipped with a 330-kips MTS actuator installed on a steel reaction frame designed for this type of experimental project.



Figure 11-1. CUIRE laboratory at the University of Texas at Arlington.

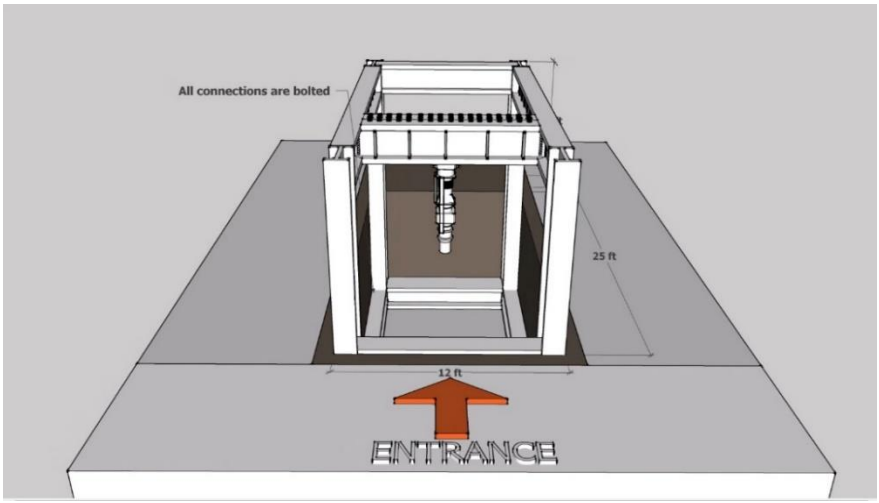


Figure 11-2. Soil box details.

The material testing program included tensile and flexural resistance evaluations of polymer and compressive strength evaluation of cementitious SAPLs. The

experimental structural testing program consisted of five sets of full-scale laboratory tests including (1) control test, (2) circular CMPs renewed with polymeric SAPL, (3) CMP arch pipes renewed with polymeric SAPL, (4) circular CMPs renewed with cementitious SAPL, and (5) CMP arch pipes renewed with cementitious SAPL.

The control test consisted of one intact circular CMP, one invert-cut circular CMP, and one invert cut CMP arch. The circular and CMP arch cementitious SAPL test series consisted of three separate invert-cut CMP samples each, renewed with 1, 2, and 3-in. thick cementitious SAPL. The SAPL liner thickness for the polymeric circular and arch pipe samples were 0.25, 0.5, and 1-in. To acquire the structural capacity of the SAPLs, the invert section of the CMPs were cut and detached after backfilling. Therefore, no ring compression existed in the CMP sample and the load was resisted by the SAPL only (Darabnoush Tehrani 2020, Kohankar Kouchesfehani 2020). Table 11-1. lists the soil box test setups.

Table 11-1. Soil box test setups at CUIRE laboratory at UTA.

Test Name	Test Number	CMP Shape	Invert-cut	Liner type	Liner Thickness (in.)
Control Test	1	Circular	No	N/A	N/A
	2	Arch	Yes	N/A	N/A
	3	Circular	Yes	N/A	N/A
Circular Polymeric	4	Circular	Yes	Polyurethane	0.25
	5	Circular	Yes	Polyurethane	0.5
	6	Circular	Yes	Polyurethane	1
Arch Polymeric	7	Arch	Yes	Polyurethane	0.25
	8	Arch	Yes	Polyurethane	0.5
	9	Arch	Yes	Polyurethane	1
Circular Cementitious	10	Circular	Yes	Geopolymer	1
	11	Circular	Yes	Geopolymer	2
	12	Circular	Yes	Geopolymer	3
Arch Cementitious	13	Arch	Yes	Geopolymer	1
	14	Arch	Yes	Geopolymer	2
	15	Arch	Yes	Geopolymer	3

11.2 EXPERIMENTAL TEST DESIGN AND SETUP PREPARATION

The soil box was designed to minimize the experiments' setup time and for ease of SAPL installation for each set of tests. To achieve this goal, the internal area of the soil box was divided into four sections to place three CMP testing samples longitudinally along each other, as depicted in Figure 11-3. The first section was for access to the soil box and the other three sections were allocated to CMP samples. Each section was separated by a wooden partition wall with a 3 × 3 ft opening. Figure 11-4 illustrates a schematic plan of the partition wooden walls. The opening at the center of each wall was improvised to provide access to the inside of each pipe sample. All the wooden walls and soil box concrete walls were lubricated and covered with polyethylene sheets.

Placement of the CMPs longitudinally in the soil with only one opening raised safety concerns for the research team and SAPL installer crew while inside the pipes. Therefore, a ventilation system was designed to allow air circulation inside the CMPs through a network of PVC pipes and a vacuum pump. Figure 11-5 illustrates the ventilation PVC pipes installed at the south side of the soil box. The vacuum pump was installed at the end of the PVC pipe on the top of the soil box at the time of SAPL installation or instrumentation inside the CMPs.

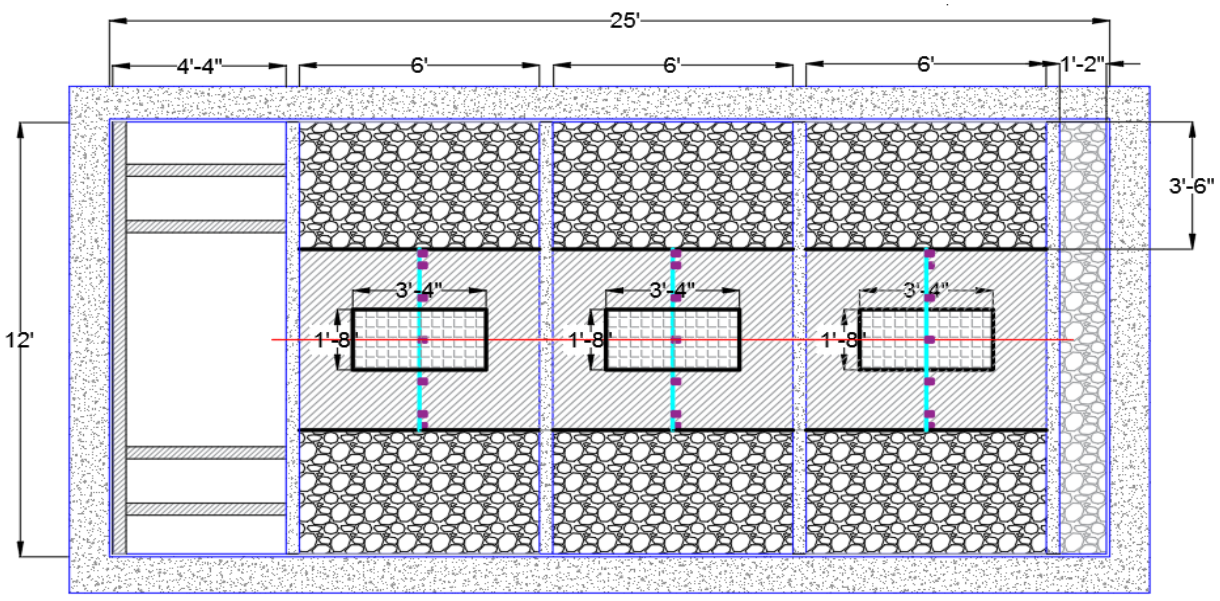


Figure 11-3. Soil box configuration for three CMP samples divided by wooden partition walls.

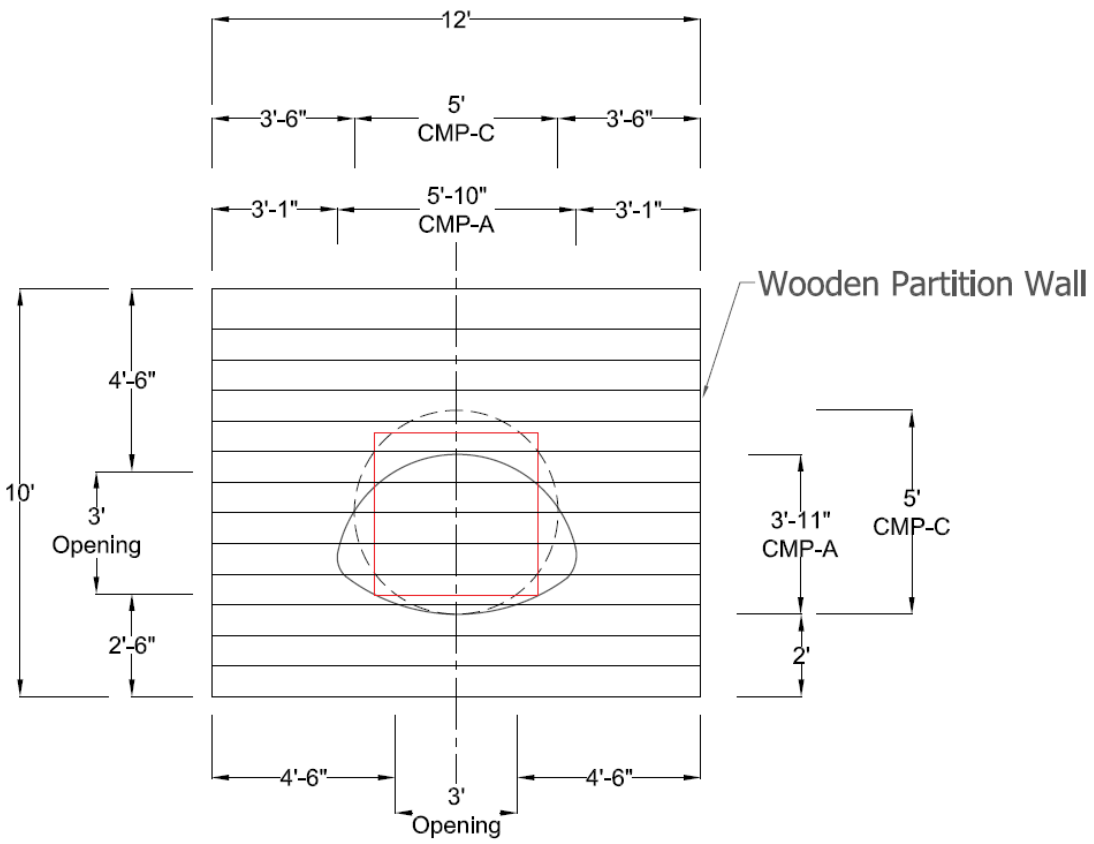


Figure 11-4. Initial schematic design of the wooden partition wall.



Figure 11-5. Soil box ventilation

11.3 BURIAL CONFIGURATION

Burial configuration of culverts depends on the type of the culvert and the project requirements. In general, a burial configuration of a culvert consists of: foundation, bedding, embedment, backfill and cover (Watkins and Anderson 1999, Moser and Folkman 2008, Whidden 2009). A foundation was suggested to be utilized with the highly compacted material, same as trench or embedment for at least 1 ft for small diameter and 2 ft for large diameter pipes (Mai et al. 2018, Syar et al. 2020). Use of this layer was suggested to mitigate the rigid response of the concrete slab on the bottom of soil box.

Two passes of a plate vibratory compactor with 4,496 lb compaction force were carried out at every 8 in. lift to achieve approximately 93% of the maximum standard Proctor dry density (SPDD), as illustrated in Figure 11-6. Since the pipe arch samples had a lower rise than the circular pipes, the foundation of the pipe arch samples was increased until their crown reached the same level of the crown of the circular CMPs. The foundation layer was placed using a 20 in. of well compacted poorly graded sand (SP) for circular CMPs, and 33 in. of SP soil for CMP arch samples.

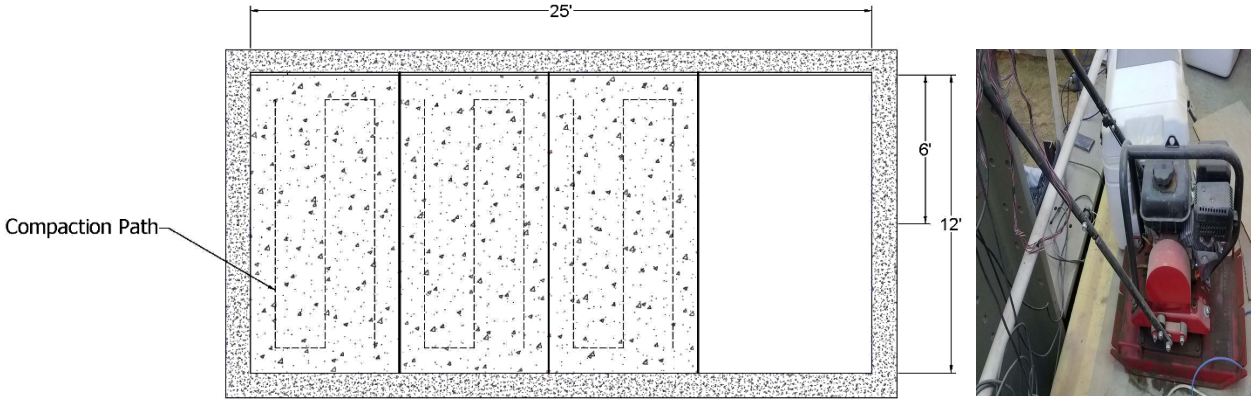
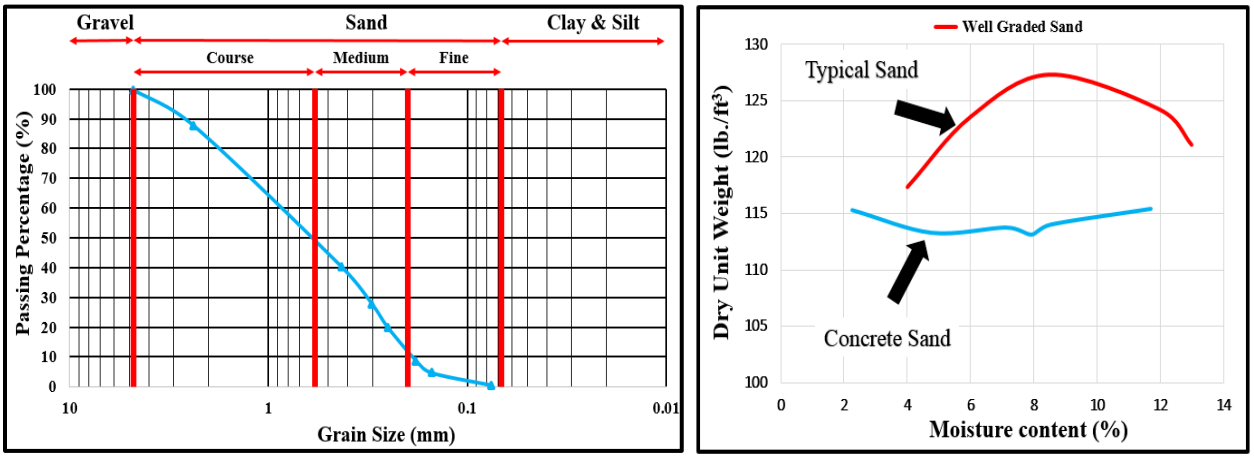


Figure 11-6. Foundation compaction: (a) schematic illustration of soil compaction, (b) soil compaction using a 4,496 lbs vibratory plate compactor.

For the foundation, loose bedding, embedment, and one ft of backfill layers, poorly graded sand (SP), known as concrete sand, were selected according to the unified soil classification system (USCS). Similar sand was used in the same application by other researchers (Mahgoub and El Naggar 2020). A particle size distribution curve was prepared according to the ASTM D6913 through sieve analysis, which is illustrated in Figure 11-7 (a). In addition, standard proctor compaction test was conducted to obtain the SPDD of the soil, illustrated in Figure 11-7 (b). The proctor test showed the maximum unit weight of the SP soil was 115 pcf. Moreover, for this type of soil that has negligible amount of silt and clay, it showed the soil sample's density did not significantly change with the alteration of the moisture content (Berney and Smith

2008). Therefore, during the soil placement in the soil box, no attempt was conducted to control the soil's water content to achieve the maximum SPDD.



(a) (b

Figure 11-7. Embedment soil characteristics: a) soil sieve analysis, and b) standard Proctor test.

Figure 11-8 (a), (b) and (c) illustrate the CMPs burial configuration in the soil box. Once the foundation was placed and compacted, a 4-in. layer of loose soil was placed at each cell. This loose bedding layer would allow the pipe sample to settle properly and to provide even bedding conditions. In addition, this layer represented loosened soil in the field under the pipe sample's invert, because of stream passage in the absence of the invert section (i.e., fully corroded invert). To consider a worst case installation scenario, where the soil is not compacted as expected, the compaction rate of 85% of SPDD was selected for embedment and the one-ft of SP backfill soil layers as specified by AASHTO (2017). In some soil material including the concrete sand, the 85% compaction value can be achieved by only dumping and spreading the soil. In-situ compaction measurement using nuclear density gauge showed the 85% compaction rate of SP soil can be achieved by dumping only. Therefore, no attempt was made to compact the soil embankment. The soil was placed and spread out at 8 in. lifts. The water content and the compaction of the soil was measured at each layer using a nuclear density meter. Since the objective of these tests were to obtain the ultimate load bearing capacity in the field, a one-ft layer of aggregate with a maximum particle size of 1.75 in., known as TxDOT 247 grade 1 type D aggregate, was placed on top of the backfill layer to prevent immature soil failure prior to pipe sample failure. This layer was representative of the base course as a part of culvert's cover in the field (Khatri et al. 2015). Figure 11-11 illustrates nuclear density measurement.

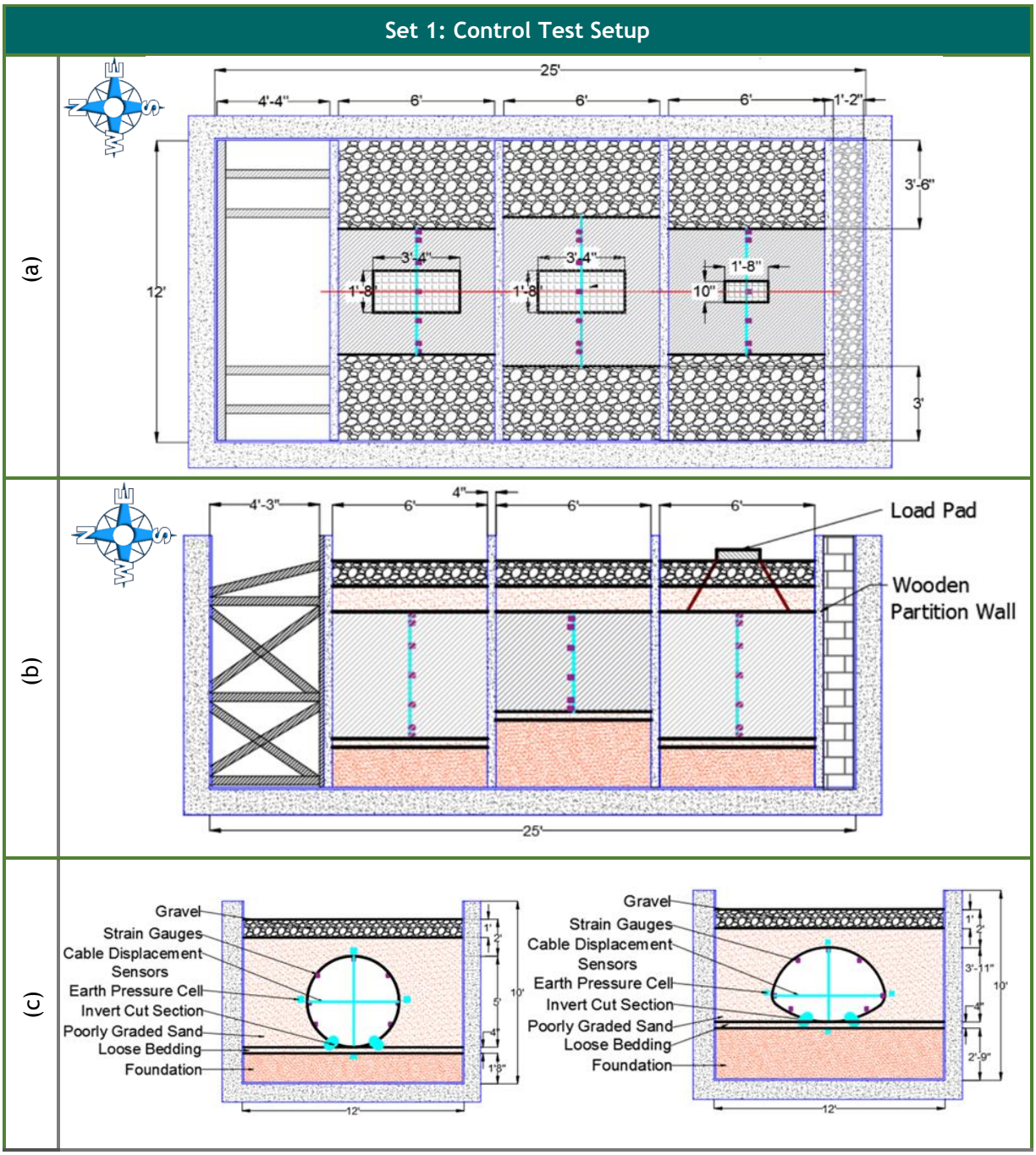


Figure 11-8. The CMPs' burial configuration (control test set): (a) plan view, (b) profile view of the aligned CMPs in the soil box, and(c) cross sectional view of both circular and CMP arch samples.

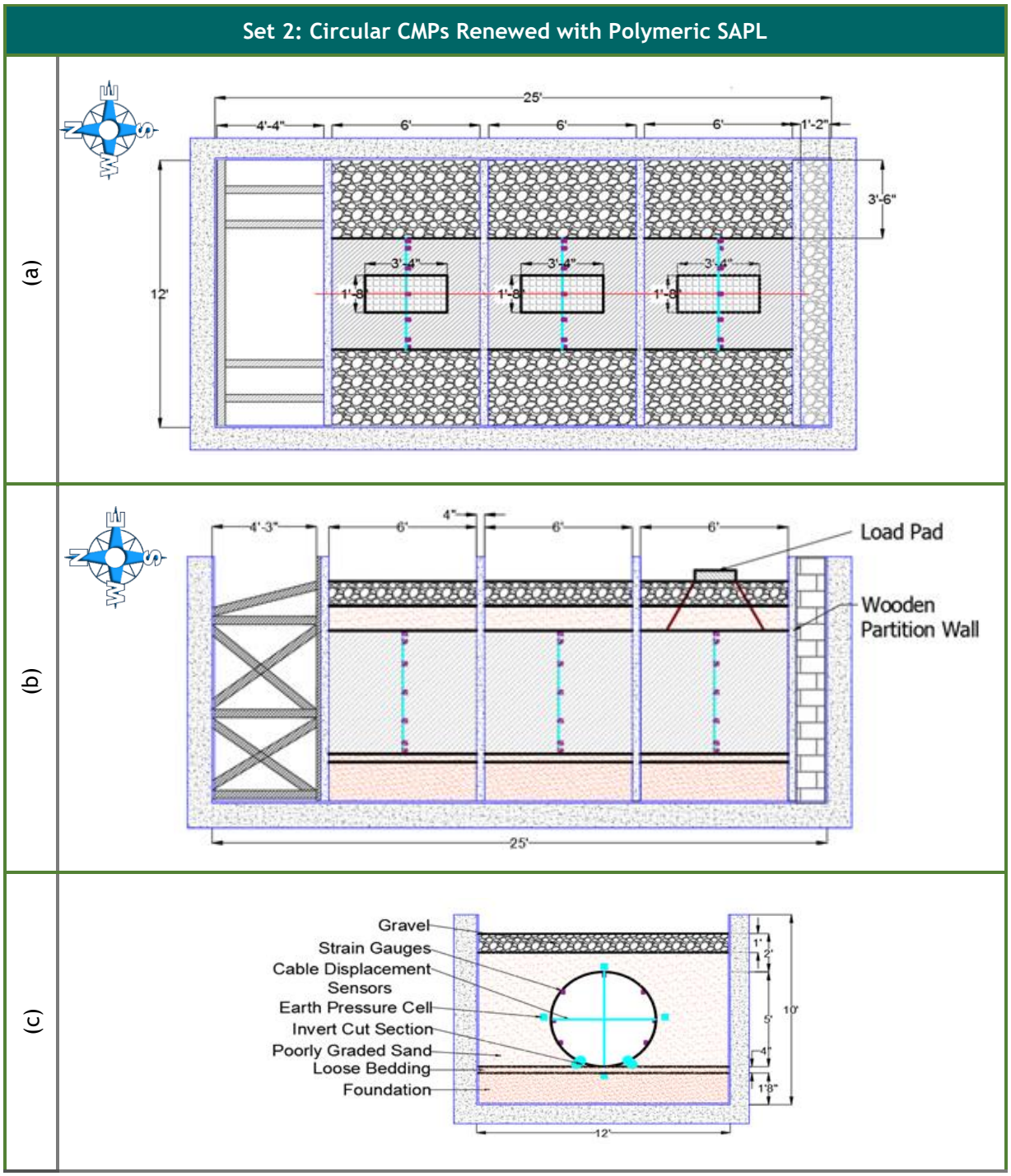


Figure 11-9. The CMPs' burial configuration (SAPL renewed testing): (a) plan view, (b) profile view of the aligned CMPs in the soil-box, and (c) cross sectional view of the circular CMP.

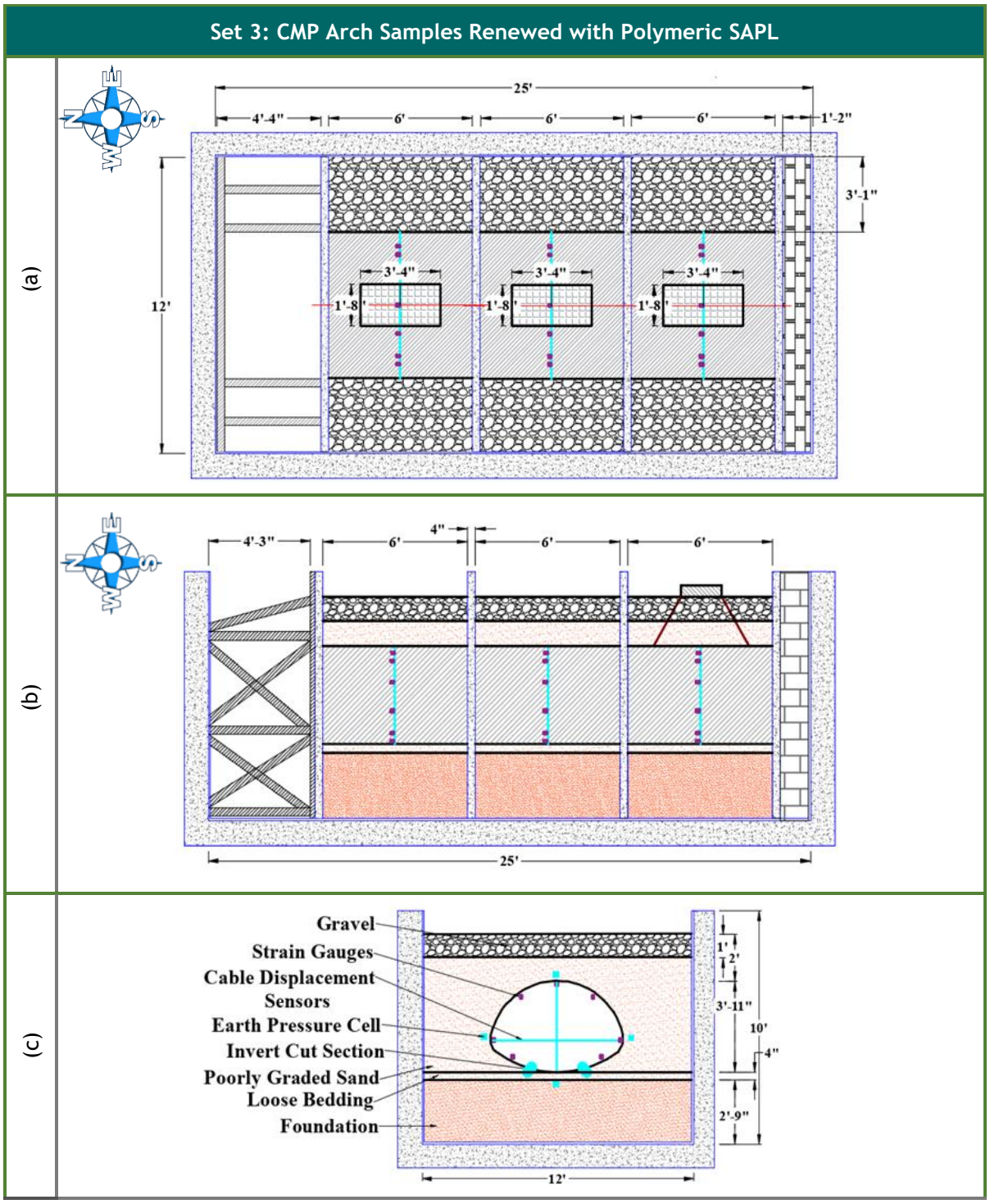


Figure 11-10. The CMP arch samples' burial configuration (SAPL renewed testing): (a) plan view, (b) profile view of the aligned CMP arch samples in the soil-box, and (c) cross sectional view of the CMP arch.



Figure 11-11. Nuclear density measurement.

11.4 COMPACTION METHODOLOGY AND MEASUREMENT

Granular soil is a term used to describe coarse grained soil like sands or gravels which have little to no clay content. These kinds of soils have no cohesive strength though, presence of some moisture may sometimes show apparent cohesion. Hence, when dry, these soils do not stick together but crumble to separate particles. Granular soils were observed to achieve maximum dry density in either oven dried or nearly saturated conditions (Drnevich, Evans, & Prochaska, July 2007). Figure 11-12 shows the typical compaction curve for granular soils.

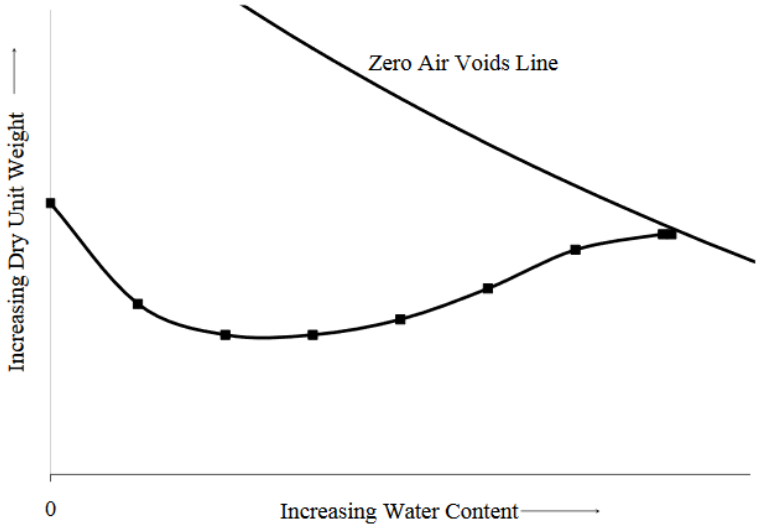


Figure 11-12. Compaction Curve for a Granular Soil (Drnevich, Evans, & Prochaska, July 2007).

11.4.1 Laboratory Compaction of Granular Soils

One of the most common methods for determining the maximum dry density of soil in laboratory is through Standard Proctor Compaction Test, the procedure for which is standardized by ASTM in the standard ASTM D698. Modified Proctor Compaction Test is the other testing approach, which uses higher energy to achieve the compaction of soil. The procedure for this test is standardized in ASTM D1557. However, since the granular soils like clean gravel and sand (i.e., without appreciable amount of fines) are free-draining in nature, the maximum unit weight achieved through these methods may not be well defined and can also be less than that obtained using Vibratory Table Compaction, the procedure for which are standardized in ASTM D4253.

For the purpose of this research project, since the soil used as backfill material was granular (sand, gravel, or mixture of both), Vibratory Table Compaction was the best way to determine the maximum unit weight of soil.

11.4.2 Field Compaction of Granular Soils

Granular soils do not possess cohesive behavior and hence, moving them requires shaking/vibration. Vibration compaction is the optimum way to perform field compaction. Additionally, considering the limited available space in the soil box, use of a vibratory plate compactor could be the most suitable method to perform compaction of soil in during soil box test (for those layers that needed compaction).

11.4.3 Soil-box Compaction

For compaction of the backfill soil in the soil box, two compaction methods of vibratory compaction and air pluviation were initially discussed at the internal meetings. Based on the available lab supplies in the CUIRE, it was more feasible to compact the soil using the vibratory plate method. During vibration compaction, the granular soils rearrange its position to achieve the desired compaction.

11.4.4 Measurement of Field Compaction

There are various methods that can be used to measure field compaction of soil. ASTM D2167 details measurement of field compaction using rubber balloon method. ASTM D1556 details measurements of field compaction using sand cone method. However, since the soil in the CUIRE soil box was cohesionless, the possibility of the test hole wall collapse made these methods unreliable. Therefore, the alternative methods that could be used to measure the field density of backfill in the soil box were through the use of a Nuclear Density Gauge (ASTM D6938) or Time Domain Reflectometry (TDR) as detail in ASTM D6780.

11.4.5 Nuclear Density Gauge

Nuclear Density Gauge (Figure 11-13) is a non-destructive method to measure the in-situ density and moisture content of soil at shallow depths. It consists of a radioactive isotope (usually 137 Cesium) that emits a cloud of particles and a sensor that counts the particles that are either reflected by the test material or pass through it. Depending on the mode of use, the gauge can be both invasive (direct transmission mode) and non-invasive (back scatter mode). For direct transmission, a small hole needs to be made in the test surface, either through drilling or in our case, by pushing a rod/needle into the soil. However, this presents the possibility of loose materials falling into the hole, which can significantly affect the accuracy of the readings. Hence, backscatter mode might be more suitable as it is non-invasive. It is also necessary to take the Standard Count of the gauge before each day's test to ensure the gauge's accuracy.

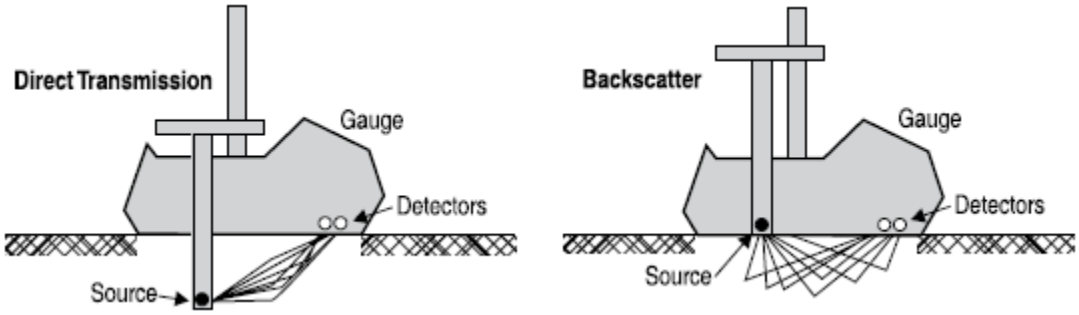


Figure 11-13. Modes of operation of nuclear density gauge (MULTIQUIP, 2018).

The disadvantage of using a nuclear density gauge for cohesionless soil is that it requires a control strip of the same fill material to be made as a reference to correct measurements obtained from the gauge (Howard, 2011). This requirement further complicates the testing procedure and increases the time required for each test. The licensing requirements that must be fulfilled to use a nuclear density gauge can also be an additional inconvenience to the method.

11.4.6 Time Domain Reflectometry (TDR)

Time Domain Reflectometry (TDR) is a measurement technique that measures electric properties like dielectric constant and electrical conductivity, both of which are strong functions of soil water content (Lin, Lin, & Drnevich, 2012).

Before the TDR setup can be used, it must be calibrated for field conditions. The calibration of a TDR setup is done by compacting soil at different moisture content into a mold and then taking the TDR measurements to get the dielectric constant and electrical conductivity at that condition. Density and moisture content measurement for the soil can then be calibrated by taking different dielectric constant and electrical conductivity measurements (Figure 11-14).

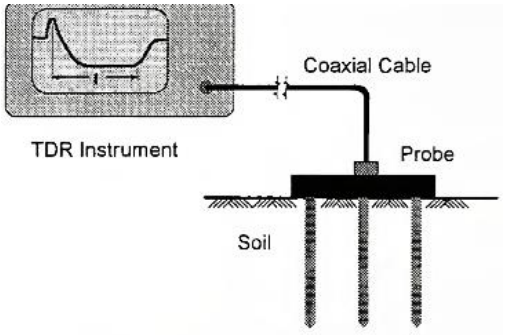


Figure 11-14. Measurement of soil moisture content using TDR method (Siddiqui & Drnevich, 1995).

There are two procedures that can be followed to obtain the in-situ water content and density of soil using TDR: Indirect approach and Direct approach (ASTM D6780). The summary of steps for indirect measurement of moisture content and density using TDR are:

- The in-situ dielectric constant of the soil is obtained using TDR.
- The soil at the measurement location is then excavated and compacted in a mold and its wet density is determined.
- Dielectric constant of the soil in the mold is measured using TDR and the water content of the soil in the mold is determined by using a correlation between dielectric constant, moisture content and soil density.
- The moisture content of in-situ soil is assumed the same as the soil in mold and the is-situ density is determined from the density of soil in the mold and the dielectric constants measure in the mold and in-situ.

The summary of steps for direct measurement of moisture content and density using TDR are:

- The apparent dielectric constant of soil in-situ, first voltage drop, and long-term voltage are determined.
- The water content and density of soil in-situ are then determined from the measured apparent dielectric constant of soil in-situ, first voltage drop and long-term voltage and five soil and in-situ pore fluid dependent constants which are determined in the laboratory.

Table 11-2. presents the summary of testing options under consideration.

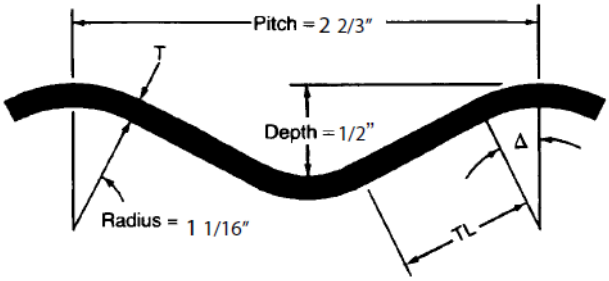
Table 11-2. Summary of materials and test options for the soil used in soil box test.

Soil Type	Compaction Method	Compaction Measurement Method	Advantages	Limitations
Poorly graded gravel (GP)	Vibratory Compaction	Nuclear Density Gauge Time Domain Reflectometry (TDR)	Higher unit weight. Significant compaction can be achieved just by dumping.	Measuring in-situ density can be problematic due to large particle size and presence of large voids.
Poorly graded sand (SP)	Vibratory Compaction	Nuclear Density Gauge Time Domain Reflectometry (TDR)	Fine grained as compared to GP and is easier to compact.	Low unit weight as compared to GP.
Mixture (GP-SP)	Vibratory Compaction	Nuclear Density Gauge Time Domain Reflectometry (TDR)	Can be compacted to a higher degree than both GP or SP.	Uniform proportion of GP/SP throughout the backfill maybe hard to achieve.

11.5 PIPE SAMPLES

A total of 15 annular corrugated metal pipe (CMP) samples were used in this research including five circular and four CMP arch samples. The circular CMP samples had an internal diameter of 60 in., and the CMP arch samples had a span of 71 in. and a rise of 47 in. (119.3 cm). All CMP samples were 6-ft long with a corrugation pitch length of 2×⅔ in. and gauge 12 thickness, fabricated from bent hot-dip galvanized steel sheets along their edges fastened by rivets. The geometric details of the CMP profile are provided in Table 11-3. . The CMP samples' steel were in compliance with the ASTM A796 (Contech 2019), with a minimum yield strength (f_y) of 33 ksi, a minimum tensile strength (f_u) of 45 ksi, and a Young's modulus of 29,000 ksi. The yield strain of 1,138 με was calculated using the elastic stress-strain relationship.

Table 11-3. CMP samples' geometric details (NCSPA 2008).



Thickness	Uncoated Thickness	Area of Section (A)	Tangent Length (TL)	Tangent Angle (Δ)	Moment of Inertia (I)	Section Modulus (S)	Radius of Gyration (r)
(in.)	(in.)	($in.^2$/ft)	(in.)	(Degree)	($in.^4$/in.)	($in.^3$/ft)	(in.)
0.109	0.1046	1.356	0.740	27.11	0.0034	0.1360	0.1741

For a culvert in field condition, the invert deterioration is a slow process and occurs over several years. As a result of this long corrosion process, the soil pipe system is stabilized and does not induce significant culvert geometry change. To simulate a culvert with entirely deteriorated invert section condition, an 18-in. wide strip of invert section of CMP samples were entirely cut out. This value was calculated based on observations that usually one-third of wetted perimeter CMPs are more vulnerable to severe corrosion (Masada 2017). Furthermore, this value was in conformity with the middle bedding section as specified in AASHTO (2017). In order to maintain the original geometry of CMPs during the installation and burial phases, the invert-cut section was left bolted to the CMPs' main body using angle sections and wood spacers. This detachable mechanism made the invert section's removal possible after burial of the CMP samples. The detachable invert section was specifically designed to withstand handling and installation forces as specified in the ASTM A796. Once the CMPs were installed and embedded, the invert sections were disassembled. Details of the detachable invert-cut section for the control tests and SAPL renewed samples were different. Figure 11-15 illustrates CMP samples prepared for this research.


Figure 11-15. Intact and invert-cut CMP samples.

For the control tests, the invert section of the pipe was cut entirely and bolted to the main body of the pipe, as shown in Figure 11-16 . However, detachment of the invert section raised the concern of pipe movement and deformation due to the applied dead load (i.e., weight of the soil). For a bare CMP sample without liner, this was not a significant issue, as it was part of the pipe behavior. However, for a renewed CMP sample, this pipe movement could result in different pipe diameters at the time of SAPL installation, which could jeopardize the repeatability of the tests. Therefore, to have the same CMPs geometry for all SAPL renewed CMP samples, two narrow strips with 3 in. width at both ends of the invert-cut section were kept bolted to hold the CMPs' geometry. Once the SAPL was installed and cured, the 3 in. end-strips were removed to eliminate ring stiffness of the host pipe (i.e., CMP) and maximize the applied force on the liner for investigation of whether the SAPL was fully structural or not. Figure 11-17 shows a plan view of the detachable invert section for SAPL renewed CMP samples, where at the stage (1) the invert was bolted to the CMP's body during backfilling. Once the backfilling task was completed and the soil-pipe system was stabilized, in the stage (2) the middle detachable invert section was removed. In the stage (3) the cementitious SAPL was installed inside the CMP and in the stage (4) after full curing of the SAPLs, the remaining invert section was unbolted to eliminate the ring stiffness of the host pipe (i.e., fully invert deteriorated pipe condition).

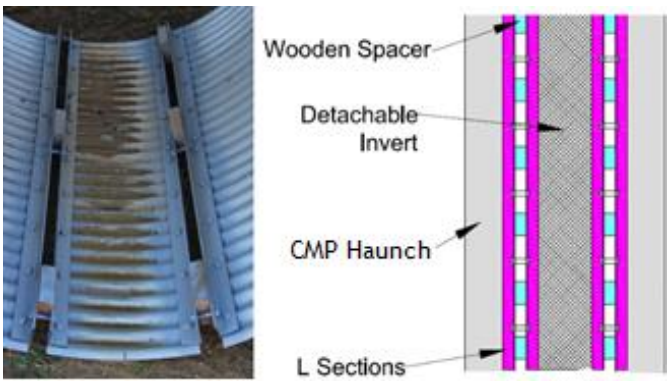


Figure 11-16. Detachable invert section for control test.

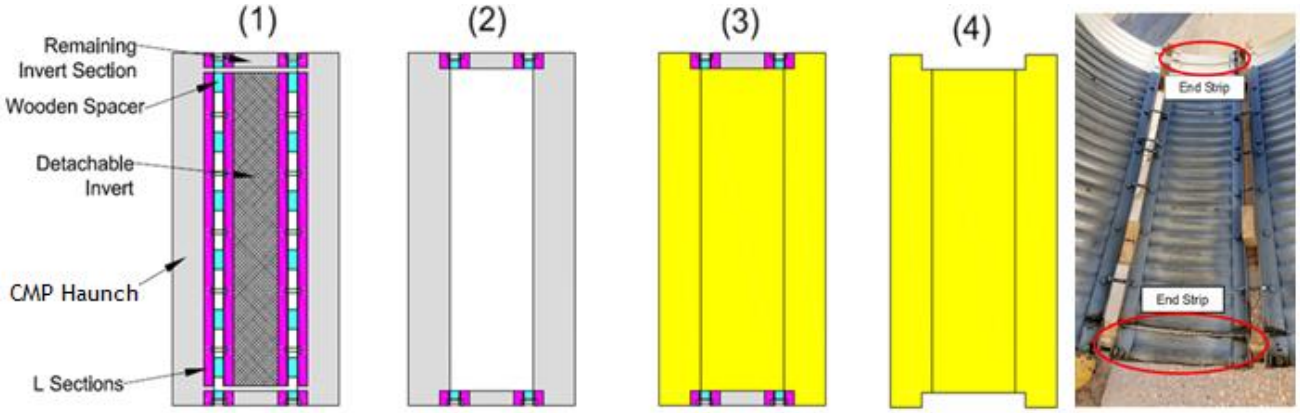


Figure 11-17. Detachable invert mechanism (in four stages) for SAPL renewed CMP samples before and during the SAPL installation.

11.6 PIPE INSTALLATION AND EMBEDMENT

The CMP samples were placed at the center of each cell in the soil box. Prior to the CMPs installation, the 4-in. loos bedding soil was perfectly leveled in every direction to provide even and uniform substratum. Once the CMPs were positioned in their location, the gaps between each pipe sample and partition walls were covered with a flexible thin plywood and Styrofoam rolls to prevent soil ingress inside the CMPs. The plywood and the Styrofoam were wrapped around the CMPs and were attached to the pipe using duct tape. The bedding leveling, pipe positioning and gap sealing are illustrated in Figure 11-18.

After the CMPs placement, positioning, and gap sealing inside the cells, the haunch area was filled with the SP soil to prevent pipe rolling during instrumentation and backfilling process. Attempts were made to fill the annular gap at the haunch area, using shovel and light hand compaction. Once the CMPs were stable in the location, the outside surface of CMPs were instrumented with strain gauges. The strain gauges' wires were clustered and attached to the valley of the pipes' corrugation and protected with both aluminum and duct tapes. To pass the wires through the soil a small duct was used to eliminate friction between wires and the soil.

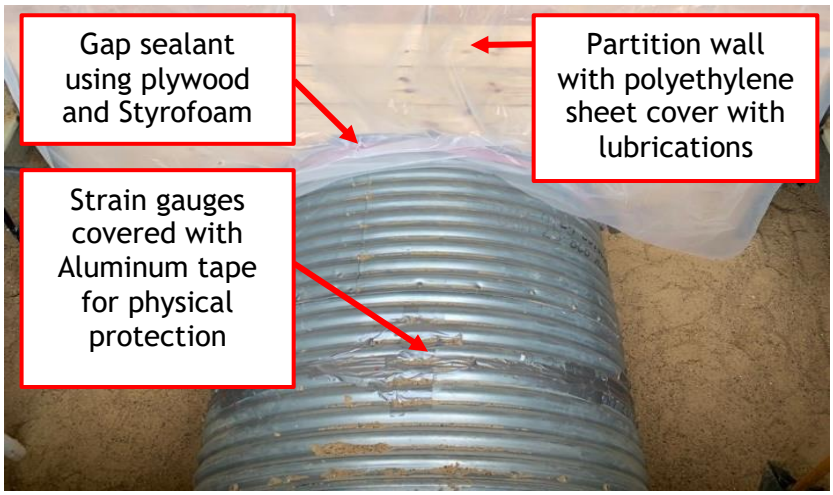


Figure 11-18. Pipe installation and preparation before backfilling.

11.7 LOAD PADS

According to the AASHTO LRFD bridge design specifications, the vehicle load on top of the culvert cover will be transferred as a uniform stress over a rectangular area equal to the contact area of the wheels. In this research project two different load pads were used: (1) a load pad size of 10 × 20 in. according to the AASHTO H-20 standard truck tire contact area, and (2) a 20 × 40 in. pad size. The 10 × 20 in. load pad was only used for bare intact (i.e., unlined and without invert cut) circular CMP and rest of the pipe samples were tested using the 20 × 40 in. pad size (Figure 11-19). The reason of using different load pad sizes was to prevent premature soil failure prior to the pipe failure. In the case of the intact CMP, soil received higher level of supports from the pipe and showed higher carrying capacity before failure. However, in the case of the invert-cut CMP samples that the pipes were severely damaged and larger deflection was expected, a larger pad was used to distribute the stress at the area of load pad-soil connection. It was to assure the testing pipes will fail sooner than the soil cover on top of the pipe. The load pads were designed and fabricated from a rigid A36 steel plates.



Figure 11-19. Steel load pads.

11.7.1 Testing Operation and Load Rate

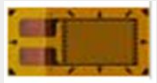
A continued static load was applied on the soil surface on top of the pipe using an MTS 330-kip hydraulic actuator attached to a reaction frame located at the CUIRE Laboratory at the University of Texas at Arlington. The static loading regime was chosen in these sets of tests since it has higher impact on the pipe sample deformation (Yeau et al. 2009). The load was applied through the rigid load pad, through a displacement-control procedure. The displacement-control method was chosen due to its advantage for obtaining the post-peak softening behavior of the specimens and it was applied by controlling the movement rate of the actuator's stroke at a certain defined rate. Choosing an appropriate load rate and loading method for these tests was one of the main challenges since in the similar studies they are not reported.

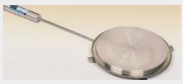
A value of 0.03 in./min was selected to be continuously applied to reach the failure and post failure of the soil-culvert system according to an study by Darabnoush Tehrani (2020). In comparison, to prevent soil lagged deformation and settlement, Masada (Masada 2017) and Regier et al. (Regier et al. 2016) applied an incremental manner. However, the chosen poorly graded sand (SP) in this research had no silt and clay, which made it insensitive to time dependent deformations. Moreover, the loading speed was slow enough to compensate the lagged settlement effect. Therefore, continuous loading was selected for this study. Prior to applying the load, actuators swivels were locked at top and bottom to prevent any possible rotation due to possible uneven deformation soil-pipe structure under the load pad.

11.8 INSTRUMENTATION

The CMP samples were instrumented with uniaxial strain gauges, linear variable differential transformers (LVDTs), cable displacement sensors (CDSs), earth pressure cells, digital image correlation (DIC) targets, and digital cameras. All the sensors used in this study were calibrated and certified by their own manufacturers. The instrumentations used in soil box testing is listed in Table 11-4.

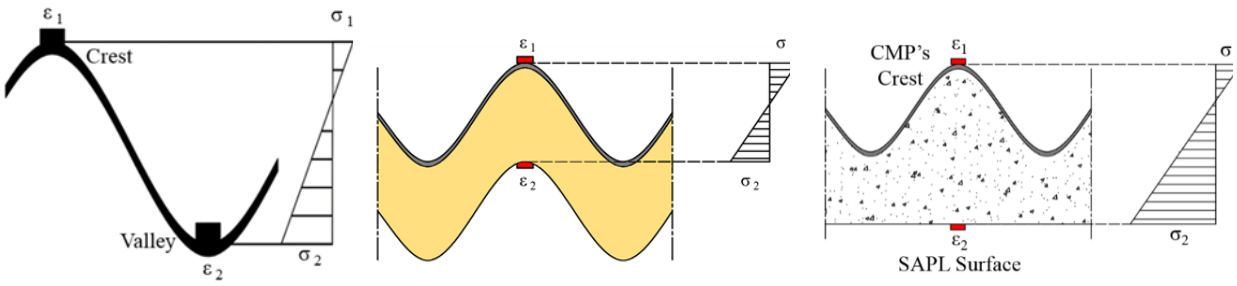
Table 11-4. Instrumentation used in the soil box testing.

Instrumentation		Number		Location
	Uniaxial Stain Gauges (Micro Measurement C2A-06-250LW-120)	Control Test	16	Circumferentially at 45° intervals at the middle section of the pipe in two layers
		SAPL Renewed	16	Circumferentially at 45° intervals at the middle section of the pipe 8 Outer Surface of CMP 8 Inner Surface of the SAPL

Instrumentation		Number	Location
	Cable Displacement Sensors (CDSs) (Micro-Epsilon WPS-500-MK30-P10)	2	Attached on the inside surface of each CMP at the middle section
	Linear Variable Differential Transformers (LVDTs) (Omega LD650)	3	All three (crown, shoulder, springline) were installed on a wooden frame, cantilevered to the middle section of each CMP
	Earth pressure cells (Geokon 4800 series)	4	Around each CMP on top, bottom, and springline within a 4 in. (10.16 cm) distance away from its outer surface
Digital image correlation (DIC) targets		40-50	Circumferentially in the middle section of each CMP
	Digital cameras (DSLR Canon Rebel T5i)	3	One at the entrance of each pipe, showing whole view of the CMP. Two were installed on a wooden frame, cantilevered to the middle section of each CMP, targeting the crown and springline

11.8.1 Strain Gauges

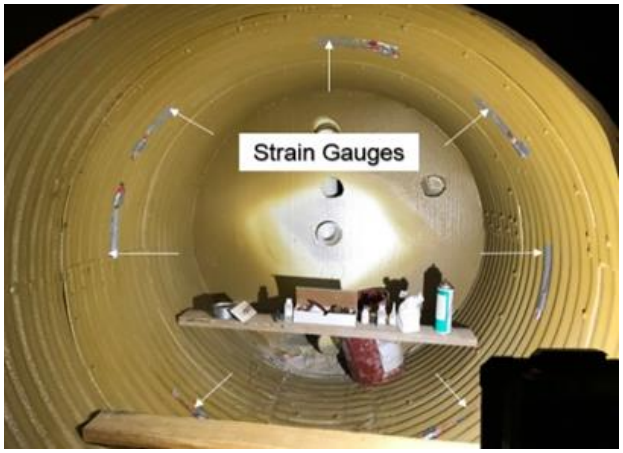
For the first set of testing (control test of bare CMPs), after placing the CMPs on the bedding layer and before backfilling, the pipe samples from both inside and outside surfaces were instrumented with a total of sixteen uniaxial strain gauges (Micro Measurement C2A-06-250LW-120). The strain gauges were installed circumferentially at 45° intervals at the middle section of the CMP sample in two layers of the valley and the crest, as illustrated in Figure 11-20 (a). For the SAPL renewed CMP samples, 8 strain gauges were installed on the outer surface of the CMP and 8 strain gauges on the inner surface of the SAPL, as illustrated in Figure 11-20 (b). After attaching the strain gauges to the samples, the Micro Measurement air drying M-Coat D was applied to protect gauges from moisture and electrical leakage. Two layers of physical protection were provided by attaching M-Coat FA Aluminum foil tape and M-Coat FN Neoprene rubber sheets to protect gauges from abrasive soil particle movement, as illustrated in Figure 11-20 (c) and (d). The strain gauges were connected to a data acquisition system that digitalized the transmitted analog signals, as illustrated in Figure 11-20 (e) and Figure 11-21.



(a) (b) (c)



(d)



(e)

Figure 11-20. Strain gauges configuration and details: (a) schematic profile view at the crown of the bare circular CMP, (b) schematic profile view at the crown of Polymeric SAPL renewed circular CMP, schematic profile view of the cementitious SAPL renewed pipe samples (d) physical protection of outer surface strain gauges, and (r) installed strain gauges on the inner surface of the SAPL renewed circular CMP.



Figure 11-21. Strain gauges connected to a data acquisition system (DAQ).

11.8.2 Earth Pressure Cells

To monitor the applied pressure at different layers of soil, four Geokon 4800 series earth pressure cells, as illustrated in Figure 11-22 (a) were embedded around each CMP at 4 locations; top, bottom, and springlines, as shown in Figure 11-22 (b). The earth pressure cells were located within a 4 in. from the outer surface of the CMP, as illustrated in Figure 11-22 (b). The earth pressure cells were connected through wires to a Geokon data acquisition system (DAQ), as illustrated in Figure 11-22 (c). DAQ digitalized the transmitted analog signals from the earth pressure cells during the tests (GEOKON 2019).



(a) (b) (c)

Figure 11-22. Earth pressure cell. (a) Geokon 4800 series, (b) 4 in. distance from the CMP at the springline, and (c) connection to a data acquisition system (DAQ).

11.8.3 LVDT and CDS

Cable displacement sensors (CDS) and linear variable differential transformers (LVDT) were utilized to measure the CMP sample deflection in the laboratory condition experimental soil box testing (Darabnoush Tehrani 2016). Two Micro-Epsilon WPS-500-MK30-P10 CDSs were attached on the inside surface of each pipe sample to measure crown and springline deflections at the mid-length of the CMPs (Micro-Epsilon 2019). Three Omega LD650 LVDTs were utilized to measure the crown, springline, and shoulder deflections of the CMP samples during the loading application (OMEGA 2019). The LVDTs were installed on a wooden frame which was cantilevered to the middle of the CMP sample, as illustrated in Figure 11-23. LVDTs and CDSs were connected to a data acquisition system that digitalized the transmitted analog signals from the sensors during the tests, as illustrated in Figure 11-24.

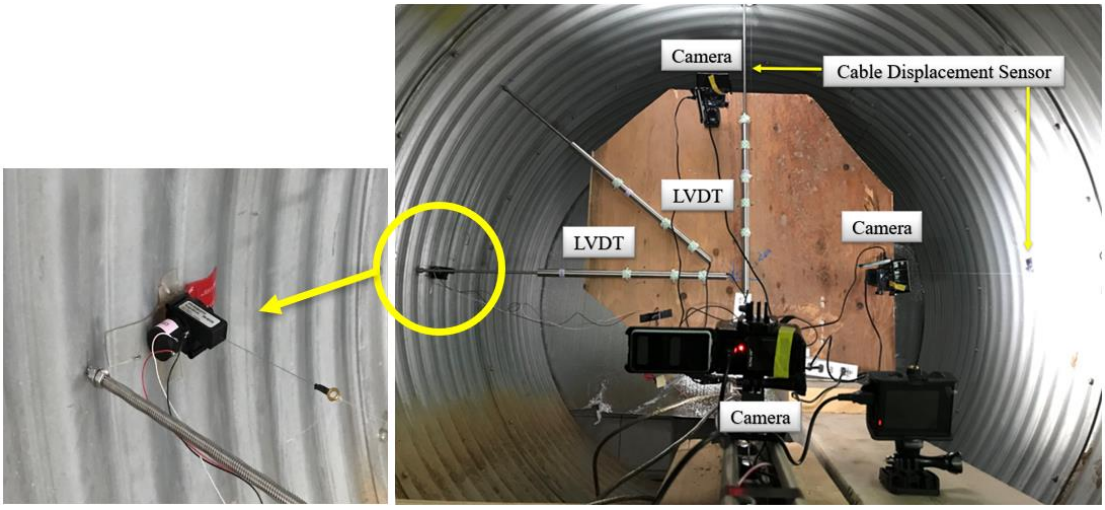


Figure 11-23. LVDTs and cable displacement sensors.

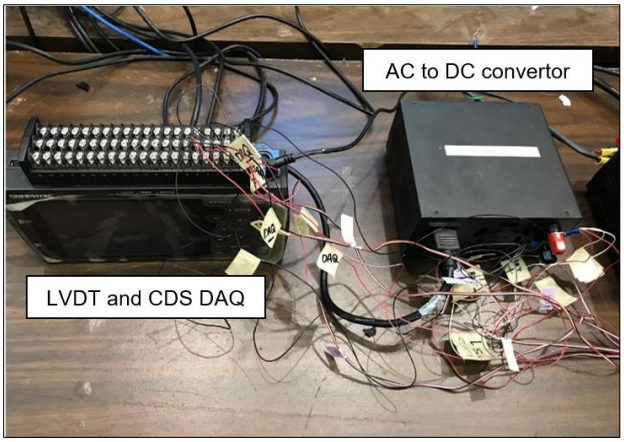


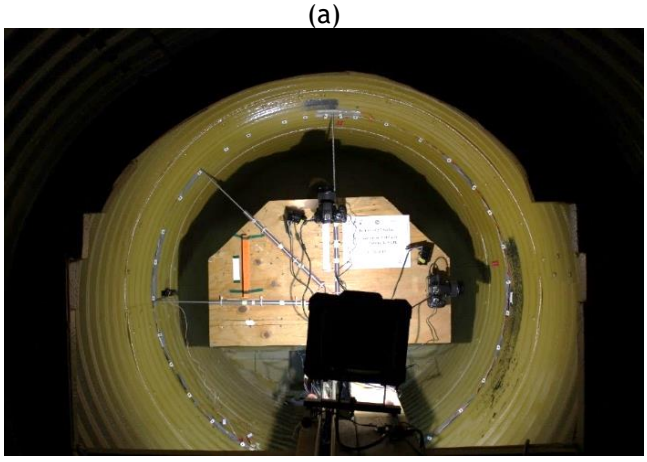
Figure 11-24. LVDT and CDS DAQ, and alternating current (AC) to direct current (DC) convertor (from left to right).

11.8.4 DIC Measurement and Pipe Monitoring

Three DSLR Canon Rebel T5i cameras were used to capture the CMP samples crown and springline changes and monitor crack initiations at the SAPLs at the middle section as well as the CMP profile changing during the tests, as illustrated in Figure 11-25 (a) and (b). A total number of around forty to fifty targets were attached circumferentially to the middle section of each CMP sample for the purpose of pipe monitoring and profiling using two-dimensional digital image correlation (DIC) technique (Ham and Darabnoush Tehrani 2019, Darabnoush Tehrani 2020, Darabnoush Tehrani et al. 2020). The DIC targets were designed and fabricated using high contrast colors of black and white. The DIC targets were attached to the inside surface of the crests of the CMP samples. The DIC technique was implemented with the use of the commercially available software of GOM Correlate and a developed MATLAB code. 2D DIC is a powerful technique that enables a multi-point deflection measurement in a 2D plane at any stage of loading (Ham and Darabnoush Tehrani 2019). The setup of DIC targets and cameras along with CDSs and LVDTs installed inside one of the circular CMP samples are illustrated in Figures 11-26 and 11-27.



(a)



(b)

Figure 11-25. Pipe monitoring: (a) cameras used for capturing changes, and (b) DIC targets for pipe profiling.

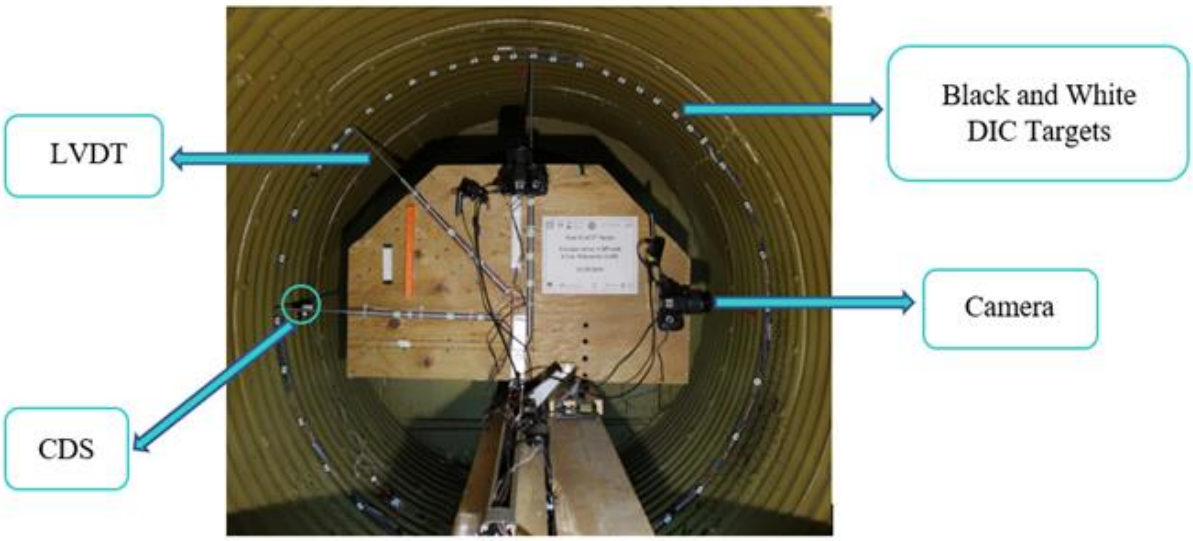


Figure 11-26. Instrumentation: LVDTs, CDSs, DIC targets and cameras inside the pipe sample.

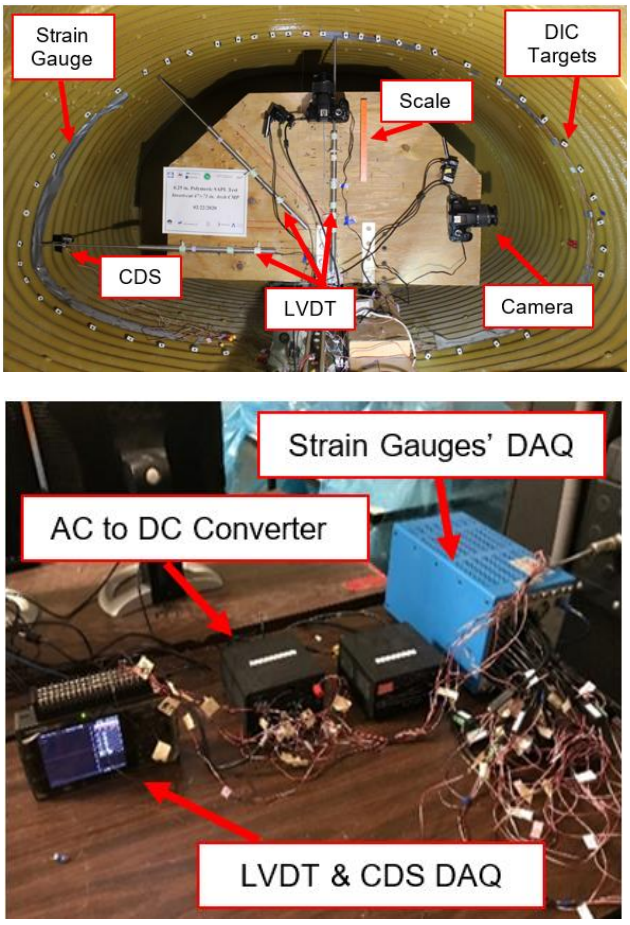


Figure 11-27. Instrumentation: (top) LVDTs, CDSs, DIC targets and cameras inside the pipe sample, (bottom) data acquisition systems.

11.8.5 SAPL Thickness Measurement

For the second and third sets of testing, the thickness measurement of the installed SAPLs were conducted using an OLYMPUS 38DL PLUS® Ultrasonic Thickness Gauge with measuring thickness range of 0.003 in. to 25 in. The SAPL thickness installed inside each CMP samples was measured at three locations longitudinally along the pipe length and circumferentially in 45˚ intervals. The ultrasonic thickness measurement gauge was calibrated using two samples of 0.25 in. and 1 in thick from the same SAPL material. Since the device probe was too large to be perfectly fitted in the valleys of CMP samples, the thickness measurements were conducted on top of the crest of corrugations at the target locations. Three measurements and readings were conducted at each point, and finally the averaged thickness value for that location was recorded. The thickness measuring locations along with the calibration SAPL samples are illustrated in Figure 11-28 for both circular and CMP arch samples.

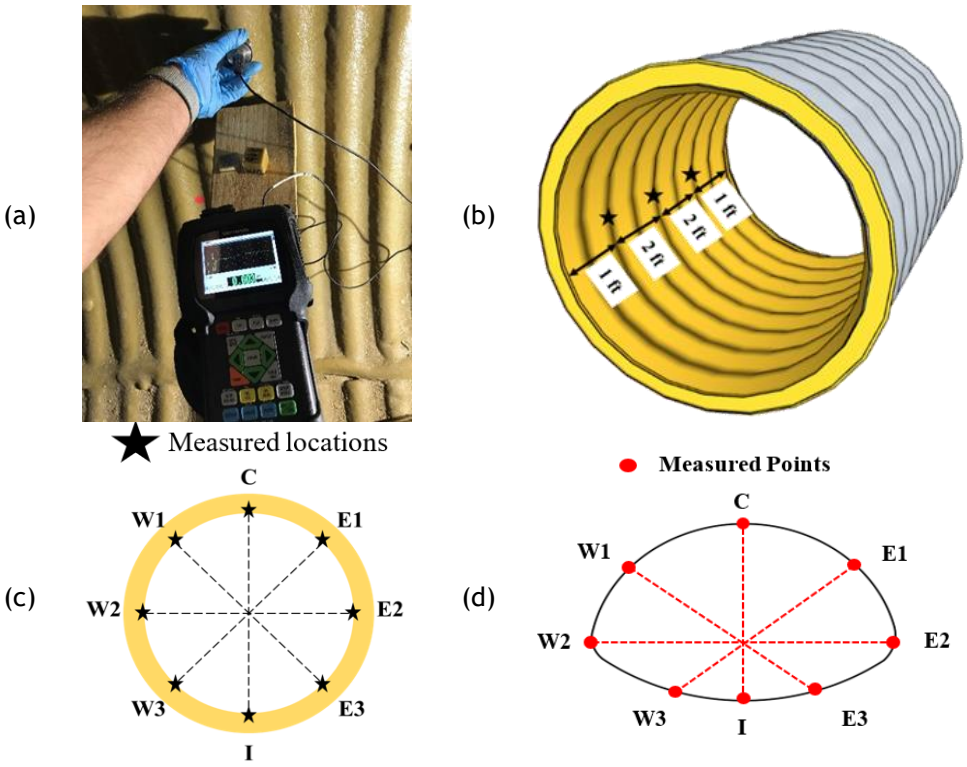


Figure 11-28. SAPL thickness measurement: (a) thickness gauge and calibration sample, (b) longitudinal measured locations, (c) circular CMP circumferential measured locations, and (d) CMP arch circumferential measured locations.

11.9 POLYMERIC SAPL

11.9.1 CMP Surface Preparation and Polymeric SAPL Installation

SprayWall (Johnson and Hammon 2017) polymeric SAPL, as a commercially available SAPL material, was selected to renew the CMPs. SprayWall® is a self-priming polyurethane lining by Sprayroq Protecting Lining System Company for pipe and manhole renewal that reinstates structural integrity, provides infiltration control and corrosion resistance. Its quick curing time enables the renewed structure to be returned to service shortly after the completion of the application, which makes it ideal for utilization in water, wastewater, and storm water pipe renewal. Sprayroq recommends cleaning the host pipe from oil, and other contaminates, which may cause formation of blisters, pinholes, foamed material, debonding, cracking, or delamination of the SAPL from the host pipe. For the second and third sets of soil box testing, after completion of CMPs' backfilling and instrumentation they were renewed with different thicknesses of SprayWall liner. CMP surface preparation was conducted prior to the pipe installation in the soil box as recommended by the Sprayroq. Hence, the CMPs were power washed using pressurized water jet to remove the dust and dirt attached to their inside surface, similar to the pipe preparation procedure for SAPL installation in field, as illustrated in Figure 11-29 (a and b).



(a) (b)

Figure 11-29. CMP surface preparation for SAPL installation: (a) dirt and dust on the CMP, and (b) CMP after power wash without any dirt and dust.

The SAPL was applied up to 0.25 in. thick in each single application or lift. The SprayWall SAPL began solidifying in about 8 seconds and its initial cure was completed within 60 minutes. In the invert section, it was not possible to spray the SprayWall directly on the soil. Therefore, the detached invert section (middle section) was kept in place to receive the liner. There was a 2 in. gap between each side of the invert section and the main body of the CMP which both gaps were filled with Styrofoam and

covered with plastic sheets and duct tape. The invert-cut section of circular CMPs before and after SAPL installation is illustrated in Figure 11-30 (a, b and c). The invert-cut section of CMP arch samples, end strips, invert preparation for SAPL installation, and the invert-cut section after the SAPL installation are illustrated in Figure 11-31 (a, b, c, d and e).



(a) (b) (c)

Figure 11-30. SAPL installation of invert-cut circular CMPs: (a) before SAPL installation (stage 1), (b) after SAPL installation (stage 2) and (c) end strips detachment (stage 3).

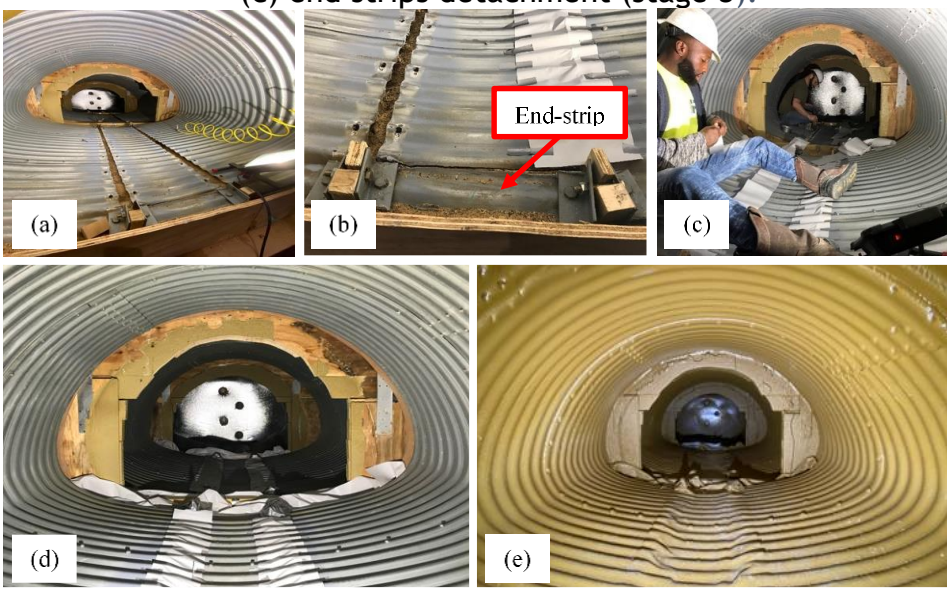


Figure 11-31. CMP arch preparation for SAPL installation: (a) CMP arch before gap sealing, (b) the invert-cut gap sealing with Styrofoam and plastic sheets, (c) Sprayroq's vendor working inside the CMP arch samples, (d) prepared pipe prior to the SAPL installation and (e) the SAPL renewed CMP arch samples.

11.9.2 Polymeric SAPL Installation

The SprayWall SAPL was installed by hand spray, as illustrated in Figure 11-32. In order to control the thickness during the installation, with respect to the volume of the sprayed material coming out of the nozzle per unit of time (i.e., second), the vendor's engineer could estimate the amount of material that was sprayed on the CMP

arch sample's inside surface in every second. In addition, by knowing the total volume of the required SAPL, the number of passes required to reach the designed thickness was estimated. However, this type of installation requires the high proficiency and experience of the SAPL installer. The Sprayroq vendor calculated an approximate amount of 179.08 lb, 358.16 lb, and 716.33 lb of SprayWall material that was required to apply 0.25 in., 0.5 in. and 1 in. thicknesses, respectively, on 60-in. CMPs. The Sprayroq vendor calculated approximate amounts of 230 lb, 460 lb, and 925 lb of SprayWall material that were required to apply 0.25 in., 0.5 in., and 1 in. thicknesses, respectively, on 47×71 in. invert-cut section. These values include a factor of safety to cover material testing sample and installation errors such as over spraying. The Sprayroq vendor installed the liner on October 29, 2019, at CUIRE Laboratory for circular CMP.



Figure 11-32. Hand spray SAPL installation.

11.9.3 Polymeric SAPL Sampling for Material Property Testing

Prior to the SAPL installation, for each test setup of circular and CMP arch samples, four plate samples of about 0.125 in. thick SAPL were sprayed from the same batch. The SAPL plate samples were collected to examine the flexural and tensile properties of the installed SAPL used for the renewal of CMPs, as illustrated in Figures 11-33 (a and b) and 11-34. Once the plate samples were fully cured, they were cut into the required plaques for flexural and tensile tests as specified by ASTM standards D790-17 and D638-14. The plaques were precision machined to exact dimensions to minimize edge effects.

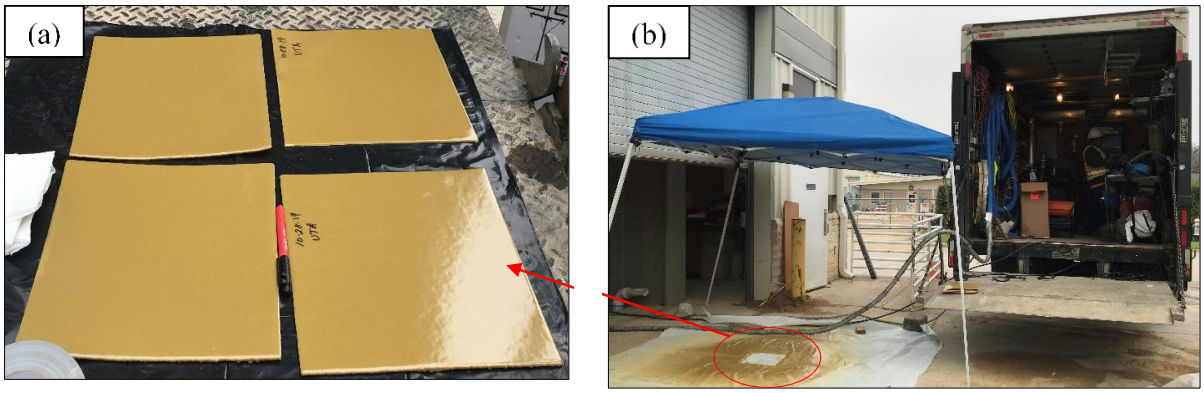


Figure 11-33. SAPL sampling for circular CMPs test setup: (a) sample plates prior to the cut into required shape for flexural and tensile test, and (b) the sampling site with Sprayroq installation truck.



Figure 11-34. Plate sampling from the SAPL batch to provide material test samples for CMP arch test setup.

11.10 CEMENTITIOUS SAPL

11.10.1 CMP Surface Preparation

The CMP samples were prepared for SAPL installation. The invert-cut section was unbolted, and the angle sections were removed completely. However, since the SAPL cannot be sprayed on soil material, the unbolted invert section was left in place to be as bas for SAPL on the invert area. The 2 in. gaps between the detached invert and the main body of CMP were filled with Styrofoam, as shown in Figure 11-35 (a).

It was essential to make sure the pipes and SAPL are both completely separated from the portion walls without any structural resistance coming from the attachment of the pipe and walls. In addition, since the inverts' end-strips were needed to be removed after hardening of the SAPL, it was crucial to keep them protected from being sprayed. Therefore, the gaps between the wooden partition walls and both ends of the

CMPs as well as the invert's end-strips were covered with duct tape to be protected from SAPL application, as shown in Figure 11-35 (b and c).



Figure 11-35. End-strip detachment: (a) end-strip preparation, (b) end-strip before SAPL installation and (c) end-strip detachment after SAPL installation.

SAPL installation on a deteriorated culvert requires cleaning and surface preparation. A common procedure is to implement sand blast or high-pressure water blast at minimum 4,000 psi pressure on the interior surface of the culverts to remove, dirt, mud and rust from the CMP surface. However, since the pipe samples were used in this study were brand new pipe and were free of surface rust or long exposure to dust and dirt, power wash and sand blast was not required. On the contrast, since they were brand new CMPs, the bonding of the cementitious SAPL to such a smooth metallic surface was a major concern. Lack of proper bonding between the SAPL and the CMP, especially on thicker thicknesses, would raise the probability of SAPL falling and detachment from the host pipe. To prevent such an issue the vendor utilized a mixture of the SAPL material with the CSI Concrete Bonder II on the surface of CMPs. The CSI Concrete Bonder II is a film forming, none re-emulsifiable liquid bonding agent and polymer modifier, which is designed to improve the adhesive and physical properties of most cementitious materials including geopolymer.

11.10.2 SAPL Installation

The cementitious SAPL installation required field equipment including a portable gas-powered engine mortar mixer, gas-powered engine rotor-stator pump, a water tank, and, if required, spine-caster machine and a portable air compressor. The Standard Cement vendor had all the required equipment mounted on a trailer connected to a medium size truck. Due to the existence of the soil box and the large steel frame that limited the access to the laboratory inside, placement of the rotor-stator pump near the mortar mixer was not possible. Therefore, except for the rotor-stator pump, all of the other equipment was kept outside. To transport the mixed

geopolymer mortar to the rotor-stator pump, a wheelbarrow was used, and the mortar was poured inside the pump using a shovel.

Each bag of geopolymer was mixed with half a gallon of water and half a gallon of concrete bonder agent and then it was pumped inside the CMPs at the pressure of 60 psi. To install the required thicknesses of 1, 2, and 3 in., for circular CMPs a total of 83 bags, and for the CMP arch samples 85 bags of geopolymer cement were used. The SAPL vendor utilized hand spray method to apply the liner in both arch pipe and circular CMPs, as illustrated in Figure 11-36. The SAPL was first sprayed to fill the CMP's corrugation. Once the corrugations were filled, the pipes were sprayed for 1 in. thickness above the corrugation's crest. At this point, they allowed the material to rest for about an hour before they apply the second 1-in. thick layer for the CMPs with design thickness of 2 and 3 in. Similar procedure was carried out until all pipe samples reached their own required design thicknesses. During the installation process, the invert of the CMPs were left unsprayed to allow the applicators move freely without disturbing the liner. Once the SAPL installation of the CMPs' main body were completed, the invert sections were filled and the surface of the bottom half section (i.e., from springline to springline) of the pipes were finished by troweling. The top half section was left untreated as it would raise the risk of SAPL falling and detachment from the CMP. Once the SAPL installation was completed, the duct tapes, attached on the gaps between the CMPs and wooden partition walls were removed to prevent hardened over-sprayed material make contact between the walls and renewed CMPs.

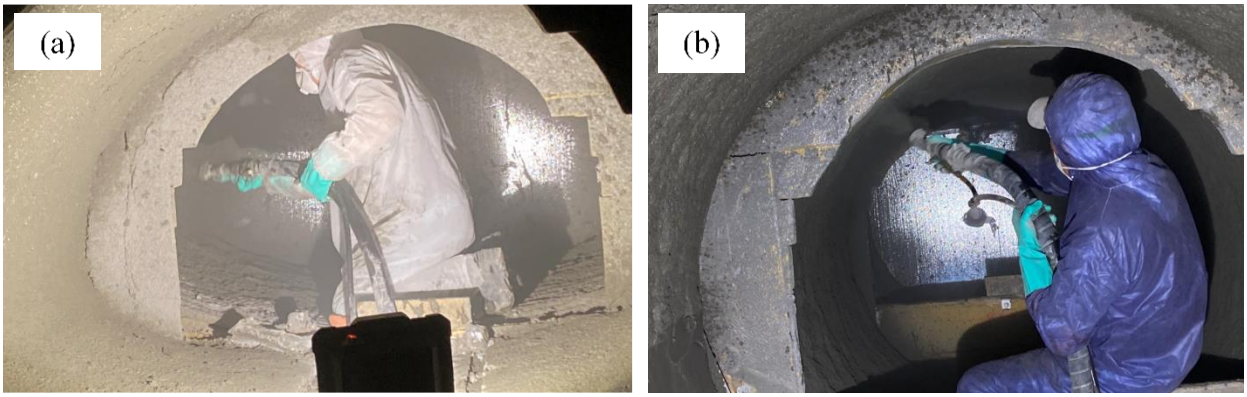


Figure 11-36. Cementitious SAPL installation on: (a) CMP arch and (b) circular CMPs.

During the installation, SAPL thickness was checked continuously using a depth gauge, illustrated in Figure 11-37. The measurements were conducted over the crest of the corrugation to inform the SAPL applicator with the applied thickness. In case of thicknesses less than the designed thickness, more material was applied. However, in case of applied thicknesses more than the required thickness, the excessive amount was not removed.

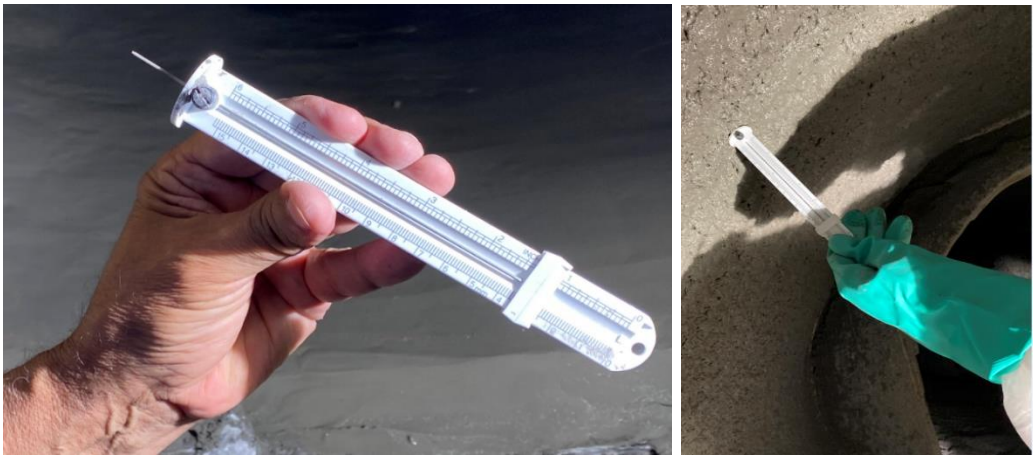


Figure 11-37. Thickness measurement using a depth gauge at the time of SAPL installation.

11.10.3 SAPL Mechanical Properties Testing Samples

A total number of 38 samples were taken from the same batch of SAPL installed on the CMP arch samples to measure compressive strength of the applied cementitious SAPL. Likewise, 41 samples were taken from the circular CMPs' SAPL batch. The samples included cubes and cylinders in different sizes, which were allocated to be tested at 24 hours, 7 and 28 days of curing. The cylinder samples were taken using both hand and spray cast methods. The sampling details and their quantity for pipe arch and circular CMP test series are presented in Tables 11-5 and 11-6, respectively. Although majority of the molds were brand new, they were washed and prepared prior to the SAPL casting. The molds were prepared with a mold release agent 24 hour before casting the SAPL, as illustrated in Figure 11-38 (a, b and c).

The cylinder and cube samples were cast, prepared, and tested in accordance with the ASTM C39 and ASTM C109, respectively. The samples were demolded and transported to a curing room 24 hour after the casting, as illustrated in Figure 11-39 (c). These samples were capped and tested right after the demolding process.

Table 11-5. Compressive testing samples for CMP arches renewed with cementitious SAPL.

Specimen Type	Specimen Size (in.)	Casting Date	Curing Time			Casting Type
			24 Hours	7 Days	28 Days	
Cube	2×2	6/13/2020	0	5	4	Hand
Cylinder	3×6		0	2	2	Hand
Cylinder	3×6		0	2	2	Sprayed
Cylinder	4×8		4	3	3	Sprayed
Cylinder	4×8		0	3	3	Hand
Cylinder	6×12		0	2	3	Sprayed
Total	-	-	4	17	17	Total = 38

Table 11-6. Compressive testing samples for circular CMPs renewed with cementitious SAPL.

Specimen Type	Specimen Size (in.)	Casting Date	Curing Time			Casting Type
			24 Hours	7 Days	28 Days	
Cube	2×2	7/18/2020	3	3	3	Hand
Cylinder	3×6		0	2	2	Hand
Cylinder	3×6		0	2	2	Sprayed
Cylinder	4×8		3	3	3	Sprayed
Cylinder	4×8		3	3	3	Hand
Cylinder	6×12		0	3	3	Sprayed
Total	-	-	9	16	16	Total = 41



Figure 11-38. Mechanical properties testing samples: (a) compressive testing cylinders molds, (b) mold preparation, and (c) sample storage at a curing room.

Both ends of the samples were capped using a sulfur capping material as specified in its corresponding ASTM standard. Extra care was made to have both sides of the cylinder perfectly leveled. The specimens were tested using a hydraulic actuator with 400 kips capacity of compression.

11.10.4 SAPL Visual Inspection and Internal Instrumentation

The SAPLs were left untouched to cure for three continuous days. On the fourth day, the entrance sealing was removed, and the research team was allowed to enter the SAPL renewed CMPs for visual inspection and internal instrumentation.

11.10.5 CMP Arch Samples Renewed with Cementitious SAPL

The visual inspection of the SAPL renewed CMP arch samples showed that all three liners had shrinkage cracks at multiple locations, mostly, in longitudinal direction. The crack width was measured using a digital image processing (DIP) method. To conduct the DIP measurement the digital camera was located perfectly

perpendicular to the crack plane. The averaged crack opening for the 3, 2, and 1-in. thick cementitious SAPLs were 0.023, 0.0325, and 0.0376 in., respectively.

11.10.6 Circular CMPs Renewed with Cementitious SAPL

The visual inspection of the SAPL renewed circular CMPs showed that all three liners had shrinkage cracks at multiple locations, mostly, in longitudinal direction. The crack width was measured using a digital image processing (DIP) method. To conduct the DIP measurement the digital camera was located perfectly perpendicular to the crack plane. The averaged crack opening for the 3, 2, and 1-in. thick cementitious SAPLs were 0.0204, 0.01848, and 0.009 in., respectively.

11.10.7 SAPL Thickness Measurement

To measure the installed SAPL thickness, after the structural testing of the soil-CMP system, the liners were drilled, and the depth of the holes were measured using a digital caliper. The thickness of the installed cementitious SAPL was measured longitudinally at three locations along the pipe length and in circumferential direction with 45˚ intervals. The measurements were conducted on the top of corrugation's crest. For each point, three measurements were conducted, and the averaged values were recorded. The measuring locations for both pipe arch and circular CMP samples are illustrated in Figure 11-39.

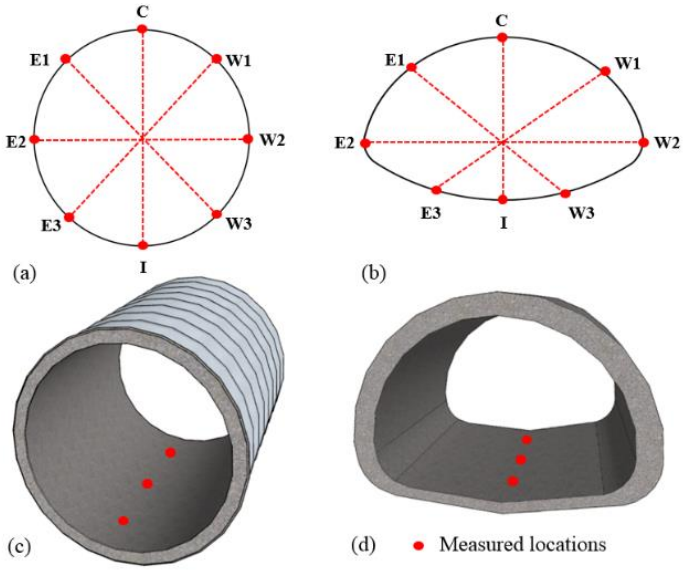


Figure 11-39. SAPL thickness measurement: (a) measurements in circumferential direction on circular and, (b) pipe arch SAPL samples, (c) measurements in longitudinal direction on circular and, (d) pipe arch SAPL samples.

11.11 TESTING RESULTS AND DISCUSSIONS

11.11.1 CMP Control Test

11.11.1.1 Invert Detachment Effect

The invert-cut sections of both circular and CMP arch samples were detached and removed prior to the loading of the pipe samples. Once the invert-cut sections were detached completely, the CMP samples suddenly moved and squeezed to the presence of active soil pressure on the sides of CMP walls, as illustrated in Figure 11-40. The CMP samples inside diameters were measured before and after the invert detachment. A laser distance meter was used for the pipe diameter measurement. As for the invert-detachment operation was a manual task and for the sake of safety, the utilization of CDS and LVDT was not possible in the confined space of CMP samples. The pipe diameter measurements revealed that the vertical and horizontal diameters of the circular CMP sample were reduced by 3.1 in. downward and 3 in. inward. The rise and span of CMP arch after the invert detachment were reduced by 2.23 in. downward and 5.24 in. inward. As the invert section of the CMP arch has a flat shape compared to the circular CMP, after the invert detachment and in the absence of the ring stiffness, the bottom of the CMP arch was slipped on the soil surface. Hence, due to the invert detachment, the CMP arch registered a smaller change in diameters compared with the circular CMP. With utilization of the digital image correlation (DIC) technique, it was measured that the circular CMP was rotated clockwise to a magnitude of approximately 0.45 in. (arc length) as illustrated in Figure 11-41.



Figure 11-40. CMP movement due to the invert detachment (without any end strips) before loading.

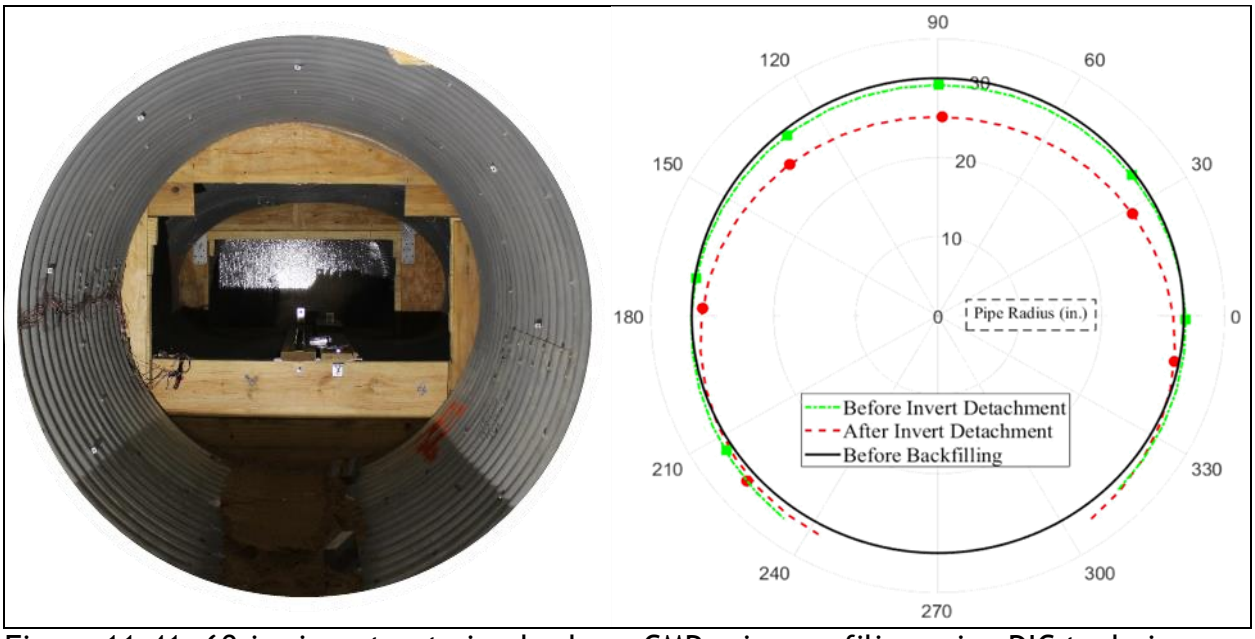


Figure 11-41. 60-in. invert-cut circular bare CMP, pipe profiling using DIC technique.

11.11.1.2 Bare CMP Behavior under the Static Load

The comparison of soil-pipe system settlement under the applied static load for the intact circular, invert-cut circular and invert-cut CMP arch samples in terms of the load-displacement graphs are illustrated in Figures 11-42, 11-43, and 11-44. The applied pressures through the load pad on the soil surface at the middle section of the soil cells for intact circular, invert-cut circular and invert-cut CMP arch samples are illustrated in Figure 11-43. The registered pressures by the earth pressure cells on top of the CMP samples (within a 4-in. gap away from the outer surface of the CMP) at the crown locations of the intact circular, invert-cut circular and invert-cut CMP arch samples are illustrated in Figure 11-44.

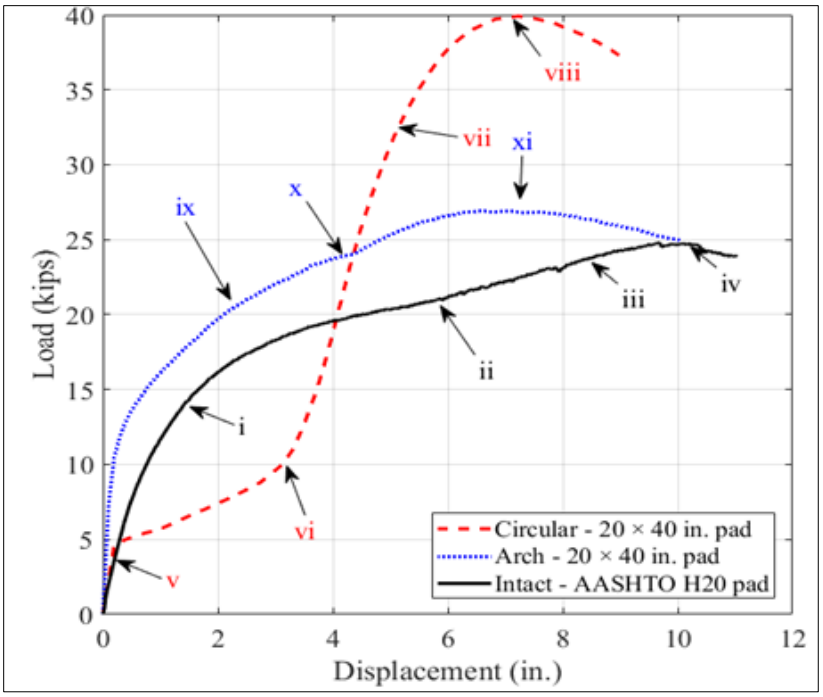


Figure 11-42. Control test: applied load through the steel load pad vs. soil settlement.

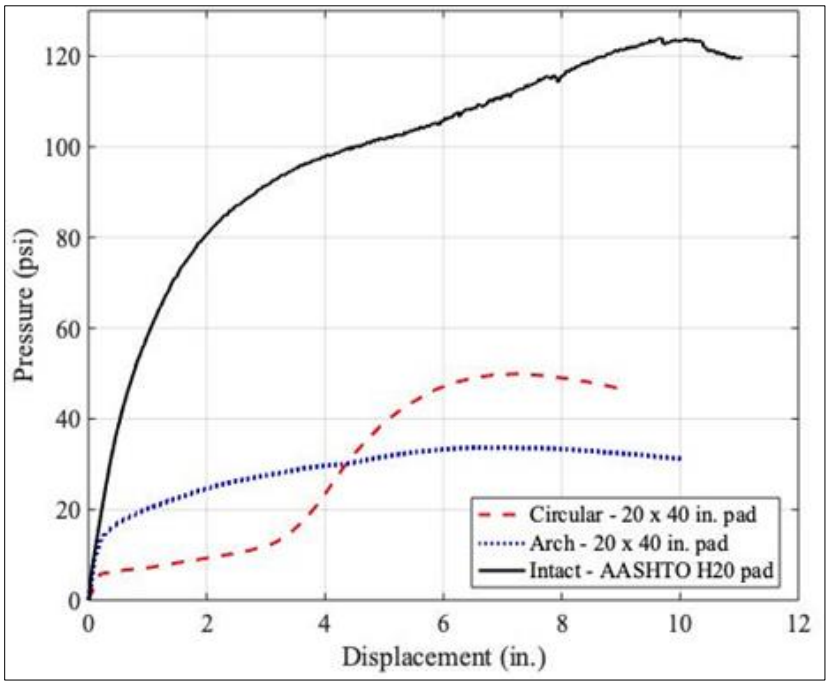


Figure 11-43. Control test: pressure on the soil surface under the load pad vs. soil settlement.

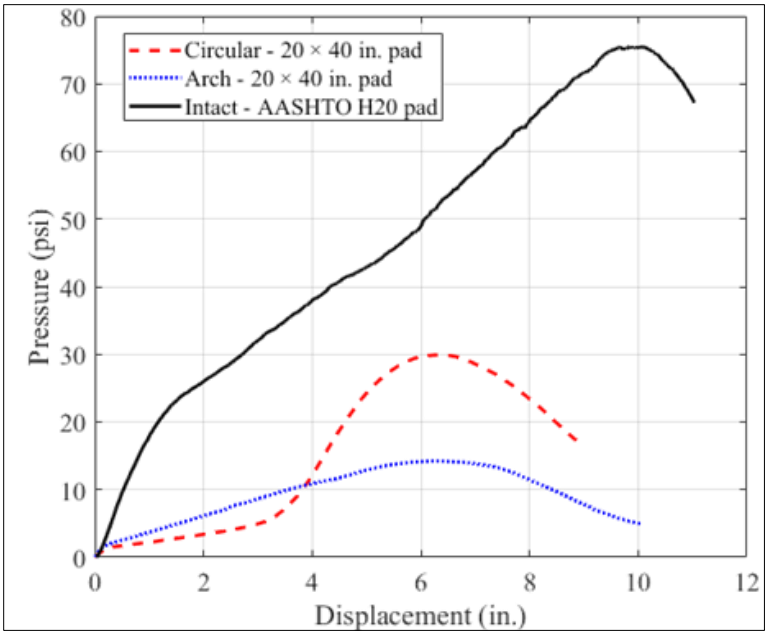


Figure 11-44. Control test: pressure on top of the CMP samples vs. soil settlement.

As it is illustrated in Figures 11-42 and 11-43 the bare intact CMP, invert-cut circular CMP and invert-cut arch CMP could withstand the ultimate load of 24.85, 39.9, and 26.9 Kips, respectively. Earth pressure cells registered the maximum pressure of 75.38, 29.95, and 14.23 psi for the intact, invert-cut circular and invert-cut arch CMP samples at the crown location at the time of failure.

11.11.1.3 Bare Intact Circular CMP

For the intact circular CMP, the soil-pipe system showed a stiff response to the AASHTO H20 truck service load up to 16 kips, with approximately 1.95 in. of soil displacement, as illustrated in Figure 11-42 by the notation of 'i'. For the intact bare circular CMP after passing the service load, the soil-pipe system showed a softened response to the applied load until the occurrence of the soil failure at point (notation of "ii" in Figure 11-42). Once the soil failed, all the applied load was carried by the intact bare CMP that caused the stiffening of the system (notation of "iii" in Figure 11-42) and ultimately the failure at the load of 24.8 kips (notation of "iv" in Figure 11-42). The results of DIC measurement and pipe profiling for the 60-in. intact circular CMP is illustrated in Figure 11-45.

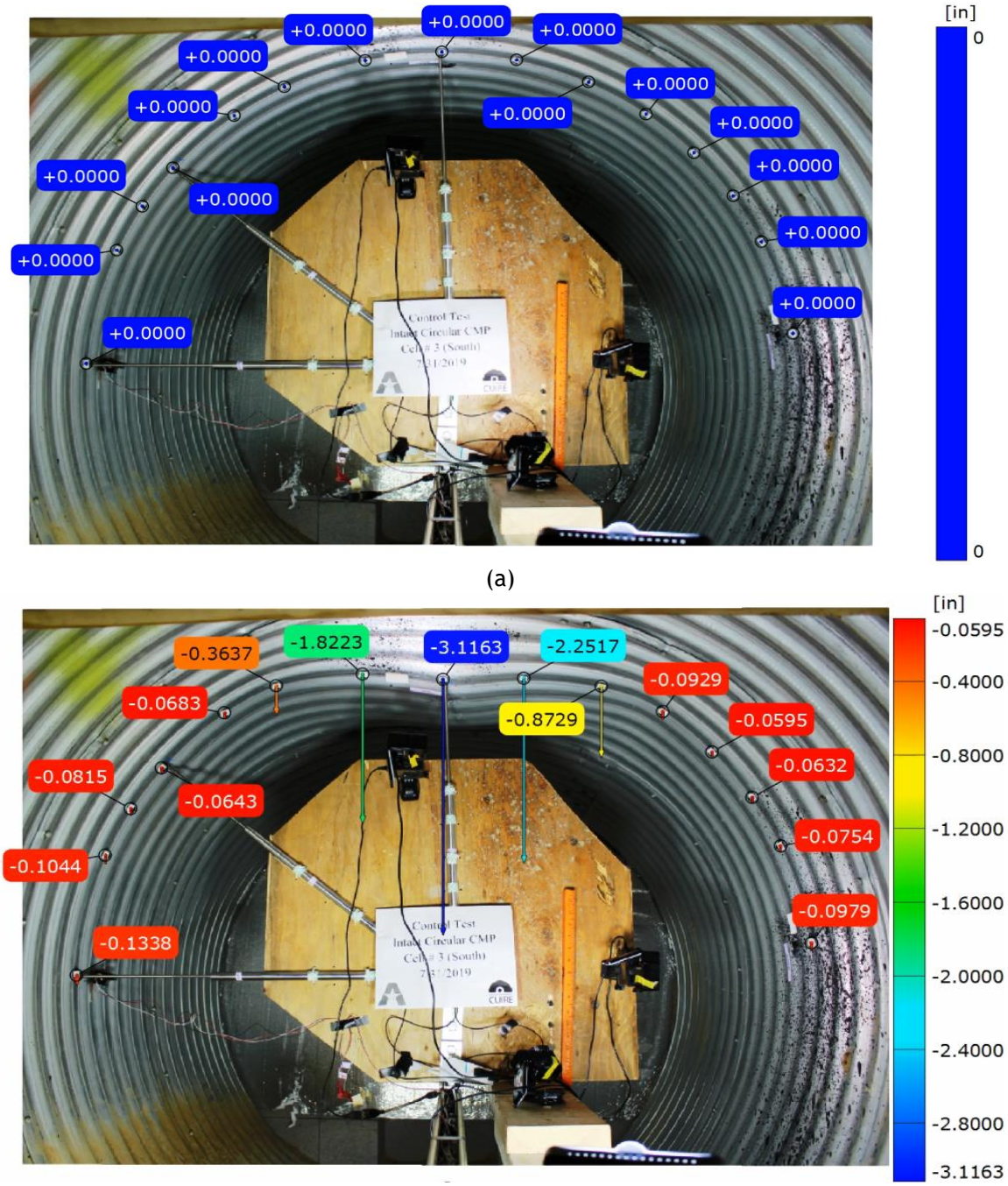


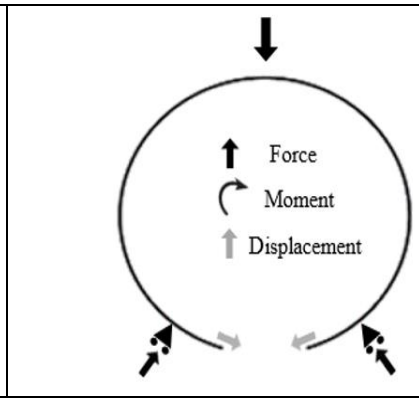
Figure 11-45. Results of DIC measurement for the 60-in. intact circular CMP: (a) before loading, and (b) after loading at the end of the test.

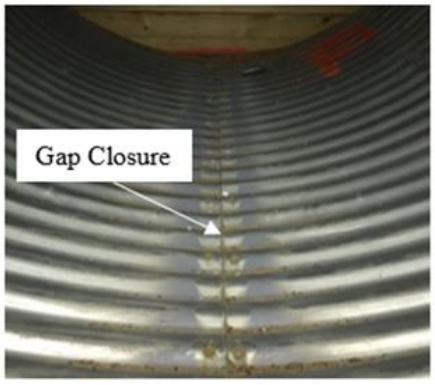
11.11.1.4 Bare Invert-cut Circular CMP

The invert-cut circular bare CMP compared with intact circular bare CMP under the static live load showed a different behavior. The invert-cut circular bare CMP sample under the applied load initially showed a stiffer response (v), due to the friction resistance force of the soil-pipe system. After reaching the limit of 4.58 kips, in the absence of pipe ring stiffness, there was no other resisting force to prevent the circumferential movement of the CMP sample. Hence, the invert-cut circular bare CMP sample under the load after passing the load of 4.85 kips, continuously moved until both sides of the invert-cut sections meet each other and the pipe ring stiffness was recovered (vi). Due to the circumferential movement of the CMP sample, the vertical diameter of the pipe reduced by 3.1 in. After contacting both edges of the pipe at the invert-cut sections (vi), the system significantly showed a stiffer response to the applied load (vii) until the failure at the load of 39.9 kips. At the failure point the system registered a 7.22-in. soil settlement (viii). The movement mechanism of the invert-cut circular CMP sample is illustrated in Figure 11-46 (a). The gap closure of the invert-cut circular CMP sample at the cut location due to vertical loading is illustrated in Figure 11-46 (b).

Figure 11-47 (a and b) illustrates the invert-cut circular CMP sample before and after loading. The structural failure mode of the invert-cut circular CMP sample was local buckling at the crown, as illustrated in Figure 11-47 (b). Figure 11-48 illustrates the results of DIC measurement for the invert-cut circular CMP sample at the end of the test.

(a)





(b)

Figure 11-46. Circular CMP movement due to the invert detachment: (a) the movement mechanism, and (b) The gap closure at the cut location due to vertical loading.

The designed laboratory soil box testing in this research was a simulation of the worst-case scenario in the field condition. In the actual field condition, the magnitude of the pipe circumferential movement in a fully deteriorated invert condition, is lower than the laboratory condition. In the actual field condition, the soil-pipe system is stabilized and usually the existing pavement layer on top of the soil cover distributes traffic loads on the pipe structure. Therefore, the circumferential movement of a fully deteriorated pipe happens at a low pace compared to the laboratory condition.

Moreover, the CMP external corrosion increases the pipe roughness as well as the circumferential friction between the pipe wall and surrounding soil. This friction has a direct relationship with the length of the pipe. Hence, in the actual field conditions that pipes are much longer than a test pipe sample in a laboratory condition, the resistance of frictional forces between the pipe and soil reduces the circumferential movement of the pipe. Consequently, the probability of the local buckling occurrence will be increased.

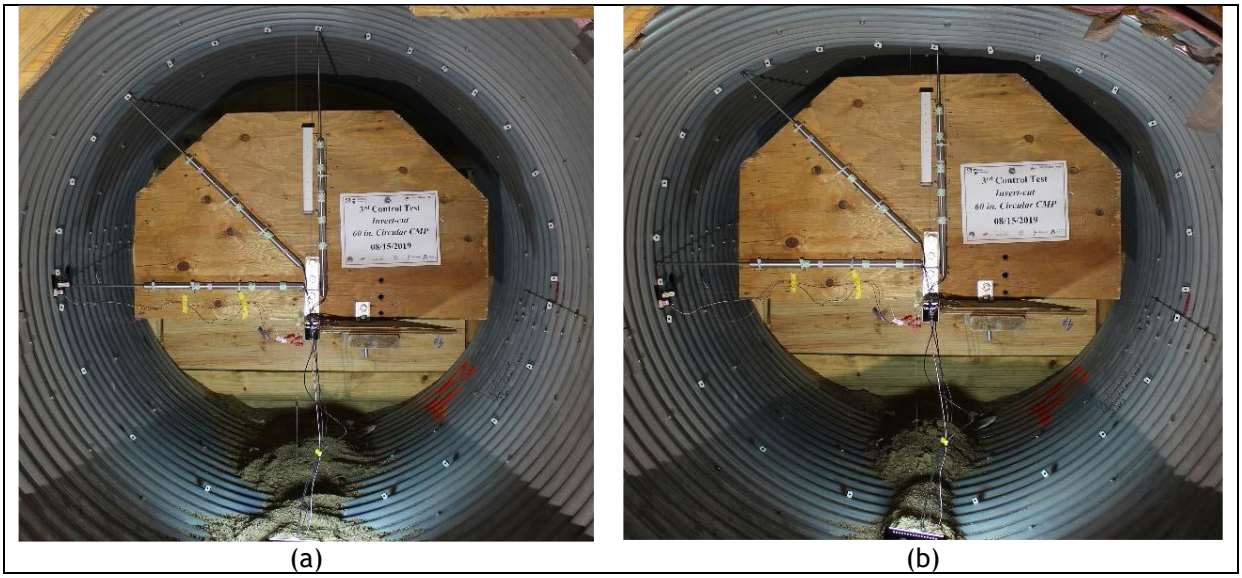


Figure 11-47. 60-in. Invert-cut circular CMP soil box testing: (a) before loading and (b) after loading.

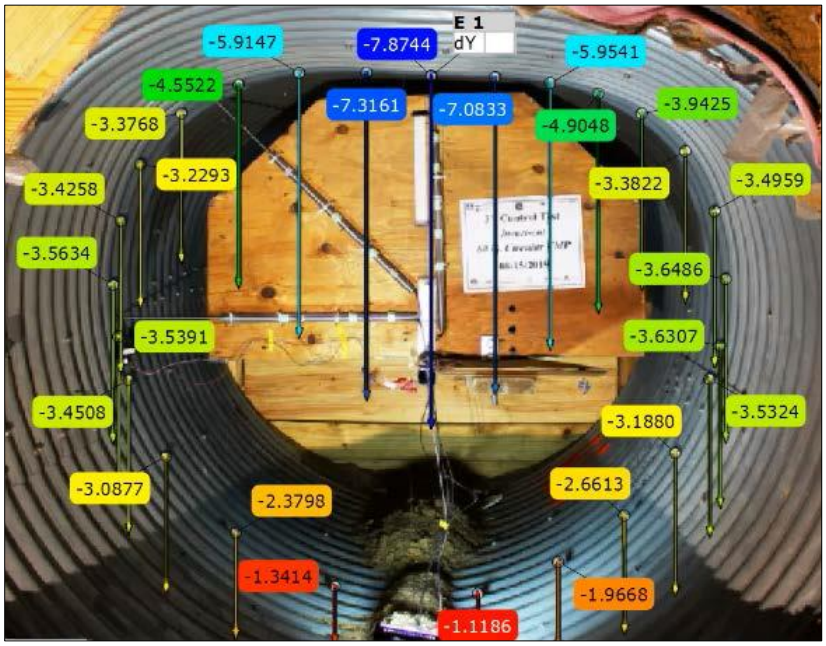


Figure 11-48. Results of DIC measurement at the end of the test (60-in. invert-cut circular CMP).

11.11.1.5 Bare Invert-cut CMP Arch

The invert-cut arch CMP, in the absence of ring stiffness, maintained its stability under the applied loading. It could take the advantage of its geometry (flat bottom) and no significant horizontal displacement was observed, as illustrated in Figure 11-42. by the notation of "ix". The low slope area at the CMP arch shoulder and the flat area at the bottom, enabled the CMP sample to resist the applied vertical load. The movement mechanism of the invert-cut arch CMP sample is illustrated in Figure 11-49 (a). Figure 11-49 (b) depicts the uplift of the invert-cut arch CMP after loading and soil compaction.

As illustrated in Figure 11-49 (a), a positive movement as well as upward forces at the invert section of the arch CMP was generated due to the applied vertical force on top of the pipe sample. Hence, the movement of the invert-cut CMP arch sample at the free ends of the invert section with a uniform upward displacement of approximately 2.2 in. occurred, as illustrated in Figure 11-49 (c). A gap was generated due to this upward displacement at the invert-cut area of the arch CMP that previously misunderstood as a result of soil erosion (Matthews et al. 2012). However, in the actual field conditions this gap could be possibly due to the combination of both soil erosion and CMP upward movement at the invert location. The invert-cut arch CMP failed at a load of 26.9 kips with a 6.54 in. soil surface settlement. Same as the invert-cut circular CMP sample, the structural failure mode of the invert-cut arch CMP sample was also local buckling at the crown. The crown of the CMP sample was the critical location under the load pad as formation of the three-hinge plastic collapse mechanism was occurred there, illustrated in Figure 11-50. The result of DIC measurement and pipe profiling for the invert-cut arch CMP at the end of the test is illustrated in Figure 11-51

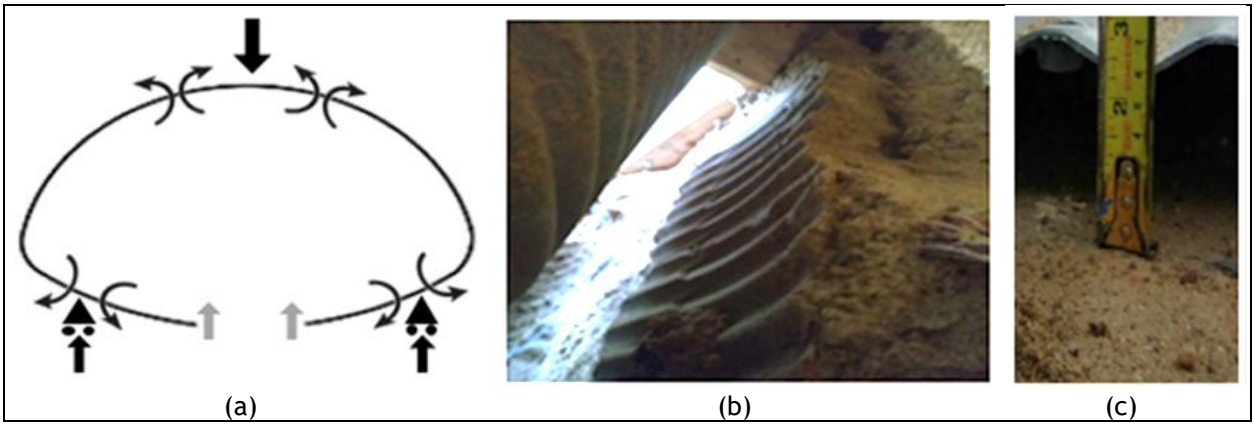
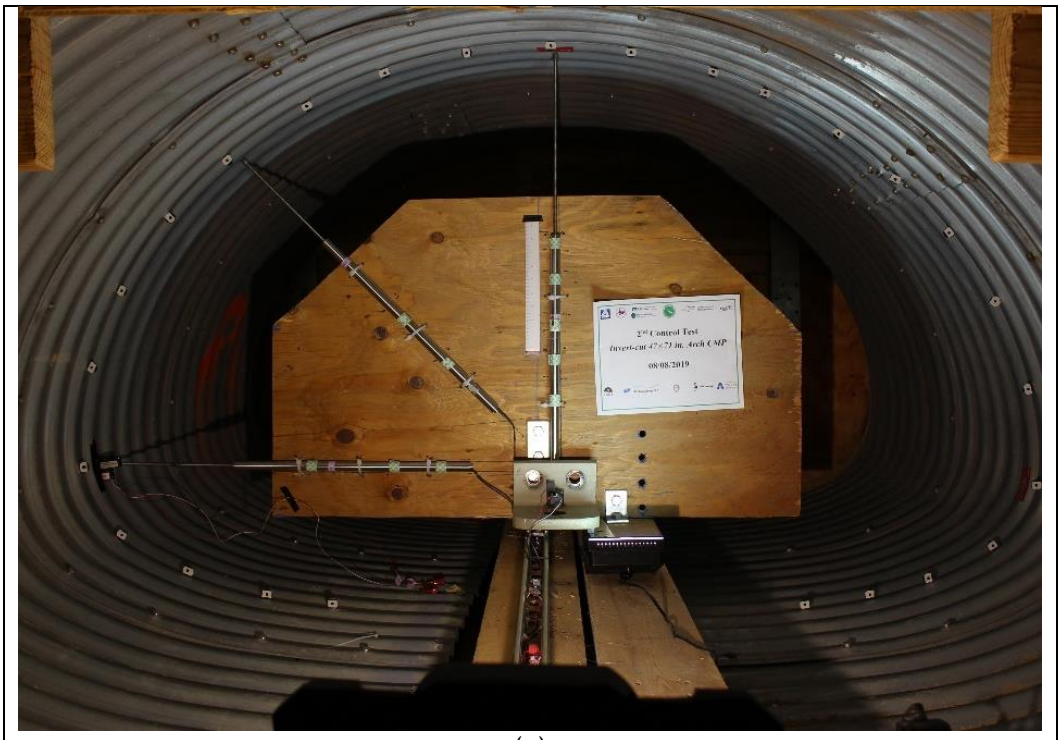


Figure 11-49. CMP arch movement due to the invert detachment: (a) the movement mechanism, and (b) the uplift of the invert-cut CMP arch after loading and soil compaction under the haunch area after exhuming the CMP.



(a)



(b)

Figure 11-50. 47×71 in. invert-cut CMP arch soil box testing: (a) before loading, and (b) the local buckling failure of the pipe sample after loading.

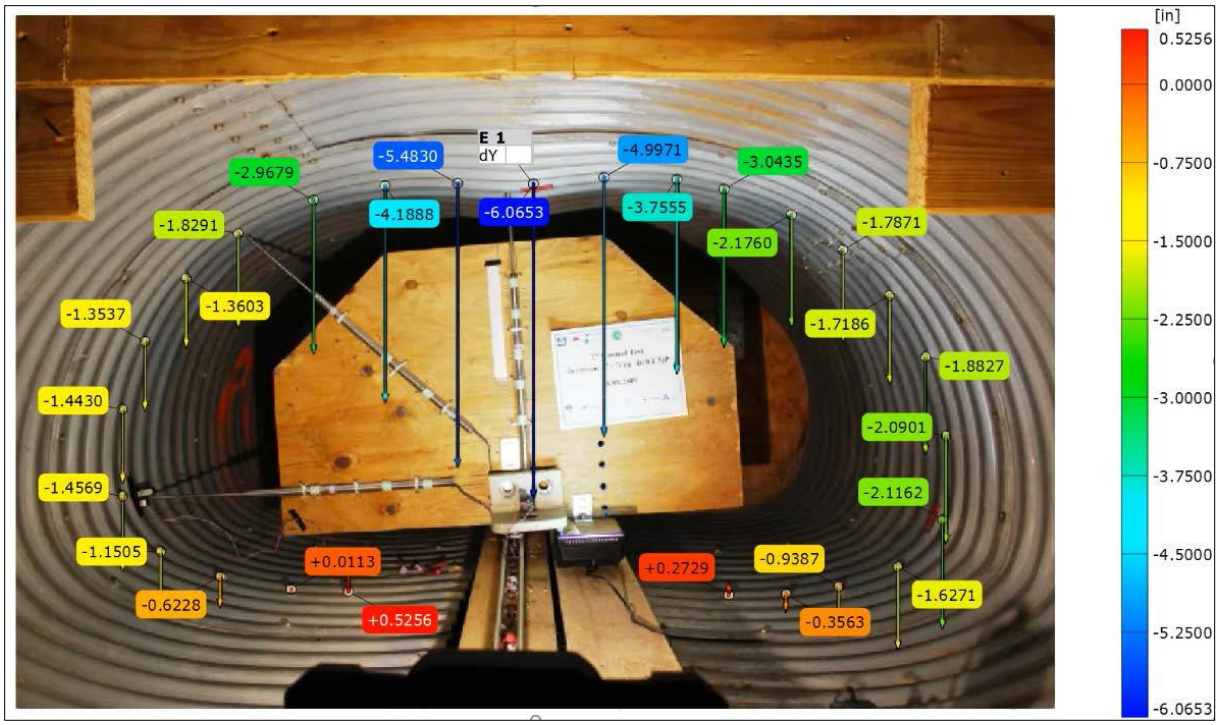


Figure 11-51. Result of DIC measurement at the end of the test (47×71 in. invert-cut arch CMP).

11.11.1.6 Bare CMPs Load Carrying Capacity

Figure 11-52 (a, b and c) illustrates the applied load on the soil surface versus the deflection of CMPs at different locations of crown, springline and shoulder along with the soil settlement for the first set of soil box testing (CMP control test). It should be noted that in this figure, a negative displacement means the CMP sample had an upward movement.

The difference in the strength of CMP and soil materials caused a discrepancy between the obtained load-displacement graphs from the CMP samples and soil, as illustrated in Figure 11-52. The soil, as the softer material, deformed or compressed more than the CMP as the stronger material.

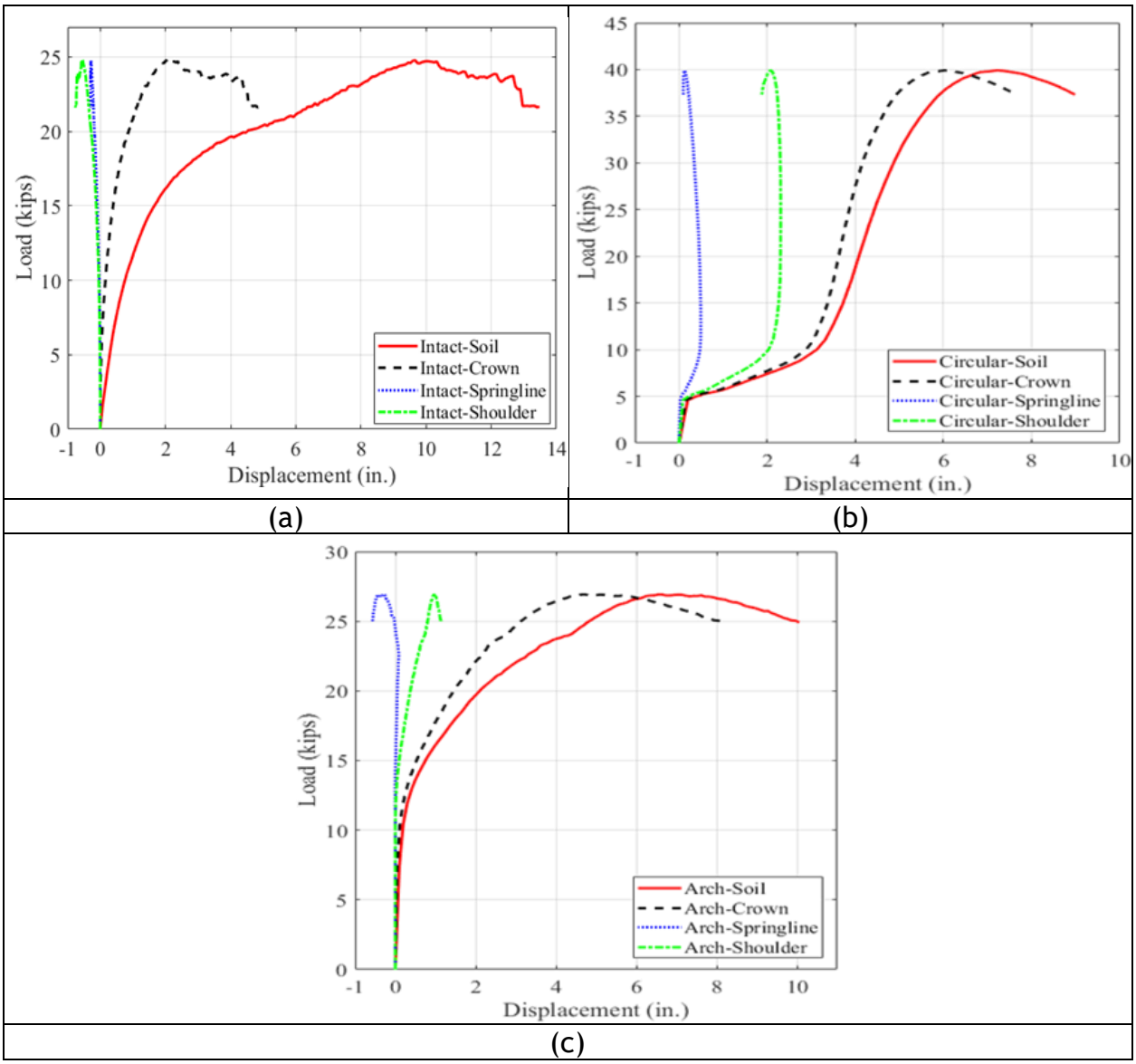


Figure 11-52. Load versus displacement of CMPs at different locations for the control test: (a) intact 60 in. circular CMP under a 10×20 in. steel load pad, (b) invert-cut 60 in. circular CMP under a 20×40 in. steel load pad, and (c) invert-cut 47×71 in. arch CMP under a 20×40 in. steel load pad.

11.11.1.7 Bare Intact Circular CMP

The intact circular CMP, under the AASHTO H20 truck load (under the steel load pad size of 10 × 20 in.), reached the service load of 16 kips with a vertical deflection of 0.46 in. at the crown of the pipe and soil settlement of 1.97 in. on the soil surface. The ultimate load carrying capacity of the intact circular CMP was reached to the load of 24.77 kips with the vertical deflection of 2.03 in. at the crown of the intact circular CMP and soil settlement of 9.96 in. on the soil surface. The soil box testing results of

the intact circular CMP showed that the CMP sample did not reach the deflection limit of 5%, prior to the occurrence of the local buckling failure at the crown.

11.11.1.8 *Bare Invert-cut Circular CMP*

The invert-cut circular CMP registered a horizontal pipe deflection of 0.12 in. at the springline and a vertical deflection of 6.03 in. at the crown for both LVDT and CDS. However, by disregarding the initial movement of the CMP sample, the absolute displacement of the invert-cut circular CMP sample pipe at the shoulder, springline, and crown are 0.07, -0.33, and -3.15 in. (positive sign is taken for inward movements), respectively.

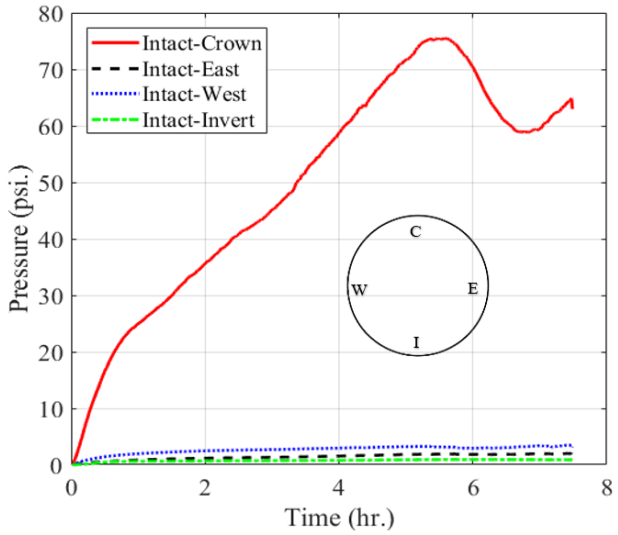
11.11.1.9 Bare Invert-cut CMP Arch

The invert-cut CMP arch sample failed at approximately the load of 26.9 kips with the vertical deformation of 4.64 in. at the crown of CMP sample and the soil settlement of 6.54 in. on the soil surface under the steel load pad. LVDTs registered the horizontal inward displacement of -0.7 in. from the east side of the springline towards the center of the pipe and CDS registered a reduction of -1.35 in. in the span of the invert-cut CMP arch sample.

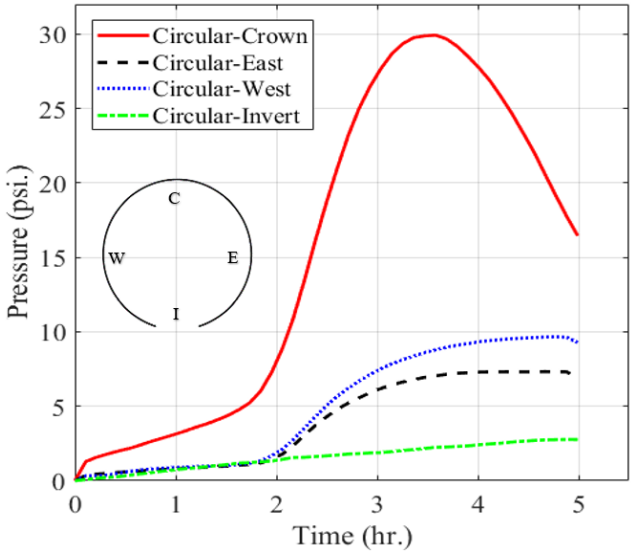
11.11.1.10 Results of Earth Pressure Cells

The earth pressure cell results are illustrated in Figure 11-53 (a, b and c). The maximum pressure at the crown of the intact CMP, invert-cut circular CMP and invert-cut arch were registered 75.38, 29.95 and 14.23 psi, respectively. As can be observed on the pressure graphs, in each cell the maximum pressure was carried out by the crown of CMP samples, and compared with the crown, no significant pressure was transferred to the springline and invert.

(a)



(b)



(c)

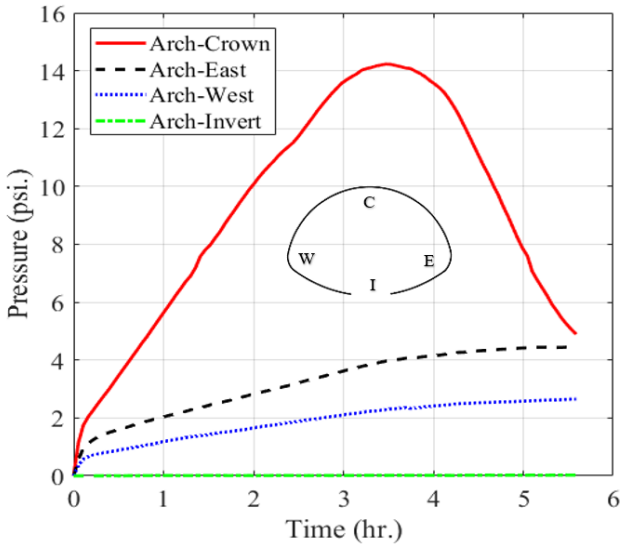


Figure 11-53. Results of earth pressure cells for the CMP control test: (a) intact circular CMP, (b) invert-cut circular CMP, and (c) invert-cut CMP arch.

The soil-structure interaction system of the invert-cut CMP arch, in comparison to the invert-cut circular CMP, showed a stiffer response to the initial stages of loading. After regaining its ring stiffness, the invert-cut circular CMP showed a stiffer response which was almost twice of its initial stiffness in the absence of ring stiffness. The earth pressure cells located at the East and West sides, for both invert-cut circular CMP and invert-cut CMP arch samples, showed that the passive pressures applied on both sides for the invert-cut circular CMP were almost twice the invert-cut CMP arch. This comparison of pressure values on both sides of the invert-cut samples indicated that the invert-cut CMP arch had less tendency towards horizontal expansion. The discrepancy between the results of the earth pressure cells located at the East and West sides of the invert-cut samples, as was illustrated in Figure 11-53, could be due to the uneven movement of the pipe samples after the invert-section detachment.

As it was illustrated in Figure 11-53 (c), the magnitude of pressure at the invert location shows a value of zero. The zero-pressure value indicates that in the absence of invert section no pressure was applied from the invert-cut CMP arch to the soil at the invert location. As illustrated in Figure 11-53 (b), the magnitude of the ultimate pressure in the existence of the pipe ring stiffness at the invert location for the invert-cut circular CMP sample showed a value of 2.7 psi that was not significant compared to the maximum registered pressure at the crown of the pipe sample. This could be due to a relatively larger movement of the circular CMP, in compare with the CMP arch, at the time of invert detachment and during the loading phase. As a summary, Table 11-7 presents the ultimate load and pressure and the maximum displacement of bare CMPs at the time of failure for the control test.

Table 11-7. Control test of bare CMPs - the ultimate load and pressure and the maximum displacement at the time of failure.

Pipe Sample	Ultimate Load (kips)	Pressure on Crown (psi)	Crown Deflection (in.)	Soil Surface Settlement (in.)
Intact CMP	24.8	75.38	4.87	9.68
Invert-cut Circular CMP	39.9	29.95	5.35	7.22
Invert-cut CMP arch	26.9	14.23	4.38	6.54

11.11.1.11 Results of Strain Gauges

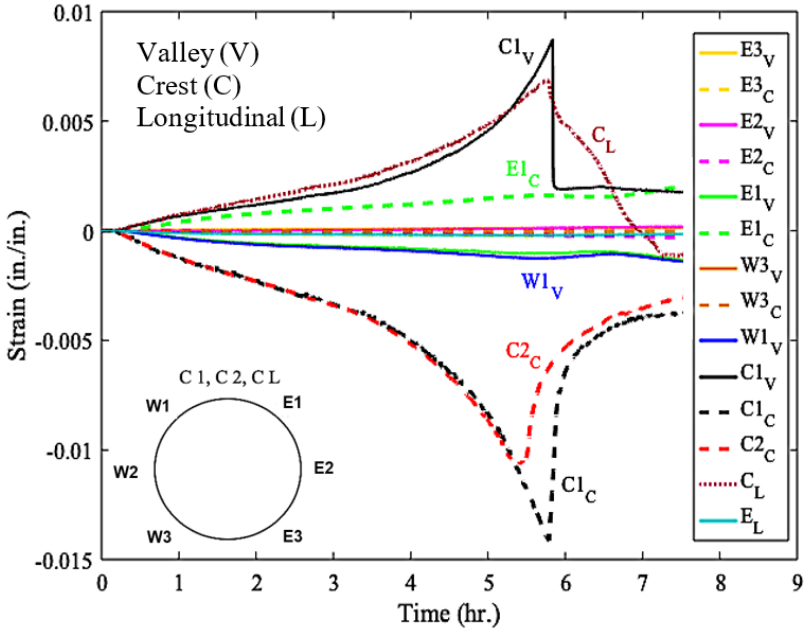
The results of strain gauges for the control test of CMPs are illustrated in Figure 11-54 (a, b and c). The intact circular CMP under the loading through a smaller load pad, compared with the invert-cut CMP samples under a bigger load pad, experienced relatively larger longitudinal strain (noted by "CL" in the figure) at the crown of the pipe, as shown in Figure 11-54 (a). The exerted load on the pipe through a smaller load pad resulted in a larger buckling curvature in longitudinal direction at the crown of the pipe.

The invert-cut circular CMP experienced the same pattern of buckling failure at the crown of the pipe. However, the invert-cut circular CMP, unlike the intact circular CMP and the invert-cut CMP arch, registered a lower strain value at the valley of the crown of the pipe compared to the shoulder locations. This could have resulted from the 2 in. circumferential movement due the invert detachment of the invert-cut circular CMP prior to the loading. Consequently, tensile stress on the exterior extreme fiber of the crest and a compressive stress on the interior extreme fiber of the valley at the crown of the pipe were exerted. Due to the vertical displacement of the crown of the pipe under the static load, the crest and valley were subjected to compressive and tensile stresses, respectively. These stress reversions (the existed stress in the pipe due to the pipe circumferential movement and the applied stress due to the static load) counteracted each other and caused a lower strain value at the crown of the pipe.

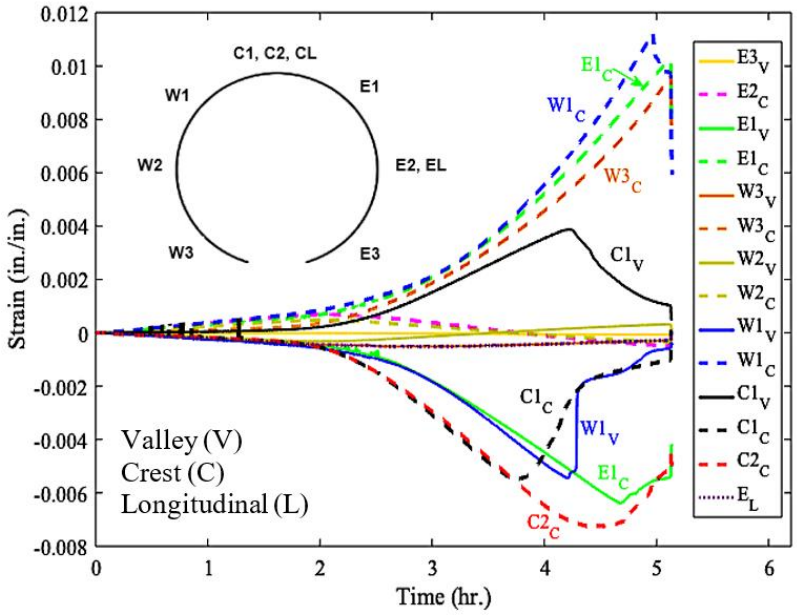
The invert-cut arch CMP registered a large strain value at the crown of the pipe and both shoulder locations, as shown in Figure 11-54 (c) that indicates the formation

of a three-hinge plastic collapse mechanism due to the local buckling at the crown. The same trend was also observed on the intact circular CMP sample.

(a)



(b)



(c)

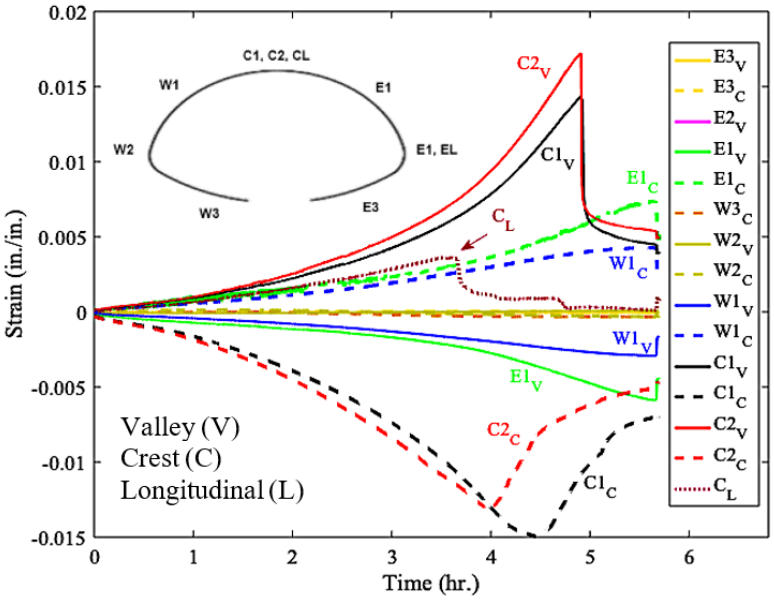


Figure 11-54. Results of strain gauges for the CMP control test: (a) intact circular CMP, (b) invert-cut circular CMP, and (c) invert-cut arch CMP.

11.11.1.12 Thrust Force and Bending Moment

For each CMP sample, once the first strain gauge registered the yield strain value of 1,138 με, the thrust force and bending moment values were calculated at seven locations around the pipe. Figure 11-55 (a and b) illustrates the thrust force and bending moment values around the CMP samples. It should be noted that a spline distribution was used to connect the seven available data points of bending moment and thrust force and estimate these values for other locations in between.

The intact circular CMP, invert-cut circular CMP and invert-cut CMP arch samples reached their yield strain at the soil pressure values of 26, 14.9 and 5.2 psi, on top of the pipes. At these pressures and at the time of reaching the yield strain, the CMP samples registered the values of 0.448, 0.304 and 0.474 kip-in./in. on top of the pipes, respectively, for the maximum positive bending moments of intact circular CMP, invert-cut circular CMP and invert-cut CMP arch. However, the shoulder areas registered the negative values of -0.175, -0.339 and -0.236, respectively, for bending moments of intact circular CMP, invert-cut circular CMP and invert-cut CMP arch. These sign changes are in conformity with the formation of the three-hinge plastic collapse mechanism at the crown of the CMP samples.

The thrust force values of -0.416, -1.002 and -1.027 kip/in. were calculated at the crown of the pipe samples, respectively, for the intact circular CMP, invert-cut circular CMP, and invert-cut CMP arch. It is noted that some of the strain gauges were damaged due to the soil backfilling and compaction. Hence, it was impossible to report their results.

(a)

(b)

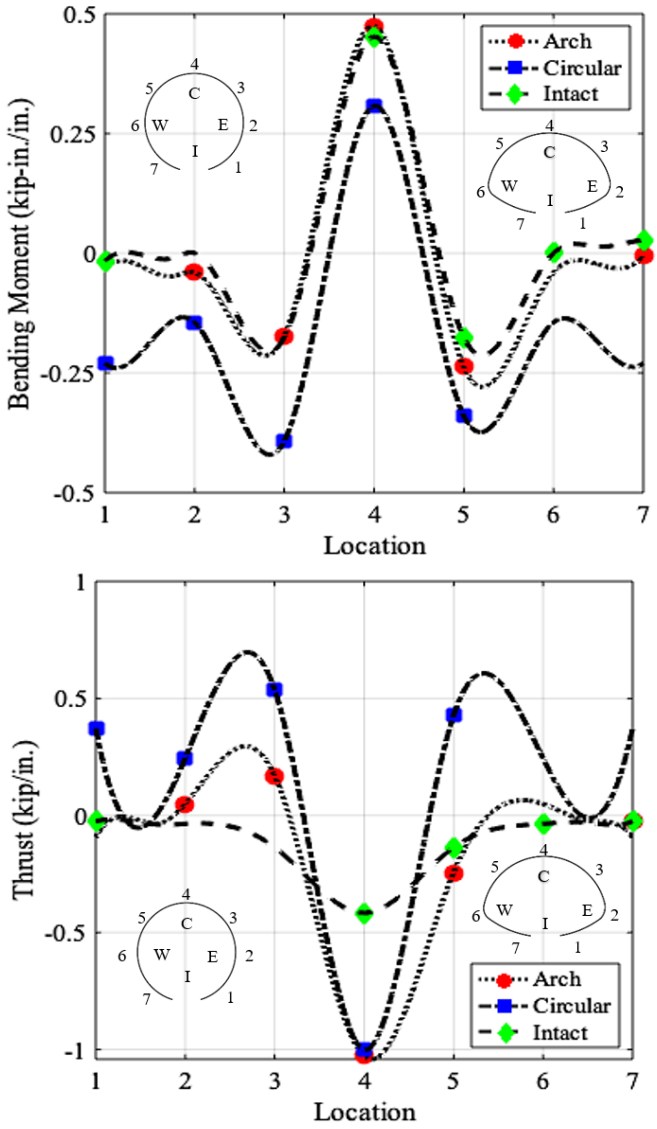
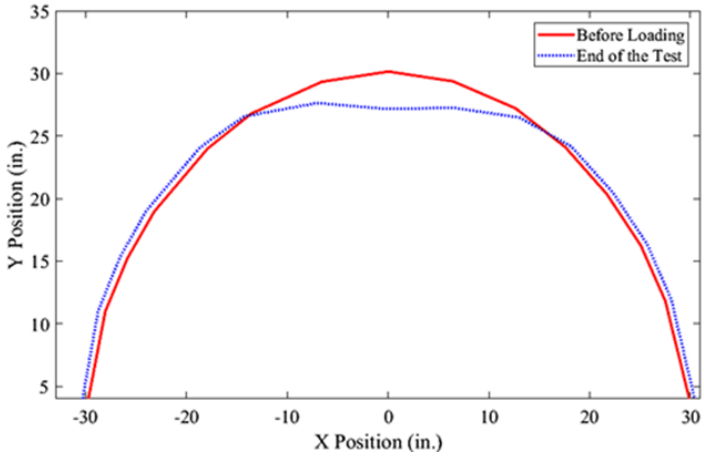


Figure 11-55. Internal forces on intact, invert-cut circular and invert-cut CMP arch samples: (a) bending moment, and (b) thrust forces for the invert-cut arch, invert-cut circular and circular intact CMPs.

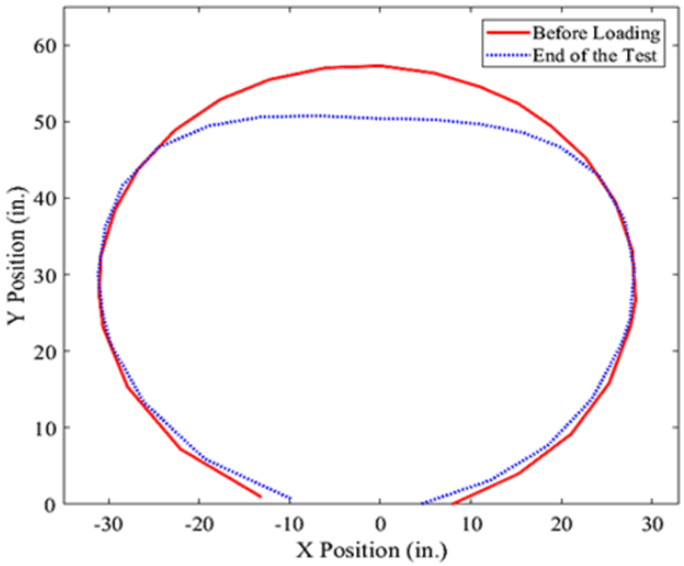
11.11.1.13 Results of DIC Deflection Measurement

The pipe profiling and deflection measurement using digital image correlation (DIC) results were illustrated in Figure 11-56. The readings are obtained from the middle section of the CMP samples under the load pad area. The failure mode of all CMP samples was local buckling at the crown of the pipe as it was clearly evident in Figure 11-55 (a and b). Due to the soil extrusion from the invert-cut section of the circular CMP sample under the loading (as a result of invert detachment), the installation of DIC targets was not possible at that location. Therefore, the invert gap closing was not captured with the DIC technique.

(a)



(b)



(c)

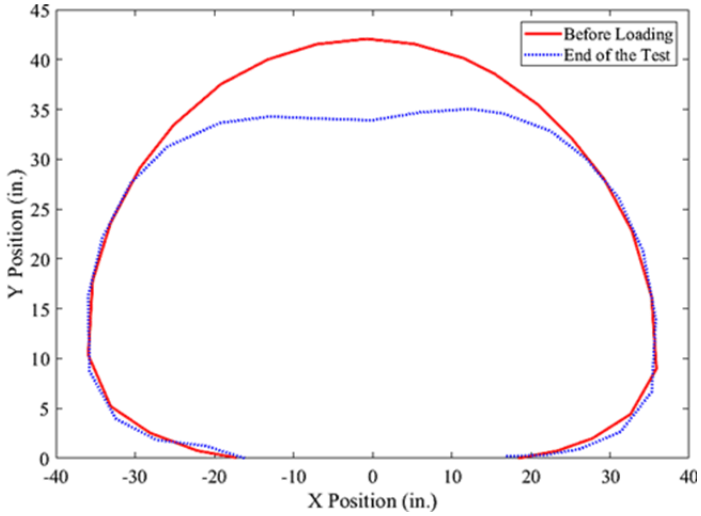


Figure 11-56. Pipe profiling using DIC results before loading and after loading at the ultimate load carrying capacity of the samples: (a) intact CMP, (b) invert-cut circular CMP, and (c) invert-cut CMP arch.

11.11.1.14 Summary of Bare CMP Control Tests

- The intact circular CMP could withstand the AASHTO H20 truck load and ultimately failed with a local buckling at the crown.
- The invert-cut circular CMP could withstand the equivalent AASHTO H20 truck load.
- The invert-cut circular CMP at the failure registered a larger horizontal movement in the absence of its ring stiffness compared with the invert-cut CMP arch that did not exhibit a significant horizontal movement.
- The invert-cut CMP arch could not reach the equivalent AASHTO H20 truck load prior to the ultimate failure. The ultimate load of the invert-cu CMP arch was 47% lower than the ultimate load of invert-cut circular CMP.
- The invert-cut CMP arch carried the superimposed loads by taking advantage of its flat area at the bottom for transferring the vertical loads to the soil, while the strength of invert-cut circular CMP was dependent on its ring stiffness.
- The initial load carrying capacity of the invert-cut circular CMP was due to the existence of frictional resistance between the outer surface of the CMP and soil. The frictional resistance is a function of the contact area between the CMP and soil, as well as the length of the pipe. A culvert in the actual field condition is longer than tested CMPs in the laboratory condition. Hence, a longer CMP in the field will experience a higher frictional resistance which can lock the pipe in place and therefore, it may reduce or eliminate the circumferential movement of the pipe. Resistance to circumferential movement of the CMP may facilitate or increase the chance of local buckling failure.

11.11.2 Polymeric SAPL

11.11.2.1 SAPL Renewed Circular CMP

11.11.2.1.1 SAPL Material Property Testing Results

The polymeric beam and dog-bone samples were tested according to the related ASTM standards. The results of the polymeric SAPL material property test are illustrated in Figure 11-57 (a and b). The polymeric SAPL's uniaxial tensile test showed the averaged maximum tensile stress was 8,671 psi with the standard deviation of 624 psi. The samples failed with the averaged maximum tensile strain of 0.0443 with standard deviation of 0.0031. Average elastic modulus of 329,210 psi was calculated through slop of the stress-strain line at initial stage.

The averaged maximum force resisted by the polymeric SAPL samples under the flexural test using 3-point bending configuration was 53.99 lb with the standard deviation of 2.23 lb. Consequently, the calculated averaged flexural modulus was

855,639 psi. The results of the tests are close to the manufacturers specifications (Johnson and Hammon 2017; TRI / Environment 2012).

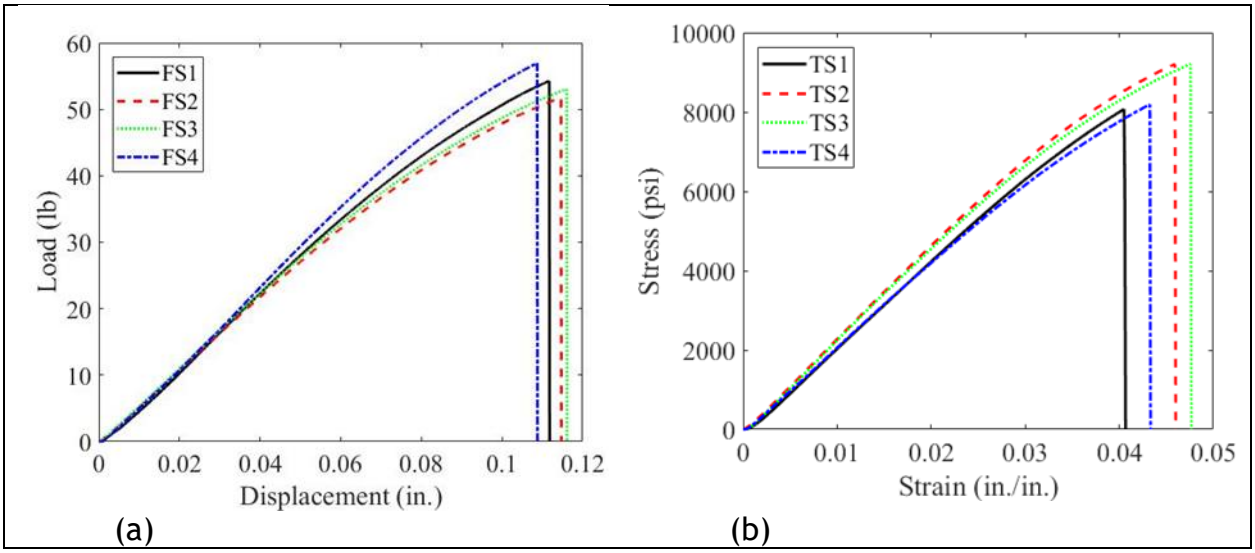


Figure 11-57. Polymeric SAPL material property test results: (a) flexural test (ASTM D790), and (b) tensile test (ASTM D638).

11.11.2.1.2 SAPL Thickness Survey Installed Inside Circular CMP

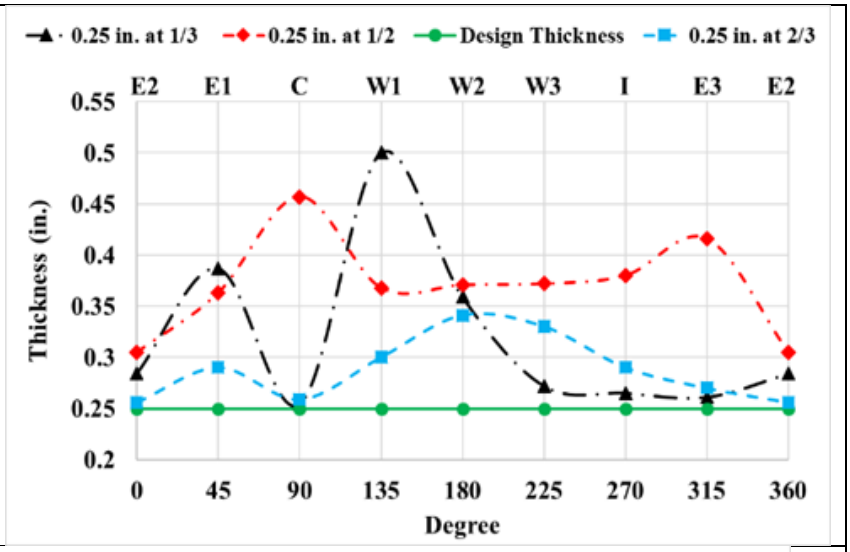
The thickness of the SAPL installed on the pipe samples were measured at three locations of approximately 1/3, 1/2, and 2/3 of the pipe sample's length. The measurement results showed that the applied thickness is usually higher at springline (i.e., locations W2 and E2 in Figure 11-58) than the design thickness. Opposite trend was observed at the crown locations (i.e., location C in Figure 11-58) where the thickness was lower than the required thickness. This alteration is more evident in the pipe sample with thicker SAPL which downward gravity force could result in the movement of the sprayed material toward the springline. Figure 11-58 (c) illustrates the thickness variation of SAPL on the 1.0 in. SAPL renewed CMP sample that shows the thickness was more uniformly applied at the center of the pipe in compare with both ends of the CMP. The same trend was observed for the 0.5 in. and 0.25 in. SAPL renewed CMP samples that could stem from the nature of hand-spray installation method of the polymeric SAPL. On the other hand, the installer had more space and ease of movement at the center of the pipe in compare with the pipe ends where the partition walls were located.

Once the structural test was carried out, the measured thickness locations with the ultrasonic thickness measurement device were drilled down to the CMP surface. A manual thickness measurement was conducted using a digital caliper to verify the accuracy of the ultrasonic thickness measurement. The results comparison showed an excellent correlation between both measuring methods, especially for thicker liners. For the 0.25-in. thick SAPL renewed CMP sample, the ultrasonic device was not able to

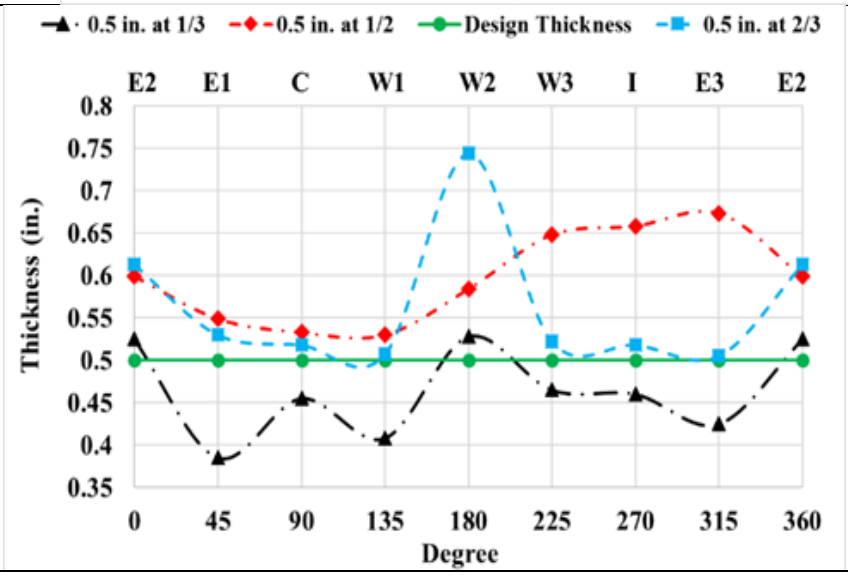
accurately measure the thickness at the location, 2/3 of the pipe's length, as was illustrated in Figure 11-9 (a). One possible reason could be due to the received higher volume of backscattered waves in low thickness such as 0.25 in. or lower that made the device unable to calculate the thickness accurately. Therefore, for this location (i.e., 0.25 in. at 2/3) the results of manual thickness measurements are presented in Figure 11-58 (a).

The visual observation on 0.25 in. SAPL renewed CMP showed the applied SAPL thickness on the seam of CMP was not sufficient and, in many sections, there was discontinuity on the liner at the seam locations. However, this issue was not observed on the 0.5 in., and 1.0 in. thick SAPL pipe samples, which implies the quarter inch thickness may not be sufficient or requires additional coverage at the seam locations.

(a)



(b)



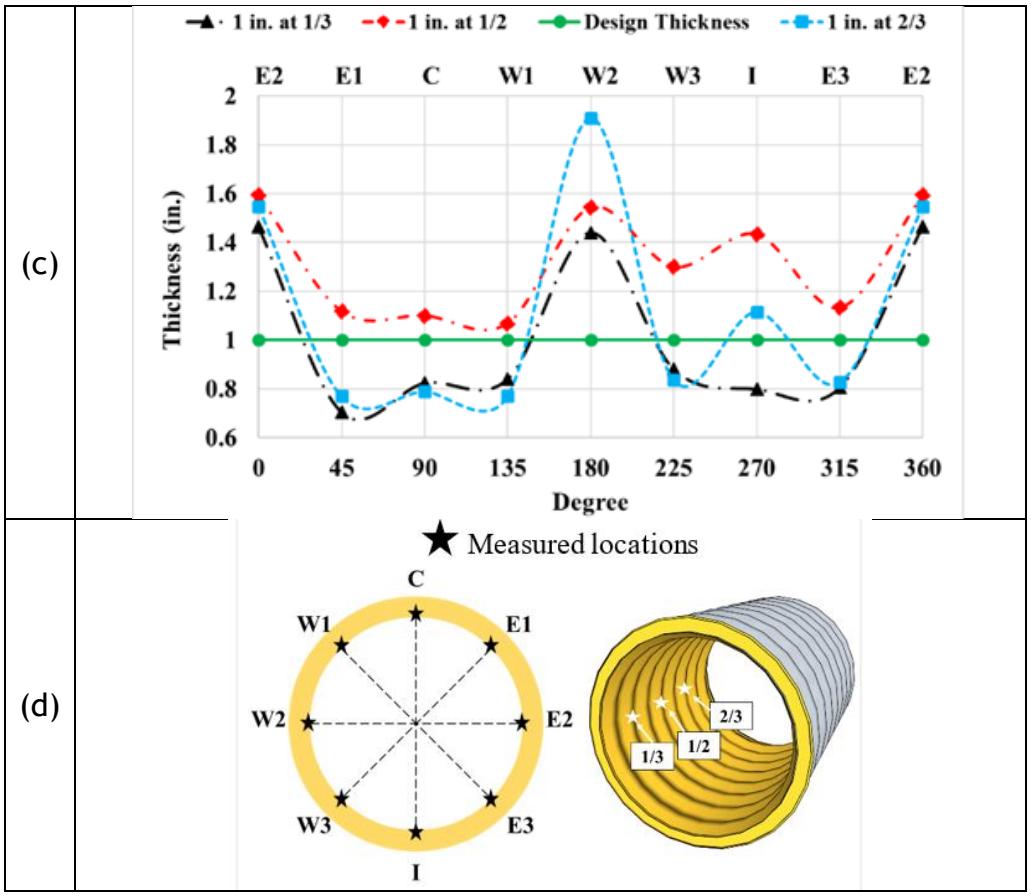


Figure 11-58. Thickness measurement results of polymeric SAPL renewed circular CMPs: (a) 0.25 in. thick SAPL, (b) 0.5 in. thick SAPL, (c) 1 in. thick SAPL, and (d) measured locations in circumferential and longitudinal direction.

11.11.2.1.3 Comparison of Bare and SAPL Renewed Circular CMPs Load Bearing Capacities (Responses to Static Load)

The static load was applied on the soil surface at the middle section of the CMP through a 20×40 in. steel load pad. The load was continuously applied with a load rate of 0.03 in./min. Figure 11-59 (a, b, c and d) illustrates the results of load-deflection of soil-CMP samples due to the applied load for the bare invert-cut CMP, and all three SAPL renewed circular CMPs. The invert-cut bare CMP, in the absence of the invert section and its ring stiffness, initially resisted the applied load on the soil surface until about 5 kips, which is believed to be due to the friction resistance force of the soil-pipe system. Once this limit was reached there was no other resisting force to prevent the pipe sample circumferential movement. Therefore, with progression of the load, the CMP moved continuously until both sides of the invert-cut section contacted each other and as a result the CMP's ring stiffness was restored. Afterward, the system showed a significantly stiffer response to the applied load and resisted until 39.9 kips of load. At this load, the corresponding soil surface settlement was almost 7.22 in. and the crown's deflection was 5.8 in.

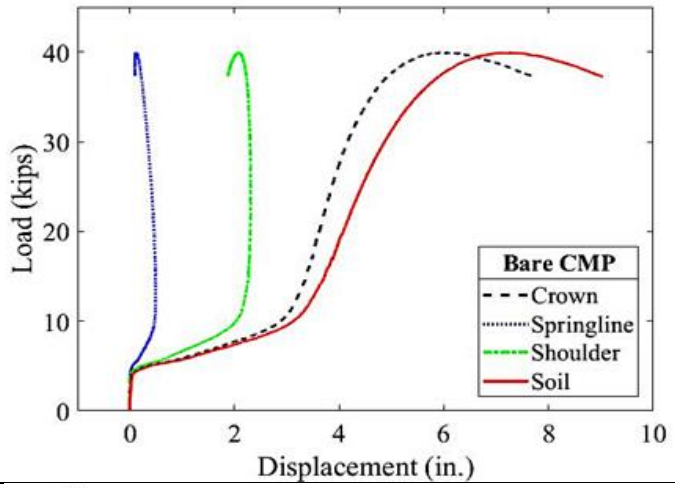
Contrary to the invert-cut bare CMP, the SAPL renewed CMP samples were able to resist the applied load without any sign of cracking or fracture at the invert location, which is not protected by the host pipe. This indicates that the polymeric SAPL was structurally capable to solely withstand the applied ring compression. In the 0.25 in. SAPL renewed CMP, the first structural crack was observed at the load of 39 kips with 2.12 in. of SAPL-CMP deflection at the crown. The CMP sample buckled at the crown, along with the SAPL crack that initiated and propagated in the longitudinal direction, as shown Figure 11-59 (a). Once the crack reached the interlocking seam of the CMP, it was diverted along the seam direction in the circumference of the CMP. This is due to the insufficient SAPL thickness at the seam location that cause SAPL discontinuity at these locations. The 0.25 in. renewed pipe sample failed at the load of 46.38 kips, as illustrated in Figure 11-59 (b).

The 0.5-in. SAPL showed a similar response to the applied surface load and cracked longitudinally at the crown when 42.78 kips of load was applied on the soil surface that induced 1.75 in. crown deflection. The SAPL-CMP system reached its ultimate load carrying capacity prior to the soil failure and eventually failed at the load of 52.43 kips. Although it was expected to observe larger load carrying capacity enhancement from 0.25 in. SAPL to 0.5 in. SAPL, the ultimate load bearing capacity was improved by 13%. This can be due to the relatively small difference between the applied SAPL thicknesses on 0.25 and 0.5 in. SAPL renewed CMPs at the crown locations, as discussed in the SAPL thickness survey section. The 0.5 in. SAPL renewed CMP's response to the applied soil surface load is illustrated in Figure 11-59 (c). It is noteworthy that the initial drop in Figure 11-59 (c) between the loads 25 to 35 kips was due to the detachment of the over sprayed SAPL material between the CMP and the partition walls. Exercise were made to keep the renewed CMPs fully disconnected form the partition walls including installation of plastic sheets at the edges prior to the SAPL installation and make a thin notch after the installation. However, a few points remained connected at the shoulder area as it was highly concerned that a deep cut would tear the Styrofoam placed at the CMP-partition wall area which would cause soil ingress into the pipes. Therefore, it was decided to only have the notches instead of a full cut at those locations.

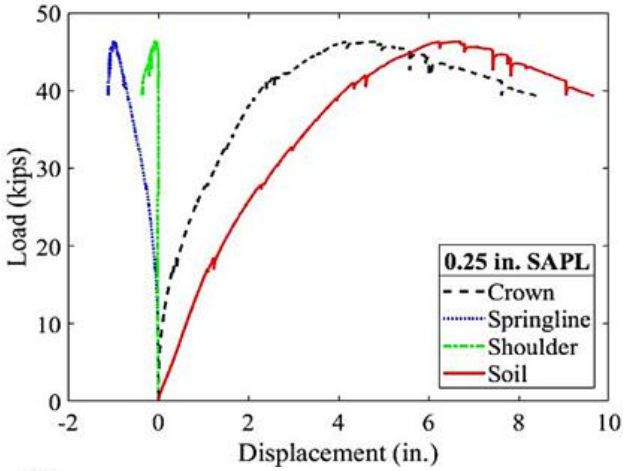
The 1-in. SAPL showed relatively stiffer response compared with the other renewed CMP samples and cracked longitudinally at the crown with the load of 66.26 kips and the 2.12 in. of pipe deflection that released a relatively larger amount of energy. The energy release is also evident in Figure 11-59 (d), where a large drop in the load displacement graph at the time of the first crack initiation was registered by LVDT sensor. This phenomenon can be related to the lower diameter over thickness ratio of the SAPL-CMP system that provides higher stiffness to the system. On the contrary, the higher diameter to thickness ratio of the lower SAPL thickness (i.e., 0.25 and 0.5 in.) resulted in more flexible behavior of the SAPL-CMP system. The higher stiffness of the 1-in. SAPL resulted in an instantaneous crack throughout the crown, while for the ¾-in. and ½-in. SAPL samples, a small crack initiated at the center of the pipe at the crown and propagated with the increase of the load, as shown in Figure 11-60 (a, b, and c). The 1-in. SAPL eventually failed at the load 72.15 kips, which was

about 20 kips higher than the 0.5 in. SAPL renewed sample. The circular CMPs' load bearing capacity, crown deflection at initial crack and failure as well as the soil displacement in both initial crack and failure stages are summarized in Table 11-8.

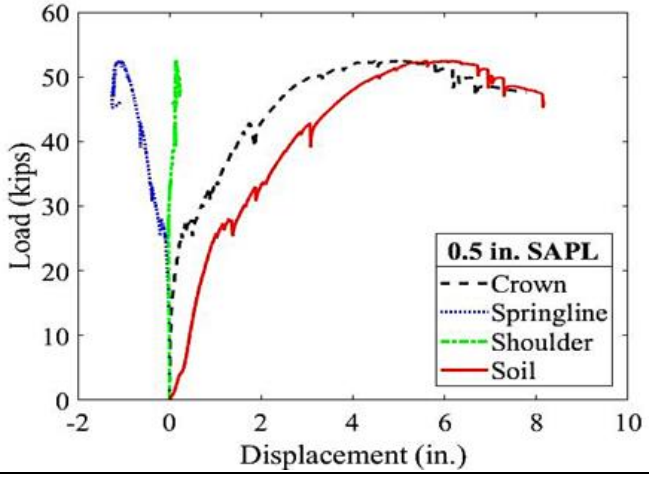
(a)



(b)



(c)



(d)

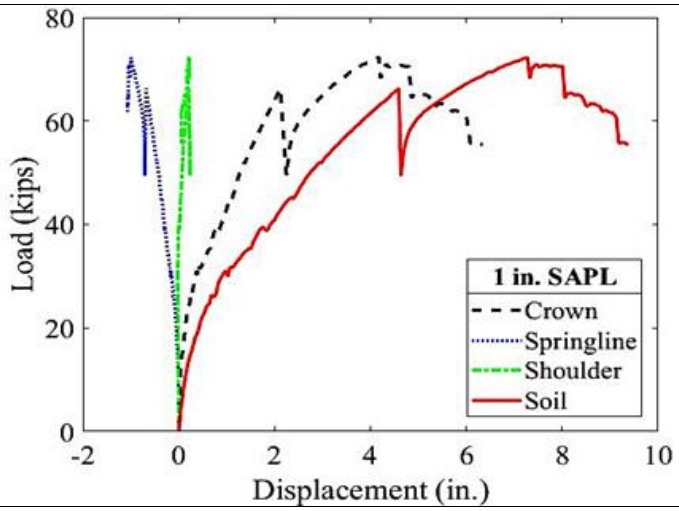
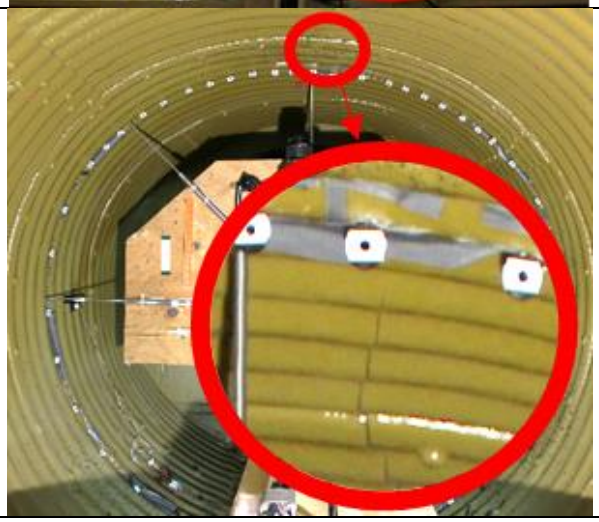


Figure 11-59. Load vs. displacement results for CMP samples and soil: (a) bare invert cut CMP, (b) 0.25 in. SAPL renewed CMP, (c) 0.5 in. SAPL renewed CMP and (d) 1 in. SAPL renewed CMP.

(a)



(b)



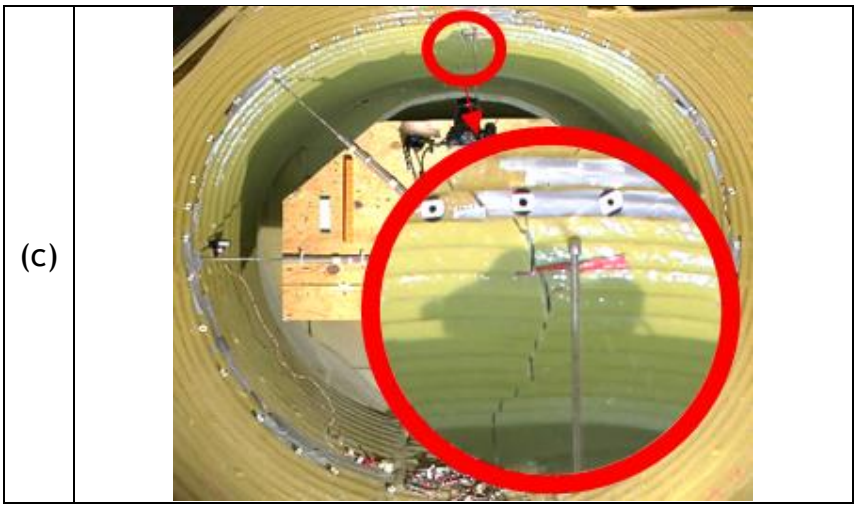


Figure 11-60. Formation of the first structural crack. It shows (a) 0.25 in. SAPL renewed circular CMP at 39 kips, (b) 0.5 in. SAPL renewed circular CMP at 42.78 kips, and (c) 1 in. SAPL renewed circular CMP at 66.26 kips.

The circular CMPs' load bearing capacity, crown deflection at initial crack and failure as well as the soil displacement in both initial crack and failure stages are summarized in Table 11-8.

Table 11-8. The circular CMPs' load bearing capacity, crown deflection and the soil displacement at initial crack and failure.

Test Setup		Initial Structural Cracking Stage			Failure Stage		
		Load (kips)	Pipe Deflection at Crown (in.)	Soil Displacement (in.)	Load (kips)	Pipe Deflection at Crown (in.)	Soil Displacement (in.)
Bare Invert-cut CMP		-	-	-	39.9	5.8	7.22
SAPL Renewed CMP	0.25 in. SAPL	39	2.12	3.95	46.38	4.83	6.69
	0.5 in. SAPL	42.78	1.75	3.06	52.43	4.43	5.61
	1 in. SAPL	66.26	2.12	4.58	72.15	4.17	7.27

Comparison between the ultimate loads of the SAPL renewed circular CMPs and the bare invert-cut CMP showed that the application of SAPL increases the ultimate load bearing capacity of the invert corroded CMP. The improvement rate for the quarter, half, and one-inch thick SAPL is 16.24, 34.4, and 80.82%, respectively, which is illustrated in Figure 11-61 (a). Considering the pipe deflection at the time of the first crack in Figure 11-59 shows all SAPL renewed pipes were cracked at about 2 in. of pipe deflection, which is 3% of pipe diameter. The bare CMP's load response at 2 in.

deflection was 7.34 kips. Figure 11-61 (b) illustrates that the application of 0.25 in., 0.5 in., and 1 in. polymeric SAPL increased the load carrying capacity at this pipe deflection for 471.7, 482.8, and 802.7%, respectively.

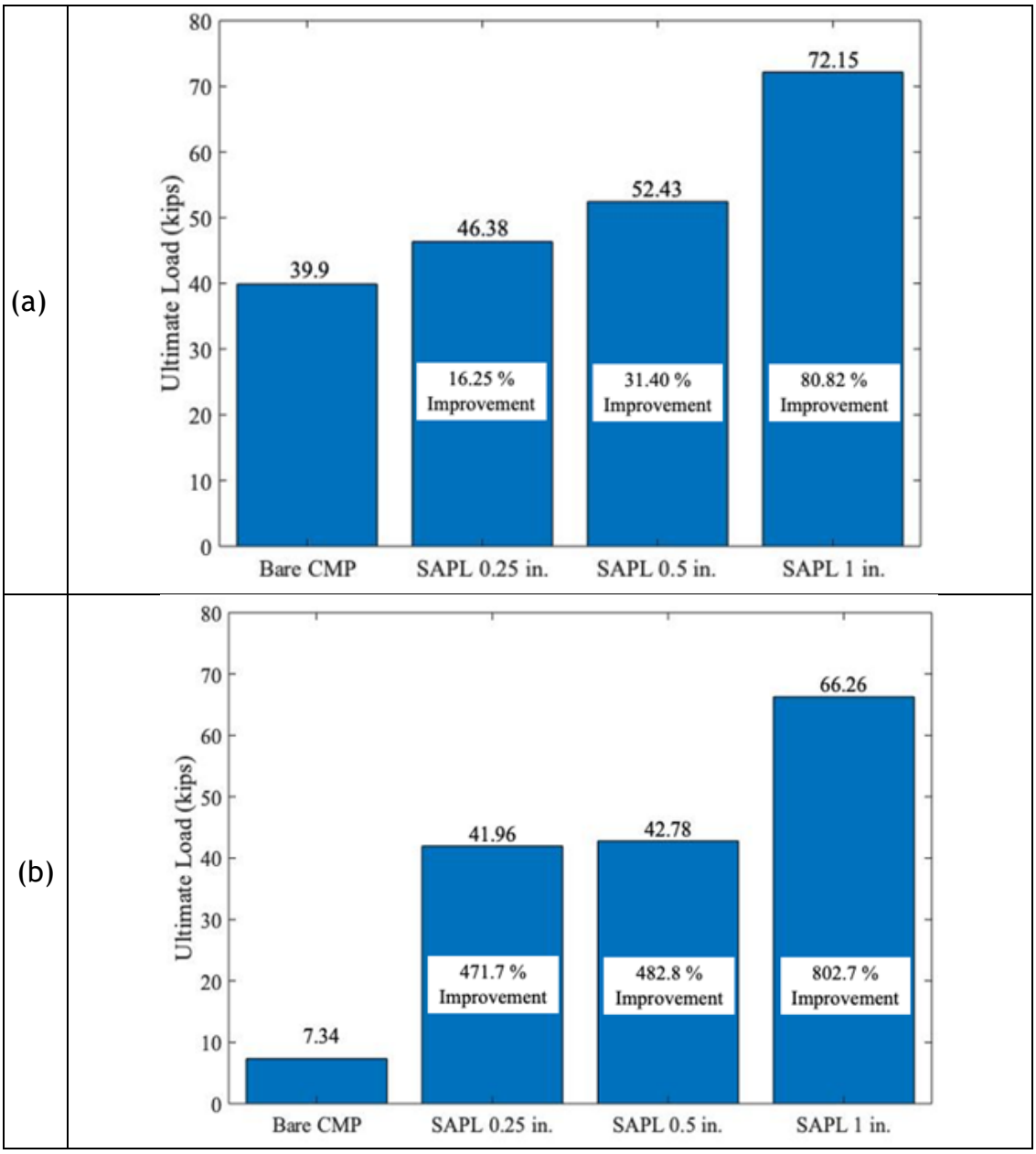


Figure 11-61. Load improvement by SAPL application: (a) ultimate load comparison of renewed SAPL circular CMPs with bare CMP, and (b) load comparison of renewed SAPL CMPs with bare CMP at 2 in. pipe deflection.

11.11.2.1.4 Pressure around the circular CMPs (Earth Pressure Cell Results)

During the tests, the earth pressure cells recorded the applied pressure around the CMP samples. Figure 11-62 (a, b, c, and d) illustrates the applied pressure all around the pipes. The maximum pressure registered by the earth pressure cell on top (i.e.,

crown) of the bare CMP was 30 psi. The maximum pressure value for the 0.25 in., 0.5 in., and 1 in. SAPL renewed CMPs were 42, 42.11 and 71.61 psi, respectively. Similar to the load-deflection graphs, there is no substantial pressure difference between the crown pressures of 0.25 in. and 0.5 in. SAPL renewed CMP samples. This could be due to the minimal thickness difference of both SAPL samples at the crown locations. However, the applied thickness at both sides of the springline (i.e., East and West) in the 0.5 in. SAPL renewed samples was almost two times greater than the 0.25 in. SAPL renewed sample that could be the reason for the pressure difference between two CMPs. The 0.25 in. SAPL renewed CMP experienced 4.6 psi at the west location and 4.93 psi at the East location. While the applied pressures on the East and West locations of the 0.5 in. SAPL renewed CMP were 6.19 psi and 8.86 psi, respectively, which were relatively higher than the 0.25 in. sample. The pressure values for the East and West sides of the 1 in. SAPL renewed CMPs were 13.93 psi and 8.407 psi, respectively. The results of the earth pressure sensors at the crown of the CMPs implied that the pressure response of the soil-CMP system was directly affected by thickness of the applied SAPL. The soil pressure around the CMPs were recorded by the earth pressure cells and are summarized in Table 11-9.

Table 11-9. Soil pressure results around the circular CMPs at the time of failure.

Test Setup		Pressure (psi)			
		Crown	Invert	East	West
Bare CMP		30	2.78	7.33	9.66
SAPL Renewed CMP	0.25 in. SAPL	42	1.34	4.93	4.6
	0.5 in. SAPL	42.11	5.06	6.19	8.86
	1.0 in. SAPL	71.61	1.72	13.93	8.407

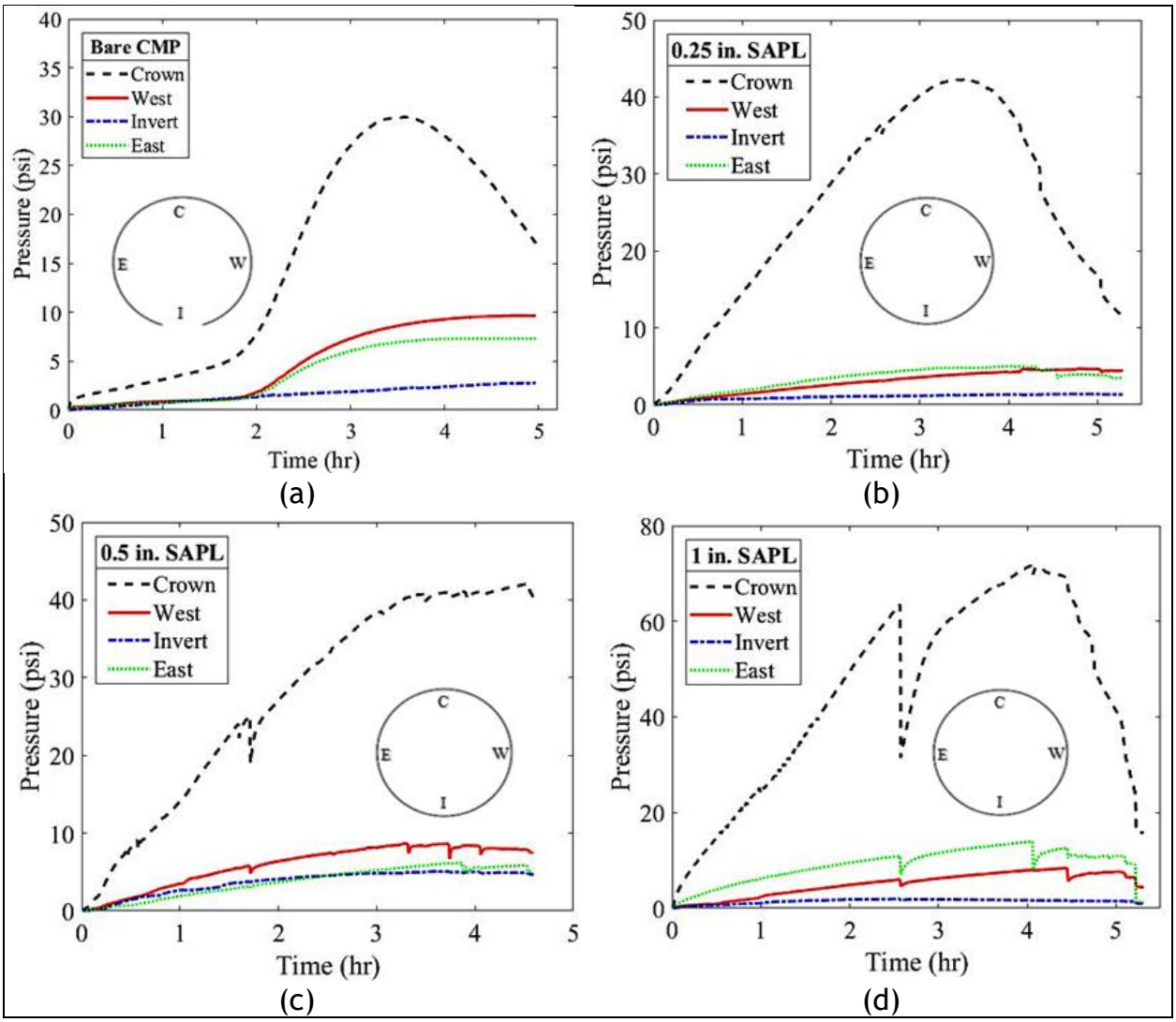


Figure 11-62. Earth pressure cells' results: (a) bare circular CMP, (b) 0.25 in. SAPL renewed circular CMP (c) 0.5 in. SAPL renewed circular CMP and (d) 1 in. SAPL renewed circular CMP.

11.11.2.1.5 Strain Gauges Results for SAPL Renewed Circular CMPs

The strain values of the crown for circular CMPs and liners are illustrated in Figure 11-63 (a). The maximum strain was registered by the host pipe of the 0.25-in. SAPL sample at the time of failure. The 1-in. SAPL renewed CMP registered relatively lower strain value compared with the 0.25-in. SAPL renewed CMP sample. However, the 1-in. SAPL sample registered the largest strain at the time of the first structural crack at the crown location. Figure 11-63 (b) illustrates the results of the SAPL strain values at time of first structural crack for other locations, such as shoulders, springline, haunches, and invert. The maximum strain occurred at the crown which is located directly under the load area. In addition, it can be observed that the thicker SAPL resulted in higher strain value at the time of cracking. It should be noted that due to the aggressive environment of the soil box and existence of moisture

content, some strain gauges outside of host pipe, including the crown of 0.5-in. SAPL, were either damaged or not responsive.

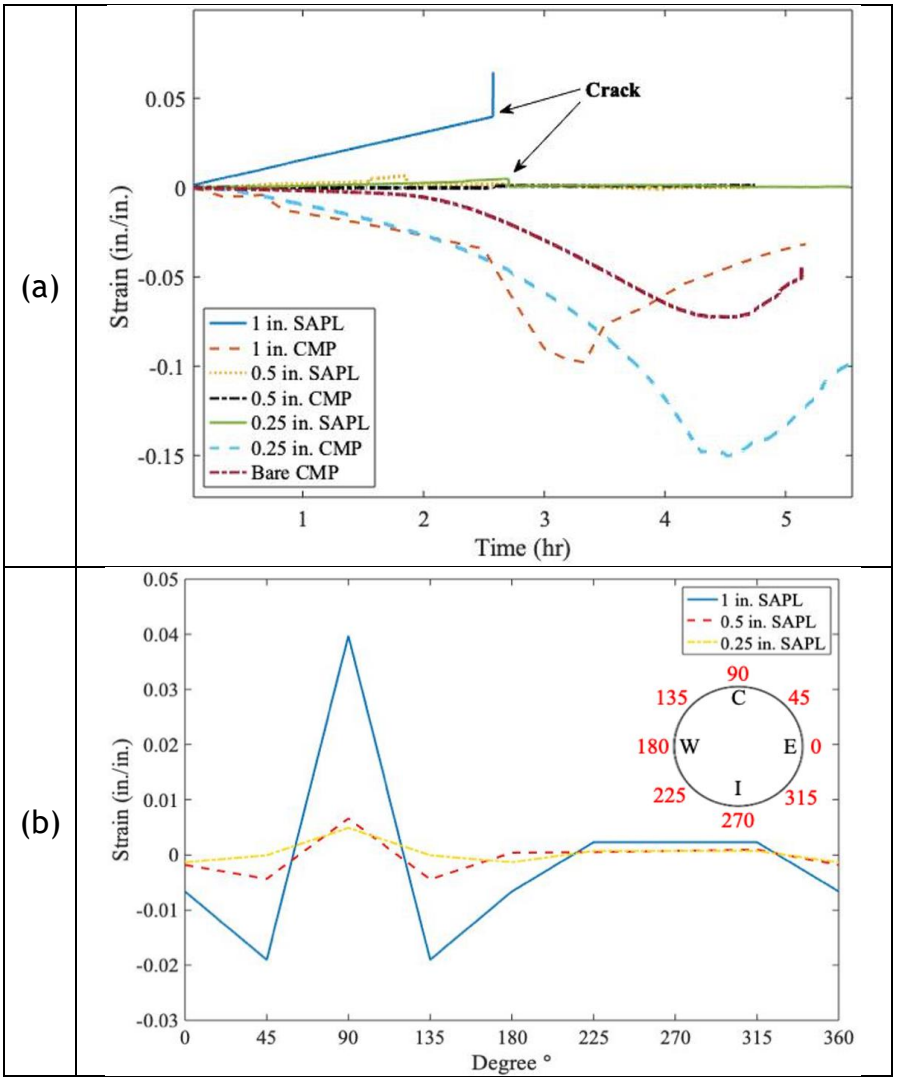


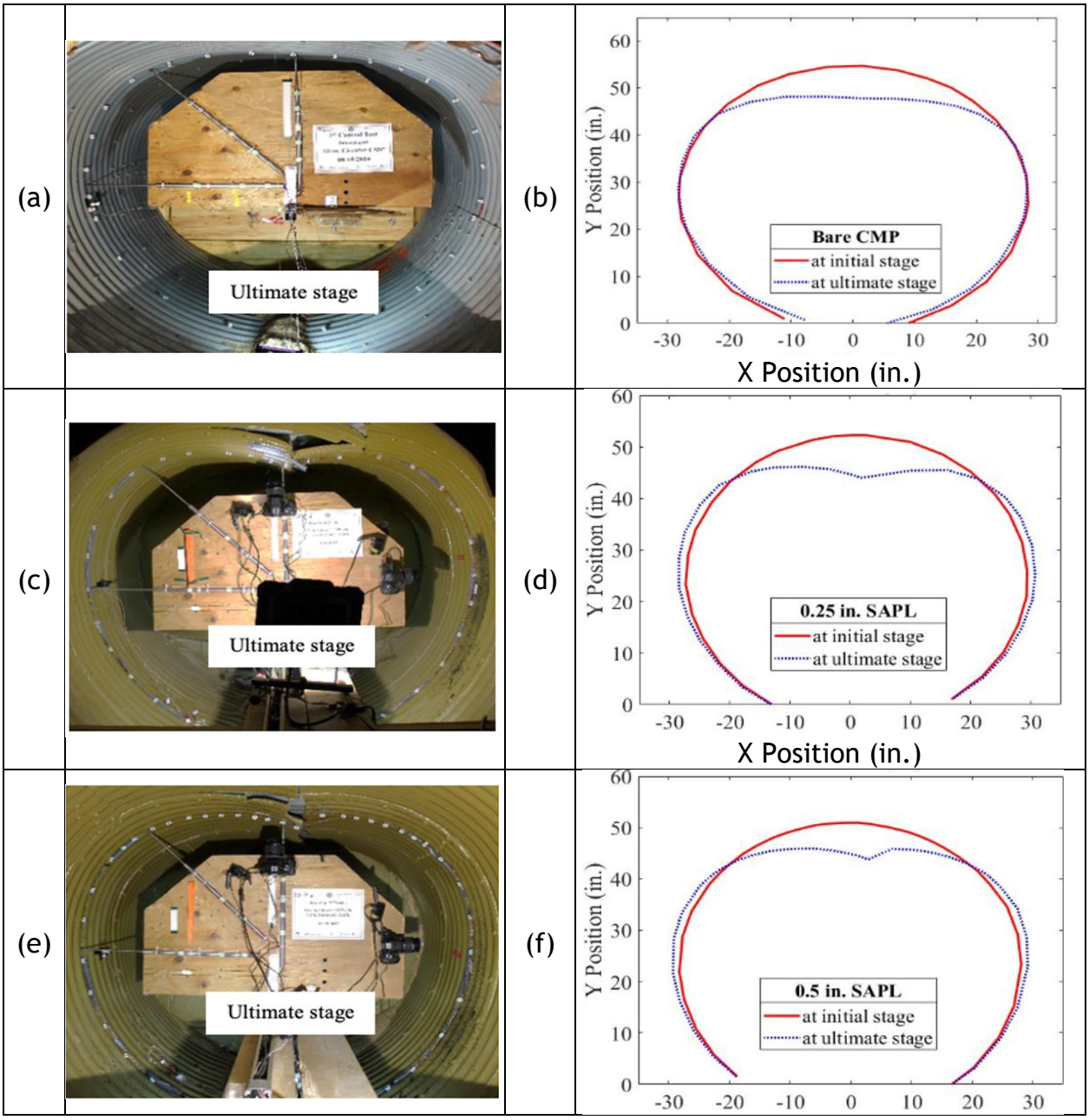
Figure 11-63. Strain gauge results for SAPL renewed circular CMP: (a) at the crown and (b) around the SAPL at the time of first structural crack.

11.11.2.1.6 Pipe Profile Measurement using DIC for SAPL Renewed Circular CMPs

The middle ring profile renewed pipe profile was measured during the test using digital image correlation (DIC) technique. Figure 11-64 illustrates the results of pipe deflection measurement before and after the loading. The comparison of crown deflection measurement DIC technique with mechanical sensors (i.e., LVDT & CDS) revealed that the both measuring methods have an excellent conformity (Darabnoush Tehrani et al. 2020b).

Pipe profiling showed that the bare CMP had movement in both horizontal and vertical directions during the loading. The bare CMP sample failed due to the buckling

at the crown, which is evident in the invert of the plotted CMP profile in the Figure 11-64 (b). Application of SAPL sustained the pipe's ring stiffness and as the result, no movement in the invert of all three SAPL renewed samples was observed. In addition to that, the SAPL renewed samples had horizontal expansion at the springline and shoulder areas as well as vertical deflection. The fracture at the crown is evident in Figure 11-64 (d), (f), and (h). The DIC results implied that for all CMP samples, the mode of failure was local buckling of the crown section. The buckling caused CMP deformation in the bare CMP and cracking and fracture of the crown of the SAPL samples. It is noteworthy that due to the existence of the instrumentation frame's beam and wires, illustration of the full pipe's ring was not possible. Figure 11-65 (a, b, and c) illustrates pipe profiling of SAPL renewed circular CMPs at the time of failure.



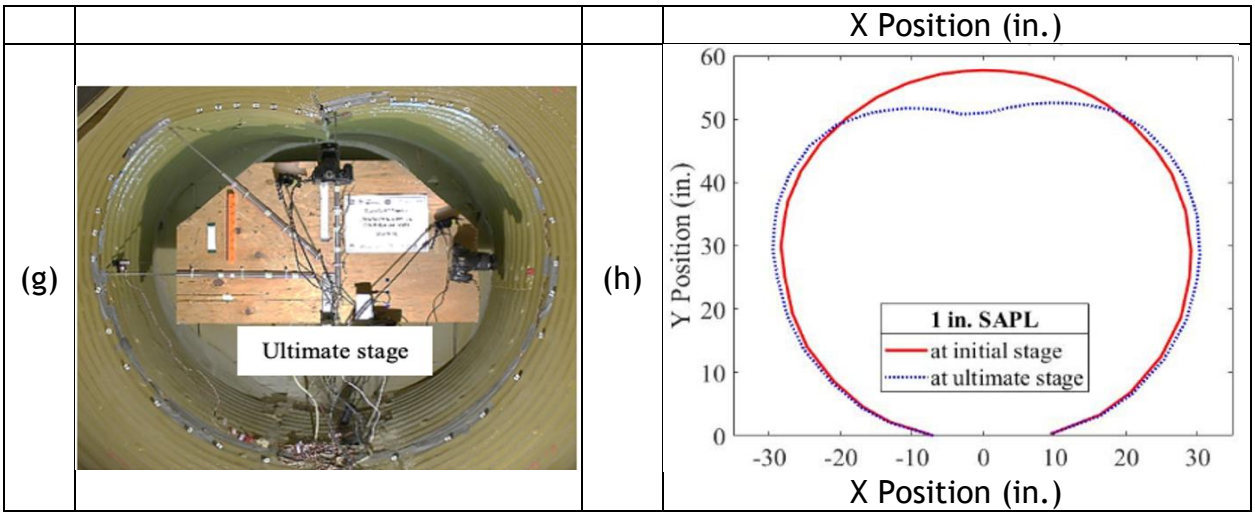
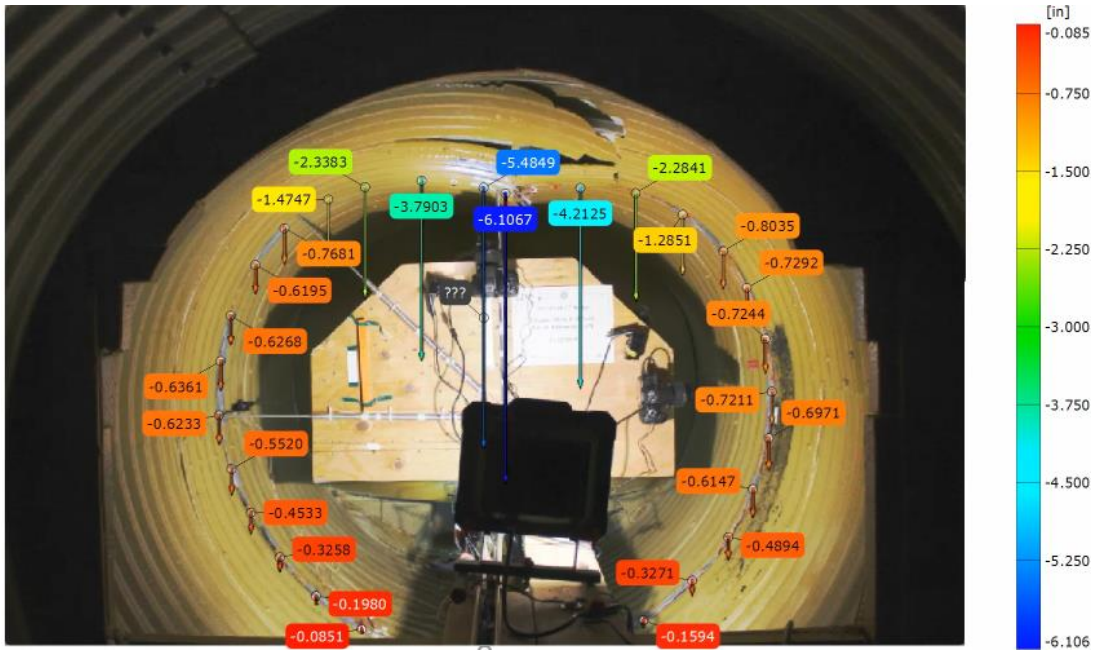
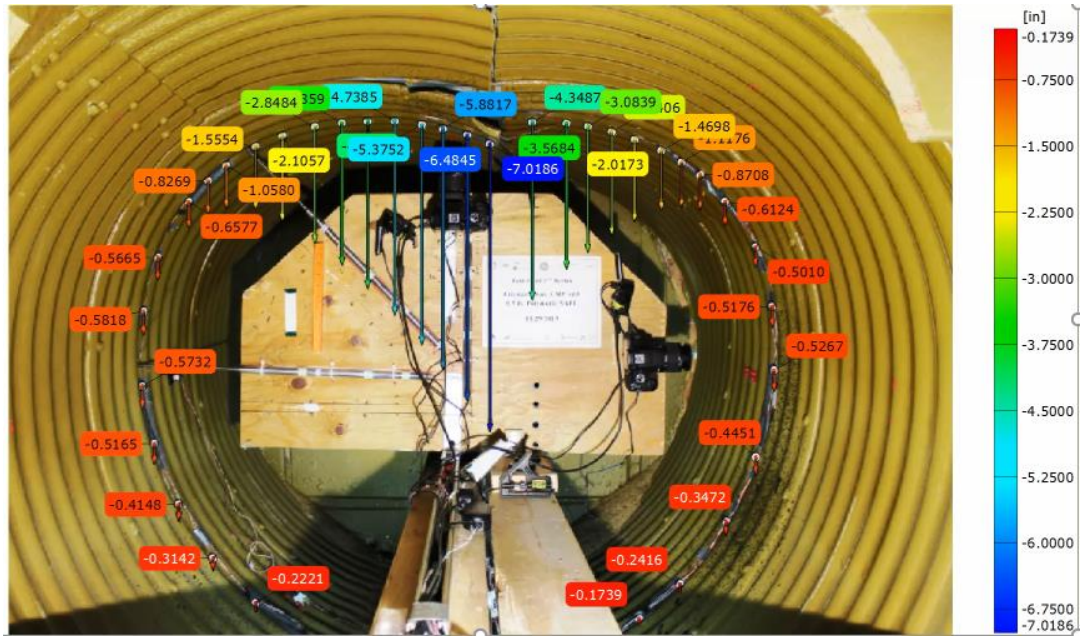


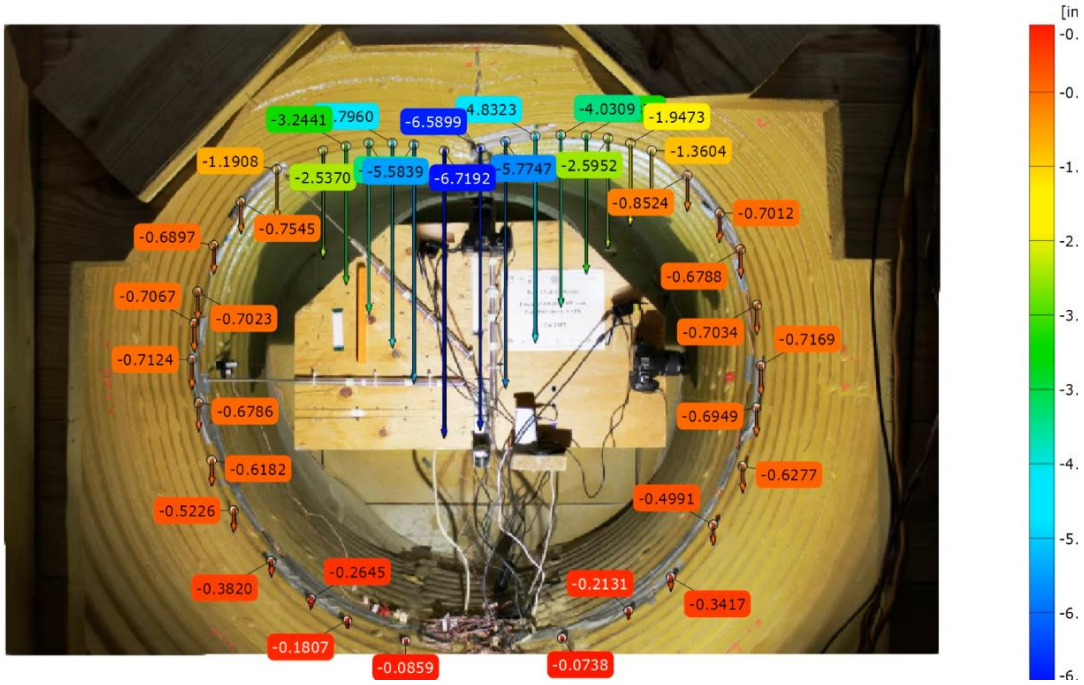
Figure 11-64. DIC results of SAPL renewed circular CMP: (a) and (b) bare CMP, (c) and (d) 0.25 in. SAPL renewed CMP, (e) and (f) 0.5 in. SAPL renewed CMP, (g) and (h) 1 in. SAPL renewed CMP.



(a)



(b)



(c)

Figure 11-65. Pipe profiling using DIC technique at the time of failure: (a) 0.25 in. SAPL, (b) 0.5 in. SAPL, and (c) 1.0 in. SAPL renewed circular CMP.

11.11.2.1.7 Summary of Polymeric SAPL Renewed Circular CMP Testing

- The physical property test results demonstrated that the polymeric SAPL had the averaged maximum tensile stress of 8,670.78 psi, elastic modulus of 489,500 psi, and flexural modulus of 855,639 psi.

- The results of thickness measurement showed that the utilization of hand spray for installation of the polymeric SAPL resulted in a thicker liner at the springline for all renewed CMPs than the designated thickness. However, the SAPL was installed closer to the required thickness at crown and both shoulders. One of the possible reasons for the inconsistent thickness installation could be due to the sagging and movement of the SAPL material at the initial stage (i.e., before hardening) of installation due to gravity.
- All SAPL renewed pipes cracked at about 3% of the SAPL-CMP system deflection, where at this deflection the application of 0.25 in., 0.5 in., and 1 in. polymeric SAPL increased the load carrying capacity for 471.7, 482.8, and 802.7%, respectively.
- Application of the polymeric SAPL increased the stiffness of the invert-cut CMP. The SAPL renewed CMPs with the thicknesses of 0.25 in., 0.5 in., and 1 in. increased the ultimate load bearing capacity of the invert deteriorated CMPs for 16.24, 31.4, and 80.82%, respectively.
- The CMP with thinner liner (i.e., 0.25 in.) was susceptible to crack at the seam locations, where the liner's thickness was not sufficient to prevent cracking. Although the first crack was initiated in the longitudinal direction, once it reached the seam locations, it was diverted towards the circumferential direction.
- The CMP with 1 in. thick SAPL showed stiffer response to the applied load as compare with thinner SAPL renewed pipe samples. In contrast with the other samples, no circumferential crack was observed in the pipe sample.
- The SAPL renewed CMP samples with the thicknesses of 0.25 in., 0.5 in., and 1 in. cracked at 3.52, 2.9, and 3.65% of crown deflection, respectively.
- In the absence of the host pipe's ring stiffness, the SAPL was able to resist the ring compression solely. Therefore, the polymeric SAPL can be considered structurally sufficient to withstand the applied load and improve the overall load bearing capacity of the fully deteriorated host pipe.

11.11.2.2 SAPL Renewed Arch CMP

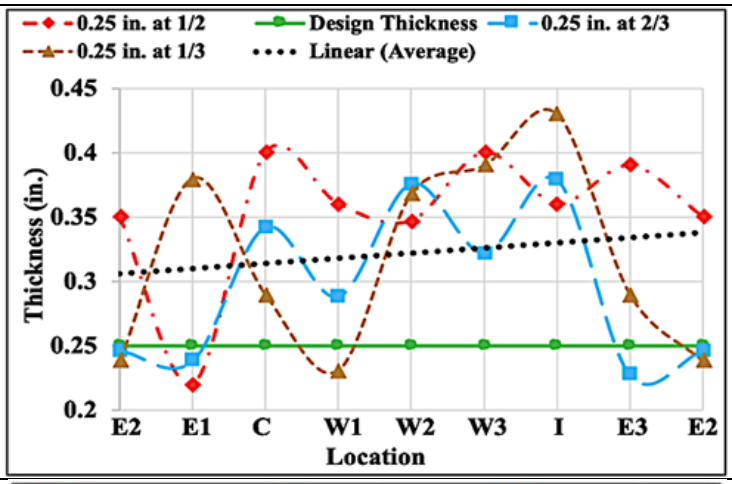
11.11.2.2.1 SAPL Thickness Survey Installed Inside Arch CMP Samples

Figure 11-66 (a, b, c and d) Illustrates the results of the SAPL thickness measurement that was conducted by an ultrasonic gauge at three locations of approximately 1/3, 1/2, and 2/3 of the pipe sample's length, and eight location on the pipe circumference. It was observed that in almost all locations, the applied thickness was higher than the design thickness could be due to the factor of safety, considered in the required SAPL quantity calculation presented in section 11.9.2. For the quarter inch SAPL renewed CMP arch the average thickness was approximately 0.33 in., where

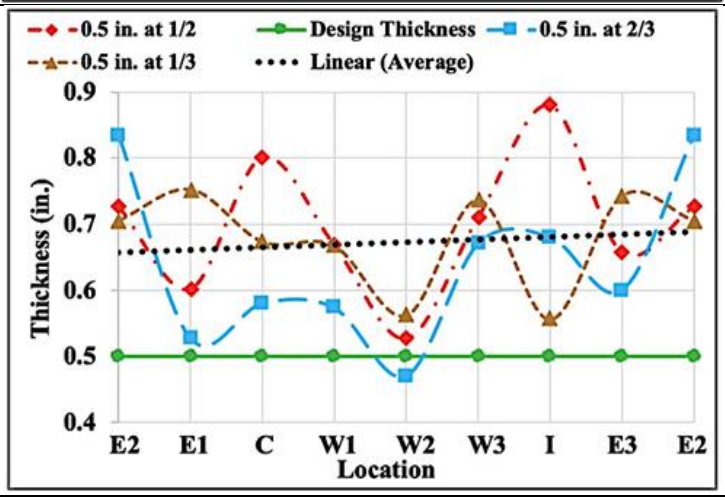
the liner thickness was higher on the invert section. The average thicknesses for half and one inch SAPL renewed CMP arch samples were 0.66 and 1.2 in., respectively.

A digital caliper was used to conduct a manual thickness measurement after the structural testing was carried out. The results showed an excellent agreement between both manual and ultrasonic measurement methods. The visual observations on quarter inch SAPL renewed CMP arch showed the applied SAPL thickness on the seam locations were not sufficient and discontinuities were observed on the liner. For the half and one inch thick SAPL pipe samples, this issue was completely resolved. That implies the 0.25 in. thickness requires additional consideration on the seam locations.

(a)



(b)



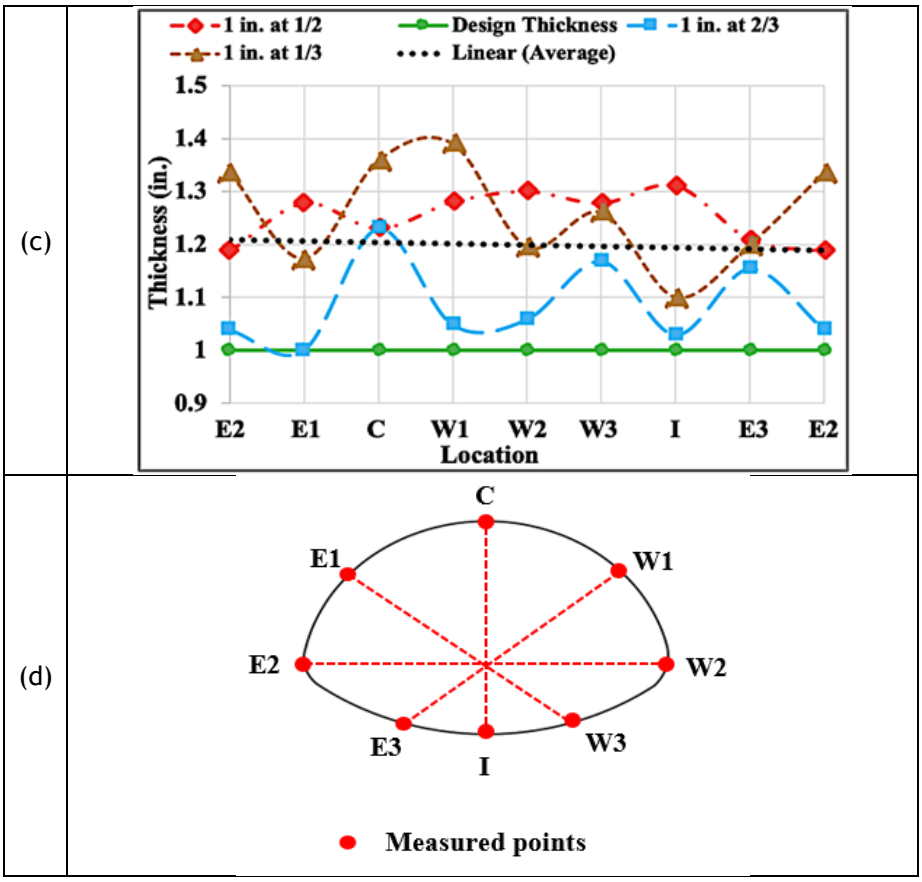


Figure 11-66. Thickness measurement results of polymeric SAPL renewed CMPAs: (a) quarter, (b) half, (c) one inch SAPL renewed CMP arch samples, and (d) measured locations in circumferential direction.

11.11.2.2.2 Arch CMP Invert Detachment Response

For the SAPL renewed arch CMP samples, the main parts of the inverts (i.e., the invert-cut and angle sections excluding the end-strips) were detached prior to the SAPL installation. The remaining two end-strips were kept bolted to maintain the pipes geometry at the time of SAPL installation. Once the SAPL was sprayed and cured, the end-strips were detached, as illustrated in Figure 11-67 (a and b). At this stage, no sign of CMP movement, SAPL crack or damage was observed.

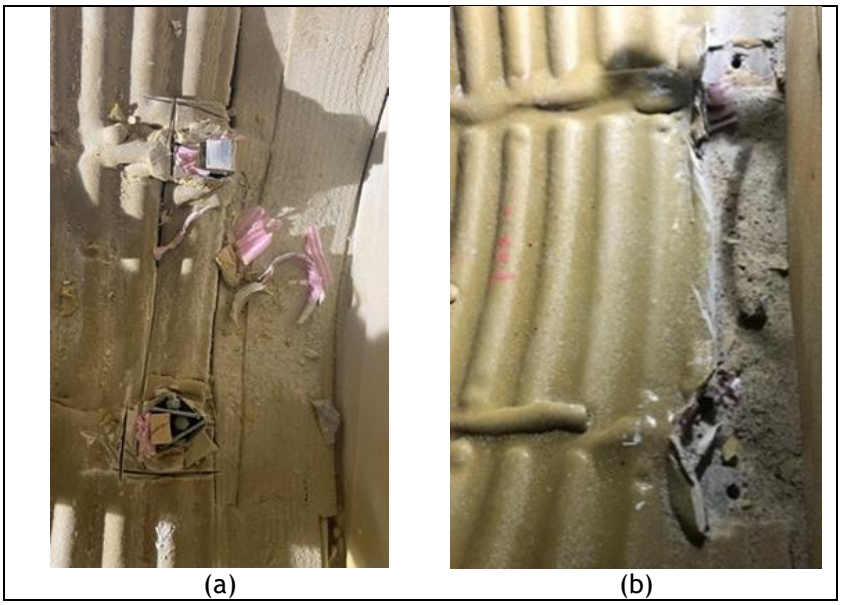


Figure 11-67. Invert-cut CMP arch end-strip detachment to remove the host pipe's ring stiffness: (a) over-sprayed SAPL and cutting process on the end-strip location, and (b) unbolted end-strip.

11.11.2.2.3 Comparison of Bare and SAPL Renewed Arch CMP Samples Load Bearing Capacities (Responses to Static Load)

The soil-CMP system was loaded through a 20×40 in. steel load pad. The continuous static load was applied on the middle ring of the CMPs on the soil surface using a load rate of 0.03 in./min. Figure 11-28 illustrated the CMP deflection in both horizontal and vertical directions due to the applied load for the bare invert-cut CMP arch, and all three SAPL renewed arch CMP samples. In the absence of the invert section and ring stiffness, the bare invert-cut CMP arch showed a stiff response to the applied load which could be due to the CMP arch's low slope at the shoulder and large flat area at the invert section. The bare arch CMP softening initiated from 12.5 kips and ultimately the soil-CMP system failed at 26.97 kips with about a 4-in. of CMP's crown deflection.

The quarter inch SAPL renewed arch CMP sample showed a stiff response to the applied load initially and then showed softening behavior starting at 15 kips of load. The first crack formed in the longitudinal direction at the load of 29.32 kips at the crown with 2.1 in. of crown displacement. The crack was further propagated with the load progression until it reached to the seam of the CMP, where the SAPL's thickness was not covered the seam and as a result, the crack was diverted in circumferential direction. The formation of the first crack is illustrated in Figure 11-69 (a). The renewed arch CMP ultimately failed at 33.2 kips of load with 4.75 in. of crown deflection.

The one inch SAPL renewed arch CMP showed relatively stiffer response compared with the quarter and half an inch renewed CMP samples. The first crack formed on the crown of the SAPL at 41.08 kips of load with 0.33 in. of pipe vertical

deflection and released relatively larger amount of energy than the quarter inch SAPL renewed arch CMP. This is evident in Figure 11-68 (d), where a large drop in the load displacement graph at the time of the first crack initiation was registered by the crown's LVDT. This can be related to the greater stiffness of the thicker SAPL due to its lower diameter overall thickness ratio. As illustrated in Figure 11-69 (c), the one inch SAPL renewed arch CMP cracked instantaneously throughout the length of the pipe at the crown. The pipe ultimately failed at 53.66 kips of static load with a 5.2 in. of crown deflection.

The half inch SAPL renewed arch CMP had a relatively lower structural capacity than expected and cracked at 26.27 kips of load with a 0.838 in. of pipe's crown deflection. This could be due to the reason that the renewed arch CMP at this thickness is neither a fully flexible pipe like the quarter inch SAPL renewed CMP sample, nor a fully rigid pipe like the one inch SAPL renewed arch CMP.

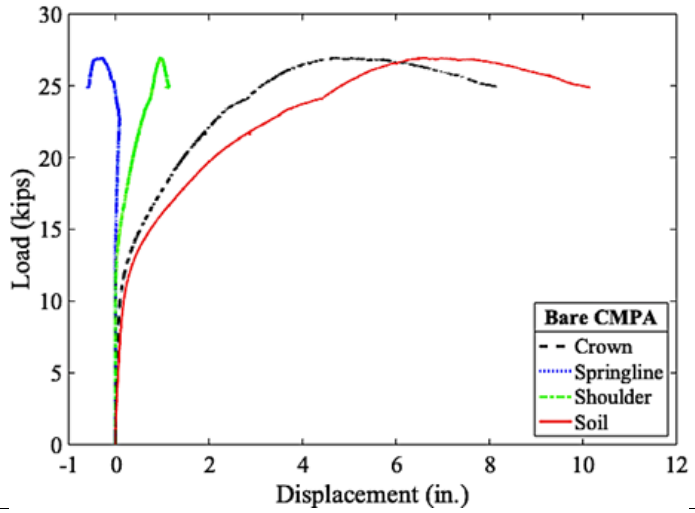
In the case of the half inch SAPL renewed arch CMP, the pipe had a 1.26 in. less crown deflection than the quarter inch SAPL renewed arch CMP and a 0.5 in. more crown deflection than the one inch SAPL renewed CMP arch at the time of first structural crack. This comparison implies that the half inch SAPL renewed CMP might fall in the transition zone between a flexible pipe to a rigid pipe behavior, where the renewed CMP arch did not received stiffness from the passive pressure activation nor the SAPL wall stiffness.

The other possible reason for the relative low cracking load of the half inch SAPL renewed CMP arch could be due to the unrepaired circumferential crack's effect on the structural bearing capacity of the renewed CMP arch. However, the likelihood of a structural capacity lose due to the a circumferential crack located at the end of a pipe is low.

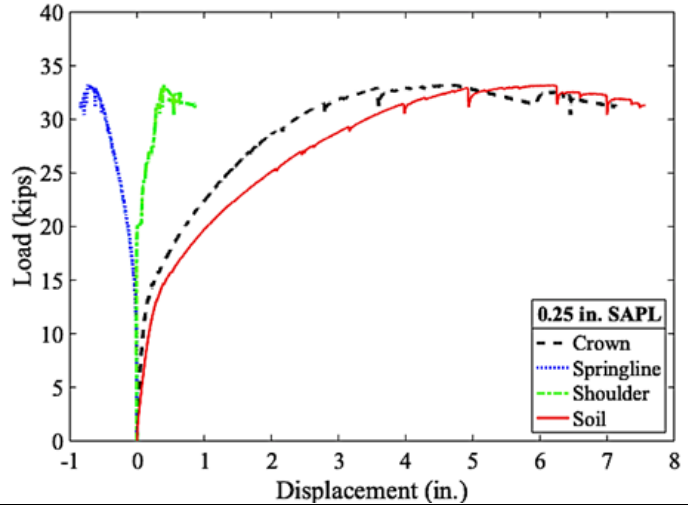
The structural crack (i.e., due to loading) of the half inch SAPL renewed CMP arch occurred throughout the crown instantaneously, as shown in Figure 11-69 (b), similar to the both 1 in. SAPL renewed circular and CMP arch samples. The renewed half inch SAPL CMP arch failed eventually at the load of 35.62 kips with a 5.07-in. of crown's deflection.

At the end of the tests, many hairline cracks were observed in circumferential, longitudinal, and 45° directions (similar to shear crack) at both shoulder areas. All of these cracks were formed after the first crack initiation at the crown that could be due the formation of three-point bending failure mechanism. In addition, no crack was observed at the invert-cut area, where the invert of host pipe was cut entirely. This can imply that the SAPL was a fully structural liner. It should be mentioned that during the load application no sign of crack was observed in the patched (repaired) area, which demonstrates the repair performed well.

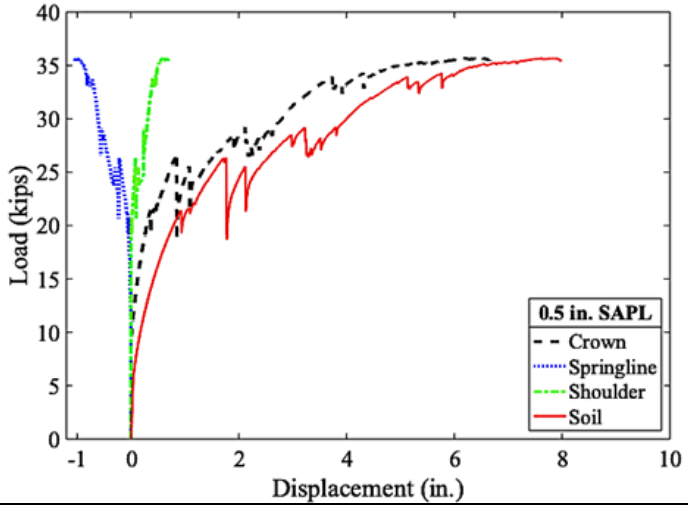
(a)


Load (kips)
Displacement (in.)
Bare CMPA
Crown
Springline
Shoulder
Soil

(b)


Load (kips)
Displacement (in.)
0.25 in. SAPL
Crown
Springline
Shoulder
Soil

(c)


Load (kips)
Displacement (in.)
0.5 in. SAPL
Crown
Springline
Shoulder
Soil

(d)

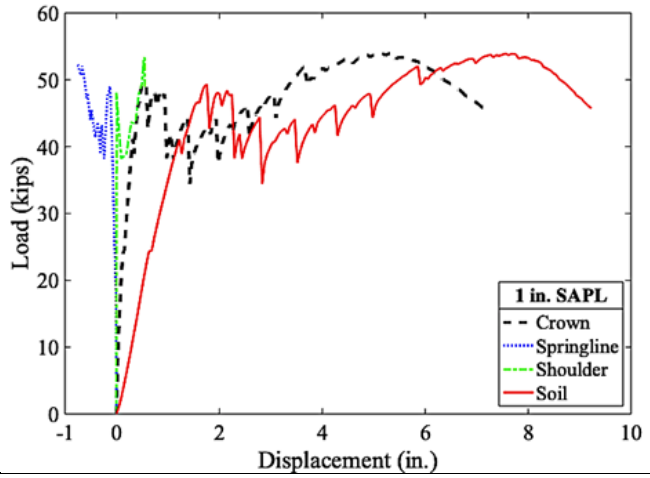
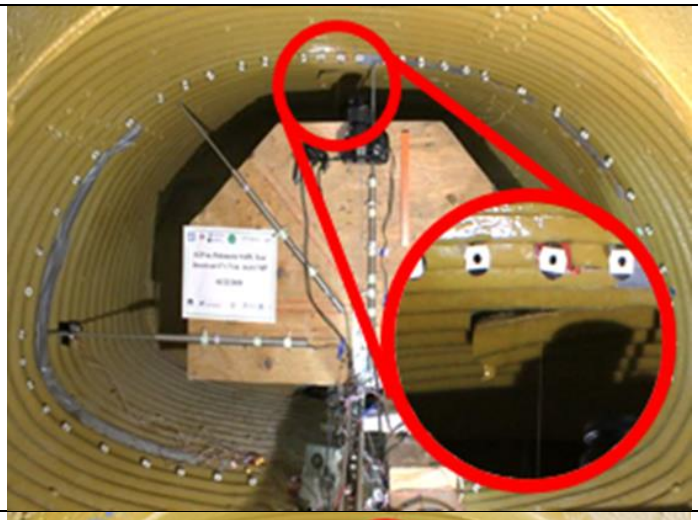
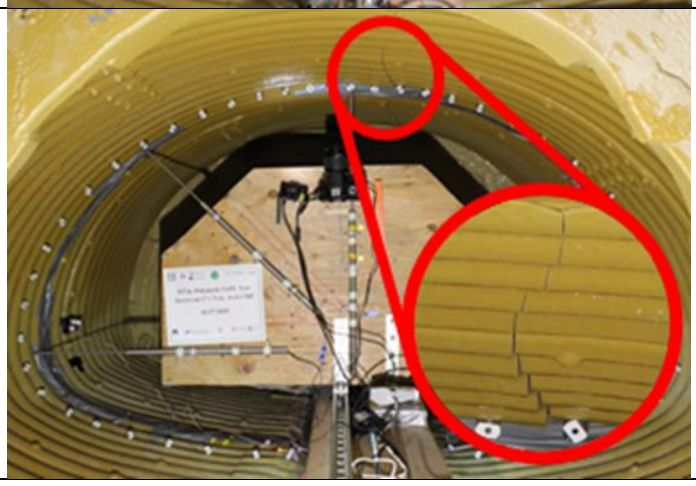


Figure 11-68. Bare and SAL renewed CMP arch samples Load-Displacement graphs: (a) invert-cut bare CMP arch, (b) 0.25 in. SAPL renewed CMP arch, (c) 0.5 in. SAPL renewed CMP arch, and (d) 1 in. SAPL renewed CMP arch.

(a)



(b)



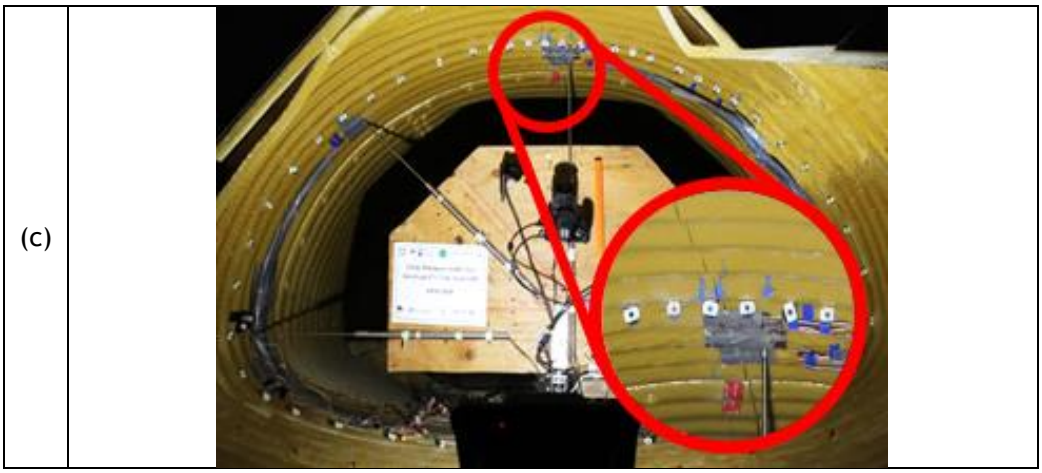


Figure 11-69. Formation of the first structural crack: (a) 0.25 in. SAPL renewed CMP arch at 29.32 kips, (b) 0.5 in. SAPL renewed CMP arch at 26.27 kips, and (c) 1 in. SAPL renewed CMP arch at 41.08 kips.

Figure 11-70 illustrates the ultimate load comparison between the bare CMP arch (i.e., control test) and all three SAPL renewed CMP samples. It was observed that the application of polymeric SAPL increased the ultimate load bearing capacity of the invert corroded CMP arch. The SAPL improvement rates for the 0.25, 0.5, and 1-in. thick SAPLs were 23.1, 32.1, and 98.9 %, respectively.

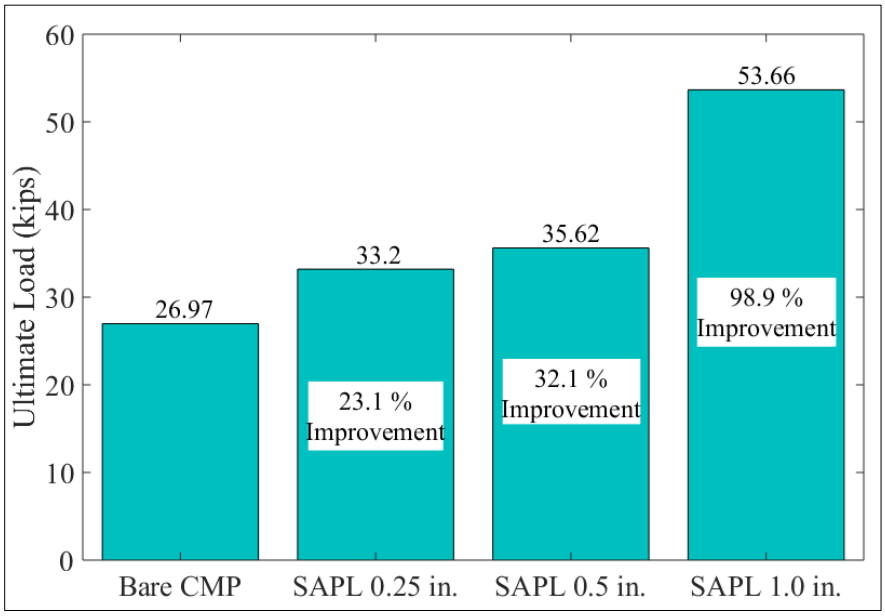


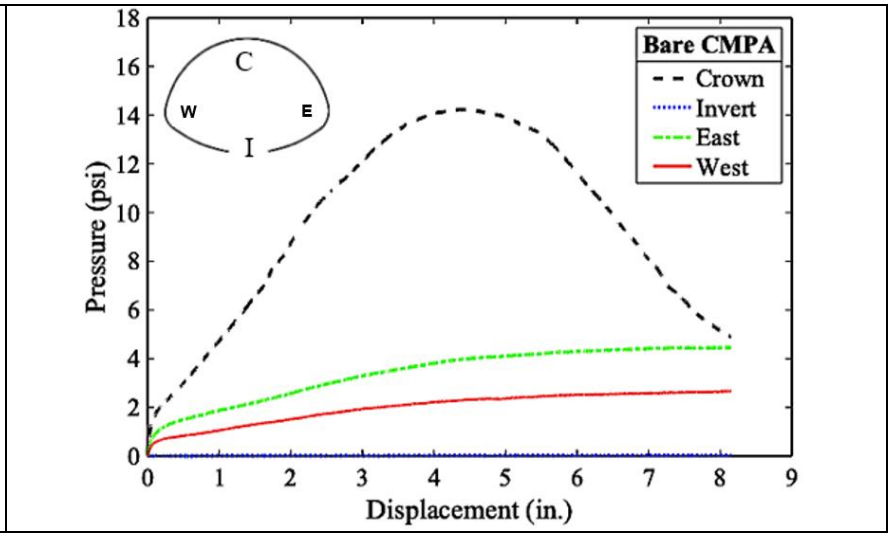
Figure 11-70. Fully Invert deteriorated CMP arch samples ultimate load carrying capacity improvement through SAPL application.

11.11.2.2.4 Pressure around the CMP Arch Samples (Earth Pressure Cell Results)

Figure 11-71 shows the applied pressures around the CMP arch samples, measured by earth pressure cells. In all four CMP arch samples the maximum pressures were registered at top of the pipes, where the pressure cells were buried 20 in. deep under the steel load pad. The maximum applied pressure on top of the bare CMP arch was 14.23 psi. The side pressures on West and East locations were 1.9 and 4 psi, respectively. No pressure was registered at the bottom of the CMP arch since in the absence of the invert section no pressure was applied on the soil underneath of that area.

The quarter, half, and one in. SAPL renewed CMP arch samples reached the failure pressure on top of the CMP at 24.32, 32.92, and 51.23 psi, respectively. Figure 11-71 illustrates the pressure-displacement graphs for bare, and all three SAPL renewed CMP arch samples. No pressure was registered by earth pressure cells on the bottom of the pipes in all CMP arch samples. This was expected for the bare CMP arch since its invert section was entirely removed. However, for the SAPL renewed samples where the invert section was rehabilitated the pressure on the bottom of the pipe was still zero. This is due to the closed-arch behavior under a vertical load which produced an uplift force on the bottom and consequently no pressure was applied to the soil bellow. The free body diagram of an CMP arch subjected to a vertical load on its top is illustrated in Figure 11-72. The load developed positive bending moment on the crown and negative bending moment on the invert section of the CMP. Therefore, an upward force is generated that uplifted the invert section as a result of the negative bending moment. This upward movement was also observed in the soil box tests through measuring the gap between the CMP arch samples invert at the cut end-strip location and the soil below. Figure 11-72 also illustrates the CMP arch samples' invert uplift after loading. DIC also capture the renewed CMP arch samples' invert upward movement.

(a)



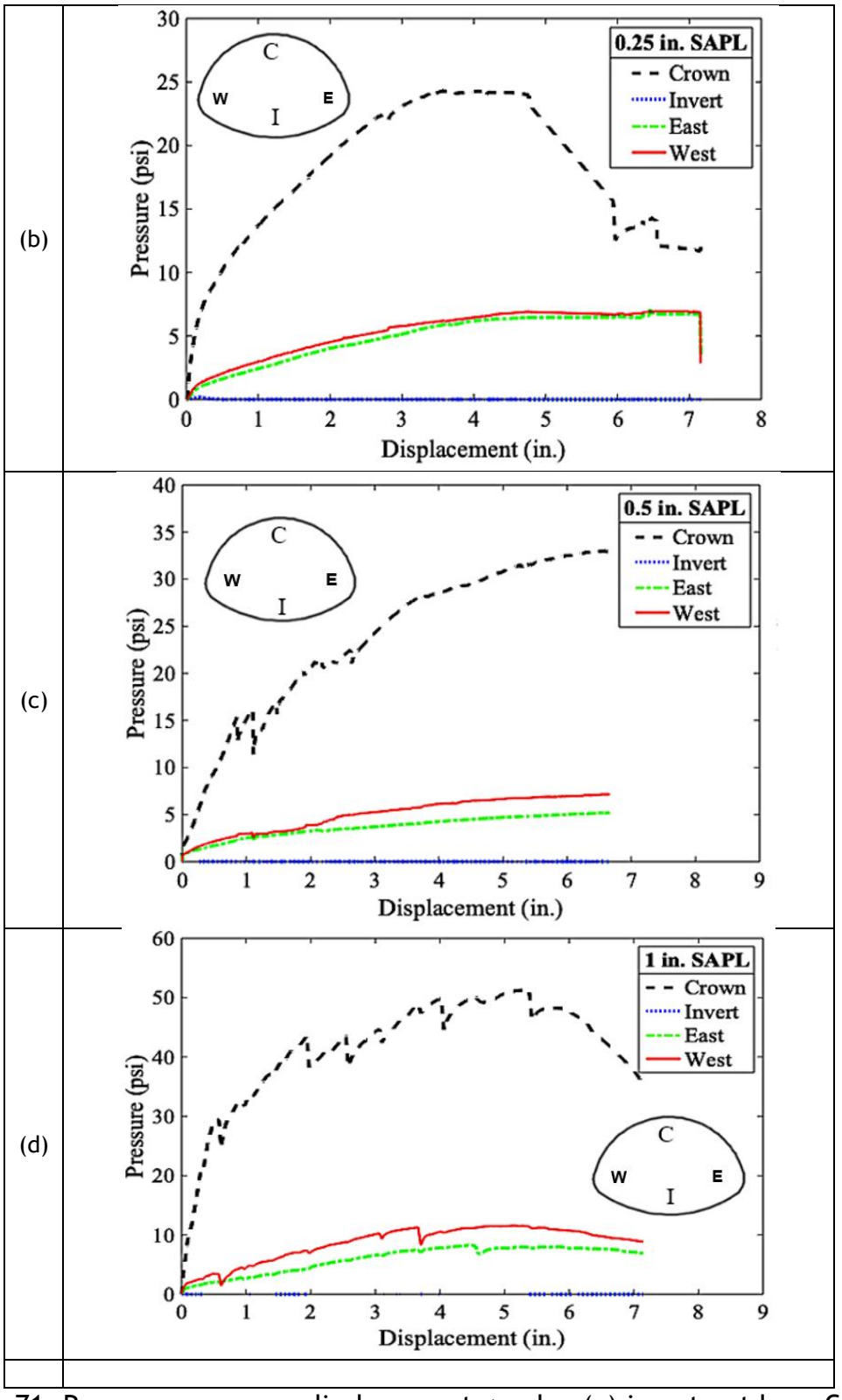


Figure 11-71. Pressure vs. crown displacement graphs: (a) invert-cut bare CMP arch, (b) 0.25 in. SAPL renewed CMP arch, (c) 0.5 in. SAPL renewed CMP arch, and (d) 1 in. SAPL renewed CMP arch.

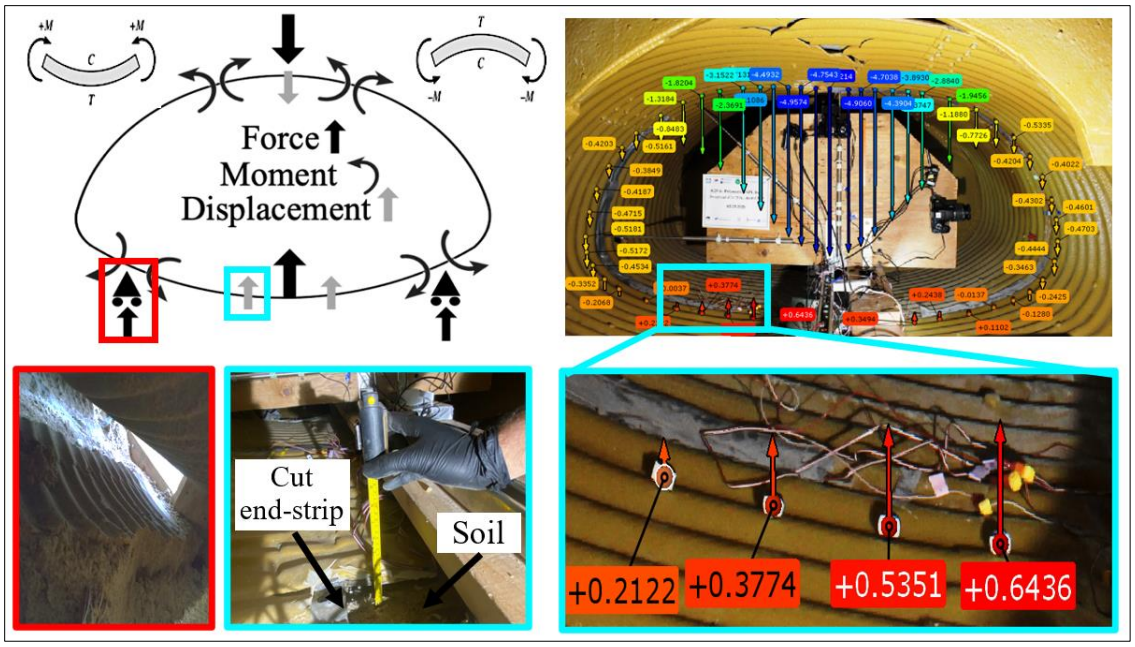


Figure 11-72. CMP arch behavior due to the vertical load, where the red boxes show the soil support under the pipe on the west haunch area and the blue boxes illustrates the pipe upward movement.

The CMP arch samples' load carrying capacity, crown deflection at initial crack and failure as well as the soil displacement in both initial crack and failure stages are summarized in Table 11-10.

Table 11-10. The circular CMPs' load bearing capacity, crown deflection and the soil displacement at initial crack and failure.

Test Setup		Initial Structural Cracking Stage				Failure Stage		
		Load (kips)	Pipe Deflection at Crown (in.)	Soil Displacement (in.)	Pressure at Crown (psi)	Load kips	Pipe Deflection at Crown (in.)	Soil Displacement (in.)
Bare Invert-cut CMP		-	-	-	-	26.97	4	6.47
SAPL Renewed CMP	0.25 in. SAPL	29.32	2.1	3.15	20.01	33.2	4.75	6.23
	0.5 in. SAPL	26.27	0.838	1.71	15.23	35.62	5.07	7.61
	1 in. SAPL	41.08	0.33	1.22	21.85	53.66	5.2	7.56

The soil pressure around the CMP arch samples were recorded by the earth pressure cells and are summarized in Table 11-11 for the time of failure at the ultimate load.

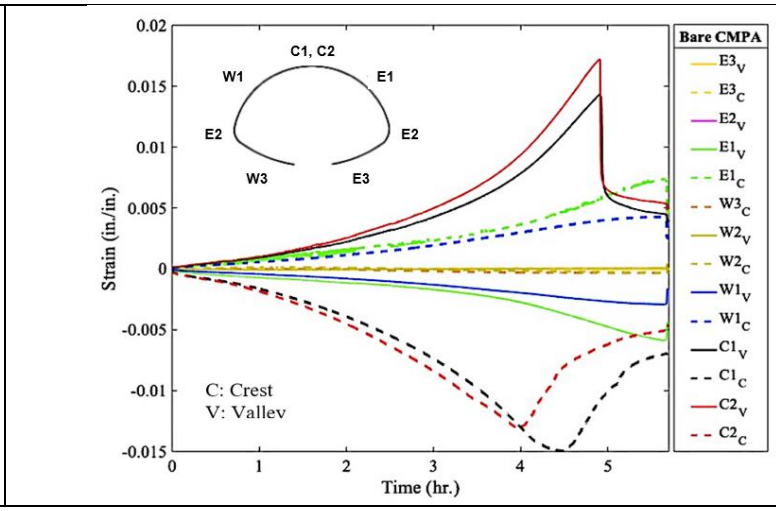
Table 11-11. Soil pressure results around the CMP arch samples at the time of failure.

Test Setup		Pressure (psi)			
		Crown	Invert	East	West
Bare CMP		14.23	0	4.05	2.34
SAPL Renewed CMP	0.25 in. SAPL	24.32	0	6.45	6.9
	0.5 in. SAPL	32.92	0	5.05	6.99
	1.0 in. SAPL	51.23	0	8.01	11.53

11.11.2.2.5 Strain Gauges Results for SAPL Renewed CMP Arch Samples

Figure 11-73 illustrates the results of strain values. The bare CMP arch experienced a large strain at the crown and both shoulder locations which indicates the formation of a three-hinge plastic mechanism (i.e., local buckling) at the crown. Likewise, the host CMP arch samples of SAPL were subjected to large amount of strains at the crown and both shoulder locations. Strain results comparison at the crown and shoulder of the CMP arch samples indicate that the sprayed polymeric material increased the stiffness of the fully invert deteriorated (i.e., invert-cut) CMP arch samples. Cracking of the ½ and 1 in. SAPL renewed CMP arch samples at the crown locations with a large drop are evident in Figure 11-73 (c) and (d), respectively. The arch SAPLs cracked with the strain values of approximately 0.003 in./in. In Figure 11-73, some strain gauges' values are not illustrated which were due to the harsh abrasive nature of the soil-pipe system.

(a)



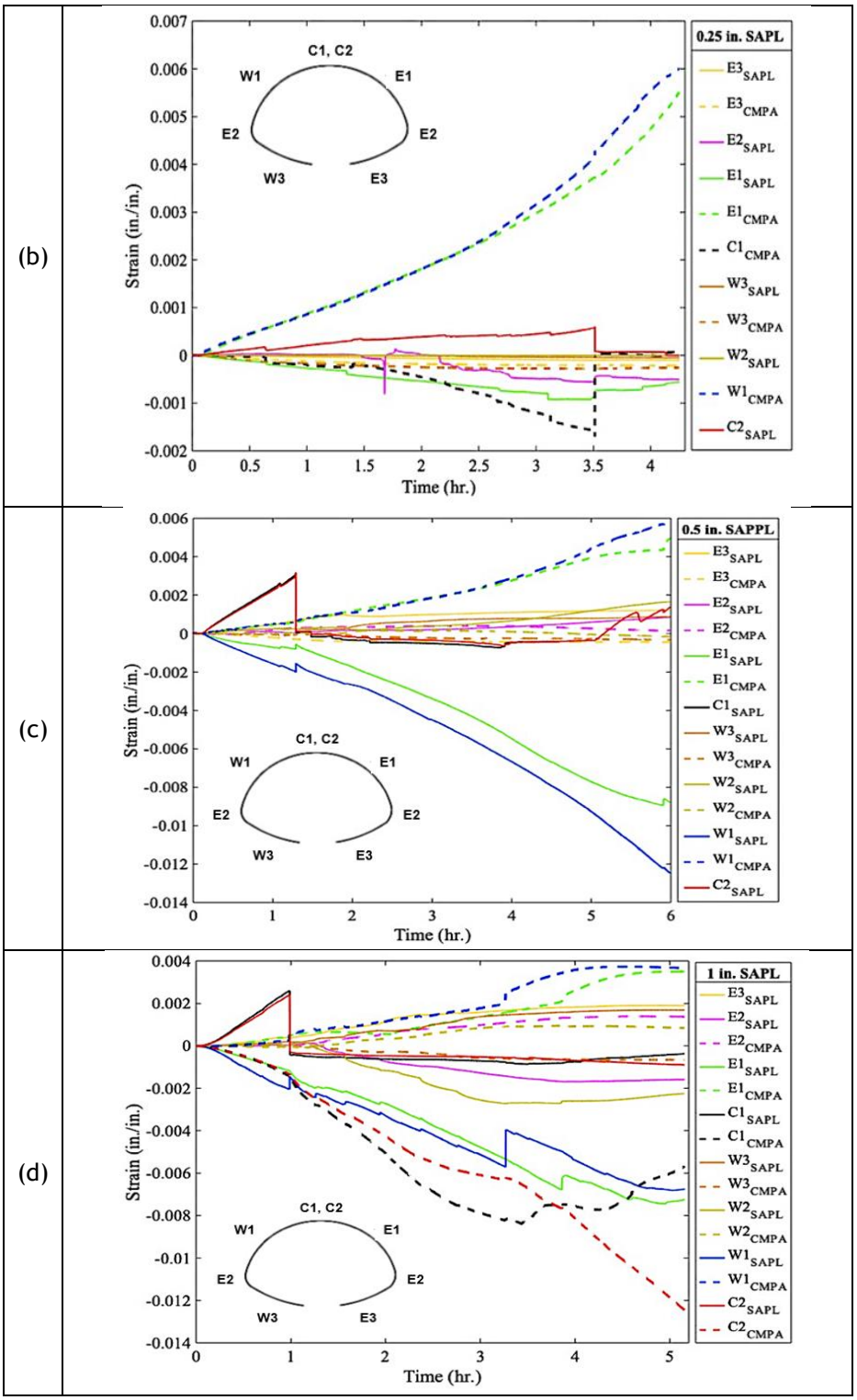
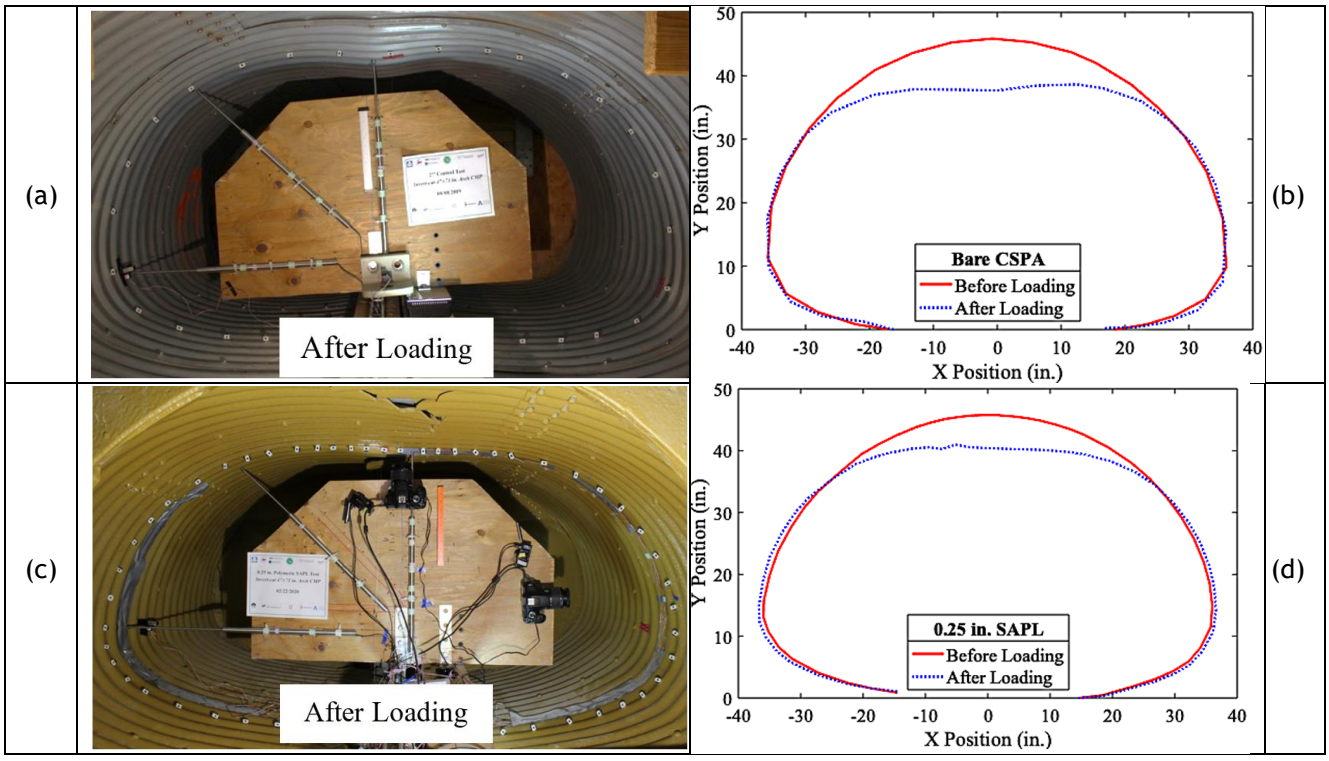


Figure 11-73. Strain gauge results: (a) invert-cut bare CMP arch, (b) 0.25 in. SAPL renewed CMP arch, (c) 0.5 in. SAPL renewed CMP arch, and (d) 1 in. SAPL renewed CMP arch.

11.11.2.2.6 Pipe Profile Measurement using DIC for SAPL Renewed CMP Arch Samples

Figure 11-74 illustrates the results of pipe deflection measurements at the middle ring of the CMP arch using DIC technique prior and after the loading. The accuracy of the DIC measurement was investigated by direct comparison with mechanical sensors (i.e., LVDT & CDS) that revealed both techniques are in an excellent conformity (Darabnoush Tehrani et al. 2020b). The SAPL renewed CMP arch samples had movement in both vertical and horizontal directions that the movements are evident in the DIC profiling. The pipe profiling for the after the test stage shows that the SAPL renewed pipe samples had horizontal expansion at the springline due to the vertical load. The magnitude of this horizontal expansion in the bare CMP arch was inconsequential. This is due to the fully detached invert section which released the restrain from the pipe. The modes of failure for all CMP arch samples were local buckling at the crown locations, which is evident in the DIC results. In case of the bare CMP arch the buckling caused pipe deformation (i.e., ductile failure) and in case of SAPL renewed CMP arch samples it caused cracking and fracture at the crown locations (i.e., brittle failure). It should be noted that, due to the existence of the mechanical sensors' frame and its holding wooden beam, implementation of DIC and illustration of the invert section of pipes' profile were not possible. Figure 11-75 illustrates pipe profiling of SAPL renewed circular CMPs at the time of failure.



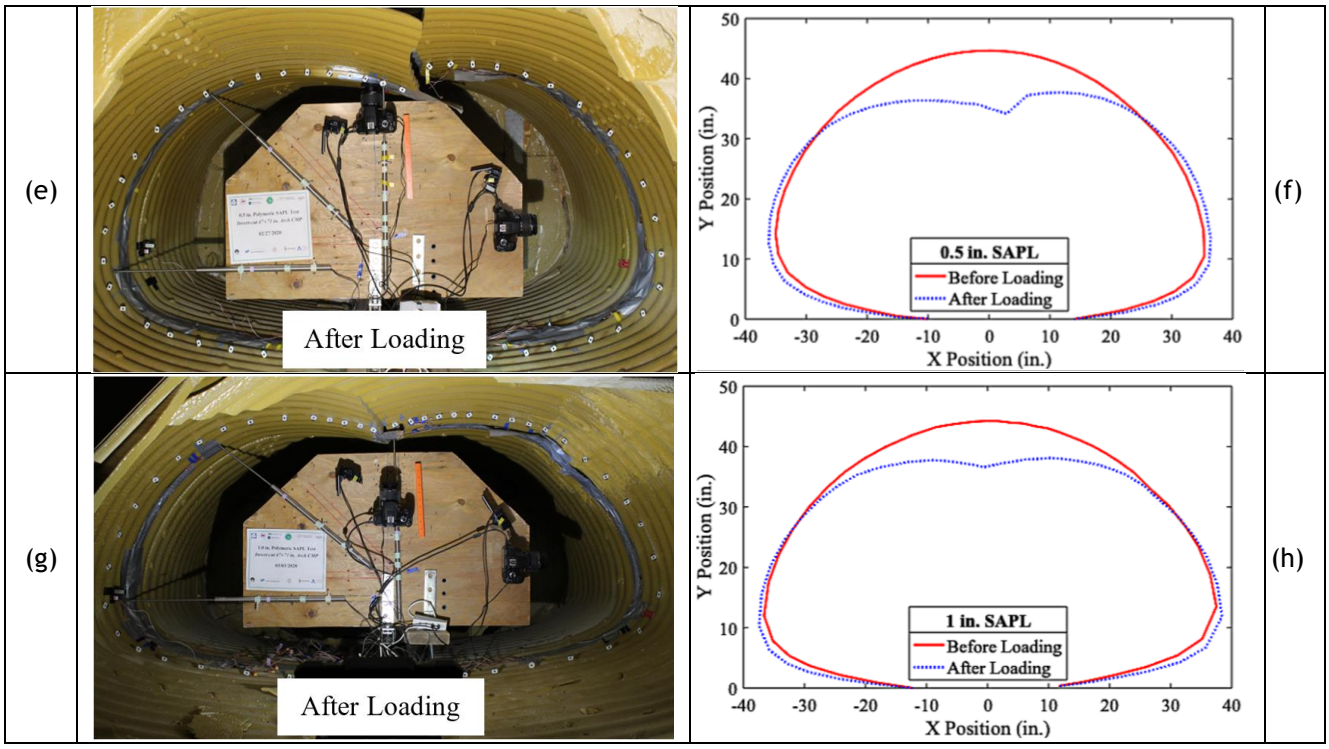
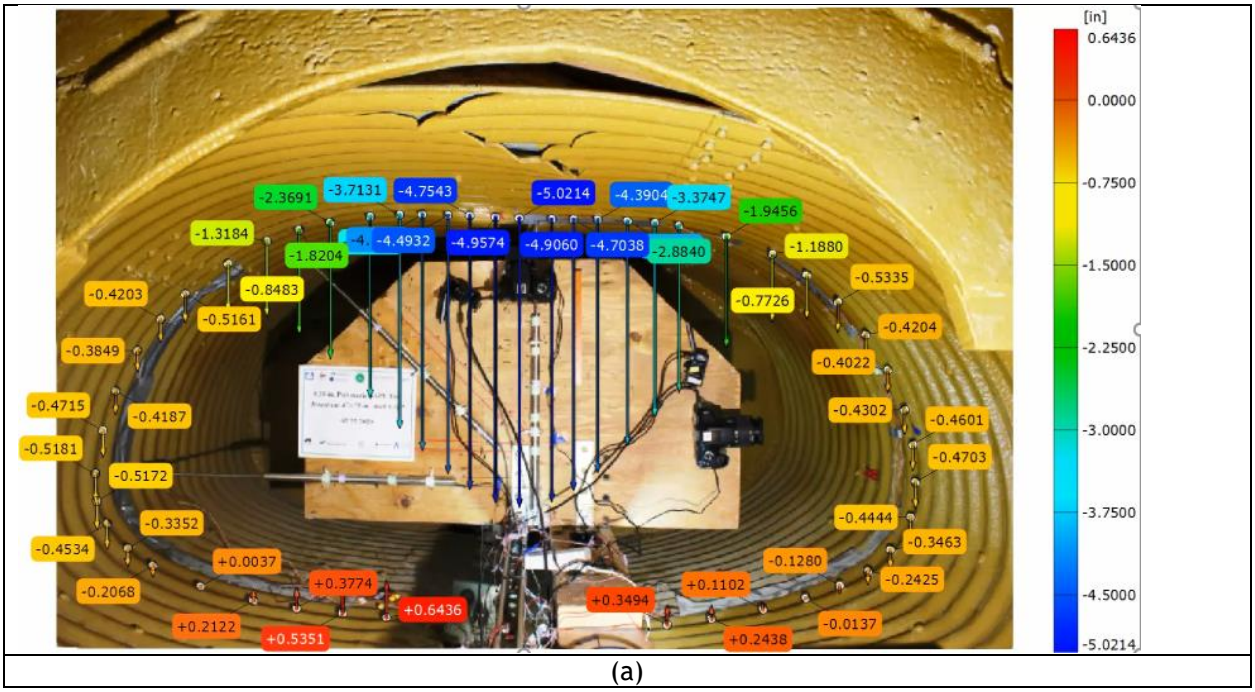
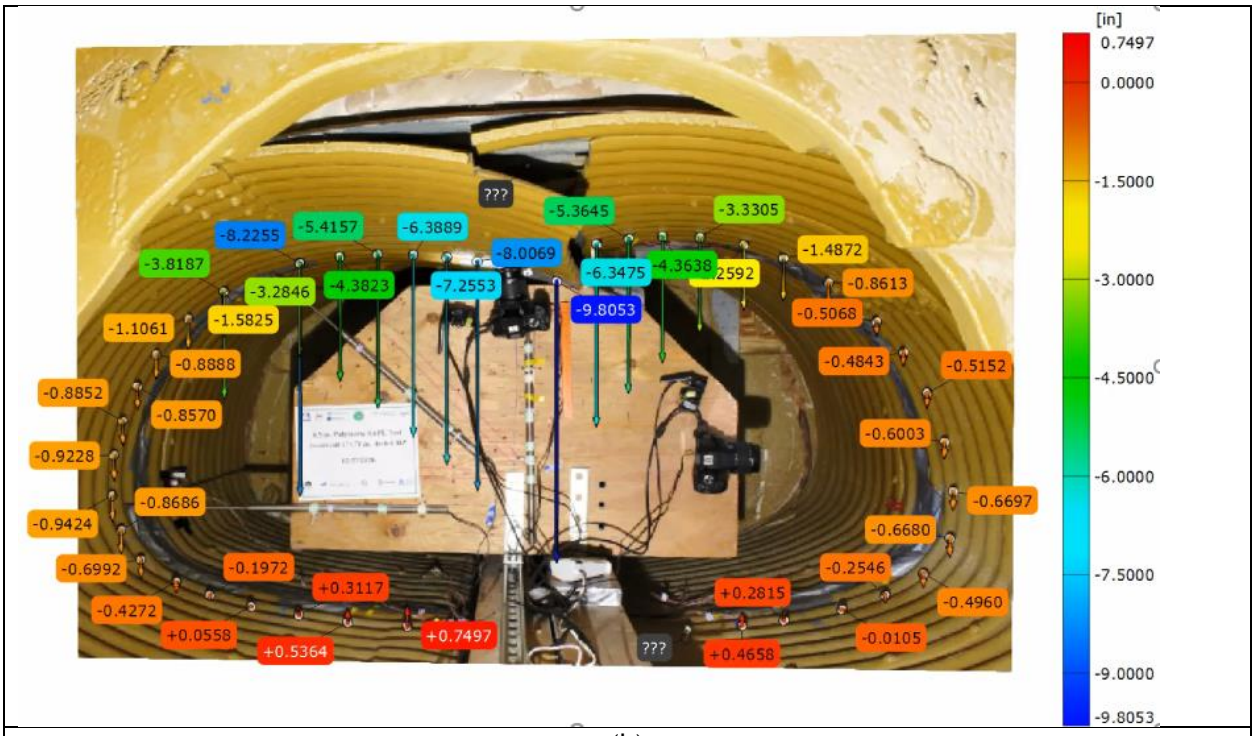


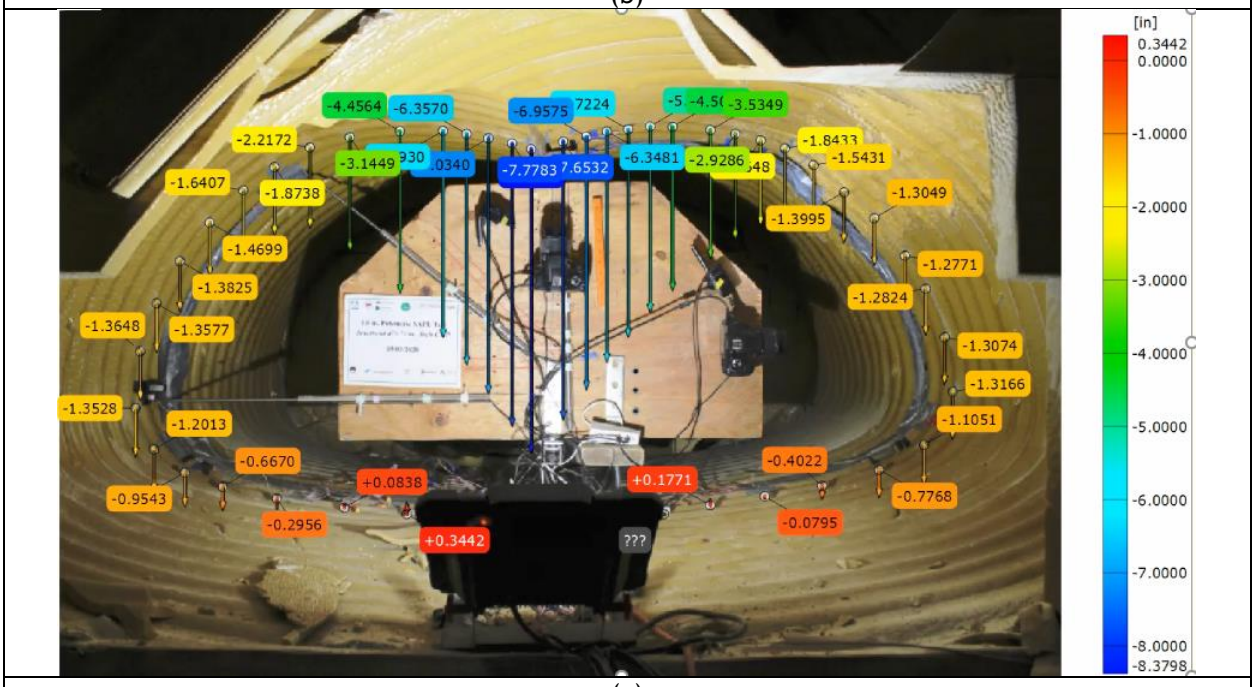
Figure 11-74. Pipe profiling using DIC results: (a) and (b) bare CMP arch, (c) and (d) 0.25 in. SAPL renewed CMP arch, (e) and (f) 0.5 in. SAPL renewed CMP arch, and (g) and (h) 1 in. SAPL renewed CMP arch.



(a)



(b)



(c)

Figure 11-75. Pipe profiling using DIC technique at the time of failure: (a) 0.25 in. SAPL, (b) 0.5 in. SAPL, and (c) 1.0 in. SAPL renewed CMP arch samples.

11.11.2.2.7 Summary of Polymeric SAPL Renewed CMP Arch Testing

Three invert-cut arch corrugated metal pipe samples (CMPs) renewed with polymeric spray applied pipe liner (SAPL) application and one invert-cut bare CMP arch were buried under 2-ft of soil cover including layers of poorly graded sand (SP), and TxDOT 247 grade 1 type D aggregates. The invert of CMP arch samples were cut before SAPL application to simulate a fully deteriorated invert condition. Static load in a displacement-control regime was continuously applied with a load rate of 0.03 in./min through a rigid 20 × 40 in. steel load pad. The experimental test simulated a poor pipe installation condition (i.e., uncompacted soil) in the absence of pavement to maximize the applied load on the renewed pipe. The results and discussions were presented in this chapter and the conclusions are summarized as follow:

- The results of thickness measurements showed that the utilization of hand spray installation method for the polymeric SAPL resulted in about 0.2 in. thicker liner than the design thickness, which could be due to the inclusion of a factor of safety in SAPL's quantity calculation.
- Under the shallow cover condition, the invert-cut bare CMP arch, in the absence of ring stiffness, was able to resist the vertical load up to the 26.97 kips of the applied static load.
- Application of the polymeric SAPL increased the stiffness of the invert-cut CMP arch. The SAPL renewed CMP arch samples with the thicknesses of 0.25 in., 0.5 in., and 1 in. increased the ultimate load bearing capacity of the invert deteriorated CMPs for 23.1, 32.1, and 98.9%, respectively.
- The CMP arch with 0.25 in. of SAPL was susceptible to crack at the seam locations, where the SAPL was either discontinued or the thickness was not as thick as design thickness. Although, the first crack was initiated in the longitudinal direction, once it reached the seam locations, it diverted towards the circumferential direction.
- In comparison with the bare CMP arch, the application of SAPL reduced the strain of the host pipes, especially at the crown and shoulder locations.
- The DIC results implied that for all CMP arch samples the modes of failure were local buckling at the crown locations, where in case of the bare CMP arch the buckling caused pipe deformation (i.e., ductile failure) and in case of SAPL renewed CMP arch samples it caused cracking and fracture at the crown sections (i.e., brittle failure).
- The 0.25, 0.5, and 1 in. SAPL renewed CMP arch samples cracked at pressures of 19.77, 16.26, and 21.95 psi, respectively. Cracking pressures of all the SAPL renewed CMP arch samples were higher than the applied pressure by the AASHTO H20 truck, calculated through AASHTO LRFD, AWWA, and NCSPA design guidelines.

- In the absence of the host pipe's ring stiffness, the SAPL was able to resist the ring compression solely. No sign of cracking was observed at the invert area, where the host pipe was entirely cut and detached. Therefore, the polymeric SAPL can be considered structurally sufficient to withstand the applied load and improve the overall load bearing capacity of the fully invert deteriorated host CMP arch.

11.11.3 Cementitious SAPL

11.11.3.1 SAPL Renewed CMP Arch

11.11.3.1.1 SAPL Renewed Invert-cut CMP Arch Test Results

The invert-cut CMP arch samples renewed with the cementitious SAPL were tested using the same load rate and load pad as invert-cut bare CMP arch samples. Due to required time for test preparation, instrumentation, and operation, conducting all the three tests of this set in one day was not possible. The first test was conducted on the 3-in. thick SAPL renewed CMP arch samples after 7 days of curing. The 2 and 1-in. thick SAPL renewed CMP arch samples were conducted with a 2-day interval, respectively. It is noteworthy that none of the existing shrinkage cracks were repaired before the loading and the soil-pipe systems were tested with existed cracks.

In general, due to the applied vertical load all three invert-cut CMP arch samples experienced a large crack width in both crown and invert. The crown is located right under the applied load that generates larger deformation than other sections of the CMP, which makes the crown susceptible to crack and buckle. The invert section also is susceptible to crack as the applied vertical load on the CMP generates a negative bending moment on the invert, which causes a relatively large uplift in the invert section. Due to this negative bending moment, the bottom of the pipe arch in the invert section does not receive any pressure, and therefore, the pressure reading at the invert of all three SAPL renewed pipe arch tests are zero. Figure 11-76 illustrates free body diagram of a SAPL renewed pipe arch, which is validated with the DIC results, that includes both positive and negative bending on the crown and invert of the pipe arch.

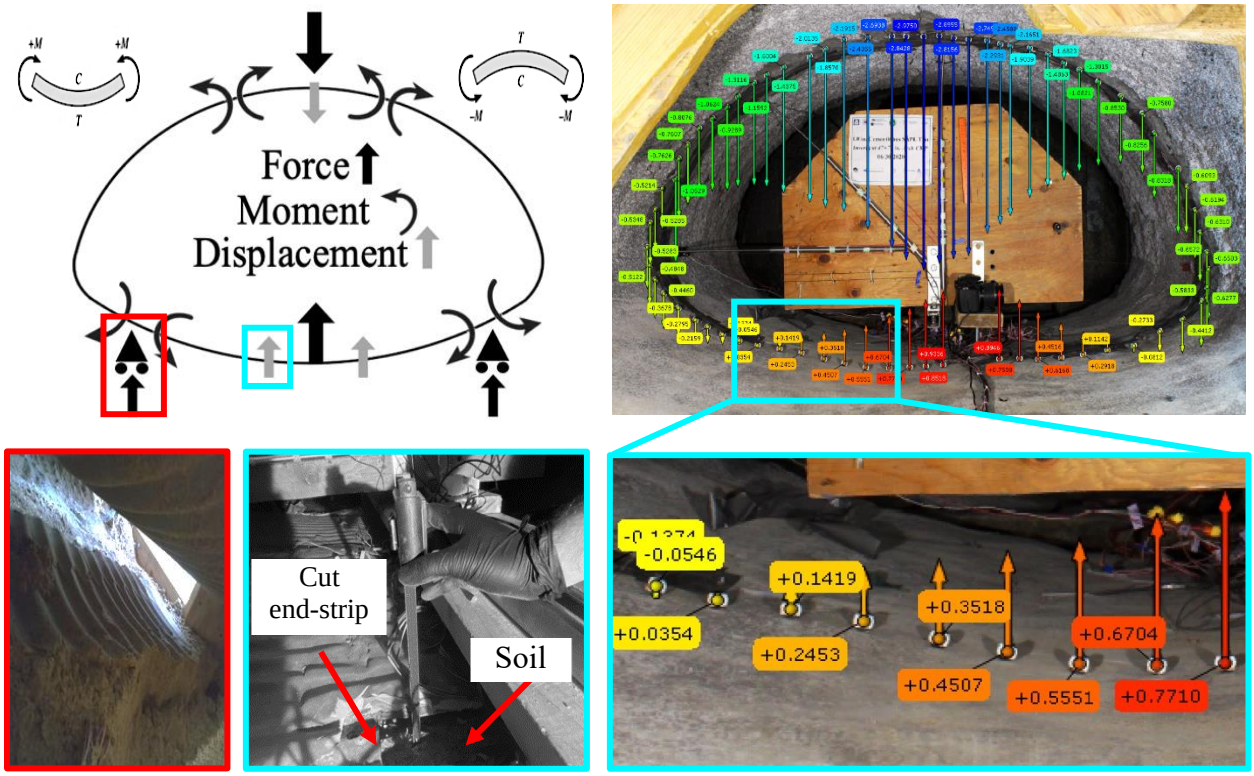


Figure 11-76. CMP arch behavior due to the vertical load, where the red boxes show the soil support under the pipe on the west haunch area and the blue boxes illustrates the pipe upward movement.

11.11.3.1.1.1 3-in. Thick SAPL Sample

The 3-in. thick SAPL renewed invert-cut CMP arch was tested on Jun 24th, 2020, using the 20 × 40 in. load pad. The test duration was 5.04 hours. During the test, due to the existence of shrinkage cracks no major drop in the load-displacement graphs was observed, and the cracks width were increasing with load progression. The SAPL renewed CMP sample failed at the load of 67.84 kips with 6.606 in. of soil settlement. The failure occurred due to the buckling and large deflection of the crown. Figure 11-77 (a) and (b) illustrate the test sample before and after the loading stage. Once the SAPL-CMP system was failed, the test was continued until about 15% load drop. Then the test was stopped, as further deflection would increase the chance of the liner detaching and falling, which would damage the mechanical sensors and cameras inside the pipe. Once the load was released from the soil surface, the pipe had an upward movement and relaxed. However, this upward movement resulted in a large delamination from the West shoulder and springline which is illustrated in Figure 11-77 (c) and (d). Figure 11-78 also illustrates the load and soil settlement graph, registered by the actuator's load cell and LDVT.

The earth pressure cell results registered the maximum pressure of 93.32 psi at the crown location. The maximum pressure applied on the West and East locations were 4.37, and 4.59 psi, respectively. Figure 11-79 illustrates earth pressure results for the invert-cut circular test.

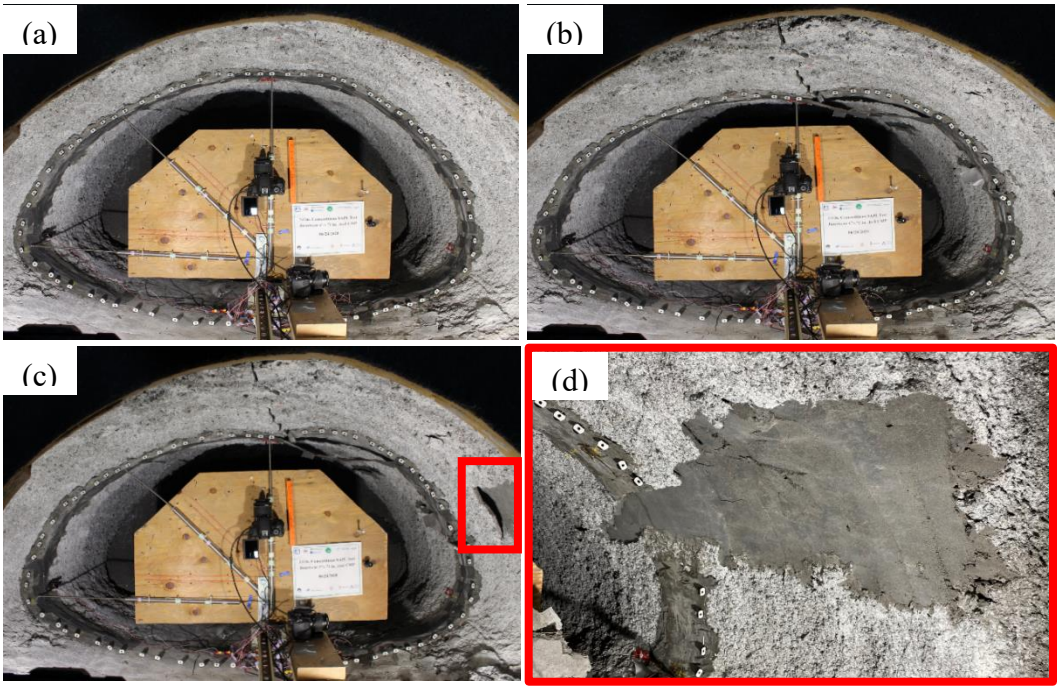


Figure 11-77. Invert-cut CMP arch renewed with 3 in. cementitious SAPL: (a) before loading, (b) after loading, (c) after unloading, and (d) delamination in the West springline.

Figure 11-80 illustrates the results of the mechanical sensors. The LVDT results show that the pipe was subjected to 4.224 in. of crown and 0.722 in. of springline deflection. The shoulder had 0.33 in. downward movement. The CDS showed 4.77 in. of crown movement, which is 0.546 in. higher than the LVDTs reading. This discrepancy is due to the fact that the LVDT could move along the SAPL surface as the liner was deflecting, while the CDS was glued to certain location. The result of the DIC is also closer to the CDS result for this experiment. At the end of the test once the load was released from the surface, the pipe's crown, and springline had reverse movement of 0.863 and 0.07 in., respectively.

The strain gauge results showed the invert-cut CMP arch samples experienced a large strain at the crown and both shoulder locations as well as springline that indicates the formation of buckling at the crown, as illustrated in Figure 11-81. The crown of the CMP was the first location that reached the steel yielding point (i.e., 1138 με) at the load of 35.22 kips. The west shoulder of the CMP also yielded at 49.27 kips. Eventually, the East shoulder of the CMP yielded at the load of 60.38 kips, which was reached after the ultimate failure of the SAPL-CMP system. Other locations did not reach the steel yield point. The strain gauges on the SAPL surface showed that the cementitious liner cracked at the load of 15.79 kips, which resulted in a drop in strain reading of the springline and shoulder of the East and West (i.e., W3, W2, and E2) locations. At this load, a drop in the load-displacement graph (Figure 11-78) can be observed. The Figure 11-81 also illustrates a sudden strain reduction in the crown of the SAPL at the load of 26.12, which can be due to a crack at this location.

Figure 11-82 illustrates the 3-in. thick SAPL renewed CMP arch profile before and after the static load. The pipe profile at end of the test clearly illustrates the crown flattening. In addition, the roughness and irregularity of the SAPL is explicitly evident in the profiling result. The deflection results captured by the DIC method is in an excellent conformity with the CDS sensor.

Figure 11-84 illustrates the applied load on the soil surface versus its corresponding pressure at the crown of the renewed CMP arch, where the recursive part of the graph represents a drop in both pressure and load at the same time. The load-displacement values for soil surface, crown, springline, and shoulder of the 3-in. thick SAPL renewed CMP arch due to the applied static load is illustrated in Figure 11-83.

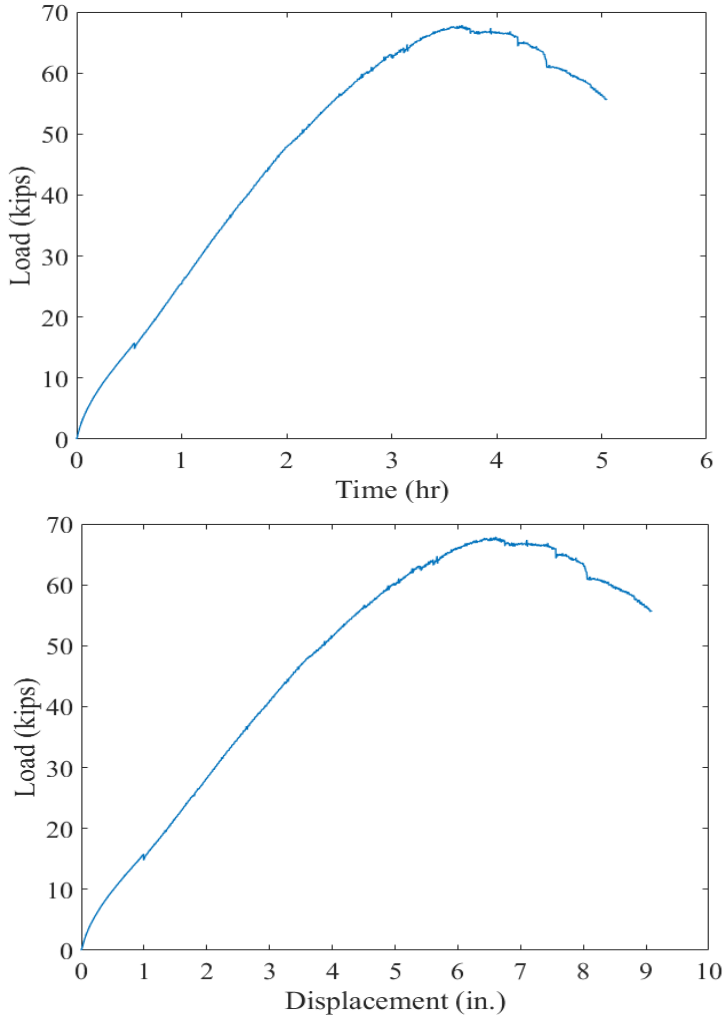


Figure 11-78. Invert-cut CMP arch renewed with 3-in. thick cementitious SAPL subjected to static live load: (top) load-time and (bottom) load-soil displacement graphs.

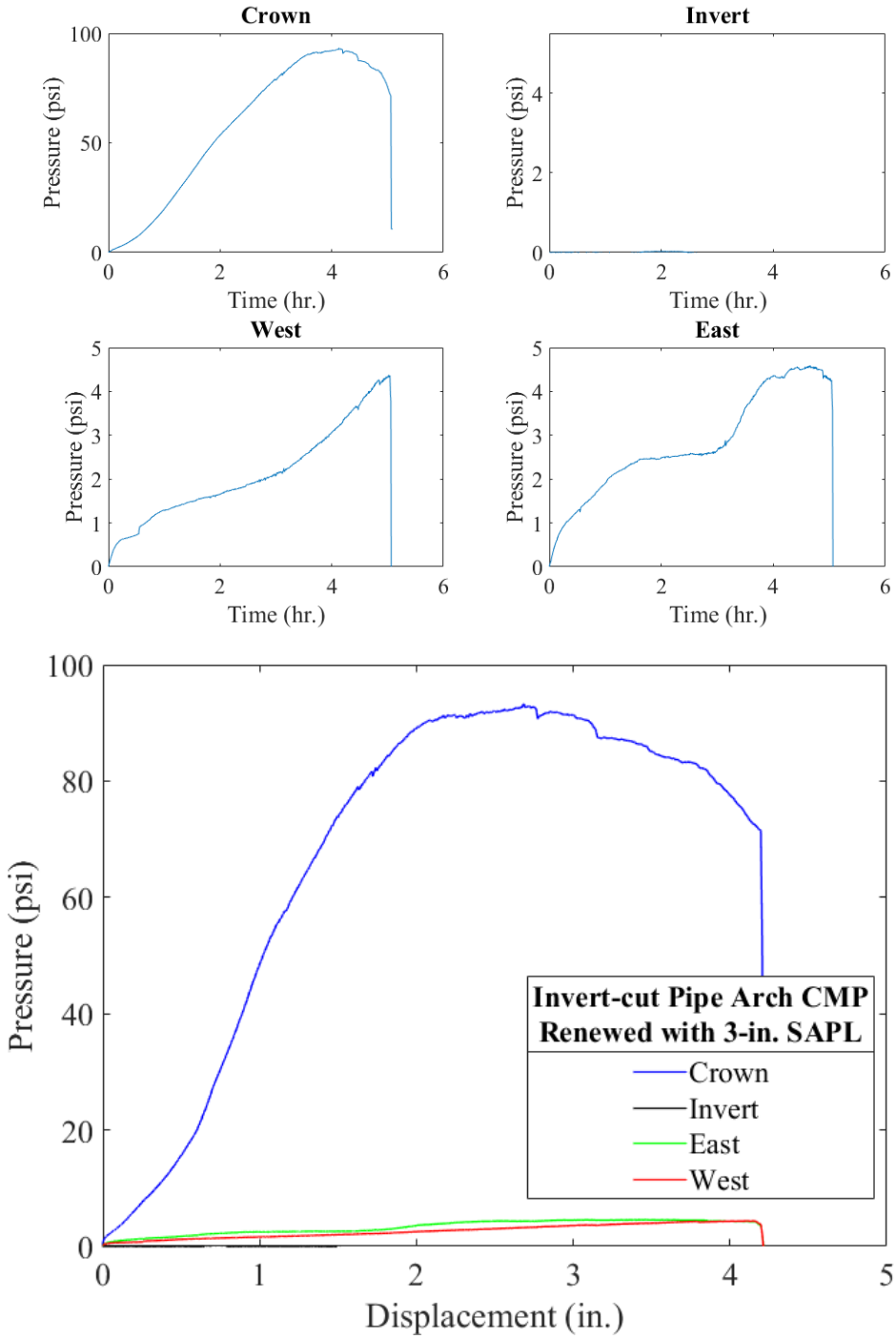


Figure 11-79. Earth pressure cell results for the 3-in. thick SAPL renewed invert-cut CMP arch with respect to: (top) time, and (bottom) crown displacement.

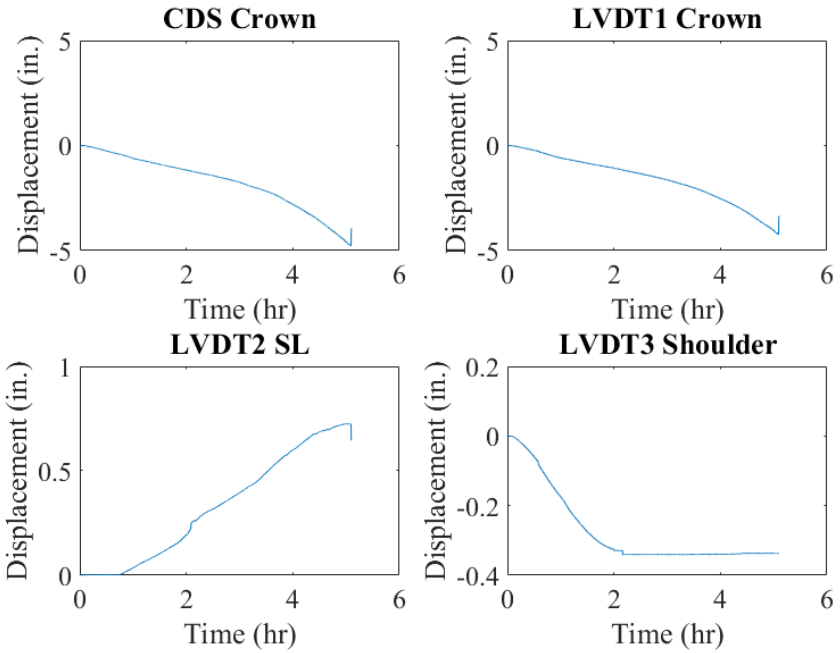


Figure 11-80. Mechanical sensors result for 3-in. thick SAPL renewed invert-cut CMP arch.

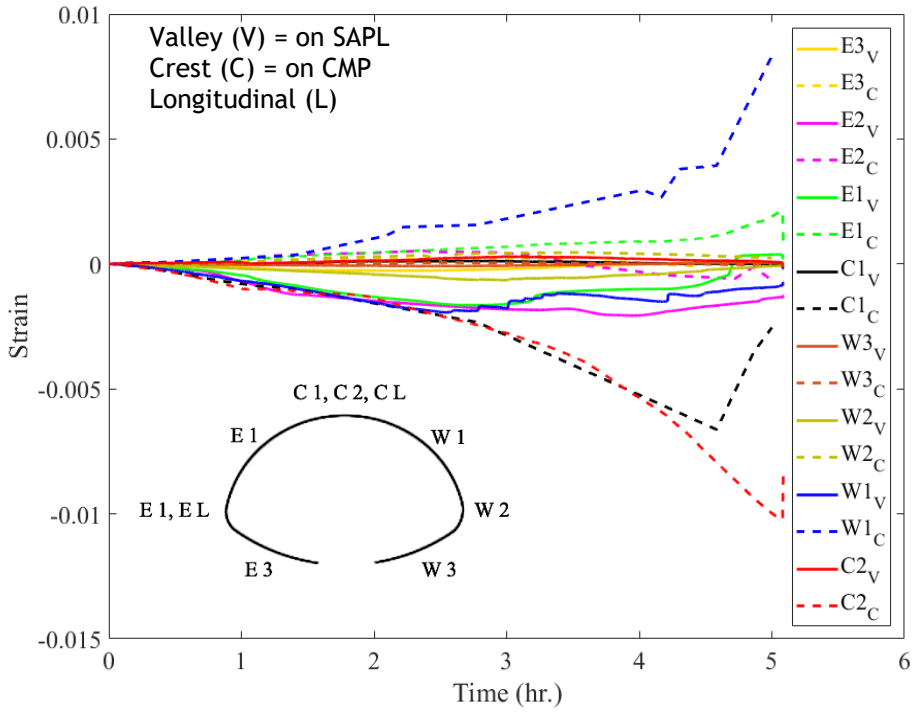


Figure 11-81. Strain gauges reading for the 3-in. thick SAPL renewed invert-cut CMP arch.

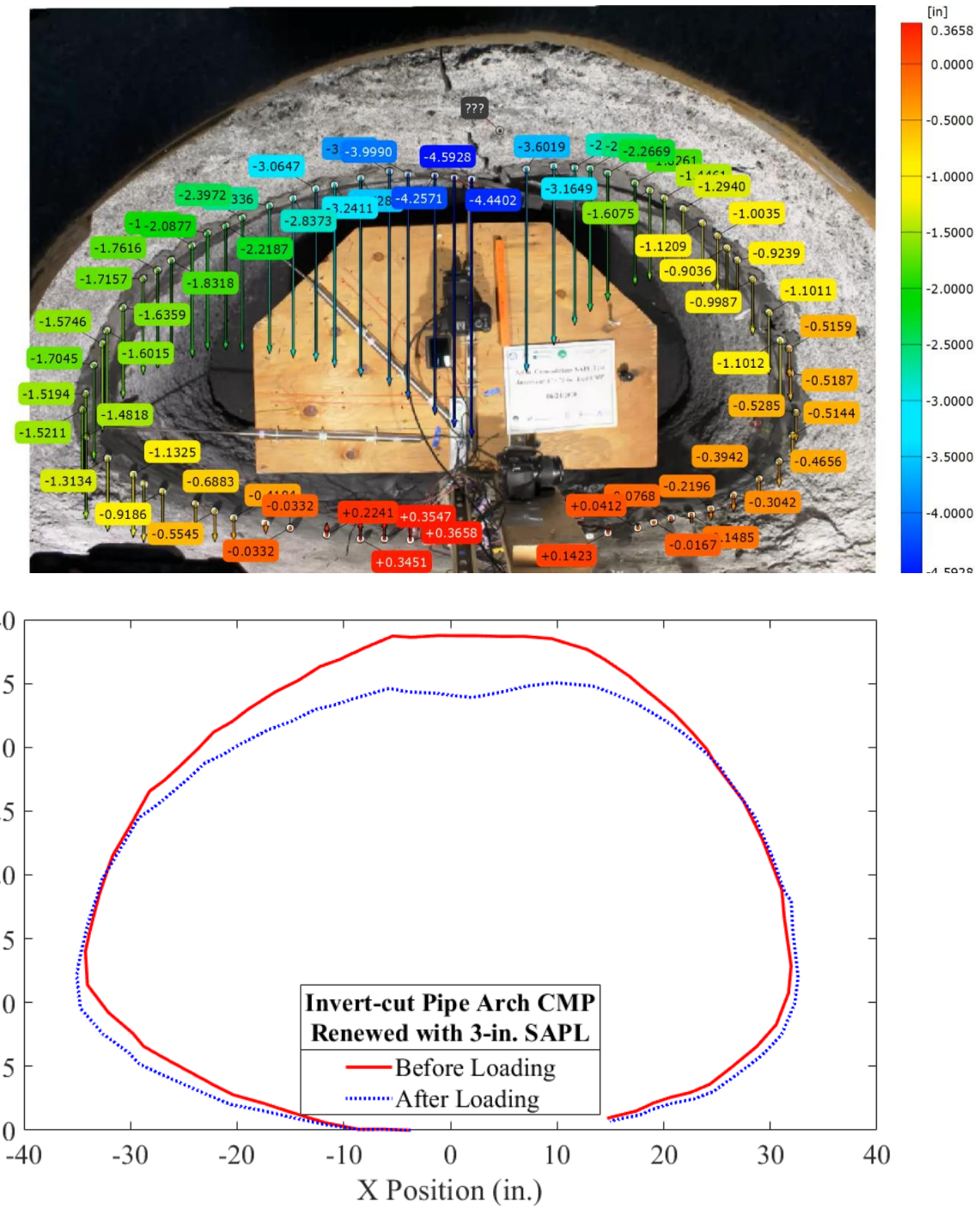


Figure 11-82. Pipe profiling using DIC for the 3-in. thick SAPL renewed invert-cut CMP arch.

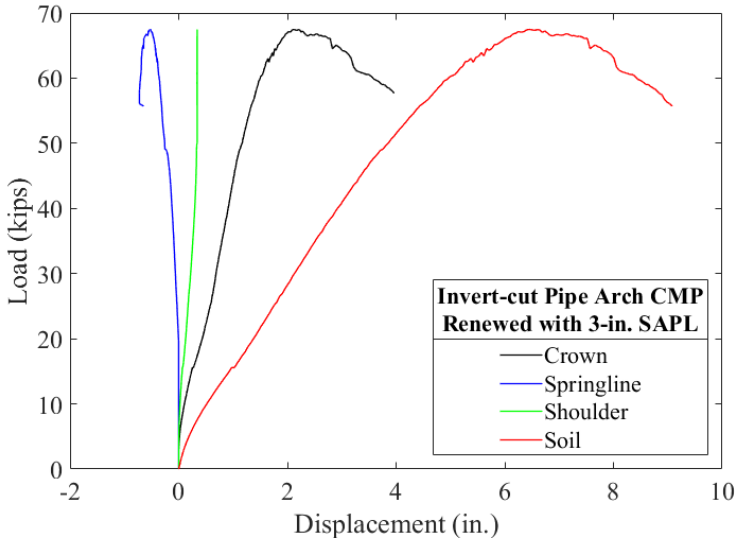


Figure 11-83. Load vs. displacement of the soil surface, crown, springline, and shoulder of the 3-in. thick SAPL renewed invert-cut CMP arch due to the applied static load.

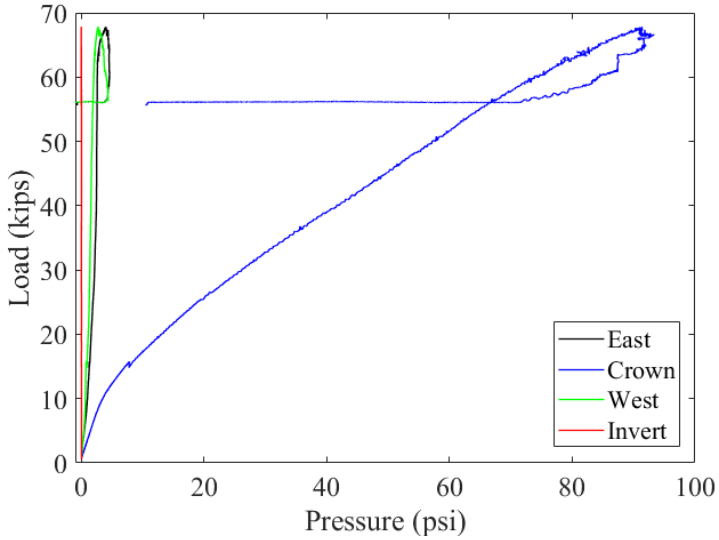


Figure 11-84. Load vs. pressure for the 3-in. thick SAPL renewed invert-cut CMP arch.

11.11.3.1.1.2 Thickness Measurement (3-in. SAPL)

The thickness of the 3-in. thick cementitious SAPL renewed CMP arch was measured after the structural test and before exhumation. Figure 11-85 illustrates the thickness measurements results for all three locations along the length of the pipe (i.e., north, center and south). The results showed that the liner's thickness varied from 2 to 3.4 in. The SAPL was thicker at the West springline and was thinner at crown and invert. In general, the averaged thickness was slightly lower than the required design thickness.

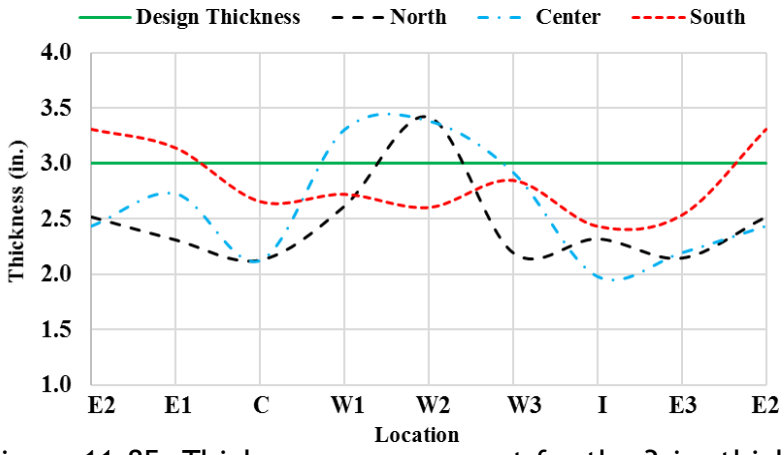


Figure 11-85. Thickness measurement for the 3-in. thick cementitious SAPL renewed CMP arch.

11.11.3.1.1.3 2-in. Thick SAPL Sample

The 2-in. thick SAPL renewed invert-cut CMP arch was tested on Jun 26th, 2020, using the 20 × 40 in. load pad. The test duration was 5.48 hours. During the test, the first visible crack was observed on East side of invert section, at the load of 20 kips. The West side of the crown also cracked at the load of 21 kips at the soil displacement of 0.87 in. The existing cracks' (due to shrinkage) width were increasing with load progression. The SAPL renewed CMP sample failed at the load of 55.16 kips with 7.391 in. of soil settlement. The failure occurred due to the buckling and large deflection of the crown. Figure 11-86 (a) and (b) illustrate the test sample at before and after loading stage. Once the SAPL-CMP system failed, the test was continued until about 20% load drop. Then the test was stopped, as further deflection would increase the chance of liner the detaching and falling, which would damage the mechanical sensors and cameras inside the pipe. Once the load was released from the soil surface, the pipe had an upward movement and relaxed. At this stage, unlike the 3-in. thick sample, no delamination or spalling was observed. Figure 11-87 also illustrates the load and soil settlement graph, registered by the actuator's load cell and LDVT.

The earth pressure cell results registered the maximum pressure of 64.63 psi at the crown location. The maximum pressure applied on the West and East locations were 7.96, and 4.158 psi, respectively. Figure 11-88 illustrates earth pressure results for the invert-cut circular test.

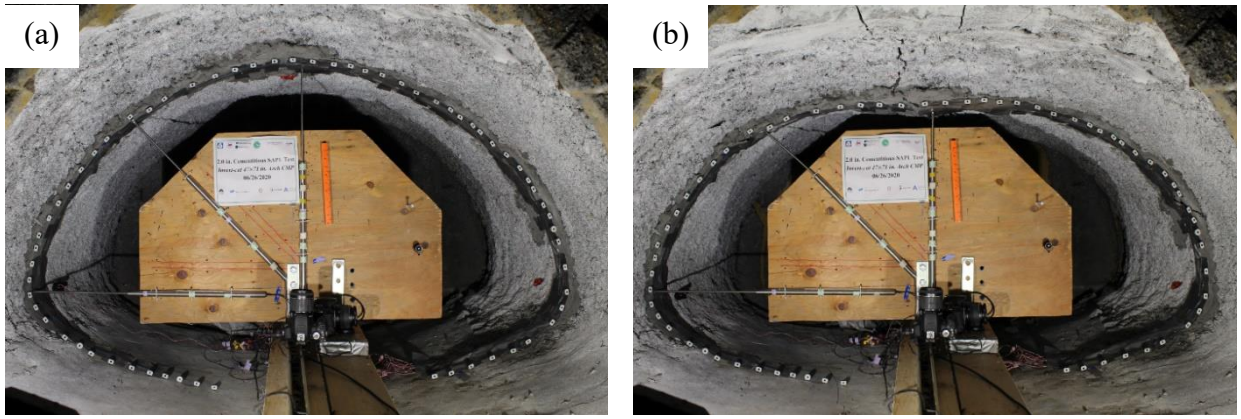


Figure 11-86. Invert-cut CMP arch renewed with 2 in. cementitious SAPL: (a) before loading, and (b) after loading.

Figure 11-89 illustrates the results of the mechanical sensors. The LVDT results show that the pipe was subjected to 5.819 in. of crown and 1.01 in. of springline deflection. The shoulder had 1.07 in. downward movement. The CDS showed an exact similar result as the crown LVDT. At the end of the test once the load was released from the surface, the pipe's crown, and springline had reverse movement of 1.048 and 0.068 in., respectively.

The strain gauge results showed the invert-cut CMP arch experienced a large strain at the crown and both shoulder locations as well as springline that indicates the formation of buckling at the crown, as illustrated in Figure 11-90. The crown of the CMP was the first location that reached the steel yielding point (i.e., 1138 με) at the load of 32.35 kips. East shoulder of the CMP also yielded at 52.38 kips. Other locations of the CMP did not reach the steel yield point. The strain gauges on the SAPL surface of the showed that the cementitious liner cracked at the load of 14.59 kips. At this load, a small drop in the load-displacement graph (Figure 11-87) can be observed. The Figure 11-90 also illustrates a sudden strain reduction in both East and West shoulders of the SAPL at the load of 19.82, which can be due to a crack at this location.

Figure 11-91 illustrates the 2-in. thick SAPL renewed CMP arch profile before and after the static load. The pipe profile at end of the test clearly illustrates the crown flattening. In addition, the roughness and irregularity of the SAPL is explicitly evident in the profiling result. The deflection results captured by the DIC method is in an excellent conformity with the CDS sensor.

The load-displacement values for soil surface, crown, springline, and shoulder of the 2-in. thick SAPL renewed CMP arch due to the applied static load is illustrates in Figure 11-92. In addition, Figure 11-93 illustrates the applied load on the soil surface versus its corresponding pressure at the crown of the renewed CMP arch, where the recursive part of the graph represents drop in both pressure and load at the same time.

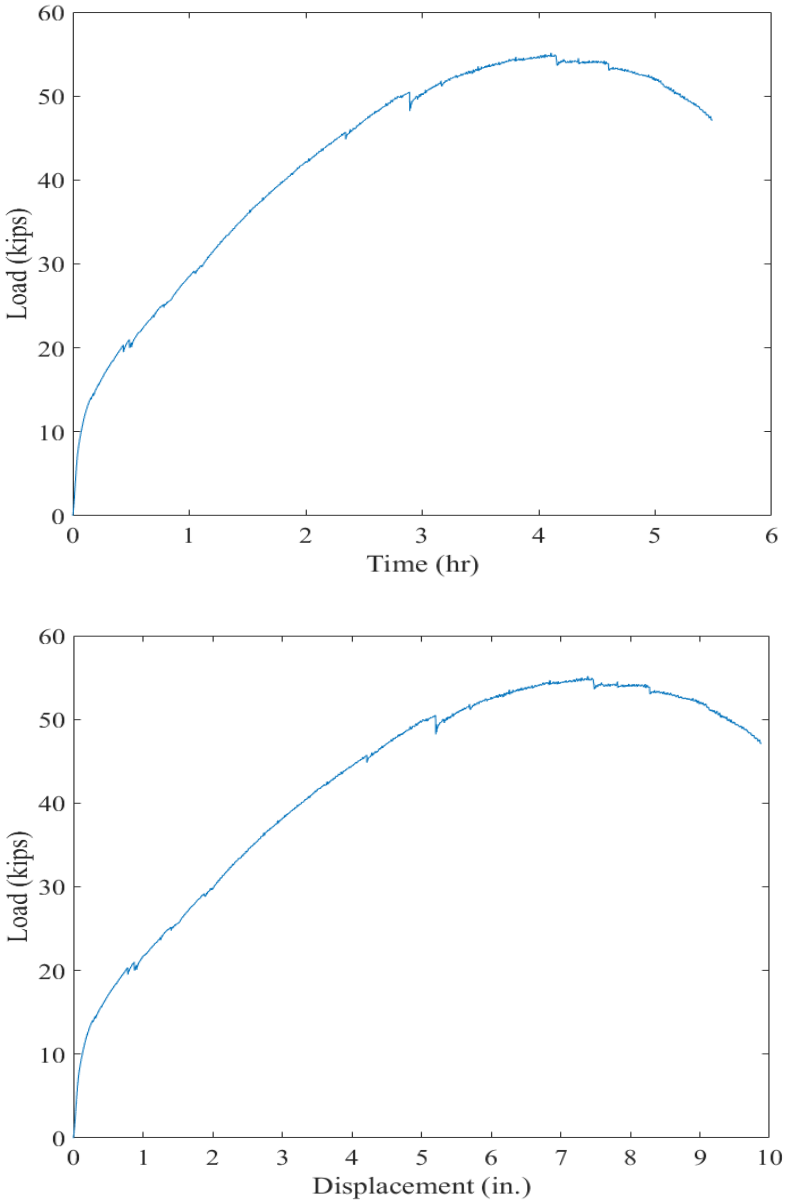


Figure 11-87. Invert-cut CMP arch renewed with 2-in. thick cementitious SAPL subjected to static live load: (top) load-time and (bottom) load-soil displacement graphs.

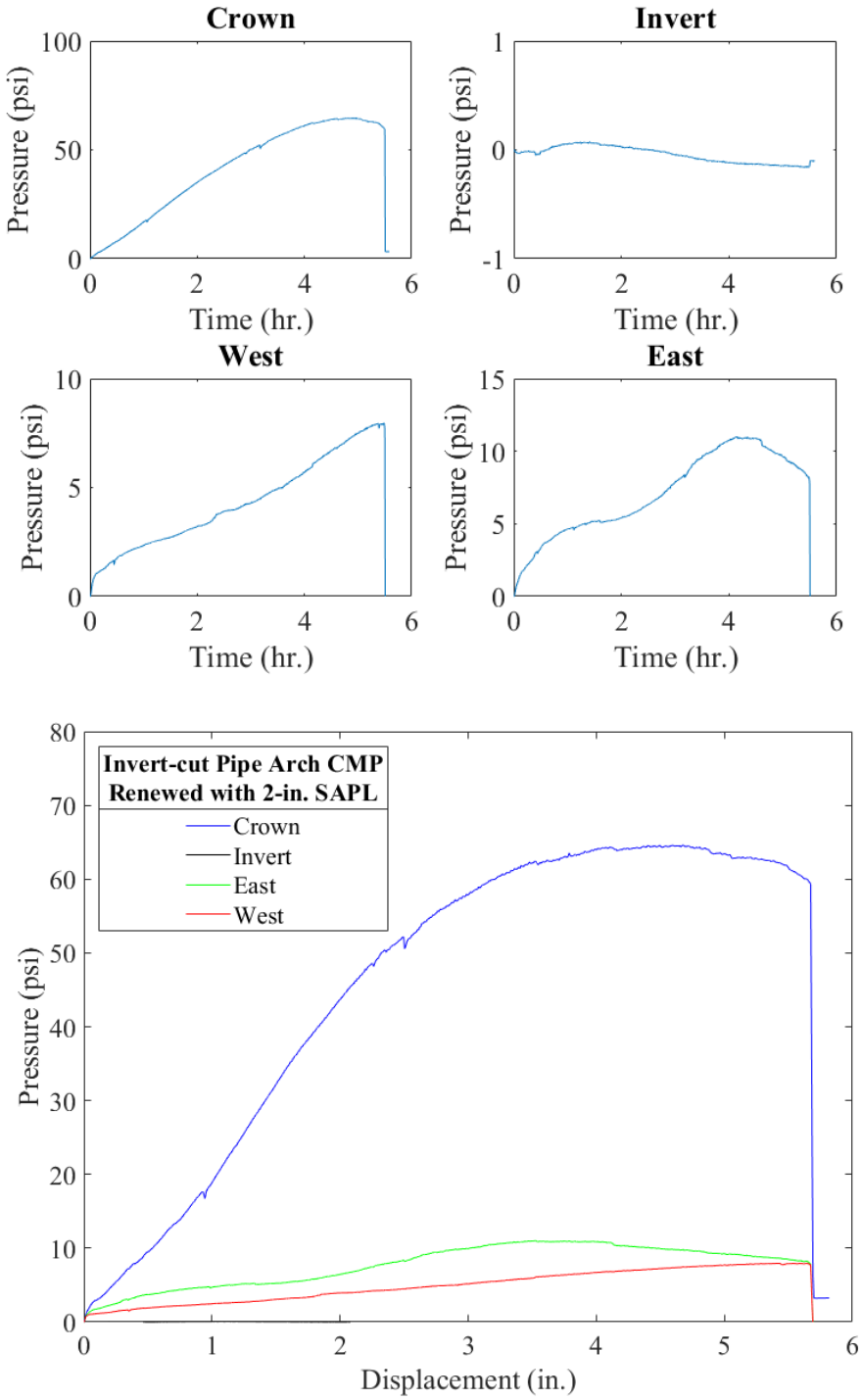


Figure 11-88. Earth pressure cell results for the 2-in. thick SAPL renewed invert-cut CMP arch with respect to: (top) time, and (bottom) crown displacement.

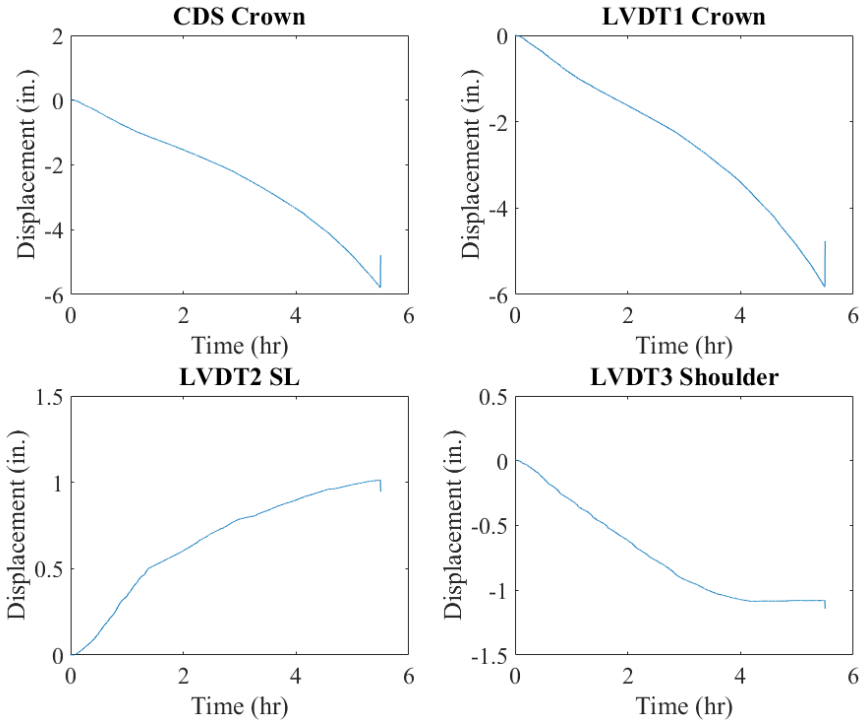


Figure 11-89. Mechanical sensors result for 2-in. thick SAPL renewed invert-cut CMP arch.

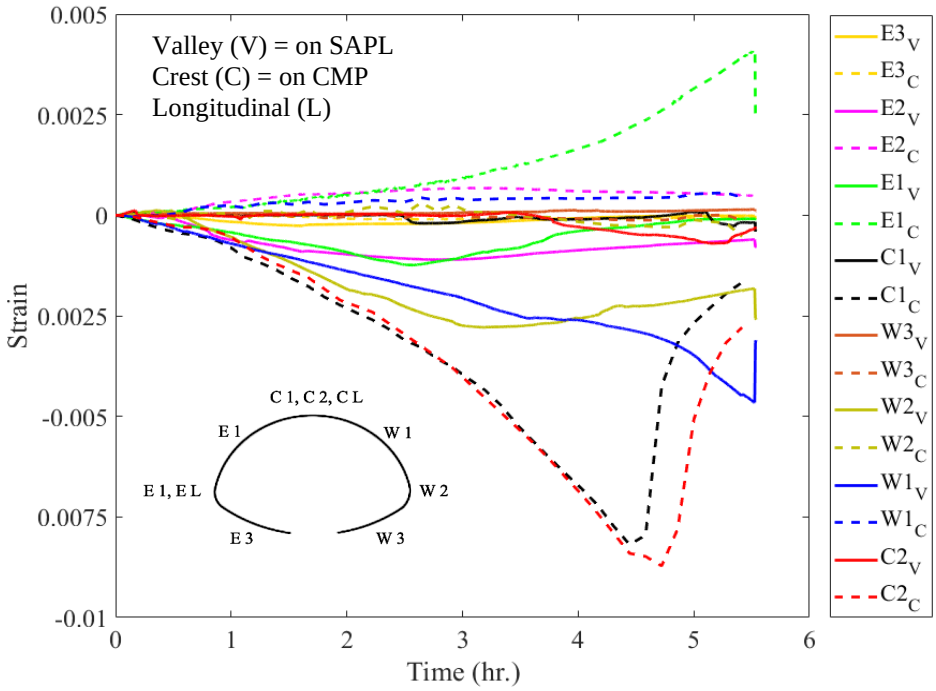


Figure 11-90. Strain gauges reading for 2-in. thick SAPL renewed invert-cut CMP arch.

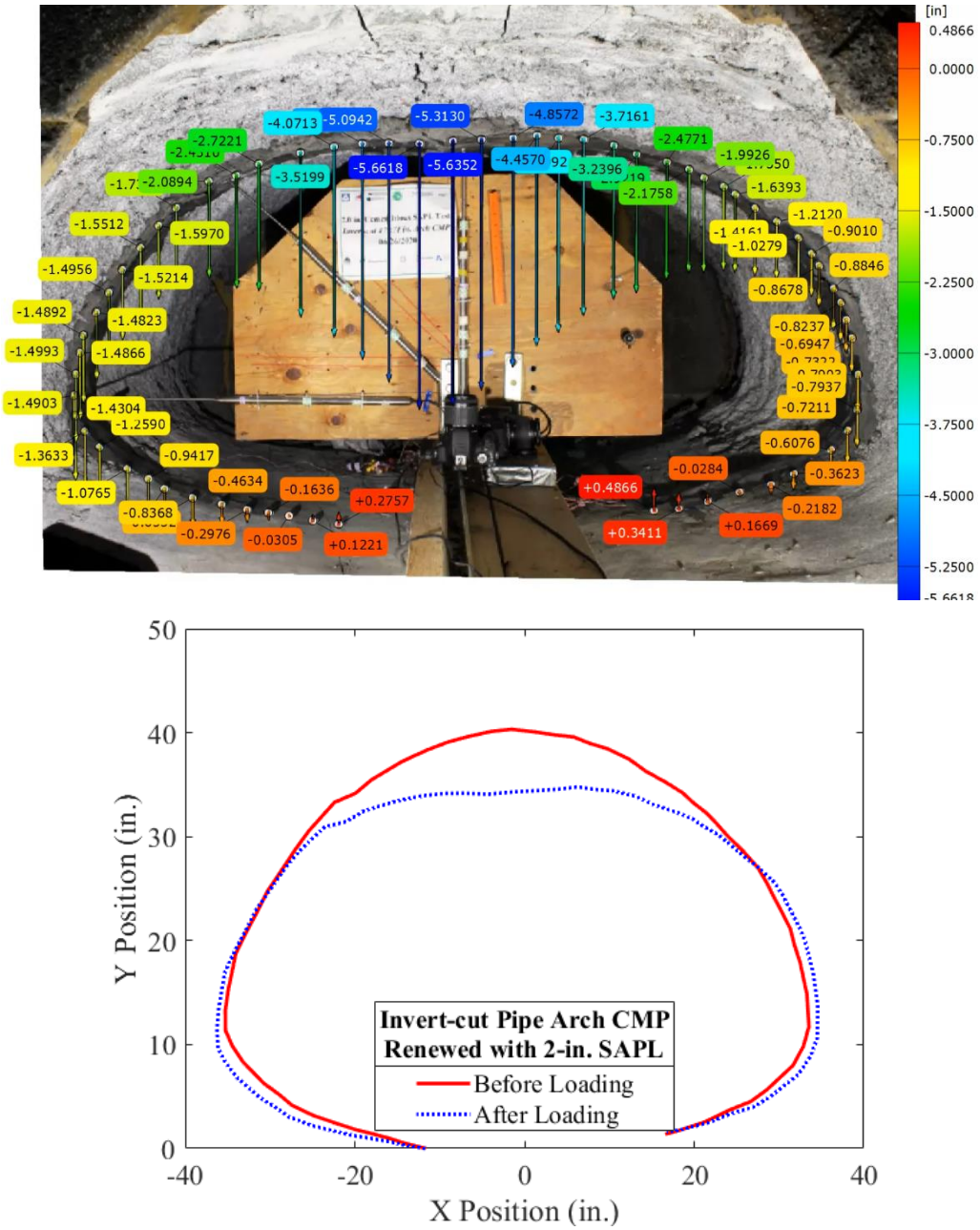


Figure 11-91. Pipe profiling using DIC for the 2-in. thick SAPL renewed invert-cut CMP arch.

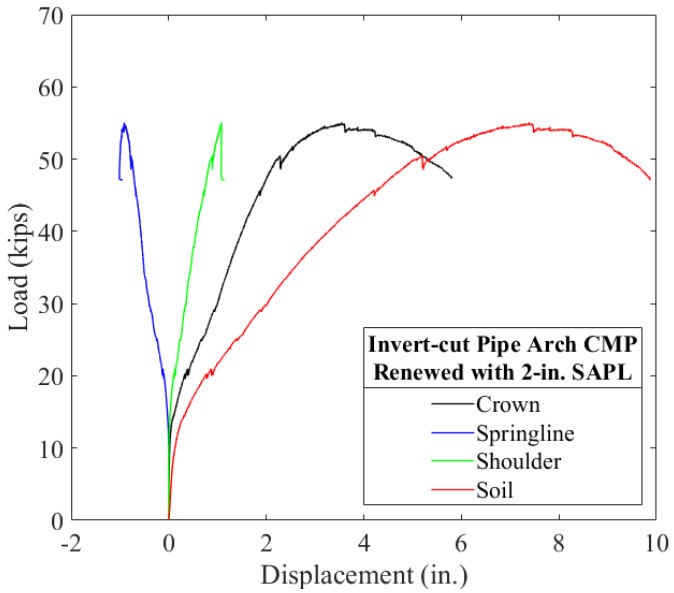


Figure 11-92. Load vs. displacement of the soil surface, crown, springline, and shoulder of the 2-in. thick SAPL renewed invert-cut CMP arch due to the applied static load.

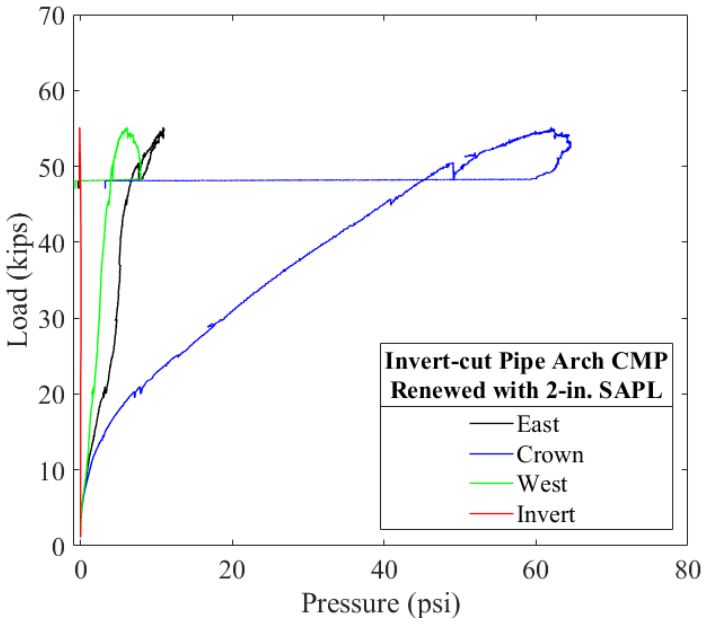


Figure 11-93. Load vs. pressure for the 2-in. thick SAPL renewed invert-cut CMP arch.

11.11.3.1.1.4 Thickness Measurement (2-in. SAPL)

The thickness of the 2-in. thick cementitious SAPL renewed CMP arch was measured after the structural test and before exhumation. Figure 11-94 illustrates the thickness measurements results for all three locations along the length of the pipe (i.e., north, center and south). The results showed that the liner's thickness variation ranged from 1.6 to 2.2 in. The SAPL was more uniformly applied than the 3-in. thick pipe sample. The SAPL was generally thicker towards south side and was thinner towards south side of the CMP. In general, the averaged thickness was slightly lower than the required design thickness.

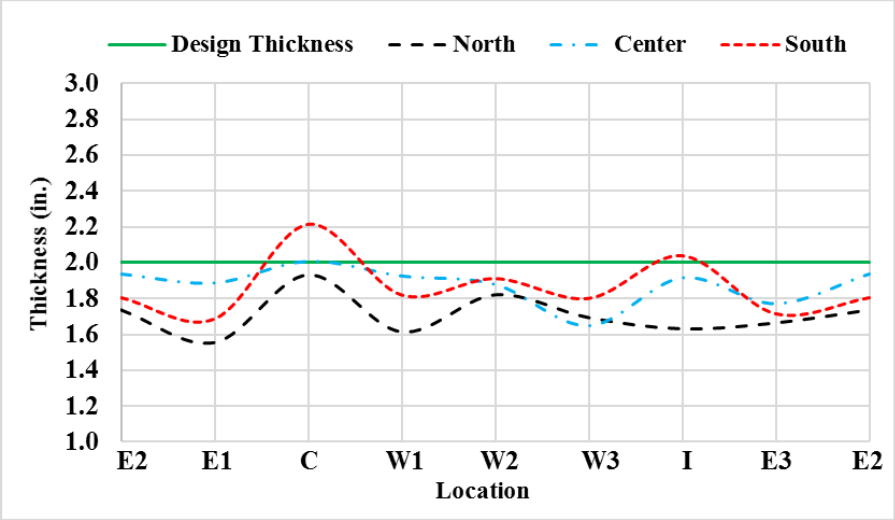


Figure 11-94. Thickness measurement for the 2-in. thick cementitious SAPL renewed CMP arch.

11.11.3.1.1.5 1-in. Thick SAPL Sample

The 1-in. thick SAPL renewed invert-cut CMP arch was tested on Jun 30th, 2020, using the 20 × 40 in. load pad. The test duration was 2.9 hours. The SAPL renewed CMP sample failed at the load of 46.5 kips with 3.9 in. of soil settlement. The failure occurred due to the buckling and large deflection of the crown. In contrast with the 2 and 3 in. SAPL renewed CMP arch samples, where the SAPL experienced two full pipe length longitudinal cracks, the 1 in. SAPL had only a single crack in the invert section. In addition to that, in this test, the longitudinal shrinkage crack at the East haunch area was entirely closed at the end of the test. This implies that due to the applied vertical load, the haunch area near the springline was subjected to compression. Figure 11-95 (a) and (b) illustrate the test sample at before and after loading stage. Once the SAPL-CMP system was failed, the test was continued until about 20% load drop. Then the test was stopped, as further deflection would increase the chance of the liner detaching and falling, which would damage the mechanical sensors and cameras inside the pipe. At this stage, a minor delamination at the East and West shoulders were observed. Figure 11-96 also illustrates the load and soil settlement graph, registered by the actuator's load cell and LDVT.

The earth pressure cell results registered the maximum pressure of 62.88 psi at the crown location. The maximum pressure applied on the West and East locations were 5.014, and 3.253 psi, respectively. Figure 11-97 illustrates earth pressure results for the invert-cut circular test.

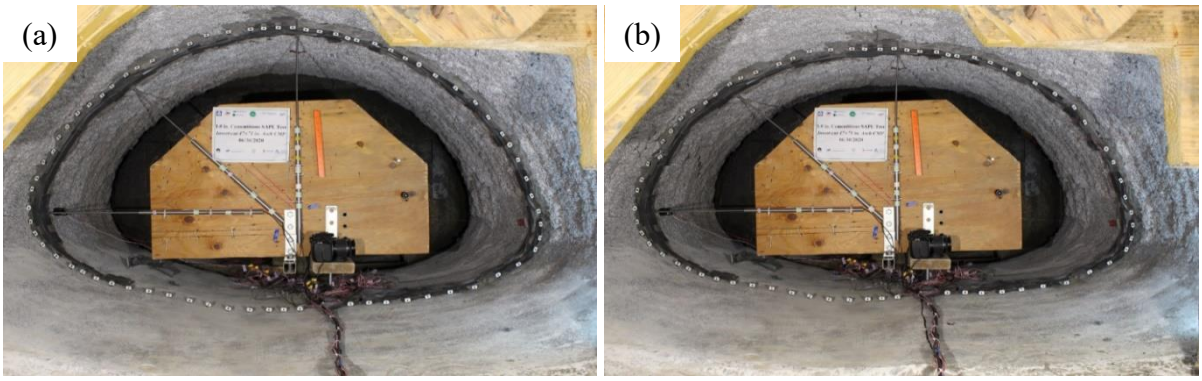


Figure 11-95. Invert-cut CMP arch renewed with 1 in. cementitious SAPL: (a) before loading, where the East haunch had a shrinkage crack and (b) after loading, where the shrinkage crack is closed.

Figure 11-98 illustrates the results of the mechanical sensors. The LVDT results show that the pipe was subjected to 2.811 in. of crown and 0.602 in. of springline deflection. The shoulder had 0.53 in. downward movement. The CDS showed an exact similar result as the crown LVDT. At the end of the test once the load was released from the surface. Unlike the other SAPL renewed CMP arch samples, this pipe did not have reverse movement.

The strain gauge results showed the SAPL cracked at the crown location at the loads of 9.5 and 12.64 kips. The West shoulder of the SAPL also cracked at the load of 12.64 kips, as illustrated in Figure 11-99. The crown of the CMP was the only location that reached the steel yielding point (i.e., 1138 με) at the load of 27.01 kips. At the time of SALP-CMP failure, strain drop is evident on the SAPL surface at the East shoulder and springline. In addition, negative strain value at these locations justifies the shrinkage crack closure as discussed above.

Figure 11-100 illustrates the 1-in. thick SAPL renewed CMP arch profile before and after the static load. The pipe profile at end of the test clearly illustrates the pipe's ovality. In addition, the roughness and irregularity of the SAPL is explicitly evident in the profiling result. The comparison between the mechanical sensors and DIC shows an excellent conformity with the CDS sensor.

The load-displacement values for soil surface, crown, springline, and shoulder of the 1-in. thick SAPL renewed CMP arch due to the applied static load is illustrated in Figure 11-101. The applied load on the soil surface versus its corresponding pressure at

the crown of the renewed CMP arch are depicted in Figure 11-102, where the recursive part of the graph represents drop in both pressure and load at the same time.

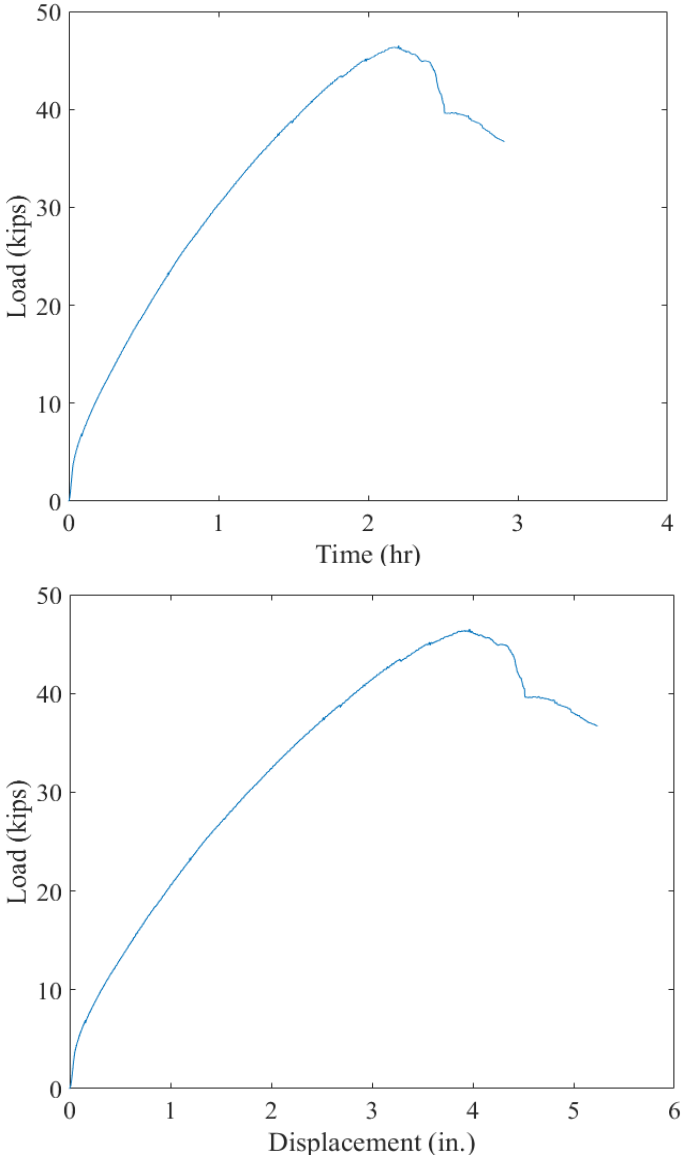


Figure 11-96. Invert-cut CMP arch renewed with 1-in. thick cementitious SAPL subjected to static live load: (top) load-time, and (bottom) load-soil displacement graphs.

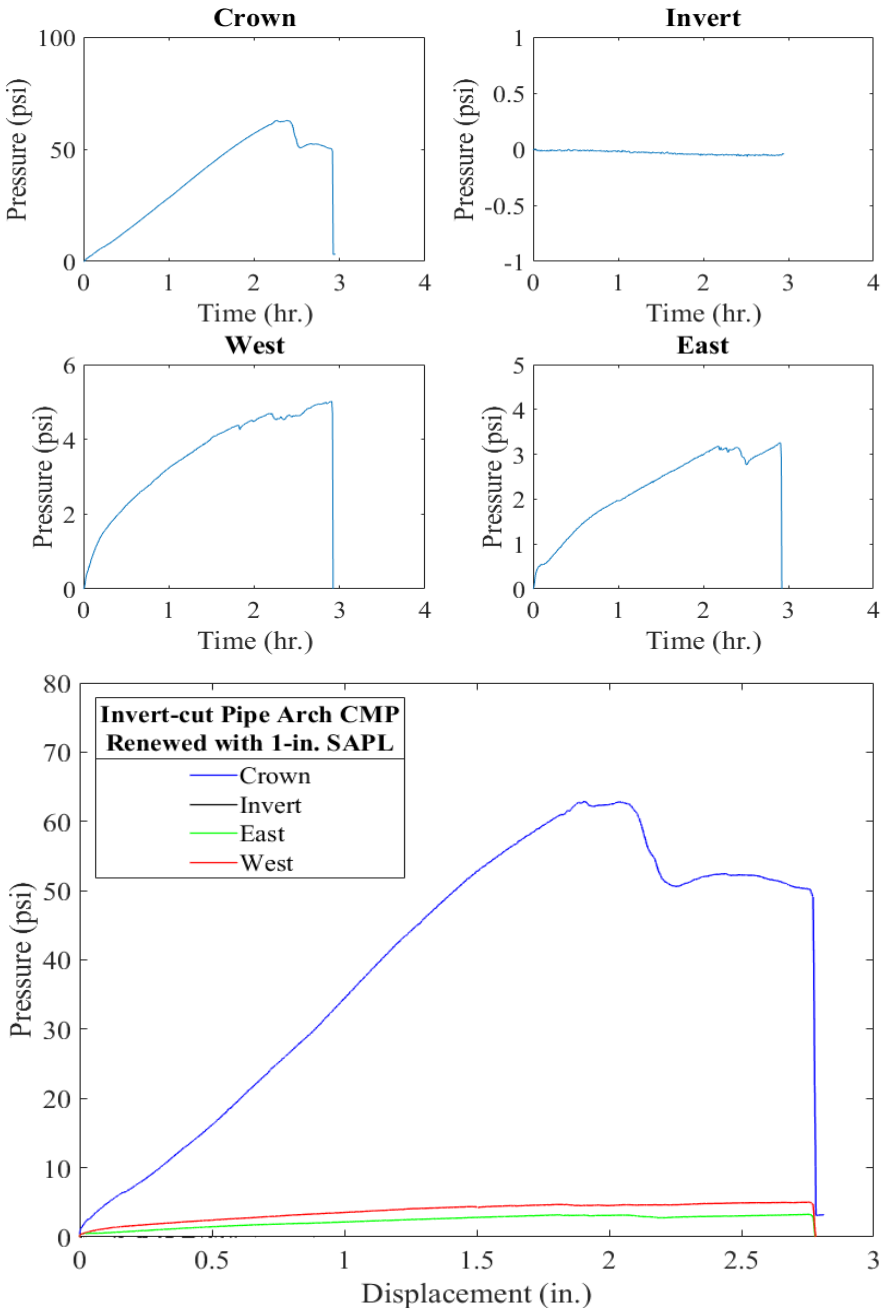


Figure 11-97. Earth pressure cell results for the 1-in. thick SAPL renewed invert-cut CMP arch with respect to: (top) time, and (bottom) crown displacement.

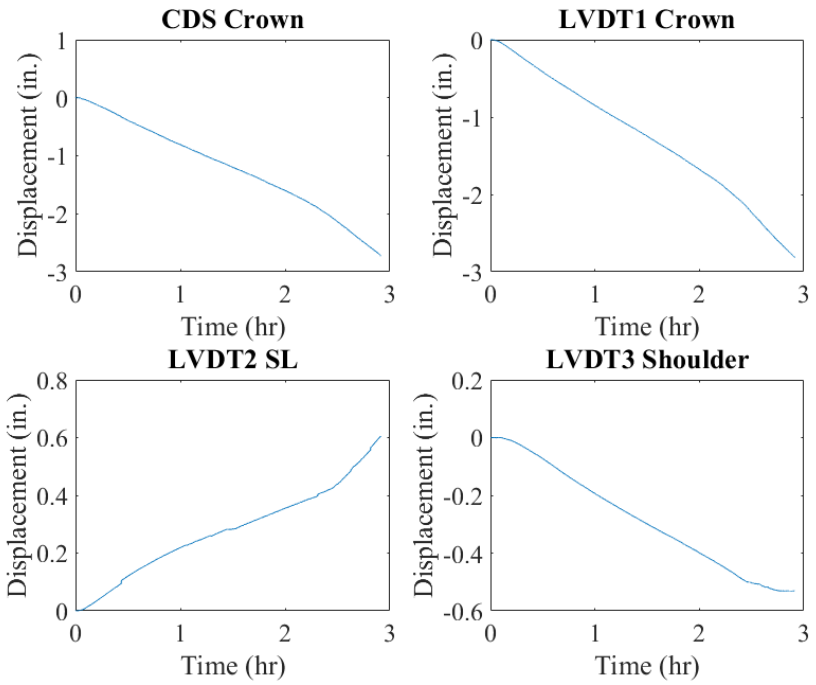


Figure 11-98.Mechanical sensors result for 1-in. thick SAPL renewed invert-cut CMP arch.

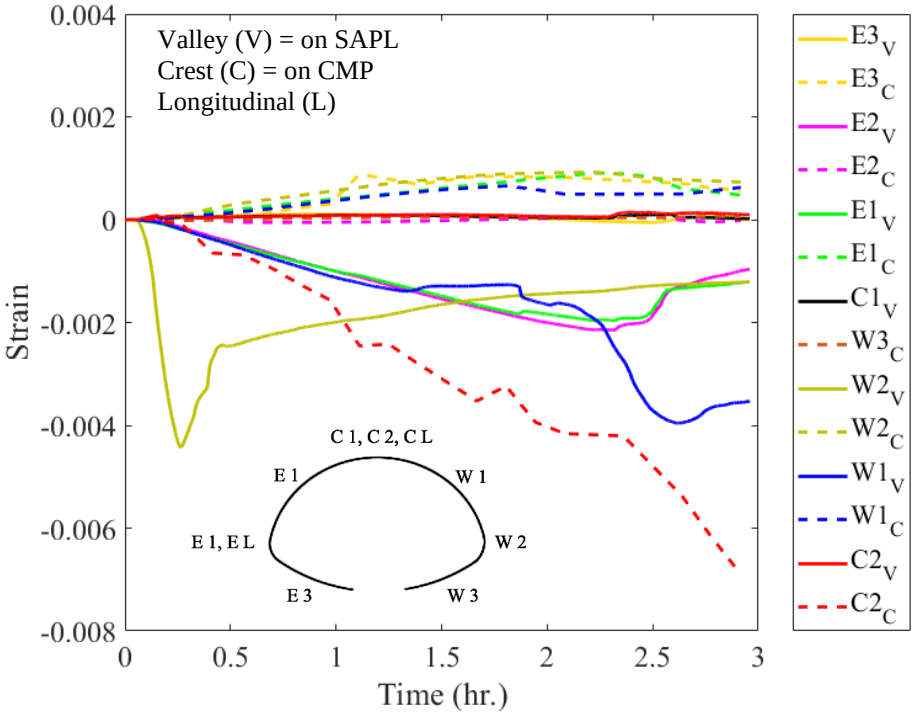
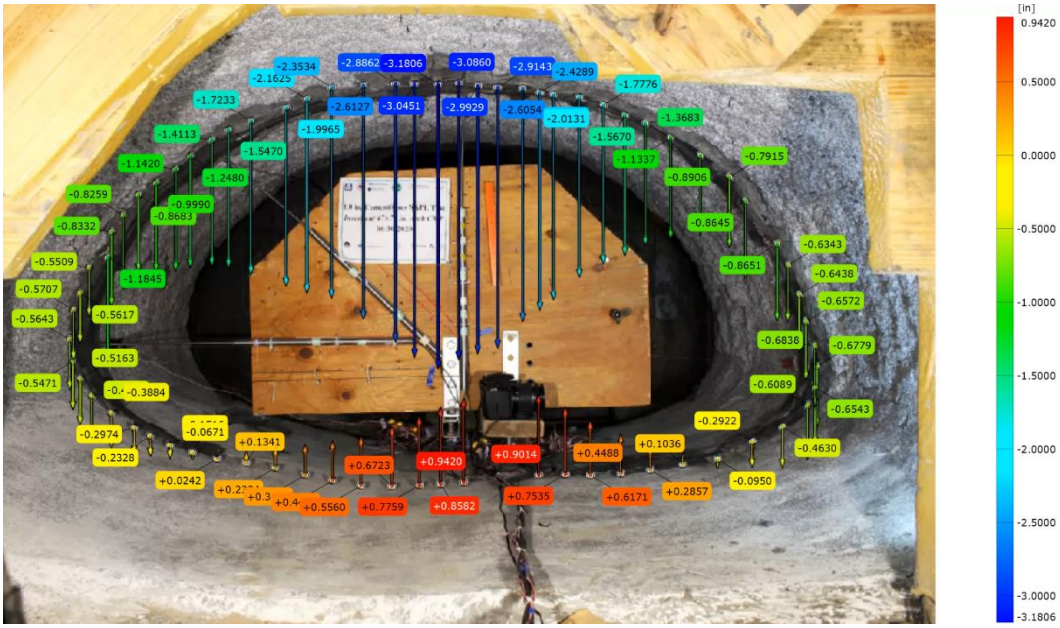


Figure 11-99. Strain gauges reading for 1-in. thick SAPL renewed invert-cut CMP arch.



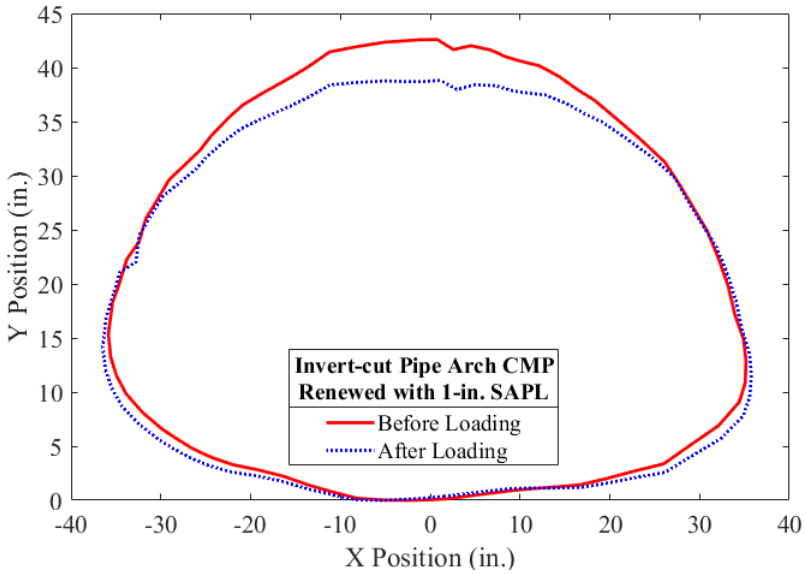


Figure 11-100. Pipe profiling using DIC for the 1-in. thick SAPL renewed invert-cut CMP arch.

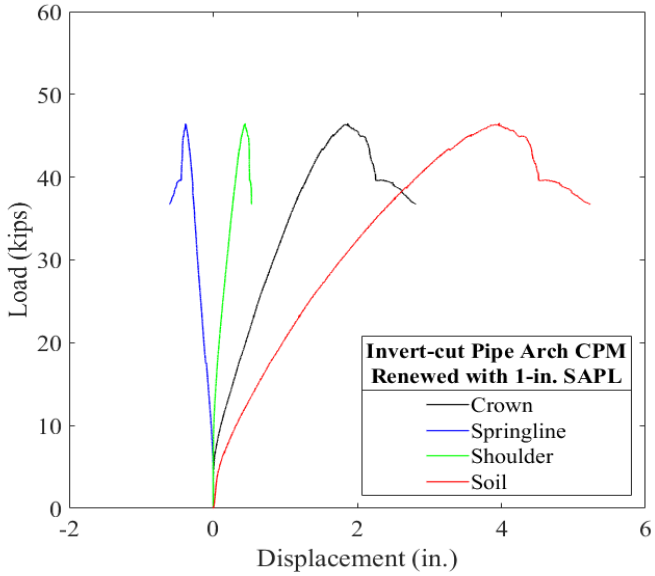


Figure 11-101. Load vs. displacement of the soil surface, crown, springline, and shoulder of the 1-in. thick SAPL renewed invert-cut CMP arch due to the applied static load.

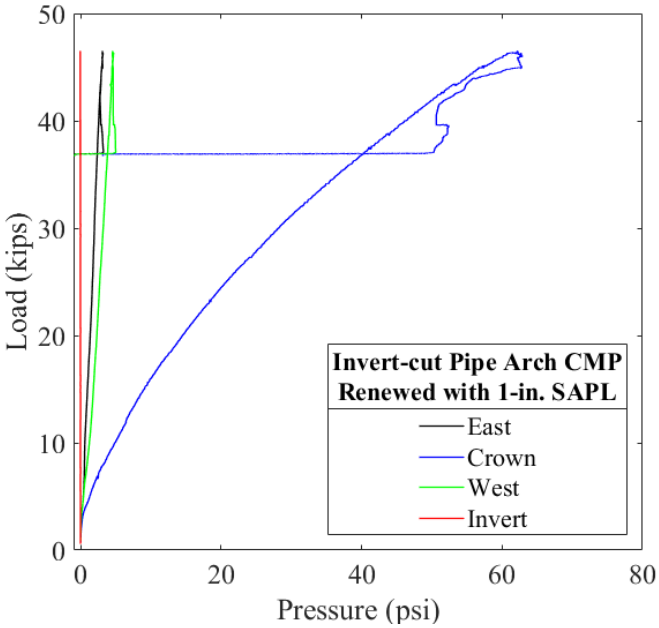


Figure 11-102. Load vs. pressure for the 1-in. thick SAPL renewed invert-cut CMP arch.

11.11.3.1.1.6 Thickness Measurement (1-in. SAPL)

The thickness of the 1-in. thick cementitious SAPL renewed CMP arch was measured after the structural test and before exhumation. Figure 11-103 illustrates the thickness measurements results for all three locations along the length of the pipe (i.e., north, center and south). The results showed that the liner's thickness variation ranged from 0.6 to 1.8 in. In compare with north and south location, the SAPL was generally thicker at center of the CMP. In general, for this pipe, the averaged thickness of the SAPL was about the required design thickness.

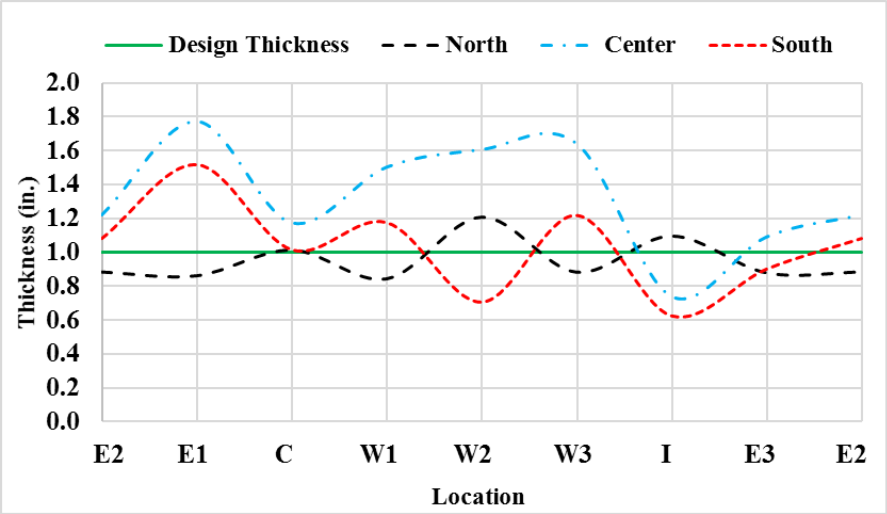


Figure 11-103. Thickness measurement for the 1-in. thick cementitious SAPL renewed CMP arch.

11.11.3.1.1.7 Comparison of SAPL Renewed Invert-cut CMP Arch Test Results

Results comparison between the bare (i.e., unlined) invert-cut CMP arch and SAPL renewed samples showed that application of 1, 2 and 3-in. thick cementitious SAPL on the invert-cut CMP arch samples increased the load carrying capacity for 72.34, 104.4, and 151.44 %, respectively.

Table 11-12 presents the ultimate load results and the load carrying capacity enhancement using different SAPL thickness.

Table 11-12. CMP arch samples test results.

Testing Pipe Samples	SAPL Material	Ultimate Load (Kips)	Improvement (%)
Bare CMP Arch	-	26.98	-
1 in. Thick SAPL	Geopolymer	46.50	72.34
2 in. Thick SAPL	Geopolymer	55.16	104.4
3 in. Thick SAPL	Geopolymer	67.84	151.44

The comparison between the soil settlement at the time of soil-CMP failure with different SAPL thicknesses show that the application of SAPL increased the required soil settlement to achieve failure of the system. Figure 11-104 illustrates a graph presenting the load versus soil settlement for all CMP arch samples. The result also showed that the soil settlement value for the 2 and 3-in. thick SAPL at the time of failure is about the same. One of reasons could be due to the fact that the actual crown thickness of both pipe samples is very close. However, it was observed that the crown displacement of the 2-in. thick pipe sample, presented in Figure 11-105, at the time of soil-CMP failure is higher than the both 1 and 3-in. thick pipe samples. The main reason of this behavior is yet unknown to the research team, however, one of the possible reasons could be due to the higher level of thickness variation and geometry irregularity of the 3-in. thick SAPL, illustrated in Figure 11-82. The result of horizontal diameter changes of different SAPL renewed thicknesses and the bare invert-cut CMP arch is presented in Figure 11-106, where the 2-in SAPL renewed CMP sample had the highest horizontal expansion.

Figure 11-107 illustrates the result of the applied static load on the soil surface versus the applied pressure over the crown of the pipe. The AASHTO H20 truck equivalent pressure, obtained from the intact CMP test, is compared from the SAPL renewed CMP arch samples and it can be observed that, unlike the bare invert-cut CMP arch, the SAPL renewed CMP arch samples could resist the equivalent AASHTO H20 truck pressure. The figure shows that the thicker the liner the higher load is required to fail the SAPL-CMP system. It can be concluded that all three thicknesses are sufficient for the AASHTO H20 truck load.

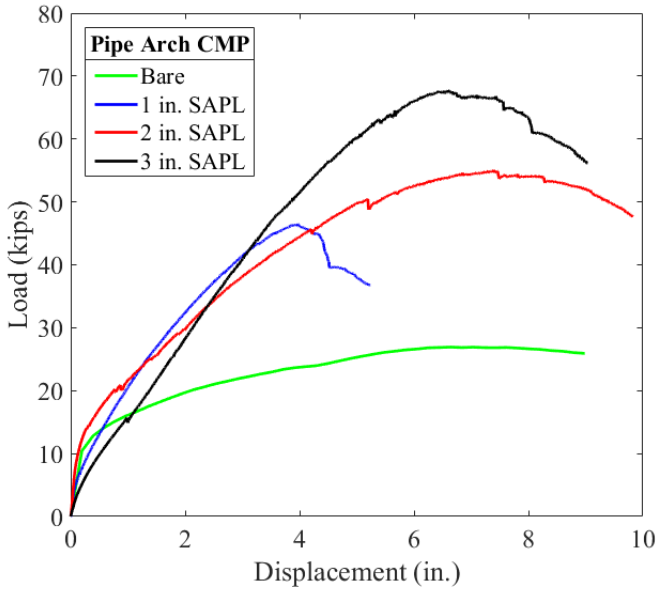


Figure 11-104. Load vs. soil settlement comparison graph.

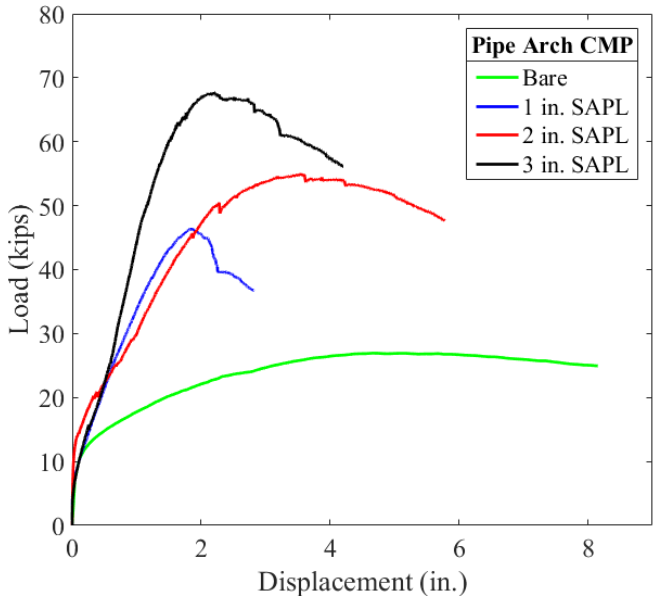


Figure 11-105. Load vs. crown displacement comparison graph.

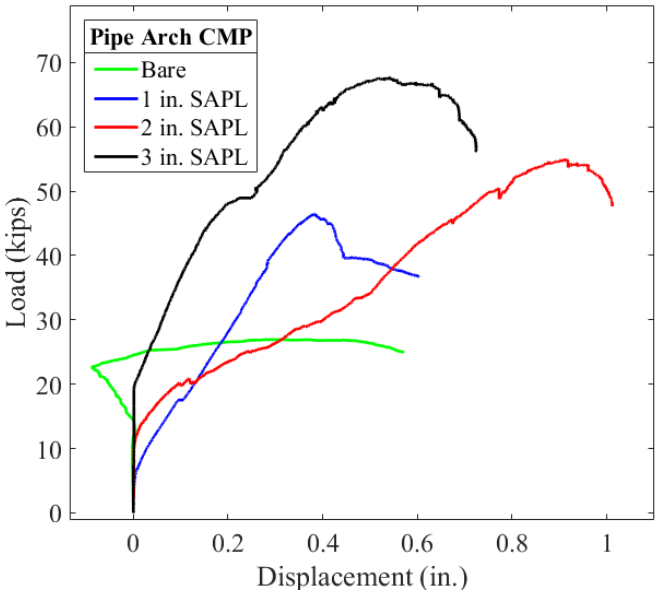


Figure 11-106. Load vs. springline displacement comparison graph.

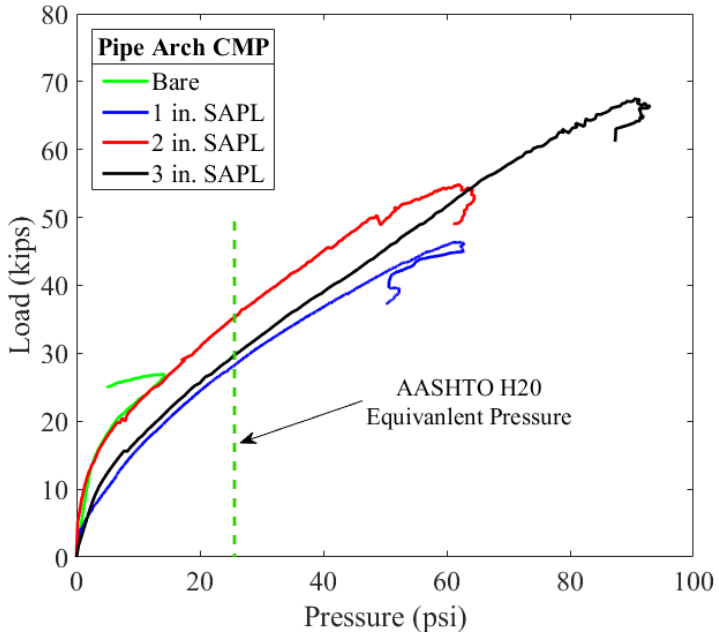


Figure 11-107. Load vs. pressure comparison graph.

11.11.3.1.2 SAPL Renewed Invert-cut Circular CMP Test Results

The invert-cut circular CMPs renewed with the cementitious SAPL were tested using the same load rate and load. Due to required time for test preparation, instrumentation, and operation, conducting all the three tests of this set in one day was not possible. The first test was conducted on the 3-in. thick SAPL renewed circular CMP after 7 days of curing. The 2 and 1-in. thick SAPL renewed circular CMPs were conducted with a 2-day interval, respectively.

In general, a circular pipe subjected to vertical load will experience tension in the crown, invert and both exterior surfaces of the springline, as illustrated in Figure 11-108. In conformity to the expected cracking locations in the tension zones, it was observed in all three tested SAPL renewed circular CMPs that the majority of the cracks formed crown, invert (at the invert-cut's gaps) and in the transition zones at shoulders and haunches area.

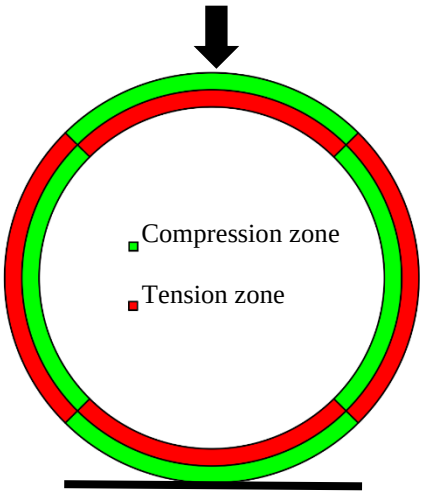


Figure 11-108. Compression and tension zones of a circular pipe subjected to a vertical load.

11.11.3.1.2.1 3-in. Thick SAPL Sample

The 3-in. thick SAPL renewed invert-cut circular CMP was tested on July 27th, 2020, using the 20 × 40 in. load pad. The test duration was 5.97 hours. During the test, due to the existence of shrinkage cracks no major drop in the load-displacement graphs was observed, and the cracks width were increased with the load progression. The SAPL renewed CMP sample failed at the load of 109.7 kips with 10.83 in. of soil settlement. The failure occurred due to the large deflection and cracking of the crown. Figure 11-109 (a) and (b) illustrate the test sample at before and after loading stage. Once the SAPL-CMP system was failed, the test was continued until about 20% load drop. Then the test was terminated, as further deflection would increase the chance of liner detachment and fall, which would damage the mechanical sensors and cameras inside the pipe. Once the load was released from the soil surface, the pipe had an upward movement and relaxed. Figure 11-110 also illustrates the load and soil settlement graph, registered by the actuator's load cell and LDVT.

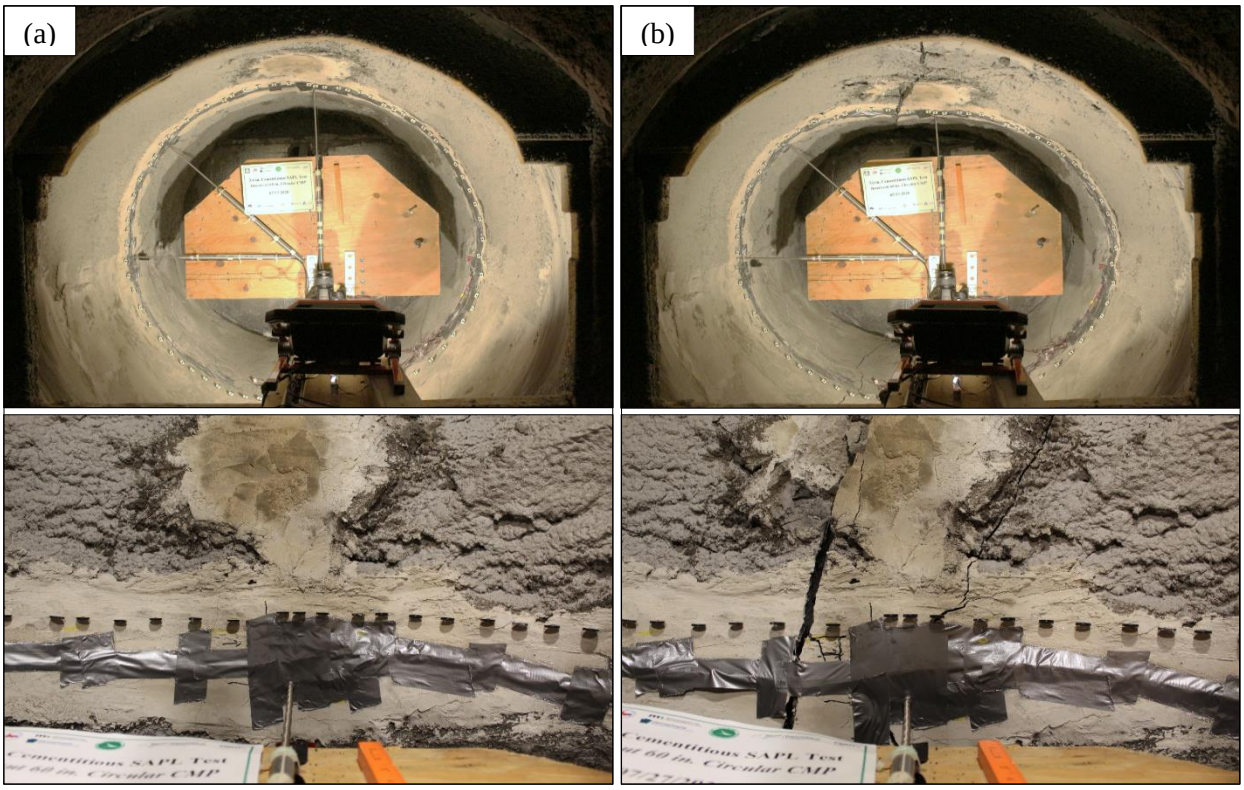


Figure 11-109. Invert-cut circular CMP renewed with 3 in. cementitious SAPL: (a) before loading, and (b) after loading.

The earth pressure cell results registered the maximum pressure of 106.8 psi at the crown location. The maximum pressure applied on the West and East locations were 23.17, and 16.51 psi, respectively. Figure 11-111 illustrates earth pressure results for the invert-cut circular test. It also shows that the pressure was dropped after 106 psi. At this pressure, the corresponding surface load and pressure, were 92 kips and 115 psi.

Figure 11-112 illustrates the results of the mechanical sensors. The LVDT results show that the pipe was subjected to 4.356 in. of crown and 1.683 in. of springline deflection. The shoulder had 0.469 in. downward movement. The CDS showed a similar result (4.348) as the crown LVDT. At the end of the test, once the load was released from the soil-pipe system, a reversal movement in crown and springline for 0.77 and 0.106 in., respectively, were observed.

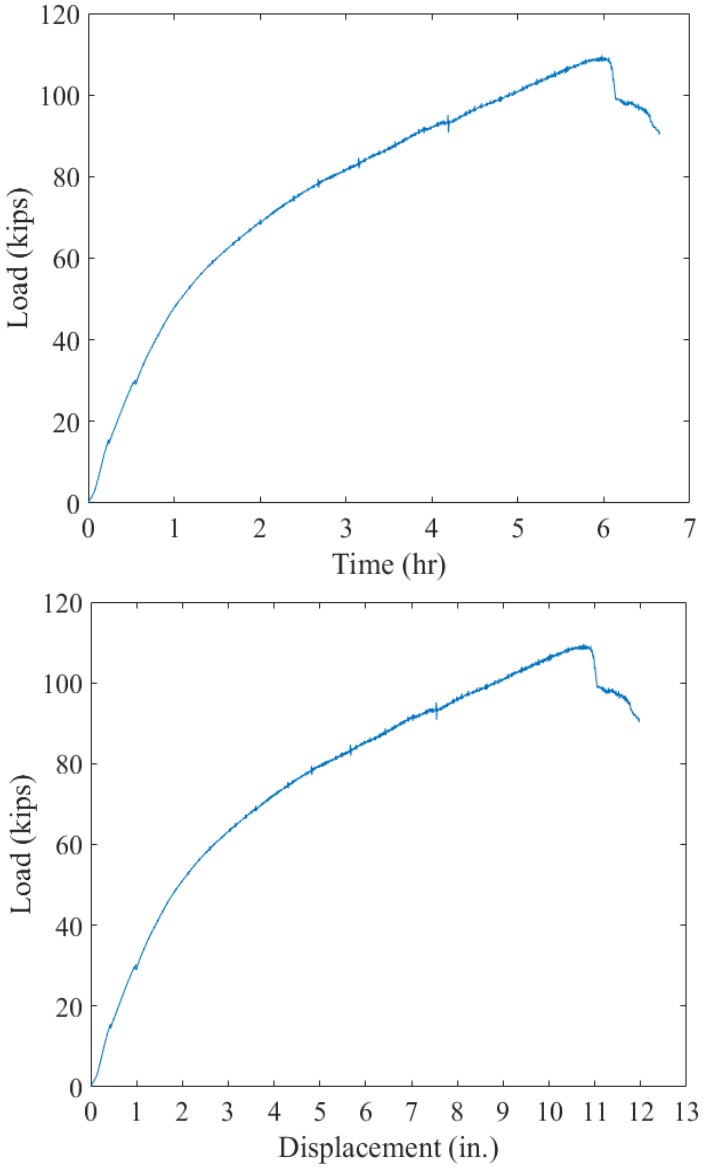


Figure 11-110. Invert-cut circular CMP renewed with 3-in. thick cementitious SAPL subjected to static live load: (top) load-time, and (bottom) load-soil displacement graphs.

The strain gauge results showed the SAPL cracked at the invert on the West side of the invert at the load of 18.71 kips. In addition to that, the East side of the invert most likely cracked at the load of 30 kips as at this load all the strain gauges show a drop in their reading, while they did not show stress relaxation that implies somewhere the liner is cracked other than installed strain gauge locations. Live monitoring of the SAPL using a digital camera revealed that at this load the invert section cracked. In addition to that, the East haunch cracked at 33 kips. Due to the harsh and abrasive nature of the soil, both strain gauges installed at the crown of CMP were damaged and were unable to measure the strain. At the load of 92 kips, which failed the soil cover on top of the CMP, a rise in all strain values were observed. After this point, the East

shoulder and springline reached the steel yielding point (i.e., 1138 με). No other location in the CMP reached the yield point.

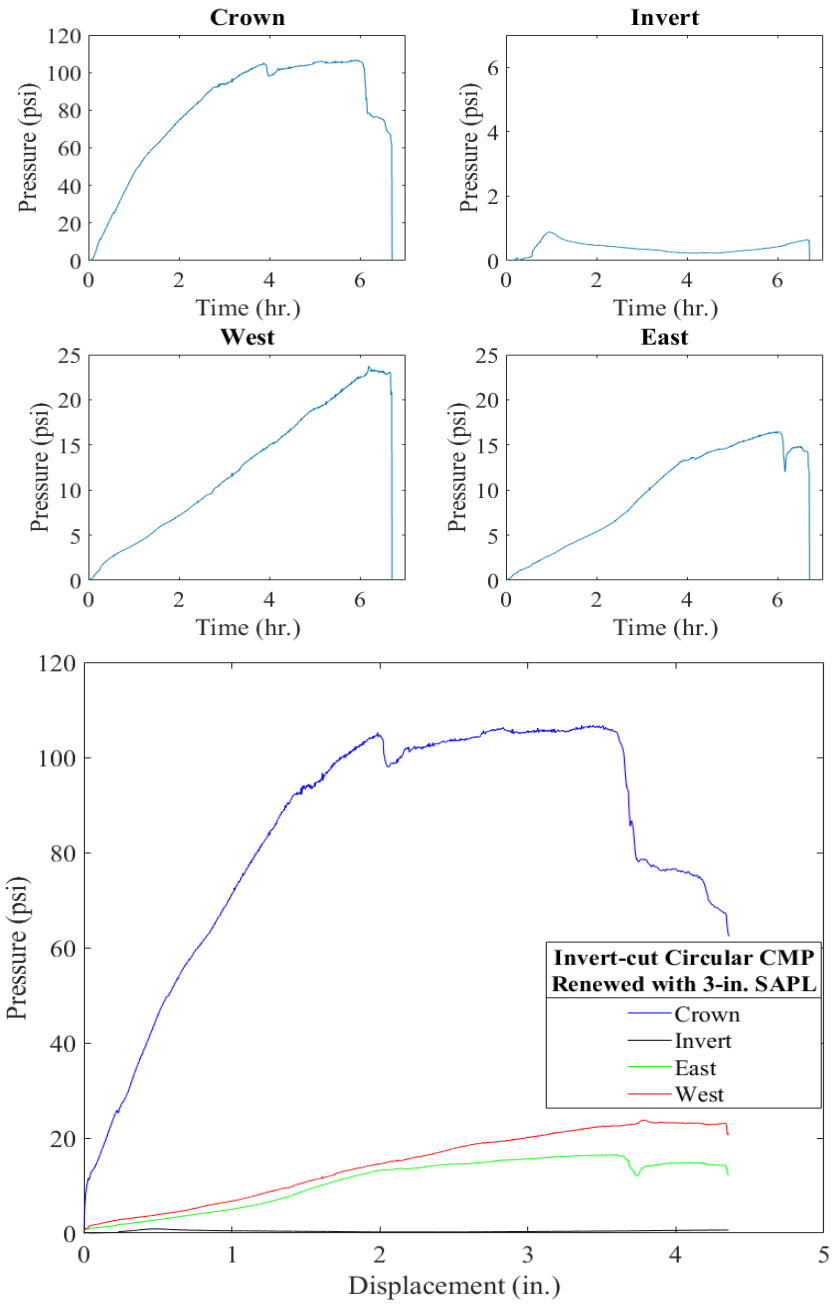


Figure 11-111. Earth pressure cell results for the 3-in. thick SAPL renewed invert-cut circular CMP with respect to: (top) time, and (bottom) crown displacement.

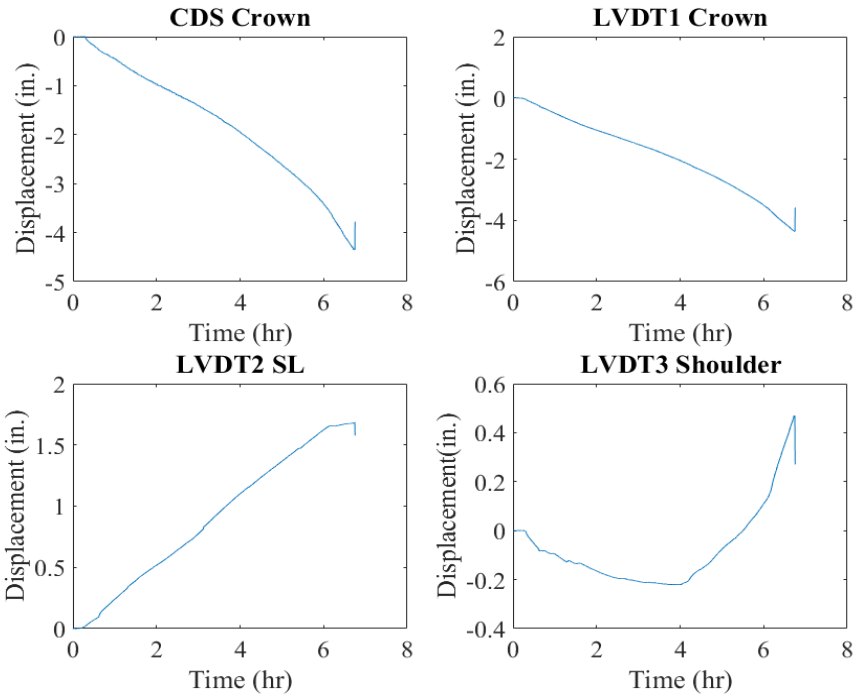


Figure 11-112. Mechanical sensors result for 3-in. thick SAPL renewed invert-cut circular CMP.

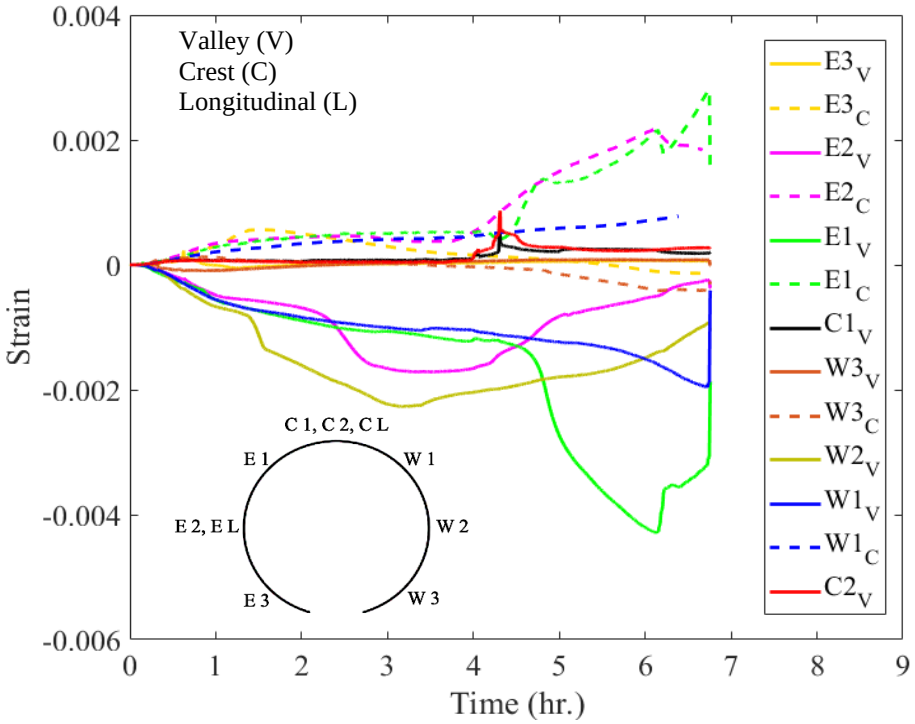


Figure 11-113. Strain gauge result for 3-in. thick SAPL renewed invert-cut circular CMP.

Figure 11-114 illustrates the 3-in. thick SAPL renewed circular CMP profile before and after the applied static load. The pipe profile at end of the test clearly illustrates the pipe's ovality. In addition, the roughness and irregularity of the SAPL is explicitly evident in the profiling result.

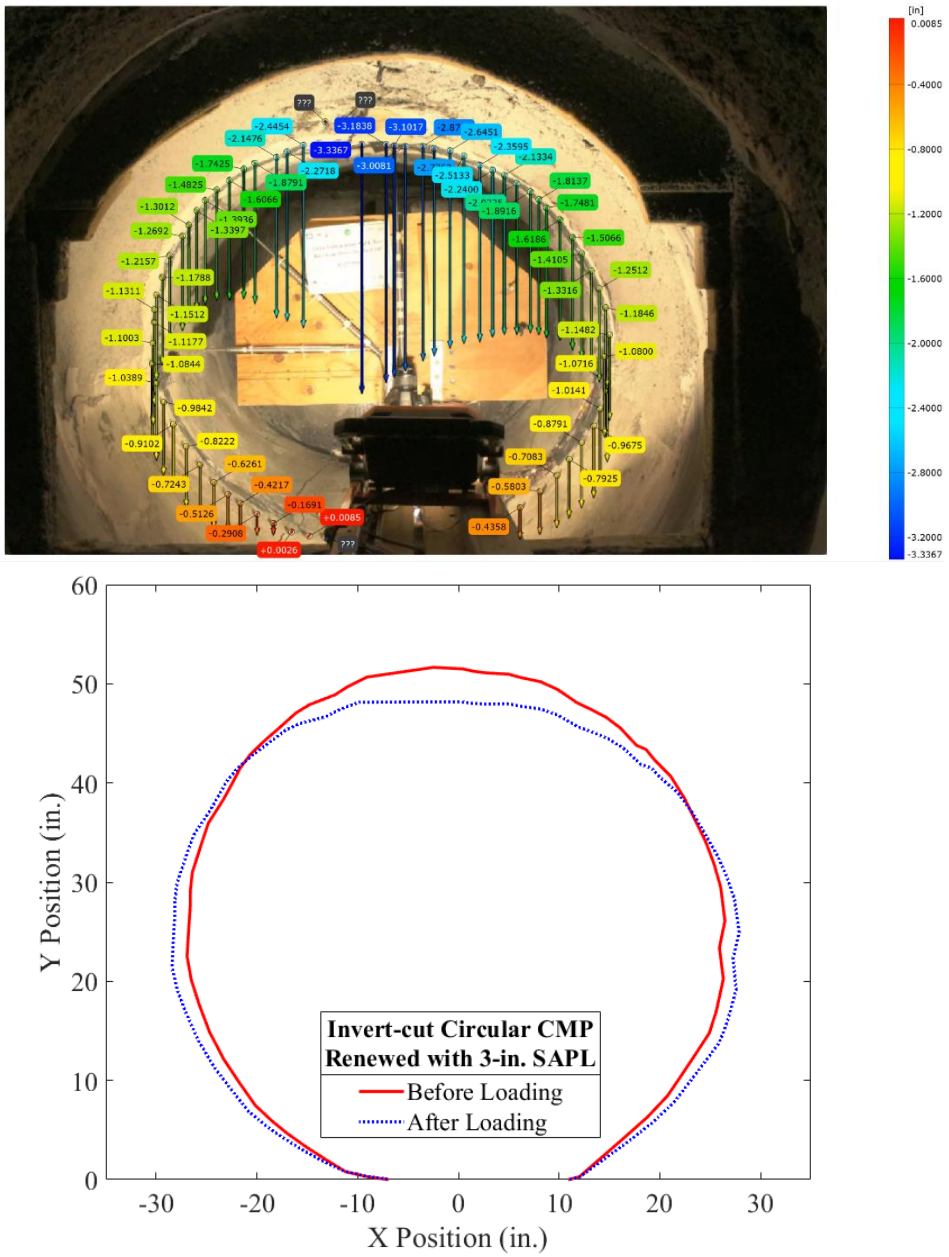


Figure 11-114. Pipe profiling using DIC for the 3-in. thick SAPL renewed invert-cut circular CMP.

The load-displacement values for soil surface, crown, springline, and shoulder of the 3-in. thick SAPL renewed circular CMP due to the applied static load is illustrates in Figure 11-115. The applied load on the soil surface versus its corresponding pressure

at the crown of the renewed circular CMP the recursive part of the graph represents drop in both pressure and load at the same time.

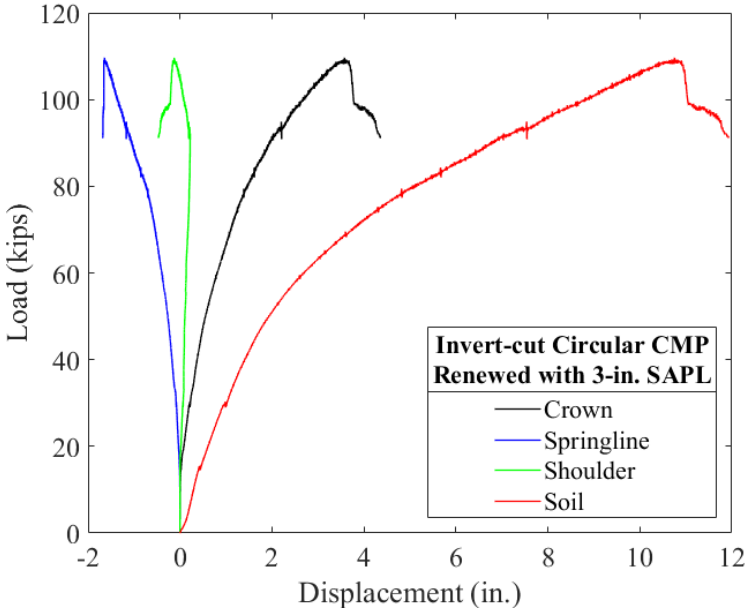


Figure 11-115. Load vs. displacement of the soil surface, crown, springline, and shoulder of the 3-in. thick SAPL renewed invert-cut circular CMP due to the applied static load.

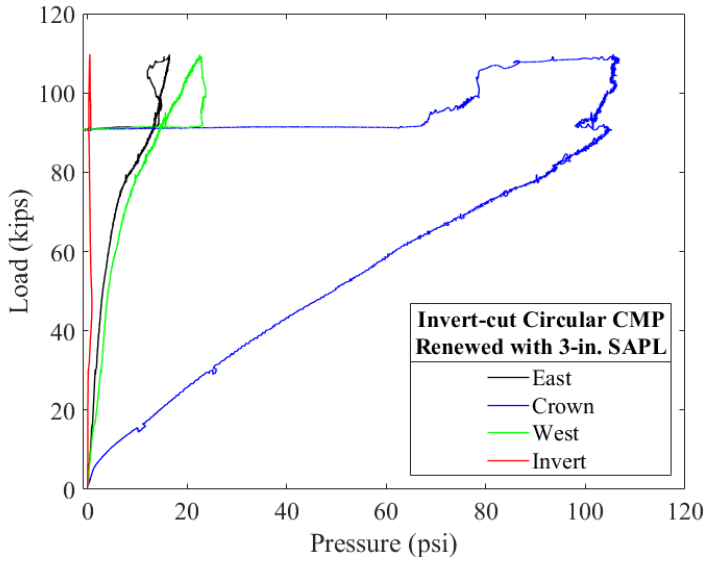


Figure 11-116. Load vs. pressure for the 3-in. thick SAPL renewed invert-cut circular CMP.

11.11.3.1.2.2 Thickness Measurement (3-in. SAPL)

The thickness of the 3-in. thick cementitious SAPL renewed circular CMP were measured after the structural test and before exhumation. Figure 11-117 illustrates the thickness measurements results for all three locations along the length of the pipe (i.e.,

north, center and south). The results showed that the liner's thickness variation ranged from 1.5 to 3.6 in. The applied thickness was generally either higher or about the design thickness on the crown and both shoulder locations. However, the applied thickness was lower at the haunches and invert area. One of the possible reasons could be due to the troweling and finishing the surface of the half bottom portion of the pipe (i.e., from springline to springline) that either compressed or reduced the finished thickness.

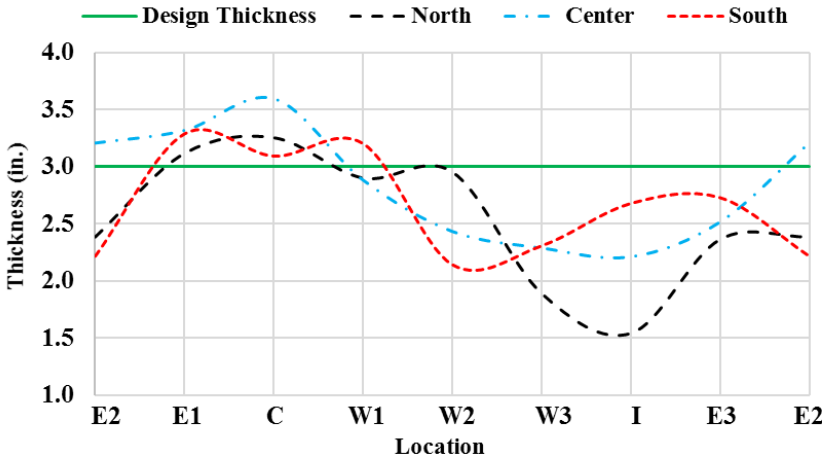


Figure 11-117. Thickness measurement for the 3-in. thick cementitious SAPL renewed circular CMP.

11.11.3.1.2.3 2-in. Thick SAPL Sample

The 2-in. thick SAPL renewed invert-cut circular CMP was tested on July 29th, 2020, using the 20 × 40 in. load pad. The test duration was 6.38 hours. In this pipe sample, unlike the 3-in. thick sample, no shrinkage crack existed in the crown. The SAPL renewed CMP sample cracked at the crown in 14 kips of load and failed at the load of 85.42 kips with 8.5 in. of soil settlement. The failure occurred due to the large deflection and cracking of the crown. Figure 11-118 (a) and (b) illustrate the test sample at before and after loading stage. Once the SAPL-CMP system was failed, the test was continued until about 20% load drop. Then the test was terminated, as further deflection would increase the chance of liner detaching and falling, which would damage the mechanical sensors and cameras inside the pipe. Once the load was released from the soil surface, the pipe had an upward movement and relaxed. Figure 11-119 also illustrates the load and soil settlement graph, registered by the actuator's load cell and LDVT.

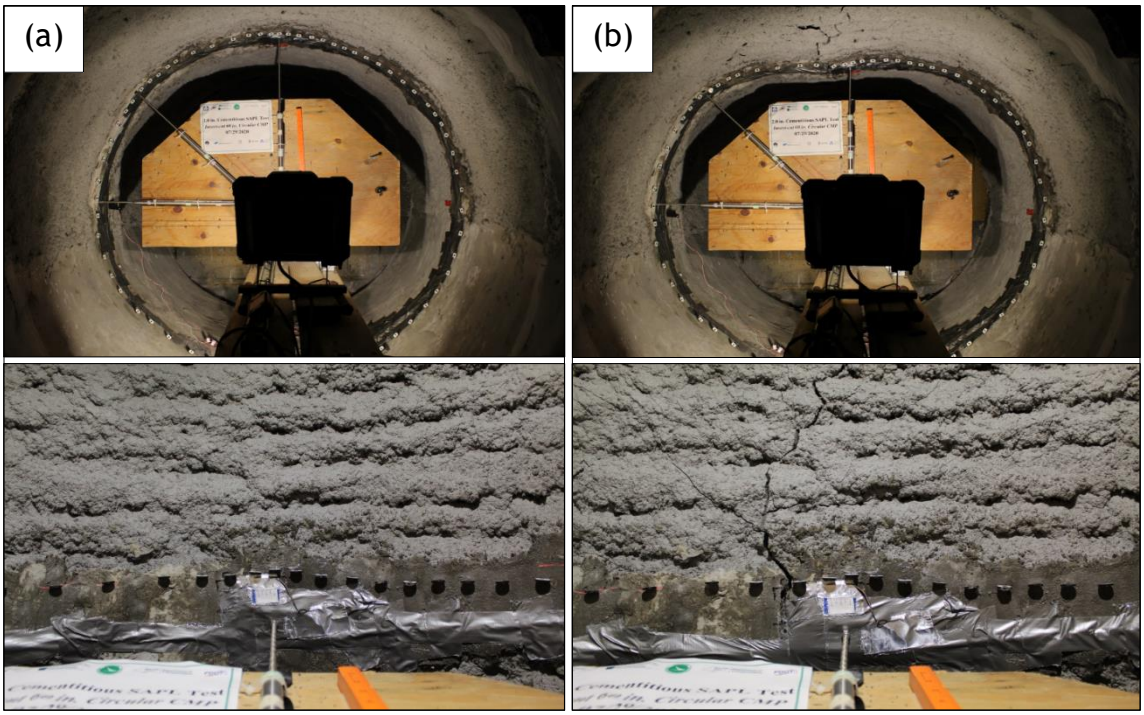


Figure 11-118. Invert-cut circular CMP renewed with 2 in. cementitious SAPL: (a) before loading, and (b) after loading.

The earth pressure cell results registered the maximum pressure of 116.3 psi at the crown location, which was 10 psi higher than the 3 in. SAPL renewed sample. Once the ultimate load was reached, the earth pressure sensors failed to capture data thereafter. However, since the pressure was about to drop after the yield point and it occurred at the time of load drop registered by the actuator's load cell, it can be implied that the 116.3 psi was the maximum pressure that the pipe experienced over the crown. In addition, the value 116.3 is larger than the maximum surface pressure, which is 106.8 psi. The most probable reason could be due to the possible soil failure at the 80 kips of load which forms a prism-like failure plane under the pad and applies the load under a smaller surface that resulted in higher pressure reading of the earth pressure cell on top of the pipe. The maximum pressure applied on the West and East locations of the CMP were 10.2, and 5.93 psi, respectively. Figure 11-120 illustrates earth pressure results for the invert-cut circular test.

Figure 11-121 illustrates the results of the mechanical sensors. The LVDT results show that the pipe was subjected to 4.727 in. of crown and 1.357 in. of springline deflection. The shoulder had 0.0566 in. downward movement. The CDS showed a similar result (4.589) as the crown LVDT. At the end of the test once the load was released from the surface a reverse movement in crown and springline of 0.159 and 0.0869 in., respectively, were observed.

The strain gauge results showed the SAPL was cracked at the invert on the crown with 14 kips of load. The West haunch (W3) experience a tensile strain at the load of

36.55 kips and it was subjected to compressive strain afterwards. This shows that the W3 location, illustrated Figure 11-122, is located on the transition zone as depicted in Figure 11-108. The crown of the CMP was the first location that reached the steel yielding point (i.e., 1138 με) at the vertical load of 36.2 kips. The East springline and shoulder also yielded at 63.36, and 67.88 kips, respectively. The West Shoulder of the CMP also yielded at 79.73 kips. No other location in the CMP reached the yield point.

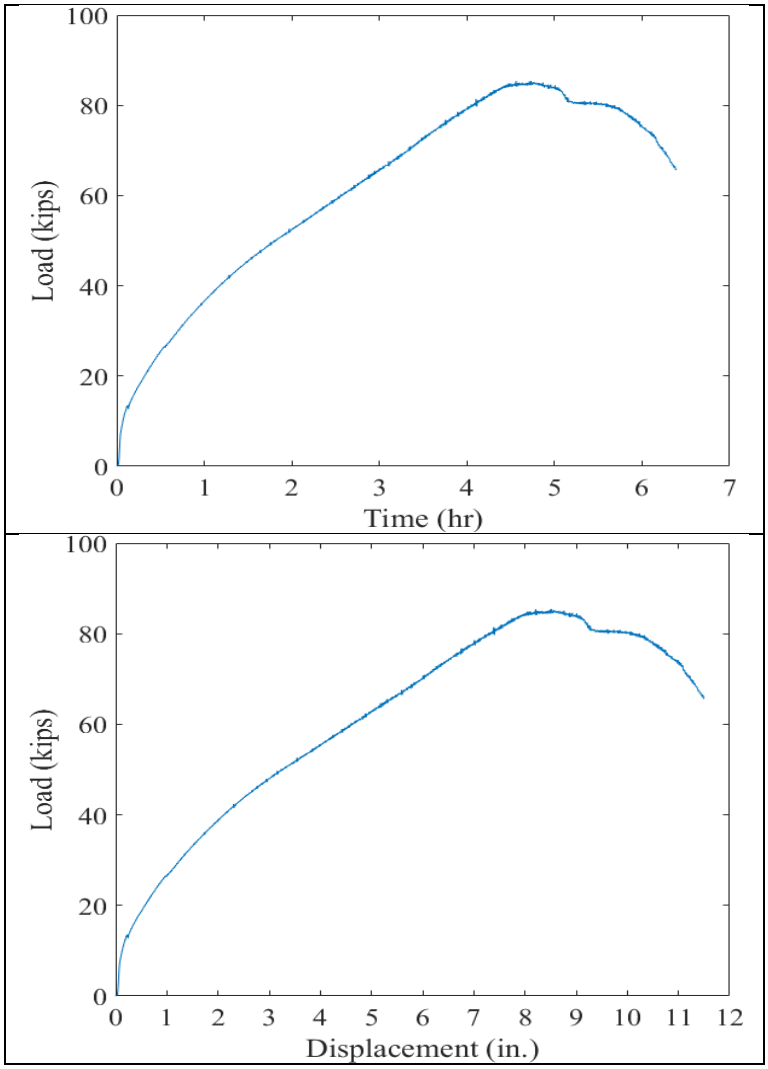


Figure 11-119. Invert-cut circular CMP renewed with 2-in. thick cementitious SAPL subjected to static live load: (top) load-time, and (bottom) load-soil displacement graphs.

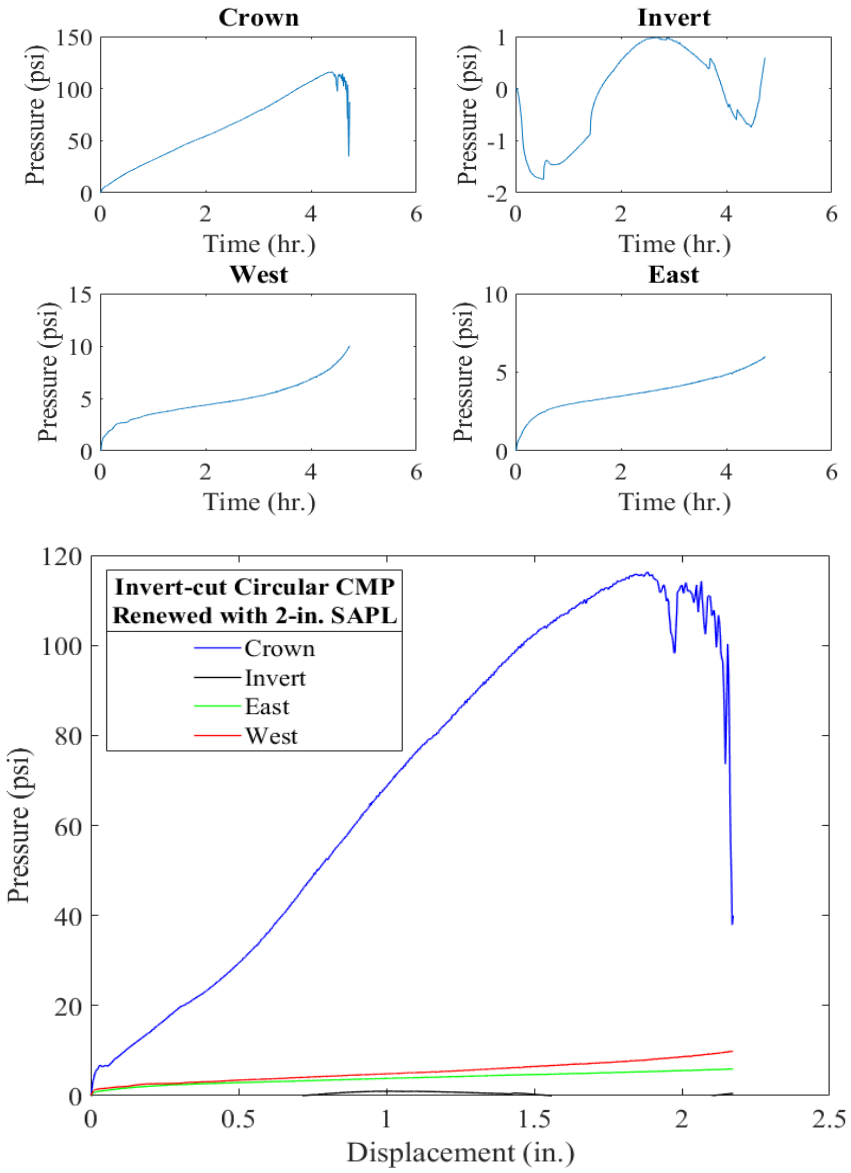


Figure 11-120. Earth pressure cell results for the 2-in. thick SAPL renewed invert-cut circular CMP with respect to: (top) time, and (bottom) crown displacement.

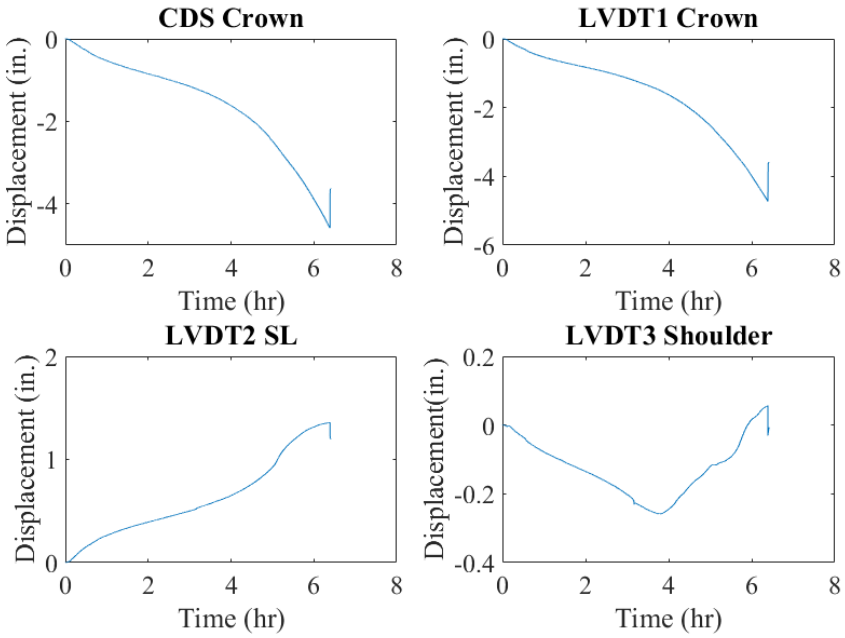


Figure 11-121. Mechanical sensors result for 2-in. thick SAPL renewed invert-cut circular CMP.

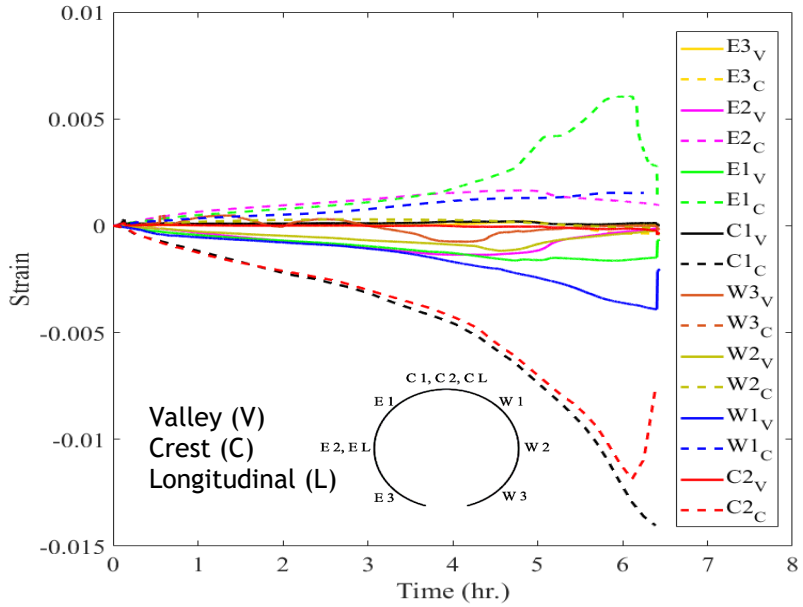
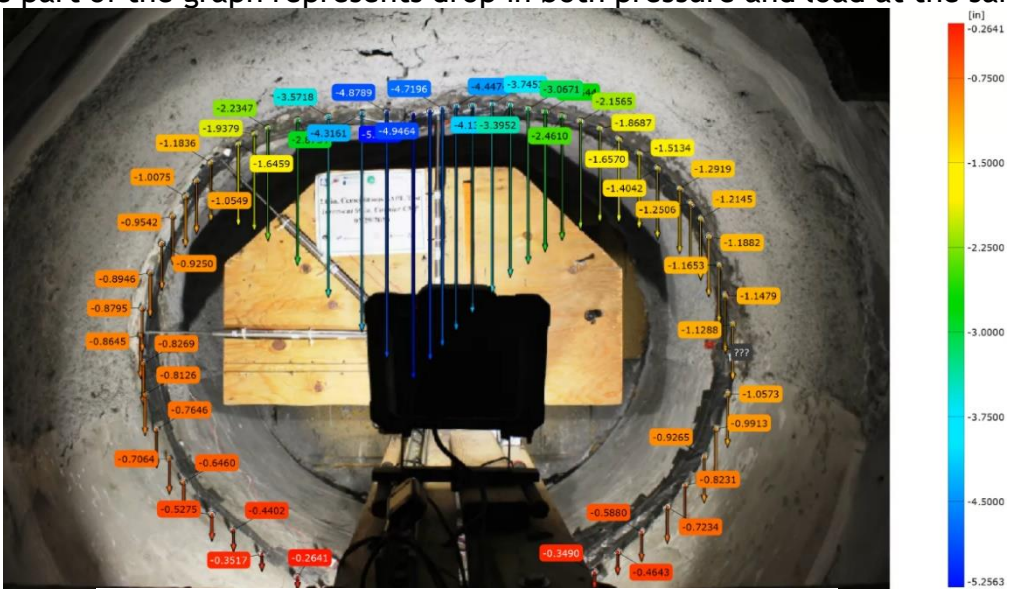


Figure 11-122. Strain gauges result for 2-in. thick SAPL renewed invert-cut circular CMP.

Figure 11-123 illustrates the 2-in. thick SAPL renewed circular CMP profile before and after the applied static load. The pipe profile at end of the test clearly illustrates the pipe's ovality. In addition, the roughness and irregularity of the SAPL is explicitly evident in the profiling result. The comparison between the mechanical sensors and DIC shows an excellent conformity with the CDS sensor.

The load-displacement values for soil surface, crown, springline, and shoulder of the 2-in. thick SAPL renewed circular CMP due to the applied static load is illustrates in Figure 11-124. The applied load on the soil surface versus its corresponding pressure at the crown of the renewed circular CMP are depicted in Figure 11-125, where the recursive part of the graph represents drop in both pressure and load at the same time.



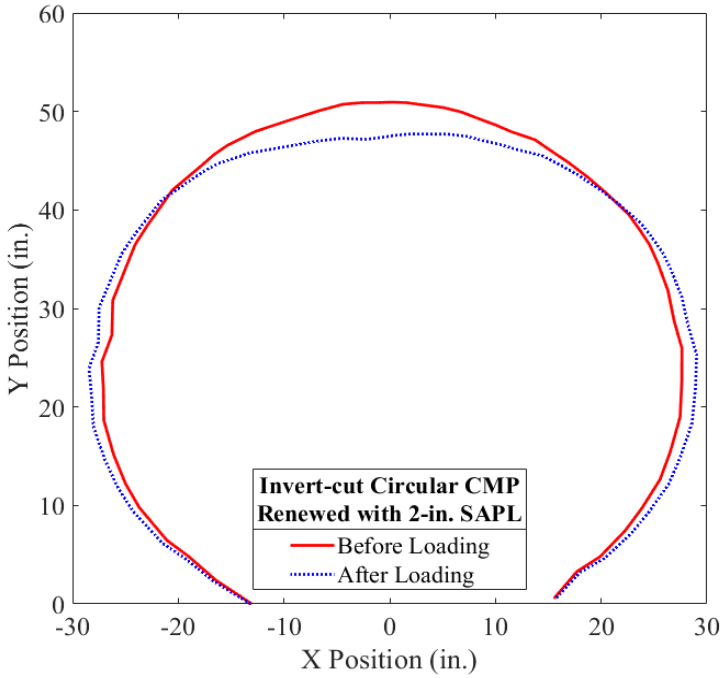


Figure 11-123. Pipe profiling using DIC for the 2-in. thick SAPL renewed invert-cut circular CMP.

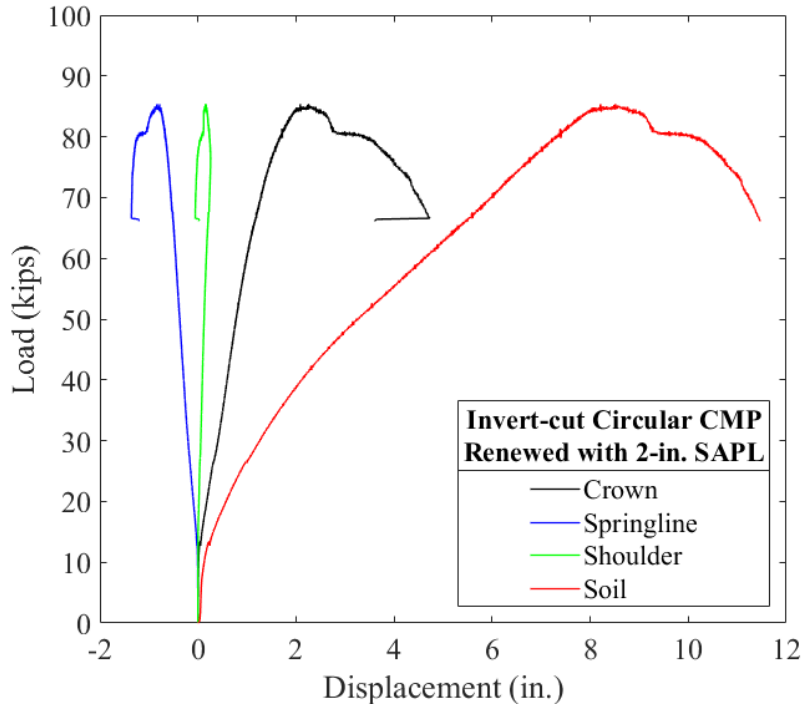


Figure 11-124. Load vs. displacement of the soil surface, crown, springline, and shoulder of the 2-in. thick SAPL renewed invert-cut circular CMP due to the applied static load.

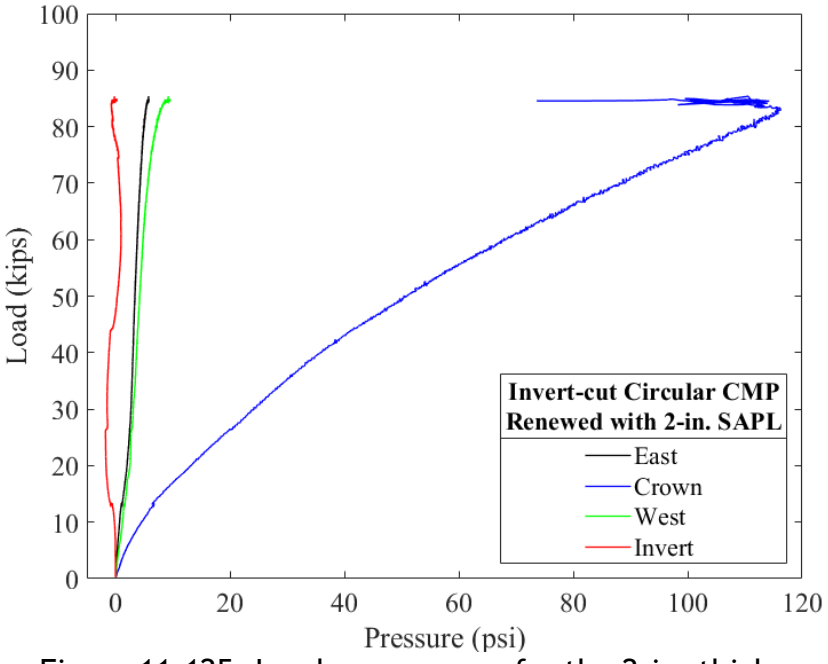


Figure 11-125. Load vs. pressure for the 2-in. thick SAPL renewed invert-cut circular CMP.

11.11.3.1.2.4 Thickness Measurement (2-in. SAPL)

The thickness of the 2-in. thick cementitious SAPL renewed circular CMP were measured after the structural test and before exhumation as elaborated in section 3.4.6. The detailed result of the measurements is presented in APPENDIX 5. Thickness Measurement Results. Figure 11-126 illustrates the thickness measurements results for all three locations along the length of the pipe (i.e., north, center and south). The results showed that the liner's thickness variation ranged from 1.5 to 2.6 in. Except the West springline, the applied thickness was generally either higher or about the design thickness in all sections of the pipe. Similar to the 3-in thick SAPL, the applied SAPL was thicker on the crown and both shoulders, which can be due to the importance of this section that entices the attention of the applicator to this location more than the other locations.

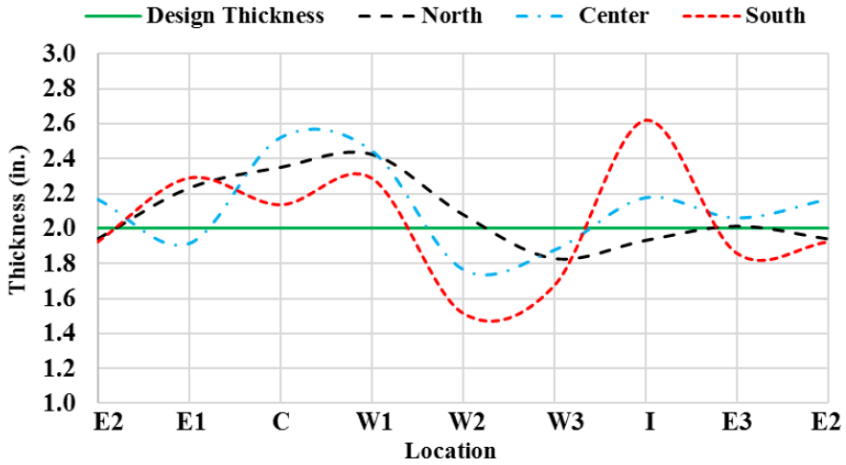


Figure 11-126. Thickness measurement for the 2-in. thick cementitious SAPL renewed circular CMP.

11.11.3.1.2.5 1-in. Thick SAPL Sample

The 1-in. thick SAPL renewed invert-cut circular CMP was tested on July 31st, 2020, using the 20 × 40 in. load pad. The test duration was 5.283 hours. In this pipe sample, unlike the 3-in. thick sample, no shrinkage crack existed in the crown. The SAPL renewed CMP sample cracked at the crown in 10 kips of load and failed at the load of 71.76 kips with 8.05 in. of soil settlement. The failure occurred due to the large deflection and multiple cracks at the crown location. Figure 11-127 (a) and (b) illustrate the test sample in before and after loading stage. Once the SAPL-CMP system was failed, the test was continued until about 20% load drop. Then the test was terminated, as further deflection would increase the chance of the liner detaching and falling, which would damage the mechanical sensors and cameras inside the pipe. Once the load was released from the soil surface, the pipe had an upward movement and relaxed. Figure 11-128, also illustrates the load and soil settlement graph, registered by the actuator's load cell and LDVT.

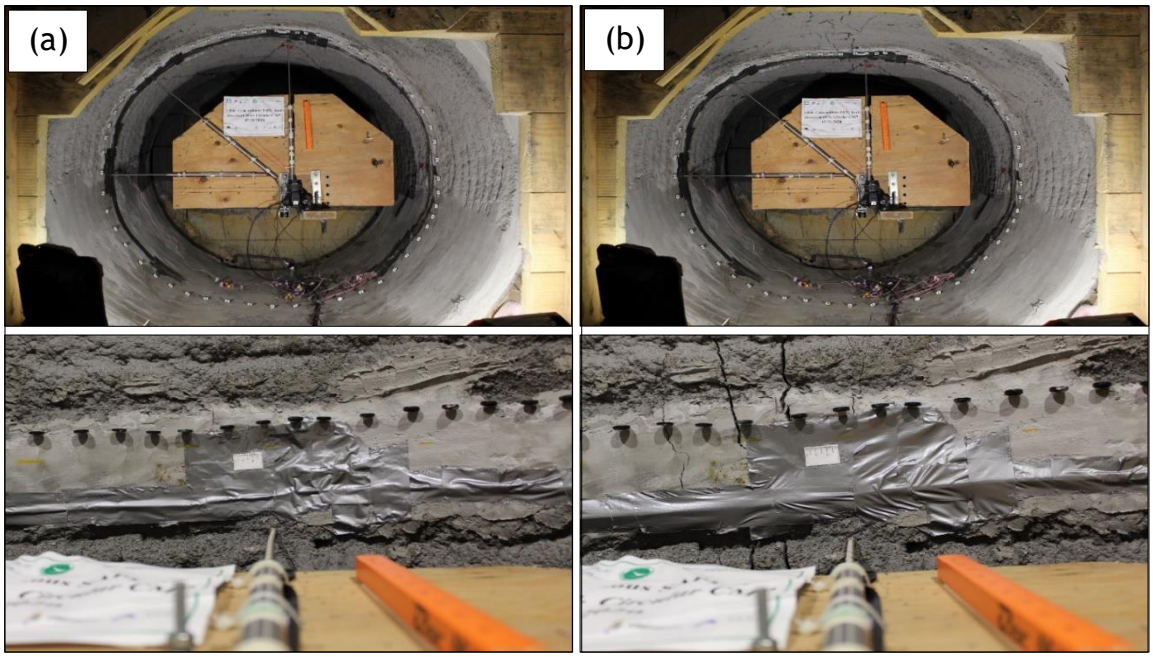


Figure 11-127. Invert-cut circular CMP renewed with 1 in. cementitious SAPL: (a) before loading, and (b) after loading.

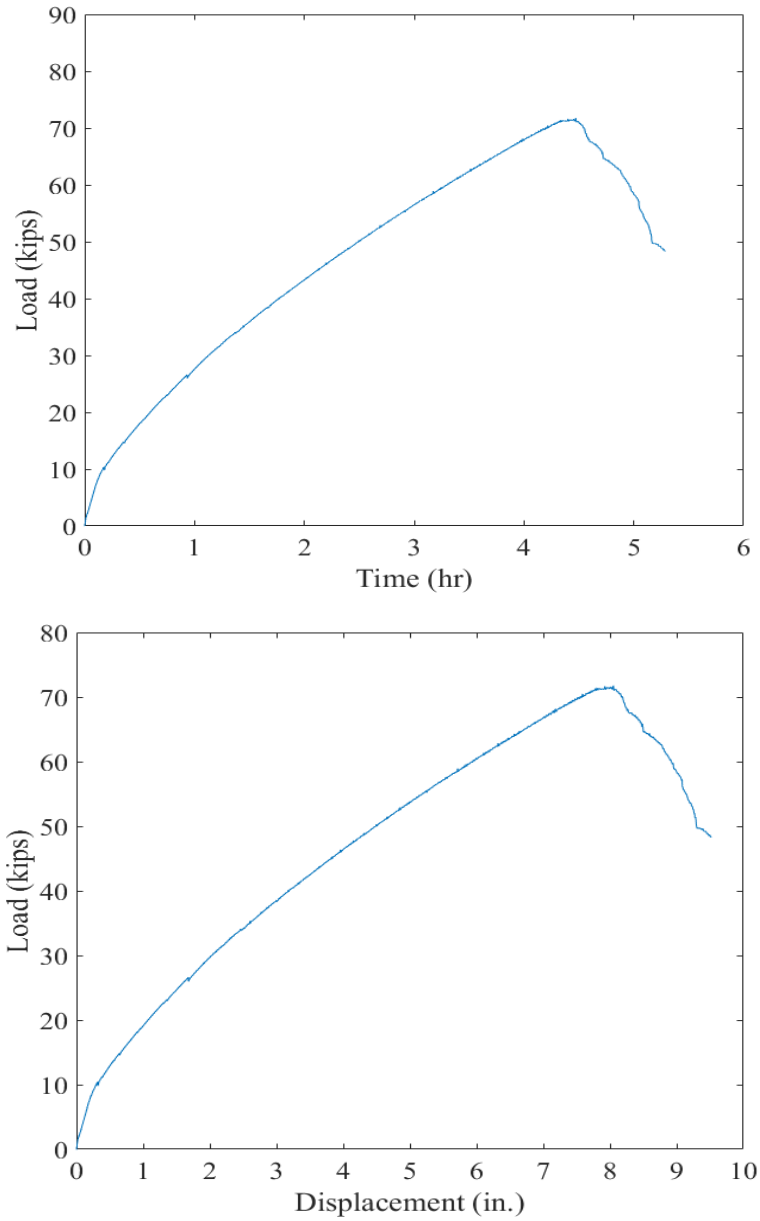


Figure 11-128. Invert-cut circular CMP renewed with 1-in. thick cementitious SAPL subjected to static live load: (top) load-time, and (bottom) load-soil displacement graphs.

The earth pressure cell results registered the maximum pressure of 102.2 psi at the crown location, which was 14 psi lower than the 2 in. SAPL renewed sample. The maximum pressure applied on the West and East locations of the CMP were 8.66, and 10.93 psi, respectively. In this test, immature soil failure was not observed. Figure 11-129 illustrates earth pressure results for the invert-cut circular test.

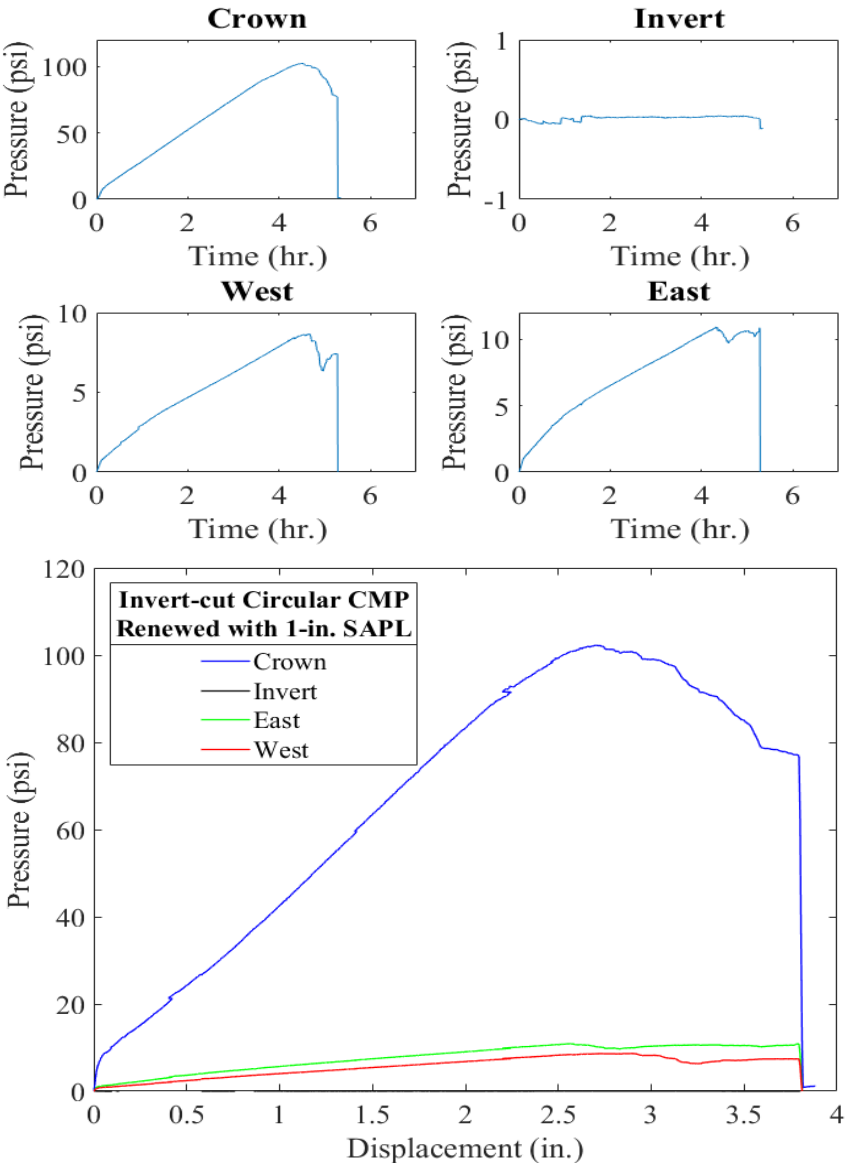


Figure 11-129. Earth pressure cell results for the 1-in. thick SAPL renewed invert-cut circular CMP with respect to: (top) time, and (bottom) crown displacement.

Figure 11-130 illustrates the results of the mechanical sensors including LVDT and CDS. The LVDT results show that the pipe was subjected to 3.889 in. of crown and 1.1133 in. of springline deflection. The shoulder had 0.055 in. downward movement. The CDS showed a similar result (3.862) as the crown LVDT. At the end of the test, once the load was released from the soil-pipe system, a reverse movement in crown and springline of 1.07 and 0.1582 in. was observed.

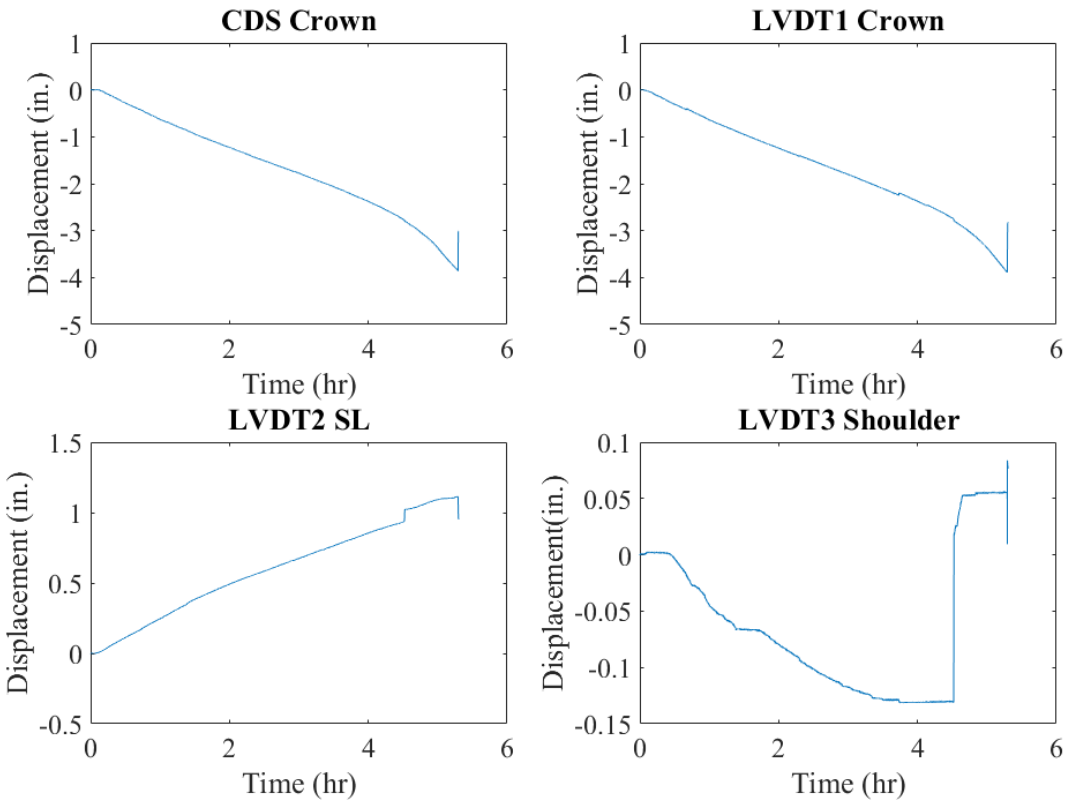


Figure 11-130. Mechanical sensors result for 1-in. thick SAPL renewed invert-cut circular CMP.

The strain measurement results of the CMP and SAPL are presented in Figure 11-131. The strain gauge results showed the SAPL cracked at the crown with 10.42 kips of load. The West haunch (W3) cracked at the load of 18.84 kips which increased the tensile strain value of the host pipe's (i.e., CMP) West haunch area. A similar situation also occurred for the East haunch of the SAPL, which cracked with 22.74 kips of load. It is noteworthy that from the strain gauge results, cracking load estimation of the invert section were not possible. The crown of the CMP was the first location that reached the steel yielding point (i.e., 1138 με) at the vertical load of 20.52 kips. The West haunch was the next location that yielded at the load of 38.99 kips. Eventually, East shoulder was the last location that yielded at the load of 66.95 kips. It should be noted that in this test the strain gauge sensors at the locations W1 and W2 were damaged.

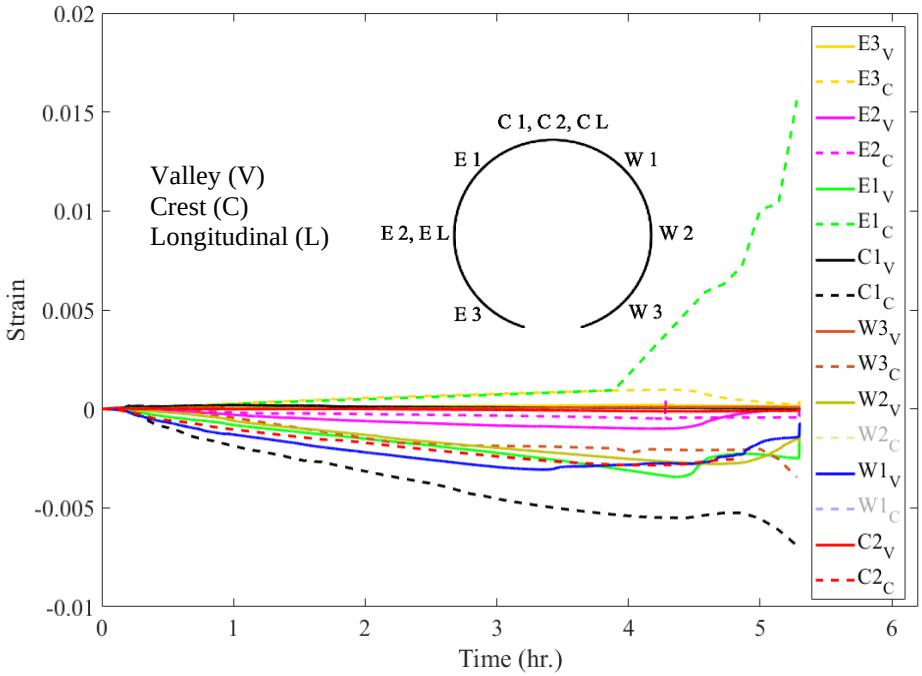


Figure 11-131. Strain gauges result for 1-in. thick SAPL renewed invert-cut circular CMP.

Figure 11-132 illustrates the 1-in. thick SAPL renewed circular CMP profile before and after the applied static load. The pipe profile at end of the test clearly illustrates the pipe's ovality. In addition, the roughness and irregularity of the SAPL is explicitly evident in the profiling result. The comparison between the mechanical sensors and DIC shows an excellent conformity with the CDS sensor.

The load-displacement values for soil surface, crown, springline, and shoulder of the 1-in. thick SAPL renewed circular CMP due to the applied static load is illustrated in Figure 11-133. The applied load on the soil surface versus its corresponding pressure at the crown of the renewed circular CMP the recursive part of the graph represents drop in both pressure and load at the same time.

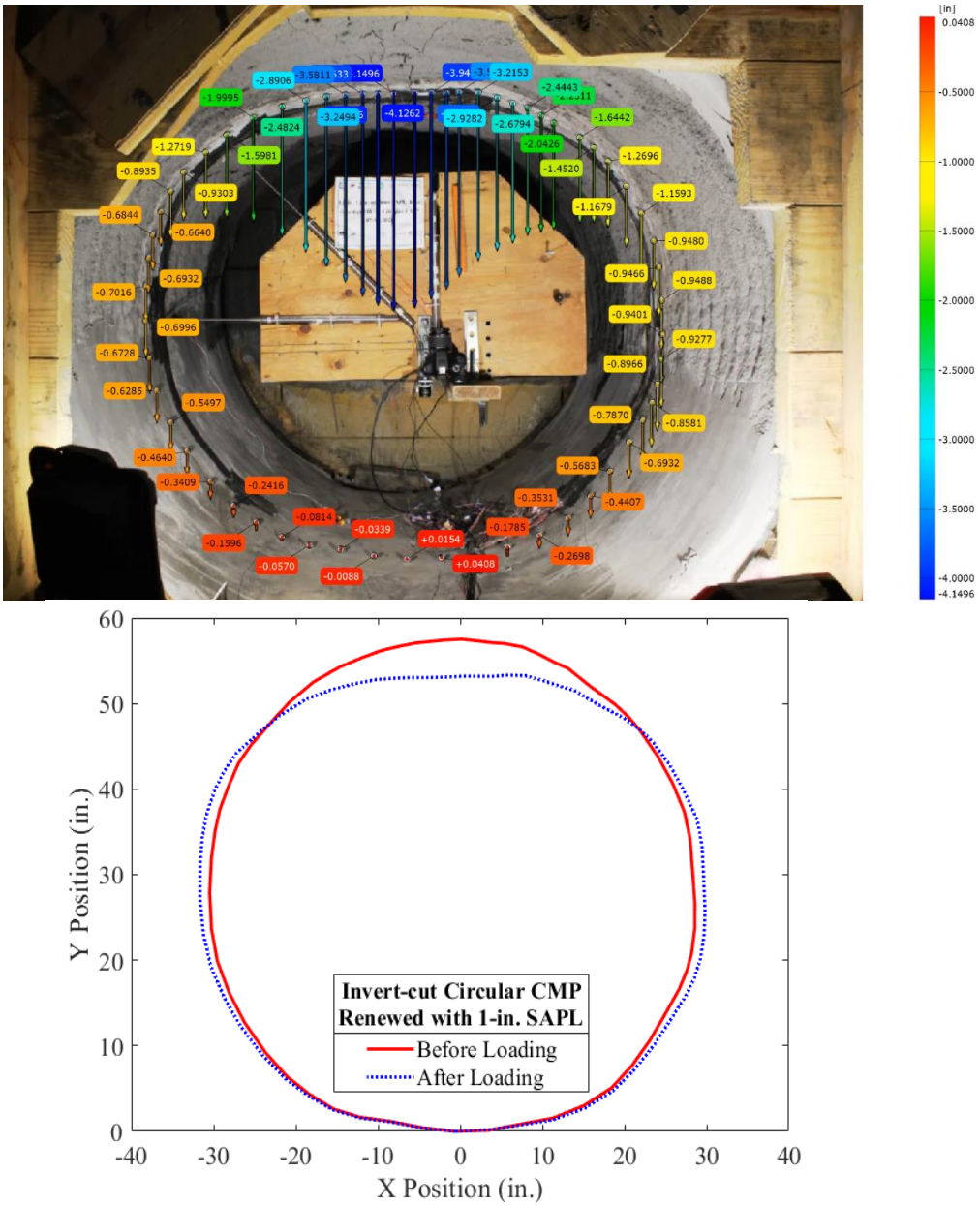


Figure 11-132. Pipe profiling using DIC for the 1-in. thick SAPL renewed invert-cut circular CMP.

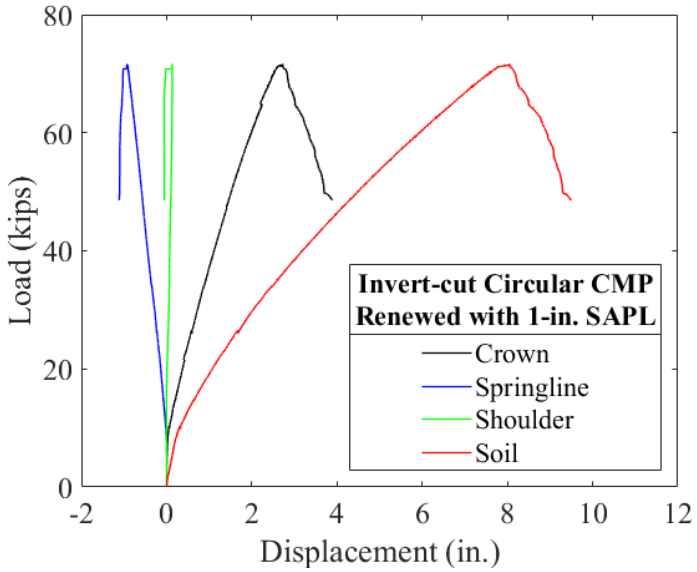


Figure 11-133. Load vs. displacement of the soil surface, crown, springline, and shoulder of the 1-in. thick SAPL renewed invert-cut circular CMP due to the applied static load.

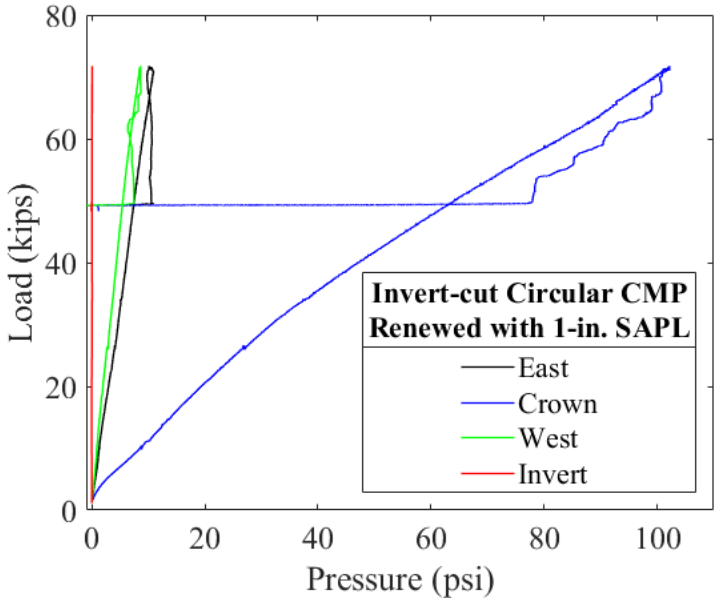


Figure 11-134. Load vs. pressure for the 1-in. thick SAPL renewed invert-cut circular CMP.

11.11.3.1.2.6 Thickness Measurement (1-in. SAPL)

The thickness of the 1-in. thick cementitious SAPL renewed circular CMP was measured after the structural test and before exhumation. Figure 11-135 illustrates the thickness measurements results for all three locations along the length of the pipe (i.e., north, center and south). The results showed that the liner's thickness variation ranged from 0.4 to 1.6 in. The applied thickness on the center ring of the pipes was more uniformly applied in compare with North and South rings. At this section, the thickness alteration was ranging from 1.1 to 1.6 in., which were all above the required thickness. The South ring had the similar condition, except the West springline which had 0.3 in. less than the required thickness. The North ring had the largest thickness variation inside the 1-in thick renewed CMP. In general, the half upper section of the pipe in the North ring had a thickness less than the designed thickness (i.e., 1 in.).

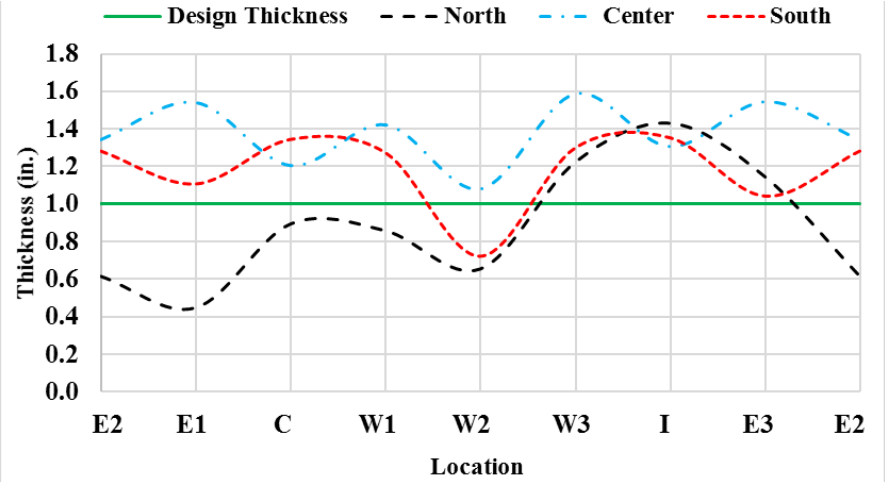


Figure 11-135. Thickness measurement for the 1-in. thick cementitious SAPL renewed circular CMP.

11.11.3.1.2.7 Comparison of SAPL Renewed Invert-cut CMP Arch Test Results

Results comparison between the bare (i.e., unlined) invert-cut circular CMP and SAPL renewed samples showed that application of 1, 2 and 3-in. thick cementitious SAPL on the invert-cut CMP arch samples increased the load carrying capacity for 79.71, 113.9, and 174.73%, respectively. In all the applied thicknesses, the improvement rate for the SAPL renewed circular CMPs were higher than the SAPL renewed CMP arch samples. Table 11-13 presents the ultimate load results and the load carrying capacity enhancement using different SAPL thickness.

Table 11-13. Circular CMP test results.

Testing Pipe Samples	SAPL Material	Ultimate Load (Kips)	Improvement (%)
Bare CMP Arch	-	39.93	-
1 in. Thick SAPL	Geopolymer	71.76	79.71
2 in. Thick SAPL	Geopolymer	85.42	113.9
3 in. Thick SAPL	Geopolymer	109.7	174.73

Figure 11-136 illustrates the results of load versus crown deflection of the bare invert-cut CMP, 1, 2, and 3-in. thick SAPL renewed invert-cut CMPs. Similar data, for springline expansion is presented in Figure 11-137. In both figures it can be observed that the 2 in. thick SAPL renewed CMP had lower crown deflection and springline expansion as expected. One of the possible reasons could be due to the irregularity of the geometry and existed shrinkage cracks in different locations which caused different failure pattern for this pipe.

Figure 11-138 illustrates the application of the SAPL increases the soil settlement value to fail the SAPL-CMP system. In other words, more soil settlement is needed to fail the SAPL renewed CMP. It can be observed that more soil settlement is also needed for thicker SAPL and the thickness of the SAPL affects the soil surface displacement.

Figure 11-139 illustrates the results of the applied static load on the soil surface versus the applied pressure over the crown of the pipes. The AASHTO H20 truck equivalent pressure, obtained from the intact CMP test, is shown in Figure 11-139. As the figure shows, all the SAPL renewed circular CMP samples could resist the equivalent AASHTO H20 truck pressure. The figure shows that the thicker the liner the higher load was required to fail the SAPL-CMP system. It can be concluded that all three thicknesses are sufficient for the AASHTO H20 truck load.

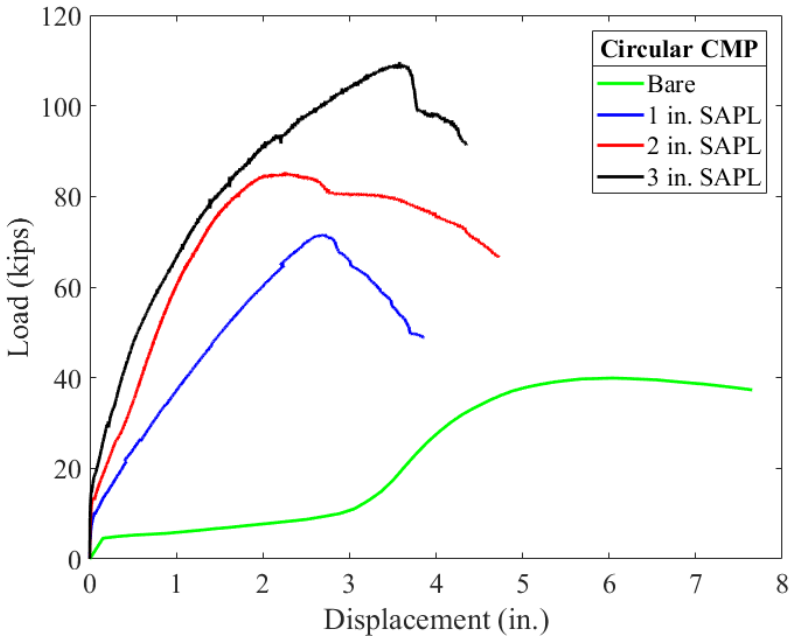


Figure 11-136. Load vs. crown displacement comparison graph.

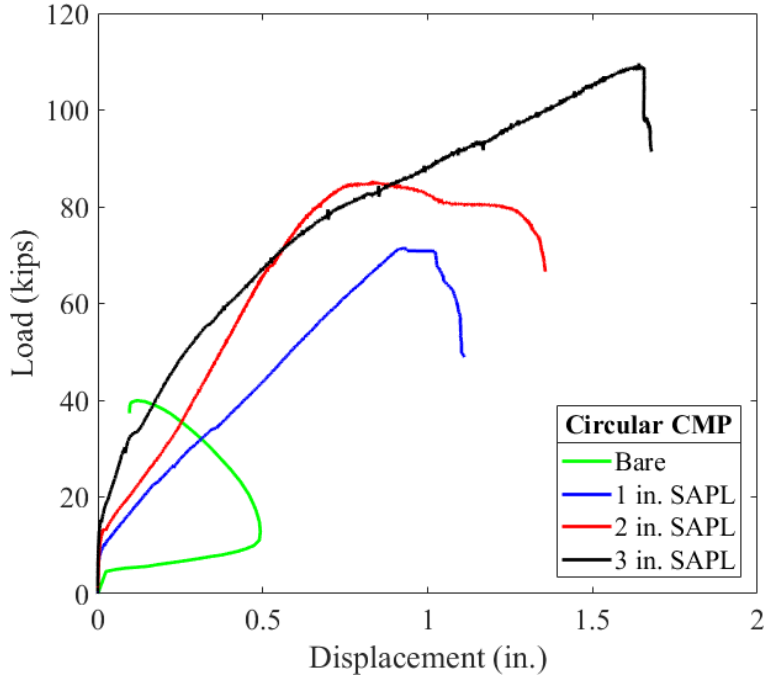


Figure 11-137. Load vs. springline displacement comparison graph.

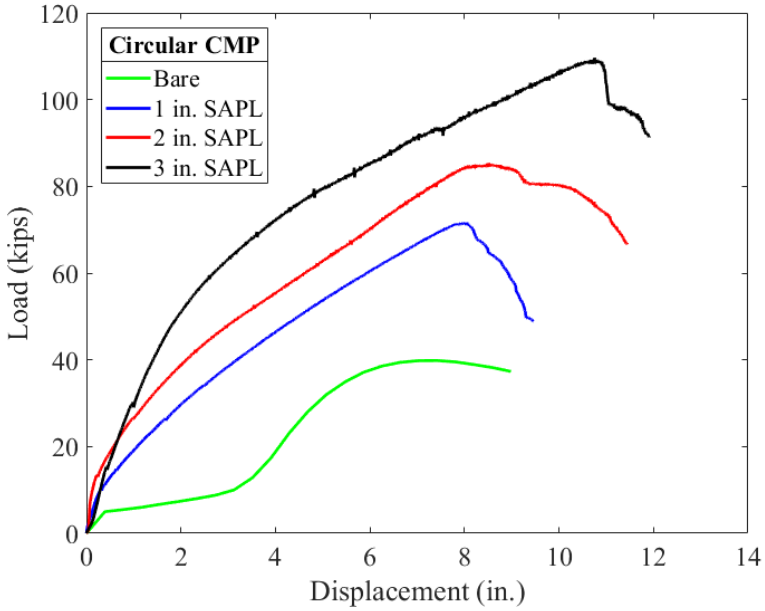


Figure 11-138. Load vs. soil surface settlement comparison graph.

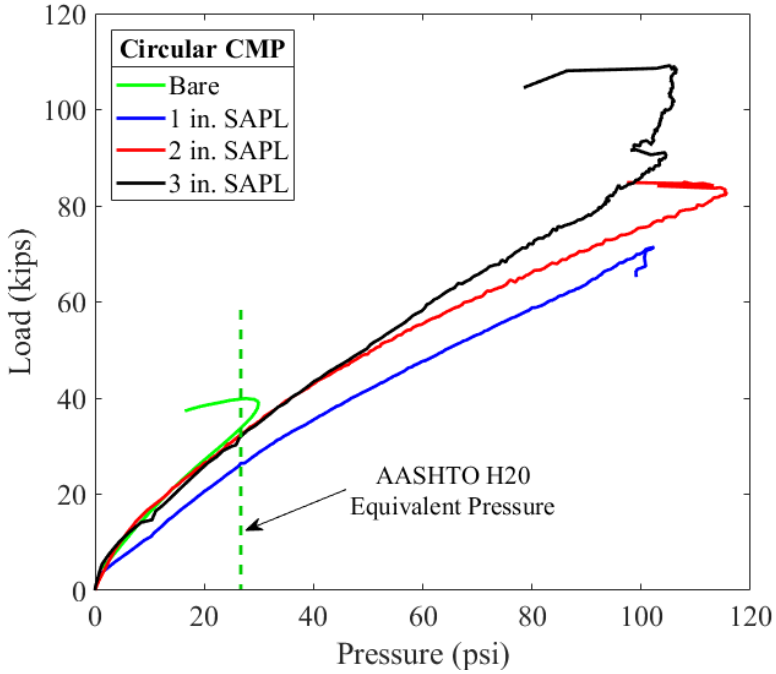


Figure 11-139. Load vs. pressure comparison graph.

11.11.3.1.3 Test Results for Mechanical Properties of Cementitious SAPL

The compressive strength of the samples was evaluated for the cubes, 3 × 6, 4 × 8, and 6 × 12 in. samples. The strength of the cubes and 4 × 8-cylinder samples were examined for 24-hour, 7- and 28-day curing time. Rest of the samples were tested only for 7 and 28-days.

The cube samples were tested according to the ASTM C109. The load was applied at the rate of 300 lb/sec, as described in the test guideline. Figure 11-140 illustrates the box plot of the cube samples result that shows the cube samples had an average compressive strength of 2753 psi after 24 hours of curing. After 7 days the strength of the samples was increased up to 4442 psi. The compressive strength increased further for 56.6% at the end of 28 days where the compressive strength reached average value of 6958 psi. Figure 11-141 (top) the samples were broken at 45-degree planes that implies the load were applied uniformly over the samples.

All the cylinder samples were tested according to the ASTM C39 at the pressure rate of 30 psi/sec. The 3 × 6 in. spray-cast cylinder samples were able to reach 3163 psi at the 7 days and 4331 psi at the end of 28 days. The sprayed cylinders showed about 36.92% increase from 7 to 28 days of curing. The hand-cast cylinders showed relatively higher compressive strength than the spray-cast cylinders at 7-day curing period and relatively lower strength at the 28-day curing time where the compressive strength of the hand-cast cylinders were 3977 and 4190 psi at 7 and 28 days, respectively. Figure 11-141 illustrates the box plot of the 3 × 6 in. samples test results.

The 4 × 8 in. spray-cast cylinder samples showed that the geopolymer was able to achieve 1906 psi compressive strength within 24 hours. The 7- and 28-days test specimens showed 4724, and 6027 psi, respectively. The comparison between the results showed that the geopolymer could increase its strength 216.2% during the 28 days of curing time. The hand-cast cylinders also showed similar results to the spray-cast samples. The results are presented in Figure 11-142. The hand-cast had compressive strength of 2476, 4966, and 5373 psi for the 24 hours, 7, and 28 days, respectively. Direct comparison between the spray-cast and hand-cast specimens showed that the hand-cast samples had 29.9% higher, 5.12% higher, and 12.17% lower strength than the spray-cast specimens in 24 hours 7 and 28 days, respectively.

The 6 × 12 in. spray-cast cylinder samples achieved 4742 psi at the end of 7 days curing time which was 11.9% lower than the 28 day cured samples. The 6 × 12 in. samples at the end of 28 days had the average value of 4,176 psi that are illustrated in Figure 11-143.

The results from all different specimens are compared for both 7- and 28-days curing time and are presented in Figure 11-144. The result comparison illustrates that in the absence of large aggregates the smaller samples could resulted in higher compressive strength. In addition, the lower compressive strength of larger samples revealed that although the geopolymer was reinforced with microfibers, the fibers could not contribute to the compressive strength. The total average compressive strength value for all the specimens at 7 and 28 days were 4,336 and 5,176 psi, respectively.

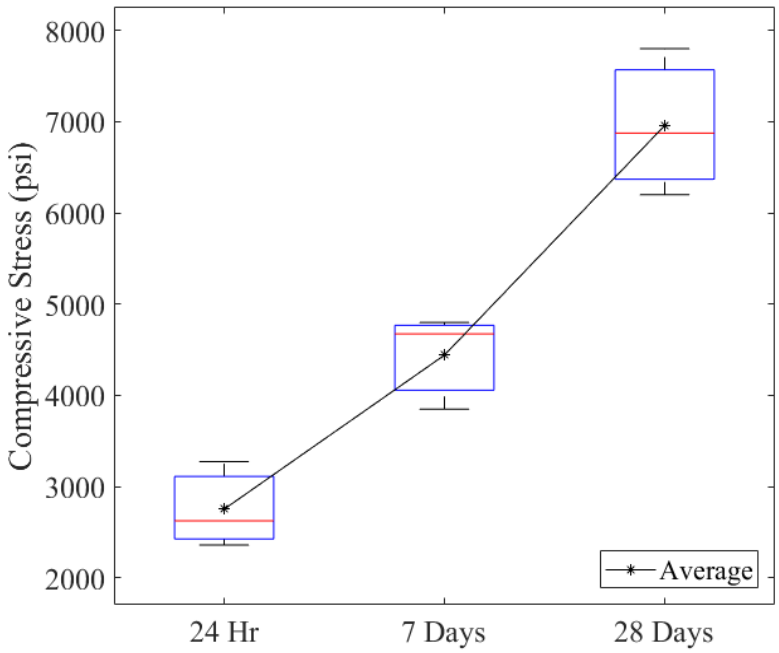


Figure 11-140. Cube samples taken from SAPL batch sprayed on circular CMPs.

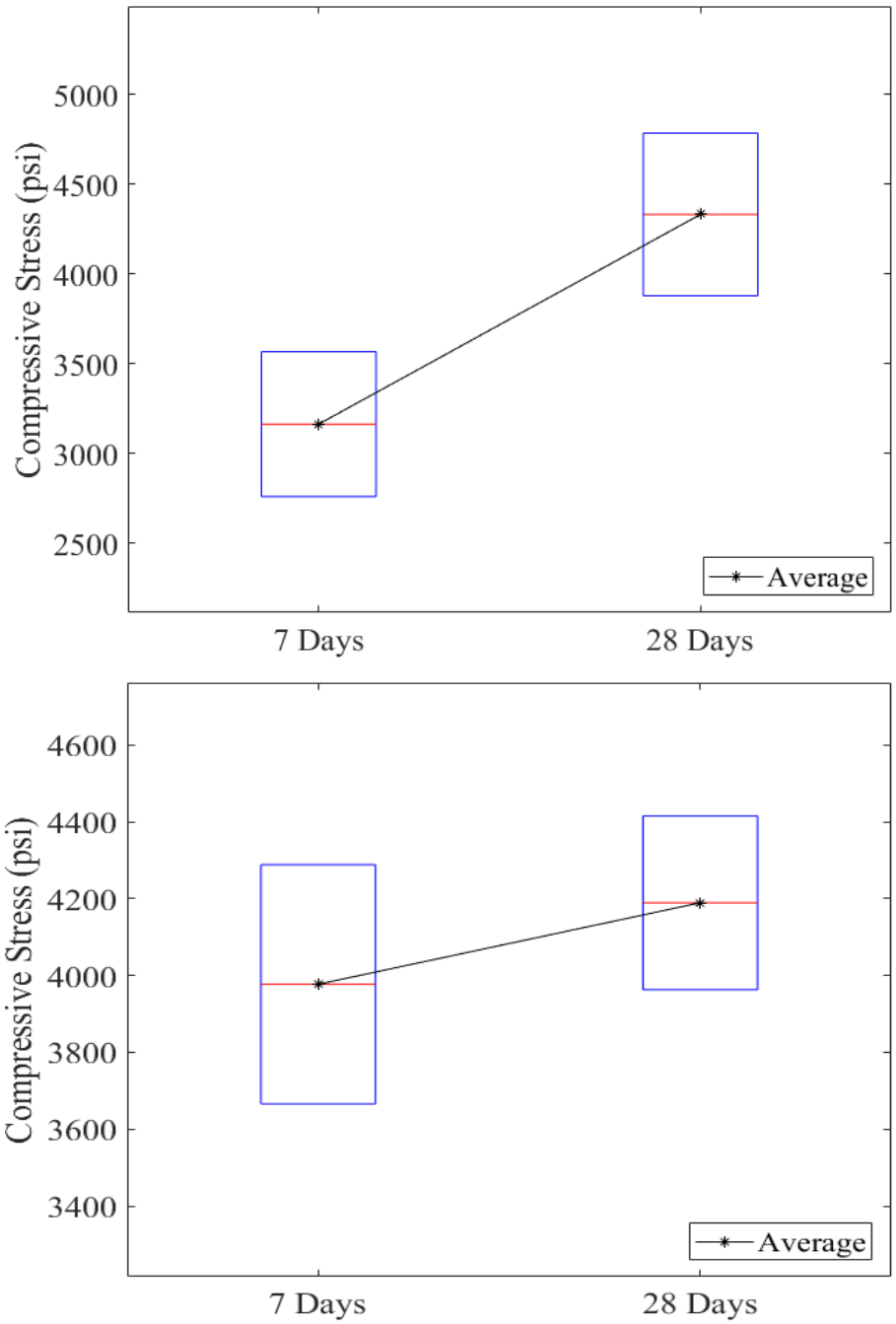


Figure 11-141. Box plot for the 3 × 6-cylinder samples taken from SAPL batch sprayed on circular CMPs: (top) spray cast, (bottom) hand cast.

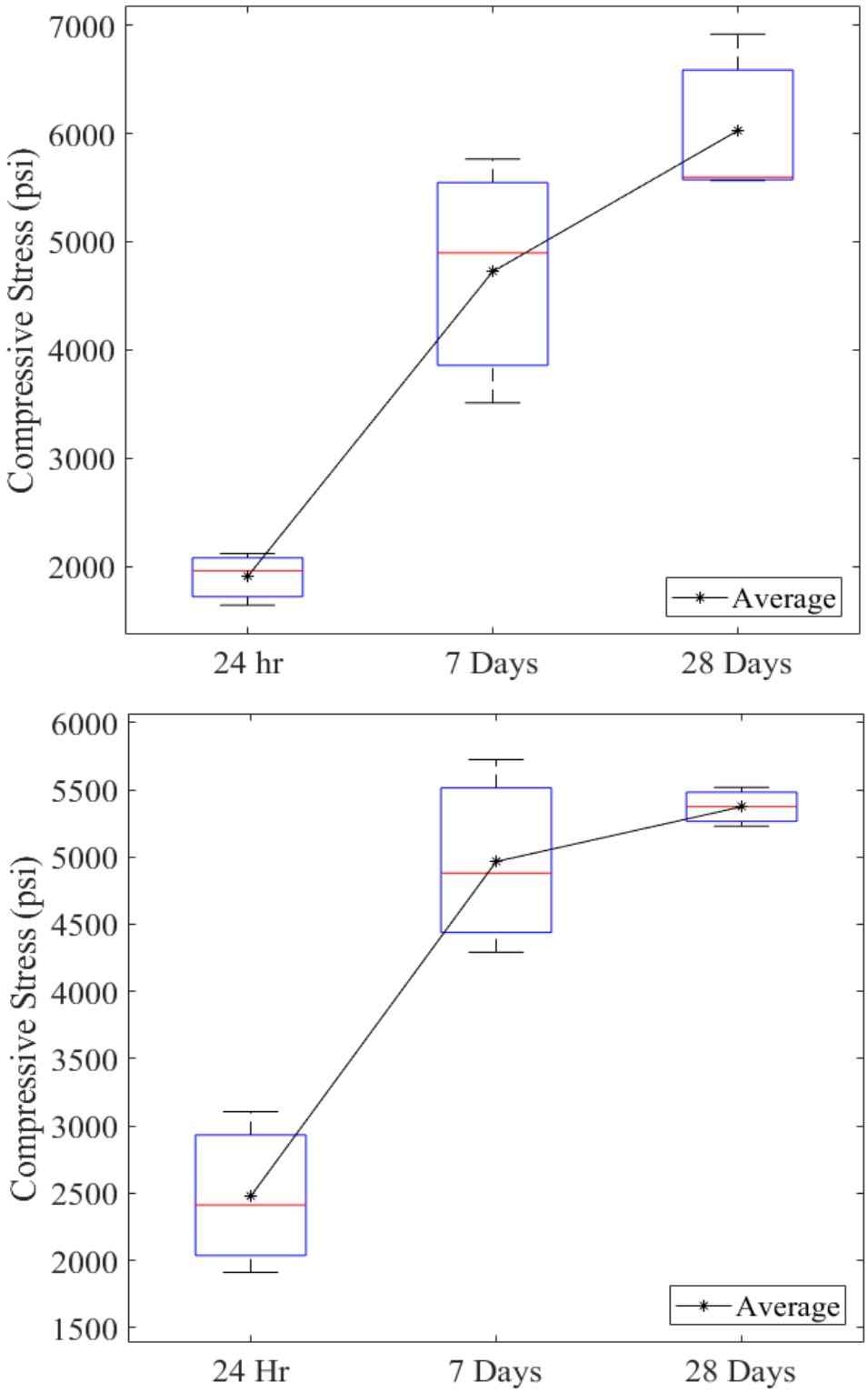


Figure 11-142. Box plot for the 4 × 8-cylinder samples taken from SAPL batch sprayed on circular CMPs: (top) spray cast, (bottom) hand cast.

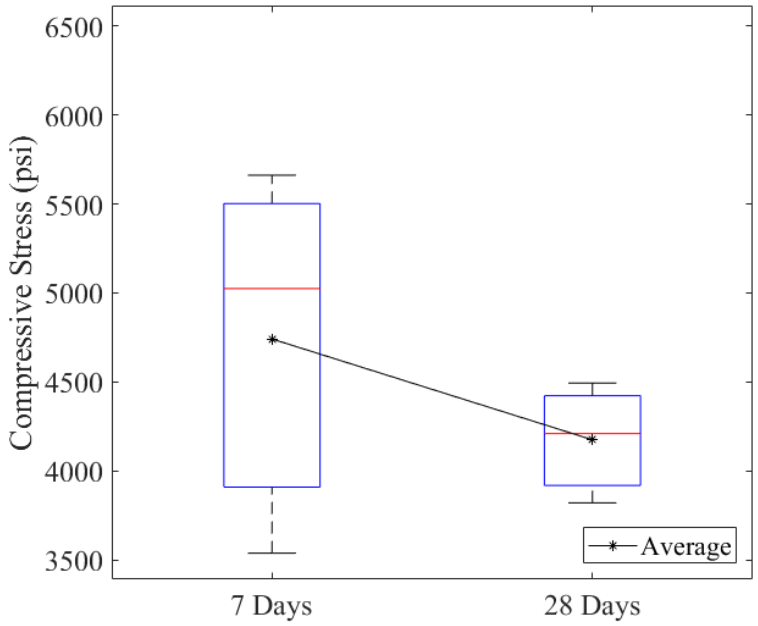


Figure 11-143. Box plot for the 6 × 12-cylinder samples taken from SAPL batch sprayed on circular CMPs.

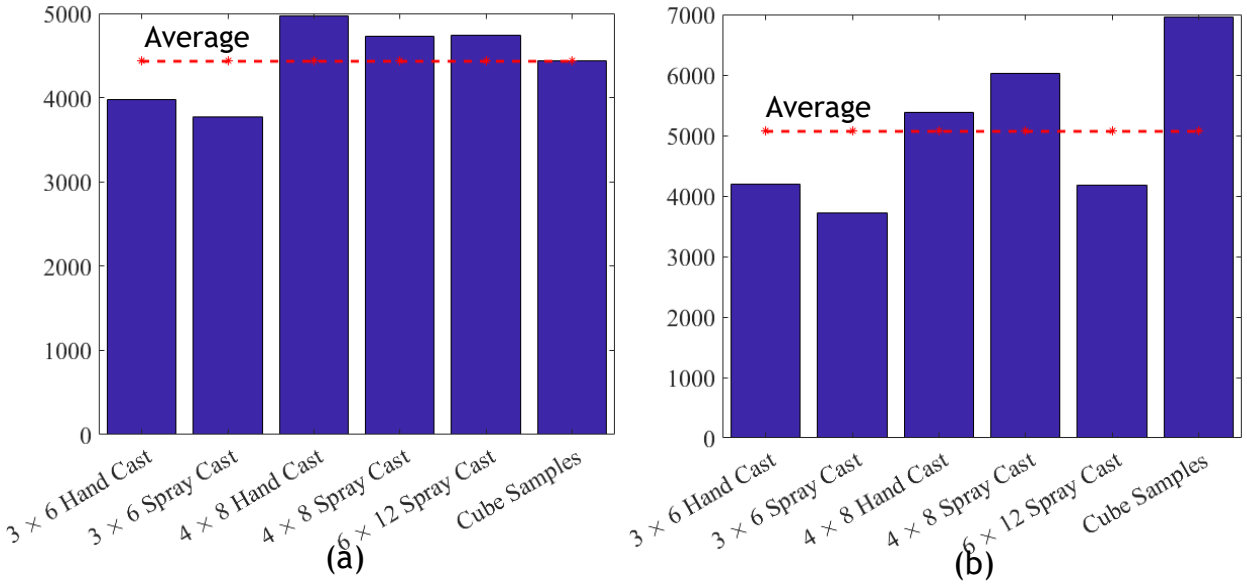


Figure 11-144. Bar chart results for: (a) 7 days, and (b) 28 days samples.

11.12 Conclusions

A total of 15 large diameter corrugated metal pipes (CMPs), including 3 bare (control samples) and 12 SAPL renewed, were buried under 2 ft of soil cover comprising layers of poorly graded sand (SP) and TxDOT 247 grade 1 type D aggregates. A static load with a displacement-control regime was continuously applied with a load rate of 0.03 in./min through a rigid 20 × 40 in. steel load pad on the soil surface over crown of the pipe. The results and discussions were presented in this report and the conclusions are summarized as follows:

- The test results for mechanical properties showed that the polymeric SAPL had the flexural modulus of 855,639 psi, the averaged maximum tensile stress of 8,671 psi, and the elastic modulus of 329,210 psi.
- The physical property test results showed that the cementitious SAPL had an average compressive strength of 2,753 psi after 24 hours of curing. After 7 days the strength of the samples was increased up to 4,442 psi. The compressive strength increased further for 56.6% at the end of 28 days where the compressive strength reached average value of 6,958 psi.
- For polymeric SAPL, the results of thickness measurement showed that the utilization of hand spray installation of the polymeric SAPL resulted in a thicker liner at the springline for renewed CMPs than the designated thickness. However, the SAPL was installed closer to the required thickness at crown and both shoulders.
- For cementitious SAPL, the liner's thickness was variable along the circumference of the pipes, which emphasizes on the superiority of centrifugal casting machine over the hand sprayed method to provide uniform thickness in large thicknesses. However, the applied thickness was generally either higher or about the design thickness on the crown and both shoulder locations.
- The invert-cut bare CMP in the absence of the ring stiffness was not able to resist the applied load beyond its frictional resistance limit. The CMP continuously squeezed until both sides of the invert-cut sections contacted the main body of the CMP and retrieved the ring stiffness. The invert-cut bare CMP structurally failed at the load of 39.9 kips.
- All polymeric SAPL renewed circular CMPs cracked at about 3% of pipe deflection, where at this deflection the application of 0.25 in., 0.5 in., and 1 in. polymeric SAPLs increased the load carrying capacity for 471.7, 482.8, and 802.7% respectively.
- Application of the polymeric SAPL increased the stiffness of the invert-cut circular CMP. The SAPL renewed CMPs with the thicknesses of 0.25 in., 0.5 in., and 1 in. increased the ultimate load bearing capacity of the fully invert deteriorated CMPs for 16.24, 31.4, and 80.82%, respectively.

- Application of the polymeric SAPL increased the stiffness of invert-cut pipe arch CMPs. The SAPL renewed CMPAs with the thicknesses of 0.25 in., 0.5 in., and 1 in. increased the ultimate load carrying capacity of the invert deteriorated pipe arch CMPs for 23.1, 32.1, and 98.9%, respectively.
- The cementitious SAPL with the thicknesses of 1 in., 2 in., and 3 in. increased the ultimate load bearing capacity of the invert-cut circular CMPs for 79.7, 113.9, 174.7% respectively. These values for the pipe arch CMPs were 72.3, 104.4, and 151.4% respectively.
- It was observed that both polymeric and cementitious SAPLs were able to increase the structural capacity of the fully invert deteriorated CMPs and retrieve the ring compression resistance of the renewed pipes. In addition to that, since the polymeric SAPL did not crack at the invert-cut location, even at the ultimate loading stage, it can be concluded that the polymeric liner was structurally capable to perform as a new pipe inside the host pipe (i.e., pipe-in-pipe) and could solely resist the applied ring compression.

APPENDIX A - Design Spreadsheet

SAPL Design

Structural Design for Liner Thickness Using Cementitious Materials
Arch Corrugated Metal Pipe

Project:	
Trial:	
Location:	
DOT:	Select DOT
Latitude:	
Longitude:	
Date:	

Input / Output — Save — Print

Live and Dead Loads Calculation:

Select Standard Pipe Arch Sizes	71 x 47	in.
Pipe Arch - Top Radius	35.750	in.
Pipe Arch - Bottom Radius	110.250	in.
Pipe Arch - Span	71.00	in.
Pipe Arch - Rise	47.00	in.
Mp Multiple Presence Factor, typically equal to 1.2 *Refer to AASHTO LRFD Bridge Design Specifications, 8th Ed. Table 3.6.1.1.2.1.*	1.20	
P Design Wheel Load *Refer to AASHTO Bridge Design Specifications, 8th Ed., Section 3.6.1.2.6b.* *P Load is the weight an AASHTO design truck imposes on a single wheel (or pair of wheels in the case of dual wheels).* *Typical HL-93 Design Truck has 3 axles, front axle load of 8 kips, and two rear axles with a load of 32 kips each (rear wheel load of 16 kips each)*	16,000.00	lb
h Depth of Cover over Culvert *Distance from top of the pipe to top of the soil*	24.00	in.
LLDF Live Load Distribution Factor *Refer to AASHTO Bridge Design Specifications, 8th Ed., table 3.6.1.2.6a-1* *For Concrete Pipe with fill depth 2.0ft or greater, linearly interpolate between these limits:* *1.15 for diameter 2.0ft or less* *1.75 for diameters 8.0ft or greater* *All other culverts and buried structures: 1.15*	1.15	
l_t Tire Patch Length *Refer to AASHTO LRFD Bridge Design Specifications, 8th Ed. Section 3.6.1.2.5.*	10.00	in.
W_t Tire Patch Width *Refer to AASHTO LRFD Bridge Design Specifications, 8th Ed. Section 3.6.1.2.5.*	20.00	in.
Sw Spacing between the Wheel Pairs on the Axle *Refer to AASHTO LRFD Bridge Design Specifications, 8th Ed. Section 3.6.1.2.3.*	72.00	in.
S_a Axle Spacing *Refer to AASHTO LRFD Bridge Design Specifications, 8th Ed. Section 3.6.1.2.3.*	48.00	in.
δ_{soil} Soil Unit Weight	120.00	pcf
c Soil Cohesion *Cohesion per ASCE Manual of Practice (MOP) 60. Standard values:* *Clay, very soft: 40 psf* *Clay, medium: 250 psf* *Clay, hard: 1,000 psf* *Sand, loose dry: 0 psf* *Sand, silty: 100 psf* *Sand, dense: 300 psf*	0.00	psf
k_μ' Select k_μ' - Refer to Figure 9-13 in ASCE MOP 60 *k_μ'=0.1924 min for granular material without cohesion* *k_μ'=0.165 max for sand and gravel* *k_μ'=0.150 max for saturated top soil* k_μ'=0.130 max for ordinary clay *k_μ'=0.110 max for saturated clay*	0.1924	
H_w Height of the Groundwater above the Top of the Pipe *H_w = 0 if no groundwater*	0.00	ft
Select if it is a Single Span culvert or Multiple Span culverts?	Single Span	

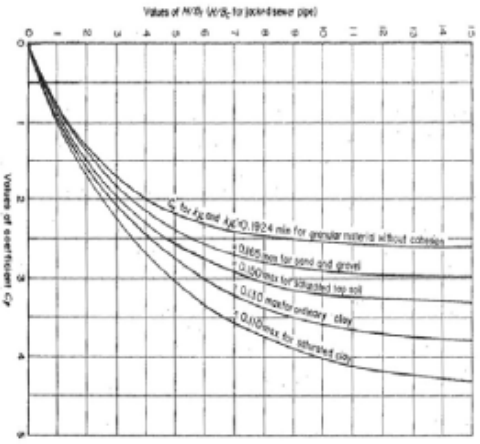


Figure 8-1

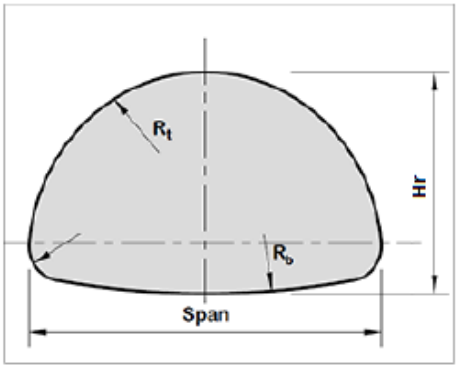


Figure 8-2

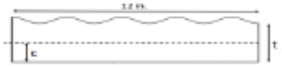


Figure 8-3

Live and Dead Loads Results:

C_t Coefficient *(Figure 9-13 in ASCE MOP 60)*	0.32	
P_L Live Load on Pipe	12.28	psi
P_E Earth Load acting on the Horizontal Soil Plane at the Top of the Pipe	0.53	psi
P_w External Hydrostatic Pressure acting on the Pipe	0.00	psi

Design Assumptions (Cementitious Liner):

t Wall Thickness of the Liner - *See figure 8-3* *Note: Wall thickness is above the corrugation crests.*	1.00	in.
Assume only the liner above the corrugation crests is effective? Select Yes or No	No	
c Distance from the Centroid of the Liner Pipe Wall Profile to the Interior Wall Surface - See figure 8-3	0.6370	in.
I SAPL Area Moment of Inertia of the Liner Wall Section	0.1814	in.4/in

σ_{cs} Compressive Stress Strength of the Liner Material *Compressive strength value to be provided by manufacturer in accordance with Pipe Liner Special Provision.*	-8,390.00	psi
σ_{flex} Flexural Stress Strength (Modulus of Rupture) of the Liner Material *Flexural strength value to be provided by manufacturer in accordance with Pipe Liner Special Provision.*	1,665.00	psi
γ_{EV} Load Factor for Soil Prism Load - Service, 1.0	1.00	
γ_{EV} Load Factor for Soil Prism Load - Strength, 1.30	1.30	
γ_{WA} Load Factor for Groundwater Load, 1.0	1.00	
γ_{LL} Load Factor for Live Load - Service, 1.0	1.00	
γ_{LL} Load Factor for Live Load - Strength, 1.75	1.75	
η_{EV} Load Modifier for Soil Prism Load, use 1.0 per Article 1.3.2 of the BDS	1.00	
η_R Load Modifier for Redundancy, 1.05 for Strength Limit State under Earth Loads	1.05	
η_R Load Modifier for Redundancy, 1.0 for Strength Limit State under Live Loads	1.00	
η_{LL} Load Modifier for Live Load, use 1.0 per Article 1.3.2 of the BDS	1.00	

Results (Cementitious Liner)

Service

Top Radius

$T_{service}$ Thrust in Liner	209.27	lb/in.	
A Area of the Cross-Section of the proposed Liner per linear inch	1.00	$in.^2/in.$	
$M_{service}$ Moment	51.55	in.-lbs/in.	
σ_{crown} Normal Stress (Service)	-28.27	psi	Stress within limits. The 1-in. thick liner is sufficient.

Bottom Radius

$T_{service}$ Thrust in Liner	67.39	lb/in.	
A Area of the Cross-Section of the proposed Liner per linear inch	1.00	$in.^2/in.$	
$M_{service}$ Moment	16.48	in.-lbs/in.	
σ_{crown} Normal Stress (Service)	-9.51	psi	Stress within limits. The 1-in. thick liner is sufficient.

Strength

Top Radius

$T_{strength}$ Thrust in Liner	360.18	lb/in.	
A Area of the Cross-Section of the proposed Liner per linear inch	1.00	$in.^2/in.$	
$M_{strengthe}$ moment	90.21	in.-lbs/in.	
σ_{crown} Normal Stress (Strength)	-43.42	psi	Stress within limits. The 1-in. thick liner is sufficient.

Bottom Radius

$T_{strength}$ Thrust in Liner	115.98	lb/in.	
A Area of the Cross-Section of the proposed Liner per linear inch	1.00	$in.^2/in.$	
$M_{strengthe}$ Moment	28.84	in.-lbs/in.	
σ_{crown} Normal Stress (Strength)	-14.69	psi	Stress within limits. The 1-in. thick liner is sufficient.

SAPL Design

Structural Design for Liner Thickness Using Flexible Polymeric Materials
Arch Corrugated Metal Pipe

Project:	
Trial:	
Location:	
DOT:	Select DOT
Latitude:	
Longitude:	
Date:	

Input / Output

Save

Print

Live and Dead Loads Calculation:

Select Standard Pipe Arch Sizes	71 x 47	in.
Pipe Arch - Top Radius	35.750	in.
Pipe Arch - Bottom Radius	110.250	in.
Pipe Arch - Span	71.00	in.
Pipe Arch - Rise	47.00	in.
Mp Multiple Presence Factor, typically equal to 1.2 *Refer to AASHTO LRFD Bridge Design Specifications, 8th Ed. Table 3.6.1.1.2.1.*	1.20	
P Design Wheel Load *Refer to AASHTO Bridge Desgin Specifications, 8th Ed., Section 3.6.1.2.6b.* *P Load is the weight an AASHTO design truck imposes on a single wheel (or pair of wheels in the case of dual wheels).* *Typical HL-93 Design Truck has 3 axles, front axle load of 8 kips, and two rear axles with a load of 32 kips each (rear wheel load of 16 kips each)*	16,000.00	lb
h Depth of Cover over Culvert *Distance from top of the pipe to top of the soil*	24.00	in.
LLDF Live Load Distribution Factor *Refer to AASHTO Bridge Desgin Specifications, 8th Ed., table 3.6.1.2.6a-1* *For Concrete Pipe with fill depth 2.0ft or greater, linearly interpolate between these limits:* *1.15 for diameter 2.0ft or less* *1.75 for diameters 8.0ft or greater* *All other culverts and buried structures: 1.15*	1.15	
l_t Tire Patch Length *Refer to AASHTO LRFD Bridge Design Specifications, 8th Ed. Section 3.6.1.2.5.*	10.00	in.
W_t Tire Patch Width *Refer to AASHTO LRFD Bridge Design Specifications, 8th Ed. Section 3.6.1.2.5.*	20.00	in.
Sw Spacing Between the Wheel Pairs on the Axle *Refer to AASHTO LRFD Bridge Design Specifications, 8th Ed. Section 3.6.1.2.3.*	72.00	in.
S_a Axle Spacing *Refer to AASHTO LRFD Bridge Design Specifications, 8th Ed. Section 3.6.1.2.3.*	48.00	in.
δ_{soil} Soil Unit Weight	120.00	pcf
c Soil Cohesion *Cohesion per ASCE Manual of Practice (MOP) 60. Standard values:* *Clay, very soft: 40 psf* *Clay, medium: 250 psf* *Clay, hard: 1,000 psf* *Sand, loose dry: 0 psf* *Sand, silty: 100 psf* *Sand, dense: 300 psf*	0.00	psf

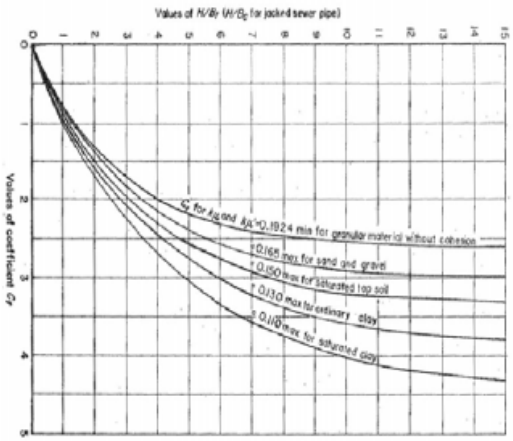


Figure 8-1

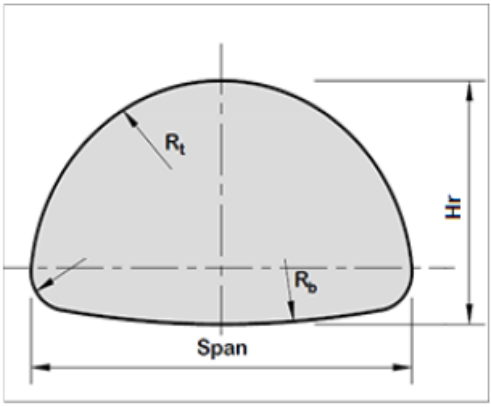


Figure 8-2

k_μ' Select k_μ' - Refer to Figure 9-13 in ASCE MOP 60 *k_μ'=0.1924 min for granular material without cohesion* *k_μ'=0.165 max for sand and gravel* *k_μ'=0.150 max for saturated top soil* *k_μ'=0.130 max for ordinary clay* *k_μ'=0.110 max for saturated clay*	0.1924	
H_w Height of the Groundwater above the Top of the Pipe *H_w = 0 if no groundwater*	0.00	ft

Select if it is a Single Span culvert or Multiple Span culverts?	Single Span

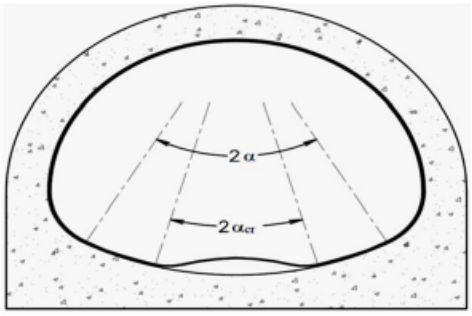


Figure 8-3

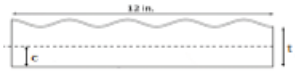


Figure 8-4

Live and Dead Loads Results:

C_t Coefficient *(Figure 9-13 in ASCE MOP 60)*	0.32	
P_L Live Load on Pipe	12.28	psi
P_E Earth Load acting on the Horizontal Soil Plane at the Top of the Pipe	0.53	psi
P_w External Hydrostatic Pressure acting on the Pipe	0.00	psi

Design Assumptions (Flexible Polymeric Materials):

t Thickness of the Liner - *See figure 8-4* *Note: Wall thickness is above the corrugation crests.*	1.00	in.
I_{SAPL} Moment of Inertia of Liner Profile per unit length of Liner	0.0456	in^4/in
$\Gamma_{(\alpha,g)}$ Amplification Factor for the Critical Angle due to Initial Gap, for SAPL = 1	1.00	
k Deformation Mode, k = 1 for a Pipe Arch Shape	1.00	
P Perimeter of the Lining	188.50	in.
α Half Arc Angle where Blister Develops *See figure 8-3*	13.00	degree°
E_{SAPL} Short-Term Circumferential Flexural Modulus of Liner Material *For determining long term and short term modulus of elasticity, use ASTM D790 standard test methods for short term, and ASTM D2990 standard test methods for long term. In the absence of the ASTM D2990 standard tests, it is a common practice to use 50% of the short term modulus of elasticity as a value for the long term modulus of elasticity.*	735.00	ksi
$\Gamma_{(d,g)}$ Amplification Factor for the Critical Deflection due to Initial Gap, for SAPL = 1	1.00	
$\Gamma_{(M,g)}$ Amplification Factor for the Critical Moment due to Initial Gap, for SAPL = 1	1.00	
ϕ_{buck} Resistance Factor to Buckling, recommend a value of 0.5	0.50	
σ_R Stress Strength of Material Corresponding to 95% Lower Confidence Limit	14,000.00	psi
ϕ_M Strength Resistance Factor for Material, use 0.67 in absence of testing	0.67	
Deflection Limit: Percentage of the Straight Section (flattest arc element)	3.00%	%

Results (Flexible Polymeric Materials):

Δ_t Total Deflection of Liner	1.56	in.	
Δ_A Total Allowable Deflection of Liner (Δ_A = 0.05 R_{top})	1.79	in.	The 1-inch thickness is good for the deflection performance
α_{cr} Calculated Half Blister Angle just before Buckling occurs	15.07	degree°	
α_{cr} / α	1.16		Eq. 8-33 is satisfied: αcr / α ≤ 1.5
p Design Pressure	2.28	psi	
p_{cr} Buckling Pressure of a Critical Lining	11.43	psi	
ϕ_{bck} p_{cr}	5.71	psi	Condition of stability is verified: P ≤ (ϕbck Pcr)
ϕ_M σ_R	9333.33	psi	
$\sigma_u = \sigma_{(u,b)} + \sigma_{(u,d)}$	818.38	psi	Condition of strength is verified: σu ≤ (ϕM σR)
d_s Maximum Deflection	0.17	in.	
d_L Permissible Deflection for Flexible Polymeric Liners	0.75	in.	Deflection is within the suggested limit of 3%

SAPL Design

Structural Design for Liner Thickness Using Cementitious Materials
Circular Corrugated Metal Pipe

Project:	
Trial:	
Location:	
DOT:	Select DOT
Latitude:	
Longitude:	
Date:	

Input / Output

Save Print

Live and Dead Loads Calculation:

Mp Multiple Presence Factor, typically equal to 1.2 *Refer to AASHTO LRFD Bridge Design Specifications, 8th Ed. Table 3.6.1.1.2.1.*	1.20	
P Design Wheel Load *Refer to AASHTO Bridge Desgin Specifications, 8th Ed., Section 3.6.1.2.6b.* *P Load is the weight an AASHTO design truck imposes on a single wheel (or pair of wheels in the case of dual wheels).* *Typical HL-93 Design Truck has 3 axles, front axle load of 8 kips, and two rear axles with a load of 32 kips each (rear wheel load of 16 kips each)*	16,000.00	lb
h Depth of Cover over Culvert *Distance from top of the pipe to top of the soil*	24.00	in.
LLDF Live Load Distribution Factor *Refer to AASHTO Bridge Desgin Specifications, 8th Ed., Table 3.6.1.2.6a-1* *For Concrete Pipe with fill depth 2.0ft or greater, linearly interpolate between these limits:* *1.15 for diameter 2.0ft or less* *1.75 for diameters 8.0ft or greater* *All other culverts and buried structures: 1.15*	1.15	
l_t Tire Patch Length *Refer to AASHTO LRFD Bridge Design Specifications, 8th Ed. Section 3.6.1.2.5.*	10.00	in.
W_t Tire Patch Width *Refer to AASHTO LRFD Bridge Design Specifications, 8th Ed. Section 3.6.1.2.5.*	20.00	in.
Sw Spacing between the Wheel Pairs on the Axle *Refer to AASHTO LRFD Bridge Design Specifications, 8th Ed. Section 3.6.1.2.3.*	72.00	in.
S_a Axle Spacing *Refer to AASHTO LRFD Bridge Design Specifications, 8th Ed. Section 3.6.1.2.3.*	48.00	in.
D_i Inside Diameter or Clear Span of the Culvert	60.00	in.
δ_{soil} Soil Unit Weight	120.00	pcf
c Soil Cohesion *Cohesion per ASCE Manual of Practice (MOP) 60. Standard values:* *Clay, very soft: 40 psf* *Clay, medium: 250 psf* *Clay, hard: 1,000 psf* *Sand, loose dry: 0 psf* *Sand, silty: 100 psf* *Sand, dense: 300 psf*	0.00	psf
kμ' Select kμ' - Refer to Figure 9-13 in ASCE MOP 60 *kμ'=0.1924 min for granular material without cohesion* *kμ'=0.165 max for sand and gravel* *kμ'=0.150 max for saturated top soil* *kμ'=0.130 max for ordinary clay* *kμ'=0.110 max for saturated clay*	0.1924	
H_w Height of the Groundwater above the Top of the Pipe *See figure 8-2* *H_w = 0 if no groundwater*	0.00	ft

Select if it is a Single Span culvert or Multiple Span culverts?	Single Span

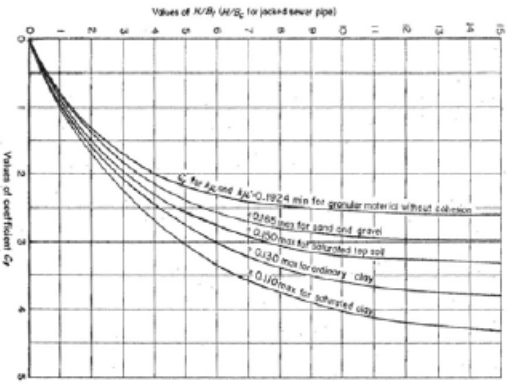


Figure 8-1

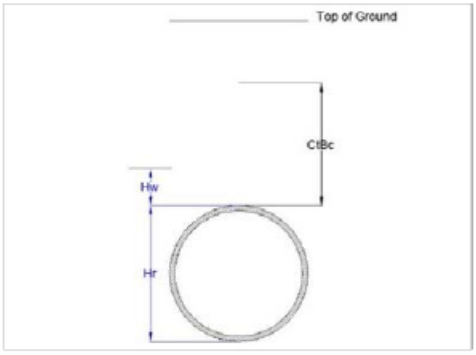


Figure 8-2

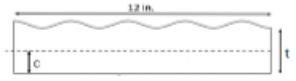


Figure 8-3

Live and Dead Loads Results:

C_t Coefficient *(Figure 9-13 in ASCE MOP 60)*	0.37	
P_L Live Load on Pipe	12.44	psi
P_E Earth Load acting on the Horizontal Soil Plane at the Top of the Pipe	0.62	psi
P_w External Hydrostatic Pressure acting on the Pipe	0.00	psi

Design Assumptions (Cementitious Liner):

t Wall Thickness of the Liner - *See figure 8-3* *Note: Wall thickness is above the corrugation crests.*	1.00	in.
Assume only the liner above the corrugation crests is effective? Select Yes or No	No	
c Distance from the Centroid of the Liner Pipe Wall Profile to the Interior Wall Surface - See figure 8-3	0.6370	in.
I SAPL Area Moment of Inertia of the Liner Wall Section	0.1814	in.4 /in.

σ_{cs} Compressive Stress Strength of the Liner Material *Compressive strength value to be provided by manufacturer in accordance with Pipe Liner Special Provision.*	-8,390.00	psi
σ_{flex} Flexural Stress Strength (Modulus of Rupture) of the Liner Material *Flexural strength value to be provided by manufacturer in accordance with Pipe Liner Special Provision.*	1,665.00	psi
γ_{EV} Load Factor for Soil Prism Load - Service, 1.0	1.00	
γ_{EV} Load Factor for Soil Prism Load - Strength, 1.30	1.30	
γ_{WA} Load Factor for Groundwater Load, 1.0	1.00	
γ_{LL} Load Factor for Live Load - Service, 1.0	1.00	
γ_{LL} Load Factor for Live Load - Strength, 1.75	1.75	
η_{EV} Load Modifier for Soil Prism Load, use 1.0 per Article 1.3.2 of the BDS	1.00	
η_R Load Modifier for Redundancy, 1.05 for Strength Limit State under Earth Loads	1.05	
η_R Load Modifier for Redundancy, 1.0 for Strength Limit State under Live Loads	1.00	
η_{LL} Load Modifier for Live Load, use 1.0 per Article 1.3.2 of the BDS	1.00	

Results (Cementitious Liner)

Service

$T_{service}$ Thrust in Liner	210.11	lb/in.	
A Area of the Cross-Section of the proposed Liner per linear inch	1.00	$in.^2/in.$	
$M_{service}$ Moment	43.51	in.-lbs/in.	
σ_{crown} Normal Stress (Service)	-57.33	psi	Stress within limits. The 1-in. thick liner is sufficient.

Strength

$T_{strength}$ Thrust in Liner	361.75	lb/in.	
A Area of the Cross-Section of the proposed Liner per linear inch	1.00	$in.^2/in.$	
$M_{strength}$ Moment	76.14	in.-lbs/in.	
σ_{crown} Normal Stress (Strength)	-94.39	psi	Stress within limits. The 1-in. thick liner is sufficient.

SAPL Design

Structural Design for Liner Thickness Using Flexible Polymeric Materials
Circular Corrugated Metal Pipe

Project:	
Trial:	
Location:	
DOT:	Select DOT
Latitude:	
Longitude:	
Date:	

Input / Output

Save

Print

Live and Dead Loads Calculation:

Mp Multiple Presence Factor, typically equal to 1.2 *Refer to AASHTO LRFD Bridge Design Specifications, 8th Ed. Table 3.6.1.1.2.1.*	1.20	
P Design Wheel Load *Refer to AASHTO Bridge Desgin Specifications, 8th Ed., Section 3.6.1.2.6b.* *P Load is the weight an AASHTO design truck imposes on a single wheel (or pair of wheels in the case of dual wheels).* *Typical HL-93 Design Truck has 3 axles, front axle load of 8 kips, and two rear axles with a load of 32 kips each (rear wheel load of 16 kips each)*	16,000.00	lb
h Depth of Cover over Culvert *Distance from top of the pipe to top of the soil*	24.00	in.
LLDF Live Load Distribution Factor *Refer to AASHTO Bridge Desgin Specifications, 8th Ed., table 3.6.1.2.6a-1* *For Concrete Pipe with fill depth 2.0ft or greater, linearly interpolate between these limits:* *1.15 for diameter 2.0ft or less* *1.75 for diameters 8.0ft or greater* *All other culverts and buried structures: 1.15*	1.15	
l_t Tire Patch Length *Refer to AASHTO LRFD Bridge Design Specifications, 8th Ed. Section 3.6.1.2.5.*	10.00	in.
W_t Tire Patch Width *Refer to AASHTO LRFD Bridge Design Specifications, 8th Ed. Section 3.6.1.2.5.*	20.00	in.
Sw Spacing between the Wheel Pairs on the Axle *Refer to AASHTO LRFD Bridge Design Specifications, 8th Ed. Section 3.6.1.2.3.*	72.00	in.
S_a Axle Spacing *Refer to AASHTO LRFD Bridge Design Specifications, 8th Ed. Section 3.6.1.2.3.*	48.00	in.
D_i Inside Diameter or Clear Span of the Culvert	60.00	in.
δ_{soil} Soil Unit Weight	120.00	pcf
c Soil Cohesion *Cohesion per ASCE Manual of Practice (MOP) 60. Standard values:* *Clay, very soft: 40 psf* *Clay, medium: 250 psf* *Clay, hard: 1,000 psf* *Sand, loose dry: 0 psf* *Sand, silty: 100 psf* *Sand, dense: 300 psf*	0.00	psf
kμ' Select kμ' - Refer to Figure 9-13 in ASCE MOP 60 *kμ'=0.1924 min for granular material without cohesion* *kμ'=0.165 max for sand and gravel* *kμ'=0.150 max for saturated top soil* kμ'=0.130 max for ordinary clay *kμ'=0.110 max for saturated clay*	0.1924	
H_w Height of the Groundwater above the Top of the Pipe *See figure 8-2* *H_w = 0 if no groundwater*	0.00	ft

Select if it is a Single Span culvert or Multiple Span culverts?	Single Span

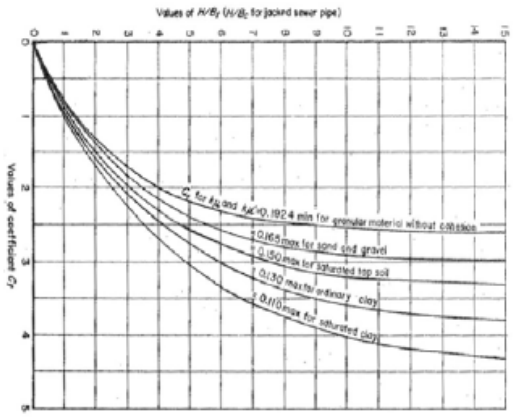


Figure 8-1

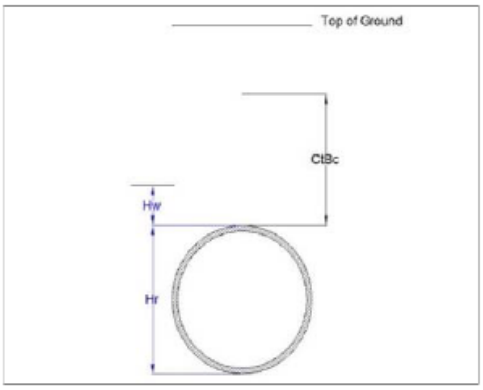


Figure 8-2

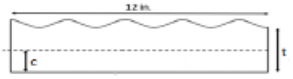


Figure 8-3

Live and Dead Loads Results:

C_t Coefficient *(Figure 9-13 in ASCE MOP 60)*	0.37	
P_L Live Load on Pipe	12.44	psi
P_E Earth Load acting on the Horizontal Soil Plane at the Top of the Pipe	0.62	psi
P_w External Hydrostatic Pressure Acting on the Pipe	0.00	psi

Design Assumptions (Flexible Polymeric Liner):

Deflection Verification

t Wall Thickness of the Liner - *See figure 8-3* *Note: Wall thickness is above the corrugation crests.*	1.20	in.
I_{SAPL} Moment of Inertia of Liner Profile per unit length of Liner	0.0456	in^4/in
D_L Deflection Lag Factor, a value of 1.0 is recommended for rehabilitation lining *Refer to AASHTO LRFD Bridge Design Manual, 8th Ed., Section 12.12.2.2*	1.00	
K_B Bedding Coefficient, a value of 0.083 is recommended for rehabilitation lining *Refer to AASHTO LRFD Bridge Design Manual, 8th Ed., Section 12.12.2.2*	0.083	
E_{SAPL} Short-Term Circumferential Flexural Modulus of Liner Material *For determining long term and short term modulus of elasticity, use ASTM D790 standard test methods for short term, and ASTM D2990 standard test methods for long term. In the absence of the ASTM D2990 standard tests, it is a common practice to use 50% of the short term modulus of elasticity as a value for the long term modulus of elasticity.*	735.00	ksi
M_s Secant Constrained Soil Modulus, as specified in Article 12.12.3.5 *A conservative value for Ms is 0.503, which assumes sandy soil at 85% compaction.* *Alternately, use the Pe value above to determine Ms from Table 12.12.3.5-1 of AASHTO LRFD Bridge Design Specifications.*	0.503	ksi
Δ_A Maximum Percentage of the Allowable Deflection [Δ_A = % x D_I]	5.0%	%

Results

Δ_A Total Allowable Deflection of Liner, Reduction in Vertical Diameter	3.00	in.	
Δ_t Total Deflection of the Pipe, expressed as a Reduction of the Vertical Diameter	1.31	in.	$\Delta t \leq \Delta a$ - Deflection within limits

Design Assumptions (Flexible Polymeric Liner):

Strength limit state for global buckling

γ_{WA} Load Factor for Hydrostatic Pressure, as per Article 3.4.1, use 1.0	1.00	
γ_{EV} Load Factor for Vertical Pressure from Dead Load of Earth Fill, recommend 1.3 for rehab *See Table 3.4.1-2 of AASHTO LRFD Bridge Design Specifications for the range of possible values. Values range from 1.95 to 0.9 for Thermoplastic Pipe, with 1.95 being more conservative.*	1.30	
γ_{LL} Load Factor for Live Load , as specified in Article 3.4.1	1.75	
η_{EV} Load Modifier for Vertical Pressure from Dead Load of Earth Fill on a Buried Structure per Article 1.3.2, recommend 1.0 for rehab	1.00	
η_{LL} Load Modifier as Specified in Article 1.3.2, as they apply to live loads on culverts *use 1.0 per Article 1.3.2*	1.00	
C_n Scalar Calibration Factor, 0.55	0.55	
ϕ_s Resistance Factor of the Soil to account for variability, 0.9 *Refer to AASHTO LRFD Bridge Design Specifications 8th ed. Table 12.5.5-1.*	0.90	
ϕ_{bck} Resistance Factor for Global Buckling as defined in Table 12.5.5-1, use 0.70	0.70	
E_{SAPL} Long-Term Circumferential Flexural Modulus of Liner Material *For determining long term and short term modulus of elasticity, use ASTM D790 standard test methods for short term, and ASTM D2990 standard test methods for long term. In the absence of the ASTM D2990 standard tests, it is a common practice to use 50% of the short term modulus of elasticity as a value for the long term modulus of elasticity.*	529.00	ksi
v Poisson's Ratio of the Soil, 0.3	0.30	

Results

ε_{fb} Factored Buckling Strain Demand	0.000669	in./in.	
ε_{bck} Nominal Strain Capacity for Buckling	0.001306	in./in.	The strength buckling limit state is satisfied by the 1.2 inch-thick liner

Design Assumptions (Flexible Polymeric Liner):

Strength limit state for flexure

ϕ_f Resistance Factor for Flexure, 0.90 (Table 12.5.5-1, BDS)	0.90
S_b Long-Term Ring-Bending Strain for Product under Design per the Manufacturer's Testing *Sb is obtained from manufacturer's ASTM D5365 test results.*	0.0130
D_f Shape Factor (dimensionless) See Table 12.12.3.10.2b-1 of AASHTO LRFD Bridge Design Specifications *A conservative value is 5.5 for poorly compacted gravel.*	5.50

Results

ε_f Factored Long-Term Strain due to Flexure	0.007445	
$\phi_f S_b$	0.011700	$\varepsilon f \leq \phi f$ Sb: The long-term strain due to the estimated deflection is acceptable

This Page Left Intentionally Blank.

REFERENCES

AASHTO. 2017. AASHTO LRFD bridge design specifications. Fourth edition with 2008 interim revisions. Washington, D.C. American Association of State Highway and Transportation Officials, [2008] ©2007.

Adhikari, S. (2013). “Mechanical and Structural Characterization of Mini-Bar Reinforced Concrete Beams,” A dissertation presented to the Graduate Faculty of the University of Akron, 350 pages.

Aggarwal, S.C. & Cooper, M.J. (1984), "External Pressure Testing of 'Insituform' Linings," Internal Report, Coventry (Lanchester) Polytechnic.

Alam, S., Sayem, S., Aaron, S., Pierce, J., Allouche, E. and McKim, R. (2014). “Experimental Examination of Deteriorated and Rehabilitated Corrugated Metal Culverts Subjected to Service Load.” 93rd Annual Meeting, Transportation Research Board, Washington DC.

Al-Lami, B. (2020). “Performance of Cracked Reinforced Concrete Pipes Subjected to Different Environmental Conditions.” The University of Texas at Arlington.

Allouche E. (2017). “Culvert Rehabilitation to Maximize Service Life While Minimizing Direct Costs and Traffic Disruption,” Active Research, NCHRP 14, Louisiana Tech University.

American Association of State Highway and Transportation Officials, Load Resistance Factor Design, (AASHTO LRFD) Bridge Design Specifications, 8th Edition, November 2017.

American Concrete Institute (ACI), ACI 318.2-14 “Building Code Requirements for Concrete Thin Shells,” an ACI Standard and Report by the ACI Committee 318, 2014, 16 pages.

American Concrete Institute (ACI), ACI Committee 544, “Drop-Weight Impact Test.”

American Concrete Pipe Association. (1987). Concrete pipe design manual. American Concrete Pipe Association.

American Concrete Pipe Association. (2008). Concrete Pipe Stays in Shape!

Angus W., Stocking L. S. (2015). “NYSDOT Embraces Centrifugally Cast Concrete Pipe for Trenchless Storm Sewer Rehab,” Trenchless Technology Magazine.

Arnoult, J. D. (1986). “FHWA Culvert Inspection Manual.” U.S. Department of Transportation, Federal Highway Administration.

Arockiasamy, M., Chaalla, O., & Limpeteeprakarn, T. (2006). Full Scale Field Test on Flexible Pipes under Live Load Applications. Journal of Performance of Constructed Facilities, 21-27.

Arulrajah, A., J. Piratheepan, M.M.Y. Ali, & Bo, M. (2012). Geotechnical Properties of the Recycled Concrete Aggregates in Pavement Subbase Applications. ASTM, 743-750.

ASCE (American Society of Civil Engineers). (2007). Pipeline Infrastructure Task Committee. “Emerging Concepts for the Design of Pipeline Renewal Systems,” ASCE Pipeline Division. Available at:

ASCE (American Society of Civil Engineers). (2010). “Trenchless Renewal of Culverts and Storm Sewers.” Prepared by: The Pipeline Infrastructure Committee, ASCE, Reston, VA.

ASCE (American Society of Civil Engineers). (2016). “Renewal of Potable Water Pipes.” Prepared by: The Pipeline Infrastructure Committee, ASCE, Reston, VA.

ASCE Manual of Practice No. 60 / WEF Manual of Practice No. FD-5, Gravity Sanitary Sewer Design and Construction (MOP 60), 2007, 436 pp

ASCE, "Emerging Concepts for the Design of Pipeline Renewal Systems," a report from the Pipeline Infrastructure (PINS) Task Committee, June 2007, 42 pages.

ASCE. (2019). Guidelines for the Sustainable Design of Pipelines. Reston, VA (Under Print).

ASTEE 3R2014 Structural Design for Non-Circular Linings Under Groundwater Pressure.

ASTM (American Society for Testing and Materials). (2012) Standard Test Method for Flexural Toughness of Fiber Reinforced Concrete (Using Centrally Loaded Round Panel), Standard ASTM C1550−12a, ASTM International: West Conshohocken, PA, USA.

ASTM (American Society for Testing and Materials). (2015) Standard Test Method for Slump of Hydraulic-Cement Concrete, Standard ASTM C143/C143M−15a, ASTM International: West Conshohocken, PA, USA.

ASTM (American Society for Testing and Materials). (2015) Standard Test Method for Obtaining Average Residual-Strength of Fiber-Reinforced Concrete, Standard ASTM C1399/C1399M−10, ASTM International: West Conshohocken, PA, USA.

ASTM (American Society for Testing and Materials). (2015) Standard Specification for Fiber-Reinforced Concrete, Standard ASTM C1116/C1116M−10a, ASTM International: West Conshohocken, PA, USA.

ASTM (American Society for Testing and Materials). (2016) Standard Test Method for Temperature of Freshly Mixed Hydraulic-Cement Concrete, Standard ASTM C109/C109M−16a, ASTM International: West Conshohocken, PA, USA.

ASTM (American Society for Testing and Materials). (2017) Standard Test Method for Density (Unit Weight), Yield, and Air Content (Gravimetric) of Concrete, Standard ASTM C138/C138M−17a, ASTM International: West Conshohocken, PA, USA.

ASTM (American Society for Testing and Materials). (2017) Standard Test Method for Air Content of Freshly Mixed Concrete by the Pressure Method, Standard ASTM C231/C231M−17a, ASTM International: West Conshohocken, PA, USA.

ASTM (American Society for Testing and Materials). (2017) Standard Test Method for Temperature of Freshly Mixed Hydraulic-Cement Concrete, Standard ASTM C1064/C1064−17, ASTM International: West Conshohocken, PA, USA.

ASTM (American Society for Testing and Materials). (2018) Standard Specification for Reinforced Concrete Culvert, Storm Drain, and Sewer Pipe, Standard ASTM C76−18a, ASTM International: West Conshohocken, PA, USA.

ASTM (American Society for Testing and Materials). (2018) Standard Test Method for Flexural Performance of Fiber-Reinforced Concrete (Using Beam with Third-Point Loading), Standard ASTM C1609/C1609M, ASTM International: West Conshohocken, PA, USA.

ASTM A760 A760/A760M - 15. (2020). "Standard Specification for Corrugated Steel Pipe, Metallic-Coated for Sewers and Drains." American Society for Testing and Materials. ASTM International, West Conshohocken, PA.

ASTM A796 A796/A796M - 17a. (2017). "Standard Practice for Structural Design of Corrugated Steel Pipe, Pipe-Arches, and Arches for Storm and Sanitary Sewers and Other Buried Applications." American Society for Testing and Materials. ASTM International, West Conshohocken, PA.

ASTM A849 -15 (2015). "Standard Specification for Post-Applied Coatings, Pavings, and Linings for Corrugated Steel Sewer and Drainage Pipe" American Society for Testing and Materials. ASTM International, West Conshohocken, PA.

ASTM A979 – 03 (2019). "Standard Specification for Concrete Pavements and Linings Installed in Corrugated Steel Structures in the Field" American Society for Testing and Materials. ASTM International, West Conshohocken, PA.

ASTM B745/B745M - 15. (2015). "Standard Specification for Corrugated Aluminum Pipe for Sewers and Drains." American Society for Testing and Materials. ASTM International, West Conshohocken, PA.

ASTM C39 - 21. (2020). "Standard Test Method for Compressive Strength of Cylindrical Concrete Specimen" American Society for Testing and Materials. ASTM International, West Conshohocken, PA.

ASTM D1557 - 12. (2015). "Standard Test Methods for Laboratory Compaction Characteristics of Soil Using Modified Effort." American Society for Testing and Materials. ASTM International, West Conshohocken, PA.

ASTM D1633 - 17. (2017). "Standard Test Methods for Compressive Strength of Molded Soil-Cement Cylinders." American Society for Testing and Materials. ASTM International, West Conshohocken, PA.

ASTM D2412 - 11. (2018). "Standard Test Method for Determination of External Loading Characteristics of Plastic Pipe by Parallel-Plate Loading." American Society for Testing and Materials. ASTM International, West Conshohocken, PA.

ASTM D698 – 12 (2014). "Standard Test Methods for Laboratory Compaction Characteristics of Soil Using Standard Effort" American Society for Testing and Materials. ASTM International, West Conshohocken, PA.

ASTM D2487- 17. (2017). "Standard Practice for Classification of Soils for Engineering Purposes (Unified Soil Classification System)" American Society for Testing and Materials. ASTM International, West Conshohocken, PA.

ASTM D4253- 16. (2019). “Standard Test Methods for Maximum Index Density and Unit Weight of Soils Using a Vibratory Table” American Society for Testing and Materials. ASTM International, West Conshohocken, PA.

ASTM D5365 - 18. (2018). “Standard Test Method for Long-Term Ring-Bending Strain of "Fiberglass" (Glass-Fiber-Reinforced Thermosetting-Resin) Pipe” American Society for Testing and Materials. ASTM International, West Conshohocken, PA.

ASTM D6780 - 19. (2019). “Standard Test Methods for Water Content and Density of Soil In situ by Time Domain Reflectometry (TDR)” American Society for Testing and Materials. ASTM International, West Conshohocken, PA.

ASTM D6913 / D6913M - 17. (2017). “Standard Test Methods for Particle-Size Distribution (Gradation) of Soils Using Sieve Analysis.” American Society for Testing and Materials. ASTM International, West Conshohocken, PA.

ASTM D6938 – 17a. (2017). “Standard Test Methods for In-Place Density and Water Content of Soil and Soil-Aggregate by Nuclear Methods

ASTM D790 - 17. (2017). "Standard Test Methods for Flexural Properties of Unreinforced and Reinforced Plastics and Electrical Insulating Materials.” American Society for Testing and Materials. ASTM International, West Conshohocken, PA.

ASTM F1216 - 16. (2016). “Standard Practice for Rehabilitation of Existing Pipelines and Conduits by the Inversion and Curing of a Resin-Impregnated Tube.” American Society for Testing and Materials. ASTM International, West Conshohocken, PA.

ASTM. 2015. “ASTM D2850-15 Standard Test Method for Unconsolidated-Undrained Triaxial Compression Test on Cohesive Soils.” ASTM International. Vol. D2850 − 15. https://doi.org/10.1520/D2850-15.2

AWWA (American Water Works Association). (2019). “Structural Classifications of Pressure Pipe Linings”, AWWA, Denver, CO.

AWWA Manual of Water Supply Practices M45, Fiberglass Pipe Design, Third Edition, American Water Works Association, 2014, 155 pp

AWWA Standard for Fiberglass Pressure Pipe, ANSI/AWWA C950-88, The American Water Works Association, Denver, CO., 1989.

Banthia N., Chokri K., Ohama Y., and Mindess S. 1994. “Fiber-Reinforced Cement Based Composites under Tensile Impact.” Elsevier Science Ltd, Adv. Ceram. Based Mater. 1 (1994) 131–141.

Banthia N., Zanotti C., and Sappakittipakorn M. 2014. “Sustainable Fiber Reinforced Concrete for Repair Applications.” Elsevier Science Ltd, Constr. Build. Mater. 67 (2014) 405–412.

Bednar, L. (n.d.). “Plain Galvanized Steel Drainage Pipe Durability Estimation with a Modified California Chart.” 70–79.

Berney, E.S., and Smith, D.M. 2008. Mechanical and Phusical Properties of ASTM C33 Sand. In U.S. Army Corps of Engineers.

Blodgett, H. B., (1934), Moment of Inertia of Corrugated Sheets, Civil Engineering, Vol. 4, No. 9, Sept. 1934, pp. 492-493

Boot, J. C., and Gumbel, J. E. (1997). “Structural analysis of sewer linings by B. Falter (Trenchless Technology Research 11 (2), 27–41, 1996).” Tunnelling and underground space technology, Elsevier, 12, 49–52.

Conference on Experimental Mechanics, Oxford, August 1998, Balkema Rotterdam, 327–332.

Boot, J. C., and Welch, A. J. (1996). “Creep buckling of thin-walled polymeric pipe linings subject to external groundwater pressure.” Thin-walled structures, Elsevier, 24(3), 191–210.

Boot, J.C. & Gumbel, J.E. (1998), Discussion of "Structural analysis of sewer linings," by B. Falter, Trenchless Technology Research, Vol. 12, Nos. 1-2, pages 49-52.

Boot, J.C. (1998), "Elastic buckling of cylindrical pipe linings with small imperfections subject to external pressure," Trenchless Technology Research, Vol. 12, Nos. 1-2, pages 3-15.

Boot, J.C., Naqvi, M.M., Gumbel, J.E. (2014), "A new method for the structural design of flexible liners for gravity pipes of egg-shaped cross-section: Theoretical considerations and formulation of the problem," Journal of Thin-Walled Structures, Elsevier, 8 pages.

Bresse M. (1866) “Cours de méchanique appliquée. (2nd Ed), Paris, France.”

Broekaen, M. (2002). “Polyurea spray coatings, the technology and latest developments, polyurethanes for high—Performance coatings ii.” ECC, Berlin, March 14(1), 5.

Cain, A. (2016). “Make the right choice for metal coating for the right application.” <https://www.designworldonline.com/make-right-choice-metal-coating-right-application/>.

Center for Underground Infrastructure Research and Education (CUIRE). (2020). "CUIRE SAPL FEM Report." The University of Texas at Arlington.

Chaallal, O., Arockiasamy, M., and Godat, A. (2014). “Field Test Performance of Buried Flexible Pipes under Live Truck Loads.” Journal of Performance of Constructed Facilities, 29(5), 04014124.

Cheney J. (1963) “ Buckling of Restrained Pipe under External Pressure”

Chiaia B., Fantilli A. P., and Vallini P. 2009. “Combining Fiber-Reinforced Concrete with Traditional Reinforcement in Tunnel Linings.” Elsevier Science Ltd, Engineering Structures, 31 (2009) 1600-1606.

Chiaia, B., Fantilli, A. P., and Vallini, P. (2009). “Combining fiber-reinforced concrete with traditional reinforcement in tunnel linings.” Engineering Structures, Elsevier, 31(7), 1600–1606.

Chimauriya, H. R. (2019). Laboratory Test and Finite Element Modeling of the Invert removed corrugated steel culvert buried under the shallow cover. Arlington: University of Texas at Arlington.

Contech. 2019. Contech Engineering Solutions. Available from https://www.conteches.com/.

CUIRE. (2012). Testing and Evaluation of statically loaded large diameter steel pipe with native backfill. Arlington: Tarrant Regional Water Districy (TWRD).

CUIRE. (2018). Evaluation of Potential Release of Organic Chemicals in the Steam Exhaust and Other Release Points during Pipe Rehabilitation Using the Trenchless Cured-In-Place Pipe (CIPP) Method. Final Report, NASSCO's Phase 1 CIPP Steam Emissions Study, 2018.

CUIRE. (2018). Structural Design Methodology for Spray Applied Pipe Liners in Gravity Storm Water Conveyance Conduits-3rd Quarterly Progress Report. Ohio: ODOT.

Darabnoush Tehrani A. 2016. "Finite Element Analysis for ASTM C-76 Reinforced Concrete Pipes with Reduced Steel Cage." Master of Civil Engineering Thesis, The University of Texas at Arlington, DOI: 10.13140/RG.2.2.13688.08967.

Darabnoush Tehrani, A. (2020). "Development of a Structural Design Methodology for Cementitious Spray Applied Pipe Linings in Gravity Storm Water Conveyance Conduits." The University of Texas at Arlington (Doctoral dissertation)

Darabnoush Tehrani, A. (2020). "Development of a Structural Design Methodology for Cementitious Sprayed Applied Pipe Linings in Gravity Storm Water Conveyance Conduits." The University of Texas at Arlington.

Darabnoush Tehrani, A. (2020). Development of a Structural Design Methodology for Cementitious Sprayed Applied Pipe Linings in Gravity Storm Water Conveyance Conduits. The University of Texas at Arlington.

Darabnoush Tehrani, A. 2016. Finite Element Analysis for ASTM C-76 Reinforced Concrete Pipes with Reduced Steel Cage. University of Texas at Arlington.

Darabnoush Tehrani, A., Kohankar Kouchesfehani, Z., and Najafi, M. 2020. Pipe Profiling Using Digital Image Correlation. In Pipelines 2020. American Society of Civil Engineers, Reston, VA. pp. 36–45.

Darabnoush Tehrani, A., Kohankar Kouchesfehani, Z., and Najafi, M. (2020b). "Pipe Profiling using Digital Image Correlation." Pipelines 2020, American Society of Civil Engineers (ASCE), San Antonio, TX.

Darabnoush Tehrani, A., Kohankar Kouchesfehani, Z., Chimauriya, H. R., Raut, S., Najafi, M., and Yu, X. (2020a). "Structural evaluation of invert-cut circular and arch shape corrugated steel pipes through laboratory testing." Canadian Journal of Civil Engineering, NRC Research Press, (999), 1–15.

Darabnoush Tehrani, A., Kohankar Kouchesfehani, Z., Najafi, M., Syar, J. E., and Kampbell, N. E. (2019). "Evaluation of Filling the Valleys of Corrugated Metal Pipes

by Trenchless Spray Applied Pipe Linings." Pipelines, American Society of Civil Engineers.

Darabnoush Tehrani, A., Kohankar Kouchesfehani, Z., Najafi, M., Syar, J. E., and Kampbell, N. E. (2019). "Evaluation of Filling the Valleys of Corrugated Metal Pipes by Trenchless Spray Applied Pipe Linings." Pipelines, American Society of Civil Engineers.

Darabnoush Tehrani, A., Kouchesfehani Kohankar, Z., and Najafi, M. (2020c). "Review and Recommendations for Structural Testing of Buried Gravity Storm Drain Pipes and Culverts." Canadian Journal of Civil Engineering, (Soil–structure interaction of buried structures).

Darabnoush Tehrani, A., Kouchesfehani Kohankar, Z., Chimauriya Raj, H., Raut, S., Najafi, M., & Yu, X. (2020). Structural Evaluation of the Invert -Cut Circular and Arch Shape Corrugated Steel Pipes through Laboratory Testing. Canadian Journal of Civil Engineering

Davidson. S.J., Kang, J., Uday, K.V., Brian, P., and Balaji, T. (2008). "PVA Fiber Reinforced Shotcrete for Rehabilitation and Preventative Maintenance of Aging Culverts". Alabama Department of Transportation, Project 930-657, https://rosap.ntl.bts.gov/view/dot/17333, Date Accessed April 24, 2018.

Dawood, E. T., and Ramli, M. (2011). "High strength characteristics of cement mortar reinforced with hybrid fibers." Construction and building materials, Elsevier, 25(5), 2240–2247.

Drnevich, Evans, & Prochaska, (2007). "A study of effective soil compaction control of granular soil".

El Debs, M. K., and Naaman, A. E. (1995). "Bending behavior of mortar reinforced with steel meshes and polymeric fibers." Cement and Concrete Composites, Elsevier, 17(4), 327–338.

Ellison D., Sever V. F., Oram P., Lovins W., Romer A., Duranceau S. J., and Bell G. (2010). "Global Review of Spray-On Structural Lining Technologies." A Report Sponsored by Water Research Foundation and U.S. Environmental Protection Agency. Prepared by AECOM, University of Central Florida, Orlando, Florida and Schiff Associates. Published by Water Research Foundation,

Ellison, D., Sever, F., Oram, P., Lovins, W., Romer, A., Duranceau, S. J., and Bell, G. (2010). "Global review of spray-on structural lining technologies." Water Research Foundation, Denver, 1–184.

El-Sawy, K. (2003). Three-dimensional modeling of the soil-steel culverts under the effect of the truckloads. Thin-walled structures, 747-768.

Entezarmahdi, A., Najafi, M. and Sever, F. (2014). "Testing and Analysis of No-Dig Structural Manhole Rehabilitation Materials." ASCE Pipelines 2014.

F3182-16, A. (2016). "Standard Practice for the Application of Spray-Applied Polymeric Liners Inside Pipelines for Potable Water." 1–6.

Falter, B. (1996). “Structural analysis of sewer linings.” Tunneling and Underground Space Technology, Elsevier, 11, 27–41.

Federal Highway Administration (FHWA) for Federal Land Highway (FLH) (2010). “Culvert Assessment and Decision-making Procedures Manual.” Publication No. FHWA-CFL/TD-10-005. U.S. Department of Transportation. Central Federal Lands Highway Division, 12300 West Dakota Avenue, Lakewood, CO 80228.

Federal Highway Administration (FHWA). (2012). “Hydraulic Design of highway Culverts.” 3rd Edition, Publication No. FHWA-HIF-12-026. U.S. Department of Transportation.

FHWA. (2012). Hydraulic design of highway culverts. United States. Federal Highway Administration.

Fiber Reinforced Concrete Association (FRCA). 2015. “Fiber Types.” http://fiberreinforcedconcrete.org/fiber-reinforced-concrete/fiber-types/

García, B. D., and Moore I. D. (2015). “Performance of Deteriorated Corrugated Steel Culverts Rehabilitated with Sprayed-On Cementitious Liners Subjected to Surface Loads.” Tunneling and Underground Space Technology, Vol. 47, No. 3, 2015, pp. 222–232.

García, D. B., and Moore, I. D. (2015). “Performance of deteriorated corrugated steel culverts rehabilitated with sprayed-on cementitious liners subjected to surface loads.” Tunnelling and Underground Space Technology, Elsevier, 47, 222–232.

GEOKON. 2019. Pressure Cells. Available from https://www.geokon.com/4800.

GERMAN ATV-DVWK Rules and Standards, ATV-DVWK M-127 E, Part 2

GERMAN ATV-DVWK Rules and Standards, DWA A 143, Part 2, Part 2

GERMAN ATV-DVWK Rules and Standards, DWA A 143, Part 2, Part 3

Ghadban A. A., Wehbe N. I., and Underberg M. 2017. “Fiber-Reinforced Concrete for Structure Components.” Mountain-Plains Consortium (MPC) 17-342, South Dakota State University.

Glock, D. (1977), "Behavior of liners for rigid pipeline under external water pressure and thermal expansion," Der Stahlbau, Vol. 46, No. 7, 212-217.

Glock, D. (1977). “Post-critical behavior of a rigidly encased circular pipe subject to external water pressure and temperature rise.” Der Stahlbau, 46(7), 212–217.

Guan, S. W. (2003). “100% solids polyurethane and polyurea coatings technology.” Coatings World, 49–58.

Guan, S. W., Liu, D., Moreno, M., and Garneau, R. (2004). “100% solids rigid polyurethane coatings technology for corrosion protection of ballast tanks.” CORROSION 2004, NACE International.

Gumbel, J., Spasojevic, A. & Mair, R. (2003) "Centrifuge modelling of soil load transfer to flexible sewer liners," New Pipeline Technologies, Security and Safety, Ed. M. Najafi, American Society of Civil Engineers, Baltimore, MD.

Gumbel, J.E. (1998), "Structural Design of Pipe Linings 1998 – review of principles, practices, and current developments worldwide," Paper presented at the 4th ASTT Conference, Brisbane, Australia.

Gumbel, John (2001), "A New Approach to Design of Circular Liner Pipe to Resist External Hydrostatic Pressure," ASCE Pipelines Division Conference PIPELINES 2001, San Diego, CA, 18 pages.

Ha, S. K., Lee, H.-K., and Kang, I. S. (2016). "Structural behavior and performance of water pipes rehabilitated with a fast-setting polyurea–urethane lining." Tunnelling and Underground Space Technology, Elsevier, 52, 192–201.

Ham, S., and Darabnoush Tehrani, A. (2019). "2D Random Shape of Aggregate Model using Image Processing and Convex Combination Theory." Transportation Research Board (TRB).

Hard, J.O. (1984). "Field Performance of Concrete and Corrugated Steel Pipe Culverts and Bituminous Protection of Corrugated Steel Pipe Culverts." Transportation Research Record, Issue 1001, pp 40-48.

Hsie M., Tu C., and Song P.S. 2008. "Mechanical Properties of Polypropylene Hybrid Fiber Reinforced Concrete." Elsevier Science Ltd, Mater. Sci. Eng. Part A 494 (1–2) (2008) 153–157.

Izaguirre A., Lanas J., and Alvarez J.I. 2011. "Effect of a Polypropylene Fibre on the Behavior of Aerial Lime-Based Mortars." Elsevier Science Ltd, Construction and Building Materials 25 (2011) 992–1000.

Izaguirre, A., Lanas, J., and Alvarez, J. I. (2011). "Effect of a polypropylene fiber on the behavior of aerial lime-based mortars." Construction and Building Materials, Elsevier, 25(2), 992–1000.

Johnson, C., and Hammon, J. 2017. Structural Polyurethane and Rehabilitation of America's Infrastructure. Department of Defense - Allied Nations Technical Corrosion Conference.

Kampbell, E. (2016). "Lining Large Pipes with the New Generation of Cementitious Lining Materials," ASCE Pipelines 2016.

Khatri, D. K., Han, J., Corey, R., Parsons, R. L., and Brennan, J. J. (2015). "Laboratory evaluation of installation of a steel-reinforced high-density polyethylene pipe in soil." Tunnelling and Underground Space Technology, Elsevier Ltd, 49, 199–207.

Kizilkanat A. B., Kabay N., Akyüncü V., Chowdhury S., and Abdullah H. 2015. "Mechanical Properties and Fracture Behavior of Basalt and Glass Fiber Reinforced Concrete: An Experimental Study." Elsevier Science Ltd, Akça, Construction and Building Materials 100 (2015) 218–224.

Klöppel, K., and Glock, D. (1970). Theoretische und experimentelle Untersuchungen zu den Traglastproblemen biegeweicher, in die Erde eingebetteter Rohre. 1.[Text]. Techn. Hochsch., Inst. f. Statik u. Stahlbau.

Kohankar Kouchesfehani, Z. (2020). "Development of a Structural Design Methodology for Polymeric Spray Applied Linings." The University of Texas at Arlington (Doctoral dissertation)

Kohankar Kouchesfehani, Z., Darabnoush Tehrani, A., Najafi, M. (2020). “Culvert Renewal with Cementitious/Geopolymer Spray Applied Pipe Lining: Field Data Collection and Assessment”. ASCE Journal of Pipeline Systems - Engineering and Practice

Kohankar Kouchesfehani, Z., Darabnoush Tehrani, A., Najafi, M., and Syar, J. (2020). “Laboratory testing of invert-cut corrugated metal pipes renewed with polymeric spray applied pipe lining.” Transportation Geotechnics, Elsevier, 100413.

Kohankar Kouchesfehani, Z., Darabnoush Tehrani, A., Najafi, M., Syar, J. E., and Ed Kampbell, P. E. (2019). “Adding Additional Reinforcement to Improve the Structural Performance of Spray Applied Pipe Lining Rehabilitation Technology: A Review.” ASCE Pipelines, Multidisciplinary Topics, Utility Engineering, and Surveying, ASCE, Nashville.

Kohankar Kouchesfehani, Z., Darabnoush Tehrani, A., Najafi, M., Syar, J. E., and Ed Kampbell, P. E. (2019). “Adding Additional Reinforcement to Improve the Structural Performance of Spray Applied Pipe Lining Rehabilitation Technology: A Review.” Pipelines 2019: Multidisciplinary Topics, Utility Engineering, and Surveying, ASCE, Nashville.

Kohankar Kouchesfehani, Z., Tabesh, A., and Najafi, M. (2017). “Risk Identification for Pipeline Installation by Horizontal Directional Drilling.” Proc. International Congress on Underground Infrastructure, Water Management and Trenchless Technology (ICUWT), 85–92.

Kouchesfehani, Z. K., Paggioli, K., Najafi, M., & Miglio, A. (2018). Evaluation of Structural Design Methodologies for Large Diameter Pipeline Renewal Design. In Pipelines 2018: Condition Assessment, Construction, and Rehabilitation (pp. 327-332). Reston, VA: American Society of Civil Engineers.

Larrinaga P., Chastre C., Biscaia H. C., and San-José J. T. 2014. “Experimental and numerical modeling of basalt textile reinforced mortar behavior under uniaxial tensile.” Elsevier Science Ltd, Materials and Design 55 (2014) 66–74.

Kouchesfehani, Z. K., Paggioli, K., Najafi, M., and Miglio, A. (2018). “Evaluation of Structural Design Methodologies for Large Diameter Pipeline Renewal Design.” Pipelines 2018: Condition Assessment, Construction, and Rehabilitation, American Society of Civil Engineers Reston, VA, 327–332.

Kouchesfehani, Z. K., Tehrani, A. D., Najafi, M., & Syar, J. (2020). Laboratory testing of invert-cut corrugated metal pipes renewed with polymeric spray applied pipe lining. Transportation Geotechnics, 25, 100413.

Kunecki, B., and Kubica, E. (2004). “Full-scale laboratory tests and FEM analysis of corrugated steel culverts under standardized railway load.” Archives of Civil and Mechanical Engineering, 4(4), 41–53.

Law, T.C.M. & Moore, I.D. (2007), "Numerical modeling of tight-fitting flexible liner in damaged sewer under earth loads," Tunneling and Underground Space Technology, Vol. 22, pages 655-665.

Law, T.C.M., and Moore, I.D. (2003), "Guidance on design of flexible liners to repair structurally compromised gravity flow sewers," Proceedings of the 21st International No-Dig Conference, NASTT, Las Vegas.

Leonards, G. A., and Stetkar, R. E. (1978). “Performance of buried flexible conduits: Interim report.” Purdue University.

Lougheed, A. C. (2008). “Limit States Testing of a Buried Deep Corrugated Large-Span Box Culvert.” Queen’s University.

Luk G. K. (2001). “Pipeline Rehabilitation with Fiber-Reinforced Mortar Lining”, ASCE, J. Infrastruct. Syst., 7(3): 116-122.

Luo J., Li Q., Zhao T., Gao S., and Sun S. 2013. “Bonding and Toughness Properties of PVA Fiber Reinforced Aqueous Epoxy Resin Cement Repair Mortar.” Elsevier Science Ltd, Constr. Build. Mater. 49 (2013) 766–771.

Luscher, Ulrich. Buckling of Soil Surrounded Tubes, Journal of Soil Mechanics & Foundation Division, Vol. 92, No. SM6, November 1966.

Mahgoub, A., and El Naggar, H. 2020. Innovative Application of Tire-Derived Aggregate around Corrugated Steel Plate Culverts. Journal of Pipeline Systems Engineering and Practice, 11(3): 1–18. doi:10.1061/(ASCE)PS.1949-1204.0000466.

Mai, V. T., Hoult, N. A., and Moore, I. D. (2013). “Effect of deterioration on the performance of corrugated steel culverts.” Journal of Geotechnical and Geoenvironmental Engineering, 141(4), 1–11.

Mai, V.T., Hoult, N., and Moore, I. 2018. Numerical evaluation of a deeply buried pipe testing facility. Advances in Structural Engineering, 21(16): 2571–2588. doi:10.1177/1369433218783769.

Maletz, Markus (2013), "German DWA Worksheet A 143, Part 2 – what's new in structural design of CIPP" No-Dig Conference and Exhibition, Berlin, Paper 4-3, 16 pages.

Masada, T. (2017a). Structural Benefits of Concrete Paving of Steel Structural Benefit of Concrete Paving of Steel Culvert Inverts.

Masada, T. (2017b). Structural Benefit of Concrete Paving of Steel Culvert Inverts. Ohio.

Masada, T., Hurd, J. and Fekrat, A. Q. (2017), “Structural Benefits of Concrete Paving of Steel Culvert Inverts.” Prepared in cooperation with the Ohio Department of Transportation and the U.S. Department of Transportation, Federal Highway Administration. Report No. FHWA/OH-2017-21

Masada, T., Sargand, S. M., Tarawneh, B., Mitchell, G. F., and Gruver, D. (2007). “Inspection and risk assessment of concrete culverts under Ohio’s highways.” Journal of Performance of Constructed Facilities, 21(3), 225–233.

Matthews J., Selvakumar A., Vaidya S., and Condit W. (2015). “Large-Diameter Sewer Rehabilitation Using a Spray-Applied Fiber-Reinforced Geopolymer Mortar.” ASCE, Pract. Period. Struct. Des. Constr., 20(4): 04014050.

Matthews, J. C., Condit, W., Vaidya, S. and Stowe, R. (2014). “Performance Evaluation of an Innovative Fiber Reinforced Geopolymer Spray-Applied Mortar for Large Diameter Wastewater Main Rehabilitation in Houston, Texas.” A Report Prepared for U.S. Environmental Protection Agency (EPA). EPA/600/R-14/443.

Matthews, J., Simicevic, J., Kestler, M., and Piehl, R. (2012). Decision analysis guide for corrugated metal culvert rehabilitation and replacement using trenchless technology. United States Department of Agriculture, Forest Service.

Mitchell, G. F., Masada, T., Sargand, S. M., and Tarawneh, B. (2005). Risk assessment and update of inspection procedures for culverts. United States. Federal Highway Administration.

Mohammad, N. (2016). Pipeline Infrastructure renewal and asset management. McGraw Hill Professional.

Moore, I. D. and García, B. D. (2013). “Measured Response of Two Deteriorated Metal Culverts Repaired with Sprayed Cementitious Liners.” Report on performance of the GeoSpray liner system for the 407 ETR, November 2013, 117pp,

Moore, I. D. and García, B. D. (2015). “Ultimate Strength Testing of Two Deteriorated Metal Culverts Repaired with Spray-On Cementitious Liners.” Transportation Research Record: Journal of the Transportation Research Board, No. 2522, 2015, pp. 139-147,

Moore, I.D. (1998), "Tests for pipe liner stability: What we can and cannot learn," Proceedings of the North American No-Dig Conference, Albuquerque, NM, page 444 – 457.

Moore, I.D. and Becerril Garcia, D. (2013), Measured response of two deteriorated metal culverts repaired with sprayed cementitious liners, Report on performance of the GeoSpray liner system for the 407 ETR, November 2013, 117pp

Moore, I.D. and Doherty, I. (2016), Design of Cementitious Liners for Repair of Deteriorated Metal Culverts, North American Society for Trenchless Technology Conference, Dallas, Texas, March 2016, 8pp.

Moore, R.G., Bedell, P.R. and Moore I.D. (1995), “Design and Implementation of Repairs to Corrugated Steel Plate Culverts.” ASCE Journal of Performance of Constructed Facilities, Vol 9, No.2.

Moser, A.P., and Folkman, S.L. 2008. Buried pipe design. In Third. McGraw-Hill New York.

Naaman E. A. (2003). “Engineered Steel Fibers with Optimal Properties for Reinforcement of Cement Composites.” Journal of Advanced Concrete Technology, Vol 1, No. 3, 241-252.

Najafi, M. (2005). “Trenchless Technology: Pipeline and Utility Design, Construction and Renewal,” McGraw-Hill, New York, NY.

Najafi, M. (2008). An asset management approach for drainage infrastructure and culverts. Midwest Regional University Transportation Center, University of Wisconsin.

Najafi, M. (2010). Trenchless Technology Piping: Installation and Inspection: Installation and Inspection. McGraw Hill Professional.

Najafi, M. (2011). Pipeline Rehabilitation Systems for Service Life Extension - Chapter 10. University of Texas at Arlington, USA, 2011.

Najafi, M. (2013). Trenchless technology: Planning, equipment and Methods. Chicago: McGraw Hill Professional.

Najafi, M. (2016). “Pipeline Infrastructure Renewal and Asset Management,” McGraw-Hill, New York, NY.

Najafi, M. and Gokhale, S.B. (2005). Trenchless Technology: Pipeline and Utility Design, Construction, and Renewal, New York: McGraw-Hill; 2005.

Najafi, M., and Bhattachar, D. V. (2011). “Development of a culvert inventory and inspection framework for asset management of road structures.” Journal of King Saud University - Science, 23(3), 243–254.

Najafi, M., and Gokhale, S. (2005). Trenchless technology: Pipeline and utility design, construction, and renewal. McGraw-Hill New York.

Najafi, M., and Osborn, L., (2008). “Trenchless Renewal of Culverts and Storm Sewers.” ASCE International Pipelines Conference 2008, July 22-27, 2008, Atlanta, Georgia.

Najafi, M., and Sever, V. F., (2015). “Structural Capability of No-Dig Manhole Rehabilitation.” A Report for the Water Environment Research Foundation. Prepared by the University of Texas at Arlington (UTA), Center for Underground Infrastructure Research and Education (CUIRE), https://www.uta.edu/ce/cuire/INFR1R12%20web.pdf,

Najafi, M., Salem, S., Bhattachar, D., Salman, B., and Patil, R. (2008). “An Asset Management Approach for Drainage Infrastructure and Culverts.” Midwest Regional University Transportation Center, Madison, WI, http://www.wistrans.org/mrutc/files/06-08_FR.pdf, Date Accessed April 24, 2018.

Najafi, M., Sever, V. F. (2019). “D-Load Strength of Concrete Pipes with Epoxy Linings.” 10(4), 1–11.

NASSCO, P. A. (2019). “Certification Program (PACP) Reference Manual.” Version.

National Association of Sewer Service Companies (NASSCO). (2019). “Certification Program (PACP) Reference Manual.”

NCHRP SYNTHESIS 303. (2002). “Assessment and Rehabilitation of Existing Culverts,” A Synthesis of highway Practice. National Cooperative Highway Research Program (NCHRP). Transportation Research Board of the National Academes.

NCSPA. (2017). “Spiral Rib Pipe.” North Carolina State Ports Authority. The National Corrugated Steel Pipe Association.

NCSPA. 2008. Corrugated Steel Pipe Design Manual. National Corrugated Steel Pipe Association, Dallas.

Noushini, A., Samali, B., and Vessalas, K. (2013). “Flexural Toughness and Ductility Characteristics of Polyvinyl-Alcohol Fibre Reinforced Concrete (PVA-FRC).” In 8th International Conference on Fracture Mechanics of Concrete and Concrete Structures, FraMCoS. International Center for Numerical Methods in Engineering.

ODOT (2017). Ohio Department of Transportation, Culvert Management Manual, http://www.dot.state.oh.us/Divisions/Engineering/Hydraulics/Culvert%20Management/Culvert%20Management%20Manual/Culvert%20Management%20Manual%20October%202017%2011-9-17.pdf, Date Accessed April 24, 2018.

Olympus. (2020). “Olympus - Non-Destructive Ultrasonic Test Equipment, Ultrasonic, Phased Array, Microscopes, Thickness Gages, Flaw Detectors, Innov-X, NDT, Remote Visual Inspection, Eddy Current, X-ray Fluorescence, X-ray Diffraction.”

Omara, A.-A. M. (1997). “Analysis of cured-in-place pipes (CIPP) installed in circular and oval deteriorated host pipes.”

OMEGA. 2019. LVDT. Available from www.omega.com.

Ostertag, C. P., and Blunt, J. (2008). “Use of Fiber-Reinforced Concrete in Bridge Approach Slabs.” Rep. No. CA09-0632. Sacramento, CA: California Department of Transportation.

PCPIPE. (2016). “Types of Corrugation.” <www.pcpipe.com/products/typesofcorrugation.html>.

Pigeon M., Pleau R., Azzabi M., and N. Banthia. 1996. “Durability of Microfiber-Reinforced Mortars.” Cement and Concrete Research, Vol. 26, No. 4, pp. 601-609, 1996 Elsevier Science Ltd.

Piratla, K. R., Pang, W., Jin, H., and Stoner, M. (2017). Best Practices for Assessing Culvert Health and Determining Appropriate Rehabilitation Methods.

Primeaux, I. I. (n.d.). “D. (1989). Spray Polyurea–Versatile High-Performance Elastomer for the Polyurethane Industry.” Polyurethanes 89, Proceedings of the SPI–32nd Annual Technical/Marketing Conference, 126–130.

Rahman, M. M., Sameen, S., Hafisa, R. and Sadaque, M. A. (2013). “Behavior of Polymeric Fiber as an Alternative Reinforcement to Iron Wire Mesh in Ferro Cement Elements under Flexural Load,” International Journal of Chemical, Environmental, and Biological Sciences (IJCEBS), Volume 1, Issue 5, pages 715-718.

Rakitin, B., and Xu, M. (2014). “Centrifuge modeling of large-diameter underground pipes subjected to heavy traffic loads.” Canadian Geotechnical Journal, 51(4), 353–368.

Ramakrishnan V., and Tolmare N. S. (1998). “Performance Evaluation of 3-D Basalt Fiber Reinforced Concrete & Basalt Rod Reinforced Concrete.” Idea Program Final Report, NCHR-45, Transportation Research Board National Research Council.

Regier, C., Hoult, N. A., and Moore, I. D. (2016). “Laboratory Study on the Behavior of a Horizontal-Ellipse Culvert during Service and Ultimate Load Testing.” Journal of Bridge Engineering, 22(3), 04016131.

Riahi, E., Yu, X., Najafi, M. and Sever, F. (2014). “Evaluation of Structural Performance of Epoxy Linings for Manhole Rehabilitation using Laboratory Testing and FEM Simulations,” ASCE Pipeline, 2014.

Rodin H. III, Nassiri S., Englund K., Fakron O, and Li H. (2018). “Recycled Glass Fiber Reinforced Polymer Composites Incorporated in Mortar for Improved Mechanical Performance.” Elsevier Science Ltd, Construction and Building Materials 187 (2018) 738–751.

Roesler, J. R., and Gaedicke, M. C. (2004). “Fiber-Reinforced Concrete for Airfield Rigid Pavements.” Technical Note, University of Illinois, Department of Civil and Environmental Engineering, 1208 NCEL, MC-250, Urbana, IL 61801.

Royer, J. R., and Allouche, E. (2016). “Laboratory Testing and Analysis of Geopolymer Pipe-lining Technology for Rehabilitation of Sewer & Stormwater Conduits.” NASTT, Dallas, Texas. WM-T6-03

Sargand, S. M., Khoury, I., Hussein, H. H., and Masada, T. (2018). “Load Capacity of Corrugated Steel Pipe with Extreme Corrosion under Shallow Cover.” Journal of Performance of Constructed Facilities, American Society of Civil Engineers, 32(4), 4018050.

Sargand, S., Khoury, I., Jordan, B., and Hussein H. (2015). “Ultimate Load Capacity of Corrugated Steel Pipe with Extreme Corrosion.” Prepared for Ohio Department of Transportation (Ohio DOT). Prepared in cooperation with the Ohio DOT and the U.S. Department of Transportation, Federal Highway Administration.

Schluter, J. C., and Shade, J. W. (1999). “Flexibility factor or pipe stiffness: Significant stiffness considerations.” Transportation research record, SAGE Publications Sage CA: Los Angeles, CA, 1656(1), 45–50.

Schrock, B. Jay and Gumbel, John, "Pipeline Renewal – 1997," Conference Paper, Workshop 1-1, North American No-Dig '97, NASTT North American Conference and Exhibition of Trenchless Technology, April 10-21, 1997, Seattle, WA.

Sehn, A. L., and Duncan, J. M. (1994). “Investigation of large deformations of a corrugated metal pipe in silty soil: Culvert distress and failures.” Transportation research record, (1431), 3–12.

Selvakumar, A., Matthews, J.C. and Condit, W. (2014). “Demonstration of an Innovative Large Diameter Sewer Rehabilitation Technology in Houston, Texas,” NASTT 2014 NO-Dig Show, Orlando, Florida.

Sever, V. F., Najafi, M. and Jain, A. (2013). “No-Dig Manhole Rehabilitation Knowledge Gaps,” ASCE Pipelines 2013.

Sezen, H., Fox, P., Yeau, K. (2009), Verification of ODOT's Load Rating Analysis Programs for Metal Pipe and Arch Culverts", ODOT State Job Number 134225, 263 pp.

Siavash G. Motlagh, Jain, A., and Najafi, M. (2013). “Comparison of Spray-on Linings for Water Pipeline Renewal Applications.” 1114–1126.

Spadea S, Farina I, Carrafiello A, and Fraternali F. 2015. “Recycled Nylon Fibers as Cement Mortar Reinforcement, Elsevier Science Ltd, Construction and Building Materials 80 (2015) 200–209.

Spadea, S., Farina, I., Carrafiello, A., and Fraternali, F. (2015). “Recycled nylon fibers as cement mortar reinforcement.” Construction and Building Materials, Elsevier, 80, 200–209.

Spangler, M. G. (1941). “The structural design of flexible pipe culverts. Bulletin, XL (153).” Iowa State College Ames, IA.

Spangler, M. G. (1960). “Engineering Characteristics of Soils and Soil Testing.” Highway Engineering Handbook, 1st Edition. McGraw-Hill, 8.

Syar, J. E., Najafi, M., Kohankar Kouchesfehani, Z., Korky, S., and Darabnoush Tehrani, A. (2019). “Use of Spray Applied Pipe Linings as a Structural Renewal for Gravity Storm Water Conveyance Conduits.” North American Society for Trenchless Technology (NASTT), Chicago, Illinois, WM-T5-05.

Syar, J.E., Najafi, M., Kouchesfehani Kohankar, Z., and Darabnoush Tehrani, A. 2020. Soil Box Testing Details of Spray Applied Pipe Linings as a Structural Renewal for Gravity Storm Water Conveyance Conduits. In NASTT’s 2020 No-Dig Show. North American Society for Trenchless Technology (NASTT), Denver. p. WM-T4-03.

Szafran, J. and Matusiak, A. (2017), “Structural Behavior and Compressive Strength of Concrete Rings Strengthened with a Polyuria Coating System.” Monograph from Scientific Seminar Organized by Polish Chapters of International Association for Shell and Spatial Structures, University Science and Technology. Civil, Architecture and Environmental Engineering, Lodz University of Technology, Poland,

Tassew S.T., and Lubell A.S. 2014. “Mechanical properties of glass fiber reinforced ceramic concrete.” Elsevier Science Ltd, Construction and Building Materials 51 (2014) 215–224.

Tetreault J., Hoult N. A. and Moore I. D. (2018). “Pre- and post-rehabilitation behavior of a deteriorated horizontal ellipse culvert.” Canadian Geotech Journal Vol. 55, 2018. Published at www.nrcresearchpress.com/cgi.

Theis, T., & Tomkin, J. (2013). Sustainability - A Comprehensive Foundation. U of I Open-Source Textbook Initiative.

Thepot, O. (2000). “A new design method for non-circular sewer linings.” Tunnelling and Underground Space Technology, Elsevier, 15, 25–41.

Thepot, O., Bergue, J.-M., Joussin, J.-M., and Orditz, D. (2015). “Systematic comparison of the four main national methods ASTM F1216, WRc-SRM, DWA-A

143-2 and 3R-2014 applicable to flexible liners of both circular and non-circular cross-sections." No-Dig 2015.

Timoshenko, S., and Gere, J. M. (1961). Theory of elasticity stability. McGraw.

Wagener, B.D. and Leagjeld, E. E. (2014). "Culvert Repair Best Practices, Specifications and Special Provisions – Best Practices Guidelines", Published by Minnesota Department of Transportation.

Walker, D., and Guan, S. (1997). "Protective linings for steel pipe in potable water service." NACE Northern Area International Conference Corrosion Prevention, 10–11.

Ward, C.D. (2018). "The Renewal of Stormwater Systems Using Trenchless Technologies," NCHRP Synthesis 519.

Watkins, R. K. and Reeve, R. C. (1982) "Effect of Heavy Loads on Buried Corrugated Polyethylene Pipe." Advanced Drainage Systems, Inc., Columbus, Ohio,

Watkins, R.K., Anderson, L.R. (1999), Structural Mechanics of Buried Pipes, CRC Press LLC, 444pp

Whidden, W.R. 2009. Buried flexible steel pipe: Design and structural analysis. American Society of Civil Engineers.

Wisconsin DOT. (1997). Facilities Development Manual, Hydraulic Design of Culverts.

Wyant, D. C. (2002). SYNTHESIS 303 Assessment and Rehabilitation of Existing Culverts.

Yeau, K. Y., Sezen, H., and Fox, P. J. (2009). "Load performance of in situ corrugated steel highway culverts." Journal of Performance of Constructed Facilities, American Society of Civil Engineers, 23(1), 32–39.

Yoo D. Y., Banthia N. 2016. "Mechanical Properties of Ultra-High-Performance Fiber Reinforced Concrete: A Review." Elsevier Science Ltd, Cement and Concrete Composites 73 (2016) 267e280.

Zanotti C., Banthia N., and Plizzari G. (2014). "A Study of Some Factors Affecting Bond in Cementitious Fiber Reinforced Repairs." Elsevier Science Ltd, Cem. Concr. Res. 63 (2014) 117–126.